United States
Environmental Protection
Agency

Policy, Planning,
And Evaluation
(PM-221)

EPA-230-05-89-051
June 1989

EPA

The Potential Effects Of Global Climate Change On The United States

Appendix A
Water Resources

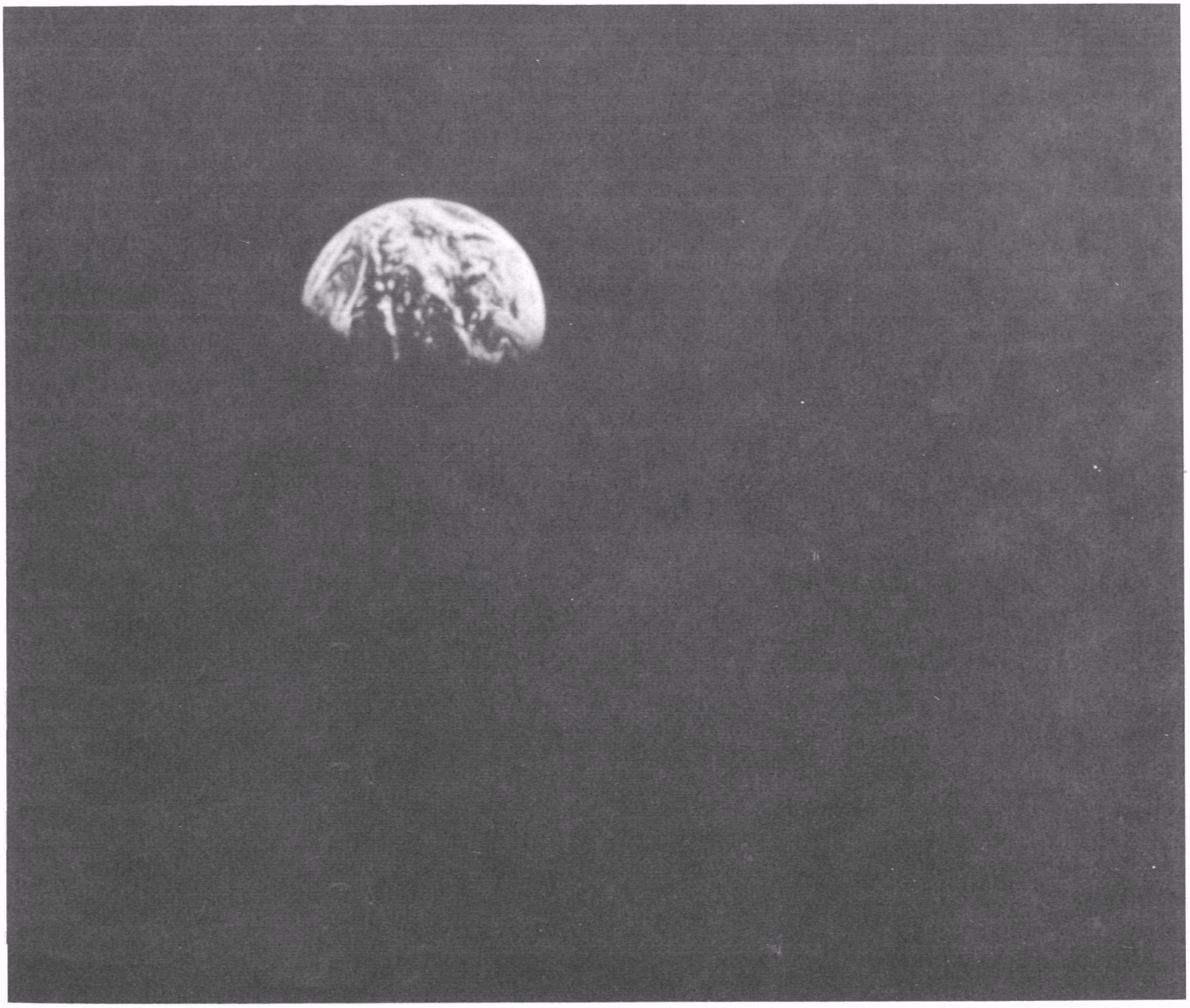

THE POTENTIAL EFFECTS OF GLOBAL CLIMATE CHANGE ON THE UNITED STATES:

APPENDIX A - WATER RESOURCES

Editors: Joel B. Smith and Dennis A. Tirpak

OFFICE OF POLICY, PLANNING AND EVALUATION
U.S. ENVIRONMENTAL PROTECTION AGENCY
WASHINGTON, DC 20460

MAY 1989

Text Printed on Recycled Paper

TABLE OF CONTENTS

Page

APPENDIX A: WATER RESOURCES

PREFACE iii

INTERPRETATION OF HYDROLOGIC EFFECTS OF CLIMATE CHANGE IN THE SACRAMENTO-SAN JOAQUIN RIVER BASIN, CALIFORNIA 1-1
Dennis P. Lettenmaier, Thian Yew Gan, and David R. Dawdy

METHODS FOR EVALUATING THE POTENTIAL IMPACTS OF GLOBAL CLIMATE CHANGE: CASE STUDIES OF THE STATE OF CALIFORNIA AND ATLANTA, GEORGIA 2-1
Daniel P. Sheer and Dean Randall

THE IMPACTS OF CLIMATE CHANGE ON THE SALINITY OF SAN FRANCISCO BAY 3-1
Philip B. Williams

EFFECTS OF CLIMATE CHANGES ON THE LAURENTIAN GREAT LAKES LEVELS 4-1
Thomas E. Croley II and Holly C. Hartmann

IMPACT OF GLOBAL WARMING ON GREAT LAKES ICE CYCLES 5-1
Raymond A. Assel

POTENTIAL CLIMATE CHANGES TO THE LAKE MIGHIGAN THERMAL STRUCTURE 6-1
Michael J. McCormick

THE EFFECTS OF CLIMATE WARMING ON LAKE ERIE WATER QUALITY 7-1
Alan F. Blumberg and Dominic M. Di Toro

IMPACTS OF GLOBAL WARMING ON RUNOFF IN THE UPPER CHATTAHOOCHEE RIVER BASIN 8-1
David K. Hains and C. F. Hains

POTENTIAL IMPACTS OF CLIMATE CHANGE ON THE TENNESSEE VALLEY AUTHORITY RESERVOIR SYSTEM 9-1
Barbara A. Miller and W. Gary Brock

PREFACE

The ecological and economic implications of the greenhouse effect have been the subject of discussion within the scientific community for the past three decades. In recent years, members of Congress have held hearings on the greenhouse effect and have begun to examine its implications for public policy. This interest was accentuated during a series of hearings held in June 1986 by the Subcommittee on Pollution of the Senate Environment and Public Works Committee. Following the hearings, committee members sent a formal request to the EPA Administrator, asking the Agency to undertake two studies on climate change due to the greenhouse effect.

> One of the studies we are requesting should examine the potential health and environmental effects of climate change. This study should include, but not be limited to, the potential impacts on agriculture, forests, wetlands, human health, rivers, lakes, and estuaries, as well as other ecosystems and societal impacts. This study should be designed to include original analyses, to identify and fill in where important research gaps exist, and to solicit the opinions of knowledgeable people throughout the country through a process of public hearings and meetings.

To meet this request, EPA produced the report entitled *The Potential Effects of Global Climate Change on the United States*. For that report, EPA commissioned fifty-five studies by academic and government scientists on the potential effects of global climate change. Each study was reviewed by at least two peer reviewers. The Effects Report summarizes the results of all of those studies. The complete results of each study are contained in Appendices A through J.

Appendix	Subject
A	Water Resources
B	Sea Level Rise
C	Agriculture
D	Forests
E	Aquatic Resources
F	Air Quality
G	Health
H	Infrastructure
I	Variability
J	Policy

GOAL

The goal of the Effects Report was to try to give a sense of the possible direction of changes from a global warming as well as a sense of the magnitude. Specifically, we examined the following issues:

- sensitivities of systems to changes in climate (since we cannot predict regional climate change, we can only identify sensitivities to changes in climate factors)
- the range of effects under different warming scenarios
- regional differences among effects
- interactions among effects on a regional level

- national effects
- uncertainties
- policy implications
- research needs

The four regions chosen for the studies were California, the Great Lakes, the Southeast, and the Great Plains. Many studies focused on impacts in a single region, while others examined potential impacts on a national scale.

SCENARIOS USED FOR THE EFFECTS REPORT STUDIES

The Effects Report studies used several scenarios to examine the sensitivities of various systems to changes in climate. The scenarios used are plausible sets of circumstances although none of them should be considered to be predictions of regional climate change. The most common scenario used was the doubled CO_2 scenario ($2XCO_2$), which examined the effects of climate under a doubling of atmospheric carbon dioxide concentrations. This doubling is estimated to raise average global temperatures by 1.5 to 4.5°C by the latter half of the 21st century. Transient scenarios, which estimate how climate may change over time in response to a steady increase in greenhouse gases, were also used. In addition, analog scenarios of past warm periods, such as the 1930s, were used.

The scenarios combined average monthly climate change estimates for regional grid boxes from General Circulation Models (GCMs) with 1951-80 climate observations from sites in the respective grid boxes. GCMs are dynamic models that simulate the physical processes of the atmosphere and oceans to estimate global climate under different conditions, such as increasing concentrations of greenhouse gases (e.g., $2XCO_2$).

The scenarios and GCMs used in the studies have certain limitations. The scenarios used for the studies assume that temporal and spatial variability do not change from current conditions. The first of two major limitations related to the GCMs is their low spatial resolution. GCMs use rather large grid boxes where climate is averaged for the whole grid box, while in fact climate may be quite variable within a grid box. The second limitation is the simplified way that GCMs treat physical factors such as clouds, oceans, albedo, and land surface hydrology. Because of these limitations, GCMs often disagree with each other on estimates of regional climate change (as well as the magnitude of global changes) and should not be considered to be predictions.

To obtain a range of scenarios, EPA asked the researchers to use output from the following GCMs:

- Goddard Institute for Space Studies (GISS)
- Geophysical Fluid Dynamics Laboratory (GFDL)
- Oregon State University (OSU)

Figure 1 shows the temperature change from current climate to a climate with a doubling of CO_2 levels, as modeled by the three GCMs. The figure includes the GCM estimates for the four regions. Precipitation changes are shown in Figure 2. Note the disagreement in the GCM estimates concerning the direction of change of regional and seasonal precipitation and the agreement concerning increasing temperatures.

Two transient scenarios from the GISS model were also used, and the average decadal temperature changes are shown in Figure 3.

FIGURE 1. TEMPERATURE SCENARIOS

GCM Estimated Change in Temperature from $1xCO_2$ to $2xCO_2$

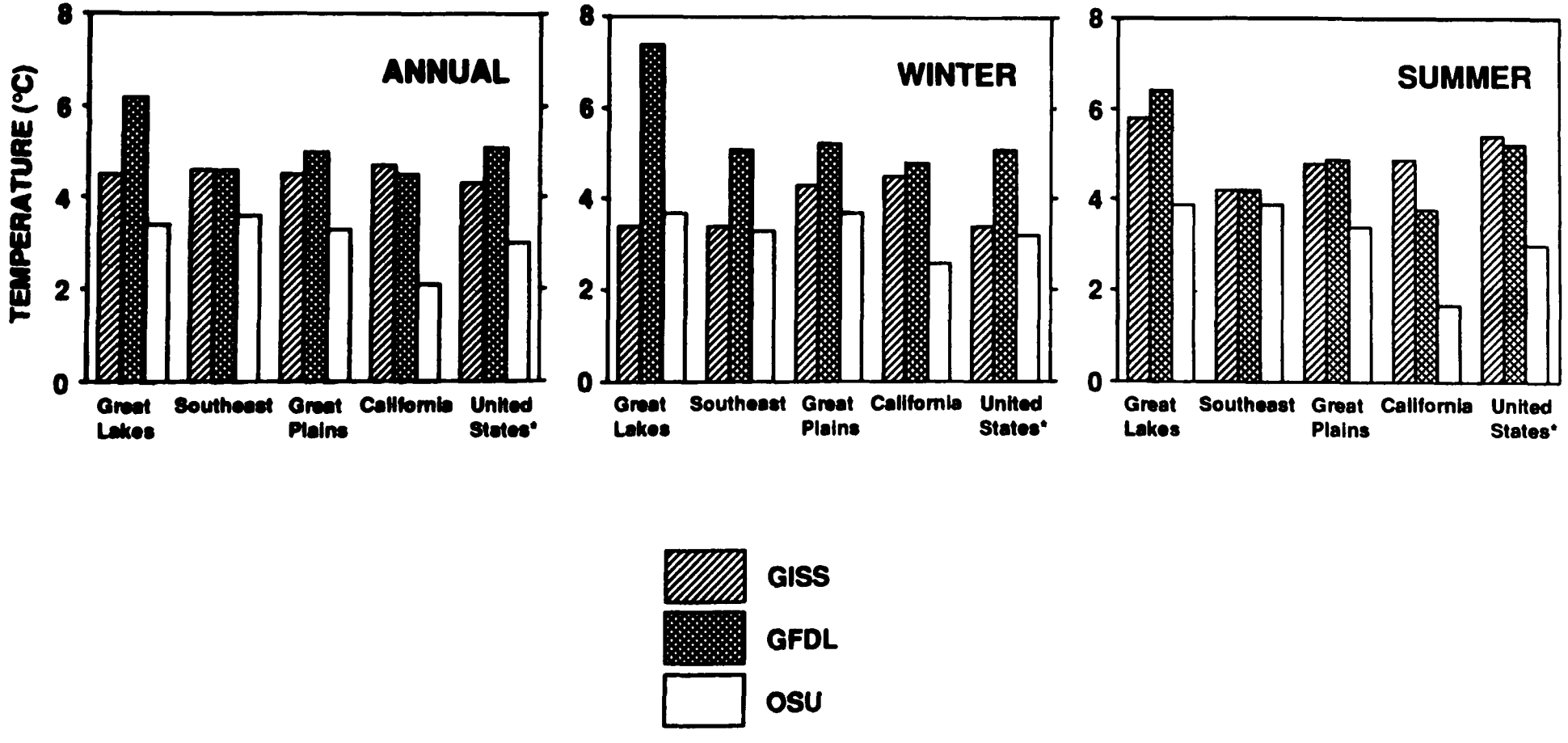

* Lower 48 States

FIGURE 2. PRECIPITATION SCENARIOS

GCM Estimated Change in Precipitation from $1xCO_2$ to $2xCO_2$

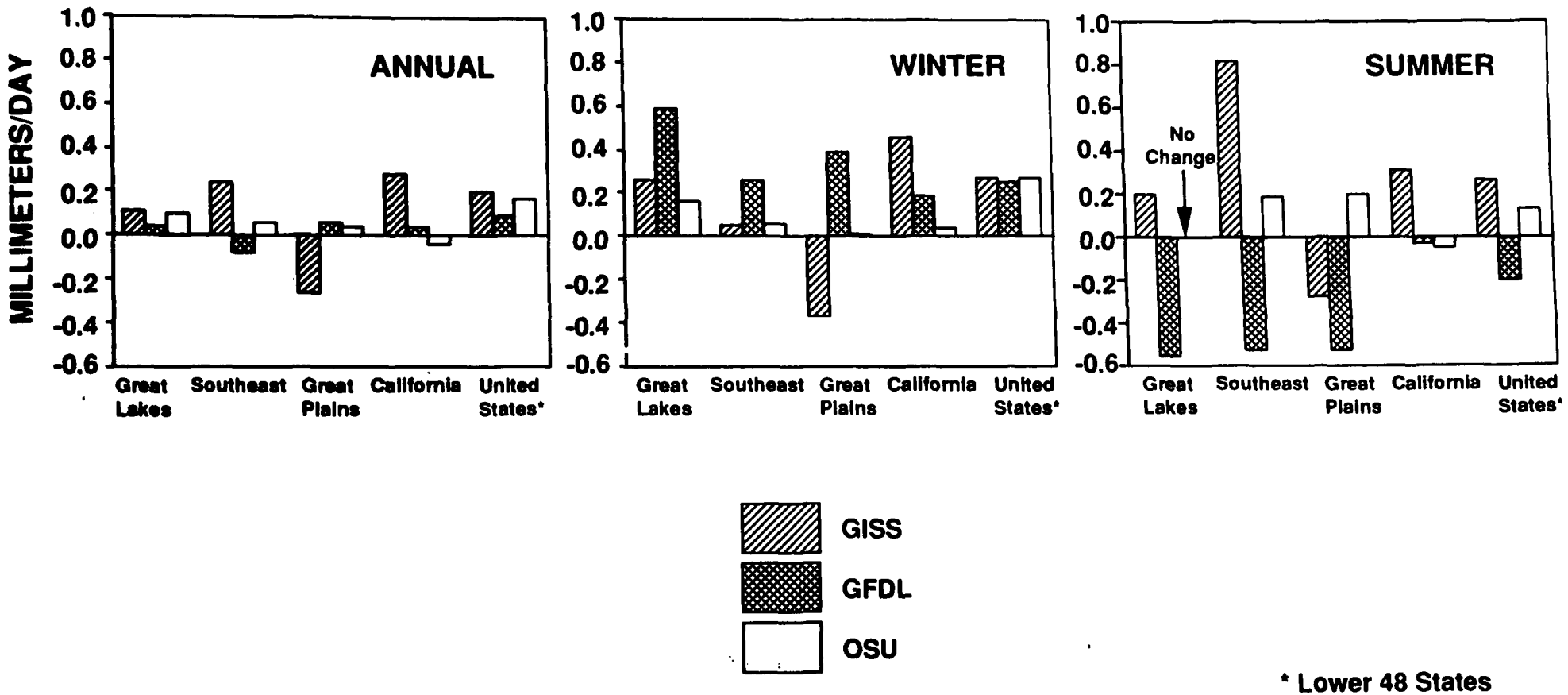

* Lower 48 States

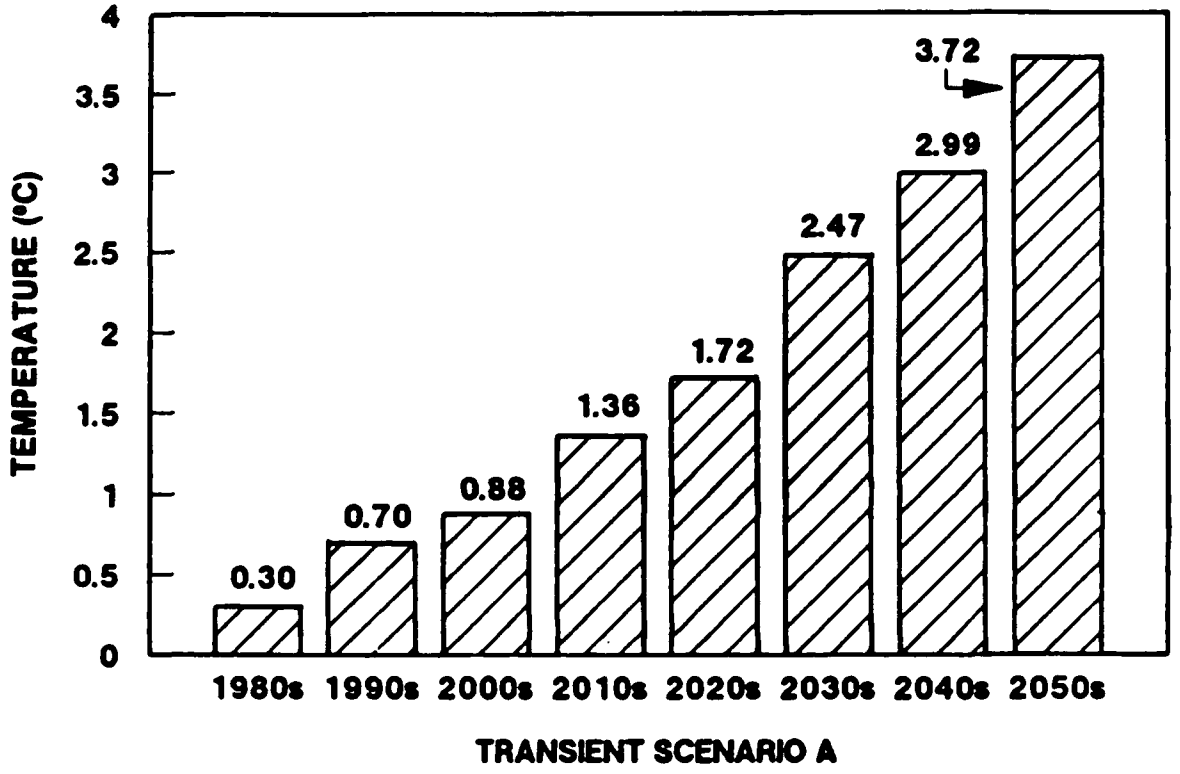

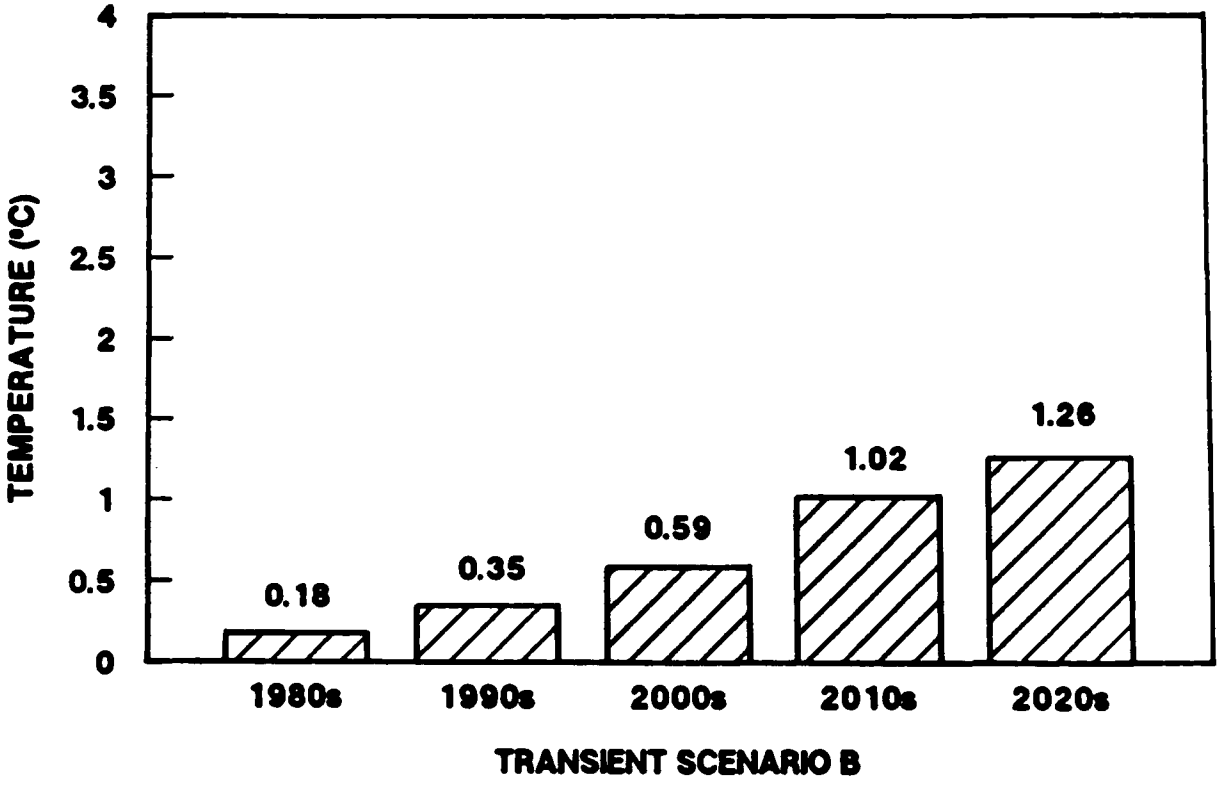

FIGURE 3. GISS TRANSIENTS "A" AND "B" AVERAGE TEMPERATURE CHANGE FOR LOWER 48 STATES GRID POINTS.

EPA specified that researchers were to use three doubled CO_2 scenarios, two transient scenarios, and an analog scenario in their studies. Many researchers, however, did not have sufficient time or resources to use all of the scenarios. EPA asked the researchers to run the scenarios in the following order, going as far through the list as time and resources allowed:

1. GISS doubled CO_2
2. GFDL doubled CO_2
3. GISS transient A
4. OSU doubled CO_2
5. Analog (1930 to 1939)
6. GISS transient B

ABOUT THESE APPENDICES

The studies contained in these appendices appear in the form that the researchers submitted them to EPA. These reports do not necessarily reflect the official position of the U.S. Environmental Protection Agency. Mention of trade names does not constitute an endorsement.

INTERPRETATION OF HYDROLOGIC EFFECTS OF CLIMATE CHANGE IN THE SACRAMENTO-SAN JOAQUIN RIVER BASIN, CALIFORNIA

by

Dennis P. Lettenmaier
Thian Yew Gan
Department of Civil Engineering
University of Washington
Seattle, WA 98195

and

David R. Dawdy
Consultant
3055 23rd Ave.
San Francisco, CA 94132

Contract No. CR814637

CONTENTS

	Page
ACKNOWLEDGMENTS	iii
EXECUTIVE SUMMARY	1-1
CHAPTER 1: INTRODUCTION	1-3
1.1 Background	1-3
1.2 Objectives	1-4
1.3 Relationship to Other Studies	1-4
CHAPTER 2: STUDY DESIGN AND METHODOLOGY	1-5
2.1 Overview	1-5
2.2 Sacramento-San Joaquin Basin Description	1-7
2.3 Study Catchment Description	1-7
2.3.1 McCloud River	1-9
2.3.2 Merced River	1-9
2.3.3 North Fork American River	1-9
2.3.4 Thomes Creek	1-12
2.4 Model Description	1-12
2.4.1 Snowmelt Model	1-12
2.4.2 Soil Moisture Accounting Model	1-13
2.4.3 Spatial Disaggregation Model	1-15
2.5 Model Implementation	1-16
2.5.1 Precipitation-Temperature Stations and Data Quality	1-16
2.5.2 Snowmelt Model Parameter Estimation	1-18
2.5.3 Soil Moisture Accounting Model Parameter Estimation	1-22
2.6 Model Input Characterization	1-22
2.6.1 Precipitation	1-26
2.6.2 Temperature	1-26
2.6.3 Potential Evapotranspiration	1-26
CHAPTER 3: RESULTS	1-28
3.1 Study Catchment Results for Initial Scenarios	1-28
3.1.1 Snow Water Equivalent	1-32
3.1.2 Runoff	1-32
3.1.3 Evapotranspiration	1-40
3.1.4 Soil Moisture Storage	1-41
3.2 Sensitivity Scenarios	1-41
3.2.1 Snow Water Equivalent	1-42
3.2.2 Runoff	1-42
3.2.3 Evapotranspiration	1-43
3.2.4 Soil Moisture Storage	1-43
3.3 Spatial Disaggregation: Primary Nodes	1-43
3.4 Spatial Disaggregation: Secondary Nodes	1-45
CHAPTER 4: SUMMARY AND CONCLUSIONS	1-48
REFERENCES	1-51

ACKNOWLEDGMENTS

The authors appreciate the assistance of a number of individuals who assisted in various aspects of the project. Dr. Richard H. Hawkins, then on leave with the EPA Environmental Research Laboratory, Corvallis, Oregon, and now with the Watershed Management Program, University of Arizona, was instrumental in the initial planning of the study. Dr. Ronald Neilson of ERL, the Project Officer, participated in the project design and management, as did Dr. Robert Worrest of ERL, and Mr. Joel Smith of EPA's Office of Policy, Planning, and Evaluation. Mr. Wendell Tangborn of the HyMet Company graciously provided computer tapes of daily meteorological data for California. Mr. Roy Jenne of the National Center for Atmospheric Research, assisted by Mr. Dennis Joseph of NCAR, provided additional meteorological data, as well as computerized summary output of the Global Climate Model results. Some of the computer simulations and preliminary analysis were performed by Dr. N. Davies Mtundu, a Postdoctoral Research Associate in the Department of Civil Engineering, University of Washington. The report was reviewed by Dr. Stephen J. Burges, of the Department of Civil Engineering, University of Washington. Notwithstanding the contributions of these individuals, the content of the report, and any opinions expressed, are the sole responsibility of the authors.

This paper is Water Resources Series Technical Report No. 110.

EXECUTIVE SUMMARY[1]

Objectives: The objectives of the study were: 1) To develop a method to interpret the possible hydrologic impacts of global climate change for catchments on the order of tens to hundreds of square miles in mountainous regions; 2) To assess the interaction of the hydrologic diversity of medium-sized catchments within a large river basin in California (the Sacramento-San Joaquin) with climate change predictions made using general circulation models (GCMs); 3) To assess differences in the hydrologic implications of different GCMs, with specific attention to the nature of predicted temperature and precipitation variations by month; and 4) To provide simulated hydrologic data at time and space scales suitable for an assessment of the possible water resource system impacts of climate change in the Sacramento-San Joaquin basin.

Approach: Four study catchments with area ranging from 203 to 358 square miles were selected in the headwaters of the Sacramento-San Joaquin basin. The study catchments were selected on the basis of their geographic and hydrologic diversity, the absence of major upstream diversions or flow regulation, and the availability of long-term hydrologic and meteorological records. Three of the study catchments, the McCloud River, the North Fork American River, and Thomes Creek, lie in the Sacramento River basin; one, the Merced River, is in the San Joaquin basin.

Snow accumulation and ablation, and runoff, were simulated under current (historical) conditions using the National Weather Service snowmelt and soil moisture accounting models. The snowmelt model operated on a six hourly time step, while the soil moisture accounting model operated on a daily time step. Once the models were calibrated to present conditions, simulations were performed under seven alternative climate scenarios. Four of these were initial cases, based on GCM climate scenarios corresponding to 1) Geophysical Fluid Dynamics Laboratory (GFDL) model results for CO_2 doubling; 2) Goddard Institute for Space Studies (GISS) model results for CO_2 doubling; 3) A transient climate predicted by the GISS model for CO_2 changing from current concentrations to double current levels over an eighty year period; and 4) Oregon State University Meteorology Department (OSU) model results for CO_2 doubling. Sensitivity analyses were performed using two additional climate scenarios: 1) the GISS model temperature predictions, with precipitation assumed to remain the same as present; and 2) a long-term climate similar to that experienced in the 1930's.

All simulations were performed using 100 years of daily temperature and precipitation data (disaggregated to a six hourly interval for the snowmelt model) consisting of the years 1951-80 supplemented by 70 additional years drawn at random from the 1951-80 record. For the alternative climate scenarios, the 100-year temperature and precipitation records were adjusted as follows: The long-term average GCM temperature and precipitation means were interpolated to 120°W, 40°N, which is approximately the centroid of the Sacramento-San Joaquin basin. For precipitation, the ratio of the GCM-predicted long-term monthly mean to the long-term mean for a base case (nominally, present conditions) for the same GCM was computed. This ratio was applied to all of the historic precipitation records. For temperature, the same approach was used, except that the difference between the long-term monthly mean temperature for a given climate alternative and the mean temperature for the same model's base case was used to adjust the historic precipitation. For the 1930's analog, the precipitation factors and temperature adjustments were based on an analysis of long-term historic data, rather than GCM results.

Results: All of the initial scenarios (based on steady-state CO_2 doubling, or a transient from present conditions to CO_2 doubling) showed that the simulated hydrologic changes were dominated by a shift in the snow accumulation pattern. Specifically, under the warmer conditions predicted by the GCMs, snow would occur only rarely at lower elevations, and the snow accumulation would be reduced at the higher elevations. For all but the highest catchment (the Merced), this resulted in a change from a snow-dominated to a rainfall-dominated

[1]Although the information in this report has been funded wholly or in part by the U.S. Environmental Protection Agency under contract no. CR814637, it does not necessarily reflect the Agency's views, and no official endorsement should be inferred from it.

hydrologic regime. Long-term mean snow accumulations were greatly reduced, and the maximum mean runoff was shifted from the spring to the winter. Spring and summer runoff were greatly reduced. In addition, soil moisture increased in the winter months and decreased in the spring and summer. Because of the reduction of summer soil moisture, and the increased potential evaporation in the spring, there was a shift in maximum evapo-transpiration earlier in the season. These general shifts were observed for all of the alternative climates. They were most severe for the GFDL and GISS CO_2 doubling scenarios, for which the temperature shifts were the greatest, and were least severe for the OSU model CO_2 doubling, for which the predicted temperature increases were less than one-half those for the GISS and GFDL models for most months.

The sensitivity analyses were designed to assess the extent to which the simulated hydrologic changes resulted from GCM-predicted temperature, as opposed to precipitation, changes. Simulations based on input from the GISS model temperature changes, with present precipitation, showed that the simulated hydrologic changes were dominantly the result of the GCM-predicted warming and not of the predicted precipitation changes. The simulations for the 1930's analog reflected a vastly different hydrologic regime than that predicted by the GCM warming scenarios: temperatures were about the same as present, but precipitation was reduced somewhat. Therefore, for this case, winter snow accumulations were slightly reduced (the reduction was much less than for CO_2 doubling scenarios), but the seasonal flow distribution remained about the same, as did the seasonal distribution of soil moisture and evapotranspiration.

Conclusions: The major conclusion of the study is that, for the snow-dominated hydrology of the Sacramento-San Joaquin basin, a general warming on the order of that predicted by all the GCMs would cause a major reduction in winter snow accumulation, and hence increases in winter runoff and reductions in spring and summer runoff. The simulated changes in annual runoff were minor, and from a practical standpoint, inconsequential in comparison to the change in the seasonal distribution of runoff. Attendant changes in the seasonal distribution of soil moisture and evapotranspiration would also occur. From a hydrologic perspective, GCM-predicted changes in precipitation, for which there is less consensus than temperature, would be less important than the predicted temperature changes.

This preliminary study suggests a number of aspects of the hydrologic cycle that require further study. These include the following: 1) The space-time distribution of precipitation under GCM-predicted altered climates; 2) The interaction of long-term shifts in vegetation, particularly as they would affect evapotranspiration and runoff; 3) Changes in the distribution of extreme floods, given the likely increased incidence of rain-on-snow events in the mid-winter period of maximum precipitation; and 4) Estimation of potential evaporation under the GCM-predicted climates.

CHAPTER 1

INTRODUCTION

1.1 Background

Modern civilizations depend critically on water for municipal and industrial supply, irrigated agriculture, natural resources recovery, and other uses. Throughout history, water shortages have had dramatic cultural effects. Periods of below-normal flow persisting for months to years are a characteristic of the hydrologic cycle that must be recognized in water resource system planning. This is normally accomplished by constructing reservoirs, sometimes augmented by groundwater withdrawals, which act as a buffer to variations in streamflow.

The reliability of a water resource system depends on the withdrawals (demand), as well as the long-term statistics of the reservoir inflows, including their means, coefficients of variations, skew coefficients, and cross- and auto-correlations. Most water resource systems are designed and operated based on a requirement that the system must perform reliably during droughts similar to those experienced in the historic streamflow record. Statistically this is equivalent to an assumption that the inflows are stationary, that is, the streamflow statistics are not time-varying.

The possibility of permanent changes in streamflow, such as might result from long-term changes in climate, complicates the problem of water resources system design and operation considerably. Although changes in climate over periods of thousands of years are well documented, there has been less agreement among hydrologists as to whether changes within typical project planning periods (on the order of a hundred years or less) can be distinguished from the random variations that are to be expected in a stationary time series (see, for example, Klemes, 1974; Lettenmaier and Burges, 1978). This issue was the topic of extensive research by hydrologists in the 1960's and early 1970's, some of which is summarized in the overview to a 1977 National Research Council report (Wallis, 1977). The general conclusion of the NRC report was that, from a practical standpoint, evidence for climate change is not detectable in historic streamflow or meteorological records, which are typically of length less than 100 years.

The advent of general circulation models (GCMs), and some consensus regarding the likely direction of future global climate change places the problem in a somewhat different light. There is now a quasi-deterministic basis for assuming the form that future climate change might take, at least with respect to changes in temperature. A GCM simultaneously solves (numerically) equations representing the conservation of mass, energy, momentum, and the equations of state on a global grid (Hansen et al., 1983, 1988). The spatial scale of the GCM results is, however, inadequate for hydrologic interpretation. GCM predictions are provided as spatial averages over areas on the order of hundreds of thousands of square kilometers. In addition, it is questionable if GCM predictions on time steps shorter than about one month reflect the observed natural variability, particularly given that they represent grid-cell averages (see, for example, Rind et al., 1988).

Interpretation of the effects of changes in meteorological inputs to a hydrologic system (and in turn, water resource developments) requires that those inputs be specified on a time scale appropriate for modeling river basin storm response. This is so because the rainfall-runoff process is highly nonlinear, and such subprocesses as infiltration and evapotranspiration, which play major roles in determining the runoff yield of a basin, depend strongly on the storage and movement of water within the soil column during storms, and the soil moisture condition at the onset of storms. For practical purposes, this implies a daily time scale for large basins (several hundreds of square kilometers and up) and hourly or less for smaller basins. While GCMs can provide grid cell average results for time steps on the order of a day or less, it is not clear whether the results at these short time scales properly reflect the short-term dynamics of the atmospheric circulation process.

Therefore, while the GCM models predict long-term changes that could have substantial impacts on water resource systems, an appropriate interface between the GCM output (most importantly, precipitation, temperature, and potential evaporation) and hydrologic models has not been developed. It is unreasonable to

use GCM results directly as input to a hydrological model to provide streamflow predictions that might be used in the same sense, for instance, as an estimate of the 100-year flood for flood plain mapping. In the absence of better space-time resolution, current hydrologic interpretations are limited to providing descriptive results that must be interpreted in an alternative scenarios context, or sensitivity analysis context. There is no basis at present to predict the hydrologic effects of long-term climate change; all results presented in this document must, therefore, be interpreted in an alternative scenarios context.

1.2 Objectives

The objectives of this work are as follows:

1. To develop a method to provide a descriptive interpretation of the hydrologic impacts of globalclimate change for medium sized catchments on the order of tens to hundreds of square miles in mountainous regions. The approach must account for the changes in snowmelt hydrology that would result from long-term temperature increases, coupled with possible changes in precipitation and evapotranspiration;

2. To assess the interaction of the hydrologic diversity of medium sized catchments within a large river basin in California (the Sacramento-San Joaquin) with GCM predictions to interpret the modes through which climate change could be evidenced in catchment hydrology;

3. To assess differences in the hydrologic implications of different GCMs, with specific attention to the nature of predicted temperature and precipitation variations by month;

4. To use the methods and results developed in 1) and 2) to provide hydrologic input at time and space scales that allow descriptive interpretation of the water resource systems impacts of climate change on the Sacramento-San Joaquin basin;

5. To develop recommendations for research needed to improve the assessment methodology, particularly in light of the relative uncertainties in the GCM predictions, and spatial and temporal resolution incompatibilities between the GCM model output and hydrologic data requirements.

1.3 Relationship to Other Studies

The primary emphasis of this work is the interpretation of the implications of global climate change as predicted by three GCMs (the models of the Geophysical Fluid Dynamics Laboratory, GFDL; the Goddard Institute for Space Studies, GISS; and the Oregon State University Department of Meteorology, OSU) on four medium sized catchments in the Sacramento-San Joaquin River basin of California. As part of this work, predictions of streamflows for larger subbasins of the Sacramento-San Joaquin system were developed and used in a companion study of the implications of global climate change on the operation of the Sacramento-San Joaquin water resource system (Sheer and Randall, 1988). Sheer and Randall applied a model of the water resource system which uses as input monthly streamflow volumes for 13 subbasins. These subbasins have drainage areas much larger than the study catchments described in this report, for which detailed hydrologic models were implemented.

For several reasons relating to data availability and time and budget constraints, it was not possible to implement, or develop, a detailed hydrologic model of each of the 13 subbasins. Therefore, to provide the input required by the water resource systems model used by Sheer and Randall, a statistical model was developed to relate the subbasin (monthly) streamflows to streamflows in the four study catchments. These subbasin flows represent the interface between this study and Sheer and Randall's work and (indirectly) with other studies based on Sheer and Randall's results. In this report, however, we emphasize the interpretation of the hydrologic implications of climate change on the four study catchments. Because the relationship between the study catchment and subbasin flows is statistical, there is no basis for a dynamical interpretation of the changed hydrologies at the subbasin level.

CHAPTER 2

STUDY DESIGN AND METHODOLOGY

2.1 Overview

The overall study design is shown schematically in Figure 2.1. The climatic inputs fall into two categories: historic data, also referred to as the base case (Case 0), and GCM climate alternatives, referred to as Cases 1-7, identified in Table 2.1. The Case 0 historic data, for the period 1951-1980, were augmented by randomly resampling (with replacement) from the years 1951-80 to provide a total record of length 100 years. The hydrologic outputs were either for one of four study catchments (with drainage areas ranging from 203 to 358 square miles), or for water resource system nodes, which are major subbasins of the Sacramento-San Joaquin of size up to several thousand square miles. The initial effort in the study was to implement hydrologic models, one for prediction of snow accumulation and ablation, and another for soil moisture accounting, which could predict the four study catchment outflows on a daily time scale, for precipitation and temperature maxima and minima on a daily time scale, and monthly average pan evaporation.

Table 2.1 General circulation model scenarios investigated

Case	Description
0	Historic conditions 1951-80
1	Geophysical Fluid Dynamics Laboratory (GFDL) $2xCO_2$ steady-state
2	Goddard Institute for Space Studies (GISS) $2xCO_2$ steady-state
3	GISS 80 year $2xCO_2$ transient
4	Oregon State University (OSU) $2xCO_2$ steady-state
5	GISS $2xCO_2$ steady-state with temperature change only (historic precipitation assumed)
6	GISS $2xCO_2$ steady-state with differential GCM node input for southern and northern study catchments
7	1930's analog precipitation and temperature

The implementation followed a standard procedure of model calibration, or parameter estimation, using a selected subset of the historic record, and an independent subset of the data for model verification. Section 2.5 gives details of the calibration and verification procedure. Once the hydrologic models were calibrated, they were run with the historic data altered by addition of a seasonal shift in the case of temperature, and by multiplication by a seasonally varying factor in the case of precipitation, to be consistent with predictions from each of seven long-term GCM predictions. For each climate alternative, study catchment outflows were predicted on a daily time step for the 100-year period indicated above.

This report focuses on the upper right quadrant of Figure 2.1, that is, on interpretation of the hydrologic model output that included soil moisture, snow accumulation, evaporation, and other variables, as well as streamflow. For the purposes of a companion study (Sheer and Randall, 1988) monthly streamflows at each of the 13 water resource system model nodes were predicted using a spatial disaggregation model applied to the study catchment monthly flows; a random noise term was included to assure that selected statistical properties of the disaggregated flows were preserved. The disaggregation model coefficients were estimated using the Case 0 study catchment predictions (summed daily flows to provide a 100-year monthly flow record) and the corresponding historic monthly flows at the water resource model nodes, as indicated in the lower left quadrant of Figure 2.1. Finally, as indicated in the lower right quadrant of Figure 2.1, the disaggregation model

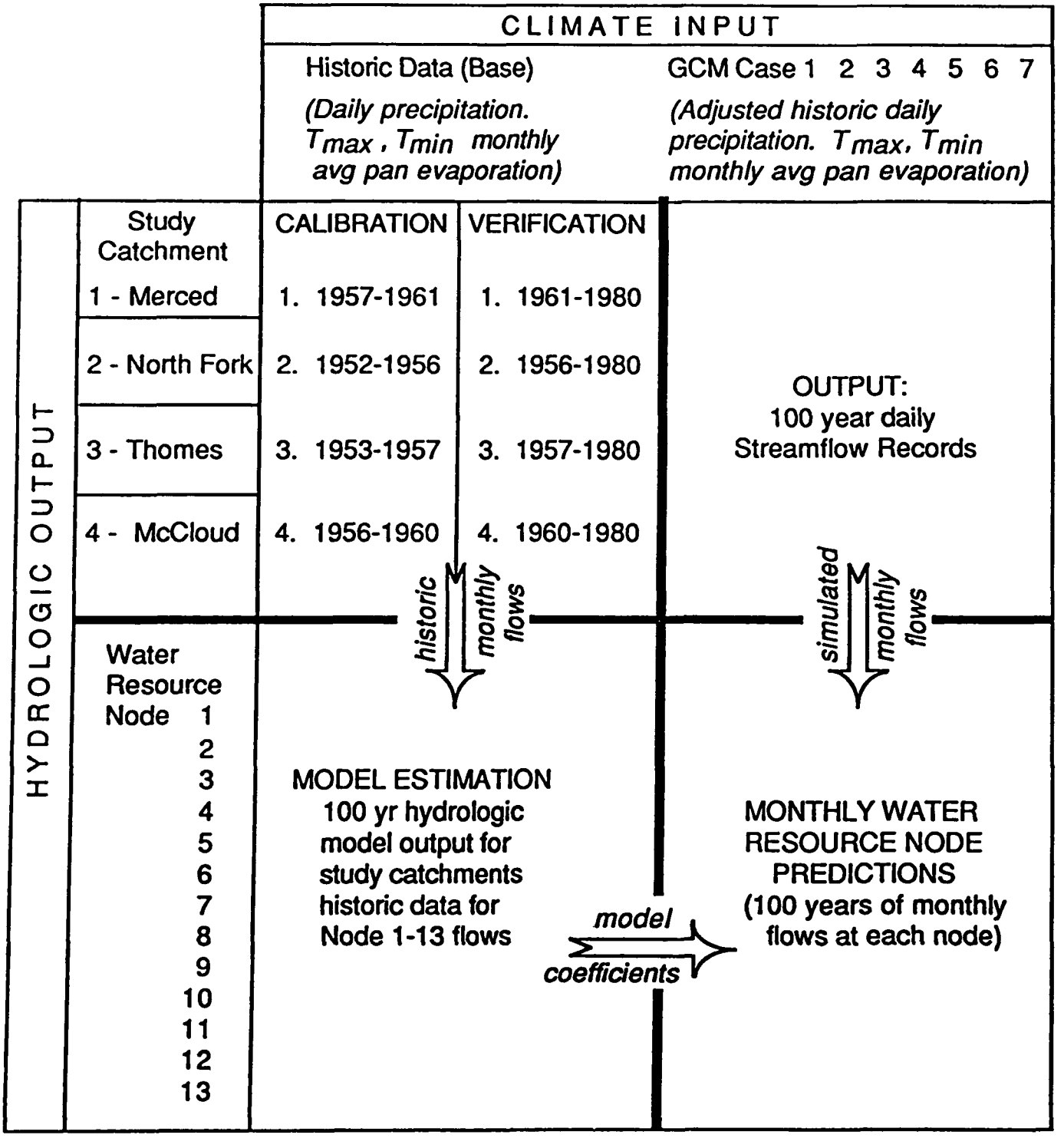

Figure 2.1. Schematic overview of study design.

was used to simulate 100-year monthly streamflow sequences at the water resource system model nodes corresponding to each of the seven climate alternatives. The climatological, hydrologic, and geologic features of the Sacramento-San Joaquin basin, and the four study catchments, are described, and the study approach is expanded, in the next section.

2.2 Sacramento-San Joaquin Basin Description

The Sacramento-San Joaquin Basin (Figure 2.2), or Central Valley, extends nearly 500 miles from north to south, with an average width of about 45 miles separating the Sierra Nevada from the Coast Range. The elevation of much of the valley floor is close to sea level. Beneath its silt and gravel cover is a thick sedimentary sequence. The Coast Range parallels the Pacific coast from the Oregon border to just north of the Los Angeles Basin. The mountains in the Coast Range rise abruptly from the narrow coastal plain to peak elevations of 8,000 feet. The Sierra Nevada, with peak elevations over 14,000 feet, form the eastern boundary of the basin. The Central Valley is terminated in the south by several transverse ranges, which are composed of many overlapping mountain blocks of nearly east-west trend. The basin terminates to the north near the Oregon-California border, where the Coast Range, the Sierra Nevada, and the Cascade range converge.

The Sierra Nevada protect the Sacramento-San Joaquin basin from the cold continental air masses that flow further east in winter. The Coast Range blocks the strong westerly air-flow and accompanying cool summer temperatures that are experienced by the western slopes of the Coast Range. Most of the precipitation in the basin is derived from frontal storms originating in the North Pacific between the months of November and March. Precipitation is strongly orographic; it is heaviest on the west facing slopes of both the Coast Range and the Sierra Nevada. The valley floor is semi-arid, with average annual precipitation generally less than 15 inches.

Temperatures are influenced by prevailing air masses, elevation, and the drainage of cold dense air from the higher elevations into the Central Valley. Although the climate on the western side of the Coast Range is dominated by the Pacific Ocean, with warm winters, cool summers, small daily and seasonal temperature ranges, and high relative humidities, the Sacramento-San Joaquin Basin experiences a more continental type of climate with colder winters, warmer summers, greater daily and seasonal temperature ranges, and generally lower relative humidities than are common for the Coast Range.

2.3 Study Catchment Description

The four study catchments (Figures A.1 to A.4) were selected to represent the geographic, climatic, and hydrologic diversity within the Sacramento-San Joaquin River basin, and to represent, via the spatial disaggregation model described in Section 2.4.3, the monthly streamflows at the water resource systems nodes. Initially, 26 candidate study catchments were identified that were upstream of all major reservoirs. Modeling of streamflow below reservoirs is complicated by the necessity to account for the effect of reservoir storage on stream flow; in practice, to implement a rainfall-runoff model successfully at a daily or shorter time scale requires streamflow data relatively unaffected by reservoirs or upstream diversions.

In addition to the requirement that upstream regulation be minimal, it was required that 1) the candidate study catchments be defined by U.S. Geological Survey (USGS) stream gaging stations rated "good" or better (interpreted by the USGS to mean that the true flow can be expected to be within 10 percent of the recorded flow 95% of the time); an exception to this criteria was allowed during periods of ice cover; and 2) that there be at most minor diversions above the stream gage; and 3) that the period of streamflow record include the years 1951-80. Further screening using these criteria reduced the number of candidate catchments to 19.

The remaining stations were then ranked based on the correlation of their annual flow with the summed annual flow over all the 13 water resource system node annual flows. The three most highly correlated basins, the North Fork of the American River at North Fork Dam (USGS 11-4270, drainage area 342 square miles), Thomes Creek at Paskenta (USGS 11-3820, 203 square miles), and the McCloud River near McCloud (USGS 11-3675, 358 square miles) were selected. Because of the desirability of representing the San Joaquin subbasin,

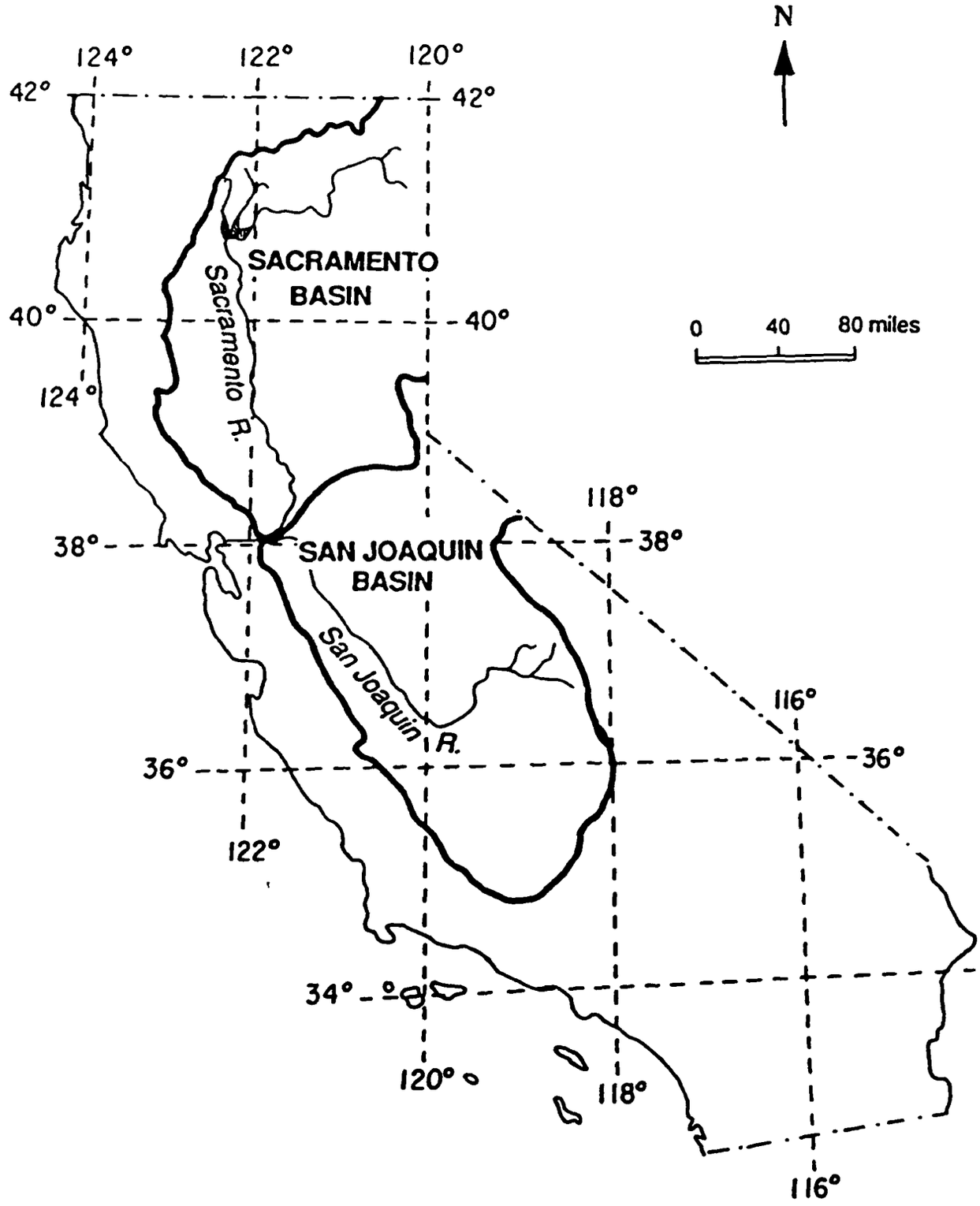

Figure 2.2. Location of the Sacramento - San Joaquin River Basin.

the southern subcatchment (the Merced River at Happy Isles Bridge, USGS 11-2645, 181 square miles) havingthe highest correlation to the total annual basin flow was selected as the fourth study catchment.

Figure 2.3 shows the locations of the index basins. Precipitation on two of the index basins, the American and the Merced River, is typical of that occurring on the west facing slopes of the Sierra Nevada; precipitation in the Thomes Creek Basin is characteristic of the east facing slopes of the Coast Range. The McCloud River, which drains the extreme northern part of the Sacramento River basin, has precipitation characteristics intermediate between those of the east facing slopes of the Coast Range and the west facing slopes of the Sierra Nevada. A brief summary of the particular characteristics of each of the study catchments is provided in the remainder of this section.

2.3.1 McCloud River

The annual precipitation, runoff, and temperature extremes (for January and July) are listed in Table 2.2. The McCloud Basin (358 mi_2) has fairly warm summers, with mean annual temperature slightly below 70°F and cool winters (annual mean of 45°F). Snow and freezing temperatures are not common except at higher elevations. The basin has annual precipitation in excess of 70 inches but rain is light in summers and more frequent in late fall and in winter, with over 80% of the annual total falling between November and May. Thunderstorms occur occasionally in summer; however, they account for only a small percentage of the total annual precipitation.

The basin is located in an area with large, gently sloping volcanoes built by outpouring of basaltic and andesitic lava. Most of these rock formations are deeply weathered, resulting in deep, well-drained soils of extremely high permeability. Even where unweathered, the lavas are highly permeable and generate little surface runoff. Consequently, the annual runoff hydrograph has extremely low variability with a peak to average flow ratio of only about 2.

2.3.2 Merced River

The climate in the Merced basin (321 mi^2) is elevation-dependent, with hot summers and mild winters at low elevations and mild summers and cold winters at high elevations. Because of its relatively higher mean elevation, its hydrology is more controlled by snowfall and snowmelt than other study catchments.

Precipitation is less in the Merced basin than in the McCloud, with an annual mean of about 64 inches. It increases with elevation, from 36 inches at 4,000 feet elevation to a maximum of about 70 inches between 8,000 and 10,000 feet. Most of the precipitation falls in winter, with almost 90% of the annual total falling between November and April. Most precipitation falls as snow at the higher elevations.

The soils in the basin are varied, but are, in general, deep and permeable; some areas are clayey and have lower permeability. The slopes range from nearly level to very steep. Because of the high permeability of the soils, the basin has a relatively dampened storm response, as evidenced by the ratio of the mean annual flood to mean annual flow of about 7.

2.3.3 North Fork American River

Figure 2.3 shows the location of the North Fork American River Basin (342 mi^2) and the main stem of the American River. The North Fork American River has the lowest median elevation (4,000 ft) of any of the study catchments. Much of the annual precipitation (50-60 inches) falls in late autumn and winter. Precipitation in summer is light and generally limited to occasional convective storms.

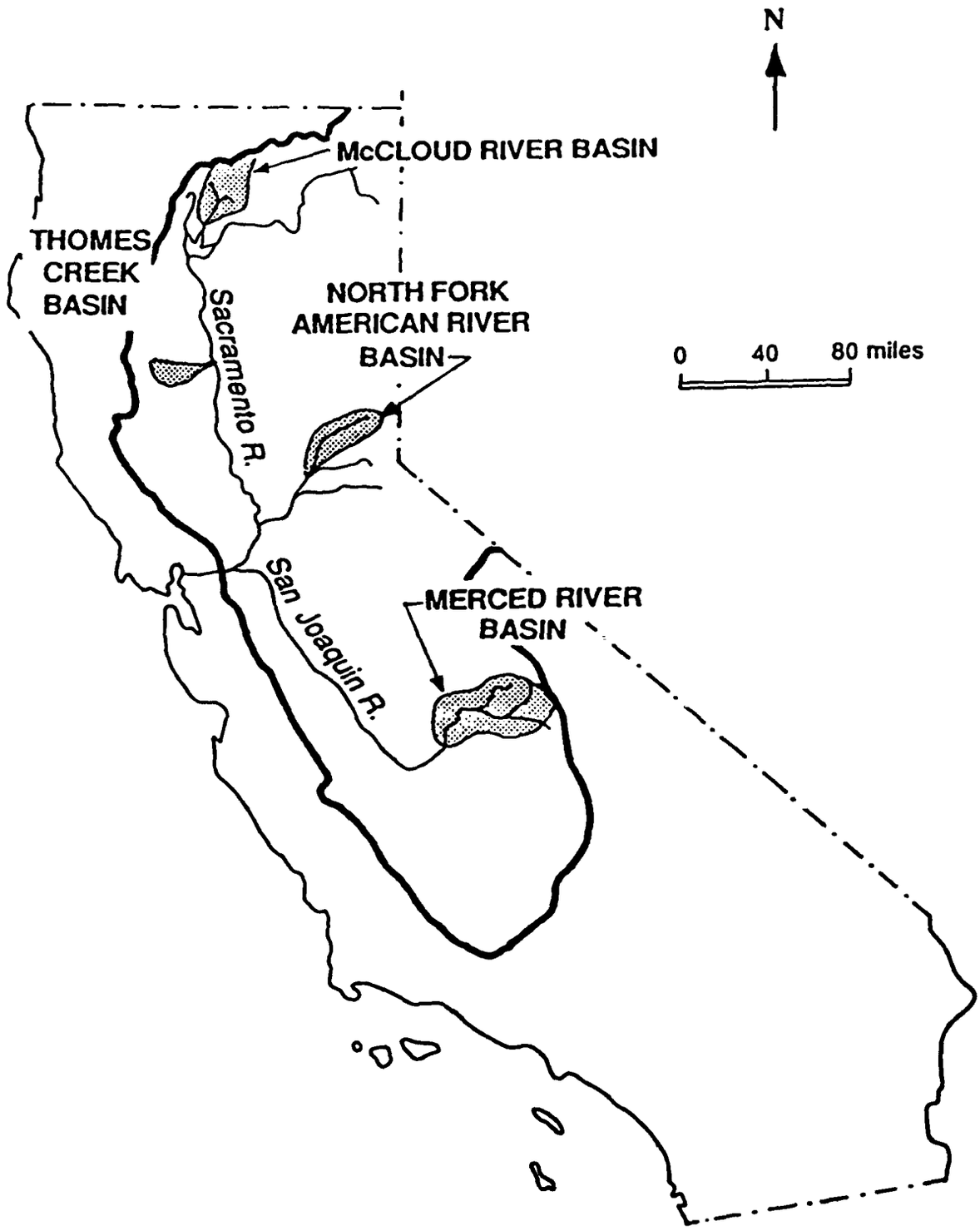

Figure 2.3. Study catchment locations.

Table 2.2. Mean annual historical precipitation, runoff and temperature of McCloud River, Merced River, North Fork American River, and Thomes Creek study catchment

Basin	Mean Annual Runoff (Inches / cfs)	Mean Annual Precipitation[a] (Inches)	Mean January Daily Temperature °F[a]			Mean July Daily Temperature °F[a]		
			Daily Average	Minimum	Maximum	Daily Average	Minimum	Maximum
McCloud	35.40 (933.6)	72.90	30.5	19.5	41.6	63.7	43.0	84.0
Merced	26.30 (621.9)	64.00	31.4	20.5	42.2	66.4	47.9	84.9
North Fork American	33.50 (844.0)	60.30	39.8	30.4	49.0	72.9	58.5	87.2
Thomes Creek	19.86 (297.0)	56.50	35.5	24.9	46.3	66.8	45.2	88.2

[a]Weighted average over elevation bands

The topography varies from nearly level to rolling old valley fill in the vicinity of the Sacramento Valley to predominantly steep dipping, faulted, and folded metamorphic rocks that have been intruded by several types of igneous rocks. Most soils in the mountainous uplands formed in place over metamorphic rock, granitic rock, or andesitic conglomerate, and are not as permeable as those in the Merced Basin. Consequently, the runoff response of the catchment is flashy, particularly in the upland mountains; the peak to average flow ratio is about 20.

2.3.4 Thomes Creek

As with the other study catchments, most of the precipitation in the Thomes Creek basin (203 mi^2) is derived from winter frontal storms. Thundershowers, most frequent in May and June, are generally of short duration but occasionally bring rainfall of high intensity. Much of the western part of the basin, which is above an altitude of 3,500 feet, has moderately deep to deep steep soils underlain by hard sedimentary and metamorphic (mainly fractured mica schist) rock. Permeability is low to moderate, resulting in relatively flashy storm response; the peak to average flow ratio is about 22.

2.4 Model Description

The models selected for this study are a snowmelt model, a soil-moisture accounting (rainfall-runoff) model, and a spatial disaggregation model. Each of the models is described briefly in this section.

2.4.1 Snowmelt Model

The snowmelt model was developed by Eric Anderson of the U.S. National Weather Service Hydrologic Research Laboratory (Anderson, 1973). The model consists of a set of equations that describe the change in storage of water and heat in the snowpack. The model inputs are ambient air temperature and precipitation at a six hourly time step. In this study, daily precipitation was interpolated to six hourly increments and six hourly temperature was estimated from daily temperature maxima and minima using equations given by Anderson (1973). The model input is limited to air temperature and precipitation because data other than temperature and precipitation needed for heat budgets are not normally available in mountainous environments.

The model can be summarized as follows. The heat exchange computations are separated into melt and non-melt periods. Melt periods are further separated into wet (precipitation) and dry periods. If precipitation occurs, the ground is bare, and the ambient air temperature is greater than 32°F, no computations are performed. If the ground is not bare, the heat exchange at the air-snow interface is computed. Two conditions are considered, warm air (air temperature (T_a) >32°F), and cold air (T_a <32°F). For T_a >32°F, the following assumptions are made: a) there is no solar radiation; b) incoming longwave radiation is equivalent to blackbody longwave radiation at T_a; c) the snow surface temperature is 32°F; d) the dew point is T_a; and e) the rain temperature is T_a. On the basis of these assumptions, the heat balance is computed as melt heat loss = Q_n + Q_e + Q_h + Q_p, where Q_n = long wave radiation, Q_e = latent heat transfer due to condensation, Q_h = sensible heat transfer (Bowen ratio based on above assumptions), and Q_p = heat transfer by rainwater (based on assumed rainwater temperature). If T_a is less than 32°F, it is assumed that the precipitation is falling as snow and that no melt occurs.

For melt during nonrain periods, the model first checks to determine whether the snowpack is isothermal at 32°F. If the snowpack is not isothermal, no melt occurs, and the net heat flux is added to the heat content of the snowpack. If the snowpack is isothermal, and the air temperature is greater than 32°F, melt is assumed to take place proportionate to a seasonally varying melt factor and the difference between the air temperature and 32°F (assumed isothermal temperature of the snowpack).

During nonmelt periods (assumed by the model to be any time T_a is less than 32°F), an antecedent temperature index (ATI) is used as an index of the temperature of the surface layer of the snowpack. The ATI is similar to the antecedent precipitation index often used for storm hydrograph prediction (see, for example, Linsley et al., 1975). The net heat exchange at the surface of the snowpack is assumed proportional to the

difference between the ATI and the current air temperature. The proportionality constant is a parameter termed "the negative melt factor," which varies seasonally in the same manner as does the melt factor used during nonrain periods.

Finally, the model accounts for the areal extent of snow cover. During periods of snow accumulation, this is assumed to be 100%. During periods of depletion, the model uses an areal depletion curve, which expresses the percent snow covered area as a function of the ratio of mean areal snow water equivalent to an index value, where the index value is the smaller of the maximum snow water equivalent since snow began to accumulate (i.e., the beginning of the snow season), or a preset maximum.

The most important parameters in the model are: a) the melt factor for nonrain period melt; b) the negative melt factor for the heat balance computation during nonmelt periods; c) the recursion parameter in the antecedent temperature index; and d) the minimum index value in the snow-covered area relationship. This brief description has omitted some details of the model: there is an expression to account for heat transfer at the base of the snowpack, and the retention of liquid water in the snowpack is also modeled. In addition, the model allows the rain-snow division to be made at other than 32°F, and also allows nonrain period melt to occur based on a threshold base air temperature which can be other than 32°F. These expressions and generalizations involve some additional parameters; however, they usually are not as important as the parameters indicated above for studies of the type being performed here. For a complete description of the algorithm, the reader is referred to Anderson (1973).

2.4.2 Soil Moisture Accounting Model

The Soil Moisture Accounting Model was developed by Burnash et al. (1973) and forms the basis of the U.S. National Weather Service's basic catchment hydrologic response model for operational forecasting. It is a deterministic, lumped parameter, conceptual model. The original model was designed for daily precipitation input but later versions allow finer time increments (6 hours or less). Input to the model is pseudo precipitation (snowmelt model output) and potential evaporation (actual, or long-term average).

The structure of the soil moisture-accounting model is shown schematically in Figure 2.4. When rainfall occurs it is considered to fall on two types of basin covers: (1) a permeable soil mantle, and (2) lakes, channel networks, and impervious areas. Rain falling on impervious areas always becomes direct runoff, whereas that which falls on the permeable soil mantle undergoes a complicated sequence which represents the infiltration process. Below the permeable soil mantle, the soil moisture storage is conceptually made up of upper and lower zones (Figure 2.4). Each zone stores moisture in two forms, tension moisture and free moisture. Tension moisture denotes water closely bound to the soil particles, while free moisture is the moisture that fills up the interstitial soil pores. For medium sized basins such as the four study basins, one set of lumped model parameters is sufficient to represent the basin hydrology.

The upper zone represents topsoils and the basin interception layer. Upper zone tension water, bound closely to the soil particles, must be filled before moisture can be stored as free water. Upper zone free water generates vertical drainage (percolation) to the lower zone and lateral drainage (interflow) to the channel. If the precipitation rate exceeds the sum of lateral and vertical drainage rates, and the upper zone free water capacity is completely filled, excess surface runoff will result. The actual percolation rate to the lower zone is governed by the interrelationship between soil drainage characteristics and the relative soil moisture conditions of the two zones.

The lower zone, which represents a groundwater reservoir, has a tension water storage zone and two free water storage zones (called primary and secondary). Water goes to the tension water zone first and then to the two free water zones, which generate primary and secondary baseflow. The reason for using three storage zones is to allow the nonlinear characteristics of baseflow recession to be represented.

Evapotranspiration (ET) extracts moisture from the upper and lower tension zones and from free water surfaces. For areas covered by surface water or phreatophyte vegetation, actual basin ET occurs at the daily potential rate. Over other areas of the soil layers, ET extraction depends on the demand and the volume and

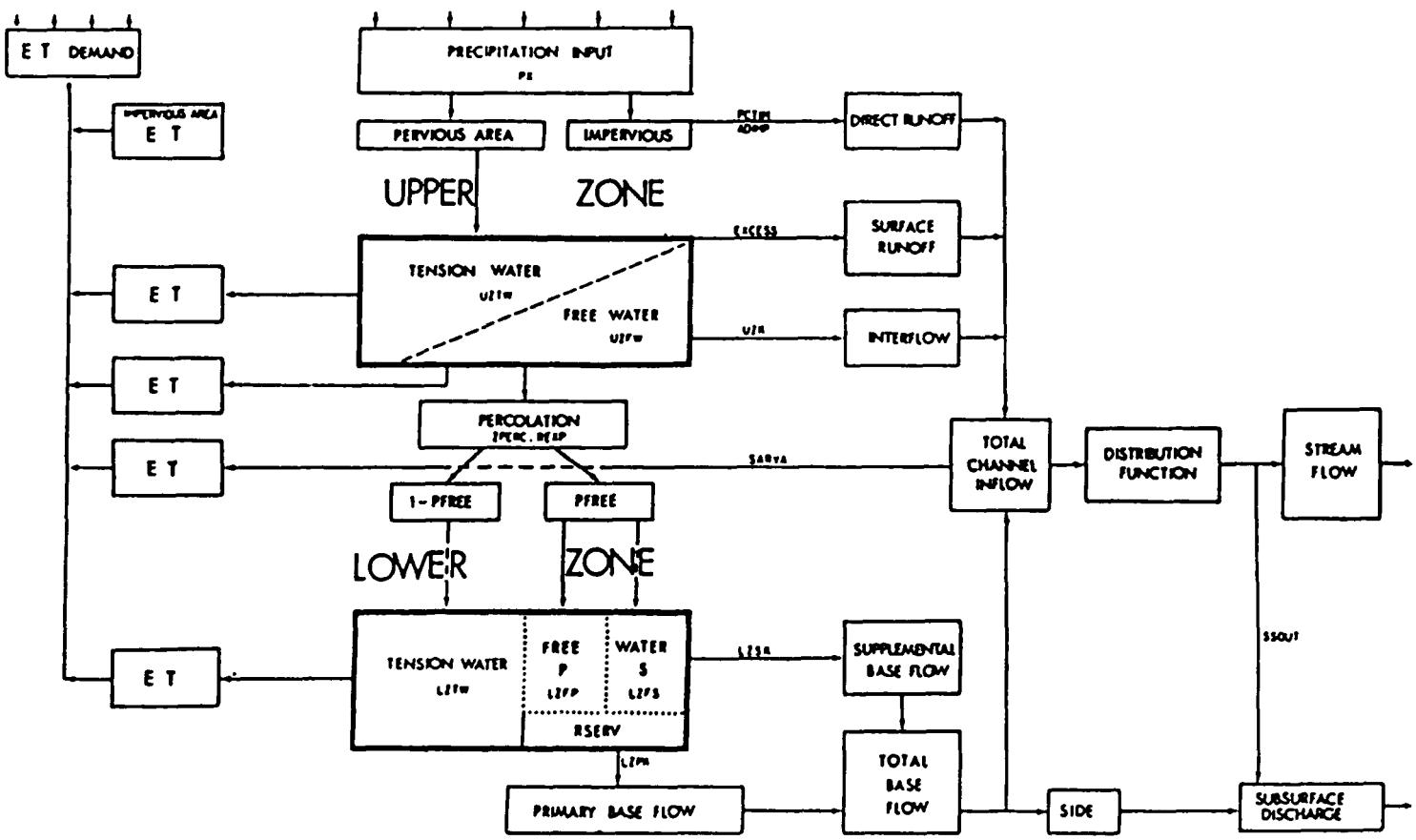

Figure 2.4. Soil-moisture accounting model schematic.

distribution of tension water storage. The upper tension zone provides ET before the lower zone. The sensitivity of ET changes to climate variations is discussed in Section 3.1.4.

Total runoff is the sum of direct runoff from impervious and water surfaces, surface runoff and interflow from the upper zone free water, and primary and secondary baseflows from the lower zone free waters. The model does not relate soil moisture explicitly to vegetation characteristics. The equations that describe the linkage between the tension zone contents, potential evapotranspiration, and actual evapotranspiration act as a surrogate for vegetation effects.

2.4.3 Spatial Disaggregation Model

The spatial disaggregation model consists of two stages. The first stage relates the monthly flows at the six water resource system model nodes (see Sheer and Randall (1988) for details) to the monthly flows at the four study catchments described in Section 2.3. These six nodes are termed "primary sites." The second stage relates the remaining seven water resource system model nodes used by Sheer and Randall (termed "secondary sites") to a selected primary site. Table 2.3 identifies the primary sites, the secondary sites, and, in the case of the secondary sites, the primary site to which they are indexed.

Monthly flow data were approximately log normally distributed, so data were transformed logarithmically to the normal domain. The model used to relate the primary site monthly flows to the monthly flows for the four study catchments is of the form

$$Y_k = A_k X_k + \epsilon_k \qquad (2.1)$$

where Y_k = 6xn matrix of n years of monthly streamflow logarithms for month k at the six primary sites, X_k = 4xn matrix of n years of monthly streamflow logarithms for month k at the 4 study catchments, A_k = 6x4 coefficient matrix, and ϵ_k = 6xn matrix of normally distributed residuals. The parameters of this model are the coefficient matrix A_k, and $G = E(\epsilon_k \epsilon_k^T)$, which is the covariance matrix of the (zero-mean) residuals (E(°) is the mathematical expectation operator).

Table 2.3 Primary and secondary sites for spatial disaggregation model

Site[a]	Name	Index Primary Site
1 (p)	Trinity River	--
2 (p)	Sacramento River at Red Bluff	--
3 (p)	American River	--
4 (p)	sum of Yuba and Bear Creeks	--
5 (p)	sum of San Joaquin basin inflow	--
6 (p)	Feather River	--
7 (s)	Sacramento Valley floor	3
8 (s)	Putah Creek	3
9 (s)	Cache Creek	3
10 (s)	Stony Creek	3
11 (s)	Sacramento Valley West Side	3
12 (s)	Sacramento Valley East Side	3
13 (s)	East Side Streams	4

[a] p = primary, s = secondary

The parameter matrices A_k and G_k can be expressed in terms of the covariances of the Y_k and X_k as

$$A_k = C_k \Sigma_{0k}^{-1} \qquad (2.2a)$$

and

$$G = S_{0k} - A\Sigma_{0k}A_k^T \qquad (2.2b)$$

where

$$S_{0k} = E(Y_k Y_k^T)$$

$$\Sigma_{0k} = E(X_k X_k^T)$$

$$C_k = E(\epsilon_k \epsilon_k^T)$$

Once the monthly streamflow logarithms at the four sites were disaggregated to the six primary sites, the disaggregated streamflow logarithms were exponentiated to provide the corresponding streamflow in real space. The disaggregation procedure explicitly preserves the means, variances, and covariances of the logarithms of streamflows (both between the primary sites, and between the study catchments and the primary basins) in each month. The model does not preserve these same statistics explicitly in real space; however, it was verified using the historic flows that these moments were preserved quite well in real space as well (Table 2.4 gives historic and simulated correlation coefficients for the six primary sites for January and July). More importantly, the model does not preserve the lagged covariances in either real or log space (the correlation between the flows in month k and month k-1 are not preserved). A more complex model of the form

$$Y_k = A_k X_k + B_k X_{k-1} + \epsilon_k \qquad (2.3)$$

explicitly preserves the lagged correlations. This model was tested, and it was found that for some months, no feasible parameter matrices existed. The possibility of using the more complex model in months where parameter solutions could be found, and the simpler model (Eq. 2.1) in the remaining months, was considered. We concluded it was better that any distortions in the covariance structure of the simulated flows relative to the historical flows be consistent through all months, so the simpler model (Eq. 2.1) was used.

Once the primary site monthly flows were estimated, the secondary site monthly flows were estimated using a simple linear regression,

$$\ln(Q_{kij}) = \alpha_{ki} q_{k,L(i),j} + \beta_{ki} + \eta_{kij} \qquad (2.4)$$

where Q_{kij} is the predicted flow in month k at site i in year j, α_{ki} and β_{ki} are coefficients estimated by ordinary least squares regression, and $q_{k,L(i),j}$ is the predicted primary site monthly streamflow logarithm at site L(i), which is specified as the index site for secondary site i. η_{kij} is a (normally distributed) random error term. This model explicitly preserves only the first two moments (mean and variance) of the historic flows; it does not explicitly preserve any of the off-diagonal covariances. The secondary sites were selected because their flows are much smaller than the primary sites, so failure to preserve statistics other than the mean and the variance at the secondary sites is of considerably less importance than at the primary sites.

2.5 Model Implementation

This section describes the selection of precipitation-temperature stations to provide representative climatic data for the four study catchments, as well as the method used to subdivide each study catchment into elevation zones. In addition, the procedure used for calibration (parameter estimation) of the Snowmelt and Soil-Moisture Accounting models is described. Characteristics of the selected precipitation-temperature stations, as well as final parameter estimates for each study catchment, are given.

2.5.1 Precipitation-Temperature Stations and Data Quality

Since precipitation input errors are among the most important source of runoff simulation errors, selection of meteorological stations is an important step in the modeling process. Few records are available for mountainous areas. For this reason, most of the meteorological stations used lie at relatively low elevations.

Table 2.4 Simulated and Historic Correlation Coefficients for the Six Primary Sites (base case)

January Historic

1.000	.950	.817	.855	.740	.907
.950	1.000	.872	.918	.812	.949
.817	.872	1.000	.989	.944	.955
.855	.918	.989	1.000	.932	.978
.740	.812	.944	.932	1.000	.900
.907	.949	.955	.978	.900	1.000

July Historic

1.000	.827	.773	.826	.746	.875
.827	1.000	.727	.750	.672	.887
.773	.727	1.000	.949	.905	.897
.826	.750	.949	1.000	.833	.897
.746	.672	.905	.833	1.000	.832
.875	.887	.897	.897	.832	1.000

January Simulated

1.000	.918	.797	.836	.613	.905
.918	1.000	.844	.895	.729	.922
.797	.844	1.000	.984	.884	.936
.836	.895	.984	1.000	.852	.955
.613	.729	.884	.852	1.000	.785
.905	.922	.936	.955	.785	1.000

July Simulated

1.000	.824	.774	.787	.688	.884
.824	1.000	.698	.676	.566	.904
.774	.698	1.000	.916	.808	.865
.787	.676	.916	1.000	.719	.829
.688	.566	.808	.719	1.000	.737
.884	.904	.865	.829	.737	1.000

The selection criteria used were data record length, quality of record (in terms of missing data), geographical locations of stations with reference to the basin topography, and distance of the stations from the study catchments. The precipitation-temperature stations selected for each of the study catchments are given in Table 2.5.

To reduce the data handling effort, only one precipitation-temperature gage station was chosen for each basin. In mountainous basins, orographic effects, which generally cause precipitation to increase with elevation, dominate the local climatology. Establishing the proper precipitation-elevation relationships is made difficult by the paucity of high-elevation meteorological stations and their susceptibility to recording errors. The approach we used was to define an elevation-dependent adjustment factor to relate precipitation at a given elevation (e.g., the midpoint of a snowmelt model elevation band) to gage precipitation as follows:

$$P_e = [1 + P_f(e-e_g)/100]P_g \qquad (2.5a)$$

where P_e is precipitation at elevation e, P_g is gage precipitation at gage elevation e_g. The (nonlinear) form of the factor $P_f(e-e_g)$ was determined by trial and error based on annual water balance considerations. In general, P_f is a monotonic function of $e-e_g$, but its second derivative is negative, reflecting the fact that the rate of increase of mean precipitation with elevation decreases at high elevations.

The relationship of temperature to elevation was described by a constant lapse rate. In fact the lapse rate is a function of meteorological conditions, e.g., wet or dry day, storm type, and other factors. However, the available data were insufficient to support more complex relationships.

2.5.2 Snowmelt Model Parameter Estimation

It is essential that mountainous catchments be divided into elevation zones, and that the snowmelt model be applied to each zone separately because low elevations might be receiving rain while higher elevations receive snow from the same storm. The weighted mean of the pseudo-precipitation from all zones was treated as the mean areal precipitation, which is the input to the Soil-Moisture Accounting Model. In general, the weighting factors used were equal to the radios of the elevation zone subareas to the total basin area.

The elevation bands were delineated as follows. First, hypsometric curves (elevations versus area fractions) were developed. Each basin was then divided into three or four zones of equal area, depending on the elevation range, and the elevation of the midpoint of each band was identified. The McCloud and North Fork American River catchments were divided into three zones while the Merced River and Thomes Creek catchments were divided into four zones (Table 2.6).

Initial values for the precipitation-elevation adjustment factors $P_f(°)$ for each elevation band were estimated from the change in mean annual precipitation with elevation of selected nearby precipitation stations. Initially, $P_f(°)$ was assumed to be a linear function of the elevation difference. Subsequently, refinements were made through a trial and error approach, which was carried out concurrently with the calibration of the soil-moisture accounting model. The final precipitation-elevation adjustment factors are given in Table 2.7.

The snowmelt model was manually calibrated for all the elevation zones. Ideally, observed snow course data could be used for calibration but in practice snow course observations are sparse in time and space, and they represent point realizations which usually are not representative of the elevation band average snow water equivalent predicted by the model. In practice, the calibration procedure involves adjusting the most important parameters to ensure that the model predicts the initiation of snow accumulation in the fall and the gradual melting of the snowpack in the late winter, and spring. The other parameters were assigned nominal values which have been used in previous studies.

Table 2.5. Precipitation/temperature Gage Stations Selected for McCloud River, Merced River, North Fork American River, and Thomes Creek Study Catchments

Basin	Station ID	Station Name	Elevation (feet)	Years of Record	
				Temp	Precip
McCloud	4-5449	McCloud	3280	76	76
Merced	4-9855	Yosemite Park HQ	3966	81	81
North Fork American	4-1912	Colfax	2410	114	117
Thomes	4-2081	Covela	1430	46	68

Table 2.6. Elevation Zones for McCloud River, Merced River, North Ford American River, and Thomes Creek Study Catchments

Basin	Zone	Elevation Range (ft)	Median Elv. (ft)	Percent Basin Area	Basin Area (Square Miles)
McCloud	1	2800-4300	3900	50	358
	2	4300-5300	4600	30	
	3	5300-12000	6500	20	
Merced	1	3900-7500	5750	25	321
	2	7500-8350	7900	25	
	3	8350-9400	8800	25	
	4	9400-12000	10050	25	
North Fork American	1	750-3350	2550	34	342
	2	3350-5250	4100	32	
	3	5250-8600	6300	34	
Thomes	1	900-3100	2000	25	203
	2	3100-4200	3750	25	
	3	4200-5500	4700	25	
	4	5500-9500	6350	25	

Table 2.7. Precipitation Adjustment Factors by Elevation Zone for McCloud River, Merced River, North Fork American River, and Thomes Creek Study Catchments

Basin	Precipitation Adjustment Factors			
	Zone 1	Zone 2	Zone 3	Zone 4
McCloud	0.304	0.443	0.786	
Merced	0.544	0.839	0.884	0.927
North Fork American	0.025	0.283	0.474	
Thomes	0.123	0.357	0.402	0.450

The lapse rate, or rate of temperature decreases with elevation, is a critical parameter. As with the function $P_f(°)$, the lapse rate is usually nonlinear. It was found that average lapse rates for four periods (each of length 6 hours) of each day for all basins vary from -0.5°C/100m to -0.8°C/100m. Together with the Pf function, lapse rates were estimated concurrently with the calibration of the Soil-Moisture Accounting Model (see Section 2.5.3).

Seasonal melt factors were interpolated between MFMAX (maximum nonrain melt factor, which occurs on June 21) and MFMIN (minimum nonrain melt factor, which occurs on Dec. 21) and were estimated to vary between 0.9 to 1.2 and 0.2 to 0.5 mm/°C/6 hours, respectively. PXTEMP, the temperature above which precipitation was assumed to be rain (°F) was taken to be 32°F. SI, the mean areal water-equivalent above which 100% areal snow cover always exists was assumed to vary between 75 and 150mm. Tables 2.8 and 2.9 give descriptions and calibrated values of the snowmelt model parameters.

2.5.3 Soil Moisture Accounting Model Parameter Estimation

Parameter estimation for the soil moisture accounting model was based on a process of initial parameter estimation suggested by Peck (1976), sensitivity analysis to determine those parameters deserving further attention, followed by automated parameter estimation using a simplex search procedure (Nelder and Mead, 1965) for the most sensitive parameters. The objective function in the search procedure was the sum of the squared difference between the logarithms of the predicted and observed (daily) streamflow over the calibration period.

The parameters estimated using the search procedure were LZFPM, LZFSM, LZPK, LZSK, UZK, UZFWM, ZPERC, REXP, UZTWM, LZTWM, and PXADJ (parameters are defined in Table 2.10). The parameters which were assigned nominal values were PCTIM, SSOUT, ADIMP, SIDE, IMPRT, and SARVA.

All parameter estimates were based on calibration periods of length four years. The calibration periods were selected to include dry, medium, and wet years so that during calibration, the model was subjected to a broad range of changes in conceptual storages.

Because of its deep and highly permeable soils, the McCloud River catchment is dominated by subsurface flow, even during intense storms. For this reason, the McCloud River catchment was calibrated manually. Calibrations for all catchments were complicated by errors in the rain and melt data produced by the snowmelt model, which itself was calibrated through trial and error. The initial and optimized values, upper and lower bounds for the sensitive parameters are reported in Table 2.10. To test whether the model had been overfit, that is, whether the simulation errors were consistent between the calibration periods and an independent verification period consisting of those years in the period 1951-80 not used for calibration, a seasonal Wilcoxon test (see Hirsch, 1988; Hettmansperger, 1984) was applied to the monthly sum of log flow differences squared. The results for all four study catchments fell within the 95% critical region for a two-tailed test, which confirmed that the performance of the model in the calibration and verification periods was comparable.

2.6 Model Input Characterization

This section describes the relationship between the upper left and right quadrants of Figure 2.1, that is, the relationship between the historic input data for the hydrologic model, and the input corresponding to the GCM alternatives. The historic input data were adjusted to reflect the altered climate predicted by each of the seven alternatives. This approach was taken in preference to using the GCM output directly, or attempting to develop a stochastic model to predict the space-time meteorological structure associated with the GCM output. The reasons for using adjustments to the historic record as input to the hydrologic models were first, in terms of the project time constraint, that it was a straightforward approach that required no new model development, and second, that the sequences might be considered a feasible realization of the (present) natural process since the historic record has actually occurred. In the remainder of this section, the specific approach used to provide the precipitation, temperature, and potential evaporation inputs is described.

Table 2.8. Snowmelt Model Parameter Description

Parameter	Description
DAYGM	Average daily ground melt at the snow-soil interface in mm
EFC	Area over which evapotranspiration can take place when there is complete areal snow cover
ELEV	Mean height of the basin elevation band
MBASE	Melt factor base temperature (assumed to be 0°C)
MFMAX(MFMIN)	Maximum and mimimum non-rain melt factors which occur on June 21 and Dec. 21 respectively
NMF	Maximum negative melt factor
PLWHC	Percent liquid-water holding capacity of ripe snow
PXTEMP	Temperature in °C to divide rain from snow
SCF	A multiplying factor to correct for gage catch deficiency in the case of snowfall
SI	Areal water quivalent in mm above which there is always complete areal snow cover
TALR	Lapse rate (°C/100m)
TIPM	Antecedent snow temperature index parameter
UDAJ	Mean wind function value during rain-on-snow periods

Table 2.9. Calibrated Values of Snowmelt Model Parameters

	McCloud River	Merced River	North Fork American River	Thomes Creek
PAYGM	0.4	0.4	0.4	0.4
EFC	0.9	0.9	0.9	0.9
MBASE	0.0	0.0	0.0	0.0
MFMAX	0.90	1.10	1.10	1.20
MFMIN	0.40	0.40	0.20	0.20
NMF	0.12	0.12	0.12	0.12
PLWHC	0.07	0.07	0.07	0.07
PXTEMP	0.5	0.5	0.5	0.5
SCF	1.03	1.03	1.03	1.03
SI	200	150	100	120
TALR	-0.5	-0.7	-0.8	-0.7
TIPM	0.3	0.3	0.3	0.3
UDAJ	0.10	0.10	0.10	0.10

Table 2.10. Initial and Optimized Final Values and Upper and Lower Bounds for the Soil-moisture Accounting Model Parameters

Thomes Creek

	LZFPM	LZFSM	LZPK	LZSK	UZK	UZFWM	ZPERC	REXP	ZTWM	LZTWM	PXADJ
Initial	6	4	.009	.02	.10	2.0	20	1.80	3	4	0.008
Optimized	1.75	1.75	.005	.053	.09	1.67	33.4	1.55	2.7	7.10	.006
Upper Bound	7.0	5.0	.03	.08	.3	3.5	43	3.0	7.0	11.0	.02
Lower Bound	1.1	1.0	.005	.01	.05	.05	10.0	1.1	1.5	2.0	.004

McCloud River Basin

	LZFPM	LZFSM	LZPK	LZSK	UZK	UZFWM	ZPERC	REXP	UZTWM	LZTWM	PXADJ
Initial	20	5.6	.003	.026	0.06	3.0	43.3	1.60	4.0	5.0	1.1
Optimized	53.0	14.7	.0022	.004	.07	2.0	81.3	1.03	5.2	6.4	0.86
Upper Bound	77.0	25.0	.03	.08	.3	9.5	98	3.0	11.0	21	1.7
Lower Bound	1.1	1.0	.0005	.003	.05	.05	10.0	1.01	1.0	2.0	0.6

Merced River Basin

	LZFPM	LZFSM	LZPK	LZSK	UZK	UZFWM	ZPERC	REXP	UZTWM	LZTWM	PXADJ
Initial	6.0	2.9	.006	.01	.11	1.9	34	1.8	4.8	7.2	0.90
Optimized	3.7	3.0	.016	.05	.08	2.80	49.5	2.30	1.2	8.1	0.98
Upper Bound	27.0	10.0	.03	.08	.3	9.5	68	3.0	11.0	21.0	1.7
Lower Bound	1.1	1.0	.0005	.004	.05	.05	10.0	1.01	1.0	2.0	.05

American River Basin

	LZFPM	LZFSM	LZPK	LZSK	UZK	UZFWM	ZPERC	REXP	UZTWM	LZTWM	PXADJ
Initial	2.17	1.88	.009	.055	0.09	1.60	36	1.10	1.68	7.27	.91
Optimized	2.70	2.6	.006	.056	.13	1.4	24.3	1.11	1.47	6.03	.92
Upper Bound	7.0	5.0	.03	.08	.3	3.5	43	3.0	7.0	11.0	1.7
Lower Bound	1.1	1.0	.005	.01	.05	.05	10	1.1	1.0	2.0	0.5

2.6.1 Precipitation

For each GCM alternative, the National Center for Atmospheric Research (NCAR) provided a disk file of the output corresponding to the center of each grid cell used by the given model, along with a program to read and print the output. This program provided, among other variables, the predicted GCM precipitation corresponding to a base case (nominally, present conditions) and the alternative climate. For all cases except Case 3 (GISS transient), the base cases and alternative climates were represented as long-term monthly averages. NCAR computed the ratio of the GCM alternative long-term precipitation to the base case long-term precipitation (or, in the case of the GISS transient, the ratio was computed for each decade over the 80-year transient run). The NCAR program was modified slightly to interpolate the results to longitude 120°W, latitude 40°N, which is approximately the centroid of that part of the Sacramento-San Joaquin basin that contributes most of the runoff. For all but the transient run, the computed precipitation ratio was then applied to all the raw input precipitation records.

In the case of the transient run, a statistical test (Spearman's rho; see for example, Conover, 1971) was applied to the 80-year sequence of decadal precipitation factors to determine whether there was a statistically significant trend. For those cases (four months) where the trend was significant, a linear regression was fit to the decadal precipitation Table 2.11, soil moisture accounting model parameter description factors, and the resulting "ramp" was used to adjust the historical precipitation records. In those cases (eight months) where the trend was not significant, the average precipitation factor (over the eight decades) was computed, and this average precipitation adjustment was used in the same way as were the NCAR-computed factors for the steady-state runs.

2.6.2 Temperature

For the steady-state runs, a temperature shift was computed as the difference between the $2xCO_2$ and base condition. These monthly differences were then applied directly to the historic data. In the case of the GISS transient run, the sequences of eight decadal shifts were tested for trend, in the same manner as were the precipitation factors. All months were found to have statistically significant uptrends, so a linear regression was fit to all months, and the resulting ramps were used as input to the hydrologic models.

2.6.3 Potential Evapotranspiration

Potential evapotranspiration (PET) was computed from the Penman equation, which is given in Veihmeyer (1964). Penman's equation is based on a theoretical energy balance approach. It predicts PET as a function of temperature, average wind speed, humidity, mean solar radiation, and the ratio of duration of bright sunshine to maximum possible duration of bright sunshine.

Penman's equation was applied on a monthly basis, using average values of the input variables. Some of the input variables (wind speed) are not well known, so they were adjusted to obtain a total annual evaporation estimate that was roughly consistent with observed pan evaporation at stations throughout the Central Valley (usually on the order of 55-65 inches of pan evaporation on the valley floor).

Once an adequate "fit" was obtained, the input values were compared with selected station values to make sure they were physically realistic. The most sensitive input value was wind speed, which can be strongly affected by local factors, so the trial and error approach seemed justified. Nonetheless, the assumed (seasonally constant) value of 200 miles per day that was used was remarkably close to the observed long-term mean at Red Bluff, which has one of the longest records in the Central Valley.

The Penman PET was then recomputed for each GCM using two sets of temperature data: the base condition for that GCM, and the predicted temperature corresponding to the CO_2 doubling. The monthly differences in the Penman PET were computed, and these differences were then applied to the historic data as input to the hydrologic models. In the GISS transient case, the differences corresponding to the base and altered climate temperatures at the beginning and end of the temperature "ramp" were computed, and the resulting Penman PET differences were used to define a PET "ramp."

Table 2.11. Soil Moisture Accounting Model Parameter Description

Soil Moisture Phase	No	Parameters	Description
Direct	1	PCTIM	Minimum impervious area (percent)
runoff	2	ADIMP	Additional impervious area (percent)
	3	RIVA	Riparian vegetation area (percent)
	4	EFC	Effective forest cover (percent)
Upper	5	UZTWM	Upper zone tension water capacity (inch)
zone	6	UZFWM	Upper zone free water capacity (inch)
	7	UZK	Daily upper zone free water withdrawal rate
Perco-	8	ZPERC	(ZPERC+1)xPBASE is the maximum percolation rate
lation	9	REXP	Exponent for the percolation equation
Lower	10	LZTWM	Lower zone tension water capacity (inch)
zone	11	LZFSM	Lower zone supplemental freewater capacity (inch)
	12	LZFPM	Lower zone primary freewater capacity (inch)
	13	LZSK	Daily supplemental withdrawal rate
	14	LZPK	Daily primary withdrawal rate
	15	PFREE	Fraction of percolation water passing directly to LZFM storages
	16	RSERV	Fraction of lower zone free water cannot be transferred to LZTW
	17	SIDE	Ratio of non-channel baseflow to channel baseflow
Initial	18	UZTWC	Upper zone tension water content (inch)
water	19	UZFWC	Upper zone freewater content (inch)
	20	LZTWC	Lower zone tension water content (inch)
	21	LZFSC	Lower zone supplemental free water content (inch)
	22	LZFPC	Lower zone primary free water content (inch)
	23	ADIMC	Tension water contents of the ASIMP area (inch)
Climatic	24	PXADJ	Precipitation adjustment factor
Index	25	PEADJ	ET-demand adjustment factor

CHAPTER 3

RESULTS

As described in Chapter 2, the long-term hydrologic response of the study catchments was simulated for climates associated with a base case (nominally, present conditions) as well as three sets of GCM predictions (Cases 1, 2, and 4) that were based on steady state climate following a doubling of current atmospheric CO_2 concentrations. In addition, the hydrologies of the study catchments associated with a transient climate resulting from doubling of atmospheric CO_2 over an 80-year period (Case 3) were also evaluated.

Three alternative climates (Cases 5-7) were used to test the sensitivity of the hydrologies of the study catchments to selected aspects of the GCM climate predictions. These included a scenario (Case 5) designed to explore the relative effect of predicted precipitation and temperature change, a scenario (Case 6) designed to explore the effect of different interpretations of the predicted geographic distribution of temperature and precipitation changes, and a scenario (Case 7) in which the long-term climate was assumed to be similar to that experienced in the 1930's. Cases 0-4 are referred to as "initial scenarios," and are discussed in Section 3.1. Cases 5-7 are referred to as "sensitivity scenarios," and are discussed in Section 3.2. The temperature shifts and precipitation scaling factors associated with Cases 1-7 are given in Tables 3.1 and 3.2, respectively.

Because the snowmelt and soil moisture accounting models operate on daily or shorter time steps, and all cases involved running the snowmelt and soil moisture accounting models for 100 years, large amounts of computer output were generated. To simplify the analysis of the results, we selected the following model (simulated) variables to summarize the alternative hydrologies: 1) average snow water equivalent over each study catchment; 2) monthly average study catchment runoff; 3) monthly average study catchment evapotranspiration; 4) average end of month study catchment soil moisture storage in selected zones (see Section 2.4.2 for description of the model soil moisture zones); 5) predicted (disaggregation model) monthly primary node streamflow; and 6) predicted (linearly regressed) monthly secondary node streamflow. In all cases, the mean of each variable was computed for the 100-year simulation period, as well as the standard deviation (expressed as a coefficient of variation in some cases). In the interest of brevity, only selected mean values are reported in this chapter; Appendix B contains a complete graphical summary of the results.

3.1 Study Catchment Results for Initial Scenarios

The hydrology of the Sacramento-San Joaquin basin in general, and the study catchments in particular, is dominated by high-elevation snow accumulation in the winter and snowmelt in the spring and early summer months. Snow water storage is especially important because of the disproportionate amount of precipitation that occurs at high elevations, and because snow water storage shifts the peak of the annual runoff hydrograph from the high precipitation winter months toward the spring and summer. Increasing winter temperature decreases the amount of precipitation falling as snow, and causes any snow that accumulates in the winter to melt earlier. This is the principal mechanism by which the alternate climates affect the hydrology of the Sacramento-San Joaquin basin. For this reason, the order of presentation of the results is as follows: predicted average snow water equivalents, monthly average runoff, monthly average evapotranspiration, and monthly average soil moisture. Before presenting the results, however, a brief discussion of the climate alternatives is in order.

All four of the initial scenarios (Case 1: GFDL $2xCO_2$, Case 2: GISS $2xCO_2$, Case 3: GISS transient, and Case 4: OSU $2xCO_2$) predicted increasing average temperature for all months (see Figure 3.1). Generally, the largest temperature changes were predicted by the GFDL and GISS models, and the smallest by the OSU model. Figure 3.1 also shows the beginning and ending values of the "ramp" fit to the Case 3 temperature transients. In general, the final values in the transient case are slightly less than the Case 1 and Case 2 steady-state values, but are larger than Case 4. Figure 3.1 shows that there was no consistency in the predicted long-term precipitation changes. The GISS model (Case 2) generally predicted an increase in precipitation in the winter months. Because the precipitation regime is highly seasonal, summer precipitation changes for the catchments are of much less importance hydrologically. The GFDL model predicted increased fall precipitation and generally decreased winter and spring precipitation. The GISS transient and the OSU model had less obvious patterns, with predicted increases in some months and decreases in others.

Table 3.1. Temperature Shifts in °C for GCM Cases 1-7

Case	Jan	Feb	Mar	Apr	May	June	July	Aug	Sep	Oct	Nov	Dec
1	3.5	4.35	4.5	4.55	5.70	6.10	4.35	3.90	4.90	4.30	4.10	3.45
2	5.9	4.6	4.6	5.4	3.1	4.1	3.9	5.50	7.20	5.3	3.4	4.4
3[a]	-.02	.33	.10	-.03	-.33	-.05	-.02	-.65	.87	-.46	.48	-1.61
	4.13	3.35	3.0	4.22	2.29	2.68	4.10	3.28	4.55	4.14	4.72	3.26
4	0.55	2.03	1.31	2.08	1.97	2.68	2.12	3.12	2.39	1.58	3.08	2.57
5	5.9	4.6	4.6	5.4	3.1	4.1	3.9	5.50	7.20	5.3	3.4	4.4
6[b]	6.60	5.06	4.78	5.15	3.14	4.0	3.31	5.98	8.55	5.33	3.47	4.69
	4.82	3.84	4.24	5.77	3.18	4.15	4.80	4.88	5.17	5.19	3.24	4.00
7	-0.16	-0.54	0.97	0.98	0.43	0.04	0.36	0.90	0.65	0.53	0.62	0.66

[a] The upper and lower entries represnt the beginning and end transient temperature shifts for the 80-year period ramp used for Case 3.
[b] The first row represents temperature shifts for the 3 nothern catchments and the second row the sourthern catchment.

Table 3.2 Precipitation Scaling Factors for GCM Cases 1-7

Case	Jan	Feb	Mar	Apr	May	June	July	Aug	Sep	Oct	Nov	Dec
1	.936	1.13	.924	.911	.710	.947	.11	.889	.818	1.084	1.189	1.096
2	1.21	1.06	1.34	.764	.976	1.28	.655	1.26	.765	1.30	1.24	1.15
3[a]	.954 1.171	1.082	1.123	.836	1.112 1.383	.864 1.564	.908	1.542	2.157	1.096	1.182	.783 1.070
4	1.03	1.13	1.04	1.36	.93	1.05	1.01	.88	1.07	0.89	0.76	0.89
5	1.0	1.0	1.0	1.0	1.0	1.0	1.0	1.0	1.0	1.0	1.0	1.0
6[b]	1.227 1.181	1.156 0.911	1.525 1.045	1.019 .363	1.106 .771	1.439 1.038	1.061 .017	1.289 1.220	0.615 0.999	1.369 1.184	1.397 .989	1.110 1.216
7	0.854	0.994	0.845	0.934	0.879	1.15	0.622	0.249	0.67	0.807	.593	.949

[a] Only months with an upper and lower entry had a statistically significant transient. For months with a significant transient, the upper and lower entries represent the beginning and end precipitation scaling factors used in the 80-year ramp for Case 3.
[b] The upper entries represent precipitation scaling factors for the three northern catchments and the lower entries represent the southern catchment (Merced River).

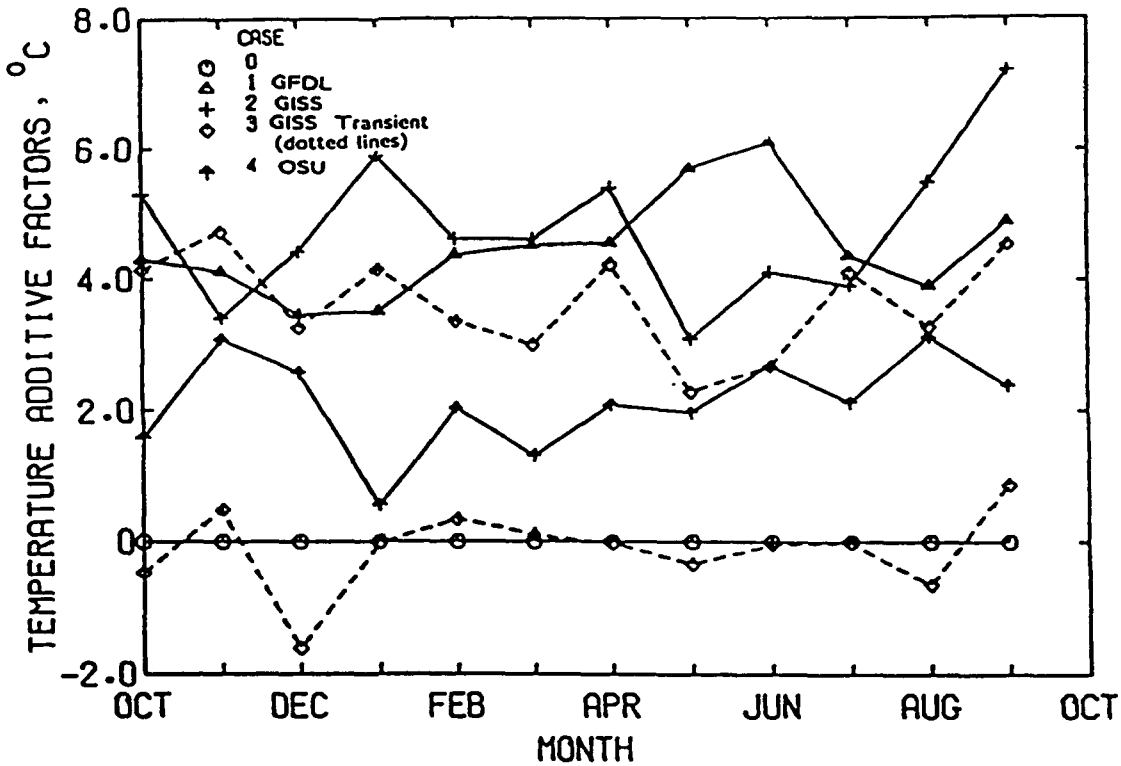

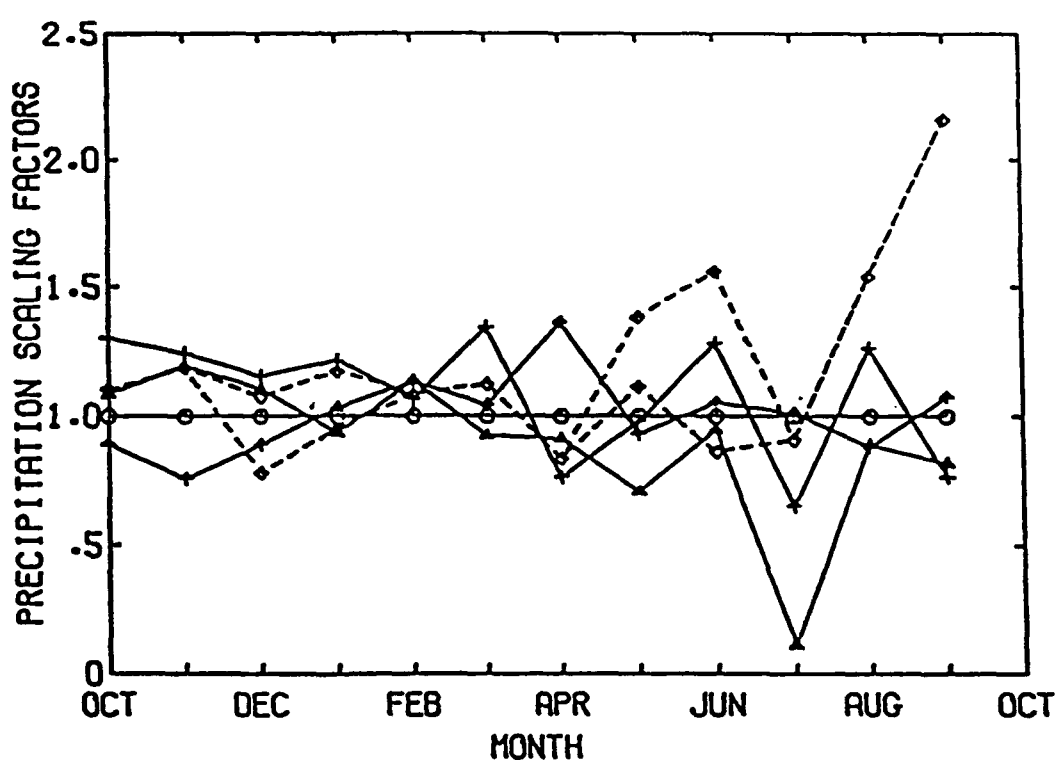

Figure 3.1 Monthly temperature shifts (1) and precipitation scaling factors (2) predicted by general circulation models for climate scenario Cases 0-4

Figures 3.2a-d show long-term study catchment-average snow water equivalent, runoff, evapotranspiration, and soil moisture storage, respectively, by month for Cases 0-4. Figure 3.3a shows the predicted average annual runoff by decades, while Figure 3.3b shows the catchment monthly mean flows of four successive 25-year periods for the transient case (Case 3). The results for Case 3 shown in Figures 3.2a-d represent averages over the 100-year simulation period and do not represent the transient nature of the Case 3 response. In Figure 3.2d, the soil moisture zone to which the model performance was most sensitive is indicated. Because of the differences in the geologic and hydrologic characteristics of the catchments, the particular subsurface zone varies by catchment. For this reason, the relative values are of greater importance than the numerical values of the predicted storages.

The results of the simulations are reported in the remainder of this chapter. In most cases, the results are reported as averages over the 100-year simulation period described in Chapter 2. For selected model variables, standard deviations over the 100 year simulation period were computed. Brief interpretations of the results for snow water equivalent, runoff, evapotranspiration, and soil moisture are given in Sections 3.1.1-3.1.4, respectively.

3.1.1 Snow Water Equivalent

Figure 3.2a shows long-term study catchment-average snow water equivalent by month for Cases 0-4. There was a marked reduction in average snow water equivalent for all of the study catchments for all of the alternative climates (Cases 1-4). The predicted changes, when expressed as a proportion of the base case average snow water equivalent, were the greatest for the North Fork American River, which has the lowest mean elevation, and the least for the Merced River, which is the highest basin. In Cases 1 and 2, snow storage is virtually eliminated in the lower elevation study catchments.

Although the proportionate reduction in mean snow water equivalent was the least for the Merced River because it is influenced more by snowfall and snowmelt than the other basins, the magnitude of the reduction in snow water equivalent was larger than for any of the other study catchments. The Merced lost more snow water equivalent than the North Fork American River or Thomes Creek had in the base case. The Case 1 and 2 temperature increases are large enough to eliminate almost all the influence of snow water storage from all study catchments but the Merced.

3.1.2 Runoff

Figure 3.2b shows the predicted changes in the seasonal distribution of study catchment runoff. The effect of reduced snow storage is immediately apparent; in all cases, the annual hydrograph peak shifted earlier in the year because of a decrease in the amount of snowfall in relation to rainfall. Runoff increased markedly in all cases for the winter months and decreased substantially in the late spring and summer. The predicted changes in annual runoff relative to the base case are reported in Table 3.3. Table 3.4 summarizes the months in which predicted runoff is reduced from present conditions.

Although the general shift in the annual streamflow hydrograph was consistent in all of the catchments, site-specific effects were observed as well. For instance, for the Merced River, which has high snowmelt-runoff between March and July, the effect of increased precipitation in Case 2 was overshadowed by the temperature increase. The North Fork American River has a mixed rainfall-runoff and snowmelt-runoff regime for the base case. This changes to a complete rainfall-runoff situation for Cases 1 and 2. The phase shift is less for Case 4 because the temperature increase is more modest. Because the North Fork American River has a large rainfall-runoff component for the base case, the increase in winter flows was not proportionally as large as for the Merced, which is snow-dominated in the base case. For Thomes Creek there was relatively less snowmelt, and the base flow in the summer approached zero for all cases including the Base Case. Case 2 resulted in the largest runoff changes, doubling the December and January mean flows and increasing February by about two-thirds. Although the mean flow and standard deviation increased, the coefficient of variation for the Thomes Creek runoff was generally reduced.

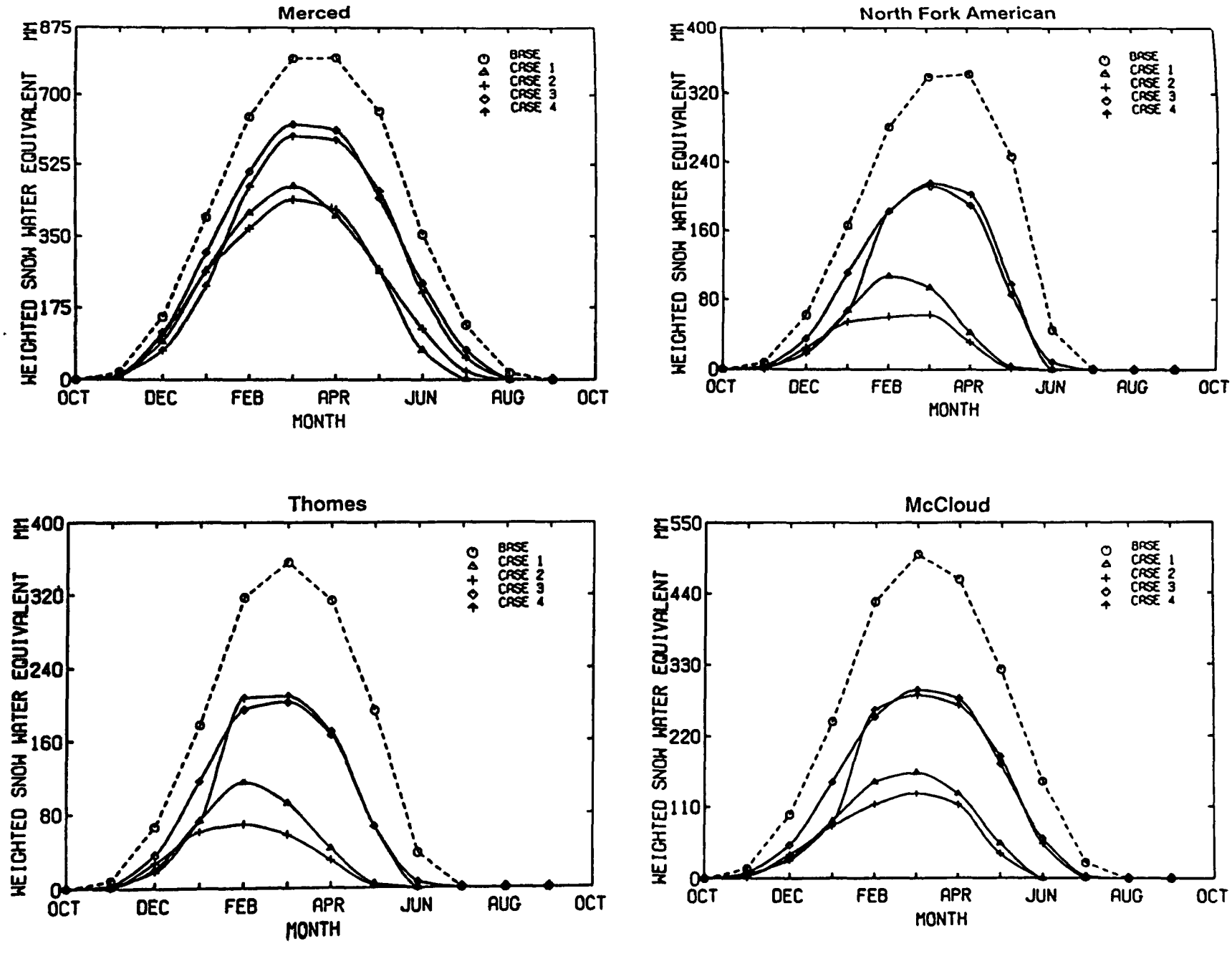

Figure 3.2a Study catchment monthly mean weighted snow water equivalent for climate scenario Cases 0-4

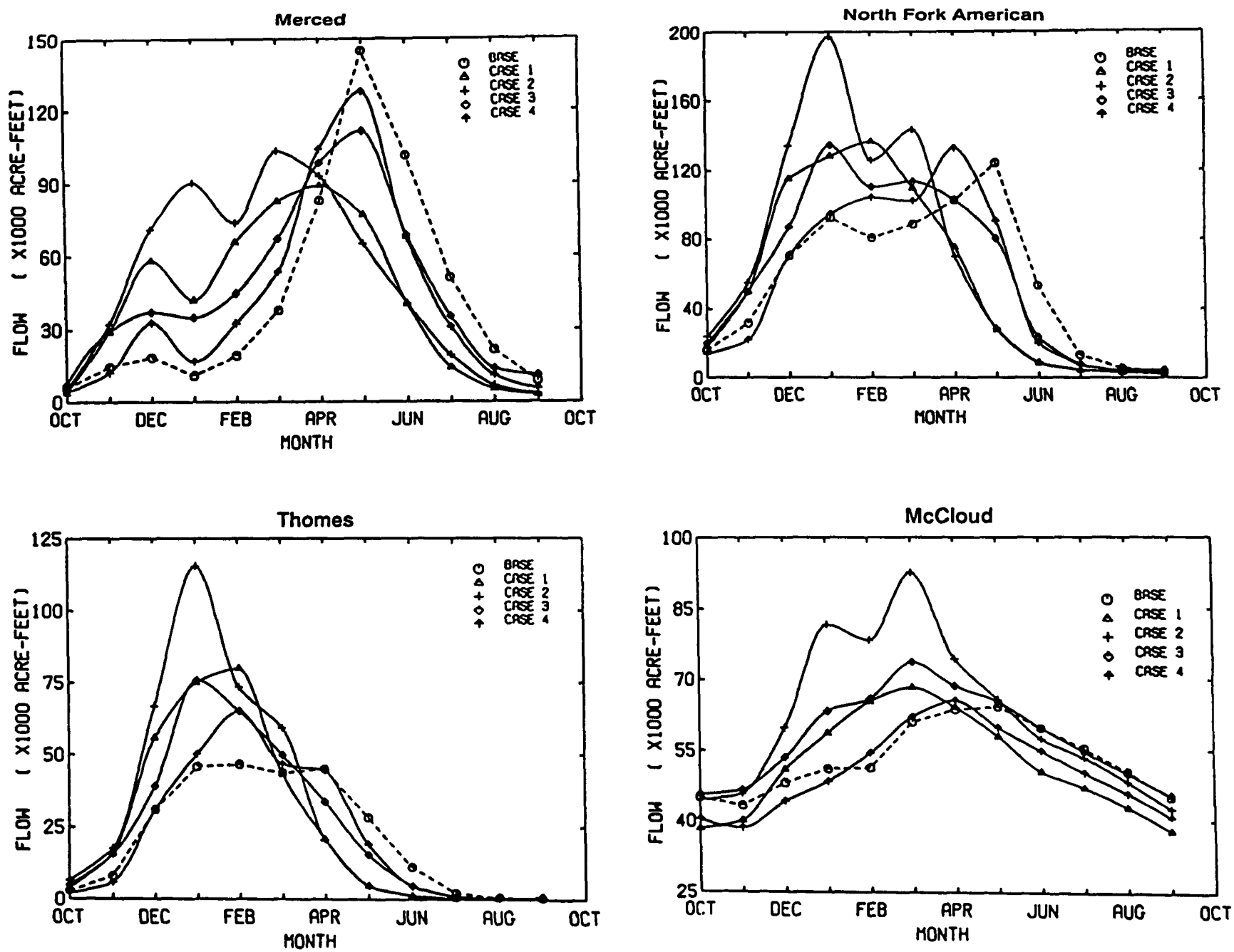

Figure 3.2b Study catchment monthly mean streamflow for climate scenario Cases 0-4

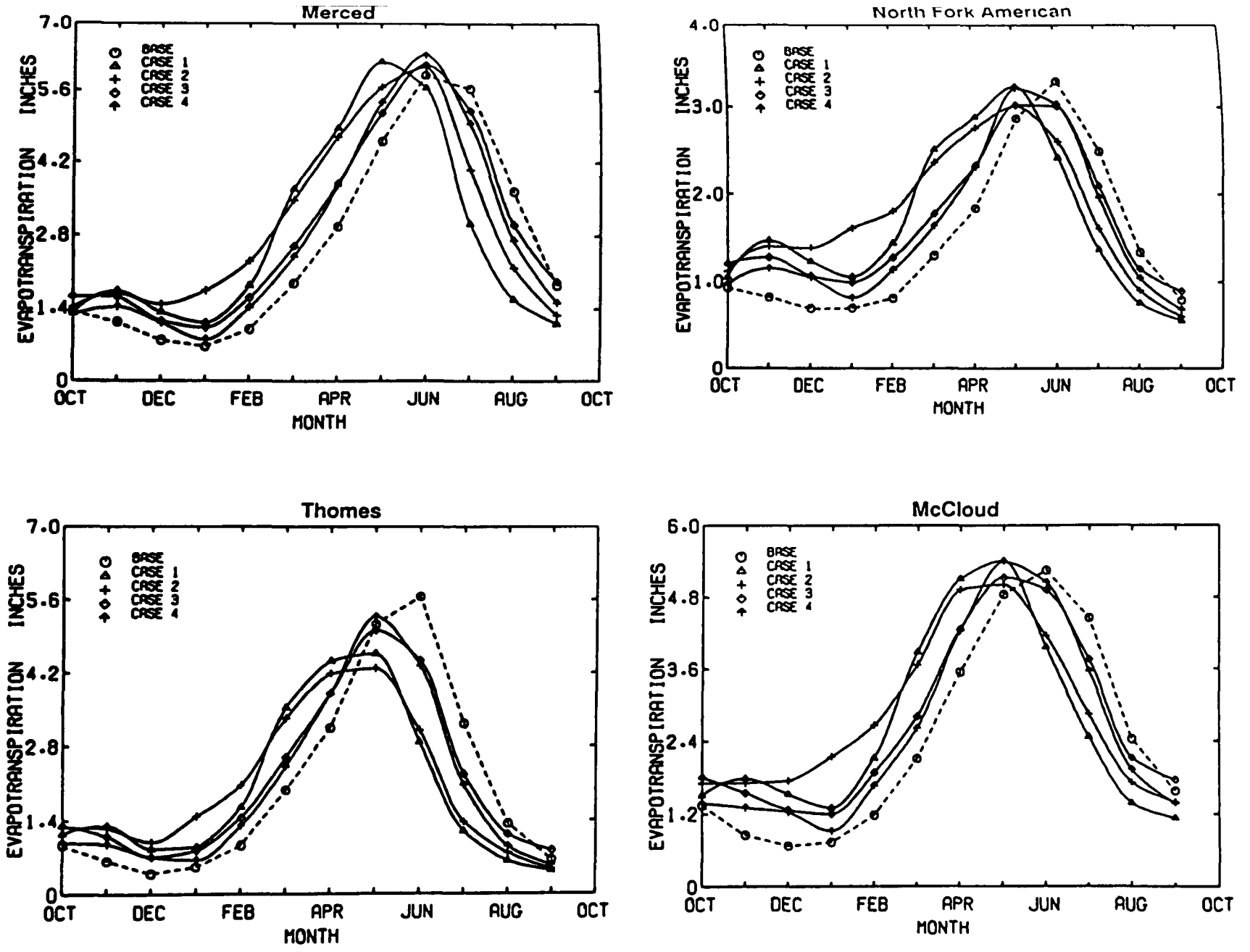

Figure 3.2c Study catchment monthly mean evapotranspiration for climate scenario Cases 0-4

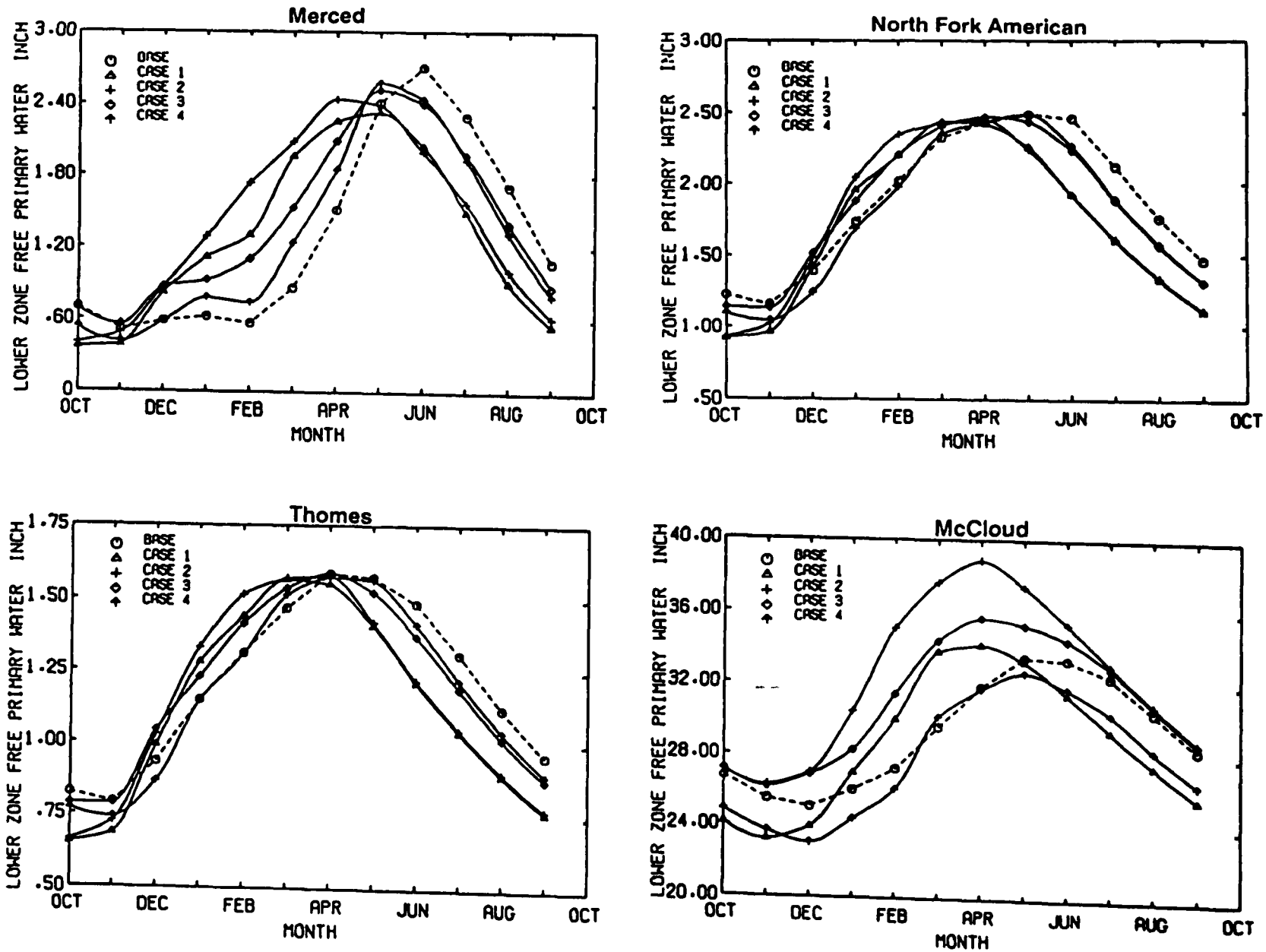

Figure 3.2d Study catchment monthly mean soil moisture for climate scenario Cases 0-4

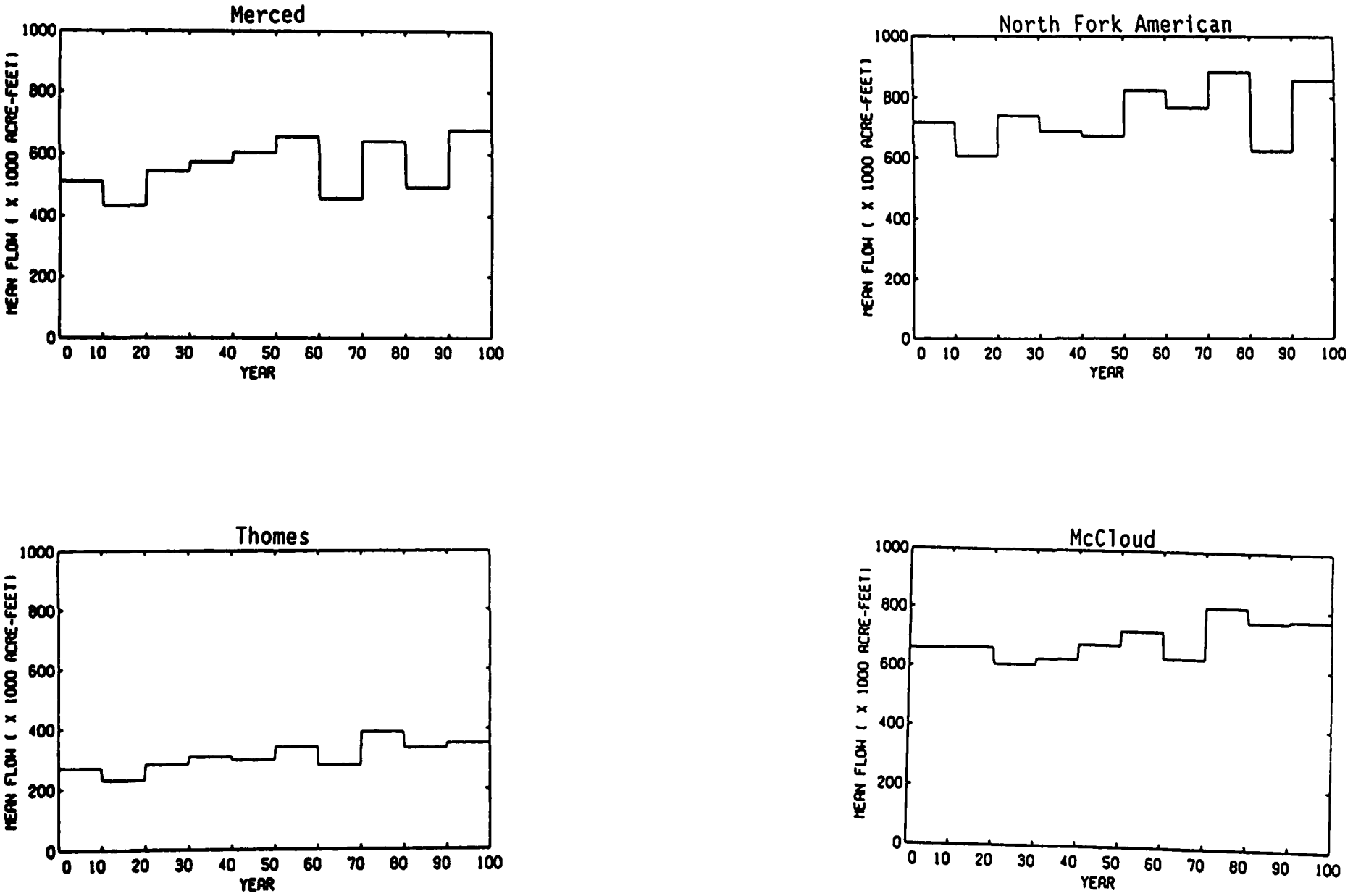

Figure 3.3a Study catchment decadal mean flows for transient climate scenario (Case 3)

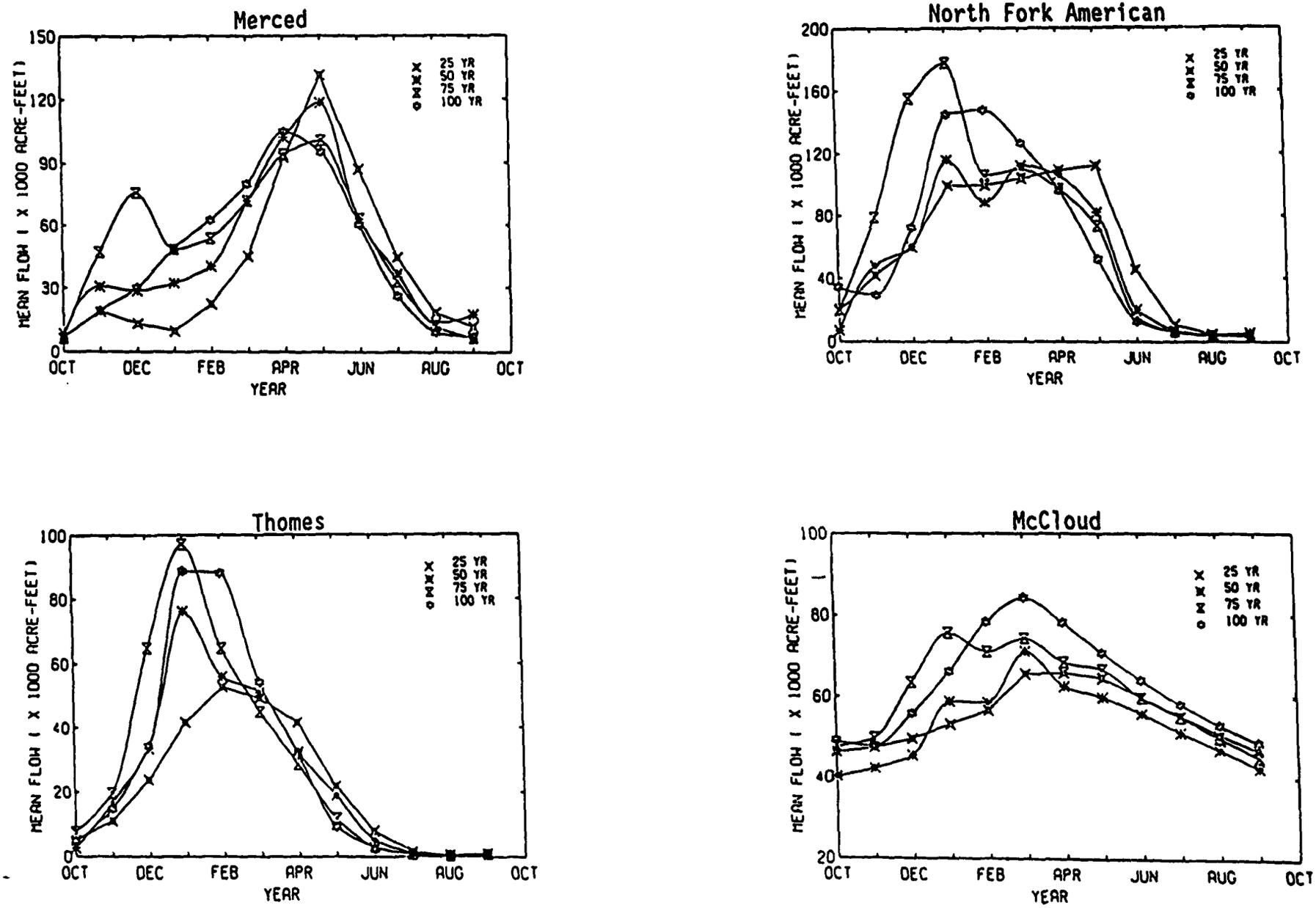

Figure 3.3b Study catchment monthly flows for four successive 25-periods for transient climate scenario (Case 3)

Table 3.3. Simulated Mean Annual Study Catchment Runoff for GCM Cases 0-4.

	Annual Runoff in Thousands of Acre-feet			
Case	Merced River	North Fork American River	Thomes Creek	McCloud River
0	518.0	679.0	267.7	448.2
1	509.3	680.0	304.4	427.7
2	596.5	795.1	367.7	591.6
3	551.2	733.3	297.1	521.7
4	500.6	669.1	269.1	406.0

Table 3.4. Months with predicted reduction in streamflow, based on the climate change predicted by the GCMs.

Basin	Case	Months
Merced	1	May to September
	2	May to September
	3	May to August
	4	May to November
NF American	1	April to September
	2	April to September
	3	May to September
	4	May to November
Thomes	1	April to August
	2	April to August
	3	April to August
	4	May to November
McCloud	1	May to November
	2	June to September
	3	None or negligible
	4	May to January

The importance of groundwater for the McCloud River is shown in Figure 3.2b. Although all scenarios shifted the flows earlier, only Case 2 overwhelmed the soil moisture storage capacity of the model. Case 2 produced peaks in January and March, with slightly lower flows in February, but the entire winter had a predominance of rainfall runoff. The standard deviation of flows generally increased also, as did the coefficient of variation.

The shift in the annual distribution of runoff is critical for water resources management; the seasonal distribution of runoff, and its variability, are more important than the annual runoff change. The implications of these changes in seasonal runoff distribution, and variability, are addressed in detail by Sheer and Randall (1988). For most of the catchments and climate change scenarios, runoff variability was substantially increased in the winter months and reduced slightly in the summer months.

3.1.3 Evapotranspiration

As described in Chapter 2, potential evapotranspiration (PET) was estimated for the alternative climate scenarios using the Penman equation with the GCM-predicted temperature changes. In all cases for all basins, the maximum actual evapotranspiration simulated by the soil moisture accounting model occurred earlier in the year (See Figure 3.2c). Case 1 generally resulted in a flatter crest for the monthly mean ET than was predicted for the base case. For Thomes Creek, Cases 1 and 2 were flatter, lower, and peaked earlier than Cases 3 and 4. ET depends on soil moisture as well as PET; therefore, although PET increased for all months for Cases 1-4 because of the increased temperature, the direction of changes in actual ET varied by month.

The soil moisture-accounting model assumes that ET depends on the moisture contents of the conceptual tension zones. The rate of ET declines as the soil dries. Therefore, the shift of the flow from spring to winter shifts the ET similarly. ET also depends upon temperature, so that wet winter soils do not yield as much ET as similarly wet spring soils. The net result, despite the change in seasonal distribution, was relatively little change in annual total ET. Although the changes in seasonal distribution of ET were similar over all the study catchments, there were differences among the cases. Cases 1 and 2 have the greatest increase in mean temperature, and they show the greatest shift in timing of ET. Case 4 predicts the least temperature change, and it shows the least change in ET. The variability of the ET increased more or less in proportion to the mean.

The increased spring ET suggests that agricultural irrigation demand might be increased over the present situation.

3.1.4 Soil Moisture Storage

Figure 3.2d shows long-term catchment-average soil moisture storage by month for Cases 0-4. As described in Chapter 2, the soil moisture accounting model has five conceptual storage zones. The capacity of the soil moisture zones strongly affects the response of the model to altered inputs. The soil moisture zone capacities were estimated through the automated calibration process described in Chapter 2. While neither their capacities nor contents are measurable physical quantities as are, for instance, snow water equivalent or runoff, the soil moisture storages do reflect, in a general sense, the physical soil moisture storage capacities of the catchments.

Figure 3.2d summarizes the results for the soil moisture zone to which the model performance was most sensitive in each study catchment. Because of the differences in the geologic and hydrologic characteristics of the study catchments, the particular subsurface zone varies by catchment. For this reason, for comparisons between catchments, emphasis is placed on the relative values.

There are few distinctive trends observed between the basins, but some general climate-related changes in most of the catchments can be seen. Some of the generalizations that follow do not apply to the McCloud catchment, which behaves differently than the others because of its extremely large soil moisture storage capacity. The warmer and generally wetter climates predicted by the GCMs cause increased rainfall relative to snowfall, making more moisture available during winter and early spring, at the expense of late spring and summer. Therefore, there is a definite phase shift in practically all storages (see Figure 3.2d). This trend is stronger among the free water zones than the tension zones, and during summers than winters. In addition, Cases 1 and 2 exhibit larger phase shifts than 3 and 4 since temperature and precipitation changes for the former are higher.

The moisture content of the upper tension zone is virtually unaffected by climate change during the wet October-March period because it has the first priority to absorb moisture and has small capacity (usually less than 2 inches). It is filled in all the climate scenarios. During the spring and early summer, the decrease in snowmelt gives rise to more severe moisture shortages, which are reflected in reduction of tension water storage. Because Cases 1 and 2 reflect the greatest warming, they result in larger phase shifts than Cases 3 and 4. The lower tension zone, which is supplied after its upper counterpart, shows larger phase shifts than the upper tension zones, in particular during the October-March period. This is partly because after supplying the upper zone, the net moisture available is reduced. Moreover, partly due to the generally larger capacities of the lower tension zones in all the catchments, the lower tension zones are more affected by the availability of moisture.

The free water zones' contents are influenced by climate change. Not only do they exhibit larger phase shifts, but the changes are also more erratic between basins and among the various cases. The upper free water zone shows larger fluctuations in moisture content than the lower zones (Figure 3.2d). The upper free water zones are comparatively more sensitive to modest changes in precipitation than are the other zones (Figure 3.1), especially for Case 2 in the McCloud River catchment.

3.2 Sensitivity Scenarios

The sensitivity scenarios were undertaken for three purposes: 1) to determine the extent to which precipitation (as opposed to temperature) change drives the simulations for the various climate scenarios (Case 5); 2) to determine the relative effect of an interpretation of the GCM predictions that provides differential input to the southern (Merced) study catchment relative to the three northern study catchments (Case 6); and 3) to evaluate the general character of the hydrologic scenarios associated with the GCM predictions relative to the historic 1930's drought (Case 7). The first issue was addressed by using the GISS GCM predictions (Case 2) with the precipitation adjustment factors set to 1.0, but with the Case 2 temperature shifts retained (this formed the new Case 5). The second issue was addressed by assigning temperature shifts and precipitation

factors associated with the GISS $2xCO_2$ model cell (Case 2) centered at 35.22°N, 120°W to the Merced River study catchment, and the GISS grid cell centered at 43.04°N, 120°W to the three northern study catchments (as opposed to an interpolated grid cell centered at 40.0°N, 120°W which was assigned to all study catchments in Cases 1-4). This formed the new Case 6. Case 7 was formed by computing the ratio of the average monthly precipitation for selected Northern California stations for the period 1931-40 to the long-term (1890-1980) precipitation at the same stations. Temperature shifts for the 1931-40 decade relative to the 1890-1980 means at the same stations were also computed. For each month, the median precipitation ratio, and temperature shift, were computed. These medians were used to define a climate scenario (Case 7) which was analogous to the GCM scenarios.

The sensitivity scenarios are summarized in Sections 3.2.1-3.2.4.

The Case 6 (geographic sensitivity to inputs) results showed that the hydrologic simulations were qualitatively the same (at least for the GISS model) regardless of whether the grid cells were interpolated as described in Chapter 2, or a nearest cell center approach was used. This result held for all variables (snow water equivalent, runoff, evapotranspiration, and soil moisture). Therefore, Sections 3.2.2-3.2.4 are devoted to a discussion of the temperature sensitivity (Case 5) and 1930's analog (Case 7).

3.2.1 Snow Water Equivalent

The difference between Case 2 and Case 5 indicates the sensitivity of the snow water equivalent to GCM-predicted temperature changes only. There was relatively little difference in this respect between Case 2 and Case 5. This confirms the earlier interpretation of cases 1-4 that changes in winter snow accumulation were primarily temperature dependent. The Case 2-predicted temperature changes were quite large; hence, there would be relatively little snow in any of the study catchments except the Merced River under the CO_2 doubling scenarios.

The Case 7 (1930's analog) results emphasize how different the 1930's conditions were from the GCM predictions; under these conditions the simulated snow water equivalents were slightly less than the base case, but were much larger than any of the GCM climate scenarios. This reflects the fact that the 1930's drought was caused primarily by a reduction in precipitation; winter temperatures were relatively little changed from the base case.

3.2.2 Runoff

For the precipitation sensitivity scenario (Case 5), the Merced River had lower mean monthly flows and standard deviations due to the reduction in winter rainfall relative to Case 2, but the phase shift in runoff was more or less the same. This is no surprise because temperature, which determines whether precipitation occurred as rainfall or as snowfall, was the same as in Case 2. Case 7 represents the precipitation and temperature analog of the relatively dry decade of 1930's. For Case 7, the temperature change was minor relative to the base case, an increase of less than 1°C. Therefore, the seasonal distribution of runoff was comparable to the base case. However, all the months had lower flows and standard deviations. This reflects the dry conditions (most precipitation factors less than 1.0) experienced in the 1930's.

For the North Fork American River, the November to March flows (mean and standard deviations) were significantly lower in Case 5 than in Case 2. Due to minimal changes in temperature, Case 7 had a similar mix of rainfall runoff and snowmelt runoff as the base case. The changes in runoff variability (standard deviations) were generally larger than the changes in runoff volumes for the 1930's analog.

The Thomes Creek responses for Cases 5 and 7 showed qualitatively similar patterns to those observed for the North Fork of the American River. This is to be expected because the hydrologies of these catchments are somewhat similar.

The McCloud River simulations showed more marked impact of the reduced precipitation in Case 5 relative to Case 2. On average, runoff occurred earlier, with increased ET and reduced soil moisture contents.

The groundwater recession began about two months earlier. Again, the McCloud catchment behaved somewhat differently than the other four catchments; the Case 5 results show that the interaction of changed temperature and precipitation was stronger in this catchment than in the other three. This is primarily a result of the damped storm response, which heightened the importance of between-storm dynamics.

3.2.3 Evapotranspiration

The Merced River is the only catchment for which there was any substantial change in ET for Case 5 compared to Case 2. This can be traced to the greater importance of snow water storage in this catchment under the alternative (warmer) climates. Reduction of precipitation in Case 5, relative to Case 2, reduced the average snowpack, and in consequence the spring and summer soil moisture. The amount of moisture available for meeting the daily ET demands was relatively unaffected by reductions in moisture supply, until the tension water storages were reduced to near zero. This was the case only for the Merced catchment. For the three catchments which are rainfall-driven in the warmer climate scenarios, ET was relatively little affected by the Case 5 reduction in winter precipitation.

For Case 7 (1930's analog) there was a slight phase shift in Case 7 ET for all the basins relative to the base case. The shift patterns was similar for all the study catchments. The 1930's analog climate had little effect on the mean ET except during summers (June to September) when the soil moisture contents of tension zones are reduced to near zero.

3.2.4 Soil Moisture Storage

More of the soil moisture reduction associated with the reduced precipitation in Cases 5 and 7 came from the upper free water zone than the lower free water zones in both Cases 5 and 7. The McCloud catchment, however, had a much larger secondary free water capacity in the lower zone than the other study catchments (about 10 inches storage capacity) to maintain its high baseflow. Therefore the reduction in precipitation in both Cases 5 and 7 gave rise to relatively higher reductions in moisture storages in the McCloud River than in the other catchments.

Generally, the lower free primary zone had larger capacities than the secondary zone. The moisture content of the McCloud catchment was as high as 40 inches, while the maxima for the other catchments were in the vicinity of only three inches. For both lower free zones, the phase shifts during summers and early autumns were more consistent than the other seasons because these seasons experience larger changes in moisture supply.

3.3 Spatial Disaggregation: Primary Nodes

Section 2.4.3 described the spatial disaggregation model used to generate monthly streamflows at the six primary sites given in Table 2.2. For the base case, the disaggregation model explicitly preserved the mean and variance of the flows at the primary nodes. Higher moments (e.g., skewness) were not preserved. The model also explicitly preserved the correlation between the sites in each month, but not the lagged correlation at a given site or between sites (for instance, the January correlations between node 1 and node 2 were preserved, but the January-February correlations at node 1 were not preserved). The model implicitly assumes that the statistical structure (moments) of the node flows relative to the catchment flows would remain the same under the alternative climates scenarios.

Figure 3.4a shows the monthly mean simulated flows for each of the six primary sites for Cases 0-4, and 5-7, respectively. These figures confirm that the disaggregated (primary node) flows were qualitatively consistent with those of the catchments. The phase shifts between various cases, as well as the high flows and low flows at the primary nodes, were generally comparable to those of the catchments. There was, of course, a substantial difference in runoff volumes, because the nodes represent much larger drainage areas than the catchments. For example, Site 2 (Sacramento River at Red bluff) had monthly runoff as high as 2.5 x 106 acre-feet, which is 10

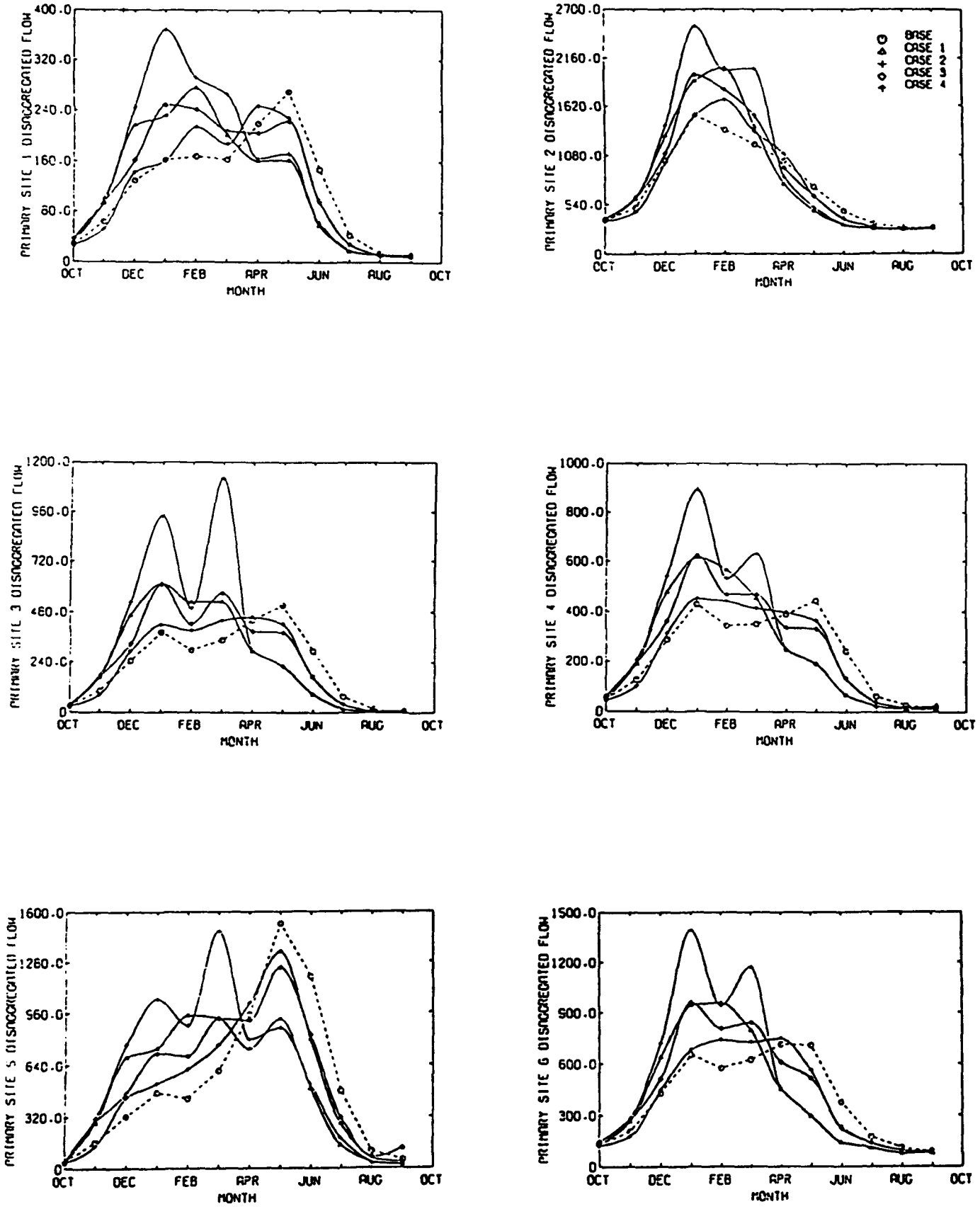

Figure 3.4a Water resources system primary node mean monthly flows for climate scenario Cases 0-4.

times higher than the highest study catchment mean flow. On a relative basis, however, the primary site annual runoff hydrographs were similar to those of the catchments.

3.4 Spatial Disaggregation: Secondary Nodes

The seven secondary nodes selected for this study are listed in Table 2.1. The secondary nodes generally represent smaller, lower elevation drainages than do the primary nodes. Because they lie at lower elevations, some of the secondary nodes have a large number of zero flows (and in some cases zero mean flow) in the historic record for the summer and fall months. Generally, the influence of the secondary site flows on the water resources management model described by Sheer and Randall (1988) is considerably less than that of the primary nodes. This consideration supported use of the simple regression model to simulate the secondary site flows conditioned on the (simulated) flow at a specified primary node (Eq. 2.4).

Figure 3.4b shows the mean simulated flows at the secondary sites for Cases 0-4. For those nodes where summer flows were nearly zero under the base condition, the net effect of the warmer climates was to increase the runoff in nearly every month. Because summer runoff was zero under the base case, no reduction was possible. Site 1 provides a good example of this effect. For those sites (for example, site 7) where there was some summer runoff for the base case, the change in the annual runoff hydrograph was more similar to those of the study catchments and the primary nodes. In Cases 1-4, the simulated increase in winter runoff exceeded the decrease in summer and fall. Cases 5-7 show similar results. Case 7 (1930's analog) showed the expected reduction in the mean flows during the winter months. This is the only case in which there was a significant reduction in the secondary site flows.

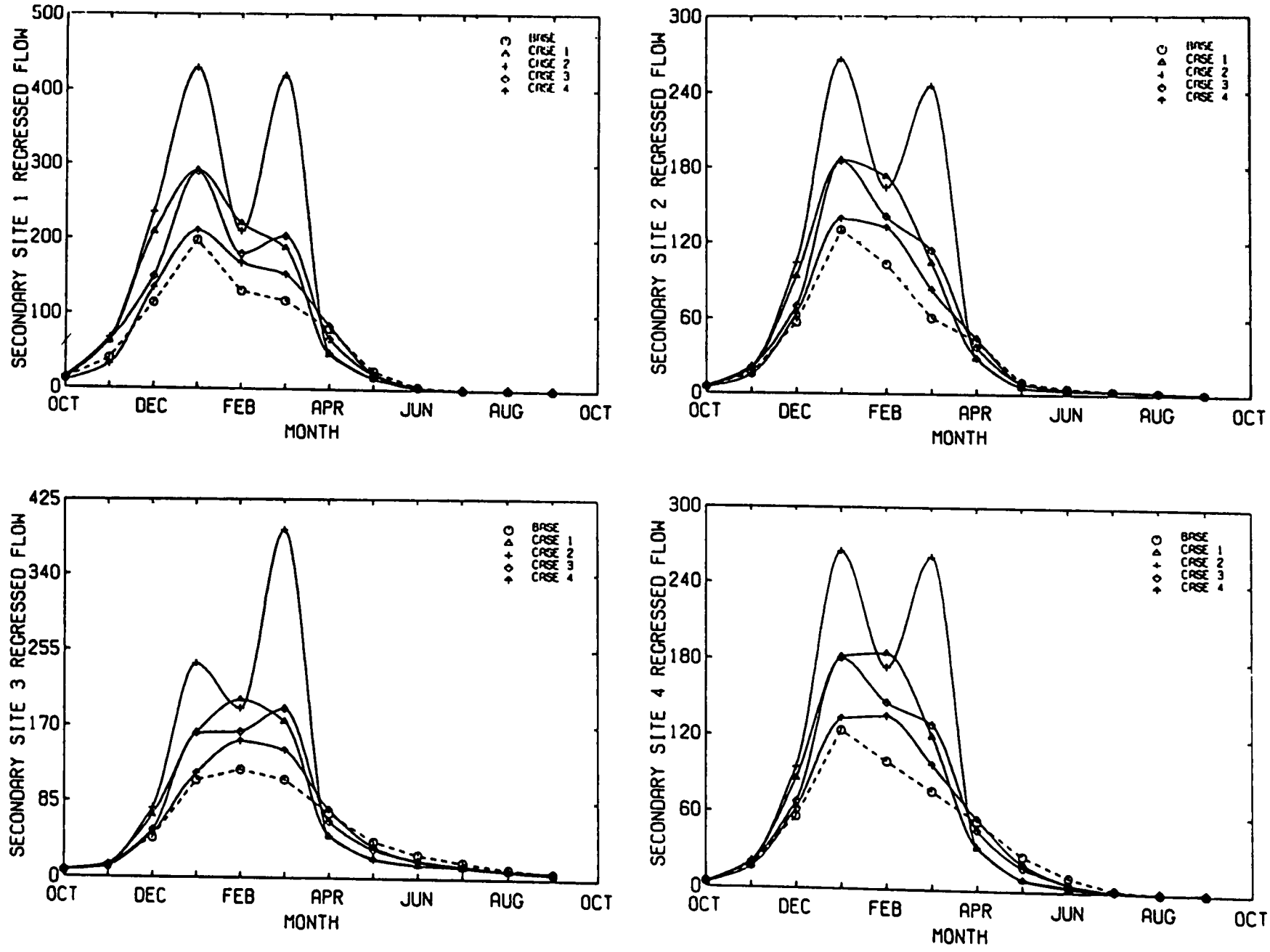

Figure 3.4b Water resource system secondary node mean monthly streamflow for climate scenario Cases 0-4

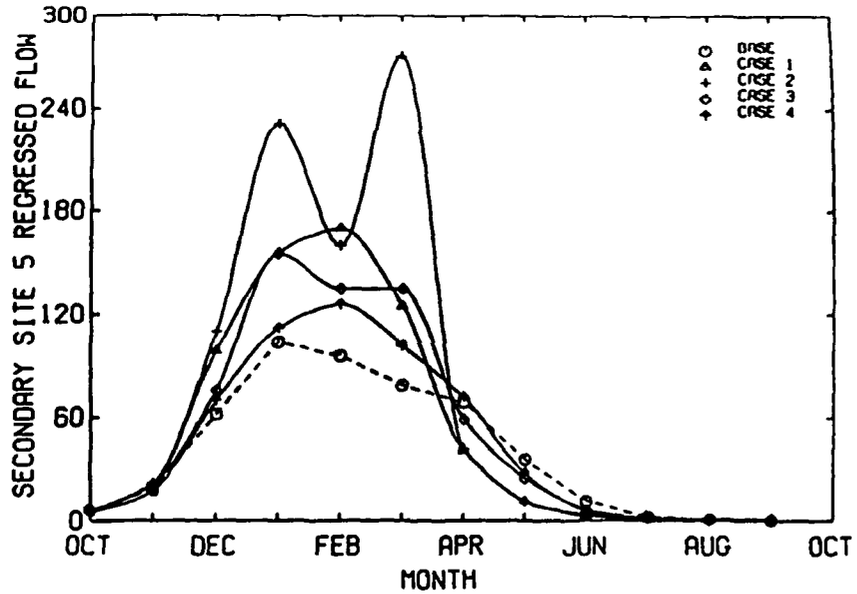

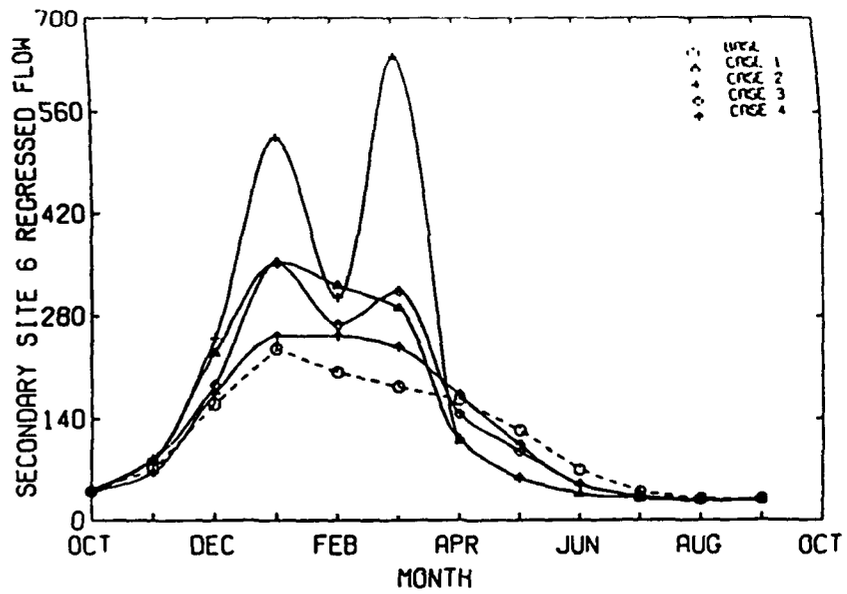

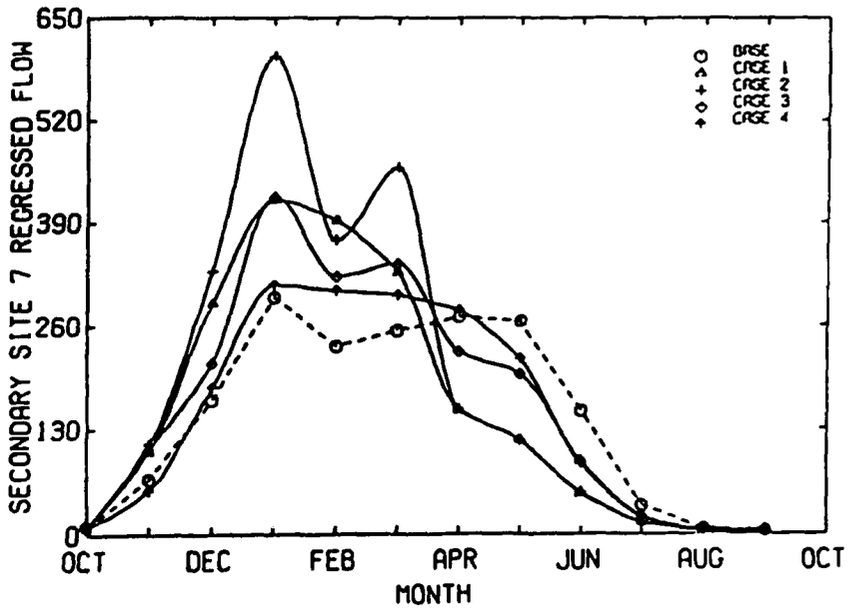

Figure 3.4b (Continued)

CHAPTER 4

SUMMARY AND CONCLUSIONS

The primary objectives of this work were to develop a methodology to provide a descriptive interpretation of the hydrologic effects of global climate change as predicted by selected GCMs, and to apply the methodology to the Sacramento-San Joaquin basin as a case study. This study is preliminary; the simulation results discussed in Chapter 3 should be interpreted in a "what if?" and not a predictive sense. Furthermore, existing hydrologic models (in particular, the National Weather Service snowmelt and soil moisture accounting models) were used, and the assumptions and simplifications incorporated in the models are reflected in the results. The following assumptions were made either implicitly or explicitly:

1) The altered climate scenarios were identical to current climate except that all precipitation was adjusted by a factor equal to the ratio of the selected GCM average monthly precipitation to the base case average monthly precipitation, and temperatures were shifted by an amount equal to the difference between the selected GCM scenario and the base case. This has the following implications for the hydrologic simulations:

- Hydrologic systems are strongly affected by the variability of the driving variables, as well as their mean. In the case of precipitation, adjustment by a fixed factor implies that the coefficient of variation (standard deviation divided by the mean) is the same for the altered climate scenarios as for the base case. For precipitation factors greater than one (as for Cases 1-4 in most of the winter months) this means that the standard deviation of the inputs will increase. This particular assumption regarding the form of the altered input affects the stochastic structure of the output, which may well have significant implications for water resources management.

- The spatial variability of the inputs was assumed to be exactly the same as in the base case. The performance of large multiple site water resource systems, such as the California State Water Project and the Central Valley Project, can be strongly affected by the spatial correlation of streamflows. If streamflows at the different sites (rivers) are highly correlated, droughts are likely to occur simultaneously at all, or many, sites. If the spatial correlation is less, and the storage locations are dispersed, the required storage will be smaller. It is unlikely that the spatial correlation of the inputs would remain the same under substantially warmer climates, but the GCM grid spacing is too coarse to allow alternative inferences to be made at present.

- The precipitation arrival process (that is, the probabilistic structure of wet and dry day sequences) was assumed to be unchanged from the historic record. While the GCMs provide precipitation predictions at time scales of one day or less, the interpretation of these predictions in terms of point precipitation (as recorded at a precipitation gage) is difficult. The GCMs provide grid cell average values, but spatial averaging over an area the size of a grid cell removes most of the information regarding the point arrival processes. Further work is needed to verify the relationship of GCM-predicted short-term precipitation to observable quantities (e.g., gage or gage-averaged precipitation corresponding to the base case). Changes in the precipitation arrival process affects catchment runoff response, even in the absence of changes in the longer term (e.g., monthly) statistics. For example, fewer storms of increased rainfall intensity are likely to lead to increased runoff, reduced soil moisture, and decreased ET in the long run.

2) The hydrologic models provide an adequate description of the catchment dynamics under the altered climate. Two major issues arise in this respect. The first regards the appropriateness of the hydrologic models to the base case. The National Weather Service River Forecast System, of which both the soil moisture accounting model and snowmelt model are part, has been widely used and verified operationally for a range of hydrologies. The soil moisture accounting model, in particular, was originally developed for use in the Sacramento basin. Although other hydrologic models might have been used, we believe the NWS models contain about the right level of detail for medium sized catchments, and can be expected to capture the essential elements of the long-term (as opposed to event) hydrologic response. The issue of applicability under alternative

climate scenarios is more difficult to address. One major problem is that the soil moisture model cannot explicitly account for long-term changes in vegetation. At a minimum, the implicit assumption that the model relationship between PET and ET will hold in warmer climates needs to be verified. In the longer term, hydrologic models capable of simulating long-term runoff need to be explored.

3) The spatial disaggregation model provides an adequate description of the relationship between the study catchment flows and the flows at the water resource system nodes. Two key limitations related to the spatial disaggregation model must be considered:

- As described in Chapter 2, the spatial disaggregation model is unable to preserve the lagged correlations in the primary basin flows. Generally, the simulated primary basin flows for the alternative climate scenarios (including the base case) were found to have lower lag-one correlations, especially during the high runoff winter months, than the historic flows. This result is of concern because correlations affect the estimated reliability of the water resource system. These correlations do not affect any conclusions regarding the hydrologic response of the study catchments to the climate alternatives. The undersimulation of the lagged correlations is the result, in part, of groundwater inflow to the water resources system nodes that is not present in the higher elevation study catchments. Selection of a different set of catchments might allow use of a more complex disaggregation model (see Chapter 2) that could resolve this problem. However, it appears likely that none of the potential catchments would be strongly enough affected by groundwater in the winter months to allow feasible parameter estimates for this model. An alternative would be to model the groundwater effect directly. This would likely be a time-consuming undertaking. In terms of the relative importance of this problem, it is probably less than changes in the stochastic structure discussed below, or any of the issues relating to the hydrologic model discussed above. One reason for this is that the study design provided that comparisons be made with a base case, rather than historic streamflows; therefore the reduced winter correlations are evidenced in the base case, as well as the alternative climate scenarios.

- The structure of the stochastic relationship between the primary water resource system node streamflows and the study catchment flows is constant under the climate alternatives. One problem with this assumption is that the study catchments lie at high elevations and are affected by changes in snow accumulation patterns. Some of the contributing areas to the water resources system nodes lie at lower elevation and are rain-affected under present conditions. Therefore, the effect on the water resources system nodes of a general warming would be different than in the catchments, resulting in a likely overestimation of the effect of the altered climate scenarios. Again, this problem affects only the water resource system node runoff predictions and not the interpretation of the catchment results (Chapter 3). In addition, because the Sacramento-San Joaquin hydrology is snow-affected, the nodes that contribute most of the inflow to the water resource system will not be much affected by this problem. The problem is likely to be greatest for the low-lying secondary nodes, whose flows under the climate alternatives will likely be somewhat overestimated. Each of these assumptions, and the related limitations imposed, suggests a direction for future research.

Recognizing the preliminary nature of the work and the limitations imposed by the assumptions, the following general conclusions can be made:

- The general warming associated with all the GCMs would result in substantial decreases in average snow accumulations in all four of the study catchments.

- Reduction in the amount of precipitation occurring as snow would increase winter runoff and decrease spring and summer runoff.

- Increased precipitation occurring as rainfall in the winter months would increase winter soil moisture storage, and would make more moisture available for ET in the early spring. Increased temperatures would increase spring ET.

- The reduction in moisture supply as snowmelt in the spring, coupled with increased spring ET, would reduce late spring, summer, and fall soil moisture, which would in turn reduce runoff during those periods.

- Although the above points suggest the general character of the changes that would occur under a general global warming for any given catchment, the specific nature of the hydrologic change would depend on physiographic characteristics (notably, the area-elevation distribution) of the catchment, as well as the geologic and topographic features that control the precipitation-runoff response. Substantial hydrologic diversity existed between catchments, especially the McCloud River, which drains an area of deep volcanic ash in the vicinity of Mount Shasta and has exceptionally persistent baseflow.

REFERENCES

Anderson, E.A., "National Weather Service river forecast system -- Snow accumulation and ablation model," NOAA Technical Memorandum NWS HYDRO-17, November, 1973.

Burnash, R.J.C., Ferral, R.L. and Mcquire, R.A., "A generalized streamflow simulation system Conceptual modeling for digital computers," U.S. National Weather Service, Sacramento, CA, 1973.

Conover, W.J., "Practical nonparametric statistics, Wiley, New York, 1971.

Foufoula-Georgiou, E., "Discrete-time point process models for daily rainfall", Water Resources Series Technical Report No. 93, Department of Civil Engineering, University of Washington, March, 1985.

Grotch, S.L., "Regional intercomparisons of General Circulation Model predictions and historical climate data", Technical Report DOE/NBB-0084, Atmospheric and Geophysical Sciences Division, Lawrence Livermore National Laboratory, April, 1988.

Hansen, J., Russell, G., Rind, D., Stone, P., Laus, A., Lebedeff, S.,
Ruedy, R. and Travis, L., "Efficient three-dimensional global models for climate studies: Models I and II", Monthly Weather Review, 111(4), 609-662, 1983.

Hansen, J., Fung, I., Lacis, A., Rind, D., Lebedeff, S., Rueddy, R.,
Russell, G. and Stone,P., "Global climate changes as forecast by Goddard Institute for space studies three-dimensional model," Journal of Geophysical Research, 93(D8), 9341-9364, 1988.

Hettmansperger, T.P., Statistical inference based on ranks, Wiley, New York, 1984.

Hirsch, R.M., "Statistical methods and sampling design for estimating step trends in surface-water quality,", Water Resources Bulletin, 24(3), 493-504, 1988.

Klemes, V., "The Hurst phenomenon: A puzzle?", Water Resources Research, 10(4), 675-688, 1974.

Leytham, K.M., "Physical considerations in the analysis and synthesis of hydrologic sequences", C.W. Harris Hydraulics Laboratory Technical Report No. 76, Department of Civil Engineering, University of Washington, 1982.

Lettenmaier D.P. and Burges, S.J., "Climate Change: Detection and its impact on hydrologic design", Water Resources Research, 14(4), 679-687, 1978.

Linsley, R.K., Kohler, M.A. and Paulhus J.L.H., Hydrology for Engineers,
2nd Ed., McGraw Hill, New York, 1975.

Nelder, J.A. and Mead, R., "A simplex method for functional minimization", Computer Journal, 9, 308-313, 1965.

Peck, E.L., "Catchment modeling and initial parameter estimation for the national weather service river forecast system", NOAA, Technical Memoandum, NWS HYDRO-31, 1976.

Rind, D., Goldberg, R.R. and Ruedy, R., "Change in climate variability in the 21st century", unpublished document, Goddard Space Flight Center, 1988.

Lettenmaier

Sheer, D.P. and Randall, D.R., "Methods for evaluating the potential impact of global climate change on water related activities: Case studies from Atlanta, Georgia and the State of California", report to U.S. Environmental Protection Agency Office of Policy, Planning, and Evaluation, May, 1988.

Veihmeyer, F.J., "Evapotrasnspiration," Chapter 11 in Handbook of applied hydrology (V.T. Chow, ed.), McGraw Hill, New York, 1964.

Wallis, J.R. (ed.) "Climate, climatic change, and water supply," National Academy of Sciences, Panel on Water and Climate, 1977.

METHODS FOR EVALUATING THE POTENTIAL IMPACTS OF GLOBAL CLIMATE CHANGE: CASE STUDIES OF THE STATE OF CALIFORNIA AND ATLANTA, GEORGIA

by

Daniel P. Sheer, Ph.D., P.E.
Dean Randall, Ph.D., P.E.
Water Resources Management Inc.
Columbia, MD 21045

Contract No: CR814637

CONTENTS

Page

FINDINGS 2-1

CHAPTER 1: INTRODUCTION 2-2
USING CIRCULATION MODEL OUTPUT TO ASSESS THE POTENTIAL IMPACTS OF GLOBAL CLIMATE CHANGE 2-2

CHAPTER 2: CALIFORNIA CASE STUDY 2-4
METHODS 2-4
RESULTS AND INTERPRETATION 2-6
SUMMARY 2-16

CHAPTER 3: ATLANTA CASE STUDY 2-17
METHODS 2-17
RESULTS AND INTERPRETATION 2-17
SUMMARY 2-25

REFERENCES 2-28

FINDINGS[1]

Case studies to evaluate the potential impacts of global climate change on water supply were performed for the Central Valley in California and the Atlanta, Georgia, metropolitan area. Streamflow traces, which were generated from the GCM models' outputs, were routed through hydrologic mass balance operation simulation models of the two systems.

In California, the total volume of streamflow for the system increased under each of the climate change scenarios. However, the seasonality of the flows changed such that the winters are wetter and the already dry summers are drier. This results in an increased probability of spring flooding and reduced water deliveries to the consumers. It is doubtful that changing operating policies for the system will significantly improve this situation.

The streamflows of the Chattahoochee River in Atlanta show the same shift in seasonality as occurs in California. However, one scenario shows an increase in total streamflow while the other two show a decrease. Under the GISS $2xCO_2$ scenario, there is more flow, and Lake Lanier levels tend to be higher. Under the GFDL $2xCO_2$ scenario, there is less flow, and the lake levels drop significantly. The effect on recreational use of Lake Lanier under this scenario would be disastrous.

---

[1]Although the information in this report has been funded wholly or in part by the U.S. Environmental Protection Agency under contract no. CR814637, it does not necessarily reflect the Agency's views, and no official endorsement should be inferred from it.

CHAPTER 1

INTRODUCTION

One of the most important goals of research on the potential for global climate change is to prepare society to adapt to such changes. Many of the most dramatic impacts of climate change, should it occur, will be caused by changes in the availability and reliability of water supplies. California, in particular, is likely to be affected by climate change because of the relatively high rate of utilization of the water resources in the state. Georgia and the remainder of the southeastern United States are continuing to feel the impacts of prolonged below-normal rainfall through the decade of the 1980s.

Unfortunately, there has been little work on the development of techniques for assessing the potential impacts of global climate change on water resources related activities. In fact, even long-term historical climatological data are neither widely nor well used in the planning or operation of water resources systems in the United States. Most facility and operations planning is based almost entirely on hydrologic records, either historical or generated. While recent advances in the analysis of water use data and rainfall runoff modeling make it desirable to use climatological data, the techniques are just beginning to find their way into practice. This lack of commonly used techniques makes it quite difficult to estimate the impacts of either potential or predicted changes in long-term climate (such as information on global warming) on water resource-related activities.

The goal of the research performed for this study is to determine how global climate changes might affect water supply availibility. Case studies were performed for the Central Valley of California and metropolitan Atlanta, Georgia. This is done by using streamflow traces generated from global circulation model output as input to hydrologic models that simulate the operation of the systems. This method was used because it allows one to analyze each area as an integrated system to show how water use might change under given climate change scenarios. It also allows the operating policies of the systems to be changed to see if operations can be improved to help counteract the climate change.

USING CIRCULATION MODEL OUTPUT TO ASSESS THE POTENTIAL IMPACTS OF GLOBAL CLIMATE CHANGE

The process of assessing the impacts of global climate change and developing options to mitigate those impacts is essentially similar to the process of using climatological data in planning. There are substantial complications, however. Most of these deal with the lack of calibration of techniques for predicting climate change (in particular global circulation models), the problems of converting output from those techniques to hydrologic traces, and finally, problems of assessing the likely changes in water use that result directly from climate change.

The basic tool for converting climatological data to hydrology is a rainfall runoff model. Such models use precipitation, temperature, and sometimes wind data at a scale comparable to that available from common sources, typically the National Weather Service. Usually there are several gauging stations proximate to the basin of interest, and data from these stations are interpolated to produce a trace of climatological data suitable for running a model. Unfortunately, the scale of techniques suitable for assessing potential global climate change is much larger than the scale of most rainfall runoff models, e.g., the area represented by a single grid point in a global circulation model may encompass several basins, which each might be calibrated using tens (or even hundreds) of weather stations. Orographic effects cause large local variations in climatology, and these effects are often magnified in the local hydrology. The level of detail of techniques for assessing future climate is simply not yet adequate to address the issues of local changes so critical to hydrology.

The calibration of techniques that convert climatological data to hydrology involves setting parameters that either directly or implicitly represent the evapotranspiration of water by local ecosystems. Techniques are generally quite sensitive to these parameters. Substantial changes in climate are likely to produce corresponding changes in ecosystems, thus invalidating calibrations based on historical data. And estimating the biological changes that might occur and affect hydrology is made more difficult by substantial impact of the hydrology itself on the kinds of ecosystems that might be supported. In preparing the hydrology for use in the California and Atlanta case studies, these issues were addressed directly (Lettenmaier, this volume; Hains, this volume), although their results show how much more research is needed in this infant field.

Just as difficult is the task of predicting water use under conditions of changed climate. Climate has direct influence on many economic variables including water requirements for cooling, cropping patterns, and population density. All of these economic factors will help determine the water use requirements. To estimate the overall impact of climate change, full consideration must be given to these items. The relationship between demand and climate was addressed in the Atlanta case study, and the results are included as an appendix. For lack of time, the results were not included in the simulation models, however.

It is most important, in assessing the impacts of global climate change, to realize that water resources systems continually adapt to new information concerning existing climate, and that if climate change happens slowly enough, the systems will adapt to the change incrementally. Indeed most predictions conclude that climate, if it does change, will change slowly, i.e., the annual rate of change in climatological norms will be much smaller than the normal interannual variation.

As a result, responses to climate change are likely to occur in the same manner as responses to more information about current climate. That is, actual changes and implementation of alternatives will be driven primarily by extreme events. Such changes can be either operational or structural, and if the best possible assessment of impacts and alternatives is to be done, the techniques used must be capable of examining both kinds of responses.

In the case studies below, we attempted to implement techniques, particularly simulation models, that could account for the factors mentioned above. This method can be used to solicit local input regarding the nature of the incremental adaptations that might occur in the face of a gradual change in the climate. In both California and Atlanta, local water managers were exposed to the results of the studies using these techniques, and the results are reported below.

It should be noted that the traces of precipitation and temperature from the global circulation models is at best a guess. The simulation models used in this study are likely far more accurate than the streamflows (which were generated from the global circulation model output) that were used as inputs.

CHAPTER 2

CALIFORNIA CASE STUDY

The State of California and the federal government have enormous investments in facilities designed to deal with the vagaries of existing climate variation in California. The federally operated Central Valley Project (CVP), and the state-operated State Water Project (SWP) (as well as other state, federal, and local projects) move water from the wet and sparsely populated northern part of the state to the dry and densely populated southern part, and hold water during wet years or seasons for use in drier periods. This water is used for irrigated agriculture and for municipal and industrial supply. In addition, under current law much of the storage in the two systems is committed to maintaining minimum levels of outflow to San Francisco Bay. Despite the investments, in recent years the demand for water has exceeded the supply. With or without climate change, this is likely to occur even more frequently in the future.

The distribution of water shortages in California is a function of the water rights of individual users under the state's water law. California is an appropriation doctrine state, so generally those who began using water first have by far the most reliable supplies. Complex arrangements have evolved, based on water rights, for water exchanges and sharing, which dictate the shortages borne by various users. Simulation models are used to test these arrangements, based on historical hydrology modified to account for future development.

These models can also be used to evaluate the impacts a climate-induced change in hydrology might have on water users and on instream flows. Before they can be used in this way, however, suitable hydrologic traces must be prepared. These traces must be consistent not only with the given climate change scenario, but also with the host of other assumptions made in developing the water resource simulation model. Finally, care must be taken in the manner in which the simulations are run and the results reported.

Operational strategies for large-scale water resource systems can have an enormous influence on the overall performance of the system. Such strategies are based, either implicitly or explicitly, on the statistics of historical hydrology. This is particularly important in California. If climate changes, it is likely to change rather gradually, and streamflow statistics will change gradually as well. Over time, operations have changed, and the changes have been driven in large part by the occurrence of occasional extreme drought or flood. Recent floods and droughts in California have, indeed, affected operations in exactly this manner. Therefore, it is vital that assessments of the potential impacts of climate change consider the opportunities available to react to those changes through changes in operating policies, including adjustment of drought management schemes and changes in reservoir rule curves.

METHODS

Existing models and previous analysis of water use in California made it possible to estimate the potential impacts of climate change on water deliveries in California, and on outflow to San Francisco Bay. The model used was developed by Water Resources Management Inc. (WRMI) for the Metropolitan Water District of Southern California (MWD), and was used with their kind permission (Sheer and Baeck, 1987). (MWD currently uses the model in its planning efforts.) The version of the model used emulates the State of California's Department of Water Resources (DWR) Planning Simulation Model (CA DWR, 1986).

The WRMI model does a mass balance simulation. It uses adjusted historical hydrologic inputs, projected water use demands, instream and Delta outflow requirements, and operating policies for determining levels of water deliveries to users in both the CVP and SWP. All of the major hydrologic features of the Central Valley are included. A schematic of that model is shown in Figure 1. The model was designed to simulate the operating policies that are currently used by both the CVP and SWP. The results of the simulation include time traces of reservoir levels, deliveries to CVP and SWP water users, flows at points in the Sacramento River and its major tributaries, and Delta outflow.

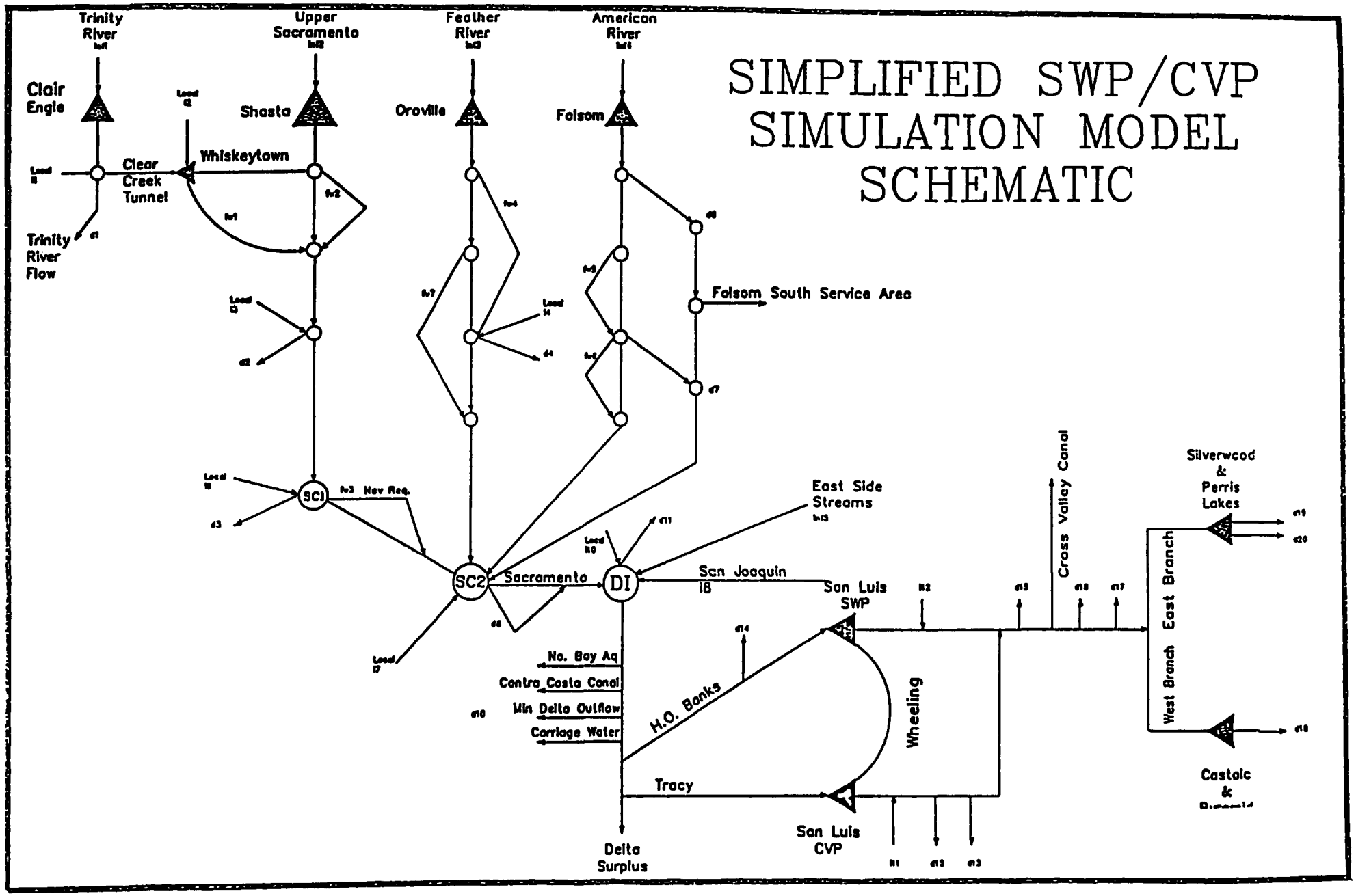

Figure 1. Simplified SWP/CVP simulation model schematic.

The hydrology used as a basis for the California case study, hereafter called the "scenario flows," was obtained from Lettenmaier (this volume). The flows he developed correspond to "virgin flows," unaltered by changes in land use. As discussed above, the flows used by the DWR model, and therefore the WRMI model, have to be adjusted to account for the projected levels of upstream water use and land development.

Five different traces have been run through the model:

1) Base run. This trace was generated using GISS output for $1xCO_2$. It represents current climate and is nearly identical to historical impaired flows.

2) GFDL $2xCO_2$. This trace was generated using GFDL output for $2xCO_2$.

3) GISS $2xCO_2$. This trace was generated using GISS output for $2xCO_2$.

4) Oregon State University $2xCO_2$. This trace was generated using OSU $2xCO_2$ output.

5) GISS Transient. This trace is intermediate between the base run and the GISS $2xCO_2$ run. It represents a gradual change in atmospheric CO_2 from current levels to $2xCO_2$ over a period of about 80 years. For this scenario it is impossible to differentiate between changes in flows due to local, short-term weather changes and long-term climate changes. Therefore, the conclusions that can be drawn from these runs are not clear, and no plots are provided.

A rather complex process for adjusting historical flows to future conditions has evolved for use by both the CVP and the DWR in California, and those will not be discussed here. Flows which correspond to the inflow at nodes in the DWR and WRMI models for 1990 conditions have been produced using this method. They are called "impaired flows." The process is also run in reverse to produced what are called "unimpaired," or "full natural" flows (CA DWR, 1987). These flows nominally represent the flows that would occur in the absence of development. To correct the scenario flows for projected "impairments," the 1990 impaired flows were subtracted from the 1990 unimpaired flows, and the resulting "impairments" were subtracted from the scenario flows to get the hydrologic traces actually used in the simulation modeling. In equation format:

Scenario - (1990 unimpaired - 1990 impaired) = new trace

Each of these scenarios was run with a monthly time step for the 57-year period from 1951 to 2007. The first 30 years of the record were derived directly from Lettenmaier's adjustment of the historical flows from 1951 to 1980. The remaining 27 years were taken by a random sampling (with replacement) for the first 30 years. A period of record longer than 30 years was developed to allow the development of adjusted operating policies that were not entirely tailored to the 30-year period being evaluated. If the adjustments to the rules were based solely on the 30 years, the rules would then be "optimal" for that particular period, and would not reflect any uncertainty as to the longer term. Fifty seven years was an arbitrary choice for period of record; it corresponds to the length of the historical record normally used in developing operating policies for the SWP. This series of runs is summarized in Figures 3 through 9, which show the response of the system to the change in inflows.

RESULTS AND INTERPRETATION

Figure 2 shows a comparison of the total monthly inflow into the Delta for the different scenarios. This graph indicates that while the total streamflow entering the Delta is greater, the seasonality of the flows for each scenario increases, with wetter falls and winters and drier springs and summers. (It should be noted that for the current climate in the Central Valley most of the precipitation falls in the winter, and the summers are very dry.) The increased seasonality is particularly strong for the GISS $2xCO_2$ case. The OSU $2xCO_2$ scenario is most like current streamflows, although there is still a seasonality shift.

FIGURE 2

Mean Monthly Delta Difference

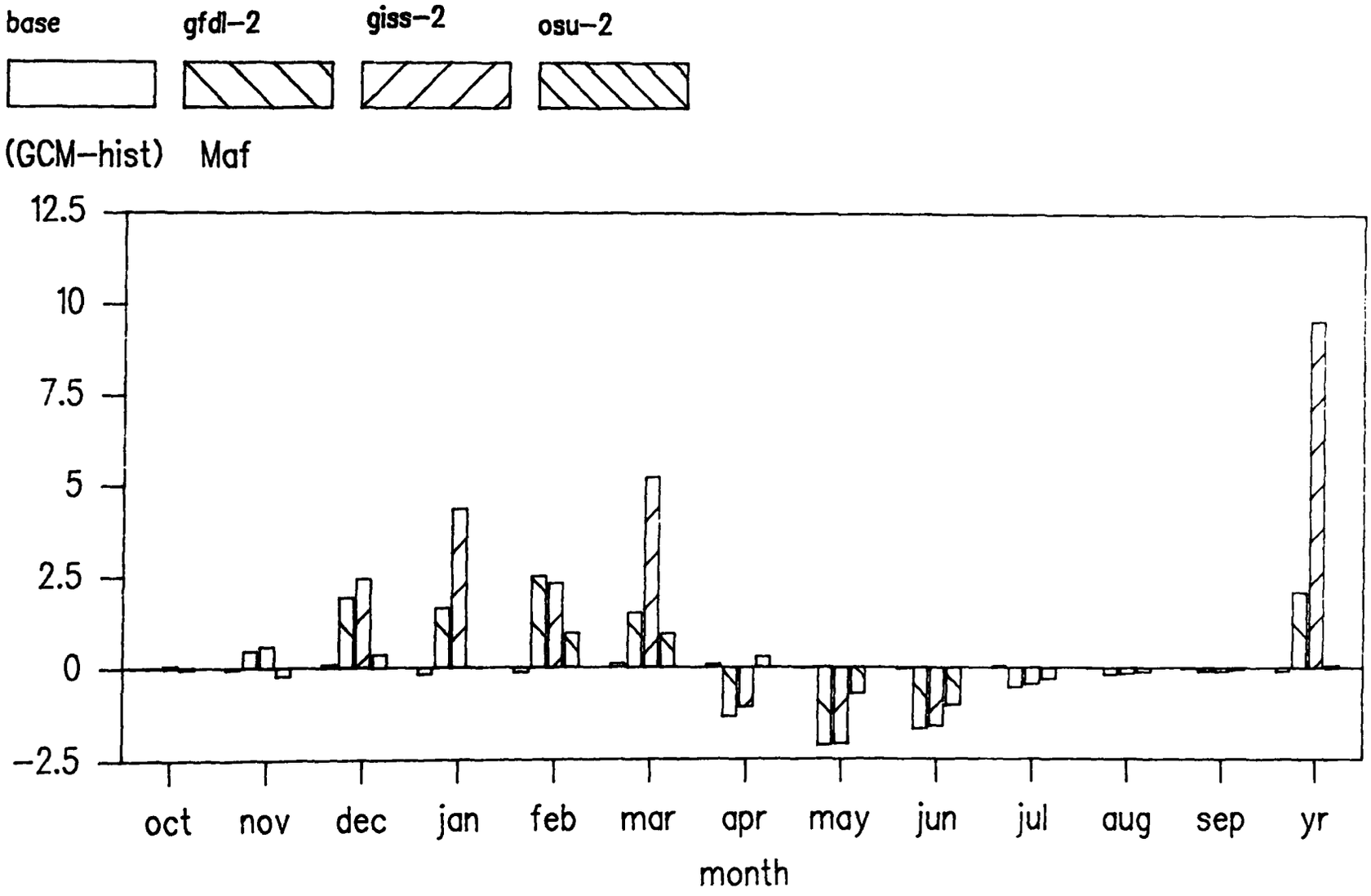

Sheer

Figure 3 shows the deliveries to SWP under the four scenarios. The $2xCO_2$ scenarios all show significantly lower deliveries, especially GISS and GFDL, despite their increased annual flow. This dramatic decrease is caused by the increased seasonality of the flows. A reasonable interpretation of this is as follows:

> Increased temperatures lead to more winter precipitation falling as rain, thus reducing snowpack. Higher winter temperatures also lead to the snowpack melting earlier. The early snowmelt spills from the reservoirs instead of going into storage and being available to augment streamflow during the early part of the irrigation season. The net effect is the loss of the large reservoir currently represented by the late spring snowpack, and a corresponding decrease in the water that can be reliably supplied by the system.

The effect of the increased seasonality of the GFDL run seems to be offset by its larger runoff volume. Figure 4 shows the mean annual volume of SWP deliveries for the four scenarios. For example, the GFDL $2xCO_2$ scenario results in about a 16% reduction in deliveries from the base case.

Deliveries to the CVP are not reduced under the scenarios. The U.S. Bureau of Reclamation estimates that it can sell an additional 1 million acre-feet of water annually, which indicates that the CVP has a surplus of storage. The SWP has much less storage, so deliveries suffer more during dry periods.

Figures 5, 6, and 7 show how the Oroville Reservoir storage, the primary storage facility for the SWP, is affected by the different scenarios. At the end of March (Figure 5), which is the last of the wet months, the storages for the scenarios are nearly identical. Storages in March are limited by the need to preserve free volume in the reservoirs for flood control, so the storage for each scenario is at the flood control rule. Figures 6 and 7 show clearly that the reservoir storage is diminished owing to the reduced spring and summer flows. Oroville reservoir is substantially lower by the end of May.

Total outflow from the Delta is shown in Figure 8. As one would expect, each of the $2xCO_2$ scenarios shows an increase in total outflow.

Carriage water is an environmental constraint that is built into the model. The H.O. Banks (SWP) and Tracy (CVP) pump plants pump water from the south side of the Delta into the California Aqueduct and the Delta Mendota Canal, respectively. At high discharges this pumping causes a southward current across the Delta. During these times of high pumpage, a minimum amount of flow must be maintained through the Delta. During times of low flow, water must be released from the reservoirs to meet this requirement. This release is called "carriage water."

One of the impacts of a warming climate is a rise in sea level, which will affect the Delta. Philip Williams, who is studying the effects of the climate change scenarios on the Delta, suggested that the Delta carriage water requirement should be doubled to counteract both the sea level rise and increasing salinity in San Francisco Bay. The base and GFDL $2xCO_2$ scenarios were done with the doubled carriage water requirement. A comparison of SWP deliveries for those two scenarios with current and doubled carriage water is shown in Figure 9. Base,1CW indicates the base run. Base, 2CW is the base case with double the doubled carriage water. GFDL2, 1CW and GFDL2, 2CW indicate the GFDL $2xCO_2$ case with current and doubled carriage water, respectively. This shows that increasing the carriage water requirement would have little bearing on the deliveries for years corresponding to the years from 1950 to 1980. It must be noted that the period from 1950 to 1980 does not include the drought of record for the Central Valley of California (1927-1934). An analysis using those years would show a substantial impact on deliveries during the drought. The carriage water will have a stronger effect over a long, sustained drought than a short, intense drought as was experienced in 1977.

Several changes in operating rules might improve the performance of the system in terms of deliveries. Reducing flood pools by increasing rule curve storage in April might reduce the relative drawdown at the end of the year, and thus increase deliveries. However, this cannot be done without increasing the storage levels in March (the wettest month), increasing the risk of a flood. With the higher flows in March, one might expect that

FIGURE 3

Annual SWP Deliveries

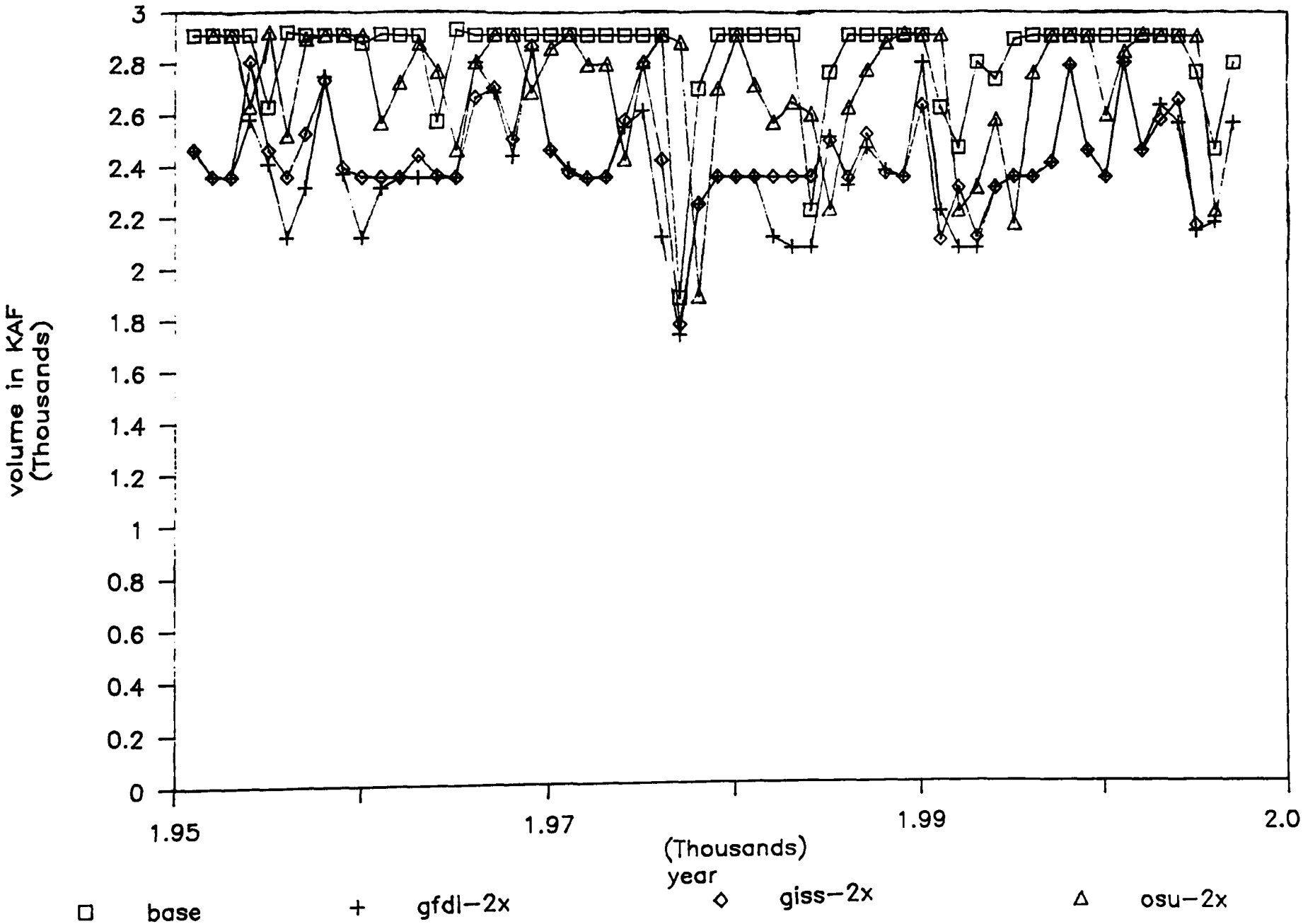

Sheer

FIGURE 4

Mean Annual SWP Delivery

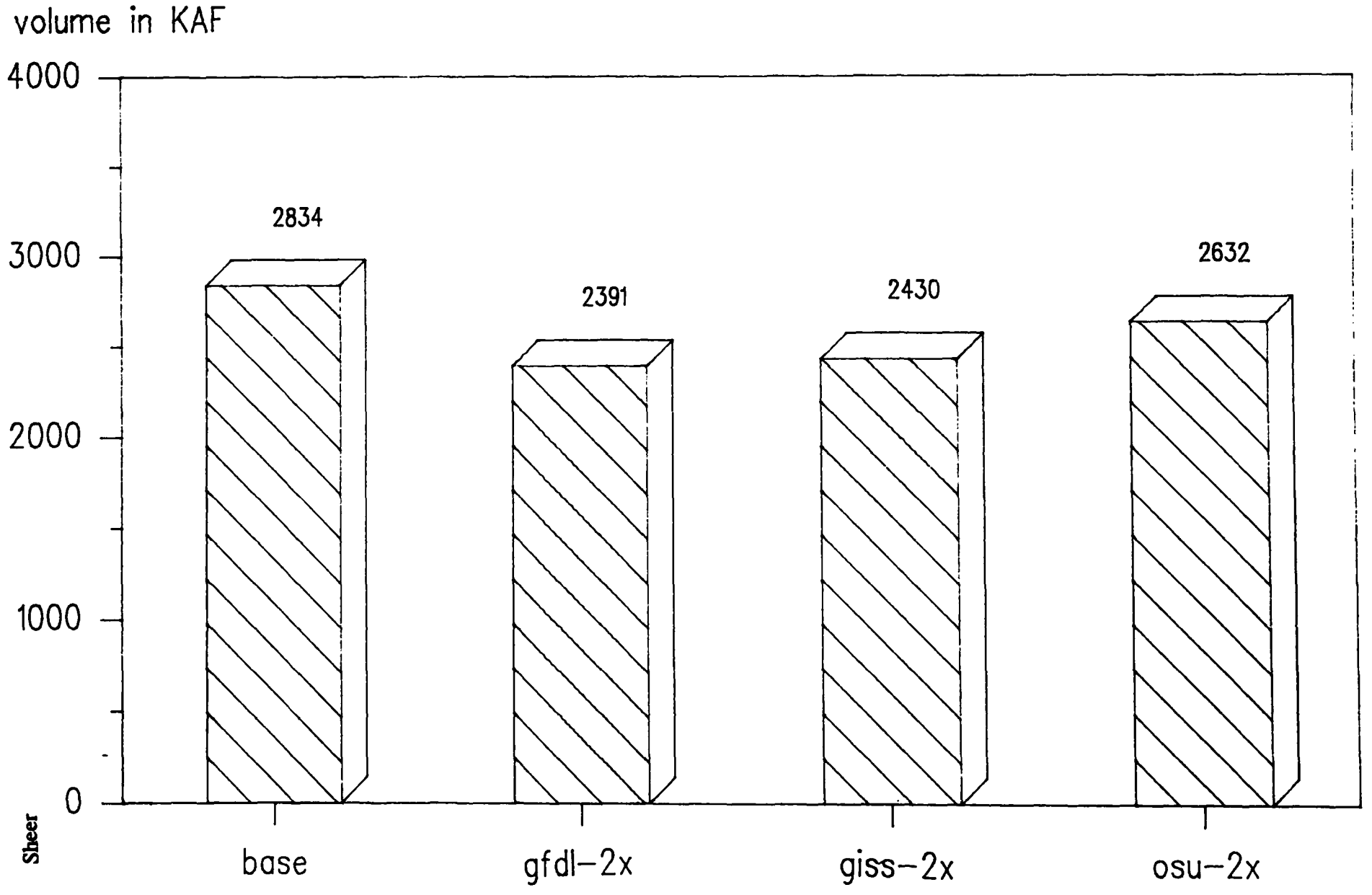

Sheer

FIGURE 5

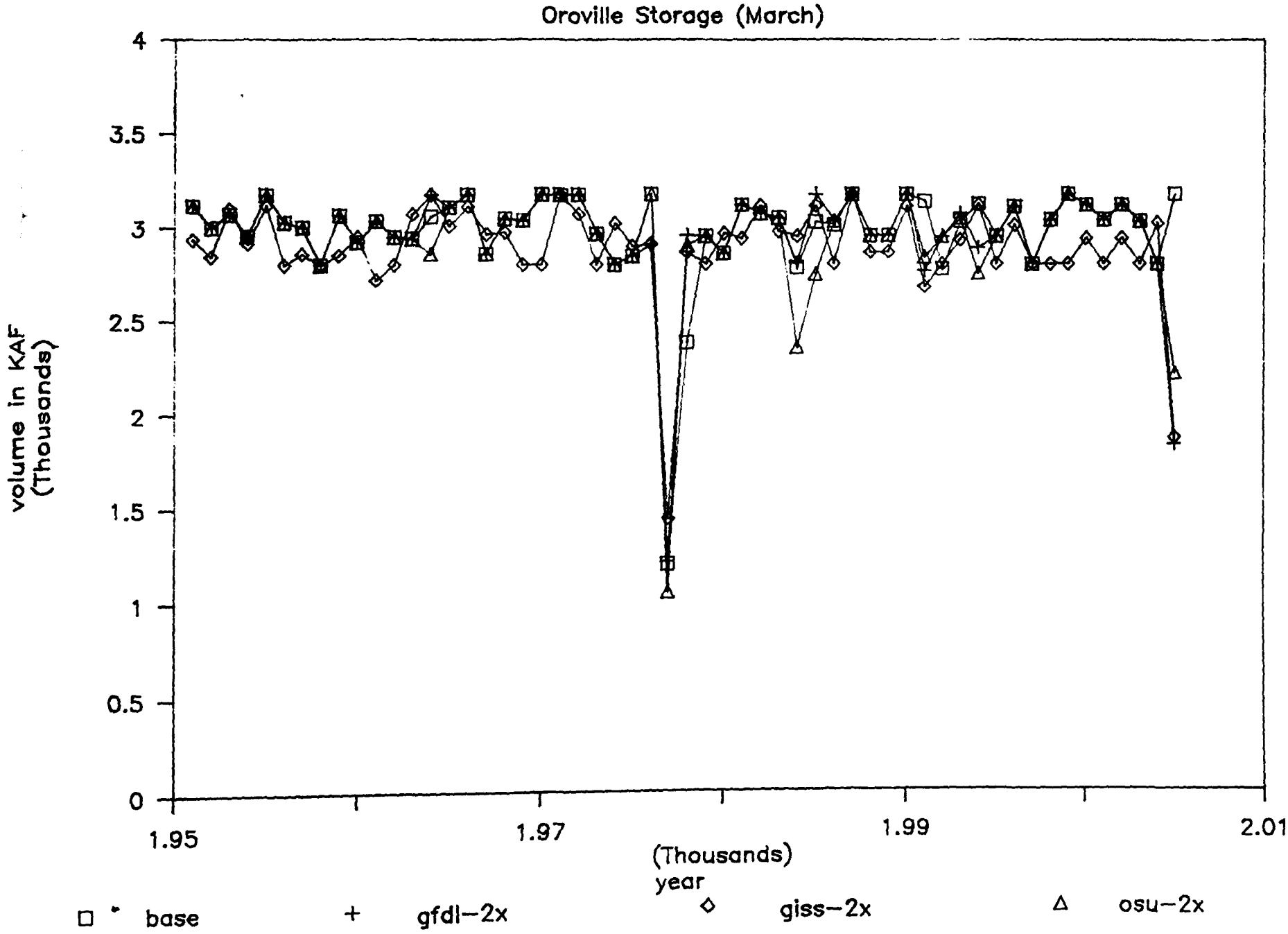

Sheer

FIGURE 6

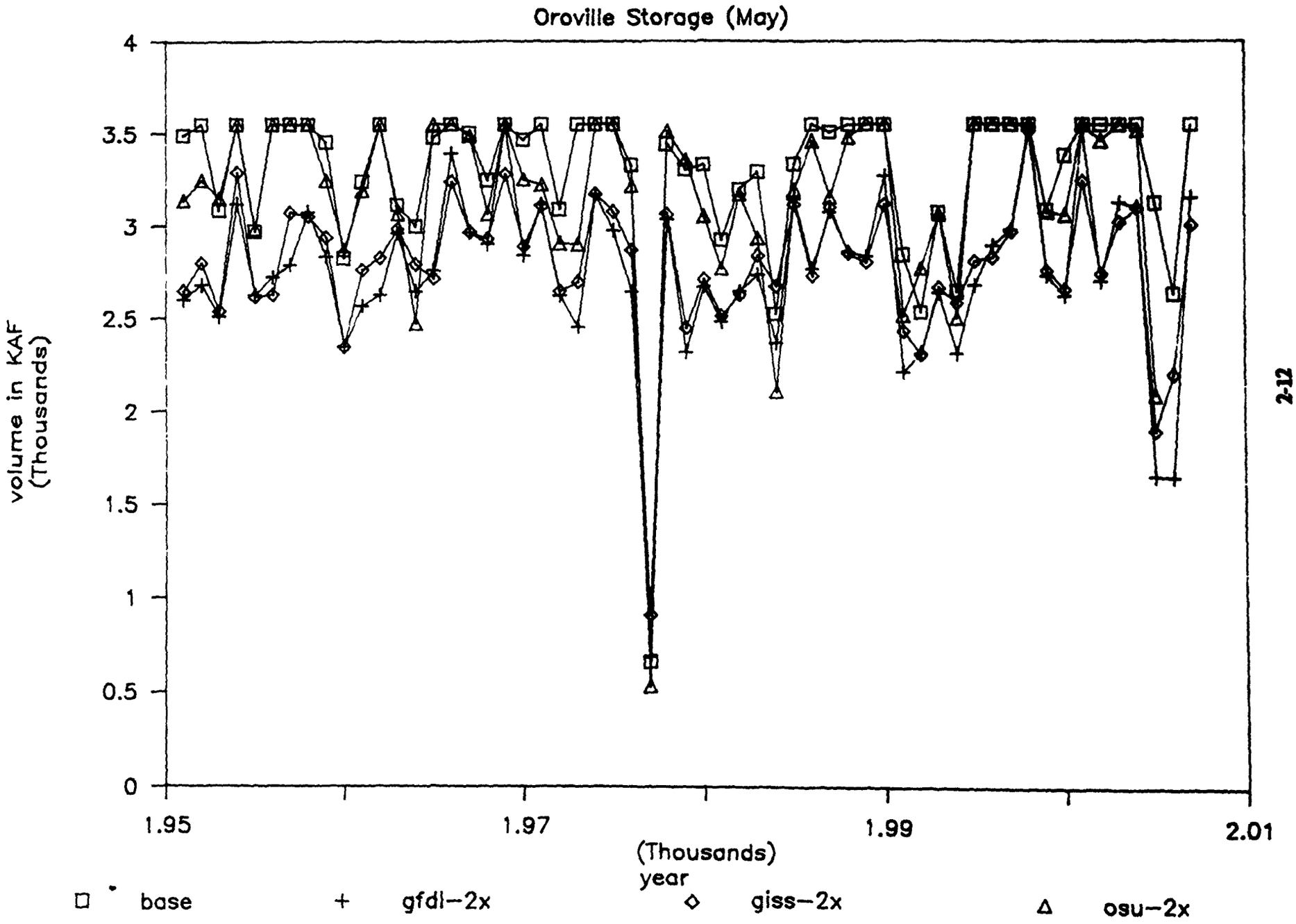

Sheer

FIGURE 7

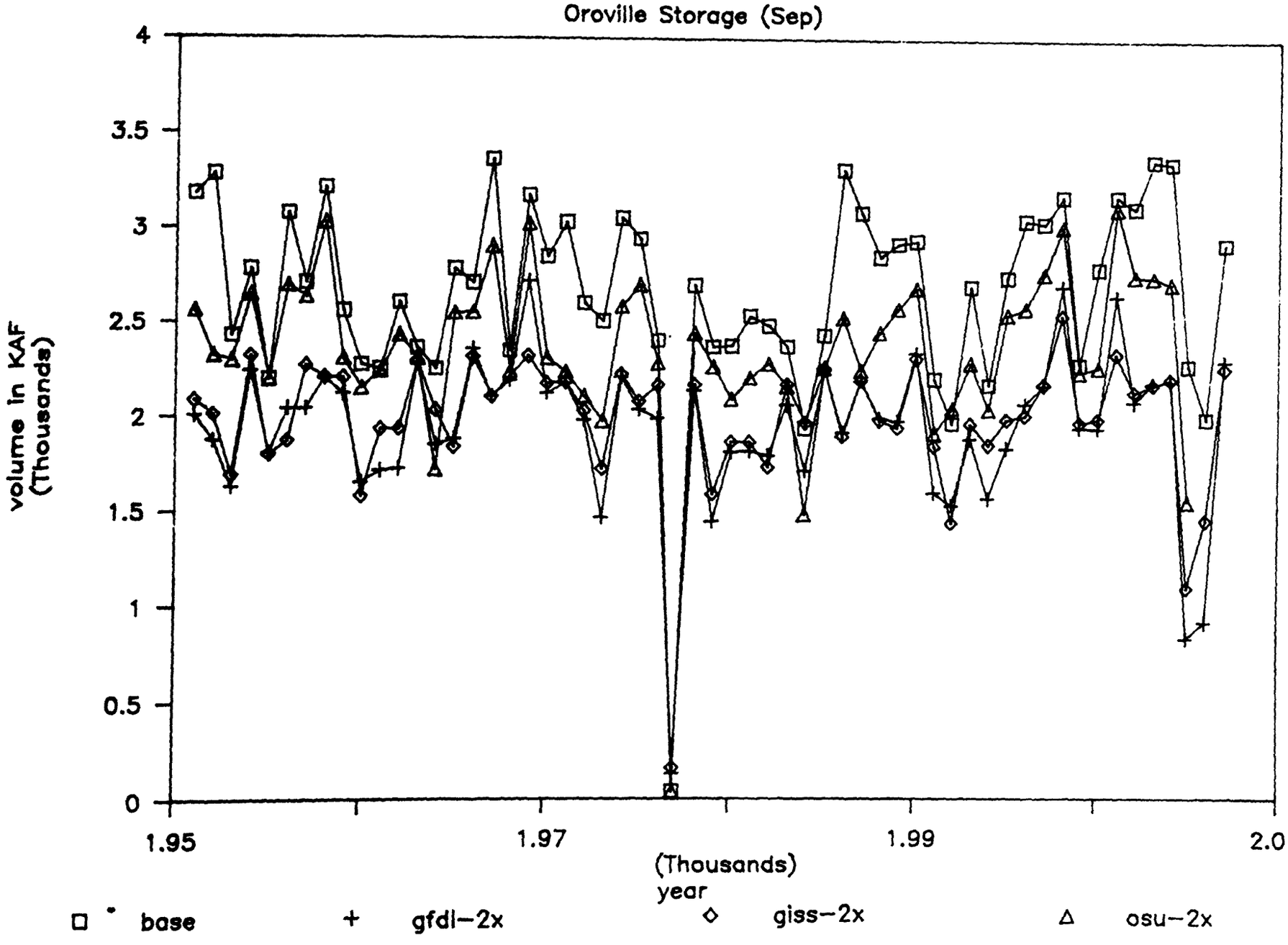

Sheet

FIGURE 8

Total Annual Outflow

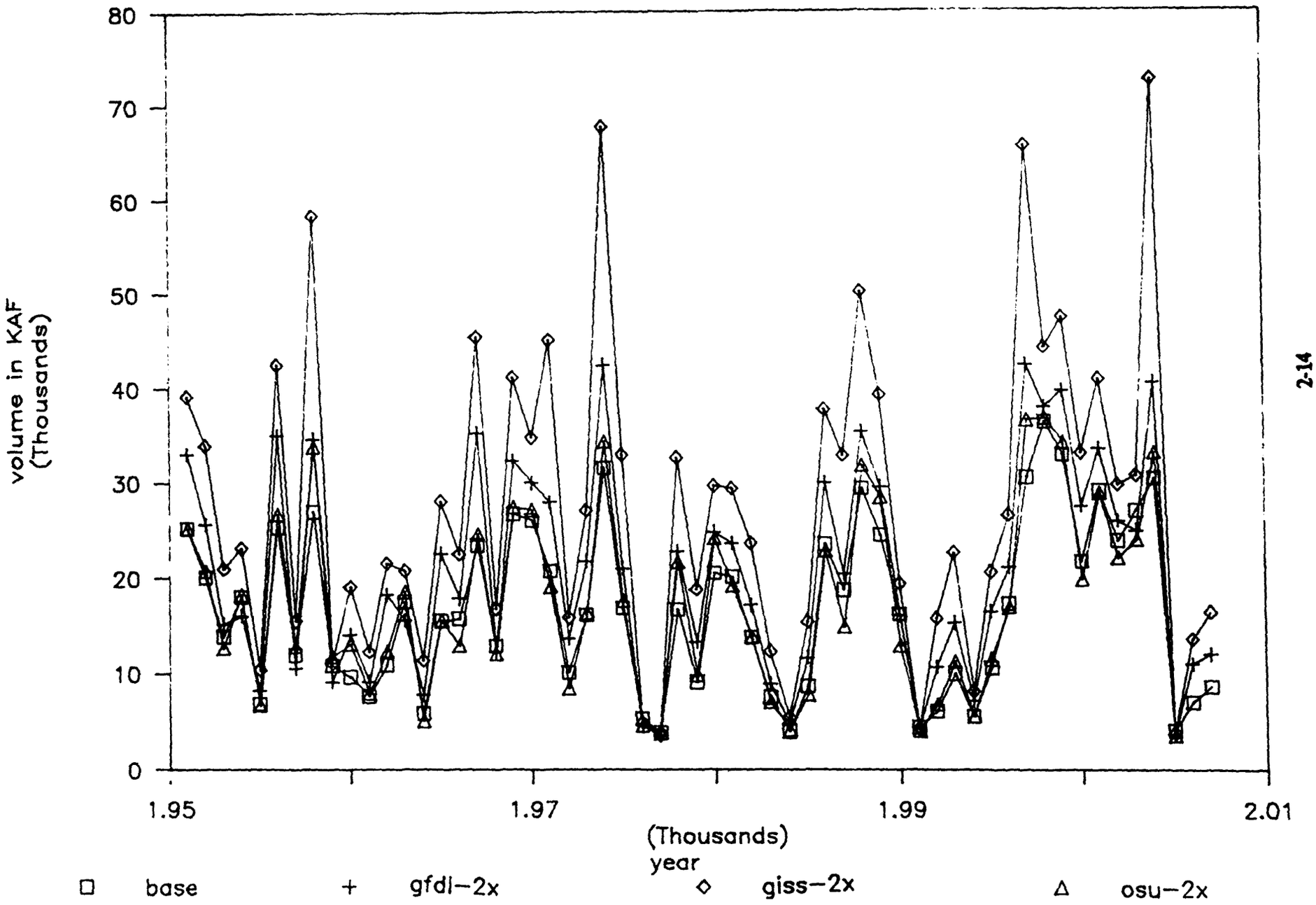

Sheer

FIGURE 9

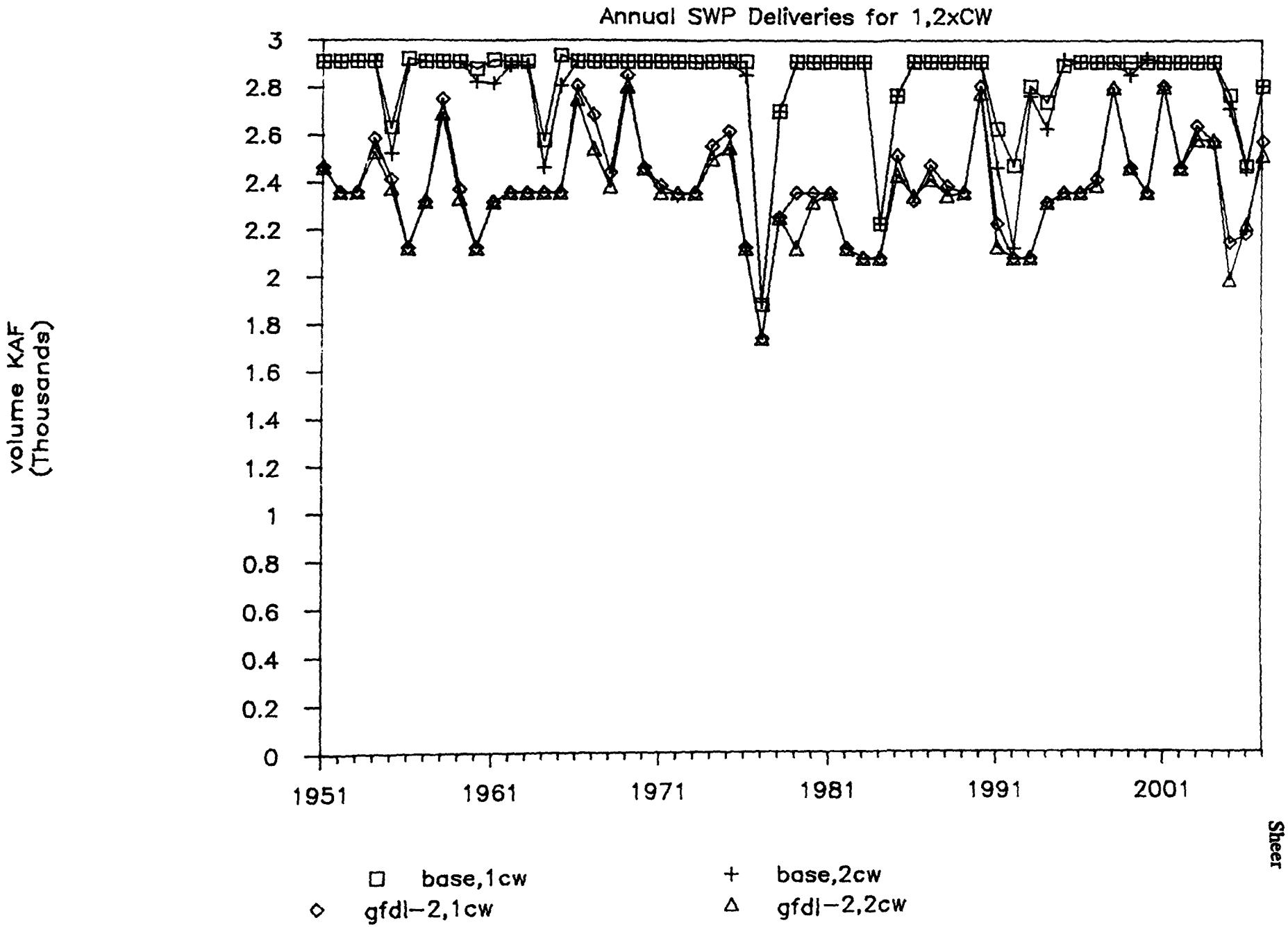

Sheer

March storages might have to be further reduced to accommodate potentially larger floods. This would only exacerbate the water supply impacts of climate change. Changing the rule curve at San Luis to increase water held in March and April might also help.

A meeting was held on March 4, 1988, with representatives of the State DWR and the Bureau of Reclamation to discuss these results. At that meeting the question of potential changes in operations to accommodate changed climate was raised. The consensus among all involved, including the current operators of the projects, was that the magnitude of the change in seasonality was such that operational changes alone would make little if any improvement in system performance. This seemed especially true in light of the potential for increased need for flood control storage.

Assuming that the scenarios are representative of the future climate, water deliveries from the CVP/SWP will decrease unless storage is added to the system. Also, unless the current operating rules for flood control storage change, there will be an increased threat of flooding, particularly in the Sacramento and Stockton metropolitan areas.

SUMMARY

Four climate change scenarios were routed through WRMI's CVP/SWP simulation model to evaluate their impacts on the California water supply system. Though the GISS and GFDL $2xCO_2$ scenarios produce more runoff, the increased seasonality of the flows will result in a substantial reduction in water delivered. One can speculate on what would be required to offset the loss in deliveries. Because the drought of record is 7 years long, it would require about 7 acre-feet of storage to support an average annual delivery of 1 acre-foot at the current reliability with the current climate, and more under a less favorable climate. Average deliveries fell some 440 thousand acre-feet (KAF) from the base run to the GFDL $2xCO_2$ run. Assuming that the less favorable climate would raise the ratio from 7:1 to 10:1, some 4.4 million acre feet of additional storage would be required to maintain current deliveries and reliability. The authors believe this estimate is low. Although sites for additional storage of this magnitude of storage are available (by enlarging Shasta Reservoir or building Auburn Dam), their political feasibility and social desirability is problematic.

CHAPTER 3

ATLANTA CASE STUDY

The Chattahoochee River is the main water supply source for the City of Atlanta and its environs. Lake Lanier is formed behind Buford Dam, located about 30 miles upstream of Atlanta on the Chattahoochee. The lake is used to maintain Chattahoochee flows, and thus reliable water supply for the region. Lake Lanier, however, is a U.S. Army Corps of Engineers (COE) reservoir authorized for flood control, navigation, and hydropower generation. No storage in the lake is specifically authorized for the purpose of water supply. Nor is any storage allocated to recreation, despite the fact that the lake is the most heavily used of any COE lake in the United States.

Minimum flows are maintained to enhance navigation on the Chattahoochee and Appalachicola Rivers downstream of Columbus, Georgia, which is about 110 miles downstream from Atlanta. Navigation releases of 1000 cfs from May through October are required. Hydropower generated at Buford Dam is sold by the Southeastern Power Administration. The minimum hydropower release is 500 ft^3/sec (cfs). The Chattahoochee is the primary water supply source for about 74% of the 2.2 million people in the seven-county metropolitan area, while about 9% of the people use water directly from the lake. The Atlanta Regional Commission (ARC) does not expect those percentages to change.

The wet nature of the 1960s and 1970s kept lake levels high. However, droughts in the 1980s have had significant impacts on recreation in the lake. Lake levels have dropped to historical lows, causing problems for boaters in particular. Power generation has also been affected, and releases to maintain instream flows have been reduced. Despite these impacts, there has always been substantial storage remaining in the lake, and water supply has never been seriously threatened.

METHODS

A mass balance model of Lake Lanier was developed for this simulation. A schematic of that model is shown in Figure 10. Current water demands from the Chattahoochee were provided by staff at the ARC. Historical inflows for the initial development were provided by the COE. Simplified rule curves for Lake Lanier operations were also provided by the COE, as well as functions for converting releases to power generation, and release requirements for navigation.

After the model was complete, a meeting was held in Atlanta involving the Georgia Environmental Protection Division, the ARC, and the COE to review the reasonableness of the operating rules to be used for the historical runs. All suggestions made at that meeting were incorporated, and the results of the model runs seemed reasonable to all concerned.

The model produces traces of lake levels, power generation, and flows below Atlanta, a reach of the river where water quality is critical. A 30-year record (1950-80) with a monthly time step was used for all the runs.

Inflows for the five scenarios, which are the same as those described in the California Case Study section of this report, were obtained from Hains (this volume). Gains were computed by multiplying the ratio of historical gains to inflows by the scenario inflows. All demands and operating rule curves remained the same for the scenarios.

RESULTS AND INTERPRETATION

Five different traces have been run through the model, which are indicated below. Figure 11 shows a comparison of the total monthly inflows into Lake Lanier. The mean annual flow for the base case, which represents current climate, is about 9% higher than historical. The GISS $2xCO_2$ scenario has stronger seasonality than the base case with wetter winters and drier summers. The mean annual flow is about 18% higher than historical. The GFDL $2xCO_2$ run exhibits the same type of seasonality as the GISS $2xCO_2$ run, but

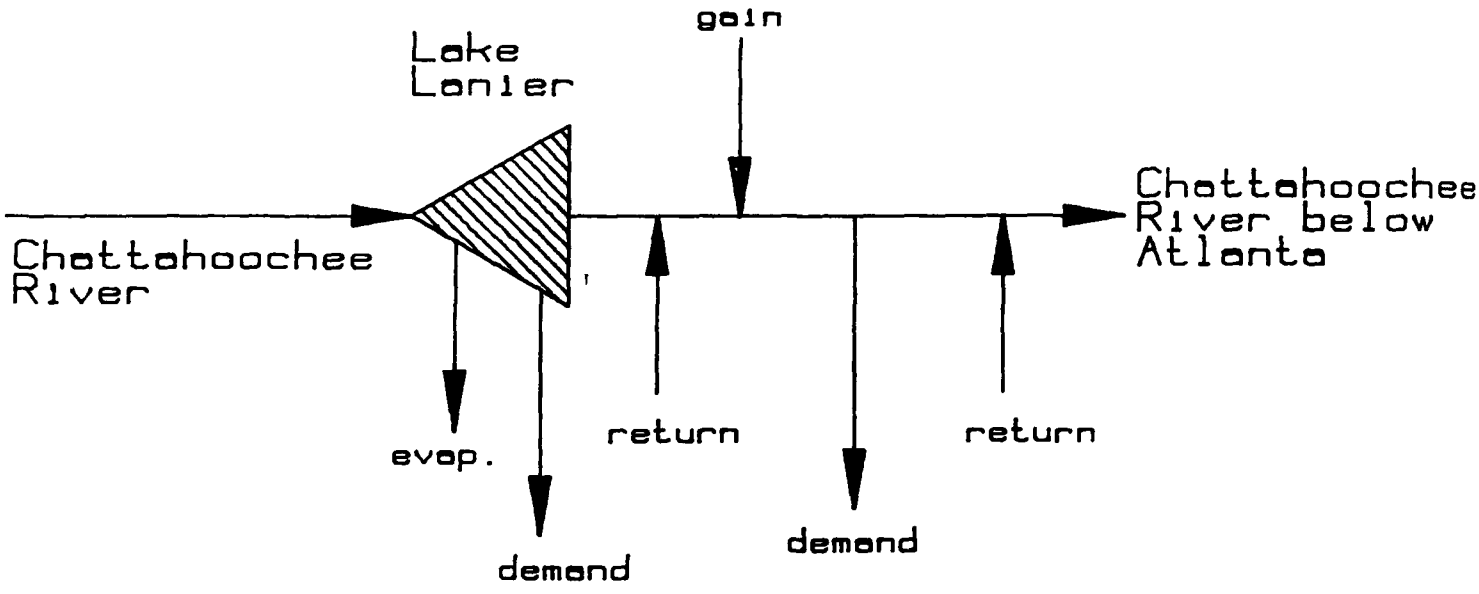

Figure 10. Lake Lanier model schematic.

FIGURE 11

Mean Inflow Difference – Lake Lanier

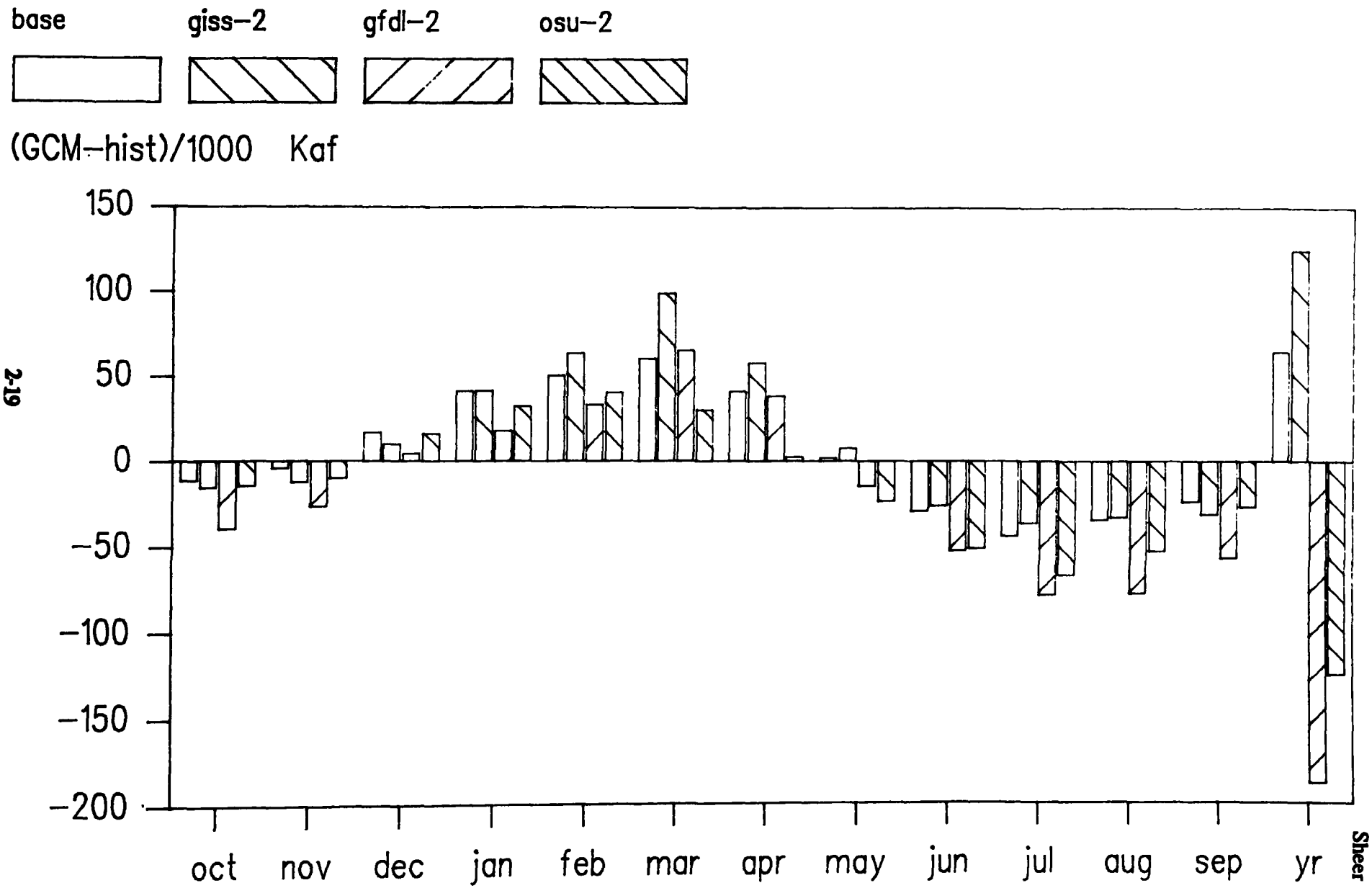

Sheer

with noticeably less mean annual flow. The OSU $2xCO_2$ run shows the same general characteristics as the GFDL $2xCO_2$, with a less pronounced reduction in mean annual flow. This scenario is not included in the plots because the GISS and GFDL $2xCO_2$ scenarios represent the extremes, so all OSU scenario traces will lie between those two, and to reduce the clutter in the graphs.

Figures 12 through 15 show the results of these runs. They include Lake Lanier elevation, power generation, and outflow below Atlanta for the base, GISS $2xCO_2$, and GFDL $2xCO_2$. All plots were done using monthly values. The COE operating rules have been used for all of the projected scenarios. It is likely that the operating rules could be changed to provide better operations under the projected scenarios. The following conclusions are drawn from these plots.

Lake Lanier elevations for September are shown in Figure 12. The target trace is the storage target for recreation, elevation 1061.32 ft. The highest target for the lake is 1067.08 ft (June) and the lowest is 1060.0 ft (October - December). The lake elevations for base and $2xCO_2$ tend to be higher than the target. The base and $2xCO_2$ traces fall below the targets 21 and 7 times in 360 months, respectively. One would expect higher lake elevations from GISS $2xCO_2$ because of the increased inflow. The levels from the GFDL scenario are noticeably lower with many more violations (261) of the lower target elevation; differences between the trace and the target of 5 to 15 ft are common. Under the GFDL scenario, the lake levels would have been continuously under the targets from 1954 through 1961. The combination of the frequency and severity of low lake levels would have a disastrous effect on recreation.

Mean annual outflows below Atlanta are shown in Figure 13. Two minimum flow requirements are used downstream of Atlanta, 750 and 650 cfs. The higher value is used under normal conditions, while the lower value is used when Lake Lanier falls below specified levels. (The rules for reducing downstream flows are explicit, but are not followed exactly in practice. In 1988, flows downstream were reduced well before the reservoir fell to the specified target level.) The outflows for GISS $2XCO_2$ are higher than base, as one would expect. Neither base nor GISS $2xCO_2$ violates the lower requirement, but they violate the upper requirement 29 and 43 times, respectively. However, these violations are slight, typically about 10 cfs. Outflows for the GFDL run violate the upper low flow requirement 117 times and the lower requirement 21 times. Again, given the lower magnitude of inflows for GFDL, this should be expected.

Power generation is shown in Figures 14 and 15. The patterns indicate that the GFDL scenario yields less energy. Figure 15 indicates that the total energy generated for the base and GISS scenarios is reasonably close, while GFDL yields about 38% less energy than base. Using a price of $0.03 to $0.10 per kilowatt hour (KWH), this results in an annual loss of between $127,000 and $424,000 in energy generation. It should be noted that the value of the power produced at Lake Lanier is not adequately reflected by a unit cost per KWH. This is because the generators at the dam produce peaking power, and if they are not reliably available, additional fossil fuel or nuclear generating units would be required at enormous capital cost. Calculating those values is beyond the scope of this study.

Two additional runs of the model were made with different operating policies. The first was done to reduce water supply withdrawals (deliveries) when lake levels are low because the COE has not authorized the reservoir for water supply. This was done by specifying the recreation target levels as the water supply constraints. When the lake level falls below the target level, no deliveries are allowed. The purpose of this model run is not to suggest that that would actually happen, but to show the effect of giving recreation lake level targets precedence over water supply. This model run is summarized in Table 1 and Figure 16.

The data shown in Table 1 indicate that the water delivery reduction policy has some effect for the base and GISS scenarios, but that the results for GFDL are disatrous in terms of water shortages. About 40% of the months have zero deliveries. One would expect that there would be fewer violations of level targets and low flow requirements as less water is being withdrawn and consumed from the system. Figure 16 shows that this policy does in fact lead to significantly higher lake levels, particularly for the GFDL scenario.

FIGURE 12
Lake Lanier Elevation (September)

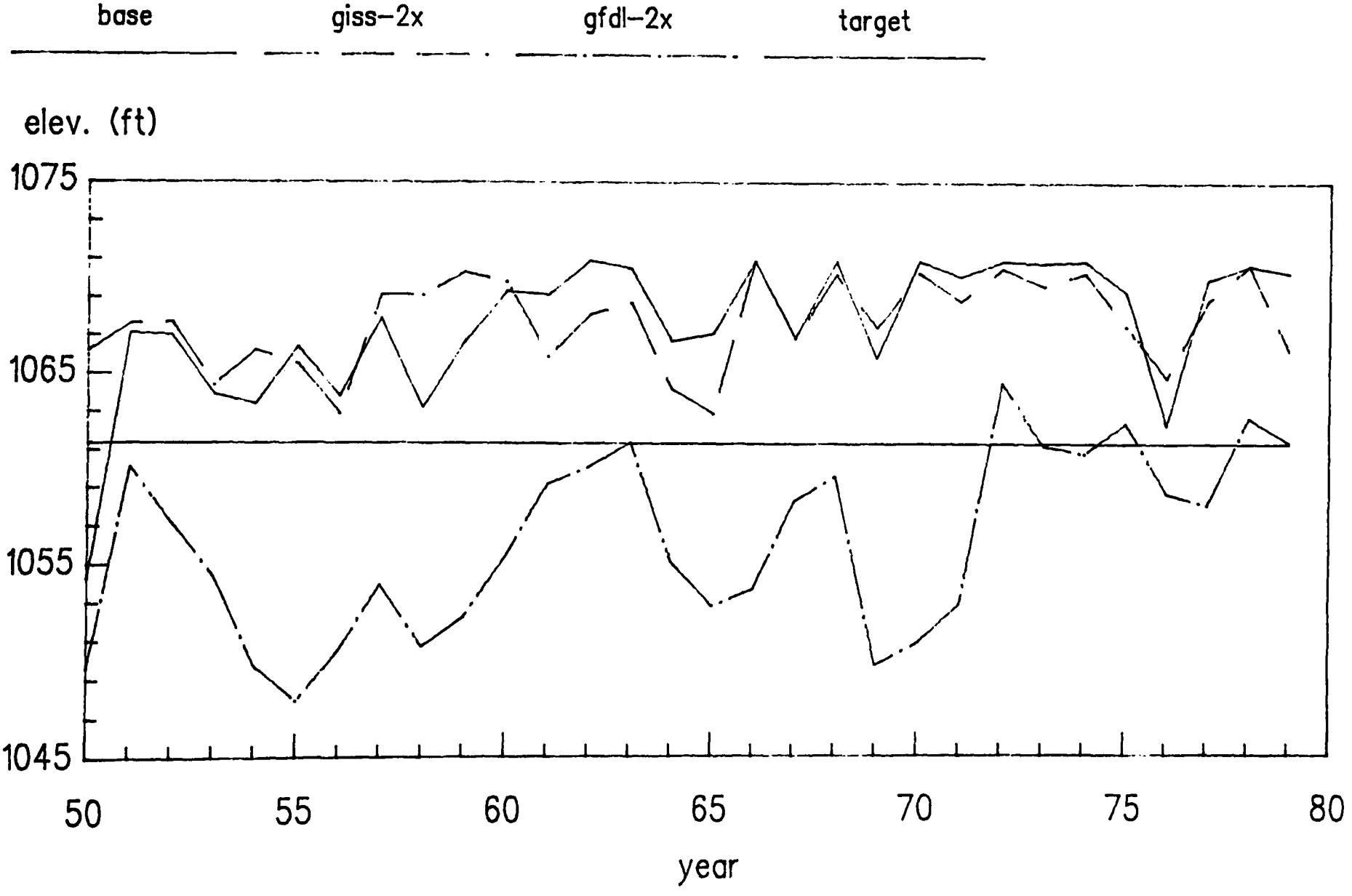

FIGURE 13

Outflow below Atlanta

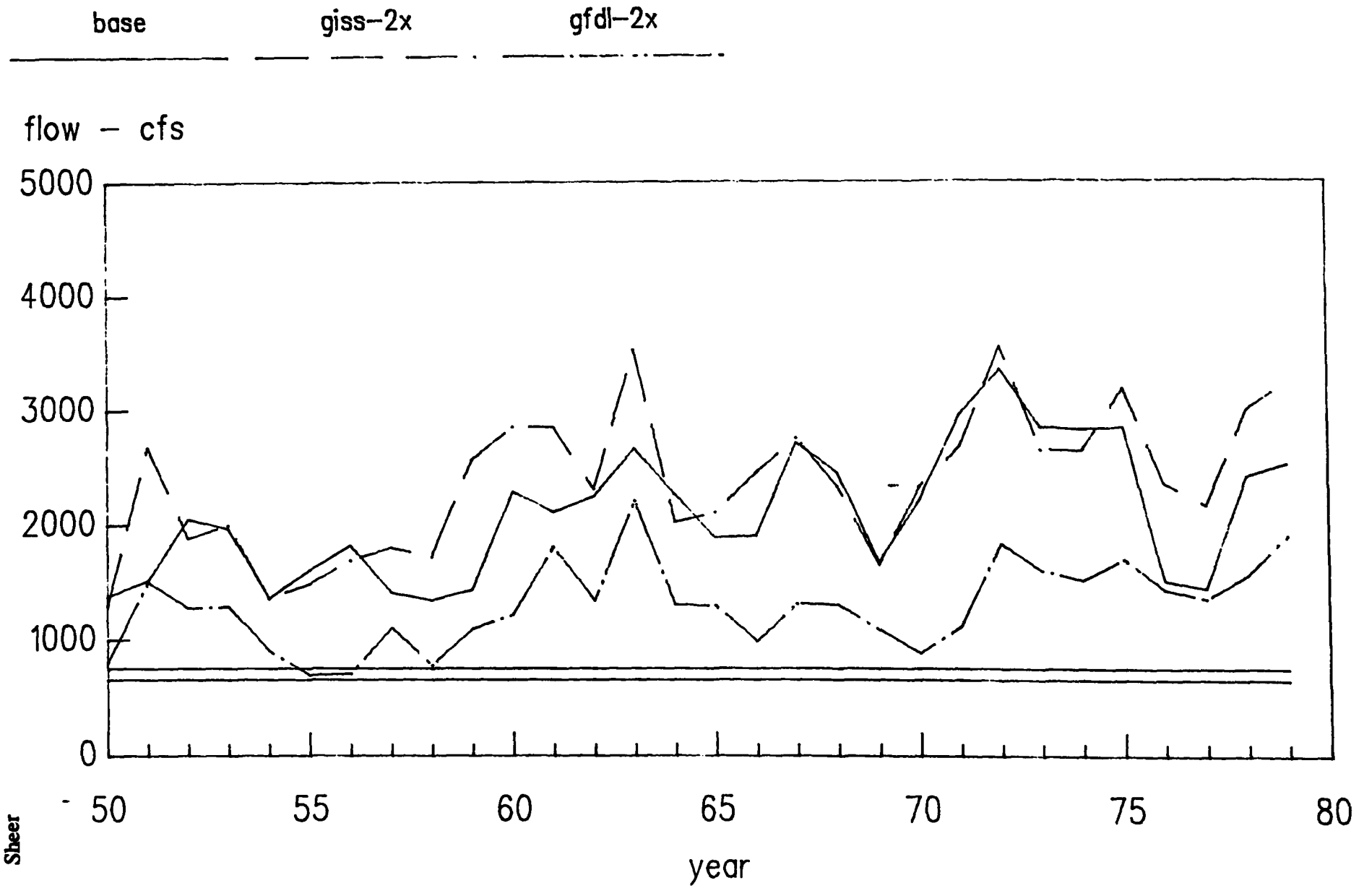

FIGURE 14
Lake Lanier Power Generation

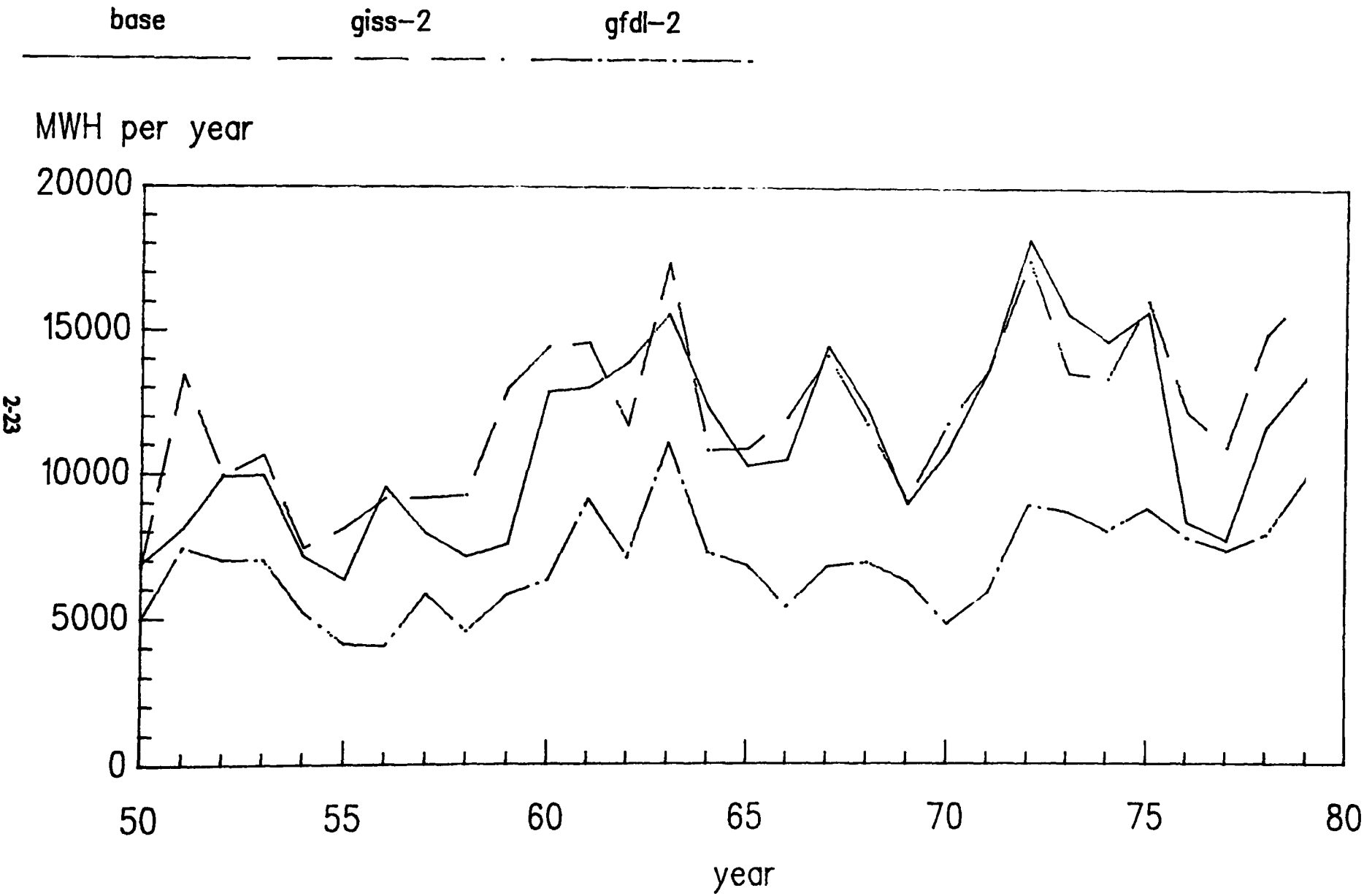

Sheer

FIGURE 15

Mean Annual Power Generation

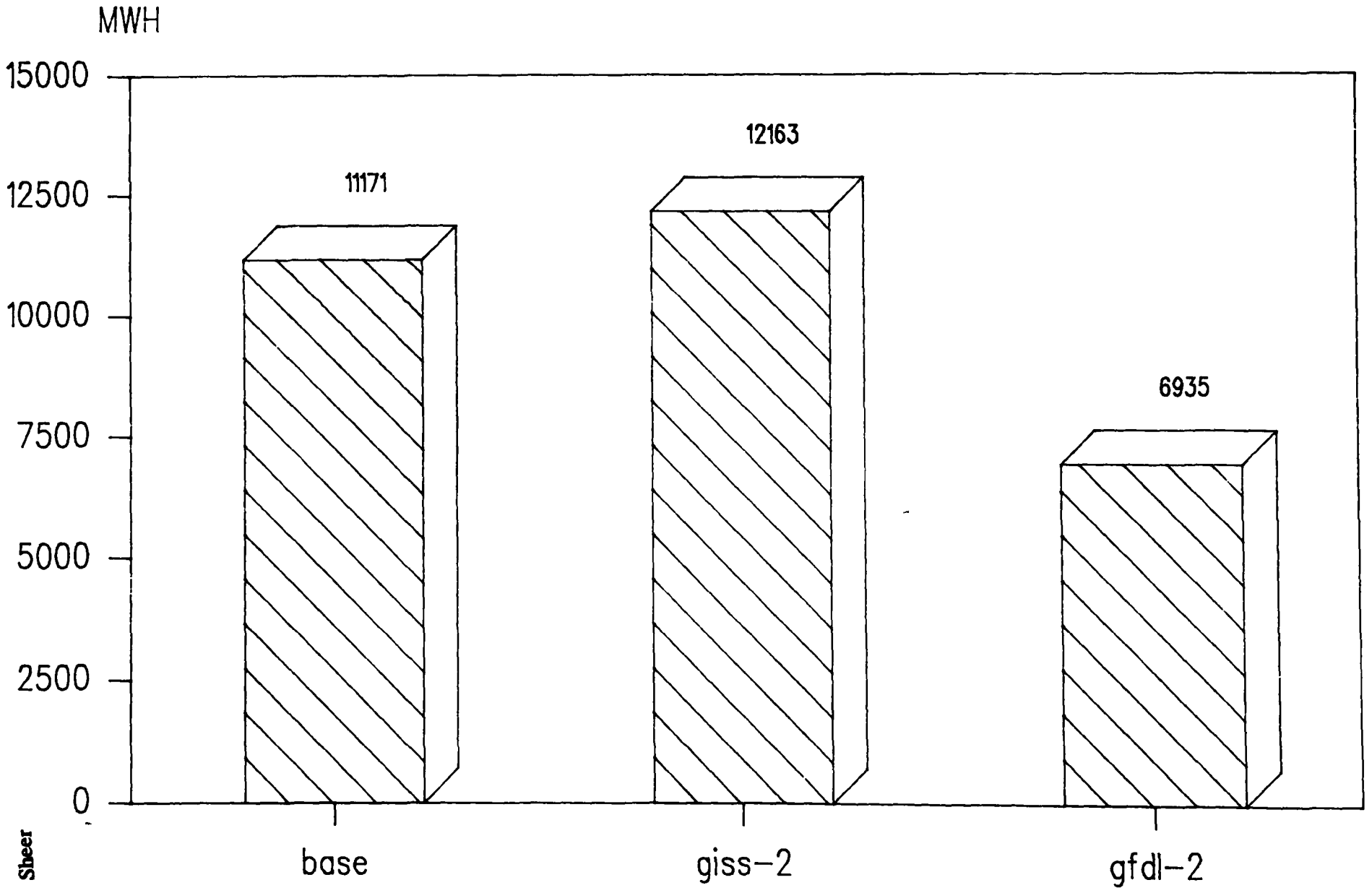

Sheer

Table 1. Comparison of Standard, Water Supply Reduction and Navigation Reduction Model Runs

	scenario	none	reduction water	navi-gation
mean annual energy (MWH)	Base	11200	11200	11200
	GISS-2	12200	12200	12200
	GFDL-2	6900	7300	7300
mean demand supplied (cfs)	Base	621	608	612
	GISS-2	621	620	620
	GFDL-2	621	379	449
# times delivery = 0	Base	0	8	0
	GISS-2	0	1	0
	GFDL-2	0	143	0
# times level < target	Base	21	16	16
	GISS-2	7	7	7
	GFDL-2	261	222	204
# times outf.< 750 cfs	Base	29	26	27
	GISS-2	43	42	42
	GFDL-2	117	10	60
# times outf.< 650 cfs	Base	0	0	0
	GISS-2	0	0	0
	GFDL-2	21	0	0

The second modified operating policy was done to see the effect of eliminating the navigation flow requirement, with the belief that there is little economic benefit in providing these releases. In this case, when the lake levels fall below the target levels, no navigation releases are made. Deliveries were handled as they were for the standard policy. The lake level graph of this policy is shown in Figure 17. Comparing this with Figure 14 again shows that this policy significantly increases lake levels.

SUMMARY

A hydrologic mass balance model was built to simulate the operation of Lake Lanier and the Chattahoochee River above Atlanta, Georgia, to address how a global climate change might affect the water supply of metropolitan Atlanta. Four climate change scenarios were routed through the model. Each scenario indicates a shift in seasonality of flows, with drier summers and wetter winters. Under the GISS $2xCO_2$ scenario, levels in Lake Lanier are similar to the base case, while GFDL $2xCO_2$ shows a definite decrease in levels.

FIGURE 16

Lake Lanier Elevation (September)

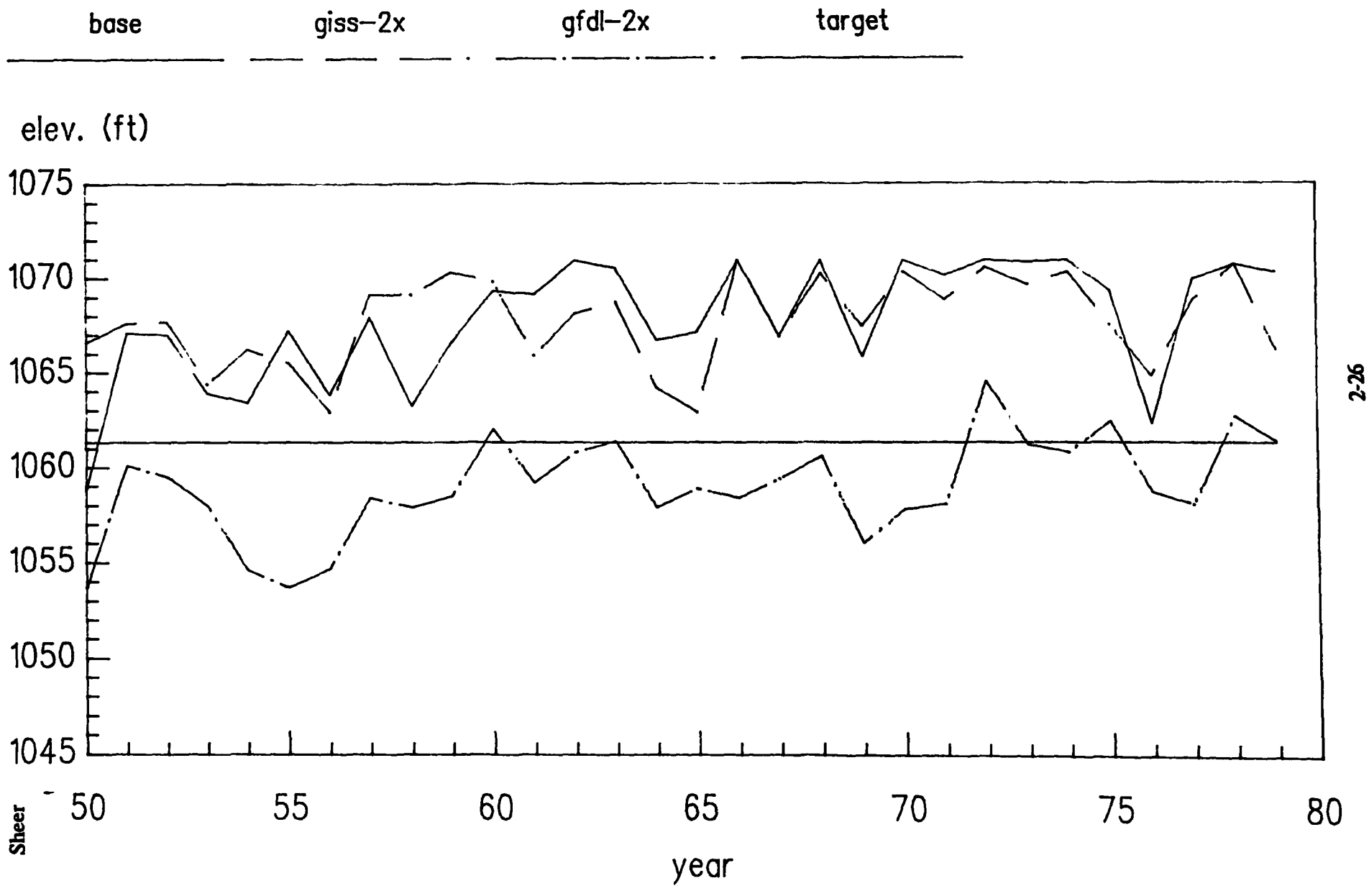

FIGURE 17

Lake Lanier Elevation (September)

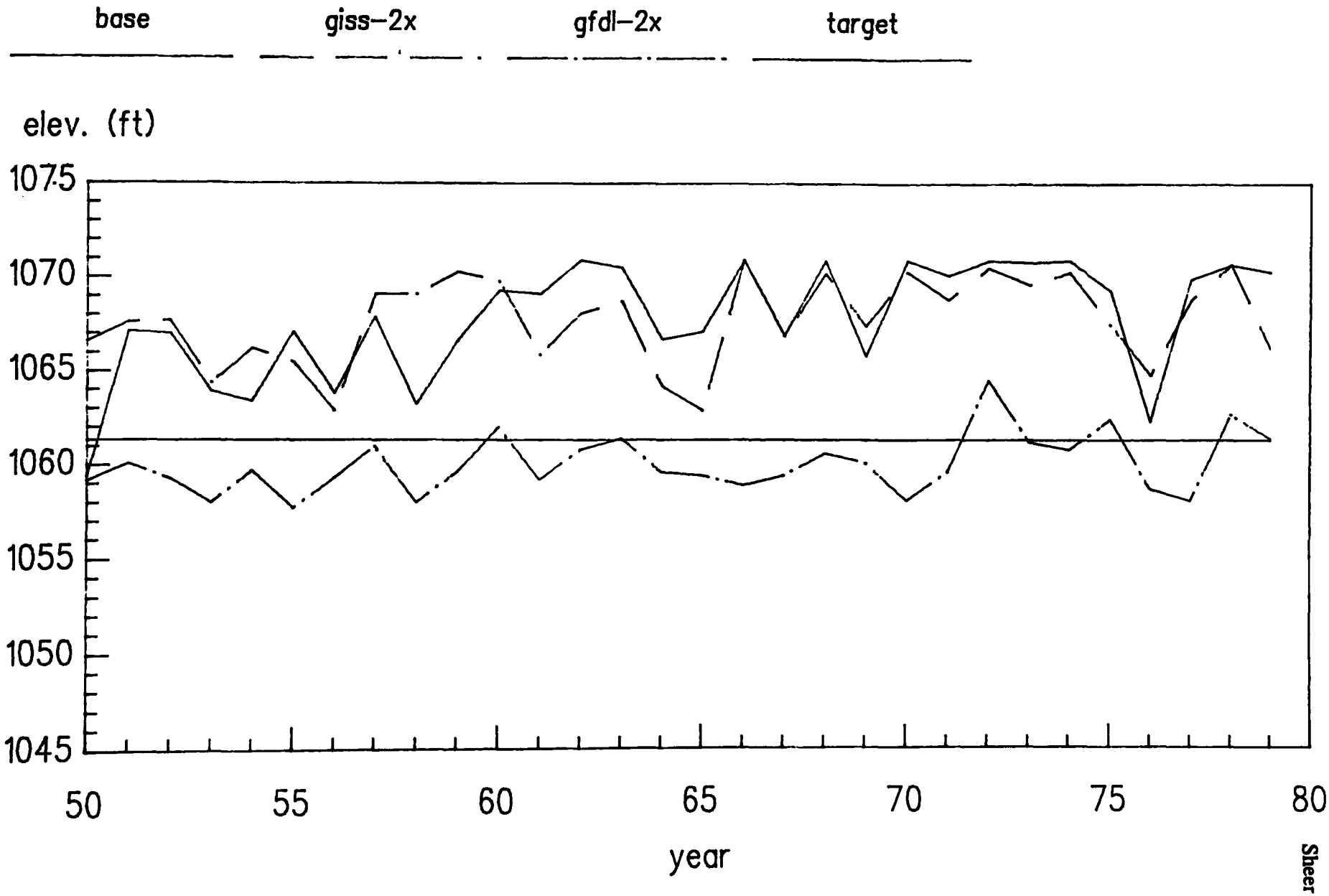

Sheer

REFERENCES

California Dept. of Water Resources, "California Central Valley Unimpaired Flow Data," Sacramento, CA, February 1987.

California Dept. of Water Resources, "Operations Criteria Applied in DWR Planning Simulation Model," Memorandum Report, Sacramento, CA, February 1986.

Sheer D.P., and M.L. Baeck, Documentation of the CVP/SWP Simulation Models developed by WRMI, Water Resources Management, Inc., Columbia, MD, September 1987.

THE IMPACTS OF CLIMATE CHANGE ON THE SALINITY OF SAN FRANCISCO BAY

by

Philip B. Williams
Philip Williams and Associates
Pier 35, The Embarcadero
San Francisco, CA 94133

Contract: University of Washington #503011

CONTENTS

Page

FINDINGS 3-1

CHAPTER 1: INTRODUCTION 3-3
STATEMENT OF PROBLEM 3-3
SAN FRANCISCO BAY MORPHOLOGY 3-3
SAN FRANCISCO BAY HYDRODYNAMICS 3-6
SAN FRANCISCO BAY HYDROLOGY 3-6

CHAPTER 2: METHODOLOGY 3-8
OVERALL APPROACH 3-8
SAN FRANCISCO BAY MORPHOMETRY 3-8
TIDAL EXCHANGE CHARACTERISTICS 3-9
SALINITY RESPONSE 3-9

CHAPTER 3: RESULTS AND INTERPRETATION 3-12
MORPHOMETRY 3-12
HYDRODYNAMICS 3-12
SALINITY 3-12
LIMITATIONS AND UNCERTAINTY 3-20

CHAPTER 4: POLICY IMPLICATIONS 3-28
THE FUTURE OF THE DELTA 3-28
THE ESTUARINE ECOSYSTEM 3-28
EXPORT OF WATER FROM THE DELTA 3-28
REDUCING THE RANGE OF UNCERTAINTY 3-28

REFERENCES 3-29

FINDINGS[1]

With future predicted climate change due to doubling of carbon dioxide levels, there would be major changes in the hydrology, morphology, tidal hydraulics, and salinity of the San Francisco Bay Estuary.

The major change in hydrology would be the alteration of freshwater inflow, primarily from the Sacramento River, which would affect estuarine circulation and salinity distribution.

Irrespective of hydrologic modifications, the San Francisco Bay Estuary would experience major changes in morphology, circulation, and salinity due to climate-induced accelerated sea-level rise.

For a sea-level rise of 1 meter (3.3 feet) associated with a doubled carbon dioxide level, the area and volume of the estuary would increase. The extent of the increase would depend on whether existing, often substandard, levees were strengthened and maintained. If they were not, and large areas were flooded, the area of the estuary could triple from approximately 1,100 to 3,500 square kilometers, and its volume double from 7 to 14 cubic kilometers. If all the existing levees were improved and maintained, the increase in area would be about 30% and volume 15%.

The exact amount of sea-level rise in the range of 1/2 to 2 meters is less important in determining the future physical characteristics of the estuary than whether or not levees are allowed to fail.

The most vulnerable part of the estuary to inundation by rising sea level is the Delta, an agricultural area whose fragile levees are susceptible to failure with the current sea level. Failure of the Delta levees in themselves would add about 1,500 square kilometers to the estuary and create a vast inland arm of the San Francisco Bay.

These morphological changes could greatly affect the movement of sediment in the Bay by capturing more sediment in the upper Bays and particularly the Delta. Secondary effects could include:

- Erosion of mudflats and salt marshes fringing the Bay, aggravating losses due to sea-level rise.
- Increased clarity of water, possibly increasing algal production.
- Increased wave energy within the Bay, causing erosion of levees.

The effects of morphologic changes could be counterbalanced by hydrologic changes. Higher winter flood flows could increase sediment delivery to the Bay.

The morphological changes would greatly alter the movement of water in the Bay. Such effects would include:

- Movement of the estuarine-induced circulation system upstream.
- Changes in tidal characteristics.
- Increased tidal current velocities.

---

[1]Although the information in this report has been funded wholly or partly by the U.S. Environmental Protection Agency under Contract #503011, it does not necessarily reflect the Agency's views, and no official endorsement should be inferred from it.

The change in hydrodynamics due to sea-level rise effects would greatly alter the salinity distribution in the estuary, causing a given average salinity level to migrate roughly 15 kilometers upstream.

Increased runoff predicted by climate models tends to partially compensate for the increase in average annual salinity caused by sea-level rise. The net result is for a given average annual salinity level to migrate up to 10 kilometers upstream.

All the climate models indicate significant average increases in salinity in the estuary in the spring and summer. Salinities formerly exceeded in 20% of years would be exceeded in about 50% of years.

Increases in salinity will greatly affect the transfer of water across the Delta for irrigation supply. In order to maintain the present low salinity levels of exports from the Delta, the amount of water released from reservoirs for salinity repulsion (carriage water) would have to be doubled and/or physical modifications made to Delta channels.

The following major policy decisions would be required to minimize economic, social, and environmental costs due to climate change:

- Determination of which low-lying areas surrounding the estuary would be protected and which abandoned.
- Identification of institutional and financial mechanisms to provide for protection of low-lying areas.
- Alteration of present water allocation and water management practices to incorporate sufficient freshwater inflow to the estuary to maintain a viable estuarine ecosystem.
- Alteration of water allocation and water management practices in order to optimize beneficial uses of water diversions from the Delta.

CHAPTER 1

INTRODUCTION

STATEMENT OF PROBLEM

San Francisco Bay is the largest estuary on the U.S. Pacific Coast. Its estuarine ecosystem is dependent on the amount and timing of freshwater inflows and the resulting salinity distribution throughout the Bay. The upper part of the estuary, the Sacramento-San Joaquin Delta, acts as a conduit for water supply transfers from the northern part of California to the arid San Joaquin Valley and Southern California. Consequently, salinity management in the estuary is vitally important to protecting the estuarine ecosystem and the quality of water exported for agriculture and urban water users.

Projected climate change due to the greenhouse effect will greatly alter the salinity distribution in the estuary. There are two primary impacts:

- The timing and amount of freshwater inflow will change.
- Sea-level rise will alter the tidal characteristics of the Bay, with dramatic changes taking place if levees protecting low-lying areas are allowed to fail.

This investigation is a reconnaissance-level study intended to provide an indication of the possible extent of these impacts. Because it was prepared in a short timeframe, and with a limited budget, simple analytic techniques were used. In addition, existing water management practices and physical facilities in place were assumed unchanged for all scenarios. It is anticipated that future studies will carry out more refined analysis to produce results that can be used for planning purposes.

SAN FRANCISCO BAY MORPHOLOGY

The San Francisco Bay Estuary was formed in the last 10,000 years as rising sea level inundated the lower valley of the Sacramento River. It has a complex morphology of interconnected bays separated by straits (see Figure 1). Hydrodynamically, the estuary is considered in two parts:

- The Northern Reach, consisting of the Central Bay, linked with San Pablo Bay by San Pablo Straits, connected to Suisun Bay by the Carquinez Straits, which in turn are linked with the tidally influenced Delta through the narrows downstream of Sherman Island. The rivers that drain the 153,000 sq. kilometers. Central Valley discharge into the Delta. The northern reach usually functions as a partially mixed to well-mixed estuary, except during very high river flows.
- South San Francisco Bay, which connects with the Central Bay through the narrows at Yerba Buena Island. Because this Bay receives little direct freshwater inflow, it usually acts as an estuarine-influenced lagoon with isohaline conditions reflecting salinity conditions in the Central Bay.

The morphology of San Francisco Bay has been greatly altered by man's activities. Almost all of the once extensive 2,200 sq. kilometers of tidal marshes have been converted primarily to agricultural land, but also to salt ponds, port development, military, and urban uses (see Figure 2). Most of the former tidal marsh area has subsided owing to compaction and in some areas owing to groundwater or natural gas extraction. Typically, 1 to 2 meters of subsidence has occurred, except in the Delta. In the central and western Delta, the freshwater tidal marshes created deep peat soils that are excellent for agriculture. However, when tilled, these soils oxidize and blow away, lowering the land elevation up to 80 mm (3 inches) per year. The Delta is now composed of

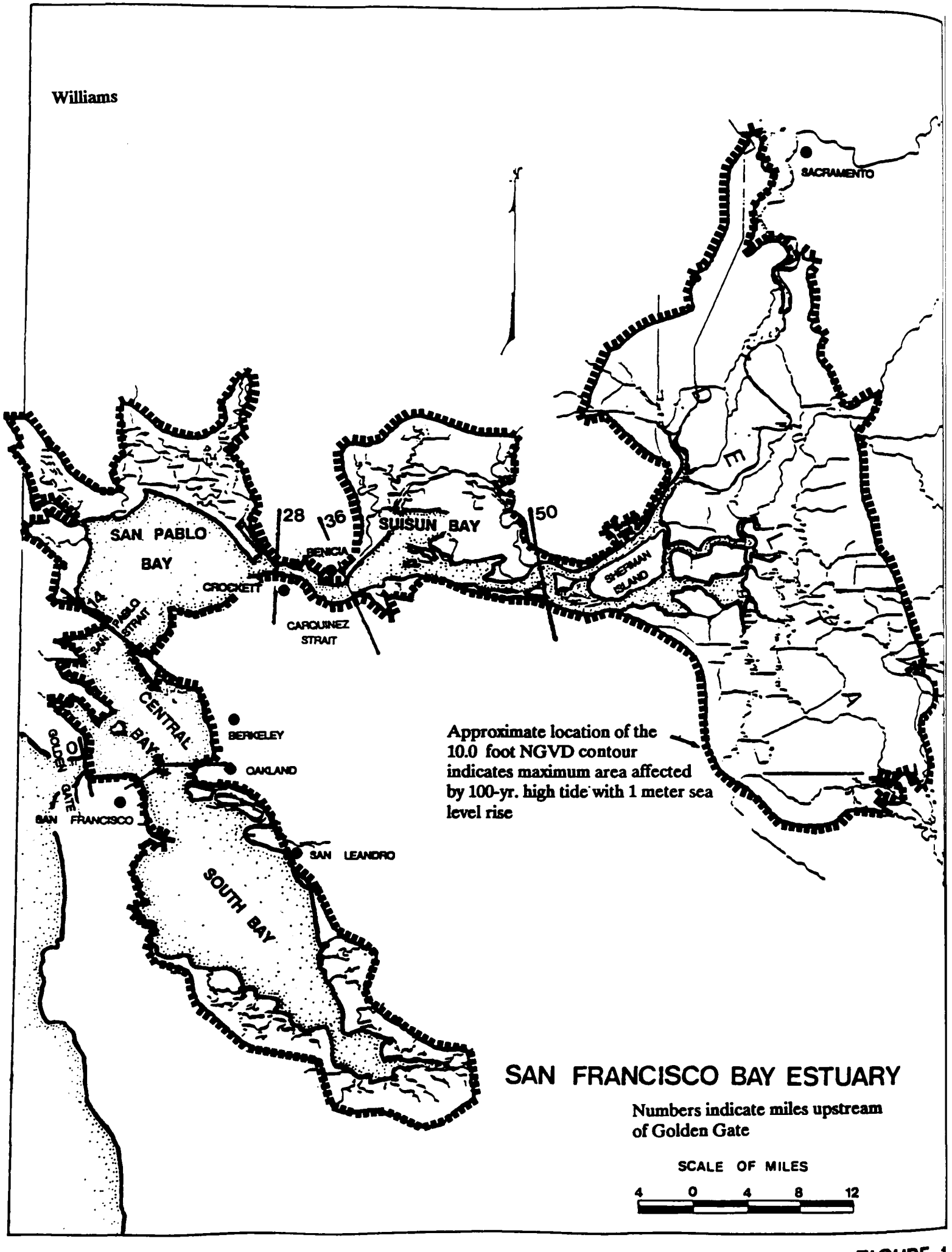
SACRAMENTO
SAN PABLO BAY
SUISUN BAY
28
36
50
14
BENICIA
CROCKETT
CARQUINEZ STRAIT
SAN PABLO STRAIT
SHERMAN ISLAND
CENTRAL BAY
BERKELEY
OAKLAND
GOLDEN GATE
SAN FRANCISCO
SAN LEANDRO
SOUTH BAY
Approximate location of the 10.0 foot NGVD contour indicates maximum area affected by 100-yr. high tide with 1 meter sea level rise
SAN FRANCISCO BAY ESTUARY
Numbers indicate miles upstream of Golden Gate
SCALE OF MILES
4 0 4 8 12

FIGURE 1

GENERALIZED AND APPROXIMATE HISTORIC CHANGES IN AEREAL DISTRIBUTION OF TIDAL MARSHES

Williams

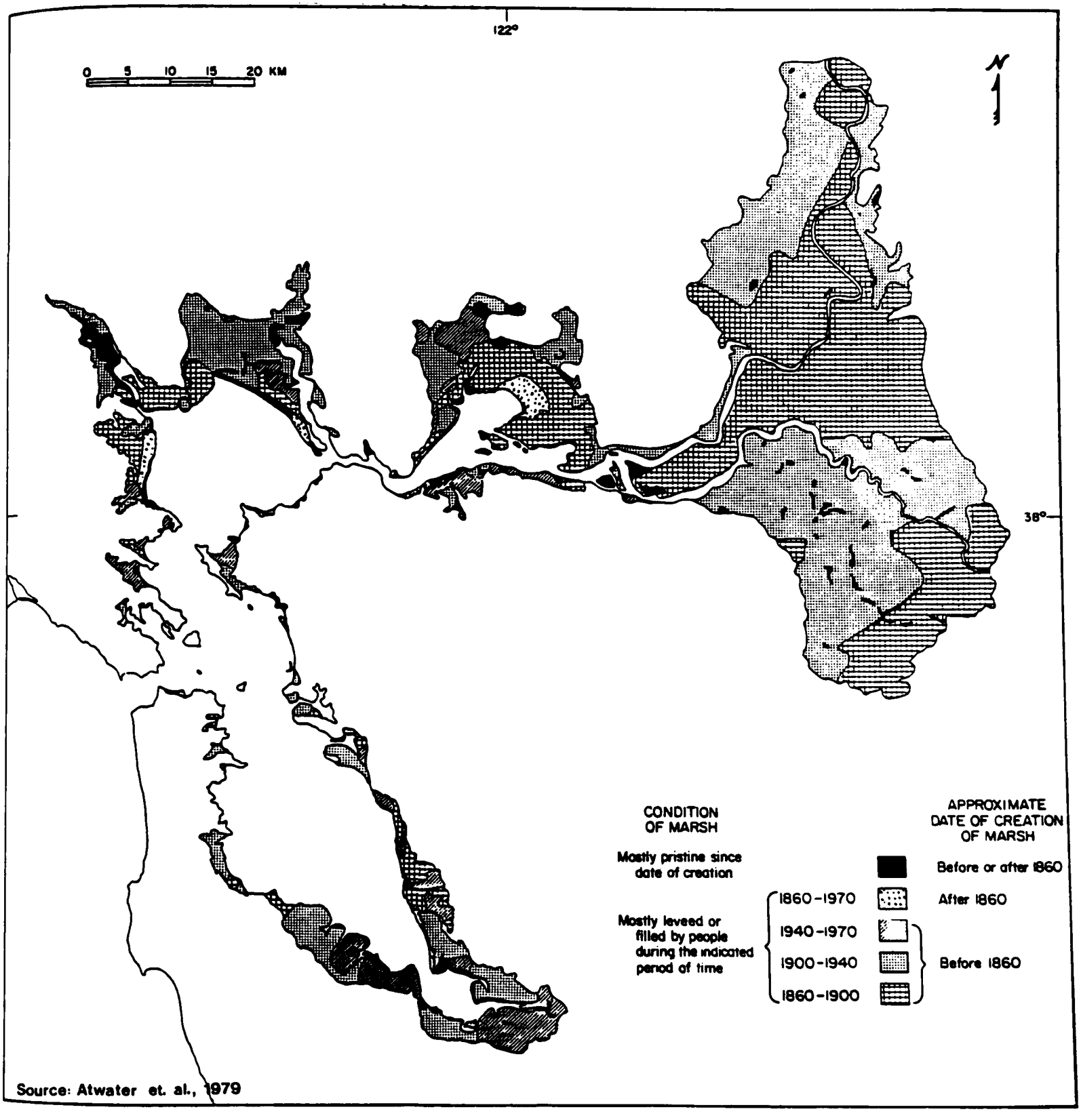

FIGURE 2

approximately 50 islands at elevations as low as 6 meters below mean sea level (NGVD)[2] (DWR, 1987). Many of these islands are separated by narrow tidal channels and are protected by fragile peat levees. Even with the existing sea level, levee failures are frequent and the islands are costly to maintain (Josselyn and Atwater, 1982). The typical 100-year high-tide flood elevation is approximately +2 meters NGVD in the Delta (DWR, 1987).

SAN FRANCISCO BAY HYDRODYNAMICS

The salinity distribution within San Francisco Bay is dictated by mixing processes governed by tidal ebbs and flows, wave action, and the freshwater flows entering the Delta. With its present configuration, the mixed semi-diurnal tides propagate up the northern reach from the Golden Gate as a progressive wave, with the tidal lag increasing and the tidal range decreasing inland to Sacramento. In the South Bay, the tides create an oscillating standing wave that tends to amplify the tidal range.

The freshwater inflow at the upstream end of the estuary creates an estuarine circulation cell upon which many estuarine species depend. During periods of high winter floods, a stratified circulation can be created with low surface salinity as far as the Golden Gate. As flows drop, the estuary rapidly mixes and at low and moderate flows becomes well to partially mixed.

During high-flow periods, lower-salinity water from the Central Bay stratifies the South Bay. This greatly reduces residence time of pollutants in the heavily urbanized South Bay and is also important in ecosystem productivity.

SAN FRANCISCO BAY HYDROLOGY

Most of the freshwater inflow to the estuary is contributed by the Sacramento River, with a lesser amount from the San Joaquin River. Except during high winter flood flows, inflows are controlled by releases from the extensive system of reservoirs upstream. Some of the inflow to the Delta is exported by the pumps of the State Water Project and Central Valley Project, some is used for irrigation on the Delta islands, and the remainder flows downstream into Suisun Bay. This amount of water is referred to as "Delta outflow." Because of the limited capacity of the Delta channels, during periods of high-export pumping some of the water that flows into the Delta from the Sacramento River flows back up the San Joaquin River. In order to prevent too much salt mixing with this flow (around Sherman Island at the western edge of the Delta), a sufficient amount of water has to be released from upstream reservoirs to ensure enough Delta outflow to repel salinity intrusion from Suisun Bay. This amount of Delta outflow is referred to as "carriage water" and is illustrated in Figure 3.

In addition to carriage water, Delta outflows are managed to maintain salinity standards for irrigation in the Western Delta, for fish migration, and to provide low-salinity water for waterfowl habitat in Suisun Marsh. These latter requirements are stated in Decision 1485 of the State Water Resources Control Board (SWRCB, 1978). However, much of the time carriage water requirements govern Delta outflow.

Much of the freshwater discharging to the estuary now occurs as winter runoff, and so salinity levels in different parts of the estuary can vary considerably throughout the year. The spring and summer freshwater flows and salinity are particularly important in maintaining the estuary productivity (Williams and Josselyn, 1987). Year-to-year flow variation is also high, and the cumulative effect of successive years of drought and consequently low runoff can greatly affect the estuary.

---

[2]NGVD means National Geodetic Vertical Datum, formerly referred to as "1929 mean sea level datum."

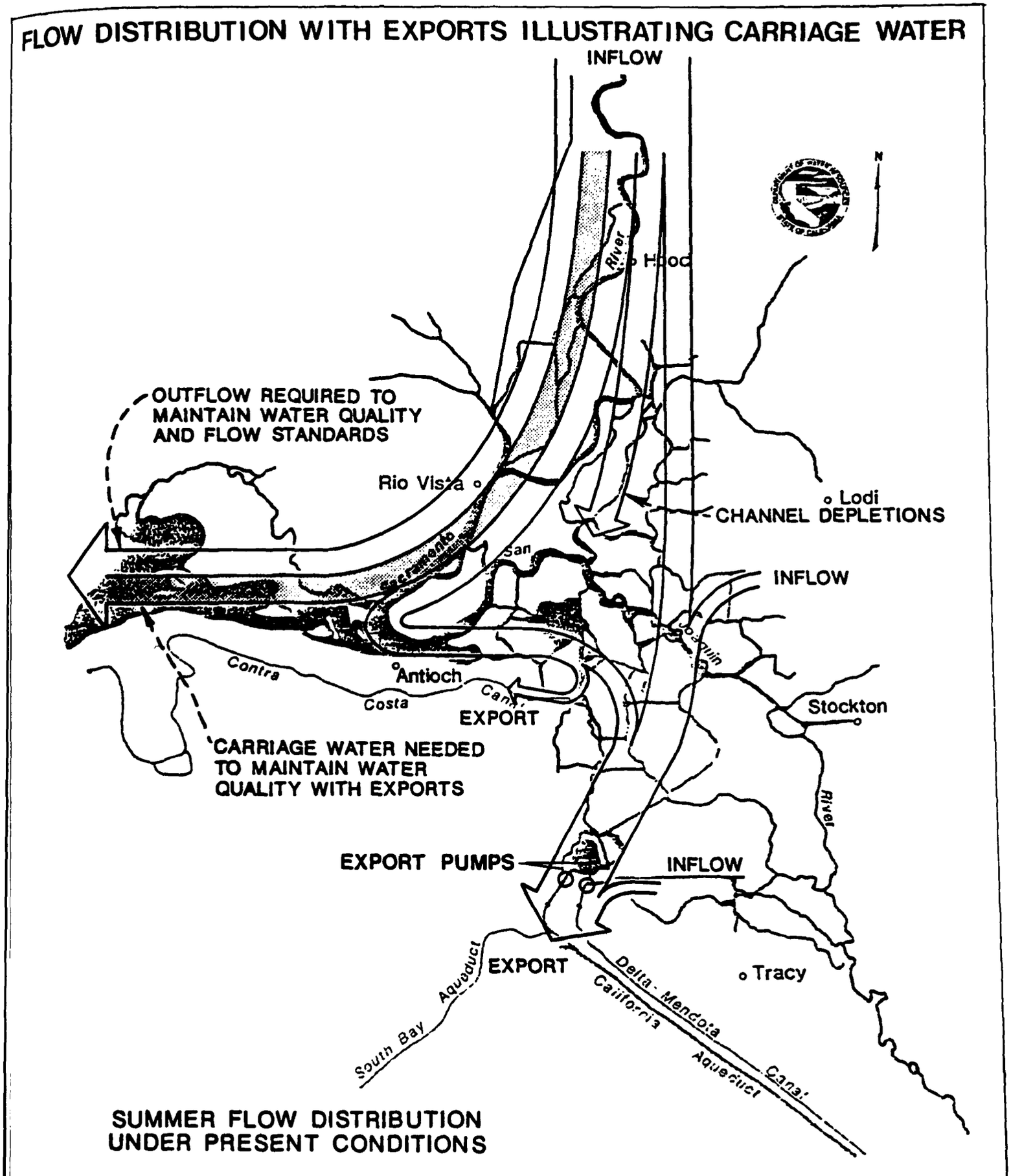

Source: DWR Exhibit 62 San Francisco Bay / Delta Hearing Process

FIGURE 3

CHAPTER 2

METHODOLOGY

OVERALL APPROACH

This study is being carried out as one component of an integrated series of studies on the effects of climate change in California. Lettenmaier et al. (Volume A) has simulated the runoff to the Central Valley for the precipitation and temperature regimes predicted by three different general circulation models run at double current carbon dioxide levels. Sheer (this volume) used these runoff predictions to simulate reservoir operation and irrigation deliveries in the Central Valley.

The main task of this study was to develop a simulation of the seasonal and annual salinities in different parts of San Francisco Bay for different future climate change and sea-level rise scenarios with the present water management system. A further study by Josselyn (Volume D) [Romberg Tiburon Center for Environmental Studies] used this analysis of salinity changes to analyze their effects on the estuarine ecosystem.

Three steps were required to simulate seasonal and annual salinities:

- Define the future morphometry (shape) of San Francisco Bay with sea-level rise.
- Determine the tidal exchange characteristics for San Francisco Bay for the future morphometry.
- Determine the salinity response of future tidal characteristics to future Delta outflow scenarios.

In addition, because carriage water requirements affect future Delta outflows, new carriage water requirements for future tidal characteristics were developed. With these new carriage water requirements, the monthly Delta outflows for three different doubled carbon dioxide climate change scenarios were modeled.

Two separate scenarios of the morphometry of the estuary were used to investigate the range of possible responses of the system. Both of these were for doubled carbon dioxide levels and assume a 1-meter rise in mean sea level.

The two scenarios are:

- 1-meter sea-level rise, no levee breaks.
- 1-meter sea-level rise with all levees failed.

A 1-meter rise was selected, as it is in the mid-range of predictions for the effect of doubled carbon dioxide levels on global sea level (National Research Council, 1987). All levees were assumed failed for the second scenario, as this is the "worst-case" condition for this analysis. Actually, it is likely that almost all levees protecting developed areas would be strengthened. However, this would only protect less than 10% of the total area.

SAN FRANCISCO BAY MORPHOMETRY

Unfortunately, no accurate analysis has been carried out of the morphometry of San Francisco Bay. Therefore, for the purposes of this study, a separate analysis of the elevation/area and elevation/volume relationships had to be carried out for all areas below +3 meters (+10.0 ft.) NGVD. This elevation was selected as it would represent the approximate elevation of the 100-year high tide after 1 meter of sea-level rise. USGS

topographic maps and NOAA bathymetric charts were used to develop the morphometric relationships for each segment of the estuary shown in Figure 1. These maps varied in age from the 1930s to 1970s and consequently may slightly underestimate areas and volumes in locations where rapid subsidence is taking place.

Using existing morphometry for future sea-level rise conditions necessarily ignores the effect of geomorphic response to sea-level rise. This would probably occur as sedimentation in the Delta and in shallower areas around the Bay, and as scouring of the deeper channels in response to increased tidal action. These variables have not been investigated.

TIDAL EXCHANGE CHARACTERISTICS

The changes in estuarine morphometry with an increase in sea level have a significant effect on tidal circulation, which in turn is a major determinant of salinity distribution.

Fischer's one-dimensional finite element tidal hydrodynamic model (Fischer, 1970) was used to simulate the tidal exchange characteristics at various points in the estuary. The estuary was represented by a nine-segment model that simulated existing morphometry and was calibrated to simulate the existing tidal range, using channel roughness as the calibration variable. The calibrated values are shown for existing conditions in Table 1 and are within approximately 0.1 meter of the predicted tidal range.

The model calculates the average ebb and flood tide flow rates at each of the straits separating the different segments of the Bay shown in Figure 1. The model was then run for the two sea-level rise scenarios using the future morphometry of the Bay.

SALINITY RESPONSE

In order to simulate the response of salinity in the estuary to different Delta outflows for future conditions, the mixing model developed by Denton (Denton and Hunt, 1986) was used.

As the model was originally formulated, the estuary was simulated as four interconnected bays separated from each other by three straits, and separated from the ocean by the straits of the Golden Gate (see Figure 4a). The model calculates the exchange of water for each bay for each tidal cycle, taking into account the volume of freshwater entering the estuary. At the end of each tidal cycle, it is assumed that each Bay is completely mixed uniformly. Because much of the water entering a bay on the flood tide leaves it on the ebb, only a portion of the water volume is exchanged in a tidal cycle from one bay to another as "new water" (Figure 4b). The "new water" ratio (explained on Figure 4b) is used as a calibration coefficient for each strait. Calibrating this simple model in this way is convenient and allows for reproducible results. The effect of many other complex mixing processes is lumped together in the calibration coefficient.

Denton's model was run for steady-state (constant freshwater outflow) conditions for the two sea-level rise scenarios, as well as a scenario with levee failure at existing sea level. The steady-state condition is a theoretical calculation of salinity that would seldom actually occur because of the large seasonal change in runoff, but is useful for systematically analyzing sea-level rise effects. For each of these runs, the volumes and tidal exchanges of each bay obtained from Fischer's model were changed to account for sea-level rise and levee failure. New water ratios were kept constant.

The change in salinity in Suisun Bay for nine different steady-state Delta outflows was determined using the model. From this, new carriage and D1485 water requirements for the sea-level rise scenarios were estimated. This was done by analyzing the additional flow required to maintain the same salinity as occurs in the existing condition immediately downstream of the Delta in Suisun Bay.

DIAGRAMS ILLUSTRATING DENTON'S MIXING MODEL

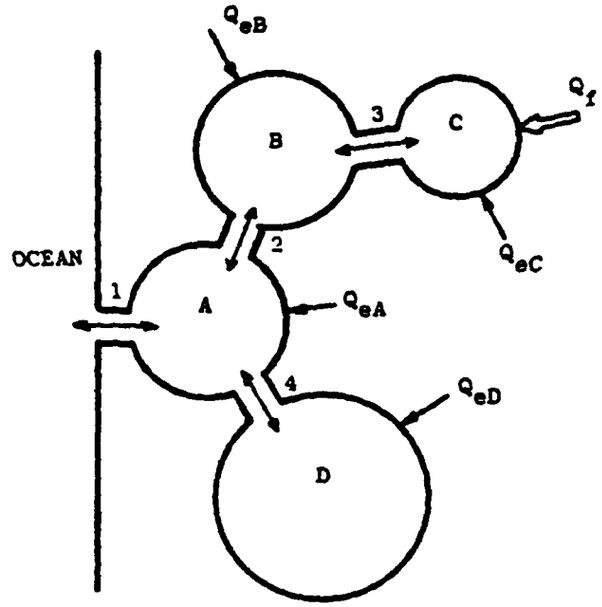

4a Sketch showing the system of four interconnected bays used to model flushing in San Francisco Bay. The main flushing mechanisms are the exchange of "new" water through the four connecting straits and the net through flow resulting from the Delta outflow Q_f. Pollutant discharges to each of the bays are also included.

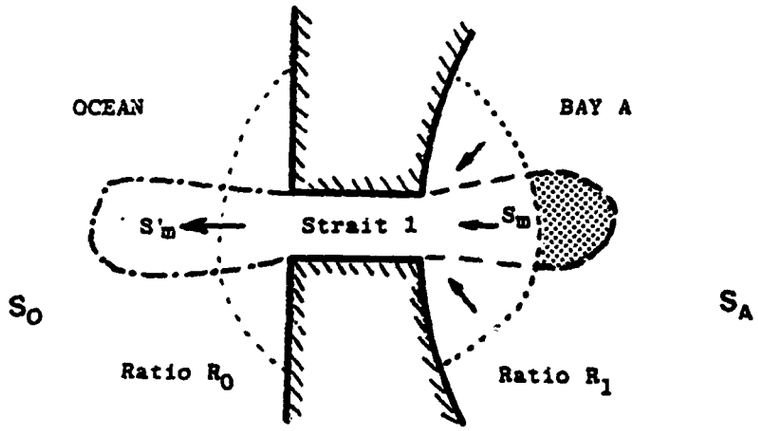

4b Definition sketch of the tidal exchange through strait 1 during the ebb tide. Strait 1 connects bay A (Central Bay) with the ocean. The water passing through the strait on the flood tide has a salinity S_m. A portion of this water ($Vol_{new}/Vol_{flood} = R_0$) is "new" water from the ocean that has not previously been in the bay. Similarly, a portion (R_1) of the water exiting the bay through strait 1 during the following ebb is "new" water from bay A. The shaded area shows the water from the flood tide that remains in bay A at the end of the tidal cycle. The average salinity S'_m of the ebb flow results from the mixture of the new water from bay A and the water from the previous flood tide.

Source: Denton and Hunt, UCB/HEL-86/01, 1986

FIGURE 4a-b

Using the new carriage water requirement in its reservoir operation simulation, Sheer (Volume A) simulated the monthly Delta outflow for the three climate change scenarios for the base period 1951 to 1980. The three scenarios were developed from the following General Circulation Models (GCMs):

- Geophysical Fluid Dynamics Laboratory (GFDL)
- Goddard Institute of Space Science (GISS)
- Oregon State University (OSU)

All of these scenarios have greater annual freshwater inflow to the estuary than occurs at present. In addition, all have a significant seasonal shift in runoff from the spring to the winter.

Denton's model was run again using the simulated monthly Delta outflows as input. The output included average monthly and average annual salinities in different bays within the estuary under the different scenarios.

CHAPTER 3

RESULTS AND INTERPRETATION

MORPHOMETRY

The elevation/area and elevation/volume relationships for the whole estuary, with and without complete levee failure, are shown in Figures 5 and 6 and summarized in Table 2. They illustrate the dramatic effect that failure of perimeter levees would have on increasing the area and volume of the estuary. As is shown in Table 2, most of this increase would occur from failure of Delta island levees. These levees are the most fragile and poorly maintained, and are susceptible to failure even at the existing sea level. The exact amount of future sea-level rise -- 0.5 meter, 1 meter, or 2 meters -- is less important to the physical characteristics of San Francisco Bay than whether or not the Delta levees are preserved.

The morphometric plots (Figures 5 and 6) illustrate that without levee failure there would be a net loss of intertidal area, including mudflats and salt marsh. This effect could be aggravated by changes in sediment transport mechanisms within the estuary. For example, possible reduced sediment concentrations entering San Pablo Bay could allow for increased wave erosion of mudflats and salt marsh. In addition, the deeper water could increase wave energy, leading to further reduction of intertidal areas by wave erosion.

The curves shown in Figures 5 and 6 include the probable effect of morphological responses to rise in sea level. Such responses would include siltation in protected areas (such as inundated Delta islands) and scouring of deeper tidal channels in response to higher tidal velocities.

HYDRODYNAMICS

The tidal transport or average tidal velocity increases dramatically with increasing sea level (Table 1). If levees are maintained, the deeper water tends to make the tidal channel hydraulically more efficient, and this tends to compensate for the increased energy losses due to the larger velocities. The net result of maintaining the levees is that tidal ranges do not appear to change dramatically from the existing condition and may even be amplified in the South Bay.

If all levees fail, the increase in tidal prism (the volume of water between high and low tides) in the Delta increases the velocities and energy losses in downstream constrictions in Carquinez Strait and Chipps Island and greatly reduce the tidal range. This reduction in tidal range largely compensates for the increased tidal volume. However, it is important to note that this analysis assumes rigid boundary channels. In fact, there would be a considerable erosion in response to the increased tidal velocities in the lower part of the Delta, causing deepening and widening of channels. These changes could substantially affect the tidal hydrodynamics and allow for an increased tidal transport in the future.

SALINITY

The steady-state salinity analysis for the two sea-level rise scenarios is summarized in Table 3. The change in steady-state salinity in Suisun Bay is shown in Figure 7. The changes in salinity throughout the northern reach of the estuary for a fixed Delta outflow of 110 m^3/sec. (4,000 cfs) is shown in Figure 8. For the 110 m^3 sec. flow, there is a landward migration of given salinity levels of about 15 kilometers (Figure 8). For Suisun Bay, it can be seen that approximately double the Delta outflow is required to maintain the same salinity as present-day conditions. Consequently, the carriage water requirement to maintain low-salinity water for export would be approximately doubled.

SAN FRANCISCO BAY ESTUARY
STAGE/AREA

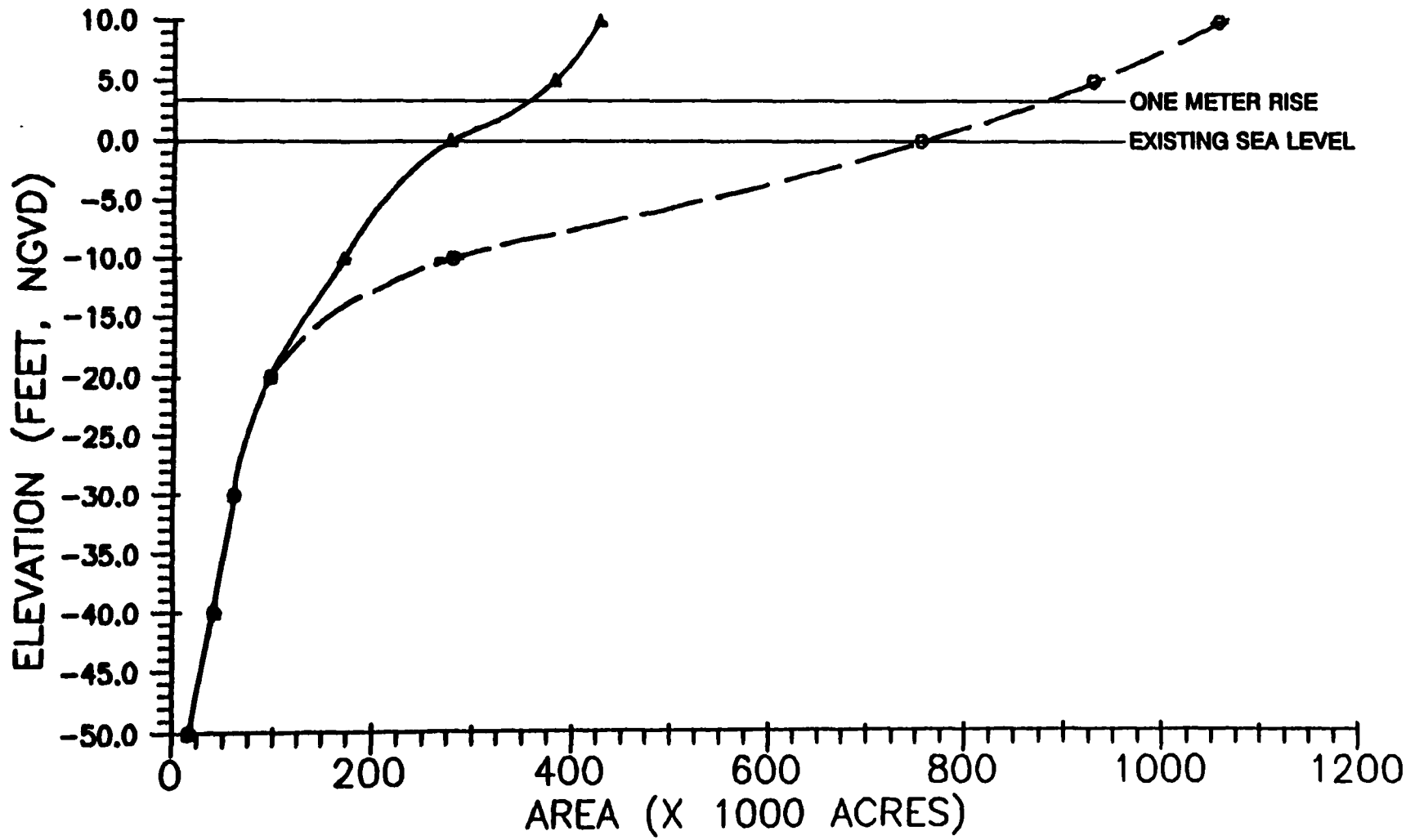

Williams

DATE: 3/18/88	EXISTING CONDITIONS COMPLETE LEVEE FAILURE	Philip Williams & Associates Pier 35, The Embarcadero San Francisco, California 94133	5

SAN FRANCISCO BAY ESTUARY
STAGE/VOLUME

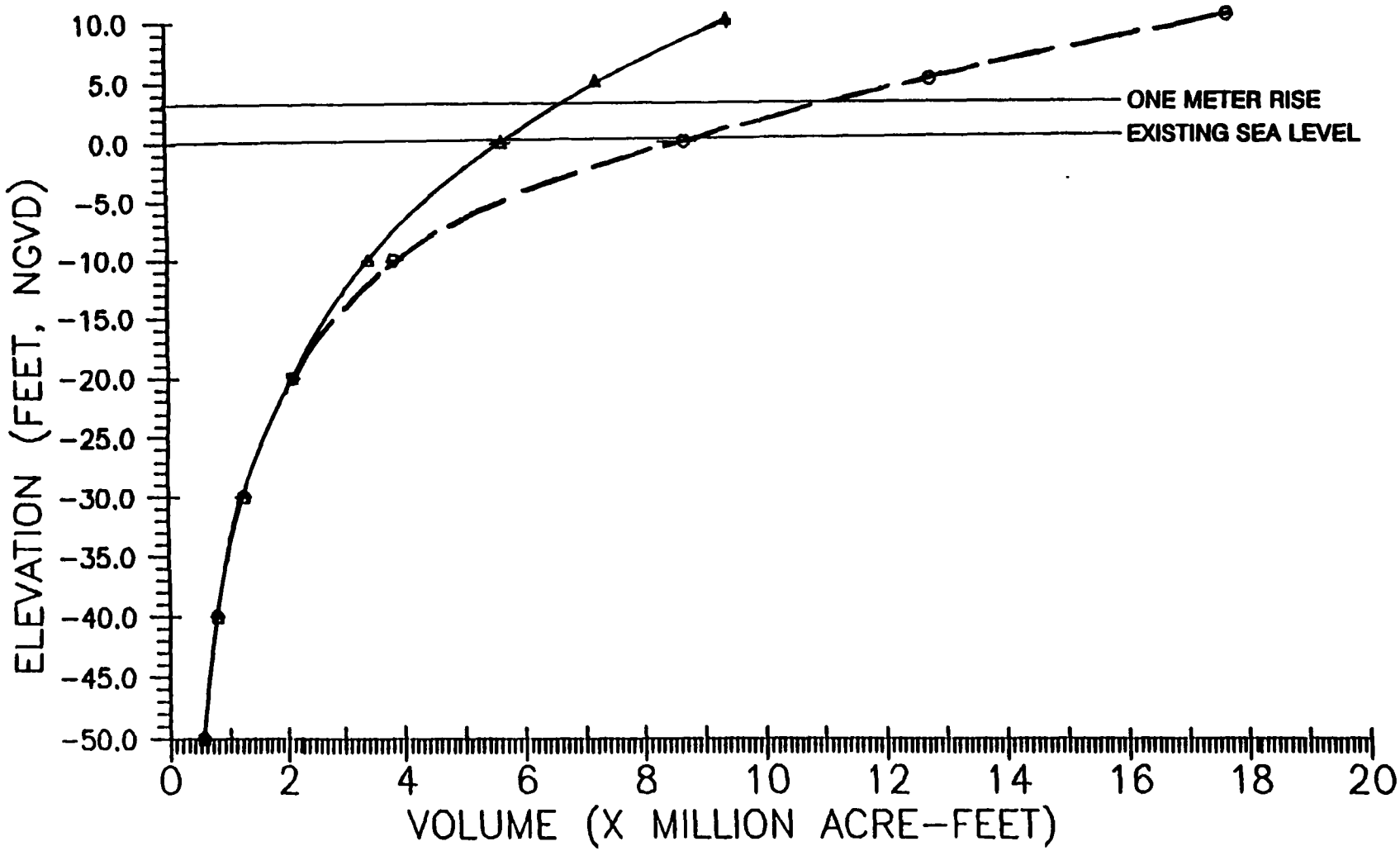

3-14

DATE: 3/02/88	EXISTING CONDITIONS COMPLETE LEVEE FAILURE	Philip Williams & Associates Pier 35, The Embarcadero San Francisco, California 94133	6

Williams

TABLE 1

CHANGE IN TIDAL CHARACTERISTICS
WITH 1 METER SEA LEVEL RISE

	Diurnal Tidal Range (m)			Avg. Tidal Transport[1] $m^3/sec \times 10^3$		
Location	Existing	No Levee Break	All Levees Failed	Existing	No Levee Break	All Levees Failed
Golden Gate	1.73	1.73	1.73	34.0	53.8	51.0
Pt. San Pablo	1.68	1.62	1.46	9.3	17.3	17.3
Benicia	1.66	1.57	1.25	4.0	6.8	7.1
Collinsville	1.40	1.21	0.30	2.3	3.4	6.2
Bay Bridge	1.84	1.87	1.59	17.6	28.3	28.3

Note:

[1] Average of ebb and flood tide flow rates

TABLE 2

CHANGES IN SAN FRANCISCO BAY AREA AND VOLUME
WITH SEA LEVEL RISE OF 1 METER

	Area km^2			Volume ($m^3 \times 10^6$)		
Location	Existing[1]	Levees[2] Intact	All[2] Levees Failed	Existing[1]	Levees[2] Intact	All[2] Levees Failed
Central Bay	206	218	218	2,368	2,529	2,529
San Pablo Bay	210	352	558	900	1,209	1,665
Carquinez Straits	15	16	16	185	202	202
Suisun Bay	85	186	384	401	506	913
Delta	166	170	1,619	839	1,011	5,242
South Bay	437	498	741	2,319	2,775	3,281
Total Bay:	1,119	1,440	3,536	7,012	8,232	13,832

Notes:

[1] Area and volume at 0.0 meter NGVD.

[2] Area and volume at 1.0 meter NGVD.

TABLE 3

SUMMARY OF STEADY-STATE SALINITIES

Location	Salinity (ppt) for Steady-State Delta Outflows								
	1,500 cfs ($40m^3/s$)			4,000 cfs ($110m^3/s$)			20,000 cfs ($560m^3/s$)		
	Exist. Sea Level	1m Sea Level Rise		Exist. Sea Level	1m Sea Level Rise		Exist. Sea Level	1m Sea Level Rise	
		No Levee Fail.	With Levee Fail.		No Levee Fail.	With Levee Fail.		No Levee Fail.	With Levee Fail.
Central	32	32	32	30	31	31	24	26	26
San Pablo	30	31	31	27	29	29	14	20	19
Carquinez	27	29	29	20	25	25	5	10	10
Suisun	24	27	27	15	21	21	2	5	6
Delta[1]	18	22	(24)[2]	8	13	(15)[2]	0.2	1.0	(1.7)[2]
South	32	32	32	30	32	32	24	26	26

Notes

1. Delta is calibrated for Western Delta salinity (see Appendix A).

2. These Delta salinity values have little meaning because of changes in channel morphology with levee failure.

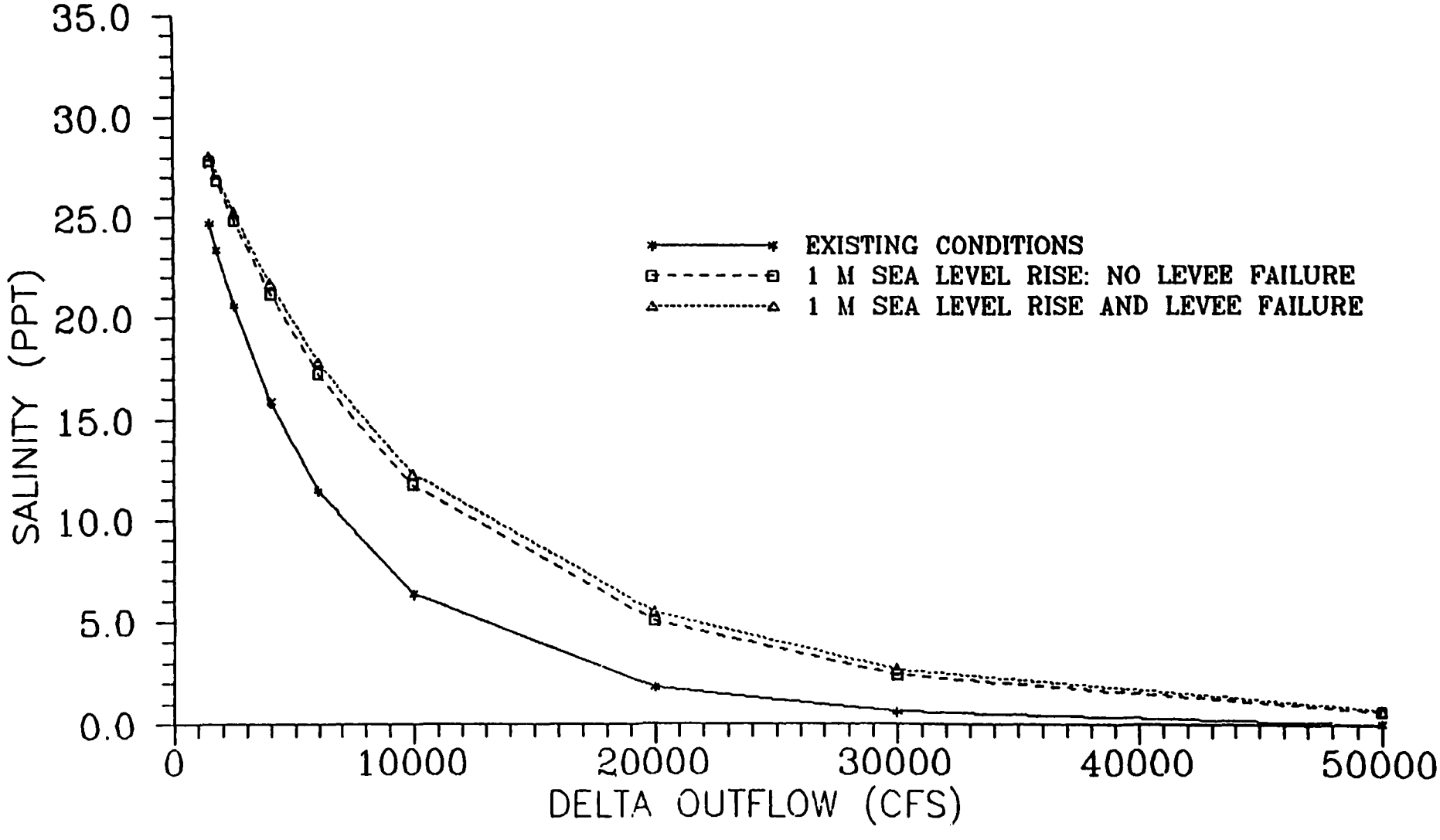

DATE: 04/26/88 BY: L. FISHBAIN		Philip Williams Associates Pier 35, The Embarcadero San Francisco, California 94133	7

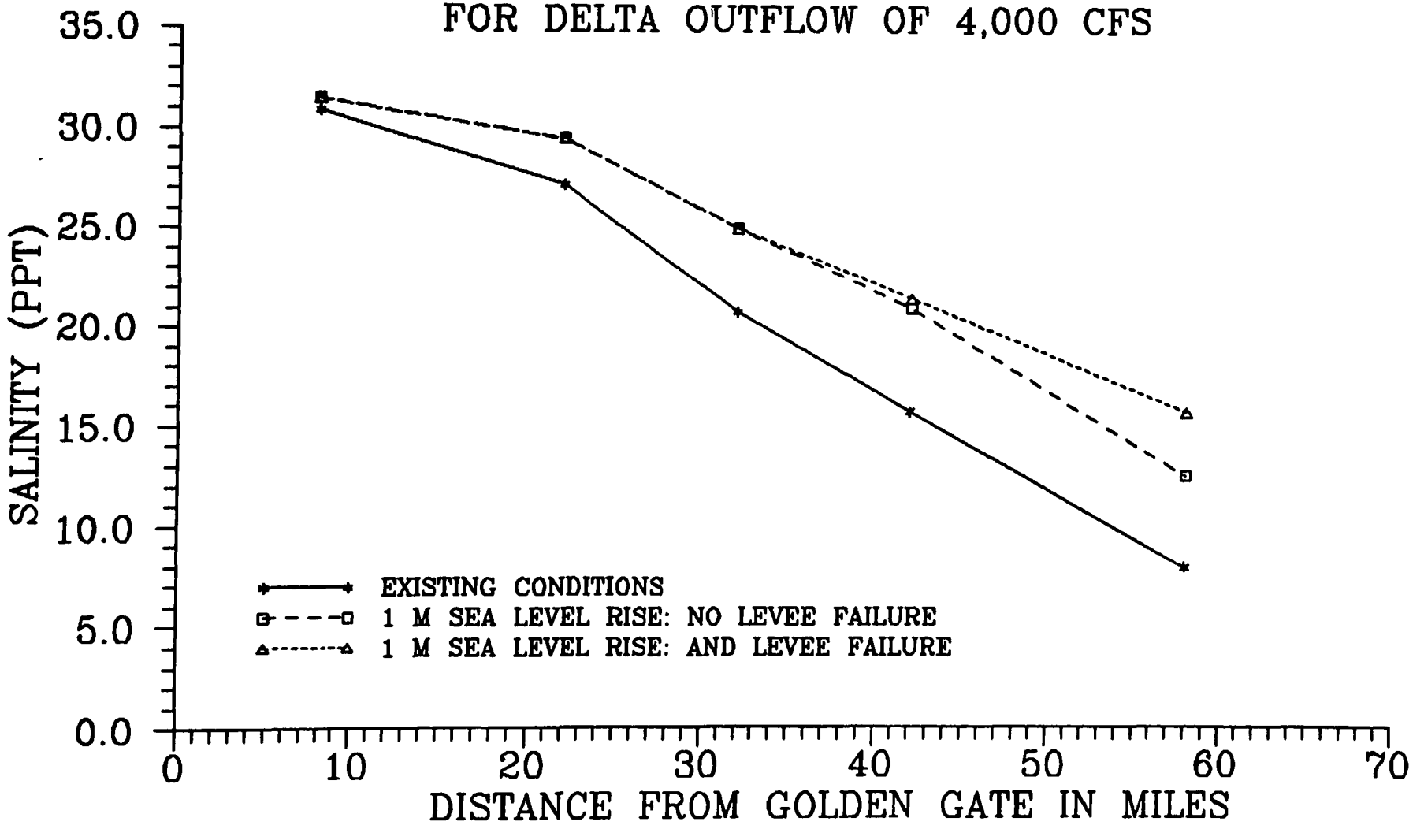

DATE: 03/20/88

BY: L. FISHBAIN

Philip Williams & Associates
Pier 35, The Embarcadero
San Francisco, California 94133

8

Williams

The modeling analysis carried out indicates that there would be little difference in the salinity regimes with sea-level rise, with or without levee failure. However, the steady-state levee failure scenario may underestimate salinity, as it does not incorporate the probable scouring of tidal channels that could allow a greater migration of salinity inland.

The steady-state analysis indicates the salinity changes due solely to sea-level rise effects. The monthly simulations of the climate change scenarios incorporate the combined effects of altered hydrology and sea-level rise as well as the seasonal changes in runoff obtained from Sheer (this volume).

The monthly simulation scenarios that were analyzed and their results are summarized in Table 4. Figure 9 shows the average annual salinity in the northern reach of the estuary for the three different hydrology scenarios. The comparatively low freshwater runoff of the OSU scenario causes the greatest increase in salinity over existing conditions. Comparison of Figure 9 with the steady-state results shown in Figure 8 indicate that the higher runoff for all three climate-change scenarios partially compensates for the sea-level rise effects. The combined hydrologic and sea-level rise effect of climate change results in a net inland migration of the average annual salinity of up to about 10 kilometers (6 miles). This shift in salinity is approximately the same magnitude as that which has already occurred due to upstream water development in the last century (Williams and Fishbain, 1987).

A closer examination of the effect on salinity of levee failure illustrates the buffering effect of the greatly increased volume of the estuary due to sea-level rise effects. The average monthly salinity in Suisun Bay with and without levee failure for the GISS hydrology scenario is shown in Figure 10. The seasonal fluctuation in average monthly salinity is 3 to 4 ppt less for the levee failure scenario (run 6) than without levee failure (run 5), even though the average annual salinity is approximately the same.

The average monthly salinity variation in Suisun Bay for the three hydrology scenarios is shown in Figure 11. In all cases, the average spring and summer salinities are higher, due to the combined effects of sea-level rise and reduced runoff. Only in the winter is the greatly increased runoff of the GISS scenario sufficient to compensate for the effect of sea-level rise.

Figures 12 and 13 illustrate the changes in frequency of a particular value in March and June in Suisun Bay. While the salinity distribution resulting from the GISS scenario shows little change from existing conditions in March, the lower runoff of the OSU scenario indicates a significant shift, with salinities that were formerly exceeded in 20% of years now occurring 50% of the time. In June, there is a significant change in frequency for both scenarios, with salinities that were formerly exceeded in 50% of years now occurring in 80% of years.

LIMITATIONS AND UNCERTAINTY

This study was a reconnaissance-level analysis carried out in a short time frame with limited resources. There are substantial limitations and uncertainties in the analysis. These are:

- Morphometric analysis. Systematic up-to-date detailed surveys could indicate errors of up to plus or minus 20% in the bays' volume.

- Sea-level rise analysis. There is a range of uncertainty in predictions of sea-level rise after doubling of CO_2, varying from 0.5 to about 2 meters.

- Geomorphic response. Siltation and erosion of estuarine sediments caused by changing tidal characteristics would alter the morphometry of the estuary and its tidal hydraulics.

- Extent of levee failure. It is likely that with sea-level rise, some levees, including those protecting urban areas, will be upgraded and the extent of inundation not as great as indicated.

TABLE 4

SUMMARY OF SALINITY RESULTS

Run No.	Sea Level Rise (m)	Levee Failure Condition	Carriage Water	Hydrology Scenario	Avg. Ann Delta Outflow[2] (km^3)	Average Salinity (ppt) Suisun Bay Ann.	Suisun Bay Mar.	Suisun Bay Sep.	San Pablo Bay Ann.	San Pablo Bay Mar.	San Pablo Bay Sep.
1	0	No	Exist	Exist[1]	19.7	7.2	2.2	12.5	19.3	12.2	25.1
2	0	Yes	Exist	Exist[1]	19.7	7.1	2.9	11.2	20.1	13.8	25.1
3	1.0	Yes	Exist	Exist[1]	19.7	8.9	4.5	12.7	21.4	16.1	25.4
4	1.0	Yes	Exist	Exist[1]	19.7	8.7	4.6	11.9	21.3	16.2	25.0
5	1.0	No	Double	GISS	33.3	8.1	1.4	13.5	19.1	8.3	25.8
6	1.0	Yes	Double	GISS	33.3	7.9	2.1	12.0	19.3	9.0	25.1
7	1.0	Yes	Double	GFDL	24.7	8.7	3.0	12.4	20.6	12.3	25.3
8	1.0	Yes	Double	OSU	20.1	9.5	4.5	12.5	21.7	15.0	25.4

Note:

[1] Existing hydrology is DWR 1990 scenario

[2] Base period 1951-1980

AVERAGE ANNUAL SALINITY VS DISTANCE FROM THE GOLDEN GATE

COMPARISON OF DIFFERENT HYDROLOGY SCENARIOS

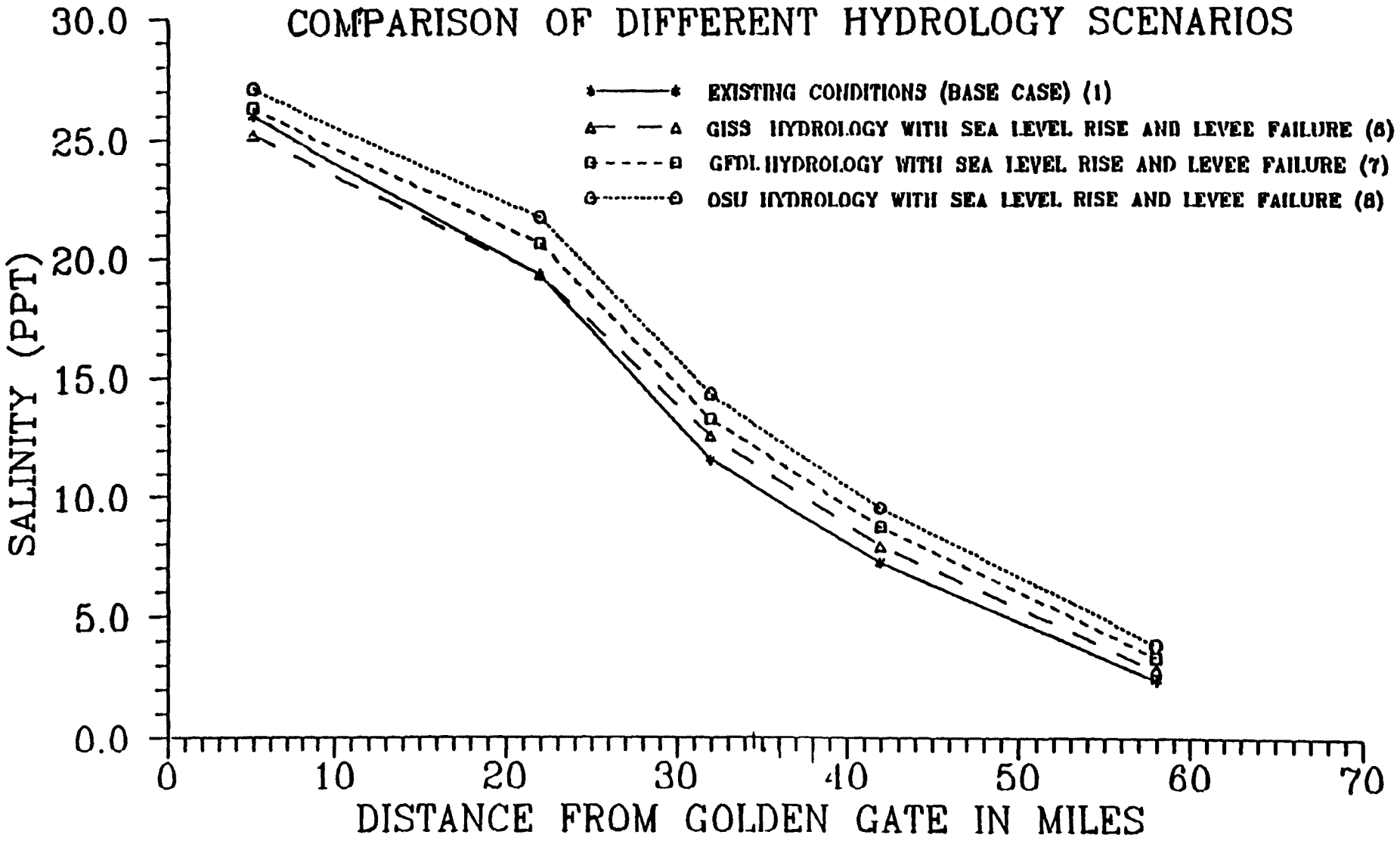

3-22

DATE: 04/18/88 BY: L. FISHBAIN		Philip Williams Associates Pier 35, The Embarcadero San Francisco, California 94133	9

Williams

AVERAGE MONTHLY SALINITY IN SUISUN BAY

EFFECT OF LEVEE FAILURE

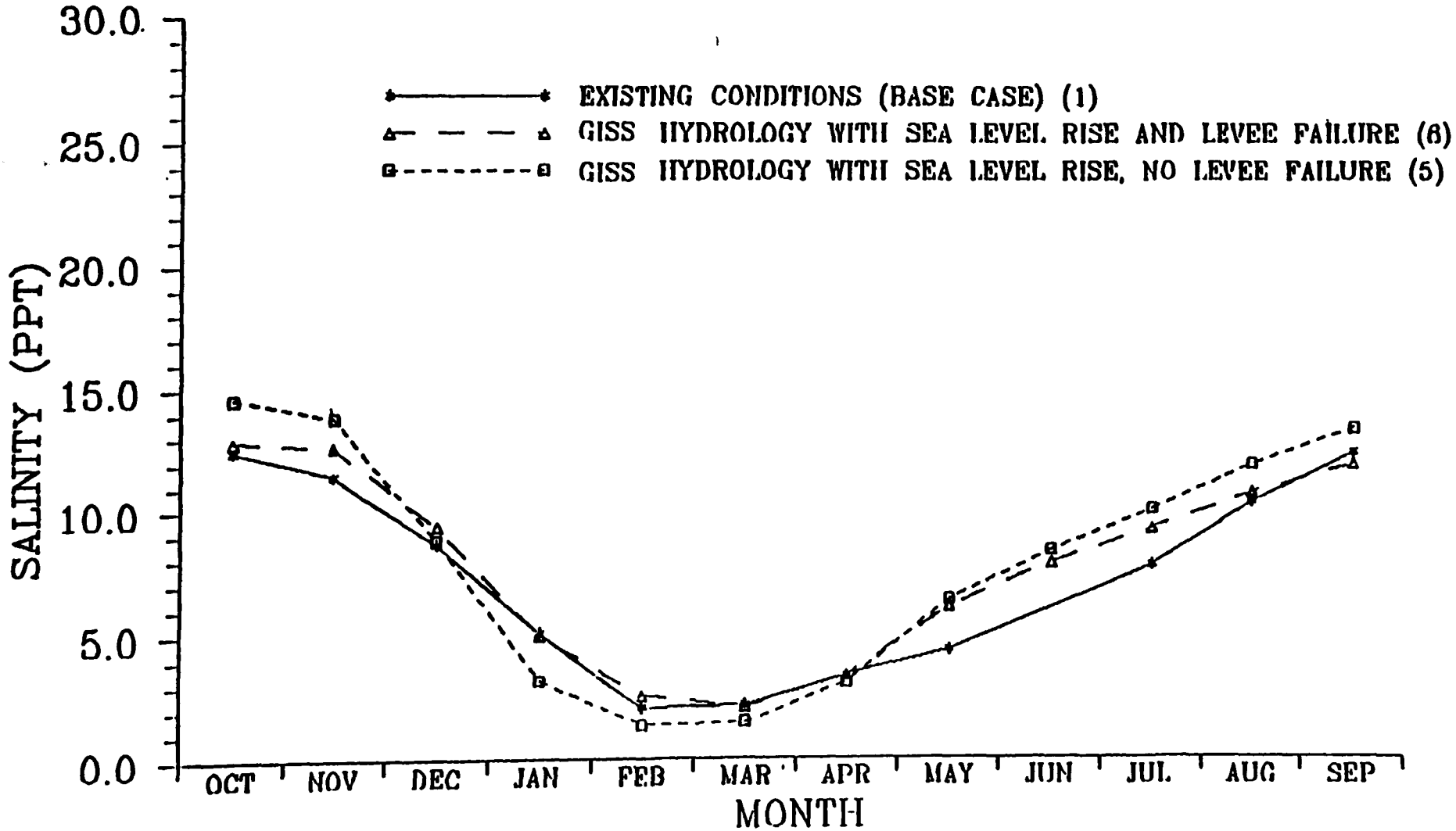

DATE: 04/18/88 BY: L. FISHBAIN		Philip Williams Associates Pier 35, The Embarcadero San Francisco, California 94133	10

Williams

AVERAGE MONTHLY SALINITY IN SUISUN BAY

COMPARISON OF DIFFERENT HYDROLOGY SCENARIOS

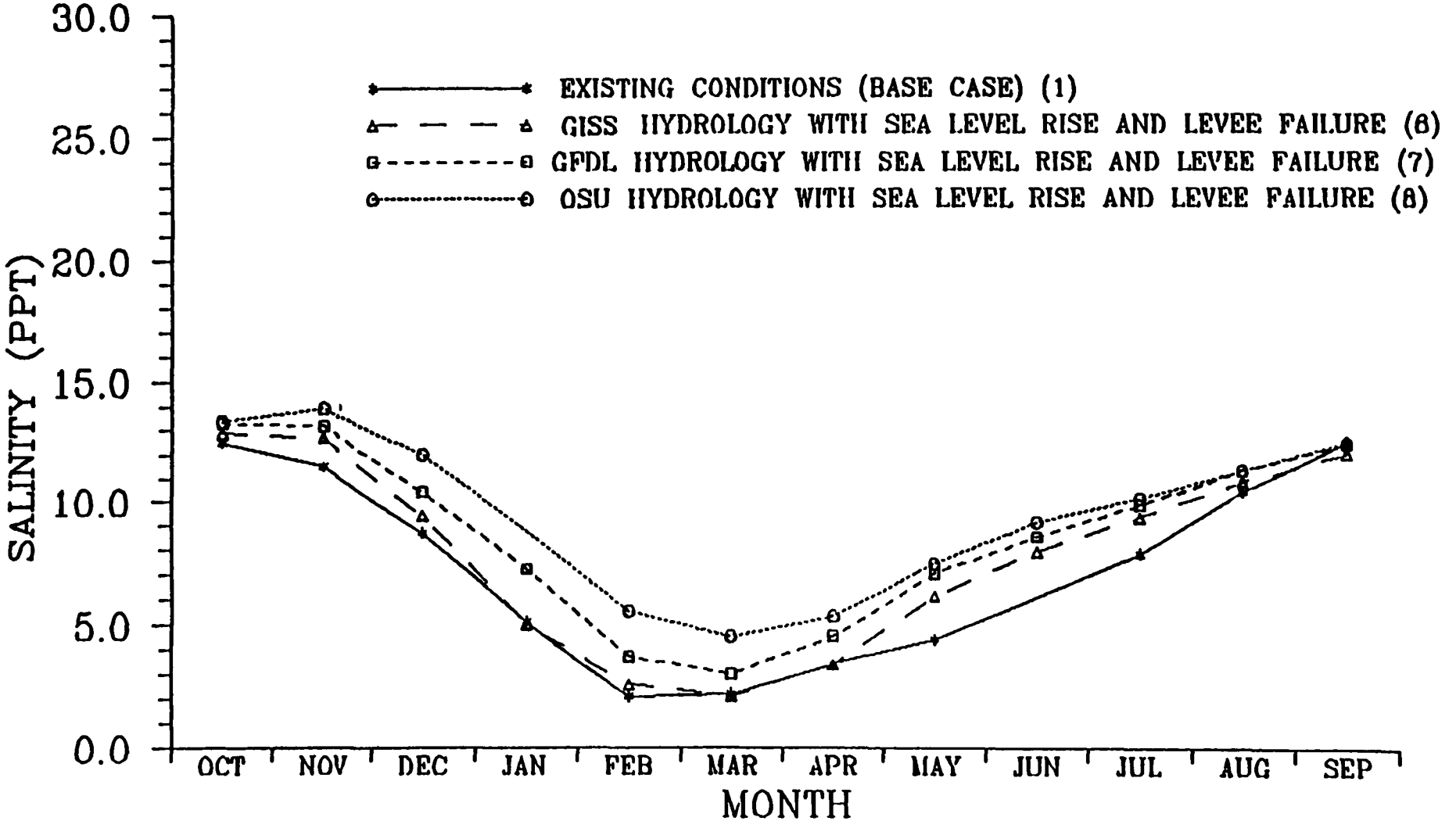

DATE: 04/12/88 BY: L. FISHBAIN		Philip Williams Associates Pier 35, The Embarcadero San Francisco, California 94133	11

Williams

3-24

SUISUN BAY SALINITY – MARCH

FREQUENCY RELATIONSHIP FOR THREE OUTFLOW SCENARIOS

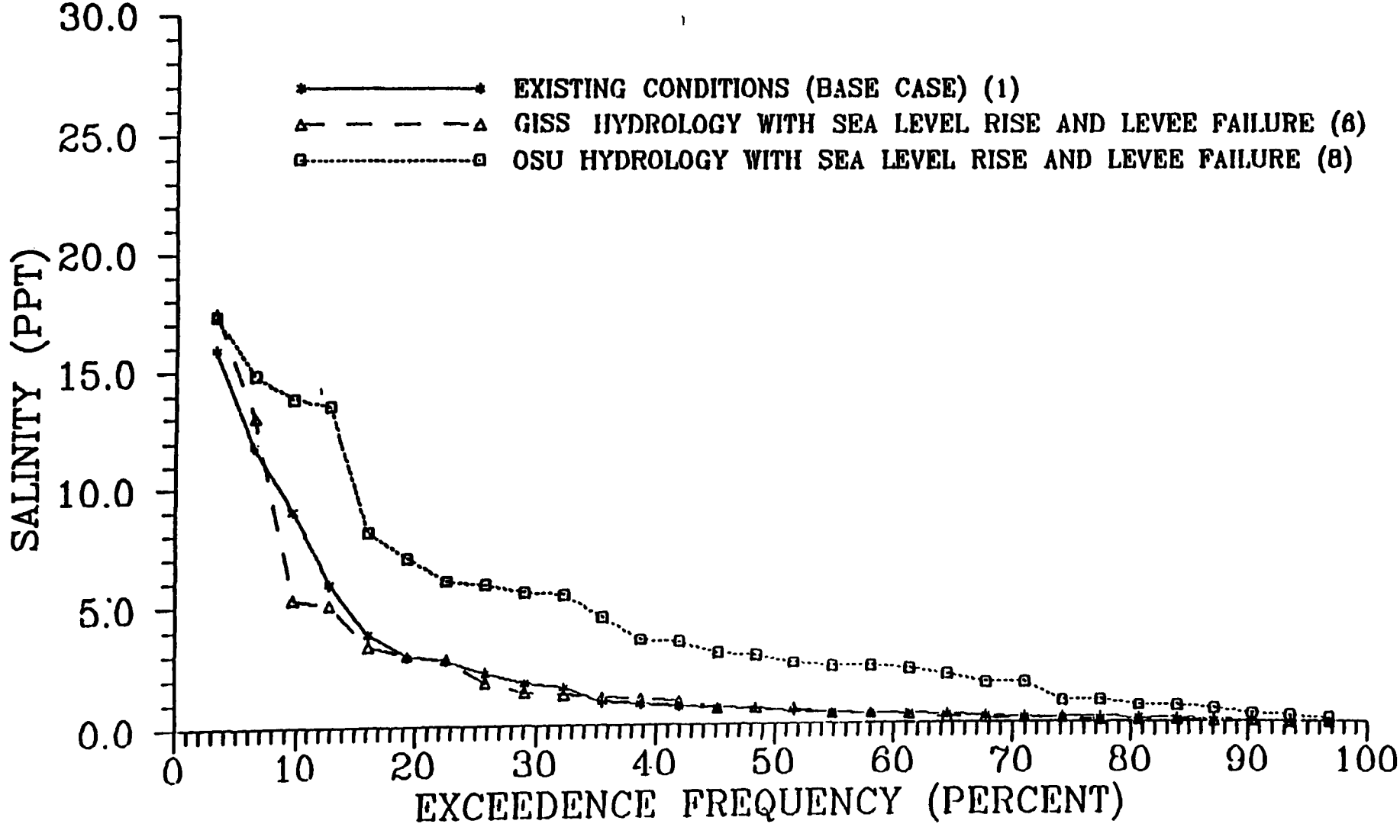

DATE: 04/18/88 BY: L. FISHBAIN		Philip Williams Associates Pier 35, The Embarcadero San Francisco, California 94133	12

SUISUN BAY SALINITY – JUNE

FREQUENCY RELATIONSHIP FOR THREE OUTFLOW SCENARIOS

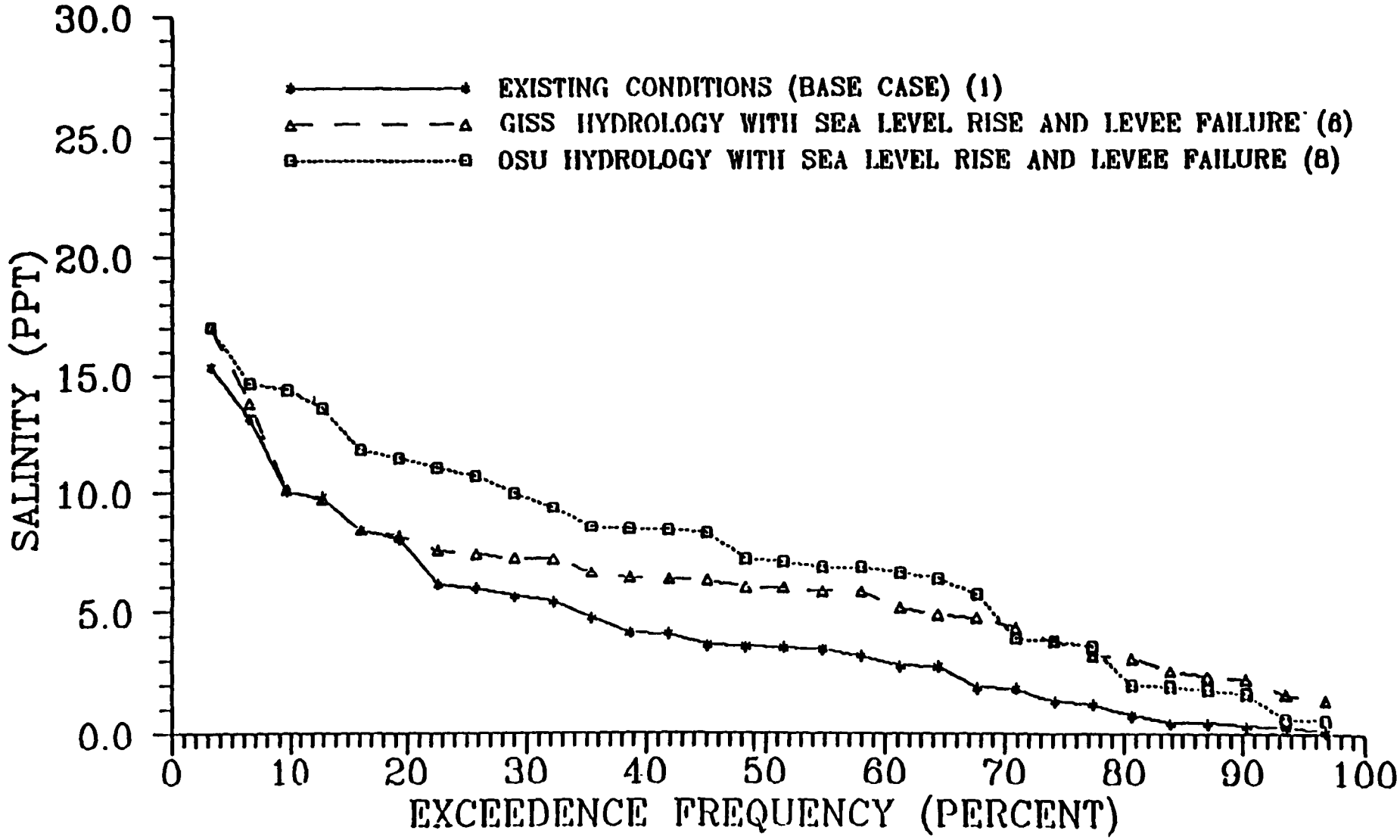

DATE: 04/25/88 BY: L. FISHBAIN		Philip Williams Associates Pier 35, The Embarcadero San Francisco, California 94133	13

Williams

- Modeling of tidal hydrodynamics. A simple model was used to achieve reasonable results in the budget and time frame available. More sophisticated physical or numerical modeling of the tidal hydrodynamics would give a better representation of tidal ranges and exchanges, particularly in the complex geometry of the Delta. The salinity distribution is particularly sensitive to the tidal exchange determined by the hydrodynamic model.

- Modeling of salinity. A simple model was used to achieve reasonable results in the budget and time frame available. A more sophisticated mixing model would give greater accuracy and more closely reflect the specific physical characteristics of each bay.

- Hydrologic base period. The hydrologic base period selected (1951-1980) is wetter than average, 20 cubic kilometers (16.0 million acre-feet) Delta outflow as compared to 16 cubic kilometers (or 13.0 million acre-feet) for the 1922-1978 average. This may tend to underestimate the long-term increases in salinity by not accounting for extended dry periods.

- Delta salinity. The salinity in the Delta at the intake to the export pumps is very sensitive to the physical characteristics of the Delta channels and islands. Although average monthly salinities in the Delta were calculated in this analysis, they are not presented in this report, because the physical significance of these results from such a simple model is unclear, considering the complexity of the geometry hydraulics of the Delta.

- Carriage water requirements. As for existing water management planning, these have been based on steady-state analysis. Complex changes in the hydraulics of the Delta and Suisun Bay such as scouring of tidal channels could increase salinity repulsion requirements.

CHAPTER 4

POLICY IMPLICATIONS

THE FUTURE OF THE DELTA

The question of the influence of the failure of the Delta island levees on salinity intrusion is already crucial in determining the justification for public expenditures to improve the existing levees. An estimate to improve these levees to protect against flooding from existing sea level is approximately $4 billion (DWR, 1982). The total valuation of property in the Delta is about $2 billion (DWR, 1987).

With accelerated sea-level rise causing major increases in salinity, the policy question becomes the following: Does the incremental value of maintaining levees in the Delta to prevent further increases of salinity in addition to protecting farmland and infrastructure justify the cost?

THE ESTUARINE ECOSYSTEM

Only in the last decade have the freshwater inflow requirements for maintaining the entire estuarine ecosystem been quantified. These requirements have not yet been incorporated into the water allocation and reservoir operating criteria of California's water system. With the major changes in estuarine hydrology, morphology, and hydrodynamics, it will become even more important to modify water resources management to incorporate protection of the estuarine ecosystem.

At the same time, climate change may allow an opportunity to restore lost environmental resources. For example, this could be done by increasing areas of tidal wetland. In addition, increased reservoir releases for salinity repulsion may also have substantial ecological benefits for San Francisco Bay.

EXPORT OF WATER FROM THE DELTA

The vulnerability of the State Water Project and Central Valley Project to salinity intrusion into the Delta was the genesis of the controversial and now-abandoned Peripheral Canal plan. The high cost of large diversion schemes that bypass the Delta probably means that salinity will continue to be managed by releases from reservoirs. Sea level rise and climate change will require that these releases be increased. The larger releases will require reallocation of water contracts and revision of present water management practices. These revisions may lead to consideration of structural modifications to the physical system such as channel modifications or off-stream storage.

REDUCING THE RANGE OF UNCERTAINTY

Because of the large economic, social, and environmental costs of these policy implications, the value of a greater degree of certainty is high. The next level of analysis for predicting the salinity response of the estuary to sea-level rise will require the following:

- Detailed morphometric description of the estuary.
- Utilization of detailed hydrodynamic and mixing models of the estuary. At present, it appears that the Corps of Engineers' Physical Model of San Francisco Bay (three-dimensional) and a version of Fischer's numerical model (pseudo-two-dimensional) are available.
- Development of a model for morphologic changes in tidal channels with changing tidal prism.
- Analysis of sediment budget and sediment dynamics in the estuary.

REFERENCES

Denton, Richard A. and James R. Hunt. "Currents in San Francisco Bay: Final Report." University of California, Berkeley, California, 1986.

Department of Water Resources. Delta Levees Investigation. Bulletin 192-82. State of California. 1982. 213 pp.

Department of Water Resources. Sacramento-San Joaquin Delta Atlas. Sacramento, California, 1987. 71 pp.

Fischer, Hugo B. "A Method for Predicting Pollutant Transport in Tidal Waters." University of California, Berkeley, Water Resources Center, Contribution No. 132. 1970. 143 pp.

Josselyn, N., and Atwater, B.F. 1982. "Physical and biological constraints as man's use of the shore zone of the San Francisco Bay estuary." In: Kockelman, W.J., T.J. Conomos, and A.E. Leviton, eds. San Francisco Bay: Use and Protection. San Francisco, CA: American Association for the Advancement of Science. p. 57-84.

Kockelman, William J., T. John Conomos, and Alan E. Leviton. San Francisco Bay: Use and Protection. American Association for the Advancement of Science. San Francisco, California, 1982. 310 pp.

National Research Council. Responding to Changes in Sea Level: Engineering Implications. National Academy Press, Washington, D.C., 1987. 148 pp.

State Water Resources Control Board. "Water Quality Control Plan: Sacramento-San Joaquin Delta and Suisun Marsh." Sacramento, California, 1978.

Williams, Philip B. and Larry Fishbain. "Analysis of Changes in Suisun Bay Salinity Due to Existing and Future Water Development." Report 412-2. San Francisco, California, 1987.

Williams, Philip B. and Michael Josselyn. "An Overview of Flow and Salinity Standards Required to Protect the Ecosystem of San Francisco Bay." San Francisco, California, 1987. 53 pp.

EFFECTS OF CLIMATE CHANGES ON THE LAURENTIAN GREAT LAKES LEVELS

by

Thomas E. Croley II
Holly C. Hartmann
National Oceanic and Atmospheric Administration
Great Lakes Environmental Research Laboratory
2205 Commonwealth Boulevard
Ann Arbor, MI 48105-1593

Interagency Agreement Identification Number DW13932631-01-0

CONTENTS

Page

FINDINGS 4-1

CHAPTER I: INTRODUCTION 4-3
THE PHYSICAL SYSTEM 4-3
RELATED WORK 4-4
STUDY APPROACH 4-4

CHAPTER II: COMPONENT PROCESS MODELS 4-6
RUNOFF MODELING 4-6
OVERLAKE PRECIPITATION 4-7
OVERLAKE EVAPORATION 4-7
CONNECTING CHANNEL FLOWS 4-9
MODELS APPLICABILITY 4-9

CHAPTER III: SIMULATION METHODOLOGY 4-11
STEADY-STATE CLIMATE CHANGE ASSESSMENTS 4-11
TRANSIENT-CASE CLIMATE CHANGE ASSESSMENTS 4-12

CHAPTER IV: RESULTS 4-13
CLIMATE CHANGE STEADY-STATE IMPACTS 4-13
Basin Meteorology 4-13
Basin Hydrology 4-13
Over-Water Meteorology 4-15
Lake Heat Balance 4-16
Net Supply Components 4-19
Lake Water Balance 4-21
CLIMATE CHANGE TRANSIENT IMPACTS 4-23
SENSITIVITIES 4-25

CHAPTER V: IMPLICATIONS OF RESULTS 4-26
ENVIRONMENTAL IMPLICATIONS 4-26
SOCIOECONOMIC IMPLICATIONS 4-26
Power Production 4-26
Navigation 4-28
Industrial Operations 4-28
Commercial Operations 4-28
Commercial Fishing 4-28
Agriculture 4-29
Recreation Interests 4-29
Riparians 4-29
POLICY IMPLICATIONS 4-29

REFERENCES 4-31

FINDINGS[1]

The Great Lakes Environmental Research Laboratory has developed conceptual model-based techniques for simulating moisture storages and runoff from the 121 watersheds draining into the Laurentian Great Lakes, overlake precipitation into each lake, and the heat storages and evaporation from each lake. We model each of these components separately and then use them in conjunction with operational regulation plans and hydraulic routing models of outlet and connecting channel flows to estimate water levels on Lakes Superior, Michigan, Huron, St. Clair, Erie, and Ontario to consider the existing basin and lake storages and possible meteorology. Integration of the models allows the consideration of climate change scenarios developed from atmospheric circulation models through linkages on air temperature, precipitation, humidity, wind speed, and cloud cover. Alternate scenarios are considered by abstracting changes in linkages, making these changes in historical data, observing the impact of the changed data in the model out puts, and comparing these to model results using unchanged data.

Three steady-state climate change scenarios corresponding to atmospheric modeling of a doubling of CO_2 in the atmosphere are considered here with the hydrologic models; they are compared to a steady-state simulation obtained with historical data representing an unchanged atmosphere. One transient climate change scenario representing atmospheric modeling of the transition from present conditions to increased CO_2 content in the atmosphere is considered here with the hydrologic models and compared to a transient simulation with historical data to assess impacts. The study results should be received with caution as they are of course dependent on the atmospheric circulation model output with large uncertainties and are only possibilities for a future with increased atmospheric CO_2 content.

The higher air temperatures under the $2xCO_2$ scenarios lead to higher overland evapotranspiration and lower runoff to the lakes with earlier runoff peaks, since snowpack is reduced up to 100% and the snow season is shortened from two to four weeks. This also results in more than a 50% reduction in available soil moisture. Water surface temperatures peak earlier on Lake Superior; since the climate becomes similar to present-day climates on the southern lakes, the lake temperature behaves similar to present-day southern deep lakes. There are larger amounts of heat resident in the deep lakes throughout the year. As a result, buoyancy-driven turnovers of the water column do not occur many times on four of the six lakes. Currently, they occur twice a year on all lakes. Ice formation also will be greatly reduced over winter on the deep Great Lakes and lake evaporation increases on all lakes. The average steady-state lake levels are seen to drop between 1/2 to 1 1/3 meters for the GISS $2xCO_2$ climate scenario, drop 2 to 2 1/2 meters for the GFDL, and drop 1/2 to 1 meters for the OSU scenario. Transient analyses of the GISS 80-yr transient scenario indicate that the lakes drop between 13 and 93 mm per decade on the average. The Lake Ontario regulation plan fails in all steady-state and transient climate change analyses, reflecting its design for regulation of current ranges of Lake Ontario water levels and St. Lawrence Seaway flows.

The climate change effects modeled herein, if they occur, will require new paradigms in water management in the Great Lakes Basin. Allocation conflicts between users of the Great Lakes will likely result. Lowered lake levels could produce large reductions in wetland areas and lower hydropower production. While reduced lake ice formation could lengthen the shipping season, lower lake levels could also increase waterborne shipping costs via lower vessel load limits, traffic backups at the Welland Canal and Sault Ste. Marie, and dredging of sediments highly contaminated with toxics. Dredging and disposal of toxic-contaminated harbor sediments may pose critical problems for municipal and private marinas and create conflicts between the many governments having jurisdiction over the lakes. To manage potential allocation conflicts, the Boundary Waters Treaty of 1909 may have to be modified to consider commercial, industrial, riparian, recreational, and ecological

---

[1]Although the information in this report has been funded partly by the U.S. Environmental Protection Agency under Interagency Agreement no. DW13932631-01-0 with the Office of Policy Analysis, it does not necessarily reflect the Agency's views, and no official endorsement should be inferred from it.

interests in addition to presently considered domestic and sanitary water supply, navigation, hydropower, and irrigation interests. The Lake Superior and Ontario regulation plans would probably have to be revised to handle persistently low water supplies.

Climate change also poses concerns unrelated to lake levels. Lake ecologies will change if the lakes do not experience their typical spring and fall water column turnovers. Changes in fish community and population structures will likely benefit some species but reduce ranges and sustainable yields for others. Winter tourism and recreation operations that require dependable snowcover may suffer total collapse throughout much of the Great Lakes region. In addition, soil moisture shortages may prove critical for agricultural operations.

CHAPTER I

INTRODUCTION

Climate change will impact on many aspects of the hydrologic cycle with consequences for mankind that are interrelated and often times difficult to discern. Impacts of climate change on water supplies have been the focus of several recent studies. The U.S. Environmental Protection Agency (EPA, 1984) and Rind (personal communication, 1988) used the hydrologic components of general circulation models to assess changes in water availability in several regions throughout North America, but the regions were very large; Rind used only four for the entire continent and indicated that assessments with smaller regions were needed. Because the Laurentian Great Lakes possess tremendous water and heat storage capacities coupled with constricted lake outlets, they respond slowly to changed meteorologic inputs. This "memory" results in a filtering or dampening of most short-term climate fluctuations with lake levels reacting primarily to longer-period fluctuations characteristic of climate change. The large Great Lakes system thus is ideal for studying regional effects of climate changes.

THE PHYSICAL SYSTEM

The Laurentian Great Lakes contain 23,000 km^3 of water (about 20% of the world's fresh surface water) and, with their surrounding basins, cover 770,000 km^2 in the United States and Canada. The lakes' surface areas comprise about one-third of the total basin area. The basin extends over 3200 km from the western edge of Lake Superior to the Moses-Saunders Power Dam on the St. Lawrence River. The water surface drops in a cascade over this distance over 182 meters to sea level. The most upstream, largest, and deepest lake is Lake Superior. Lake Superior outflows are controlled according to regulation Plan 1977, under the auspices of the International Joint Commission. The lake has two interbasin diversions of water into the system from the Hudson Bay basin, the Ogoki and Long Lake diversions. Lake Superior waters flow through the lock and compensating works at Sault Ste. Marie, Michigan, and down the St. Mary's River into Lake Huron where it is joined by water flowing from Lake Michigan.

Lakes Michigan and Huron are considered to be one lake hydraulically, because of their connection through the deep Straits of Mackinac. The second interbasin diversion takes place from Lake Michigan at Chicago. Here water is diverted from the Great Lakes to the Mississippi River basin. The water from Lake Huron flows through the St. Clair River, Lake St. Clair, and Detroit River system into Lake Erie. The drop in water surface between Lakes Michigan-Huron and Erie is only about 2.4 meters. This results in a large backwater effect between Lakes Erie, St. Clair, and Michigan-Huron; changes in Lakes St. Clair and Erie levels are transmitted upstream to Lakes Michigan and Huron. From Lake Erie the flow continues through the Niagara River and Welland Canal diversion into Lake Ontario. The major drop over Niagara Falls precludes changes on Lake Ontario from being transmitted to the upstream lakes. The Welland Canal diversion is an intrabasin diversion bypassing Niagara Falls and is used for navigation and hydropower production. There is also a small diversion into the New York State Barge Canal system, which is ultimately discharged into Lake Ontario. Lake Ontario outflows are controlled in accordance with Plan 1958-D. From Lake Ontario, the water flows through the St. Lawrence River to the Gulf of St. Lawrence and the Atlantic Ocean.

There are three primary types of fluctuations of Great Lakes levels: annual, seasonal, and short-term variations due to wind setup and storm surge. Annual fluctuations result in most of the variability leading to record high or low lake levels. There is an overall range of about 1.8 meters in the annual levels. Superimposed on the annual levels are seasonal cycles, which range in magnitude from about 0.38 meters on Lake Ontario to about 0.30 meters on Lake Michigan-Huron. In general, the seasonal cycles have a minimum in the winter, usually January or February. The levels then rise due to increasing water supplies from snowmelt and spring precipitation until they reach a maximum in June for the smaller lakes (e.g., Erie and Ontario) or in September

in the case of Lake Superior. The lakes begin their seasonal declines in the late summer and fall. The final type of fluctuation, storm surge or wind setup, is relatively short-lived, lasting only several hours. While sometimes large (Lake Erie can experience differences between levels on the eastern and western ends of the lake as large as 4.9 meters), they are too transitory to be considered by the model applications herein and are not discussed further.

The hydrologic cycle of the Great Lakes basin determines the lake levels. Runoff constitutes a significant part of the Great Lakes' water supplies, particularly during the snowmelt season, late March through early June. Because the lakes are so large, lake precipitation and evaporation are of the same order of magnitude as runoff. On a monthly scale, precipitation is fairly uniformly distributed throughout the year. Lake evaporation typically has the greatest effect on water supplies during the winter months (Derecki, 1980); cool dry air and warm water result in massive evaporation then. Condensation on the cool lake surface from the wet overlying air occurs in the summer. Net groundwater flows to each of the Great Lakes are generally negligible (DeCooke and Witherspoon, 1981). Net supplies typically reach a maximum in the late spring and a minimum in late fall. The imbalance between supplies and outflows from the lake results in rising or falling lake levels. Although the net basin supply components are of similar magnitude, their estimations are not equally sophisticated.

RELATED WORK

Preliminary estimates of the impact of climate warming on the Great Lakes water resources have been undertaken. Quinn and Croley (1983) estimated that a 3°C rise coupled with a 6.5% increase in precipitation would decrease the net basin supply to Lake Superior by 10%. A similar 3°C rise with no precipitation increase would decrease the Lake Erie net basin supply by 33%. Cohen (1986) indicated 4 to 21% decreases in net basin supply for various double-CO_2 scenarios with annual temperature changes varying between 3.1 and 4.8°C and varying projections of wind speed and precipitation changes. His computations are very sensitive to changes in precipitation, wind speed, and humidity. To examine the potential response of the unregulated Great Lakes to decreased water supplies, Quinn (1988) used two hydrometeorologic scenarios with GLERL's Hydrologic Response Model. A 15% decrease in net basin supplies reduced water levels on Lakes Michigan-Huron, St. Clair, and Erie by 77, 60, and 51 cm, respectively. A 30% decrease in supplies reduced the lakes levels by 156, 125, and 106 cm, respectively.

Environment Canada began, in 1984, a major study to assess the impacts of climate change on the province of Ontario (Allsopp and Cohen, 1986). Goddard Institute of Space Sciences double carbon dioxide climate scenarios were modified and used with models or estimators of net basin supply components. However, the water supply models used only monthly data, they assumed water temperatures rose equal to air temperatures, and, for the most part, they used a fragmented approach in that consistency between modeled processes was not preserved. While their air temperature and precipitation changes were consistent with atmospheric scenarios, dewpoint was increased arbitrarily the same as air temperature and sunshine was decreased independently; the original $4xCO_2$ scenario was used to estimate $2xCO_2$ changes by dividing monthly anomalies in temperature and wind speed by two; and alternate scenarios were used where wind speeds were unchanged or reduced an arbitrary 20%. Overall water supplies to the Great Lakes system under these conditions were about 15% lower than the base case; water levels were routinely expected to drop below the drought-period levels of the 1960s.

STUDY APPROACH

The Great Lakes Environmental Research Laboratory (GLERL) has developed conceptual model-based techniques for simulating moisture storages and runoff from the 121 subbasins draining into the Great Lakes, overlake precipitation into each of the Great Lakes and Lake St. Clair (hereafter included as a Great Lake), and the heat storages and evaporation from each of the lakes. We model each of these components separately and then use them in conjunction with operational regulation plans and hydraulic routing models of outlet and

connecting channel flows to estimate water levels on Lakes Superior, Michigan, Huron, St. Clair, Erie, and Ontario to consider the existing basin and lake storages and possible meteorology. Integration of the models allows the consideration of climate change scenarios developed from atmospheric circulation models through linkages on air temperature, precipitation, humidity, windspeed, and cloud cover. Alternate scenarios are considered by abstracting changes in linkages, making these changes in historic data, observing the impact of the changed data in the model outputs, and comparing it to model results using unchanged data. Scenarios, supplied by the U.S. Environmental Protection Agency (EPA) and obtained from three different general circulation models, are used in this manner to understand how climate warming affects lake levels through interrelated changes in the atmospheric-hydrologic linkages.

This report describes the models and methodology used and their limitations, presents and interprets the results, and addresses the potential environmental, scoioeconomic, and policy implications of the results.

CHAPTER II

COMPONENT PROCESS MODELS

RUNOFF MODELING

The GLERL Large Basin Runoff Model (LBRM) consists of moisture storages arranged as a serial and parallel cascade of "tanks" (Croley, 1983a,b); water flows from the snowpack to the upper soil zone tank, from the upper to the lower soil zone and surface storage tanks, from the lower to the groundwater and surface tanks, from the groundwater to the surface tank, and from the surface tank out of the watershed. It makes use of physical concepts for snowmelt and net supply to the watershed surface, infiltration, heat available for evapotranspiration, actual evapotranspiration, and mass conservation. As a conceptual model, the LBRM is useful not only for predicting basin runoff, but for facilitating our understanding of watershed response to natural forces as well. The main mathematical feature of the LBRM is that it may be described by strictly continuous equations; none of the complexities associated with inter-tank flow rate dependence on partial filling are introduced. For a sufficiently large watershed, these nuances are not observed owing to the spatial integration of rainfall, snowmelt, and evapotranspiration processes.

Daily precipitation, temperature, and insolation (the latter available from climatological summaries as a function of location) may be used to determine snowpack accumulations and net surface supply based on degree-day determinations of snowmelt. The net surface supply is divided into infiltration to the upper soil zone and surface runoff by taking infiltration proportional to the net supply rate and to the areal extent of the unsaturated portion of the upper soil zone. Outflow from each storage within the watershed is proportional to the moisture in storage. The evapotranspiration rate from the upper and lower soil zones is proportional to available moistures there and to the heat rate available for evapotranspiration; it also reduces the heat available for subsequent evapotranspiration. The total amount of heat in a day is split between that used for and that still available for evapotranspiration by empirical functions of air temperature based on a long-term heat balance. Mass continuity yields a first-order linear differential equation for each of the tanks (Croley, 1982) that are tractable analytically, and the model is applied to daily data.

The Great Lakes basin is divided into 121 watersheds draining directly to a lake. The meteorologic data from about 1800 stations about and in the watersheds are combined through Thiessen weighting to produce areally-averaged daily time series of precipitation and maximum and minimum air temperatures for each watershed (Croley and Hartmann, 1985b). Records for all "most-downstream" flow stations are combined by aggregating and extrapolating for ungauged areas to estimate the daily runoff to the lake from each watershed. The LBRM is calibrated to determine the set of parameters resulting in the smallest sum-of-squared-errors between model and actual daily flow volumes for the calibration period (Croley, 1983b; Croley and Hartmann, 1984, 1985a). Calibrations are repeated with initial storages equal to observed long-term averages until there is no change in the averages to avoid arbitrary initial conditions in case their calibration effects do not diminish rapidly. However, the simulation effect of the initial values greatly diminishes with the length of the period and after 1 year of simulation, the effects are nil from a practical point of view. After the LBRM is calibrated for each watershed (subbasin), the model outflows are combined to represent each Great Lake basin; this distributed-parameter model integration filters individual subbasin model errors. The LBRM calibration periods generally cover 1965-1982 depending upon flow data availability. Table 1 presents calibration results for the distributed-parameter applications. While the calibrated parameters are used for all scenarios, the statistics in Table 1 apply only to the historical calibration and verification periods.

Table 1. Large Basin Runoff Model Calibration Statistics[1].

Lake	No. of Sub-basins	Mean 1-day Flow (mm)[2]	Flow Std. Dev. (mm)[2]	Root Mean Square Error (mm)[2]	Correlation Calib.	Correlation Verif.
Superior	22	1.12	0.67	0.25	0.93	0.77
Michigan	29	0.89	0.47	0.18	0.93	0.86
Huron	27	1.06	0.69	0.26	0.92	0.69
St. Clair	7	0.90	1.36	0.62	0.89	0.87
Erie	21	1.01	1.28	0.54	0.91	0.90
Ontario	15	1.41	1.13	0.43	0.93	0.89

[1]Calibrations and statistics generally cover 1966-83; verification correlation generally covers 1956-63.
[2]Equivalent depth over the land portion of the basin.

OVERLAKE PRECIPITATION

The lack of overlake precipitation measurements means that estimates typically depend on land-based measurements and there may be differences between land and lake meteorology. Although gage exposures may significantly influence the results of lake-land precipitation studies (Bolsenga, 1977, 1979), Wilson (1977) found that Lake Ontario precipitation estimates based on only near-shore stations averaged 5.6% more during the warm season and 2.1% less during the cold season than estimates based on stations situated in the lake. Using a network that also included stations somewhat removed from the Lake Ontario shoreline, Bolsenga and Hagman (1975) found that eliminating several gages not immediately in the vicinity of the shoreline increased overlake precipitation estimates during the warm season and decreased them during the cold season. Thus, for the Great Lakes, where lake ef fects on near-shore meteorology are significant and the drainage basins have relatively low relief, the use of all available meteorologic stations throughout the basin is probably less biased than the use of only near-shore stations.

OVERLAKE EVAPORATION

Great Lakes evaporation studies typically used mass transfer formulations from the classic Lake Hefner study (U.S. Geological Survey, 1954, 1958); see Richards and Irbe (1969) and Derecki (1976). More recently, Phillips (1978) and Quinn (1979) included atmospheric stability effects on Great Lakes evaporation bulk transfer coefficients; the latter approach is used presently by both Canadian and U.S. agencies applied to monthly data for water surface temperatures, windspeed, humidity, and air temperatures (Derecki, 1976, 1979, 1981a,b; Quinn and Kelley, 1983; Atmospheric Environment Service, 1988). The present study uses that approach, applied to daily data combined with models for over-water meteorology, ice cover, and lake heat storage and with a lumped representation of a lake's heat balance (Croley, 1988). As over-water data are not available generally, over-land data are used by adjusting for over-water conditions. Phillips' and Irbe's (1978) regressions for over-water corrections are used directly by replacing the fetch (and derived quantities) with averages. Air temperatures and specific humidities over ice are used for over-ice evaporation calculations and over water for the over-water calculations; the two estimates are combined by weighting for the fraction of the surface covered in ice. Existing data on ice cover (Assel, 1983) were used to determine empirical relations between ice cover extent and air temperatures, similar to other efforts (Derecki, 1978, 1981a).

Spring turnover occurs around June for Superior and around May for Ontario (when water temperatures reach 3.98°C, at which water is most dense). As surface temperature begins increasing above 3.98°C, a stable profile develops, with water surface temperature increasing faster than temperatures at depth, until a well-defined epilemnion layer is present at the end of the summer. As the net heat flux to the surface then changes to negative, water surface temperature drops and the temperatures at depth first grow and then recede, keeping the upper part of the profile vertical. The mixed-layer (where the temperature profile is vertical) deepens until the profile again approaches a vertical line throughout at 3.98°C (representing fall turnover). Then a symmetical behaviour is observed with temperatures less than 3.98°C as the lake continues to lose heat; the surface temperature changes fastest until the net heat flux at the surface changes to positive again. Water surface temperature then increases toward 3.98°C and the temperatures at depth first decrease and then increase as the profile again approaches a vertical line (representing spring turn over). These observations enable the extension of the mixed-layer thermal structure developed for oceans (Gill and Turner, 1976; Kraus and Turner, 1967) to the Great Lakes to allow the determination of a simple one-dimensional model for surface temperature increments or decrements from past heat additions or losses, respectively (Croley, 1988). The effects of past additions or losses are superimposed to determine the surface temperature on any day as a function of heat in storage; each past addition or loss is parameterized by its age as a proxy for the wind history or accumulated mixing. Turnovers can occur as a fundamental behaviour of this superposition model, and hysteresis between heat in storage and surface temperature, observed during the heating and cooling cycles on the lakes, is preserved.

Heat in storage in the lake at the end of each day is evaluated from a daily conservation of energy by taking the change in storage equal to the sum of the fluxes integrated over the day. Short-wave radiation is interpolated from generalized maps of Canadian and northern U.S. mid-monthly clear-sky values and adjusted for daily cloudcover and average short-wave reflection is taken simply as one-tenth of the incident (Gray et al., 1973). Net long-wave radiation exchange is estimated for each day with the water and atmosphere behaving as gray bodies with cloud-cover correction only to atmospheric radiation (Keijman, 1974). Sensible heat transfers are taken as the latent heat of evaporation times Bowen's ratio, evaluated from daily air and water temperatures and associated humidities, (Gray et al., 1973) and added to evaporative advection and latent heat transfers. Energy advected with precipitation is adjusted if the precipitation is snow to account for the heat required in snowmelt. The energies advected into and out of the lake with other water flows are determined from the water surface temperature and the mass flow rates. The heat delivered to the ice pack each day is used in a heat balance over the ice to adjust the ice pack mass for accumulation, aggradation, and ablation; it is given by a simple account of energy fluxes also. Reflected short-wave radiation is taken here (Gray et. al., 1973) as a function of the ice cover. Net long-wave radiation exchange is computed each day by using ice surface temperature equal to the air temperature or zero °C, whichever is smaller. Evaporative heat transfers from ice include the heat of fusion as well as vaporization at the temperature of the ice surface. Sensible heat transfers also are calculated from the daily Bowen ratio by using ice surface temperature. Energy advected with precipitation onto the ice surface is uncorrected for melt since that is taken as occurring with the ice pack.

As both water surface temperature and evaporation over water and ice are unknown and must be determined each day, an iterative approach is used. The water surface temperature at the beginning of the day is determined inversely from the heat storage at the beginning of the day (which is equal to the heat storage at the end of the previous day). The water surface temperature at the end of the day is initially set equal to that at the beginning. Then 1) the beginning and end water surface temperatures are averaged as the water surface temperature during the day; 2) it is used with the day's meteorology to compute evaporation over water and ice; 3) stored heat at the end of the day is found from the heat balances over water and ice with fluxes determined as above; and 4) an improved water surface temperature at the end of the day is computed again. These four steps are repeated until the water surface temperature at the end of the day converges to within 0.001°C. If the water surface temperature passes through 3.98°C, turnover is considered to have occurred. Any time that either turnover occurs or the mixed layer begins developing, the age of the mixed layer is reset.

Unfortunately, there are no really good independent evaporation data to calibrate and verify evaporation models on the Great Lakes. Water balances are insufficient owing to the large errors induced by subtracting

nearly equal large inflows and outflows to each Great Lake or owing to errors of estimate in the water balance components. However, with the joint heat balance and evaporation model described here, it is possible to compare water surface temperatures with available data, now available from the National Oceanic and Atmospheric Administration's Polar Orbiting Satellite Advanced Very High Resolution Radiometer (Irbe and Saulesleja, 1982; Irbe et al., 1982; AES, 1988) and reduced for all lakes except Michigan.

The heat balance model was calibrated to determine values of the seven model parameters that give the smallest sum-of-squared-errors between model and actual daily water surface temperatures observed by satellite during a calibration period. Daily meteorological over-land data at from five to ten near-shore stations about each Great Lake are assembled and averaged for correction to over-lake data. The water surface temperature and the number of days since the last turnover must be initialized prior to modeling or calibration but for calibration or long simulations the initial values are generally unimportant. The effect of the initial values diminishes with the length of the simulation and after 1 year of simulation, the effects are nil from a practical point of view as with the runoff model. Calibrations start on 1 January 1979 and end on 31 December 1985 for all Great Lakes and start on 1 January 1979 and end on 31 December 1983 for Lake St. Clair. Nearly two years at the beginning of these periods are without surface temperature data, allowing sufficient initialization prior to computation of comparison statistics.

There is good agreement between the actual and calibrated-model water surface temperatures; correlations are greater than 0.98, means and variances both differ only by a few percent, and the root mean square error is between 1.2 and 1.5°C on the deep lakes. The period 1966-78 was used as a verification period, and statistics were computed comparing water surface temperatures to data outside of the calibration period to assess independently how well it performs; root mean square errors were 1.3 to 1.6 °C on the deep lakes (Croley, 1988); the model is judged to perform well in describing deep lake evaporation with less confidence placed in shallow lake evaporation. Lake Michigan parameters were set from the other lakes.

CONNECTING CHANNEL FLOWS

Lake Superior outflows are found by using "Plan 1977" as implemented by the U.S. Army Corps of Engineers (USACE) for simulation studies (International Lake Superior Board of Control, 1981, 1982). It tries to balance Lakes Superior and Michigan-Huron relative to their long-term levels while considering their normal variability. It requires a hydraulic routing model for the connecting channels to determine projected water levels for Lake Michigan-Huron, which then affect the control of Lake Superior outflows. The GLERL Hydrologic Response Model (HRM) (Hartmann, 1988; Quinn, 1978) uses reservoir routing concepts and discharge equations to reflect present conditions; it appropriately relates lake storage changes to lake level fluctuations and considers consumptive use rates (Hartmann, 1987). The Ogoki diversion comprises part of the gaged river flows into Lake Superior and thus is modeled by the LBRM. Constant diversions of 40, 91, and 261 cubic meters per second are used for the Long Lake, Chicago, and Welland Canal diversions, respectively. Consumptive use rates of 7, 56, 62, and 15 cubic meters per second are used for Lakes Superior, Michigan-Huron, Erie, and Ontario, respectively (International Great Lakes Diversions and Consumptive Uses Study Board, 1981). Long-term average rates of ice retardation of flows over 1937-1981 are used for the St. Clair and Detroit Rivers. Lake Ontario levels and outflows are determined using the USACE implementation of Plan 1958-D (International St. Lawrence River Board of Control, 1963). The plan attempts to satisfy many, often conflicting, interests, including riparian, shipping, and hydropower concerns, both upstream and downstream of the lake outlet; it is suspended often during times of non-normal water supplies.

MODELS APPLICABILITY

Since we have daily models derived for other purposes, we use a daily resolution of data with our models. However, basin-wide processes of runoff, lake evaporation, channel routing, and lake level change are often described with weekly or monthly models for lake-level simulation (this ignores short-term fluctuations associated with storm movement which are not addressed in this study). Likewise, spatial resolution finer than

about 1000-5000 km^2 (the present average resolution of our models and their applications) is unnecessary, and much can be done in assessing lake level changes at resolutions of 100,000-1,000,000 km^2 with lumped versions of our models. This coarse spatial resolution is still much finer than the present GCM grids.

There is some indication of model applicability outside the time periods over which the models were calibrated. The LBRM is used in forecasts of Lake Superior water levels (Croley and Hartmann, 1987) and comparisons with climate outlooks showed the runoff model was very close to actual runoff (monthly correlations of water supply were on the order of 0.99) for the period August 1982-December 1984, which is outside of and wetter than the calibration period (Croley and Hartmann, 1986). The model also was used to simulate flows for the time period 1956-63, outside the period of calibration. The correlation of monthly flow volumes between the model and observed during this verification period are also contained in Table 1. They are a little lower than the calibration correlations but quite good except for Lakes Superior and Huron (there were less than two-thirds as many flow gages available for 1956-63 as for the calibration period for these basins). Likewise, lake evaporation models were verified over time periods independent of the calibration period (Croley, 1988). To assess the applicability of the process models to a climate warmer than the one under which they were calibrated and verified requires access to meteorologic data and process outputs for the warmer climate which unfortunately do not exist. Warm periods early in this century are not sufficiently documented for the Great Lakes. In particular, data are lacking on watershed runoff to the lakes, water surface temperatures, windspeed, humidity, cloudcover, and solar insolation.

It is entirely possible that the models are tied somewhat to the present climate; empiricism is employed in the evapotranspiration component of the LBRM and in some of the heat flux terms in the heat balance and lake evaporation model. Coefficients were determined or selected in accordance with the present climate. The models are all based on physical concepts that should be good under any climate; however, the assumption is made that they represent processes under a changed climate that are the same as the present ones. These include the rainfall-runoff concepts of linear reservoir moisture storages and partial-area infiltration as well as lake heat-storage relations with surface temperature and gray-body radiation. However, the calibration and verification periods for the component process models include a range of air temperatures, precipitation, and other meteorological variables that encompass much of the changes in these variables predicted for a changed climate. Even though the changes are transitory in the calibration and verification period data sets, the models appear to work well under these conditions.

CHAPTER III

SIMULATION METHODOLOGY

We constructed a master computer procedure that integrates the Large Basin Runoff Model, overlake precipitation estimates, lake evaporation models, the Lake Superior regulation plan, the Hydrologic Response Model, and the Lake Ontario regulation plan to provide a model of the entire Great Lakes system. We developed it specifically to look at the impact of changed climate by doing simulations with changed meteorology that represent scenarios of changed climate and comparing with simulations based on historical meteorology (representing an unchanged climate). Inputs are areal-average daily precipitation and maximum and minimum air temperatures for each of the 121 watersheds about the Great Lakes and areal-average daily air temperature, cloudcover, humidity, and windspeed for each of the five Great Lakes and Lake St. Clair. Outputs are organized into three groups corresponding to basin hydrology and runoff, overlake meteorology and evaporation, and net supplies to the lake and water levels.

STEADY-STATE CLIMATE CHANGE ASSESSMENTS

As instructed by EPA, our general procedure for the investigations of steady-state behaviour under a changed climate required that we first simulate 30 years of "present" lake levels by using historical daily maximum and minimum air temperatures, precipitation, windspeed, humidity, and cloud cover data for the 1951-80 period and present diversions and channel conditions; this is called the "base case" scenario. The initial conditions were arbitrarily set but an initialization simulation period of 1 January 1948 through 31 December 1950 was used to allow the models to converge to conditions (basin moisture storages, water surface temperatures, and lake levels) initial to the 1 January 1951 through 31 December 1980 period. We also then repeated the simulation with initial lake levels set equal to their averages over the simulation period until they were unchanging to facilitate investigation of "steady-state" conditions. Then we conducted simulations with adjusted data sets.

Ratios of "future" to "present" absolute air temperature, specific humidity, cloud cover, and precipitation, and differences of "future" and "present" windspeed were supplied by EPA as GISS (Goddard Institute of Space Sciences), GFDL (Geophysical Fluid Dynamics Laboratory), and OSU (Oregon State University) atmospheric model predictions, at grid points spaced 7.83 degrees latitude by 10 degrees longitude, 4.44 by 7.5, and 4 by 5 respectively, for a "future" atmosphere with twice the CO_2 content of the "present" atmosphere. We used these ratios or differences with the historic data to estimate 30-year sequences of atmospheric conditions associated with a changed climate, referred to as the "$2xCO_2$" scenario(s). We inspected each of the 770,000 square kilometers within the Great Lakes Basin to see which of the GISS or GFDL or OSU model grid points it was closest to and applied the monthly adjustment at that grid point to data representing that square kilometer. By combining all square kilometers representing a water shed or the lake surface, we derived an areally averaged adjustment to apply to our areally averaged data sets for the watershed or lake surface, respectively. We then used each $2xCO_2$ scenario in simulations similar to the base case scenario. As for the base case scenario, we repeated the simulation until the lake level averages, also used as initial conditions, were unchanging. We then interpreted differences between the $2xCO_2$ scenarios and the base case scenario as resulting from the changed climate.

Transfer of information between the general circulation models and our hydrologic models in the manner described involved several assumptions. Solar insolation at the top of the atmosphere and through the atmosphere on a clear day were assumed to be unchanged, modified only by cloud cover changes. Over-water corrections were made in the same way, albeit with changed air temperatures, water surface temperatures, humidities, and windspeeds, which presumed that over-water/over-land atmospheric relationships were unchanged. Our procedure for transfering information from the GCM grid to our spatial data is an objective approach but simple in concept. It ignores interdependencies in the various meteorologic variables as all were averaged in the same manner. Of secondary importance, the spatial averaging of meteorologic values over a GCM grid box filters all variability that exists in the GCM output over that grid box. If GCM output at the grid

box corners were supplied and interpolation between these point values were allowed, then at least some of the patial variability might be preserved. Of course, little is known about the validity of spatial linear interpolation and, for highly variable spatial data, it may be inappropriate. However, the same is true for the spatial averaging that was used to supply GCM results to us.

TRANSIENT-CASE CLIMATE CHANGE ASSESSMENTS

We simulated one transient scenario supplied by EPA: "GISS transient A." As instructed by EPA, our general procedure for the investigation of this transient-case behaviour under a changing climate required that we first simulate 80 years of "present" lake levels and component processes over the period 1981-2060. We did this by using historical daily maximum and minimum air temperatures, precipitation, windspeed, humidity, and cloud cover data for the 1951-80 period, repeated three times, and applied to initial conditions (basin storages, water surface temperatures, and lake levels) observed 1 January 1981; only the 80 years from 1 January 1981 through 31 December 2060 are of interest. We repeated three times the procedure developed for steady-state climate change investigations (reported above). The first simulation used initial conditions observed 1 January 1981; the second used the end-of-run conditions from the first simulation as initial conditions; and the third used end-of-run conditions from the second. The three simulations were combined to represent the entire period of interest. After this "base case" scenario was completed, we conducted simulations with adjusted data sets.

The EPA-supplied GISS transient A scenario consists of nine sets of monthly ratios for precipitation, air temperature, humidity, and cloud cover, and monthly differences for windspeed, one set for each decade from 1970-9 through 2050-9. These ratios or differences were between "present" and "future" values for each of the data and represent atmospheric model predictions for an increasing atmospheric-CO_2-content over the period 1971-2059. We used these ratios or differences by interpolating between decadal averages to obtain adjustments for each month of each year of the period 1981-2059 and by applying them in three simulations as for the base case: 1981-2010 adjustments to 1951-80 data for the 1981-2010 period simulation, 2011-40 adjustments to 1951-80 data for the 2011-40 simulation, and 2041-59 adjustments to 1951-1969 data for the 2041-59 simulation. We took the 2060 adjustment as the same as the 2059 adjustment, since the GISS scenario ended in 2059, and applied it to 1970 data for the 2060 simulation. Discerning the $2xCO_2$ signal from the historical variations in the adjusted data sets is enhanced by comparing values 30 years apart, thus eliminating the (repetitive) historical variations. A differencing approach that does this is described in the presentation of results. We combined ratios for each month of each year of the simulation from the nearest atmospheric model gridpoint for all square kilometers representing a watershed or the lake surface to derive an areally averaged adjustment to apply to our areally averaged data sets for each watershed or lake surface. We then used the transient scenario segments in simulations as we did with the original historical data, combining them to represent the entire period of interest and then interpreted differences between the transient scenario and the base case scenario as resulting from the changing climate.

CHAPTER IV

RESULTS

Steady-state behaviours in all aspects of the hydrological cycle are exemplified here in figures for the Lake Erie basin for the GISS and base case comparisons and summarized for all lakes and all climate-change scenarios for the entire period in tables. Transient behaviour simulations also are summarized here in tables.

CLIMATE CHANGE STEADY-STATE IMPACTS

Basin Meteorology

The $2xCO_2$ climate (GISS) air temperatures are higher throughout the annual cycle than the $1xCO_2$ climate (base case); the difference is smaller during the summer than during the winter for all lakes but smallest for the northernmost lakes (Superior, Michigan, and Huron); see Figure 1. The average steady-state GISS air temperatures are 4.2 to 4.7°C higher, depending on the basin; see Table 2 for this and other scenarios. The $2xCO_2$ climate precipitation is similar in the winter, spring, and summer to the $1xCO_2$ climate precipitation over all of the Great Lake basins; see Figure 1. In the fall, the $2xCO_2$ climate precipitation is significantly higher than in the $1xCO_2$ climate on the Superior basin but significantly lower on the other basins. The average steady-state GISS annual precipitation is 148 mm higher over the Superior basin (expressed as a depth over the land portion of the basin) to 66 mm lower over the Ontario basin with a fairly smooth change with longitude; see Table 2. Precipitation changes are much less consistent than air temperature changes between the various GCMs and the different lakes as illustrated in Table 2.

Basin Hydrology

The resulting average steady-state GISS evapotranspiration from the land portion of the basin is higher for the $2xCO_2$ climate in all cases, with a fairly smooth change with latitude from 153 mm higher over the Superior basin to 65 mm higher over the Huron basin to 87 mm higher over the Ontario basin; see Figure 1 and Table 2. Runoff from the land portion of the basin is reduced by the $2xCO_2$ climate in all basins, changing for the GISS scenario from only 7 mm lower over the Superior basin to 153 mm lower over the Ontario basin in a smooth variation with longitude; see Table 2. The average annual cycle of runoff, depicted in Figure 1, has changed as well; run off peaks slightly earlier and with smaller magnitude under the $2xCO_2$ climate than under the $1xCO_2$ climate. This is largely the result of the very big changes observed in the snowpack accumulation and ablation as well as other basin moisture storages.

In the GFDL climate scenario, evapotranspiration sometimes appears limited by available water. Note in Table 2 on the Superior and Michigan basins that since precipitation decreases under the GFDL scenario and increases under the GISS or OSU scenarios, less water is available in these basins for evapotranspiration in the GFDL scenario than in either the GISS or OSU scenarios. Thus, even though air temperatures are higher under the GFDL scenario than under the others (and more heat is available to drive evapotranspiration), less actual evapotranspiration occurs under the GFDL scenario. On the other basins, precipitation increases under the GFDL scenario enough so that water availability is not so limiting, and evapotranspiration is greater for the GFDL scenario than for either the GISS or OSU scenarios. In comparing the OSU and GISS scenarios, water availability is not as limiting under the GISS scenario for the Superior and Michigan basins and more evapotranspiration occurs. For the other basins, GISS water availability is more limiting and less evapotranspiration occurs under the GISS scenario than under the OSU scenario.

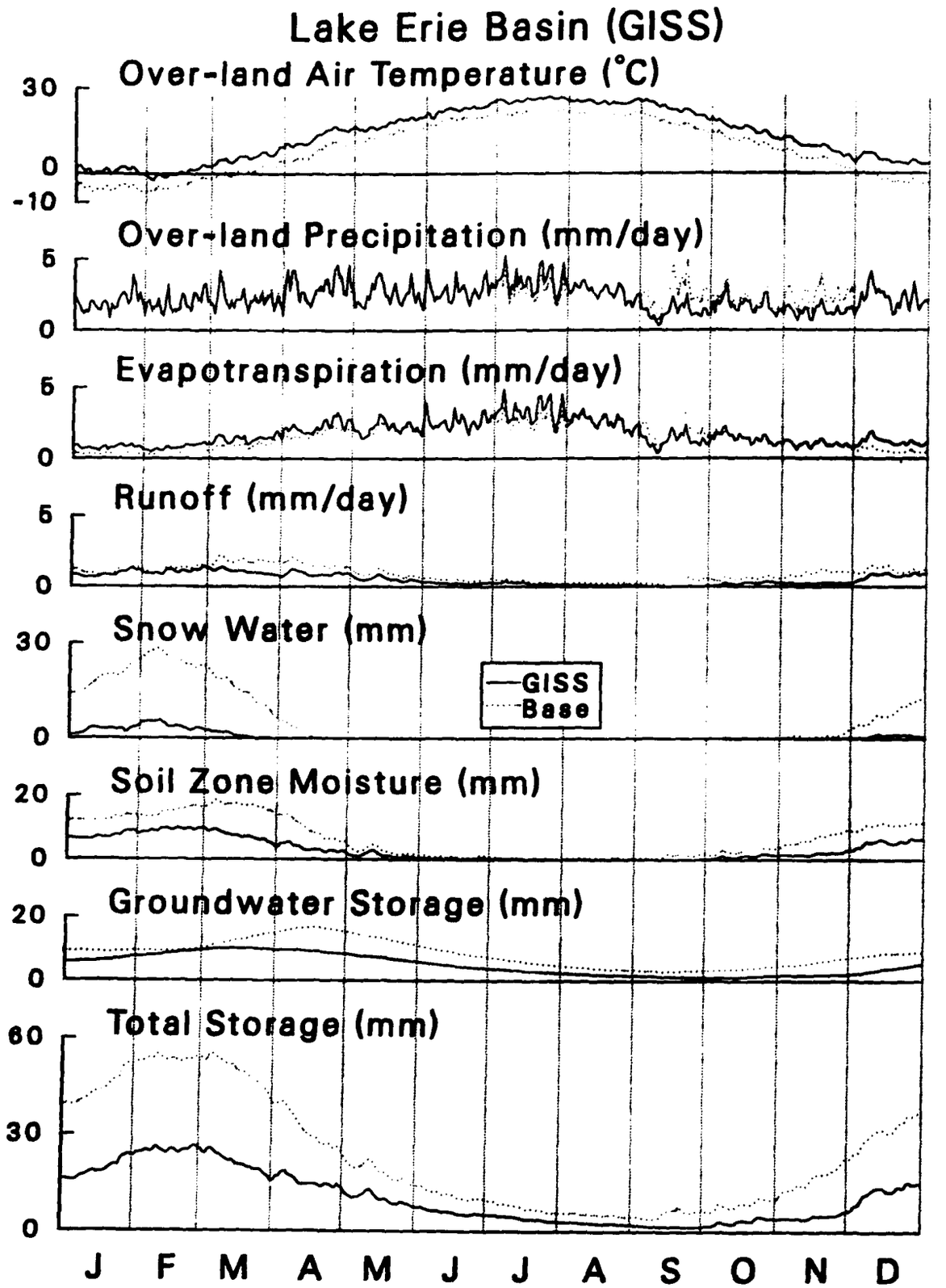

Figure 1. Steady-state GISS Lake Erie over-basin model outputs.

Table 2. Average Annual Steady-State Basin Hydrology Differences.

Basin	Air Temperature (°C)			Precipitation (mm)[1]			Evapo-transpiration (mm)[1]			Runoff (mm)[1]		
	GISS	GFDL	OSU	GISS	GFDL	OSU	GISS	GFDL	OSU	GISS	GFDL	OSU
Superior	4.3	7.2	3.4	148	-36	58	153	66	88	-7	-102	-31
Michigan	4.7	6.2	3.5	16	-8	42	92	76	85	-76	-84	-43
Huron	4.6	6.4	3.3	-43	28	46	65	99	81	-109	-71	-35
St. Clair	4.7	5.7	3.4	-53	56	51	78	119	113	-132	-64	-63
Erie	4.7	5.7	3.4	-53	48	54	85	121	119	-139	-74	-65
Ontario	4.6	5.9	3.2	-66	27	74	87	111	104	-153	-84	-30

[1]Expressed as a depth over the land portion of the basin.

On the Superior basin, the average steady-state snowpack storage is reduced by more than half; on the other basins, more to the south, the snowpack is almost entirely absent under the GISS $2xCO_2$ climate; see Figure 1 and Table 3. This reduction in snowpack accumulation results from the higher air temperatures, especially during the winter, that accompany the changed climate. The snow season (period of freezing air temperatures) is shortened also two weeks to one month under the GISS scenario. The effects on the snowpack are felt throughout the basin in terms of the derived moisture storages in the soil zone, groundwater, and surface zones. Figure 1 illustrates the general impact on all Great Lake basins of generally lower moisture storages that peak earlier in the $2xCO_2$ climate than in the $1xCO_2$ climate scenarios. This general lowering of moisture in storage in each of the basins is summarized in Table 3 and in some cases represents greater than a 50% reduction in available moisture (see "Total Basin Storage" column).

Over-Water Meteorology

The over-lake air temperature, humidity, and wind speed differ from over-land since the lower atmospheric layer is affected by the water surface over which it lies. The model corrections to over-land meteorology observations for over-water conditions depend heavily on the water surface and over-land air temperature which in turn are a function of the over-lake meteorology and heat balance at the surface of the lake. Figure 2 illustrates the GISS and base case annual cycles for Lake Erie in over-lake meteorology and heat balance effects. Note that monthly changes from the GISS scenario superimposed on a daily time series creates discontinuities between months that are reflected in some outputs in Figure 2 (e.g., November-December cloud cover and July-August wind speed). In general, for all $2xCO_2$ scenarios, the synergistic relationship that exists between air and water temperature yields a general increase in both that follows the $1xCO_2$ climate patterns, similar to over-land behaviour in Figure 1. Table 4 shows that the average steady-state air temperature difference between the GISS and base cases varies from 4.3°C on Lakes Michigan, Erie, and Ontario to 5.5°C on Lake Superior. An increase with latitude is more pronounced than variation with size of the lake in terms of volume or heat capacity, although Lake Superior not only has the largest rise in over-lake air temperatures but also has the largest rise relative to over-land air temperature rise, probably reflecting the large heat storage capacity influence on the air layer over the lake. Absolute humidities over the lakes have increased appreciably for the $2xCO_2$ climate, while cloud cover and over-water wind speed have dropped after adjustment of over-land values for over-water conditions at increased water temperatures.

Table 3. Average Annual Steady-State Basin Storages Differences.

Basin	Snow Pack Water Equivalent (mm)[1]			Soil Moisture (mm)[1]			Groundwater Moisture (mm)[1]			Total Basin Storage (mm)[1]		
	GISS	GFDL	OSU	GISS	GFDL	OSU	GISS	GFDL	OSU	GISS	GFDL	OSU
Superior	-31	-39	-19	-1	-9	-3	-1	-26	-11	-29	-86	-37
Michigan	-11	-11	-9	-8	-9	-4	-13	-14	-6	-34	-36	-20
Huron	-25	-26	-20	-14	-10	-4	-3	-2	-1	-44	-40	-25
St. Clair	-8	-8	-7	-3	-2	-2	-4	-2	-2	-16	-12	-11
Erie	-5	-5	-5	-4	-3	-2	-4	-2	-2	-13	-10	-9
Ontario	-15	-16	-13	-6	-4	-2	-4	-2	-1	-30	-24	-17

[1]Expressed as depths over the land portion of the basin.

Lake Heat Balance

The heat budget gives rise to increased water surface temperatures as seen in Figure 2 and summarized in Table 5. Since Lake Erie is a very shallow lake, the annual cycle of the $2xCO_2$ climate water surface temperatures follows a pattern very similar to the $1xCO_2$ climate but several degrees higher. The average steady-state water surface temperature increase for the GISS scenario ranges from 4.3 °C on Lake St. Clair to 5.6°C on Lake Superior, reflecting again the influence of heat storage capacity in a lake. The heat storage capacity of a lake has another influence on the increase in water surface temperatures that cannot be seen in Table 5. The higher heat content of Lake Superior earlier in the year allows the $2xCO_2$ climate water surface temperatures to peak earlier than the $1xCO_2$ climate; as over-lake air temperatures are affected by the water temperatures, they also peak ahead of the base case for Lake Superior. Lake Superior then behaves under the warmer climate as do the deep lakes to the south under the current climate; average surface temperatures peak in August (currently September for Superior) as the climate for Superior becomes more like the warmer southern climates. Large amounts of heat now reside in the deep lakes throughout the year. All of the deep lakes (Superior, Michigan, Huron, and Ontario) show water surface temperatures that stay above 3.98°C (at which water density is maximum) throughout the average annual cycle for all scenarios (actually the OSU scenario on Lake Superior did result in two out of thirty years when surface temperatures dipped below 3.98 degrees). This means that buoyancy-driven turnovers of the water column would not occur. It also means that ice formation will be greatly reduced over winter on the deep lakes.

Note that as the average air temperature increases between scenarios, the average water surface temperature increases at a reduced rate (this rate further decreases at higher air temperature rises). For example on Lake Superior, the OSU scenario increases over-land air temperatures 3.4°C over the base case, the GISS scenario increases them further an additional 0.9°C to 4.3°C over the base case), and the GFDL scenario increases them another 2.9°C (to 7.2°C over the base case, see Table 2). The rises between scenarios of 0.9 to 2.9°C result in rises in water surface temperatures, repsectively, of 0.8 and 1.8°C; see Table 5. (This is true on all lakes for all air temperature increases between scenarios with the minor exception of Lake Michigan between the OSU and GISS scenarios.) Part of the reason for this is that water sureface tempertures are lower bounded at the freezing point while air temperatures are not. However, it is also true that the deep lakes show smaller rises in water surface temperatures during the fall (including the August peak in surface temperatures) and winter than do the air temperatures, between the base case and each of the scenarios. This

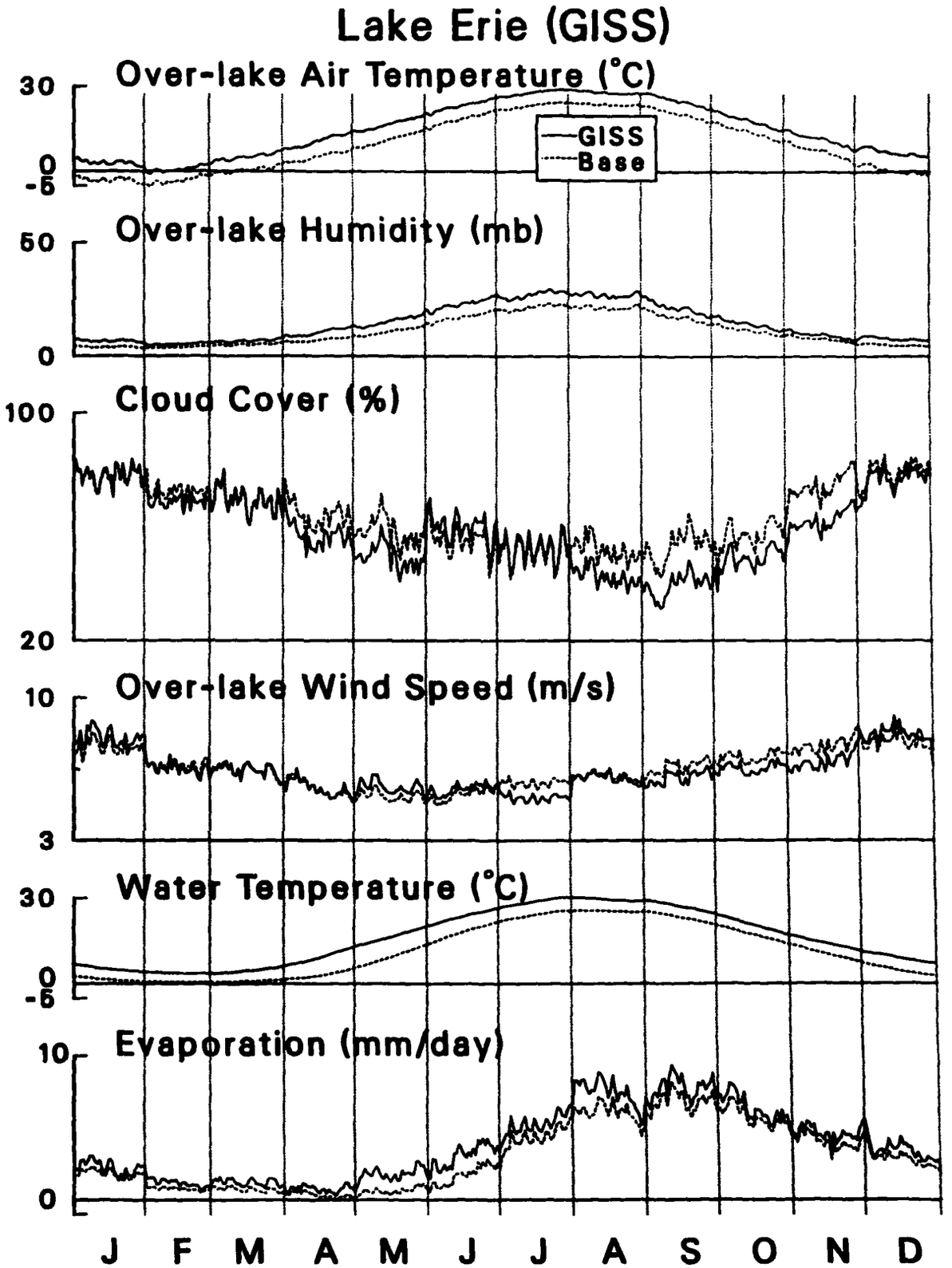

Figure 2. Steady-state GISS Lake Erie over-lake model outputs.

Table 4. Average Annual Steady-State Over-Lake Meteorology Differences.

Basin	Air Temperature (Deg C)			Absolute Humidity (mb)			Cloud Cover (%)			Wind Speed (m/s)		
	GISS	GFDL	OSU	GISS	GFDL	OSU	GISS	GFDL	OSU	GISS	GFDL	OSU
Superior	5.5	7.0	4.5	4.4	6.1	3.7	-1.1	-5.8	-4.2	-0.1	-0.2	0.0
Michigan	4.9	6.0	3.5	4.4	5.7	3.2	-0.1	-2.0	-2.6	-0.2	-0.4	-0.1
Huron	5.1	6.6	3.7	4.1	5.5	3.0	-4.4	-2.8	-3.4	-0.1	-0.2	0.0
St. Clair	5.1	5.9	3.8	5.4	6.4	3.7	-3.7	-2.9	-2.6	-0.1	-0.3	-0.1
Erie	4.9	5.6	3.4	5.1	5.8	3.5	-4.9	-4.1	-3.6	-0.1	-0.3	-0.1
Ontario	4.9	5.9	3.5	4.6	5.8	3.3	-4.8	-5.4	-3.2	-0.1	-0.3	0.0

Table 5. Average Annual Steady-State Lake Surface Temperature and Evaporation Differences.

Basin	Water Surface Temperature (Deg C)			Overlake Evaporation (mm[1])		
	GISS	GFDL	OSU	GISS	GFDL	OSU
Superior	5.6	7.4	4.8	152	284	173
Michigan	4.7	5.5	3.4	176	279	179
Huron	4.7	6.0	3.6	199	297	166
St. Clair	4.3	5.0	3.0	297	408	262
Erie	4.4	5.0	3.0	290	414	232
Ontario	4.9	5.9	3.6	213	281	172

[1]Expressed as a depth over the lake.

is not illustrated well in Figure 2 for Lake Erie, but is very prominent on all deep lakes. Even in comparing cool and warm years from the historical record, where there are comparable rises in spring and summer air and water temperatures, the fall and winter rises of surface temperature are smaller than the air temperature increases. The point is that air temperature rise is only a partial indication of what can be expected of water surface temperatures. Water temperatures depend on the total heat balance of the lake with the atmosphere which, in turn, depends on changes in humidity, wind speed, and cloud cover in addition to air temperatures. As average air temperatures increase, the average water surface temperatures (in particular, the surface temperatures during the evaporation season of fall and winter) generally increase at lower rates and the rate decreases as air temperatures rise. This is contrary to standard assumptions in other works that do not perform heat balances to determine surface temperatures but set surface temperature rises equal to air temperature rises (Cohen, 1986, 1987). However, the evaporation computations are found to be very sensitive to this assumption since the fall

and winter are when most of the evaporation occurs on all of the lakes. At high air-water temperature differences, the effects of humidity and wind speed changes are secondary to the temperature (and hence vapor pressure) differences, and large evaporation may be calculated even with offsetting humidity and wind speed changes as evident in Tables 4 and 5. At lower air-water temperatures, the effects of the humidity and wind-speed changes become primary in determining the relative magnitudes of evaporation between the various scenarios.

The higher water surface temperatures under the $2xCO_2$ climate result in increased annual lake evaporation ranging from 152 mm over Lake Superior to 297 mm over Lake St. Clair for GISS; see Table 5. The shallow lakes have the highest increase in evaporation under all $2xCO_2$ scenarios while the deep lakes have similar (but smaller) increases. Note that the Lake Michigan evaporation may be suspect because no data were used in the calibration of the Lake Michigan heat balance; calibrated parameters from Lakes Huron, Erie, and Ontario were adapted for use on Lake Michigan. Note that while average humidities are up and average windspeeds are down in Table 4 (by themselves suggesting that evaporation drops), evaporation in Table 5 is higher. This is because the water surface temperature (and associated saturated vapor pressure at the surface) has increased sufficiently to over-compensate the rise in atmospheric humidity (the average vapor pressure difference between the water and the air has increased) and drop in wind speed. Interestingly, the Lake Superior evaporation under the GISS scenario is less than that under the OSU scenario even though GISS water surface temperatures rise more than OSU (compare 5.6 to 4.8 degrees, respectively, in Table 5). However, inspection shows that with the increase in air temperatures consequent with the GISS scenario, the over-land air-water temperature difference (see Tables 2 and 5) drops less than with the OSU scenario (4.3 - 5.6 = -1.3 for GISS and 3.4 - 4.8 = -1.4 for OSU); this means that air stability over the lake is larger generally with the GISS scenario than with the OSU scenario, resulting in larger over-lake air temperature and dewpoint corrections toward the water surface temperatures. Resulting air-water vapor pressure differences and windspeeds are lower (the latter is reflected in Table 4) with consequent lower evaporation.

Net Supply Components

Over-lake precipitation, runoff, and lake evaporation sum algebraically as the net basin supply and are presented again in Figure 3 for convenience. Since over-lake precipitation is taken here as the same as over-land, Figure 3 and Table 6 show the same relations for GISS vs. base case precipitation as does Figure 1 and Table 2. Runoff in Figure 3 is the same as in Figure 1 except it is expressed as a depth rate over the lake rather than over the basin. Net basin supply in the GISS scenario in Figure 3 is seen to be uniformly less under the $2xCO_2$ climate than under the $1xCO_2$ climate; this is true for Lakes St. Clair and Erie. It is nearly true on Lakes Huron (only January supplies are higher) and Ontario (only January and February supplies are higher); Lake Michigan supplies are smaller 75% of the time and Lake Superior supplies are smaller only about half of the time. Lake Superior experiences increased net basin supplies during the fall, and winter under the $2xCO_2$ climate and Lake Michigan has increased net basin supplies during the winter. This leads to a reduced drop in the average steady-state net basin supply on Lakes Superior and Michigan for the GISS scenario; it significantly drops for all other Great Lakes and all other scenarios as shown in Table 6. The GISS scenario in Table 6 results in a larger precipitation rise and a smaller drop in basin runoff for Lake Superior than do either the GFDL or OSU scenarios, resulting in higher net basin supply (and lower difference with the base case) than for these other scenarios. Lake Michigan shows a larger precipitation rise for the GISS scenario than for either Figure 3. Steady-state GISS Lake Erie lake-level model outputs.of the other two and a smaller drop in basin runoff for the GISS scenario than for the GFDL. On the remaining lakes, the GISS scenario results in drops in over-lake precipitation (instead of rises as with the GFDL and OSU scenarios) and larger drops in basin runoff than do the other scenarios, resulting in larger drops in net basin supplies for the GISS scenario. Table 7 summarizes the changes in the net basin supply components for the entire Great Lakes basin; they were computed by converting the equivalent depths of Table 6 to annual flow rates on each lake and adding them over all the lakes. The changes from the base case are also expressed relatively in Table 7. Even though more heat is available under the GFDL scenario than under the GISS or OSU scenarios, evapotranspiration is lower because less water is available, as seen by inspection of the average precipitation in Table 7. In the OSU and GISS scenarios, water availability is not as limiting and the higher air temperatures of the GISS scenario lead

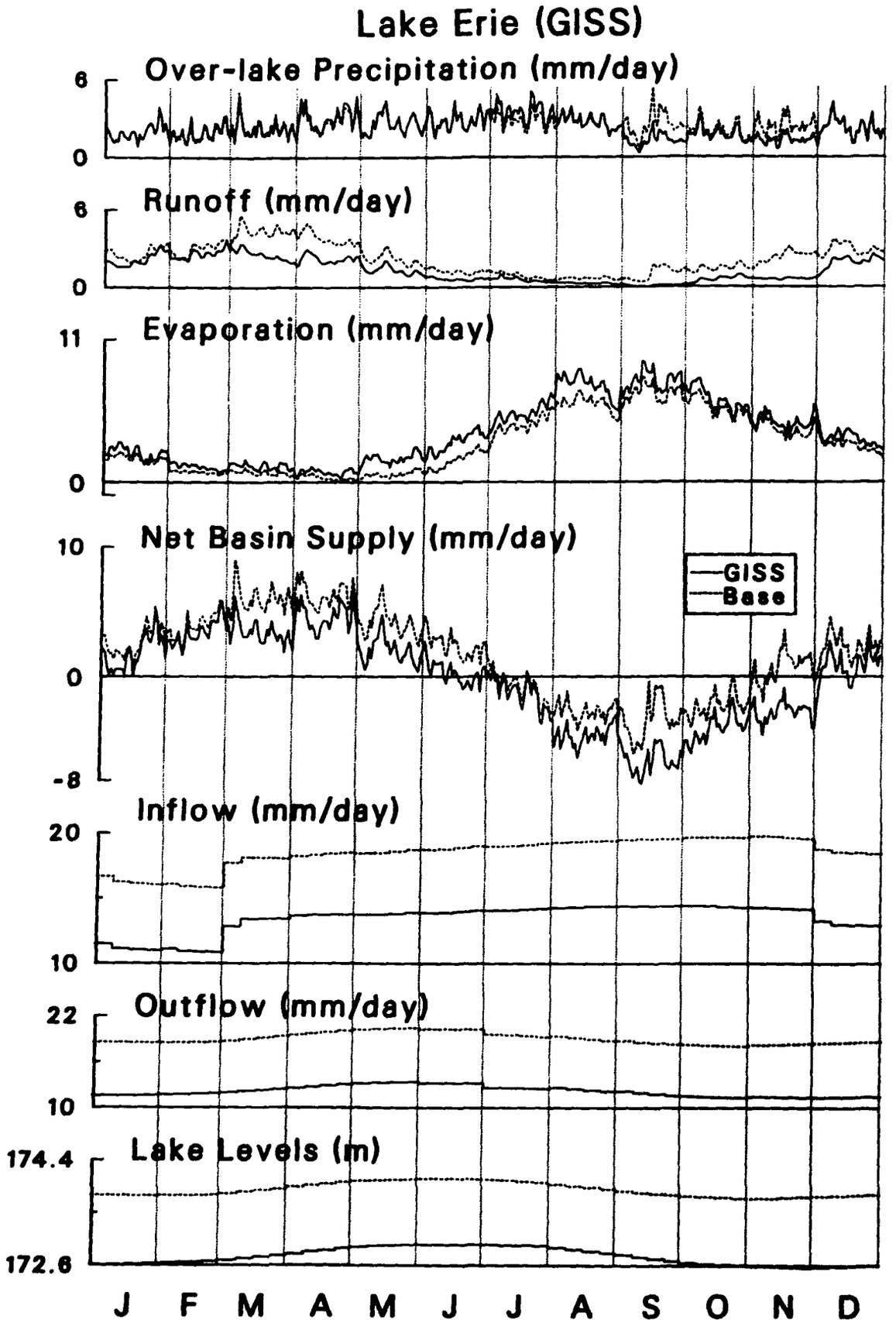

Figure 3. Steady-state GISS Lake Erie lake-level model outputs.

Table 6. Average Annual Steady-State Net Supply Components Differences.

Basin	Over-Lake Precipitation (mm)[1]			Basin Runoff (mm)[1]			Over-Lake Evaporation (mm)[1]			Net Basin Supply (mm)[1]		
	GISS	GFDL	OSU	GISS	GFDL	OSU	GISS	GFDL	OSU	GISS	GFDL	OSU
Superior	148	-36	58	-11	-159	-48	152	284	173	-16	-479	-163
Michigan	16	-8	42	-152	-168	-87	176	279	179	-312	-455	-223
Huron	-43	28	46	-241	-158	-78	199	297	166	-483	-427	-197
St. Clair	-53	56	51	-1870	-901	-891	297	408	262	-2219	-1252	-1102
Erie	-53	48	54	-328	-173	-153	290	414	232	-671	-540	-331
Ontario	-66	27	74	-565	-311	-112	213	281	172	-844	-564	-210

[1]Expressed as depths over the lake.

Table 7. Average Annual Steady-State Great Lakes Basin Hydrology and Net Basin Supply Components.

Scen-ario	Over Land Precip-itation (cms)	Evapo-trans-piration (cms)	Basin Runoff (cms)	Over Lake Precip-itation (cms)	Over Lake Evap-oration (cms)	Net Basin Supply (cms)
BASE	13637	7727	6090	6499	5352	7237
GISS	13871 +2%	9317 -21%	4658 -24%	6747 +4%	6821 +27%	4584 -37%
GFDL	13725 +1%	9176 -19%	4714 -23%	6501 +0%	7685 +44%	3530 -51%
OSU	14483 +6%	9204 -19%	5438 -11%	6903 +6%	6745 +26%	5596 -23%

to higher evapotranspiration than in the OSU scenario even though more water is available under the OSU scenario. Note also that in Table 6, the lesser drops in net basin supplies for the GISS scenario compared to the GFDL scenario for Lakes Superior and Michigan offset the greater GISS drops for all other lakes, so that the total GISS net supply drop over all basins is smaller than the overall GFDL drop and the summed net basin supplies in Table 7 are lower under the GFDL scenario than under the GISS scenario.

Lake Water Balance

Results in Figure 3 reveal that river inflow and outflow make up a large part of the water budget of Lake Erie, and drops in Lake Erie inflows are accompanied by drops in outflows. The drop in lake levels comes from the drop in net basin supplies and the net drop in inflows and outflows is only partly offsetting. Table 8 shows that Lake Erie's average GISS steady-state inflow minus its outflow rises 656 mm (compare to the drop in net basin supplies of 671 mm) while lake levels drop about 1.16 m. Similar drops in net flows are observed on all lakes under all scenarios and the lake levels drop on all of the Great Lakes. Some of the planned results were not obtainable because of failure of the regulation plan(s) under the climate change scenarios. As earlier

Table 8. Average Annual Steady-State Flows Differences.

Basin	Inflow (mm[1])			Outflow (mm[1])		
	GISS	GFDL	OSU	GISS	GFDL	OSU
Superior	-	-	-	-14	-	-162
Michigan-Huron	-10	-	-113	-386	-	-312
St. Clair[2]	-40628	-	-32892	-42831	-	-33980
Erie	-1857	-	-1473	-2513	-	-1794
Ontario	-3407	-	-2432	-	-	-

[1]Expressed as a depth over the lake.
[2]Lake St. Clair inflows and outflows are relatively large since it is such a small lake (wide spot on the river).

Table 9. Average Annual Steady-State Lake Levels Differences.

Basin	GISS (m)	GFDL (m)	OSU (m)
Superior	-0.46	-	-0.47
Michigan-Huron	-1.31	-2.48	-0.99
St. Clair	-1.21	-2.12	-0.87
Erie	-1.16	-1.91	-0.79
Ontario	-	-	-

climate change and consumptive use studies by others have found, the Lake Ontario regulation plan's mathematical algorithms behave erratically under extreme low water supply conditions (F.H. Quinn, GLERL, personnel communication, 1988; C. Southam, Environment Canada, personal communication, 1988).

The average steady-state lake-level difference summary for all $2xCO_2$ scenarios is given in Table 9. The GFDL scenario produced such low water supplies to Lakes Superior and Michigan that the rule curves of both regulation plans (Lakes Superior and Ontario) failed. The Lake Superior regulation plan uses a balancing approach that attempts to consider the impacts of regulation as well on Lakes Michigan and Huron. However, the balancing equation fails when Lake Superior's levels become too low. To get some idea of system behaviour under the GFDL scenario without using many different regulation rules to avoid ambiguity, Lake Superior outflows were taken equal to Lake Superior net supplies and other inputs (e.g., Long Lac diversions) on an annual basis. This probably is correct over long periods (actual Lake Superior net basin supplies plus diversions differ from the St. Mary's River outflows by less than 1% over 1951-80) and, for the 30-yr period used herein, gives an estimation of long-term differences in lake levels. No attempt was made to determine what Lake Ontario levels might be. The Lake Superior net supplies and Long Lac diversions (Ogoki diversions are already included in the net basin supplies) were used as the St. Marys River flows with the GLERL Hydrologic Response Model. The lakes drop more under the GFDL and GISS scenarios than under the OSU scenario because of their much larger drops in net supplies to all lakes but Superior than is observed under the GISS scenario. Lake

Superior drops more under the OSU scenario since GISS supplies are not reduced as much, as discussed above. GFDL has smaller drops in net basin supplies than GISS for Lakes Huron, St. Clair, Erie, and Ontario yet larger drops in the water levels on these lakes because of its larger drop in supplies to Lakes Superior and Michigan which affect inflows to lower lakes and offset the reduced drops in supplies there. Because the GISS scenario shows larger drops in net basin supply on the remaining downstream lakes than the GFDL and OSU scenarios, the drops in lake levels in Table 9 under the three scenarios approach each other somewhat on the downstream lakes. The lake levels drop 40 to 130 cm for the GISS scenario, 190 to 250 cm for the GFDL scenario, and 50 to 100 cm for the OSU scenario.

CLIMATE CHANGE TRANSIENT IMPACTS

There are serious difficulties in analyzing transient impacts of climate change with short historical data sets as outlined under "Methodology." In simulating 80 years (1981-2060) by using 30 years of historical data (1951-80) repeated three times (for the 1981-2010, 2011-2040, and 2041-2060 periods), the variations contained in the historical record repeat, of course. As corrections to the historical data are made to reflect the transient GISS climate changes, it is found that the repeating fluctuations of the historical record so completely dominate the superimposed climate changes that it is difficult to see the effect of climate change. Thirty-year averages could be used to filter historical variations for presentation of results; however, only two complete 30-yr periods are contained in the simulation and a 30-yr average filters some of the climate change as well. A differencing approach is used here to give a very general idea of transient behaviour; it works by comparing transient behaviours 30 years apart to eliminate the effect of the historical variations. By comparing the GISS and base cases transient simulation changes for decades 1, 4, and 7 (1981-90, 2011-20, and 2041-50, which are all based on the same 1951-60 data period), decades 2, 5, and 8 (1991-00, 2021-30, and 2051-60, which are all based on the same 1961-70 data period), and decades 3 and 6 (2001-10 and 2031-40, which are both based on the same 1971-80 data period) in the tables following, the effect of the repetitive natural variations is eliminated since the same underlying historical data segments are used in each grouping. The climate change trends then can be identified.

As an example of applying this differencing approach, decadal-average annual changes in air temperature between the 80-year base case and transient simulations are given in Table 10 for Lake Superior; air temperature is increasing on the order of about 1.6°C per 30-yr period. This is found by subtracting GISS-base changes for decade 1 from 4, 4 from 7, 2 from 5, 5 from 8, and 3 from 6 and averaging to get, respectively: 0.9 + 1.9 + 1.3 + 2.3 + 1.8 = 8.2, and dividing by 5 (the number of comparisons) to get 1.64 per 30 years. This is more conveniently expressed as 0.5°C per decade. Other hydrometeorological quantity variations are computed in the same way and are summarized in Table 11.

Table 10. Lake Superior Basin Transient GISS Decadal-Average Annual Over-Land Air Temperature Changes from Base Case (°C).

Decade	1981-90	1991-00	2001-10	2011-20	2021-30	2031-40	2041-50	2051-60
Number	1	2	3	4	5	6	7	8
	0.7	0.9	1.2	1.6	2.2	3.0	3.5	4.5

On Lake Superior, precipitation increases are partially offset by evapotranspiration increases so that annual runoff, expressed as a depth over the land portion of the basin, increases about 4 mm each decade. All other lakes show a drop in annual runoff of 7-15 mm/decade. The average snowpack accumulates about 1-4 mm less each decade, and average soil zone moisture and groundwater generally drop 0.3-1 mm/decade (except on Superior); the resultant effect is a lowering of total basin moisture storage about 0.1-5 mm/decade. Over-lake

air temperatures increase at about the same rate as over-land average air temperatures. Over-lake humidity generally increases slightly (but negligibly) each decade; note however that while it is corrected for over-water conditions in the simulations, it is not computed by taking increased evaporation into account. Rather, over-land humidity is supplied in the GISS atmospheric model outputs (inputs to this simulation).

Cloud cover generally decreases slightly (but negligibly) and is not influenced by these simulations; it is strictly an input here from the GISS atmospheric model. Over-lake wind speed is almost not affected and the water surface temperature increases by about 0.5-0.7°C each decade. Resultant annual lake evaporation increases 18-40 mm/decade. Net basin supplies are highly variable but generally drop on all lakes except Superior. These changes in net supplies are reflected in changes in outflows and lake levels. The increased supplies to Lake Superior are more than offset by increases in net outflow, which results in a small decline in Superior water levels of about 13 mm/decade. The associated rise in the combined Michigan and Huron inflows allows the annual net outflow in Table 11 to drop only 31 mm/decade; their combined net supplies drop more allowing lake levels to fall about 59 mm/decade. This is a consequence of the Lake Superior regulation plan, which endeavors to balance water levels on Lakes Superior, Michigan, and Huron about their long-term mean values. On the lower lakes, there are drops in net basin supplies, net outflows, and lake levels; Lake St. Clair drops about 64 mm/decade, while Lake Erie drops about 66 mm/decade and Lake Ontario drops about 93 mm/decade. Only the first seven decades were used in computing the average decadal difference in net outflows and lake levels for Lake Ontario, since the regulation plan failed in the eighth decade. Note that while there are similar patterns in the behaviour of the lake levels between this transient analysis and the GISS steady-state analysis (see Table 9), the magnitudes of the drops are dissimilar (while of the same general order of magnitude).

Table 11. GISS Transient Changes Summary.

Hydrological Variable	Units	Basin					
		Sup.	Mic.	Hur.	StC.	Eri.	Ont.
Basin Air Temperature	(°C/dec):	+0.5	+0.6	+0.6	+0.6	+0.6	+0.6
Annual Basin Precipita.[1]	(mm/dec):	+29	+7	+2	-0	+3	+1
Annual Basin Evapotrans.[1]	(mm/dec):	+25	+14	+12	+15	+16	+16
Annual Basin Runoff[1]	(mm/dec):	+4	-7	-9	-15	-15	-14
Snowpack[1]	(mm/dec):	-4	-1	-4	-1	-0.7	-2
Soil Moisture[1]	(mm/dec):	+0.5	-0.8	-1	-0.4	-0.4	-0.6
Groundwater[1]	(mm/dec):	+2	-1	-0.3	-0.4	-0.4	-0.3
Total Basin Moisture[1]	(mm/dec):	-0.1	-4	-5	-2	-2	-4
Lake Air Temperature	(°C/dec):	+0.7	+0.6	+0.6	+0.6	+0.6	+0.6
Lake Humidity	(mb/dec):	+0.6	+0.5	+0.5	+0.7	+0.7	+0.6
Lake Cloud Cover	(%/dec):	+0.1	-0.2	-0.5	-0.4	-0.5	-0.5
Lake Wind Speed	(m/s/dec):	+0.0	+0.0	+0.0	+0.0	+0.0	-0.0
Surface Temperature	(°C/dec):	+0.7	+0.5	+0.6	+0.5	+0.6	+0.6
Annual Lake Evaporation[2]	(mm/dec):	+18	+19	+22	+38	+40	+24
Annual Net Basin Supply[2]	(mm/dec):	+17	-27	-41	-245	-75	-75
Annual Net Outflow[2]	(mm/dec):	+20	-31		-241	-70	-57[3]
Lake Level	(mm/dec):	-13	-59		-64	-66	-93[3]

[1]Expressed as a depth over the basin.
[2]Expressed as a depth over the lake.
[3]Computed over first 7 decades since Ontario regulation plan fails in eighth.

SENSITIVITIES

Without temperatures below freezing, the snowpack is insensitive to precipitation. Although the GISS, GFDL, and OSU scenarios show conflicting estimates of possible precipitation changes, each shows increases in air temperatures that significantly reduce snowpack storage, especially in the southern Great Lakes basin. Thus, even if precipitation increases are larger than any suggested by the GCMs, snowpack will be much reduced under warmer winters. Similarly, regardless of actual changes in precipitation, the Great Lakes basin will experience reductions in soil moisture storage and runoff. Soil moisture and runoff peak shortly after snowmelt and then drop throughout the summer and fall due to high evapotranspiration demands; each climate scenario produces earlier snowmelt and a longer period of evapotranspiration. Although soil moisture and runoff certainly vary with precipitation, they are most sensitive to it in midsummer when at their annual minimums. Thus, within the limits of precipitation produced by the GCMs, soil moisture and runoff scenarios are fairly insensitive to precipitation.

Of the meteorological variables that affect lake evaporation (air temperature, humidity, cloud cover, and wind speed) wind speed is probably the most critical, although air temperature and humidity are also important. Over-lake evaporation is very sensitive to the air temperature increase inherent in the scenario, which governs the sensitivity to humidity and wind speed changes. In the range of air temperature increases considered for the steady-state scenarios, the higher temperature rises associated with the Lake Superior GISS scenario compared to the OSU scenario increased over-lake air stability to such an extent that evaportion actually decreased compared to the OSU scenario, and this was not true with smaller air temperature rises. For the smaller air temperature rises, there was more opportunity for increases in evaporation since the rise in water surface temperatures (and vapor pressure difference with the atmosphere) compensated for the slighter drop in wind speed and rise in atmospheric humidity. That this turn around point in the behaviour of evaporation occurred in the range of climate variations considered under the three climate change scenarios, showing the uncertainty that may be associated with climate change evaporation estimates.

Because net basin supplies are a simple addition of lake evaporation, runoff, and precipitation, they are equally sensitive to changes in any of the components. Inspection of Table 7 reveals much greater variability in the estimates of the net basin supplies across the different scenarios than in the components. Partly, this is because limits were reached (as in the case of limiting water availability for evapotranspiration under the GFDL scenario or in the case of air temperature increases resulting in increases in stability and drops in lake evaporation under the GISS Superior scenario), but this also illustrates the potential for uncertainty in changes in estimated net supplies (and lake levels).

CHAPTER V

IMPLICATIONS OF RESULTS

Climate change has the potential to alter many traditional activities in the Great Lakes region. Although changes in lake levels have major implications for Great Lakes users, altered precipitation, evaporation, and runoff patterns will be important as well. Environmental implications and socioeconomic implications are addressed separately herein; however, these concerns are often intimately intertwined since a healthy ecosystem is vital for the social or economic well-being of a number of interests (e.g., riparian, commerical fishing, recreation, commercial interests) and some issues (e.g., disposal of toxic dredge spoil) combine environmental, social, and economic dimensions.

ENVIRONMENTAL IMPLICATIONS

Lowering of Great Lakes levels could dramatically affect the Great Lakes' ecosystem production through dependence on the consistent availability of marshes and wetlands that serve as breeding and nursery areas for fish and wildlife. Even a 20-cm lowering of Lake Michigan-Huron levels could affect 64% of all Great Lakes wetlands in the U.S. (Manny, 1984). Although confined wetlands may be especially vulnerable to disruption from lake level declines (Wall, 1988), even open shoreline wetland extents could be permanently reduced due to their direct lake level dependence, unsuitable offshore substrates, and steep offshore dropoffs, combined with a resulting reduction in seeds and rhizomes for colonization (Manny, 1984). On the other hand, the total areas of different wetland types may remain nearly unchanged if water levels drop so slowly that the shoreline can adapt (Meisner et al., 1987).

Decreased wetland extents could significantly reduce Great Lakes fisheries production, even in deeper waters; over half of all Great Lakes fish species use wetlands for spawning and nursery habitat (Goodyear et al., 1982). Meisner et al. (1987) provide an initial assessment of the potential impacts of increased water temperatures on Great Lakes fishes. Among their general expectations are northward shifts in the geographical distribution of warm and cold water species, changes in relative abundance of species within fish communities, and changes in yields of different species. Table 12 summarizes some of these anticipated impacts.

Increased water temperatures may result in substantial changes in the Great Lakes ecosystem. With water temperatures remaining above 4°C throughout the year, buoyancy-induced turnovers in the fall and spring may not occur. Without turnover, hypolimnion chemistry may be altered; oxygen may be depleted, releasing nutrients and metals from lake sediments. On the other hand, the lakes may experience a single winter turnover even with water temperatures above 4°C if temperature gradients are small and winds are strong enough to induce turbulent mixing (Hutchinson, 1957).

SOCIOECONOMIC IMPLICATIONS

Power Production

The waters of the Great Lakes are extensively used for hydropower production. Facilities range from low-head plants on the St. Mary's River to high-head facilities in the Niagara and St. Lawrence Rivers. A climate warming would result in decreased flows and water surface elevations, which would contribute to lower hydropower production. This could be especially important since hydropower is inexpensive and nonpolluting when compared to the primary alternatives, fossil fuel or nuclear power facilities.

Table 12. Anticipated Impacts of Increased Water Temperatures On Selected Great Lakes Basin Fishes[1].

Species	Impacts
smallmouth bass largemouth bass bigmouth buffalo	- northward extension of range
lake trout lake whitefish	- northward contraction of range
brook trout	- contraction of range to stream headwaters - reduced populations due to competition with other trout for remaining habitat
whitefish yellow perch (south) walleye (south)	- decreased populations due to increased egg and larval mortality or inhibited reproduction
alewife yellow perch (north) walleye (north)	- increased populations due to increased reproduction and reduced mortality
lake whitefish northern pike walleye	- decreased sustainable yield

[1]Meisner et al., 1987

Fossil fueled and nuclear power plants sited around the lakes use lake water for cooling; conversion to these modes of power production would increase the consumptive use of water for cooling (via evaporation), which would further exacerbate the anticipated low lake levels. Coal-fired power plants additionally require the economic efficiencies provided by waterborne transportation of coal; with lower water levels, higher transportation costs would directly affect power production costs.

The full impact of climate change on power production interests depends not only on the water supplies available for hydropower, cooling, or transportation, but on the changes in peak power demands that result from the increased air temperatures. In much of the U.S. portion of the Great Lakes basin, peak power demands occur in the summertime for cooling (R. Crissman, New York Power Authority, personal communication, 1988); climate warming could increase peak power demands, making the loss of hydropower production even more critical. On the other hand, climate warming may substantially reduce the peak power demands for winter heating that occur in Canada, making replacement of hydropower facilities nonproblematic (J. Eaton, Ontario Hydro, personal communication, 1988). However, impacts on peak power demands are difficult to predict since they are so closely tied to population levels, and continued growth in the use of air conditioners in Canada could raise summer peak demands above winter levels.

Navigation

The Great Lakes/St. Lawrence Seaway is a major freshwater transportation system. This system depends upon adequate depths in the connecting channels and harbors to function at full capacity. During conditions of low levels, more trips must be made to move the same amount of cargo; this increases shipping costs, and the increased traffic could cause backups at recognized bottlenecks in the system (e.g., Welland Canal). Any impacts on the shipping industry will have direct impacts on industries that depend upon the Great Lakes for transport of production inputs or final products (e.g., iron, steel, grain).

Shipping interests suggest that industry contraction in the 1960s was related to the record low water levels of that period (Marchand et al., 1988). Under the climate change scenarios, those low levels will be typical. Climate change impacts on the shipping industry could be made even more severe if the trend toward increased vessel size continues; for dense cargos (e.g., iron ore) those ships' capacities are extremely sensitive to changes in draft. Decreased channel depths will likely require extensive dredging in both the connecting channels and harbors to maintain present shipping capabilities. However, bottom sediments in the Great Lakes are highly contaminated with toxics, creating a problem with dredge spoil disposal.

Industrial Operations

Industrial interests typically use the Great Lakes as part of the production process (e.g., water supply, waste disposal) and/or as a mode of transportation for inputs or products. These interests include companies involved in a wide range of activities, including grain shipment, food processing, pulp and paper processing, petroleum refining, organic chemicals and synthetics, inorganic chemicals, industrial minerals, metal mining and refining, iron and steel production, metal casting, metal plating, and plastics fabrication. Thus, lowered Great Lakes levels would likely have adverse effects that pervade regional and national industrial operations and economies.

Commercial Operations

For many businesses in the Great Lakes region (e.g., marinas, hotels, resorts, restaurants), economic success is intimately tied to their shoreline location. As lake levels fall, these businesses will experience problems similar to those of the 1960s: reduced scenic views, inaccessible docking facilities, and unusable water intakes or waste disposal outlets. However, these adverse effects would likely be only transitory; although individual businesses may suffer under the steady-state climate change conditions, the industry as a whole will likely be able to adapt by simply moving with the lakeshore. There may be notable exceptions, however. The lower lake levels and connecting channel water levels would greatly reduce the areas accessible to small craft, including passenger vessels. This could require extensive private dredging and the rebuilding of ramps. As in the major harbors used by the navigation industry, bottom sediments are highly contaminated with toxics. Many municipalities and private harbors would likely have to cease operation if faced with the costs associated with dredging and disposal of contaminated spoil (P. Keillor, Sea Grant Institute, personal communication, 1988).

Other types of businesses may be affected more by hydrometeorologic changes than lowered lake levels; thus, these impacts will not be limited to lakeshore businesses. Commerce that depends upon reliable snow cover (e.g., skiing, snowmobiling, ice fishing) may suffer total collapse throughout much of the Great Lakes region, especially in areas that are only climatically marginal for winter recreation at present; other areas (e.g., the more northern portions of the Lake Superior and Huron basins that are also subject to lake effect snows) may still have sufficient snow during their peak tourist season (Wall, 1988). Riverine canoe rental operations may become more seasonal as river flows become too low except during peak runoff periods.

Commercial Fishing

Commercial fishing operations (e.g., commercial anglers, fish packers, processors, exporters) use the Great Lakes to provide an essential production input. Harbor access problems will occur due to the lowered lake levels, but changes in fisheries population structures may be even more important. Fisheries production is

intimately tied to wetland extent, which may be irretrievably lost as lake levels are lowered (Manny, 1984). Even if stocking programs are used to maintain fish populations, the industry may have to adjust to use of different species since increased water temperatures and the absence of semi-annual lake turnovers may affect what fish can be harvested at marketable levels. Additionally, climate change could indirectly affect commercial fishing operations; if dredging of channels and harbors makes toxic contaminants available for uptake by fish, their market ability may be limited.

Agriculture

Agricultural interests near Great Lakes shorelines use the lakes for water supply and take advantage of the soil fertility and climate moderation provided by lakeshore locations. Climate change will likely provide both benefits and costs to agriculture. More moderate winter temperatures may provide suitable conditions for significant increases in insect and disease problems. In northern portions of the Great Lakes basin, increased air temperatures would improve growing conditions and enable major agricultural expansion (Smit, 1987). Agricultural producers located in areas without substantial moisture reserves would experience harsh growing conditions during the summer as soil moisture drops below levels suitable for traditional crops (Smit, 1987). Lakeshore producers could mitigate any short falls in soil mositure by increased use of Great Lakes water for irrigation, although possible exacerbation of lower lake levels could create conflicts with other interest groups. Under lower lake level conditions, many low-lying areas will have improved drainage and additional fertile bottom-lands will be available; however, those rich lands may also contain exceedingly high levels of toxics, limiting farming potential. Also, as agricultural products are often shipped via waterborne transport, lowered lake levels will increase transportation costs for Great Lakes farming products.

Recreation Interests

Recreation interests use the Great Lakes in such a wide variety of ways that climate change is certain to provide both benefits and costs. Recreation activities that depend upon the ecosystem production of the Great Lakes (e.g., fishing, hunting, birding) will suffer if productivity is reduced due to loss of wetlands or lack of lake turnovers. For recreation uses dependent on other lake amenities (e.g., shoreline location), adverse effects would likely be only transitory; although recreation at specific sites may suffer under the steady-state climate change conditions, the recreational activities (e.g., beach use, water sports, camping) as a whole will likely be able to adapt by simply moving with the lakeshore. There may be notable exceptions, however. Long-term loss of marina and harbor access due to lower lake levels and high costs of toxic dredge spoil disposal could affect recreational boating. Beach use could be affected if public access to the shoreline is not maintained. Winter recreation (e.g., skiing, ice fishing) would be negatively affected by the warmer winter temperatures. Riverine canoeing opportunities could be reduced as river flows become too low during all but peak runoff periods.

Riparians

Great Lakes riparian interests derive many benefits from their shoreline location, including water supplies, shore access for beach use and other recreation, and scenic vistas. Individual benefits can be very sensitive to lake levels as their property becomes inundated or far removed from the waterfront. Under the climate change scenarios examined, transitory effects for riparians may be severe. Under steady-state conditions of climate change, however, although individual property owners may suffer, riparians as a whole will likely adapt by simply moving with the lakeshore.

POLICY IMPLICATIONS

Climate warming may require new paradigms of how the Great Lakes will be viewed from social, economic, and ecological perspectives. Reduced water supplies and lake levels likely will require management strategies to resolve conflicts over the allocation of Great Lakes water. Management will be made especially difficult because different interest groups are affected differently by climate change; while some groups may experience severe negative effects, others may actually benefit. In addition, Great Lakes uses are often

conflicting; optimizing for one interest may adversely affect another. System interdependencies (i.e., changes in levels or flows in one part of the Great Lakes system affect levels and flows throughout the remainder of the system) add to the complexity of management. A major policy decision will be the distribution of benefits between commercial, riparian, recreational, and ecological interests, between upstream and downstream interests, and finally, between the many jurisdictional (e.g., U.S., Canadian, federal, state, provincial, municipal) interests. It is likely that the U.S. and Canadian governments will react based upon the relative strengths of the interest groups and the pressures they can exert.

Presently, the Boundary Waters Treaty between the U.S. and Canada mandates a specific hierarchy of Great Lakes interests to be protected or enhanced; the primary interest is domestic and sanitary uses, followed by navigation, and power and irrigation, in that order (International Joint Commission, 1965). The treaty may have to be modified to reflect the changed relative importance of those interests compared to other commercial and industrial interests, riparian, recreational, and ecological interests.

No historical analog, comparable to conditions suggested by the climate change scenarios, exists to provide insight as to what the management response will be to a prolonged period of extremely low lake levels. During the relatively mild and short-term low levels of the mid-1960s, there was an increased emphasis on bringing additional water into the system, improved regulation, and on further system-wide water level regulations to counteract lake level lowerings that resulted from historical dredging and mining operations. A major thrust of water management under a warmer climate will probably be to keep water in the system. This will require extensive revision of the existing Lake Superior and Ontario regulation plans as well as the possible regulation of Lakes Michigan-Huron and Erie. The existing regulation plans were not designed for the low net supplies expected with climate change and failed in the assessment simulations. The debate over interbasin diversions of water will also likely intensify. There will probably be demands to increase the amount of water brought into the Great Lakes through existing diversions into Lake Superior as well as the consideration of new incoming diversions. In addition, efforts will likely be made to curtail the water diversion out of Lake Michigan at Chicago. Presently, an informal agreement, "The Great Lakes Charter," between governors and premiers in the Great Lakes region exists to forestall new diversions out of the Great Lakes basin (McAvoy, 1986). With probable increased demands for water from outside the basin, that agreement will require greater authority to remain effective.

REFERENCES

Allsopp, T. R., and S. J. Cohen. "CO_2-Induced Climate Change and Its Potential Impact on the Province of Ontario." In: Preprint Volume, Conference on Climate and Water Management - A Critical Era, American Meteorological Society, Boston, Massachusetts, 1986. pp. 285-290.

Assel, R. A. "A Computerized Ice Concentration Data Base for the Great Lakes." NOAA Data Report ERL GLERL-24, Natl. Tech. Inf. Ser., Springfield, Va. 22161, 1983.

Atmospheric Enviroment Service. "Monthly and Annual Evaporation from the Great Lakes Bordering Canada." Environ. Canada, Atmos. Environ. Serv., Downsview, Ont., 1988.

Bolsenga, S. J. "Lake-Land Precipitation Relationships Using Northern Lake Michigan Data." J. Appl. Met., 16(11):1158-1164, 1977.

Bolsenga, S.J. "Determining Overwater Precipitation from Overland Data: The Methodological Controversy Analyzed." J. Great Lakes Res., 5(3- 4):301-311, 1979.

Bolsenga, S. J., and J. C. Hagman. "On the Selection of Representative Stations for Thiessen Polygon Networks to Estimate Lake Ontario Overwater Precipitation." International Field Year for the Great Lakes Bulletin 16, National Oceanic and Atmospheric Administration, Rockville, Maryland, 1975. pp. 57-62.

Cohen, S. J. "Impacts of CO_2-Induced Climatic Change on Water Resources in the Great Lakes Basin." Climatic Change, 8:135-153, 1986.

Cohen, S.J. "Sensitivity of Water Resources in the Great Lakes Region to Changes in Temperature, Precipitation, Humidity, and Wind Speed." In: Proceedings, The Influence of Climate Change and Climatic Variability on the Hydrologic Regime and Water Resources, International Association of Hydrologic Sciences publication no. 168, 1987. pp. 489-499.

Croley, T. E., II. "Great Lakes Basins Runoff Modeling." NOAA Tech. Memo. ERL GLERL-39, Natl. Tech. Inf. Ser., Springfield, Va. 22161, 1982. 96 pp.

Croley, T.E., II. "Great Lakes Basins (U.S.A.-Canada) Runoff Modeling." J. Hydrol., 64:135-158, 1983a.

Croley, T.E., II. "Lake Ontario Basin (U.S.A.-Canada) Runoff Modeling. J. Hydrol., 66:101-121, 1983b.

Croley, T.E., II. "Verifiable Evaporation Modeling on the Laurentian Great Lakes." NOAA Tech. Memo. ERL GLERL-XX, Environmental Research Laboratories, Boulder, Colorado, 1988. (in prep.)

Croley, T. E., II, and Hartmann, H. C. "Lake Superior Basin Runoff Modeling." NOAA Tech. Memo. ERL GLERL-50, Natl. Tech. Inf. Ser., Springfield, Va. 22161, 1984. 284 pp.

Croley, T.E., II, and Hartmann, H.C. "Lake Champlain Water Supply Forecasting." GLERL Open File Report, Contribution No. 450, Great Lakes Environmental Research Laboratory, Ann Arbor, Michigan, 1985a. 56 pp.

Croley, T.E., II, and Hartmann, H.C. "Resolving Thiessen Polygons." J. Hydrol., 76:363-379, 1985b.

Croley, T.E., II, and Hartmann, H.C. "Near-Real-Time Forecasting of Large-Lake Water Supplies; A User's Manual." NOAA Tech. Memo. ERL GLERL-61, Environmental Research Laboratories, Boulder, Colorado, 1986. 82 pp.

Croley, T.E., II, and Hartmann, H.C. "Near Real-Time Forecasting of Large Lake Supplies." J. Wat. Res. Plan. Manag. Div., ASCE, 113(6):810-823, 1987.

DeCooke, B. G., and D. F. Witherspoon. "Terrestrial Water Balance." In: IFGYL - The International Field Year for the Great Lakes, E.J. Aubert and T.L. Richards, eds. Great Lakes Environmental Research Laboratory, Ann Arbor, Michigan, 1981. pp. 210-219.

Derecki, J. A. "Multiple Estimates of Lake Erie Evaporation." J. Great Lakes Res., 2(1), 124-149, 1976.

Derecki, J.A. "Evaporation from Lake St. Clair." NOAA Tech. Memo. ERL GLERL-23, Natl. Tech. Inf. Ser., Springfield, Va. 22161, 1978.

Derecki, J.A. "Estimates of Lake St. Clair Evaporation." J. Great Lakes Res., 5(2), 216-220, 1979.

Derecki, J.A. "Evaporation from Lake Superior." NOAA Tech. Memo. ERL GLERL-29, Environmental Research Laboratories, Boulder, Colorado, 1980.

Derecki, J.A. "Stability Effects on Great Lakes Evaporation." J. Great Lakes Res., 7(4), 357-362, 1981a.

Derecki, J.A. "Operational Estimates of Lake Superior Evaporation Based on IFYGL Findings." Water Resour. Res., 17(5), 1453-1462, 1981b.

Gill, A. E., and J. S. Turner. "A Comparison of Seasonal Thermocline Models with Observation." Deep-Sea Res., 23, 391-401, 1976.

Goodyear, C. D., T. A. Edsall, D. M. Dempsey, G. D. Moss, and P. E. Polanski. "Atlas of the Spawning and Nursery Areas of Great Lakes Fishes, Volume 13: Reproductive Characteristics of Great Lakes Fishes." Report No. FWS/OBS-82/52, Fish and Wildlife Service, Washington, D.C., 1982.

Gray, D. M., G. A. McKay, and J. M. Wigham. "Energy, Evaporation, and Evapotranspiration." Handbook on the Principles of Hydrology, D. M. Gray, ed. Water Information Center, New York, 1973. pp. 3.1-3.66.

Gray, D.M., G.A. McKay, and J.M. Wigham. "Potential Variation of Great Lakes Levels: A Hydrologic Response Analysis." NOAA Tech. Memo. ERL GLERL, Environmental Research Laboratories, Boulder, Colorado, 1988. (in prep.)

Hartmann, H. C. "An Evaluation of Great Lakes Hydraulic Routing Models." NOAA Tech. Memo. ERL GLERL-66, Environmental Research Laboratories, Boulder, Colorado, 1987.

Hutchinson, G. E. A Treatise on Limnology, Volume I, Part 1 - Geography and Physics of Lakes, John Wiley and Sons, New York, New York, 1957.

International Great Lakes Diversions and Consumptives Uses Study Board. "Great Lakes Diversions and Consumptive Uses." International Joint Commission, Washington, D.C., 1981.

International Joint Commission. "Rules of Procedure and Text of Treaty." International Joint Commission, Washington, D.C., 1965.

International Lake Superior Board of Control. Regulation of Lake Superior: Plan 1977 Development, Description, and Testing, International Joint Commission, Washington, D.C., 1981.

International Lake Superior Board of Control. Regulation of Lake Superior: Operational Guides for Plan 1977, International Joint Commission, Washington, D.C., 1982.

International St. Lawrence River Board of Control. Regulation of Lake Ontario: Plan 1958-D, International Joint Commission, Washington, D.C., 1963.

Irbe, J. G., and A. Saulesleja. "An Operational Program for Monitoring Surface Temperatures of Lakes and Coastal-Zone Waters in Canada from Polar-Orbiting Satellite Infrared Data." Actes du symposium international de la Commission VII de la Societe internationale de photogrammetrie et teledetection, 13-17 September, Toulouse, France, International Archives of Int. Soc. Photogram. and Rem. Sens. 24(VII-1):717-724, 1982.

Irbe, J. G., R. K. Cross, and A. Saulesleja. "Remote Sensing of Surface Water Temperature of the Great Lakes and Off the Canadian East Coast." Northwest Atlantic Fisheries Organization Scientific Council Studies No. 4, Special Session on Remote Sensing, September, Dartmouth, Canada, 1982. pp. 31-39.

Keijman, J. Q. "The Estimation of the Energy Balance of a Lake from Simple Weather Data." Boundary-Layer Meteorol. 7:399-407, 1974.

Kraus, E. B., and J. S. Turner. "A One-Dimensional Model of the Seasonal Thermocline II; The General Theory and Its Consequences." Tellus. 19:98-105, 1967.

Manny, B. A. "Potential Impacts of Water Diversions on Fishery Resources in the Great Lakes." Fisheries 9(5):19-23, 1984.

Marchand, D., M. Sanderson, D. Howe, and C. Alpaugh. "Climatic Change and Great Lakes Levels: The Impact on Shipping." Climatic Change, 1988. (in press)

McAvoy, P. V. "The Great Lakes Charter: Toward a Basin-Wide Strategy for Managing the Great Lakes." In: Proceedings of the Great Lakes Legal Seminar: Diversion and Consumptive Use, The Center for the Great Lakes, Chicago, 1986.

Meisner, J. D., J. L. Goodier, H. A. Regier, B. J. Shuter, and W. J. Christie. "An Assessment of the Effects of Climate Warming on Great Lakes Basin Fishes." J. Great Lakes Res. 13(3):340-352, 1987.

Phillips, D. W. "Evaluation of Evaporation from Lake Ontario During IFYGL by a Modified Mass Transfer Equation." Water Resour. Res., 14(2), 197- 205, 1978.

Phillips, D. W., and J. G. Irbe. "Land-To-Lake Comparison of Wind, Temperature, and Humidity on Lake Ontario During the International Field Year for the Great Lakes (IFYGL)." Rep. CLI-2-77, Environ. Canada, Atmos. Environ. Serv., Downsview, Ont., 1978.

Quinn, F. H. "Hydrologic Response Model of the North American Great Lakes." J. Hydrol., 37:295-307, 1978.

Quinn, F.H. "An Improved Aerodynamic Evaporation Technique for Large Lakes with Application to the International Field Year for the Great Lakes." Water Resour. Res., 15(4), 935-940, 1979.

Quinn, F.H. "Likely Effects of Climate Changes on Water Levels in the Great Lakes." In: Proceedings, First North American Conference on Preparing for Climate Change, Climate Change Institute, Washington, D.C., 1988. pp. 481-487.

Quinn, F. H., and T. E. Croley II. "Climatic Water Balance Models for Great Lakes Forecasting and Simulation." In: Preprint Volume: Fifth Conference on Hydrometeorology, American Meteorological Society, Boston, Massachusetts, 1983. pp. 218-223.

Quinn, F. H, and R. K. Kelley. "Great Lakes Monthly Hydrologic Data." NOAA Data Report ERL GLERL-26, Natl. Tech. Inf. Ser., Springfield, Va. 22161, 1983.

Richards, T. L, and J. G. Irbe. "Estimates of Monthly Evaporation Losses from the Great Lakes, 1950 to 1968, Based on the Mass Transfer Technique." paper presented at the 12th Conference on Great Lakes Research, International Association of Great Lakes Research, Ann Arbor, Michigan, May, 1969.

Smit, B. "Implications of climatic change for agriculture in Ontario." Climate Change Digest CCD 87-02, Environ. Canada, Atmos. Environ. Serv., Donwsview, Ont., 1987.

U.S. Environmental Protection Agency. Potential Climatic Impacts of Increasing Atmospheric CO_2 with Emphasis on Water Availability and Hydrology in the United States, EPA Office of Policy, Planning, and Evaluation, Washington, D.C., 1984.

U.S. Geological Survey. "Water Loss Investigations, Vol. 1, Lake Hefner Studies. Geol. Surv. Prof. Pap. 269 U.S., 1954.

U.S. Geological Survey. "Water Loss Investigations: Lake Mead Studies." Geol. Surv. Prof. Pap. 298 U.S., 1958.

Wall, G. "Implications of climatic change for tourism and recreation in Ontario." Climate Change Digest CCD 88-05, Environ. Canada, Atmos. Environ. Serv., Downsview, Ont., 1988.

Wilson, J. W. "Effect of Lake Ontario on Precipitation." Monthly Weather Review 105:207-214, 1977.

IMPACT OF GLOBAL WARMING ON GREAT LAKES ICE CYCLES

by

Raymond A. Assel
National Oceanic and Atmospheric Administration
Great Lakes Environmental Research Laboratory
2205 Commonwealth Blvd.
Ann Arbor, MI 48105-1593
(GLERL Contribution No. 620)

Interagency Agreement Identification Number DW13932631-01-0

CONTENTS

Page

FINDINGS 5-1

CHAPTER 1: INTRODUCTION 5-2
GREAT LAKES ICE COVER AND ICE CYCLES -- A BRIEF REVIEW 5-2
ICE CYCLE MODELS 5-2

CHAPTER 2: METHODOLOGY 5-4
MODEL DEVELOPMENT AND ADJUSTMENTS 5-4
MODEL LIMITATIONS 5-7
SCENARIOS USED 5-8

CHAPTER 3: RESULTS 5-11
WINTERS WITHOUT ICE COVER 5-11
DATES OF FIRST/LAST ICE COVER AND ICE COVER DURATION 5-11
The 1951-80 Base Period 5-11
Doubled CO_2 Scenarios 5-11
The Transient Scenario 5-11
The 1930-39 Analog Scenario 5-12
DAILY AVERAGED BASIN MEAN ICE CONCENTRATION 5-12

CHAPTER 4: INTERPRETATION AND LIMITATIONS OF RESULTS 5-24
INTERPRETATION 5-24
LIMITATIONS 5-24

CHAPTER 5: IMPLICATIONS OF RESULTS 5-26
ENVIRONMENTAL IMPLICATIONS 5-26
SOCIO-ECONOMIC IMPLICATIONS 5-26

CHAPTER 6: POLICY IMPLICATIONS 5-27

GLOSSARY 5-28

REFERENCES 5-29

FINDINGS[1]

Lake basin mean depth is an index of thermal inertia, and freezing degree-days (FDD) are an index for energy loss at the water surface. Daily basin mean FDD are correlated with daily basin mean ice concentration during winter. Annual ice cover duration and daily ice concentration are simulated with FDD regression equations for Lake Erie's West, Center, and East Basins and for Lake Superior's West, East, and Whitefish Bay Basins. Models are calibrated over a 20-year (1960-79) period. Models are applied to an independent four-winter period (1980-83) to evaluate simulation error. Standard errors on the independent winters ranged from 20 to 30 percent for annual maximum ice concentration, and standard errors were 2 to 4 weeks in magnitude for annual ice cover duration.

Average monthly air temperature for doubled CO_2 scenario winters is above-freezing for Lake Erie basins. Ice cover still forms during some doubled CO_2 winters because of a sufficient number of consecutive days with below-freezing air temperatures. Ice concentration and duration trends followed the air temperature trends of the three doubled CO_2 scenarios; that is, the coldest scenario (Oregon State University) had the greatest ice concentration with the longest ice cover duration, and the warmest scenario (Geophysical Fluid Dynamics Laboratory) had the smallest ice concentration with the shortest ice season duration. Daily average ice cover under all of the doubled CO_2 scenarios is limited to the shore area and shallows of each lake basin. Doubled CO_2 scenario winters without ice cover occur 37 to 83 percent of the time in the East and Central Basins of Lake Erie and up to 17 percent of the time for the West Basin of Lake Erie and the East Basin of Lake Superior. Average winter duration for the 1951-80 base period was 13 to 16 weeks. Under the doubled CO_2 scenarios, the average winter duration is 5 to 13 weeks shorter. The shorter duration and less extensive ice covers would affect lake ecology, and loss of some cold water fish species such as lake whitefish may occur. The shipping season, which traditionally stops during the winter months, would likely be extended, perhaps to a year-round season.

Under the 79-year transient CO_2 scenario (1981-2059), only Lake Erie basins have winters without ice cover. During the last three decades of the transient (2030-59) 30 to 80 percent of the winters for Lake Erie's Center and East Basins are without ice cover. Transient scenario daily ice concentration, averaged for the years 2010-39, is significantly less than the base period for all lake basins. However, extensive ice cover will occur under many transient CO_2 winters, particularly during the first 29 years (1981-2009). Average ice cover duration is 3 to 7 weeks shorter during the next 30 years of the transient 2010-39 relative to the 1951-80 base period. During the last decade of the transient scenario (2050-59), decadal-averaged ice concentration and ice cover duration is similar to the doubled CO_2 scenarios.

Ice cover simulation of an analog climatic warming period (1930-39) shows that average ice cover duration was 1/2 to 1 week shorter than the 1951-80 base period for Lake Superior and about 3 to 4 weeks shorter for the Center and East Lake Erie Basins. Annual maximum ice concentration was less than the base period but greater than the doubled CO_2 scenario.

---

[1]Although the information in this report has been funded partly by the U.S. Environmental Protection Agency under contract DW13932631-01-0, it does not necessarily reflect the Agency's views, and no official endorsement should be inferred from it.

CHAPTER 1

INTRODUCTION

GREAT LAKES ICE COVER AND ICE CYCLES -- A BRIEF REVIEW

The Great Lakes ice cycle is divided into three periods: fall cooling, ice formation, and ice loss. During fall cooling, thermal stratification is lost as the entire water column cools to the temperature of maximum density near 4 degrees C. Subsequent cooling results in the formation of less dense surface water, winter restratification, and the start of the ice formation period. Ice loss occurs in spring owing to increasing solar radiation and above-freezing air temperature.

During the winter ice formation period, vertical ice accretion occurs as a result of heat transfer from the ice-water interface through the ice to the atmosphere. As the ice cover thickens its vertical extent reduces the rate of heat loss from the ice-water boundary and retards additional ice accretion. Under the current climate regime, the upper limit of thermodynamic ice growth appears to be about 50 to 100 cm for bay and harbor sites in the Great Lakes (Sleator, 1978). Local factors such as air temperature, water depth, winds, and snowfall are responsible for the variation of ice thickness. Winds can cause portions of an ice cover to compact and override or submerge under the remaining ice cover; the result is rafted, ridged, or jammed ice, depending upon the amount and vertical extent of ice rubble formed. The U.S. Coast Guard has reported wind-induced ice thickness of up to 8 m in the Great Lakes.

The Great Lakes' ice cover forms in the shallow bays and harbors in December and in deeper bays and along the perimeter of the Great Lakes during January. Lake Erie, with its shallow depth, forms midlake ice cover in January; midlake areas of the other Great Lakes usually form extensive ice cover in February. Annual maximum ice coverage occurs in February and early March, but even then, some areas tend to remain open water. Normal maximum ice cover expressed as a percentage of total surface area is 90% for Lake Erie, 75% for Lake Superior, 68% for Lake Huron, 45% for Lake Michigan, and only 24% for Lake Ontario (Assel et al., 1983). Lake Ontario's small annual maximum ice coverage results from the combination of (1) its large thermal inertia (mean depth of 86 m), (2) average water surface temperatures during winter near but above 0 degrees C, which make air-water temperature differences primarily a function of air temperatures, and (3) its relatively mild winter air temperatures (-4.4 degrees C, compared with -9.8 degrees C for Lake Superior). Air temperature is the single most important atmospheric climate variable affecting ice cover. The average winter temperature for all five Great Lakes in 1979 was -6.8 degrees C, and the annual maximum ice extent was nearly 100%. The average winter temperature for 1983 was -2.2 degrees C and the maximum ice extent was approximately 23% of the combined Great Lakes surface area (Assel et al., 1985).

In spring, ice loss results from melting caused by solar radiation and above-freezing air temperature. Solar radiation penetrates and is absorbed within the ice, reducing the structural strength of the ice due to preferential melting at ice crystal boundaries. The weakened ice cover can then be easily broken by winds and wave action, and melted or transported to windward (eastern) lake shores. In March, areas of open water and low ice concentration expand from the deeper, more exposed midlake areas toward the perimeter and eastern shores. By mid-April, any remaining ice is usually located in the shore zone; however, during some years, ice cover lasts into May.

ICE CYCLE MODELS

Ice cover models that lend themselves most easily to climate analysis are empirical and statistical in nature because of the availability of input data needed to calibrate and evaluate them. For this reason and because of a need to complete this analysis in a timely manner, only relatively simple empirical statistical models using cumulative air temperature in the form of degree-days are considered in this paper.

Freeze-up dates on shallow inland lakes in Canada were found to correlate with weighted mean daily air temperatures (Bilello, 1964) and accumulated freezing degree-days (FDD) (Williams, 1965). Later Williams (1971) also correlated breakup dates with previous dates of breakup and air temperatures. And Tramoni et al. (1985) and Barry (1986) found that freeze-up on shallow inland lakes in Canada and Finland are an index of fall air temperatures; an increase of 1 degree C in average fall air temperature corresponded with a 3- to 10-day delay in date of freeze-up. One of the earliest empirical ice cover studies on the Great Lakes was made by Oak and Myers (1953); they used February air temperature to forecast spring opening dates for navigation at various bays and harbors. Systematic aerial ice reconnaissance observations of Great Lakes ice cover began in the late 1950's; this established a data base for making empirical and statistical studies of large areas of the Great Lakes ice cover. Richards (1963) correlated antecedent heating degree-days for the previous summer (index of summer heating) and freezing degree-days for late fall and winter (index of water cooling and ice formation) with observations of lake-averaged Great Lakes ice cover. Snider (1971) developed threshold FDD accumulations for navigationally significant ice in specific areas of the Great Lakes, based on average heat storage in the water. Rogers (1976) used FDD and thawing degree-days to develop regression models of annual maximum lake-averaged ice concentration. More recently, Assel et al. (1985) developed a regression model of regional annual maximum ice cover of the combined area of the five Great Lakes, based on regional average winter temperature. Their model implies that a 4 to 5 degree C increase in regional average winter temperature from the 1951-80 base period average would result in regional annual maximum ice cover between 0 and 9% for the combined area of the Great Lakes. Howe et al. (1986) developed empirical models for each lake relating monthly average air temperature on the perimeter to annual maximum ice cover. They estimated the climatically "normal" annual maximum ice cover based on 1951-80 mean air temperatures and the expected annual maximum ice cover for a doubled CO_2 warming. Their results indicate that, except for Lake Erie, the expected annual maximum ice cover under a doubled CO_2 warming is nil.

The studies noted in the previous paragraphs developed models of different parts of the annual ice cycle. In this present study empirical models were developed that simulate daily mean basin ice concentration for the entire ice cycle, using some of the methods from the earlier studies. This initial analysis is limited to Lakes Erie and Superior -- the two lakes that represent the extremes in mean lake depth and air temperatures for the Great Lakes. A summary of development methodology and an assessment of model limitations are described. The range and expected values of ice concentration and ice cycle duration are presented and briefly interpreted relative to environmental and socio-economic implications.

CHAPTER 2

METHODOLOGY

MODEL DEVELOPMENT AND ADJUSTMENTS

Two important variables affecting ice formation are (1) heat stored in the water mass and (2) the energy budget at the air-water boundary. Mean lake basin depth (volume divided by surface area) is an index that reflects thermal inertia, and accumulated freezing degree-days (FDD) are an index of energy loss from the surface mixing layer. Lakes Superior and Erie are divided into basins using lake bathymetry: East, Center, and West Basins for Lake Erie, and East and West Basins for Lake Superior (Figure 1 and Table 1). In addition, Whitefish Bay is included as a separate basin of Lake Superior because of its importance to navigation.

Table 1. Lake Basin Parameters (approximate values)

	Lake Superior			Lake Erie		
	WB	EB	WFB	WB	CB	EB
Mean Depth (m)	135	152	41	9	19	27
Area (km2)	21971	58947	1182	5135	14635	5909
Volume (km3)	2966	8960	48	46	278	159
Max FDD (C)#	1299	1255	1255	318	342	368

Averaged annual maximum FDD for the 1951-80 base period.

Mean basin ice concentration is calculated for each lake basin from synoptic ice charts (Assel, 1983) for the years 1960-79. These data are used to develop regression equations between synoptic mean basin ice concentration and daily mean basin FDD accumulation through the date of the synoptic ice concentration observation (Table 2). Equation 1 was developed for Lake Superior's East and West Basins, and Equation 2 for Whitefish Bay and the three Lake Erie basin. Equations 3 and 4 differentiate between initial ice formation in the shallow and deep areas of each Lake Superior basins. Equation 3 is used for initial ice formation in the shallows of Whitefish Bay and, Equation 4 is used for initial ice formation in shallow areas of Lake Superior's East and West Basins. Equation 5 is an ice reduction factor that is part of Equation 1 and Equation 2.

The three periods of the annual ice cycle are simulated by the system of equations in Table 2. Initial ice formation is a function of threshold FDD accumulations given as part of the constraints in Equations 2, 3, and 4. Threshold FDD values are estimated from analysis of historic ice charts and corresponding FDD accumulations from November 1 to the date given on the ice chart. If these threshold FDD values are not accumulated, ice cover will not form. Threshold FDD values for Lake Erie's West, Center, and East Basins are 27, 75, and 110 FDD, respectively. Initial ice extent at these threshold values is 45%, 37%, and 30%, respectively. If less than 430 FDD accumulate for the East and West Basins of Lake Superior, ice cover will not form. The threshold FDD value needed for initial ice formation on Whitefish Bay is 350.

Ice growth is simulated by the expressions (FDD-BFDD) in Equations 1 and 2. These expressions are an index of heat loss at the air-water boundary and they also incorporate the hysteresis effect of antecedent FDD accumulations on increasing ice extent. The hysteresis effect in Equation 1 (exponential term) is a function of the number of days past the date of end-of-fall overturn because the maximum ice cover (which is usually below 100%) is related to the number of days past the date of end-of-fall overturn on Lake Superior's East and

FIGURE 1
LAKE BASINS AND TEMPERATURE STATIONS

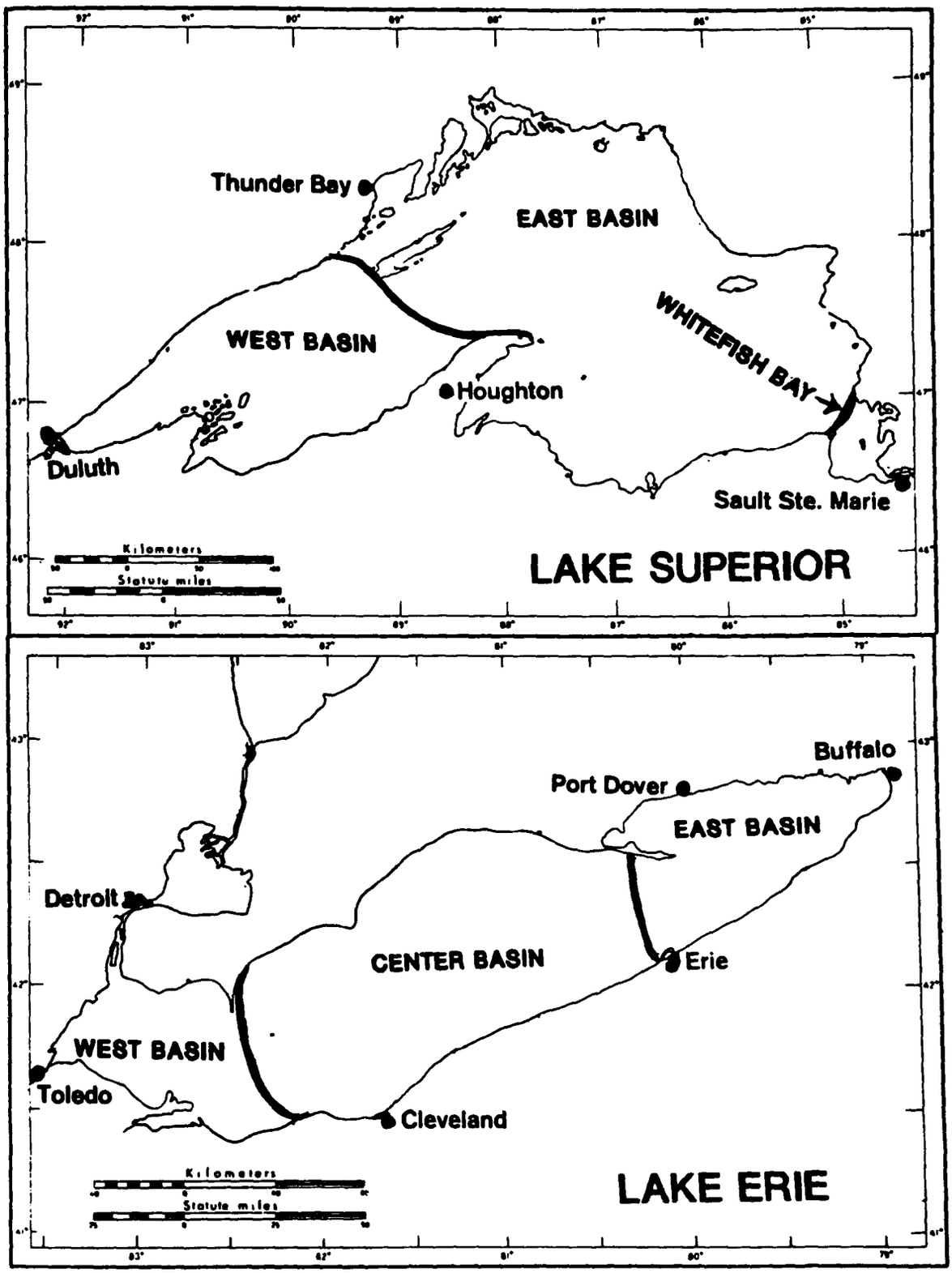

Table 2. Annual Ice Cycle Simulation Model Equations

EQ. 1 $$ICE = \frac{100}{1 + C1*\exp[C2*((FDD-BFDD)/JD)] + C3*(FDD-BFDD) + THFAC}$$

EQ. 1 constraints:
1. 730 < FDD < FDDCRIT
2. JD = 1 when FDD=BFDD and JD increments by 1 every day after that date.
3. ICE=100 if FDD > FDDCRIT

EQ. 2 $$ICE = \frac{100}{1 + FZFAC + C1*\exp[C2*(FDD-BFDD)] + THFAC}$$

EQ. 2 constraints:
1. 450 < FDD (for Whitefish Bay only)
2. FZFAC=1000 when FDD < BFDD, FZFAC=0 when FDD > BFDD
3. ICE=0 if FDD < BFDD

EQ. 3 ICE = 5*(FDD-350)/100

EQ. 3 constraints:
1. 350 < FDD < 450
2. ICE=0 if FDD <350
3. JD < DMFDD

EQ. 4a ICE = 5 + 10*(FDD-580)/150

EQ. 4a constraints:
1. 580 < FDD < 730
2. JD < DMFDD

EQ. 4b ICE = 5*(FDD-430)/150

EQ. 4b constraints:
1. 430 < FDD < 580
2. ICE=0 if FDD <430
3. JD < DMFDD

EQ. 5 $$THFAC = \frac{1}{1 - [(JD-DMFDD)/\{Sqrt(MFDD-BFDD)/MELT\}]} - 1$$

EQ. 5 constraints:
1. THFAC=0 if JD < DMFDD
2. THFAC=9999 if JD-DMFDD > a. or b. below:
   a. Sqrt[(MFDD-BFDD)/MELT]
   b. maximum historic observed value of days past annual maximum FDD to date of last observed ice.

See glossary for definition of terms.

West Basins. The hysteresis effect of antecedent FDD accumulation in Equation 2 is related to the FDD accumulation necessary for virtually 100% ice coverage because the ice cover on Lake Erie basins and Lake Superior's Whitefish Bay approaches 100% most winters. Basin ice concentration generally decreases by the date FDD accumulations reach their annual maximum value -- average air temperatures are usually above freezing after that date. Consequently, the date of annual maximum FDD accumulation defines the end of the ice growth period and the beginning of the ice decay period. A temporal ice concentration reduction factor, Equation 5, is activated in Equations 1 and 2 after the date of annual maximum FDD accumulation. Ice loss in Equation 5 is a function of average daily ice melt rate, average ice thickness on the date of maximum FDD accumulation, and number of days past the date of maximum FDD accumulation. The average ice melt rate (cm/day) during the ice loss period was optimized by trial and error during the regression analysis. The rate is 1.250 (cm/day) for Lake Superior's East and West Basins, and Whitefish Bay, and 0.889, 0.667, and 0.333, for Lake Erie's West, Center, and East Basins, respectively. Lake-averaged ice ablation rates for bays and harbors of Lakes Superior and Erie are 1.4 and 1.1 cm/day, respectively (Bolsenga, 1988). Lower ablation rates for Lake Erie's Center and East Basins apparently reflect the eastward advection of ice into these basins during the ice loss period, which in effect, prolongs the period of ice loss and reduces the average daily rate of ice ablation. A Stefan ice growth expression (the square root of the accumulated FDD) was used to estimate ice thickness. Complete ice loss occurs when the number of days past the date of annual maximum FDD exceeds the number of days needed to melt the ice at the average melt rate. The largest observed number of days between the date of annual maximum FDD accumulation and the date of ice cover loss was estimated from historic ice charts for the Lake Erie basins, and this was made a constraint for Equations 5 and 2 for simulating ice loss in Lake Erie basins.

MODEL LIMITATIONS

Model prediction error for each basin was evaluated by the cross validation method; that is, the data were divided in half and model coefficients were generated for each subset of the original data. Coefficients for one subset were used to simulate ice concentration for the second subset. The model prediction error for each data subset ranged from 15 to 28% (Table 3).

Table 3. Model Cross Validation for Root Mean Square Error (RMSE)

	Lake Superior			Lake Erie		
RMSE	WB	EB	WFB	WB	CB	EB
First half of data	25.9	20.9	14.7	17.8	24.9	19.7
Second half of data	27.8	18.8	22.8	22.1	27.0	18.1

Model prediction error over the entire data base was evaluated by simulation of annual maximum lake-averaged ice concentration during four winters outside the model calibration period. Estimates of lake-averaged annual maximum ice cover and date of occurrence for the early 1980s have been provided by the U.S. Coast Guard (personal communication, United States Coast Guard, Ninth District Headquarters, Cleveland, Ohio). Basin mean ice concentrations from simulation models for Lakes Superior and Erie were areally weighted and summed to obtain the lake-averaged ice concentration for the dates of annual maximum ice concentration provided by the Coast Guard. The four "test winters" contained both extremely high and extremely low annual maximum ice concentrations (Table 4). Models did well for both winter extremes; standard errors are 30% for Lake Superior and 20% for Lake Erie. It is significant that the models did well during the mild 1982-83 winter, since that winter is ranked as the 10th warmest winter in the Great Lakes during the 200-year period 1783-1983 (Assel et al., 1985), and thus it likely approaches conditions of some of the CO_2 global warming scenarios.

Table 4. Simulation Error for Annual Maximum Ice Extent

Lake	Winter Season	Maximum Ice Concentration Observed	Simulated	Error (Obs-Sim)
Superior	1979-80	75	34	41
	1980-81	92	62	31
	1981-82	97	96	1
	1982-83	21	13	8
Erie	1979-80	95	86	9
	1980-81	100	85	15
	1981-82	100	74	26
	1982-83	25	40	15

Errors in simulated ice cover duration were also analyzed. Ice cover duration is defined here as the difference in days between the dates of initial ice cover greater than 0.5% concentration and final and complete loss of ice cover. Dates of first- and last-ice were estimated from Canadian composite ice charts and from National Ocean Service water level gauge ice reports. Standard error in simulated ice cover duration ranged from 3 to 4 weeks for Lake Superior basins and from 2 to 3-1/2 weeks for Lake Erie basins (Table 5). Determining ice cover duration during mild winters can be difficult. The first and last dates of ice were used to determine season duration, but in mild winters this method may over-estimate the actual number of days with ice cover because of alternating periods of ice formation and ice cover loss. For example, an error of 40 days for West Basin of Lake Erie during the mild 1982-83 winter resulted from intermittent ice cover during two days in December. If those spurious data were omitted, the initial ice cover would have been on January 18th and the season duration would have been 45 days, producing an error of only 3 days.

It is difficult to quantify the magnitude of error in ice cover models caused by not considering wind effects because wind effects are highly nonlinear and depend upon physical processes that occur on time scales of a few hours to a few days. Analysis of data from Lewis (1987) indicates that for the 28-year period 1957-1985, the annual average number of storms with wind speeds of 88 km/hour or greater during the 3-month period January, February, and March is about one severe storm per winter. If winter storms of this magnitude were to increase in frequency during the climate warming scenarios, this would contribute to a reduction in both ice duration and ice concentration; a reduction in storm frequency from the present climate average of one per season would have the opposite effect. High winds during the early winter would tend to retard ice formation, particularly in the deeper lake basins; thus, models would predict initial ice formation too early and ice extent would be over-estimated. An extended period of calm conditions in early winter would have the opposite effect; initial ice covers would form earlier and be more extensive. High winds during the winter after an extensive ice cover exists could reduce ice covers temporarily, and models would over-estimate ice extent. High winds in spring could move the ice out of a basin or melt it by upwelling, resulting in an over-estimated ice coverage during part of the ice loss period and a tardy simulated date of last ice cover.

SCENARIOS USED

The 1951-80 climatological period used to define the current normal value for climate elements was used as a base period in this study. The decade of the 1930's had several years of much above normal temperatures and is used as a historic analog that approaches CO_2 global warming scenarios. Cumulative departures from long-term monthly mean temperature (1895-1977) for the contiguous United States show a increasing temperature trend from 1921 to 1954 and a decreasing trend after that (Diaz and Quayle, 1980). Mild winters

Table 5. Simulation Error for Ice Cycle Duration

	Ice Cycle Duration in Day								
Lake Superior	West Basin			East Basin			Whitefish Bay		
winter season	obs	sim	error	obs	sim	error	obs	sim	error
1979-80	105	87	18	108	88	20	108	101	7
1980-81	134	101	33	125	103	22	129	110	19
1981-82	123	119	4	139	118	21	150	121	29
1982-83	84	114	-30	91	92	-1	83	97	-14
Lake Erie	West Basin			Center Basin			East Basin		
winter season	obs	sim	error	obs	sim	error	obs	sim	error
1979-80	118	106	12	69	72	-3	76	86	10
1980-81	79	81	-3	94	80	14	121	103	18
1981-82	95	107	-12	92	89	3	113	111	2
1982-83	42	82	-40	37	16	21	28	17	11

obs = observation; sim = simulation

occurred in the Great Lakes during the early 1950's but not during the rest of the 1951-80 base period when severe winters were prevalent (Assel, 1986).

Monthly mean air temperatures ratios (doubled $CO_2/1CO_2$) for the GISS, GFDL, and OSU scenarios and for the GISS-A scenario were multiplied by daily mean air temperatures for stations on the perimeter of each basin for the 1951-80 base period data (Table 6). The closest grid point for a given global circulation model (GISS, GFDL, OSU) was determined for each meteorological station (Table 6), and the air temperature ratios at that grid were used for simulating the doubled CO_2 and transient CO_2 temperature time series. The daily observed station temperatures were converted to degrees Kelvin, multiplied by the appropriate ratio (year and month) for a given scenario, and then converted back to degrees C, following EPA instructions. Mean daily air temperatures for the 1930-39 historic analog scenario and the 1951-80 base period were abstracted from a Great Lakes Environmental Research Laboratory air temperature data base (Assel, 1986) for analysis. Mean basin daily air temperatures and FDD accumulations were calculated and the daily FDD data were used to drive the ice cycle simulation models. Winter seasons were started in November prior to the year shown as the first year of the scenario. For example, the 1951-80 base period includes air temperatures and FDD for November and December, 1950. The GISS-A scenario began November 1980; the average ice cover statistics for the first decade of these scenarios was only nine winters, 1981-89. Thirty-year monthly averaged temperatures for the 1951-80 base period, the doubled CO_2 scenarios, and decadal monthly averages for the 1930-39 analog and transient CO_2 scenario are given in Table 7 for East and West Basin of Lake Erie and East and West Basins of Lake Superior. Monthly air temperatures for the doubled CO_2 scenarios are above 0 degrees C for Lake Erie, but only during November and occasionally during March for Lake Superior. This is somewhat misleading since daily average temperatures are occasionally below 0 degrees C; consequently, global circulation model output statistics should concern a daily rather than a monthly time period. Daily values may produce significantly different results relative to ice cover simulation. The transient decadal average monthly temperatures for the first three decades are in general similar to the 1951-80 base period. November-through-March averaged temperatures for the last decade of the transient is similar to GISS doubled CO_2 scenario averaged temperatures. The 1930-39 analog temperatures are less then 2 degrees C warmer than the 1951-80 base period in most of the winter months.

Table 6. Air Temperature Stations used in FDD Analysis

Basins	Temperature Stations
Eri WB	Detroit, MI., Toledo, OH., Cleveland, OH.
Eri CB	Cleveland, OH., Port Dover, ONT.
Eri EB	Port Dover, ONT., Erie, PA., Buffalo, NY.
Sup WB	Duluth, MN., Houghton, MI., Thunder Bay, ONT.
Sup EB	Sault St. Marie, MI., Thunder Bay ONT.
Sup WFB	Sault St. Marie, MI., Thunder Bay, ONT.

Table 7. Monthly Average Temperatures (°C) for Base Case, Doubled CO_2, and Decadal Average for the Analog and Transient CO_2 Scenarios

	Lake Erie - West Basin					Lake Erie - East Basin				
	Nov.	Dec.	Jan.	Feb.	Mar.	Nov.	Dec.	Jan.	Feb.	Mar.
1951 - 80	4.9	-1.3	-4.2	-3.0	2.1	4.6	-1.4	-4.5	-4.1	0.6
GISS $2CO_2$	9.1	5.5	2.0	1.3	6.9	8.8	5.3	1.6	0.2	5.4
GFDL $2CO_2$	9.8	5.2	2.5	1.7	7.1	9.6	5.0	2.1	0.6	5.6
OSU $2CO_2$	6.7	1.6	1.3	0.9	6.3	6.4	1.2	0.7	-0.2	4.7
1930 - 39	5.3	-0.3	-1.2	-1.9	2.0	4.7	-1.0	-2.2	-3.3	0.4
1981 - 89	4.6	-0.8	-1.5	-1.0	2.3	4.6	-0.9	-2.1	-2.1	0.8
1990 - 99	6.4	-1.2	-3.4	-3.3	1.8	6.1	-1.2	-3.7	-4.5	0.3
2000 - 09	6.4	0.4	-4.9	-2.8	3.3	5.9	0.0	-5.1	-3.9	1.3
2010 - 19	6.7	2.3	-2.0	0.9	3.7	6.6	1.9	-2.6	-0.2	2.3
2020 - 29	7.2	0.4	-2.8	-0.8	4.0	6.9	0.4	-3.2	-2.0	2.5
2030 - 39	7.7	2.4	-2.6	-0.1	5.5	7.2	2.0	-2.8	-1.2	3.6
2040 - 49	8.5	3.6	-0.3	2.0	6.4	8.5	3.2	-0.9	1.0	5.0
2050 - 59	11.0	3.8	1.2	2.3	6.3	10.7	3.8	0.8	1.1	4.8

	Lake Superior - West Basin					Lake Superior - East Basin				
	Nov.	Dec.	Jan.	Feb.	Mar.	Nov.	Dec.	Jan.	Feb.	Mar.
1951 - 80	-1.9	-9.4	-13.3	-11.3	-5.2	-1.1	-8.9	-12.9	-11.4	-5.2
GISS $2CO_2$	4.1	-4.0	-8.1	-5.2	-0.5	3.9	-3.0	-7.4	-6.1	0.5
GFDL $2CO_2$	4.4	-1.9	-6.9	-4.1	1.9	5.0	-1.6	-5.8	-4.1	1.8
OSU $2CO_2$	0.5	-6.7	-8.4	-7.4	-1.2	1.3	-6.2	-8.2	-7.4	-1.2
1930 - 39	-1.3	-7.6	-11.0	-10.4	-4.9	-1.1	-7.4	-10.7	-11.0	-5.6
1981 - 89	-3.9	-9.3	-12.5	-9.6	-4.4	-2.0	-8.9	-11.6	-9.5	-4.4
1990 - 99	-1.2	-8.9	-12.4	-11.2	-4.4	-0.3	-8.3	-12.1	-11.6	-4.6
2000 - 09	-1.6	-8.8	-13.7	-9.8	-4.1	-0.4	-8.2	-13.2	-10.5	-4.4
2010 - 19	-1.8	-6.7	-10.8	-8.4	-4.5	0.0	-6.3	-10.7	-7.9	-4.0
2020 - 29	-1.0	-6.5	-10.8	-9.5	-2.8	0.5	-6.3	-11.0	-9.4	-2.8
2030 - 39	-0.6	-6.5	-10.7	-8.2	-1.0	0.7	-6.1	-10.4	-8.6	-1.6
2040 - 49	0.1	-5.4	-8.6	-6.6	-0.8	1.8	-4.7	-8.5	-6.5	-0.7
2050 - 59	3.2	-4.0	-7.4	-7.1	-0.3	4.4	-3.4	-7.1	-6.7	-0.7

CHAPTER 3

RESULTS

Daily mean basin ice concentration was simulated for the 30 winter seasons of the 1951-80 base period, the 30 winters of each doubled CO_2 scenario, the 79 winters of the transient CO_2 scenario, and for the winters of the 1930-39 analog scenario. These data and monthly statistics for all scenarios (average, median, maximum, minimum, and standard deviation) and decadal averages of monthly statistics for the transient CO_2 scenario are available at the Great Lakes Environmental Research Laboratory.

WINTERS WITHOUT ICE COVER

The winter of 1952-53 was extremely mild, and ice cover did not form in Lake Erie's East and Central Basins (International Niagara Working Committee, 1983). The ice cycle models for these basins accurately simulated the lack of ice cover that winter. This was the only winter during the base period that Lake Superior or Lake Erie lacked ice cover. Under the doubled CO_2 scenarios up to 7% of the winters for Lake Superior basins and up to 17% of the winters for the West Basin of Lake Erie lack ice. From 37 to 83% of the winters for Center and East Basins of Lake Erie also are without ice cover (Table 8). Under the transient scenario, only Lake Erie basins have winters without ice cover. During the first five decades, no more than 20% of the winters for Lake Erie basins are without ice cover. Because of the greater mean depth of the Center and East Basins of Lake Erie (compared to the West Basin), they have more winters without ice cover in the latter decades of the transient and for the doubled CO_2 scenarios. During the last three decades of the transient, 30 to 80% of the winters for Central and East Basins of Lake Erie (but no more than 10% of winters for West Basin) are without ice cover. During the 1930-39 analog decade, only the East Basin of Lake Erie had winters without ice cover, and then, for only 20% of the time.

DATES OF FIRST/LAST ICE COVER AND ICE COVER DURATION

The 1951-80 Base Period

Ice covers began forming in shore areas of Lake Superior during the first half of January and were lost near the end of April. The average annual duration of the ice cycle on Lake Superior basins was 15 to 16 weeks. Initial ice formation on Lake Erie occurred in the shallow West Basin the third week of December and was usually lost during the third week in March. On average, the West Basin of Lake Erie had ice cover for about 13 weeks. In Lake Erie's Central and East Basins, first-ice occurred early in January and it was completely lost by late March (Center Basin) or mid-April (East Basin). Average ice cover duration was about 12 weeks for the Center Basin and close to 14 weeks for the East Basin of Lake Erie.

Doubled CO_2 Scenarios

The average dates of first- and last-ice were based only on winters with ice cover, and all 30 winters were used in calculating the average annual duration of ice cover. Under the doubled CO_2 scenarios, Lake Superior ice formation starts 2-1/2 to 6-1/2 weeks later and ends 2-1/2 to 6 weeks earlier than it did in the 1951-80 base period; Lake Erie ice formation starts 3 to 4-1/2 weeks later and ends 4 to 6 weeks earlier than the 1951-80 base period (Table 9). The average duration of ice cover is 5 to 13 weeks shorter for Lake Superior and 8 to 13 weeks shorter for Lake Erie.

The Transient Scenario

GISS-A decade averages show a general trend of later first-ice and earlier last-ice dates. Because of the built-in bias of lower temperatures in the 1951-80 base temperature data used to construct the transient scenario

Table 8. Percentage of Winters Without Ice Cover

Scenarios		Lake Superior WB	EB	WFB	Lake Erie WB	CB	EB
$1CO_2$	1951-80	0	0	0	0	3	3
$2CO_2$	GISS	0	0	0	10	67	80
$2CO_2$	GFDL	0	7	7	17	73	83
$2CO_2$	OSU	0	0	0	7	37	60
GISS-A	1981-89	0	0	0	0	10	10
GISS-A	1990-99	0	0	0	0	0	0
GISS-A	2000-09	0	0	0	0	0	0
GISS-A	2010-19	0	0	0	10	10	20
GISS-A	2020-29	0	0	0	0	0	0
GISS-A	2030-39	0	0	0	0	30	30
GISS-A	2040-49	0	0	0	10	40	70
GISS-A	2050-59	0	0	0	10	70	80
Analog	1930-39	0	0	0	0	0	20

temperatures, dates of first-ice are earlier and dates of last-ice are later than the 1951-80 base period in some of the early decades of GISS-A. A 29-year (1981-2009) average and a 30-year (2010-39) average for dates of first- and last-ice and ice cover duration were calculated to filter out the effects of the bias of lower temperatures in the 1951-80 base period (Table 9). Average dates of first-ice, last-ice, and ice cover duration for 1981-2009 are virtually the same as the 1951-80 base period, with the exception of the Center and East Basins of Lake Erie. Average date of first-ice for 2010-39 is 1-1/2 to 2 weeks later and average date of last-ice is 2 to 4 weeks earlier than during the 1951-80 base period. Average ice cover duration for 2010-2039 is 3 to 4 weeks shorter for Lake Superior basins and 5-1/2 to 7-1/2 weeks shorter for Lake Erie basins. The decadal average ice cover duration for the last two decades of the transient are 6-1/2 to 9 weeks shorter for Lake Superior basins and 9 to 13 weeks shorter for Lake Erie basins, compared to the 1951-80 base period (Table 9). Average ice cover duration during the 2040-49 decade is similar to the doubled CO_2 OSU scenario, and average ice cover duration for 2050-59 is similar to the doubled CO_2 GISS scenario.

The 1930-39 Analog Scenario

The 1930-39 analog has a shift to both later first- and later last-ice dates for Lake Superior basins and the West Basin of Lake Erie, relative to the 1951-80 base period. Average ice cover duration was 1/2 to 1 week shorter than the base period for Lake Superior basins and for the West Basin of Lake Erie. Analog decadal average ice duration was 3 to 4 weeks shorter then the base period for the Center and East Basins of Lake Erie.

DAILY AVERAGED BASIN MEAN ICE CONCENTRATION

Daily averaged ice concentration was calculated for the 30-year base period, for each of the doubled CO_2 scenarios, and for consecutive 29-year and 30-year non-overlapping periods of the GISS-A transient scenario (that is, 1981-2009 and 2010-39). The standard deviation of the base period daily average ice concentration was also calculated as an estimate of ice cover variability under the current climate regime. Selected results are shown in Figures 2 through 10. The daily averaged ice concentration portrayed in these figures was set to zero before the average date of first-ice and after the average date of last-ice (Table 9). This modification was done to be consistent with the dates given in Table 9 and does not significantly alter any of the findings.

A t-test (Brownlee, 1967) at the 99% probability level was performed between the daily averaged ice concentration of the base period and each of the two non-overlapping periods of the transient, and for each of

the doubled CO_2 scenarios. During the 1981-2009 period, average daily ice cover was significantly different than the base period during late March and early April for Lake Superior basins and during the last three weeks of February for the Center Basin of Lake Erie. The daily average ice cover for the period 2010-39 was significantly different than the base period daily average most of the winter for all lake basins. The t-test analysis for the doubled CO_2 scenarios showed significant differences between the daily average ice concentration of the 1951-80 base period and the doubled CO_2 scenarios. It is probable ice cover will be restricted to shoal areas and to the shore zone of each lake basin during an average doubled CO_2 winter (Figures 5-10). However, it will still be possible, although not very likely, to have extensive ice cover formation during some doubled CO_2 scenario winters. Extensive ice cover will form during many of the transient scenario winters, particularly during the 1981-2009 year period of the transient (Figures 2-4).

Table 9. Average First-Ice/Last-Ice Dates and Ice Duration

Average First Date of Ice Cover *

Lake Basin	1951-80 $1CO_2$	Doubled CO_2 GISS	Doubled CO_2 GFDL	Doubled CO_2 OSU	1981-2009 GISS-A	2010-39 GISS-A
Sup WB	Jan 6	Feb 14	Feb 20	Jan 25	Jan 5	Jan 16
Sup EB	Jan 9	Feb 18	Feb 22	Jan 30	Jan 10	Jan 21
Sup WFB	Jan 2	Feb 6	Feb 15	Jan 19	Jan 4	Jan 12
Eri WB	Dec 17	Jan 18	Jan 17	Jan 7	Dec 19	Dec 31
Eri CB	Jan 6	Feb 4	Feb 4	Jan 27	Jan 10	Jan 16
Eri EB	Jan 12	Feb 3	Feb 7	Feb 2	Jan 15	Jan 26

Average Last Date of Ice Cover *

Lake Basin	1951-80 $1CO_2$	Doubled CO_2 GISS	Doubled CO_2 GFDL	Doubled CO_2 OSU	1981-2009 GISS-A	2010-39 GISS-A
Sup WB	Apr 27	Mar 31	Mar 15	Apr 8	Apr 24	Apr 14
Sup EB	Apr 26	Apr 1	Mar 14	Apr 8	Apr 22	Apr 13
Sup WFB	Apr 26	Apr 1	Mar 14	Apr 8	Apr 22	Apr 13
Eri WB	Mar 19	Feb 17	Feb 13	Feb 14	Mar 13	Feb 25
Eri CB	Mar 29	Feb 28	Feb 28	Feb 28	Mar 24	Mar 4
Eri EB	Apr 18	Mar 2	Mar 7	Mar 7	Apr 9	Mar 18

Average Ice Duration (Days) **

Lake Basin	1951-80 $1CO_2$	Doubled CO_2 GISS	Doubled CO_2 GFDL	Doubled CO_2 OSU	1981-2009 GISS-A	2010-39 GISS-A
Sup WB	112	46	24	75	108	88
Sup EB	108	43	19	69	103	84
Sup WFB	115	55	26	80	109	92
Eri WB	93	26	23	35	84	54
Eri CB	83	8	6	19	71	41
Eri EB	97	6	5	13	82	43

Table 9. (continued)

Decadal average ice cover duration for transient and analog

Lake Basin	Decade Starting Year 1930	1981	1990	2000	2010	2020	2030	2040	2050
Sup WB	106	110	107	109	93	86	86	66	46
Sup EB	103	103	100	105	86	82	83	61	44
Sup WFB	112	110	107	111	95	91	91	70	56
Eri WB	85	72	96	83	45	66	51	31	29
Eri CB	61	62	83	68	34	53	37	14	8
Eri EB	70	75	92	79	31	52	46	5	7

* Average dates of first- and last-ice for winters with ice cover.
** Average season length for all winters in each scenario.

FIGURE 2

DAILY AVERAGED ICE COVER 1951-80 BASE & GISS-A SCENARIO LAKE ERIE CENTER BASIN

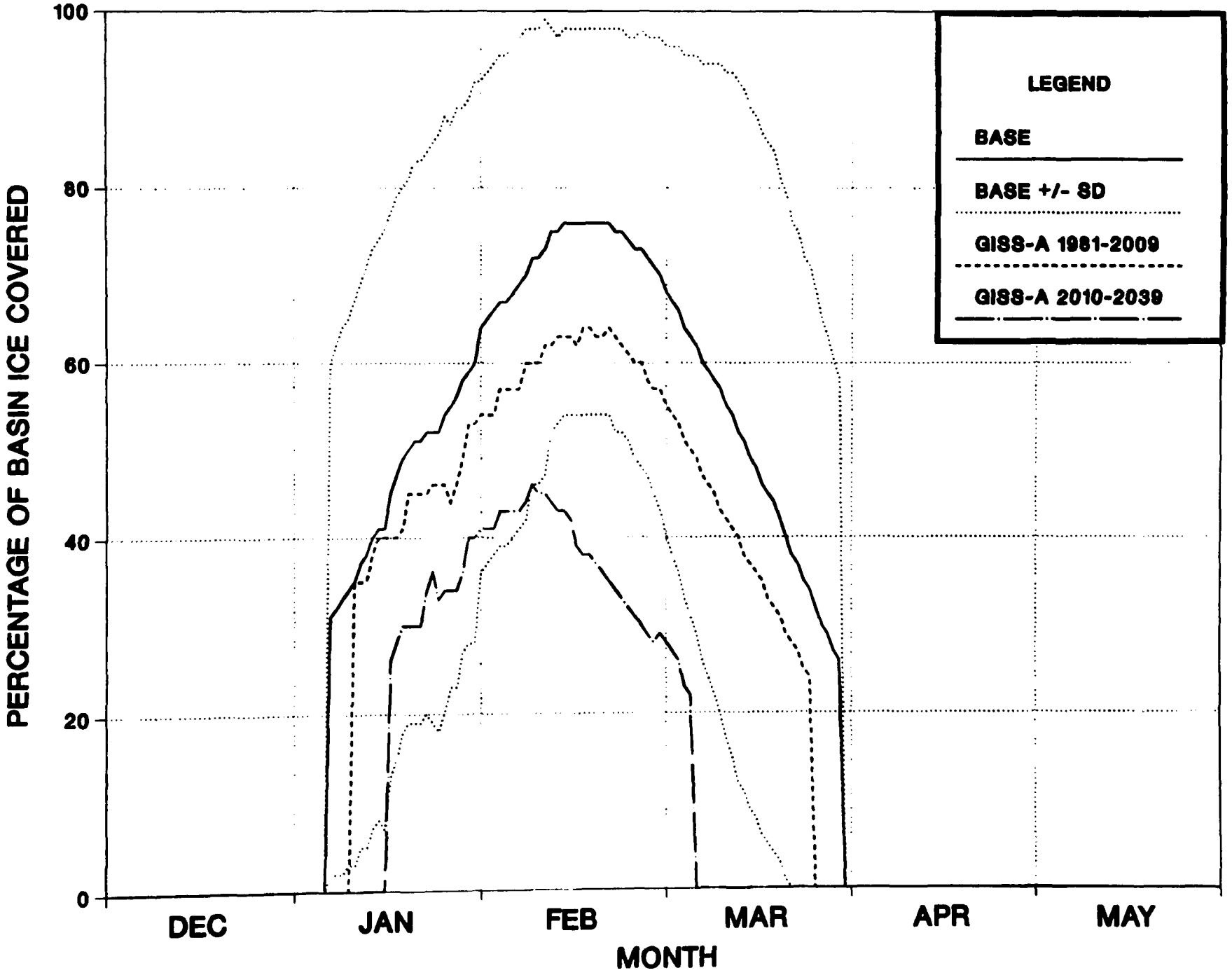

FIGURE 3

DAILY AVERAGED ICE COVER 1951-80 BASE & GISS-A SCENARIO LAKE SUPERIOR WEST BASIN

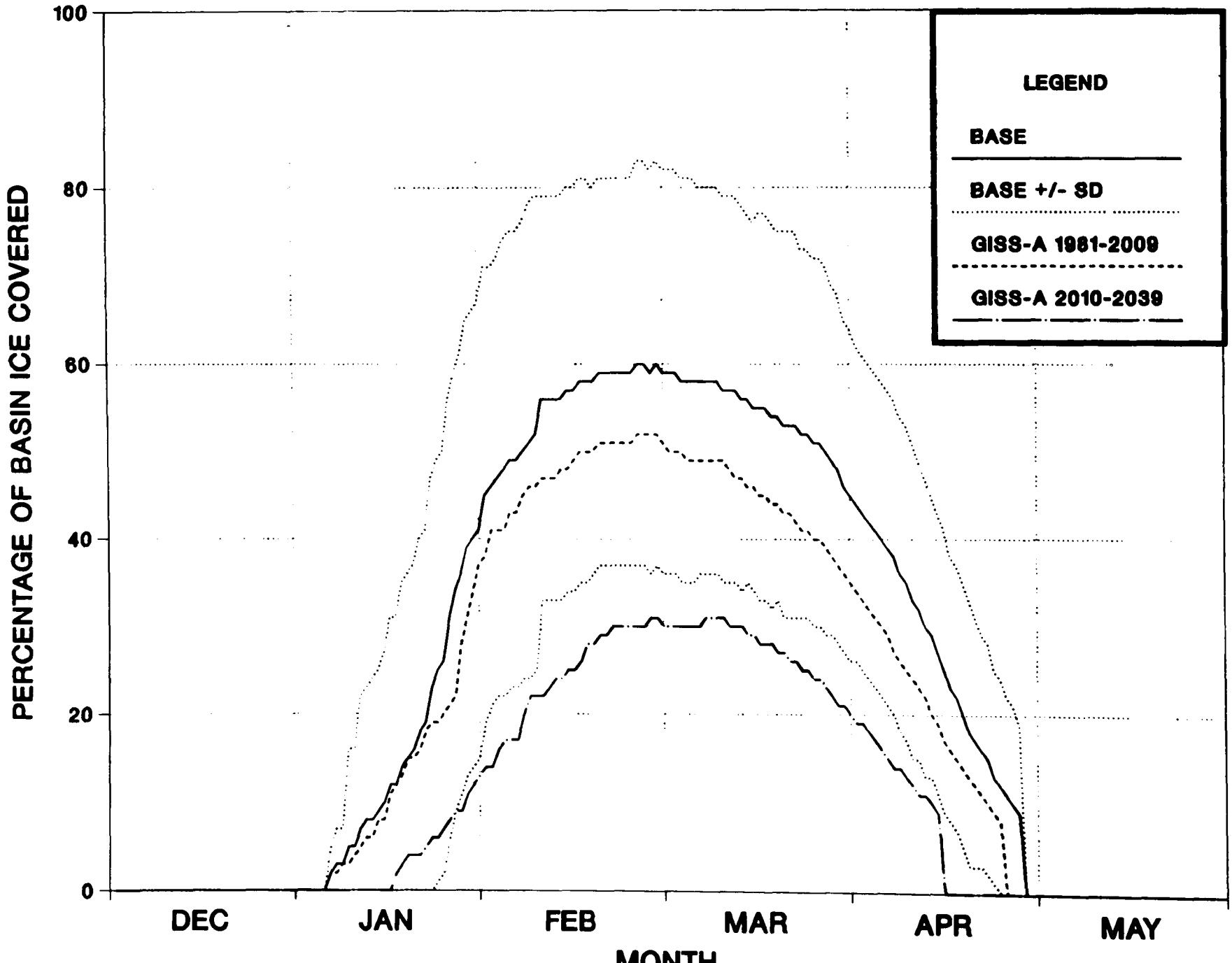

Assel

FIGURE 4

DAILY AVERAGED ICE COVER 1951-80 BASE & GISS-A SCENARIO LAKE SUPERIOR AT WHITEFISH BAY

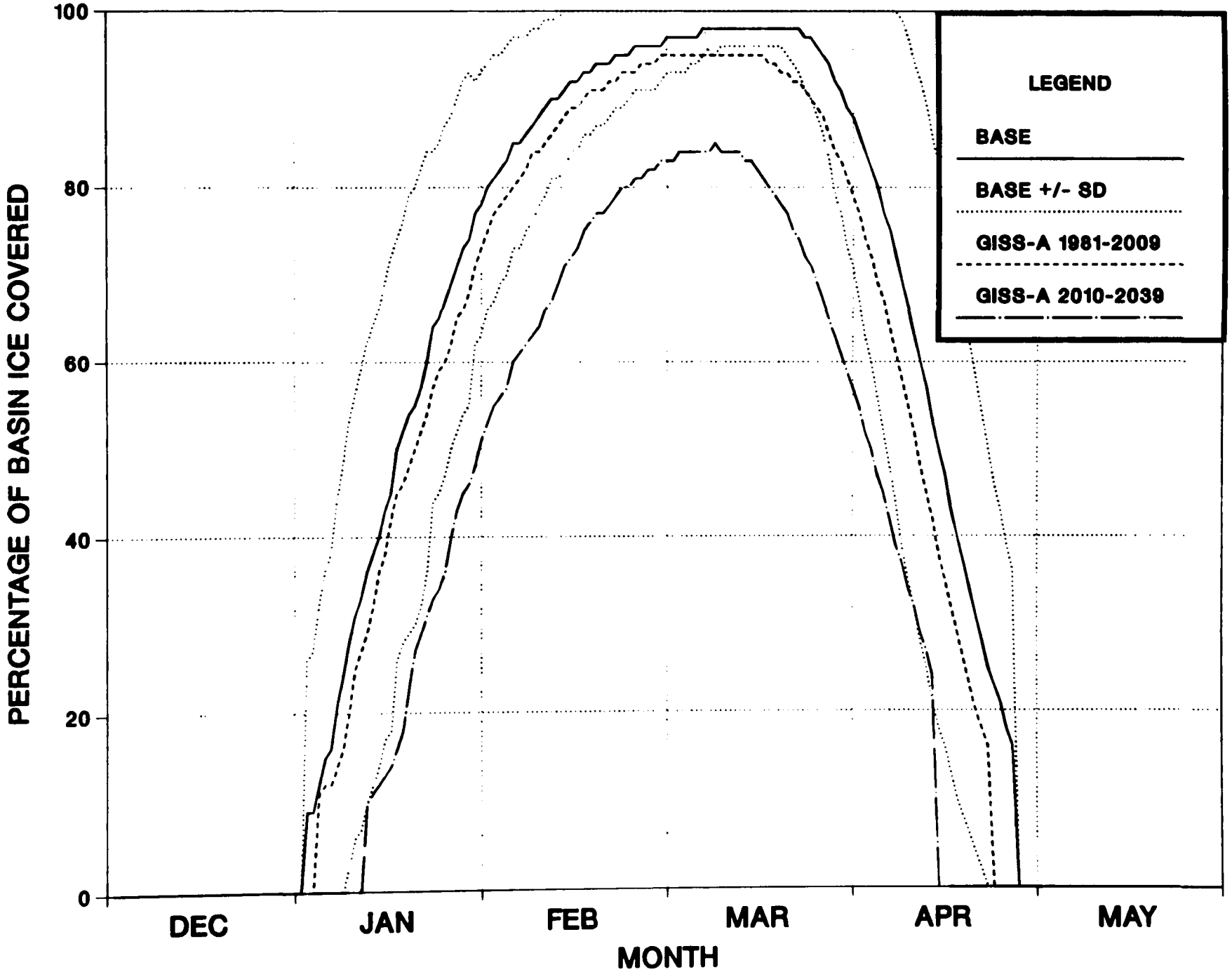

Assel

FIGURE 5

DAILY AVERAGED ICE COVER 1951-80 BASE & 2CO2 SCENARIOS LAKE ERIE WEST BASIN

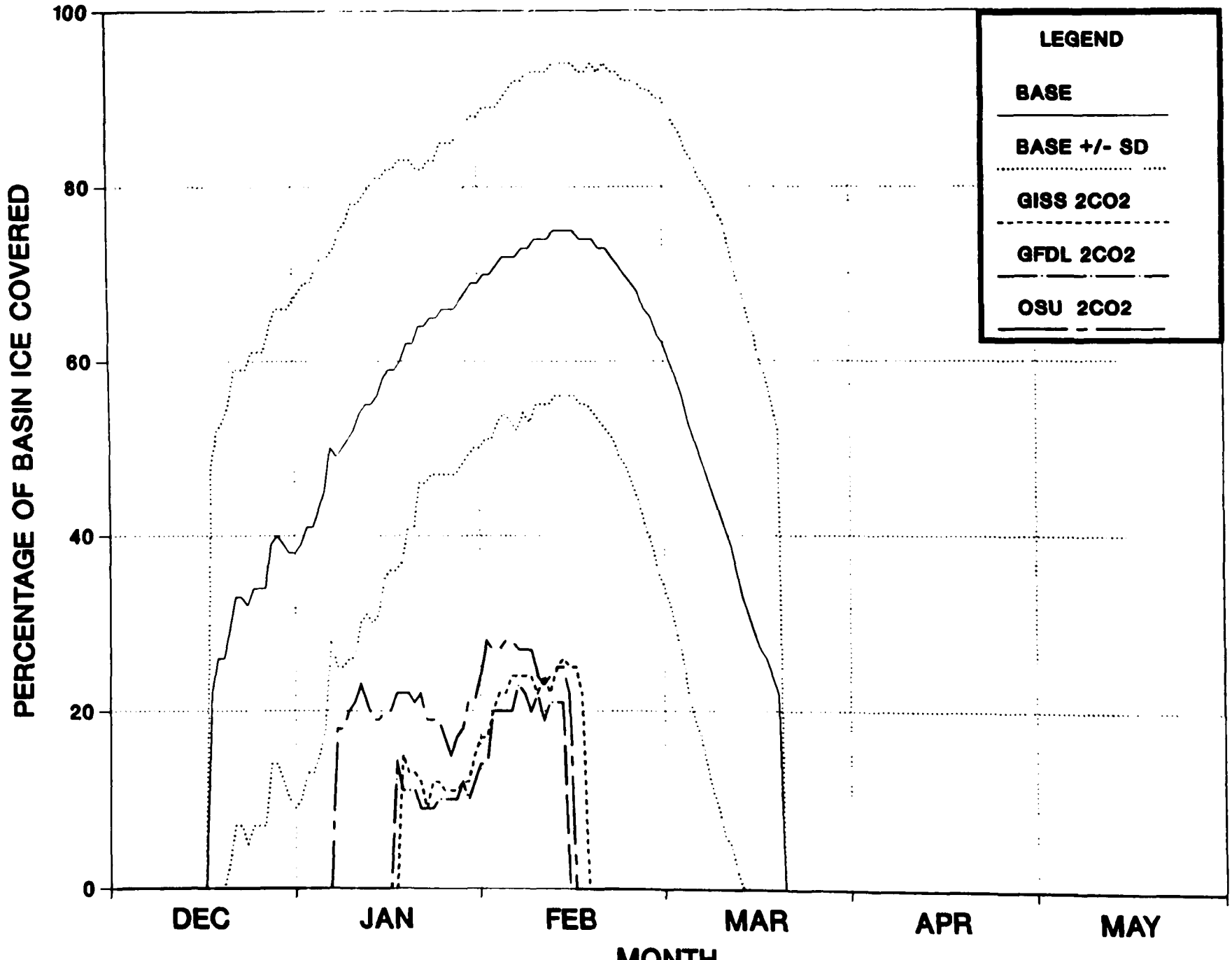

Assel

FIGURE 6

DAILY AVERAGED ICE COVER 1951-80 BASE & 2CO2 SCENARIOS LAKE ERIE CENTER BASIN

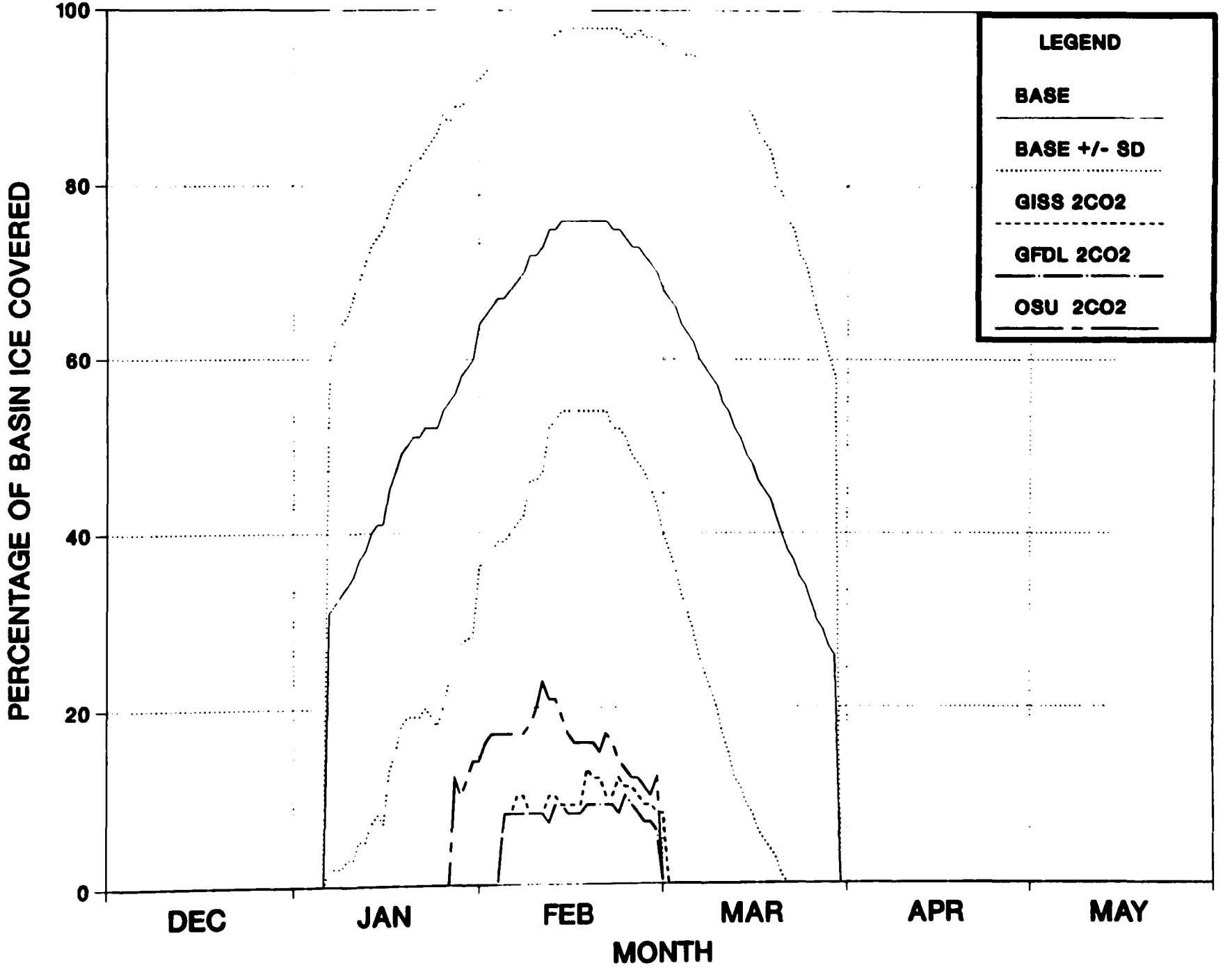

FIGURE 7

DAILY AVERAGED ICE COVER 1951-80 BASE & 2CO2 SCENARIOS LAKE ERIE EAST BASIN

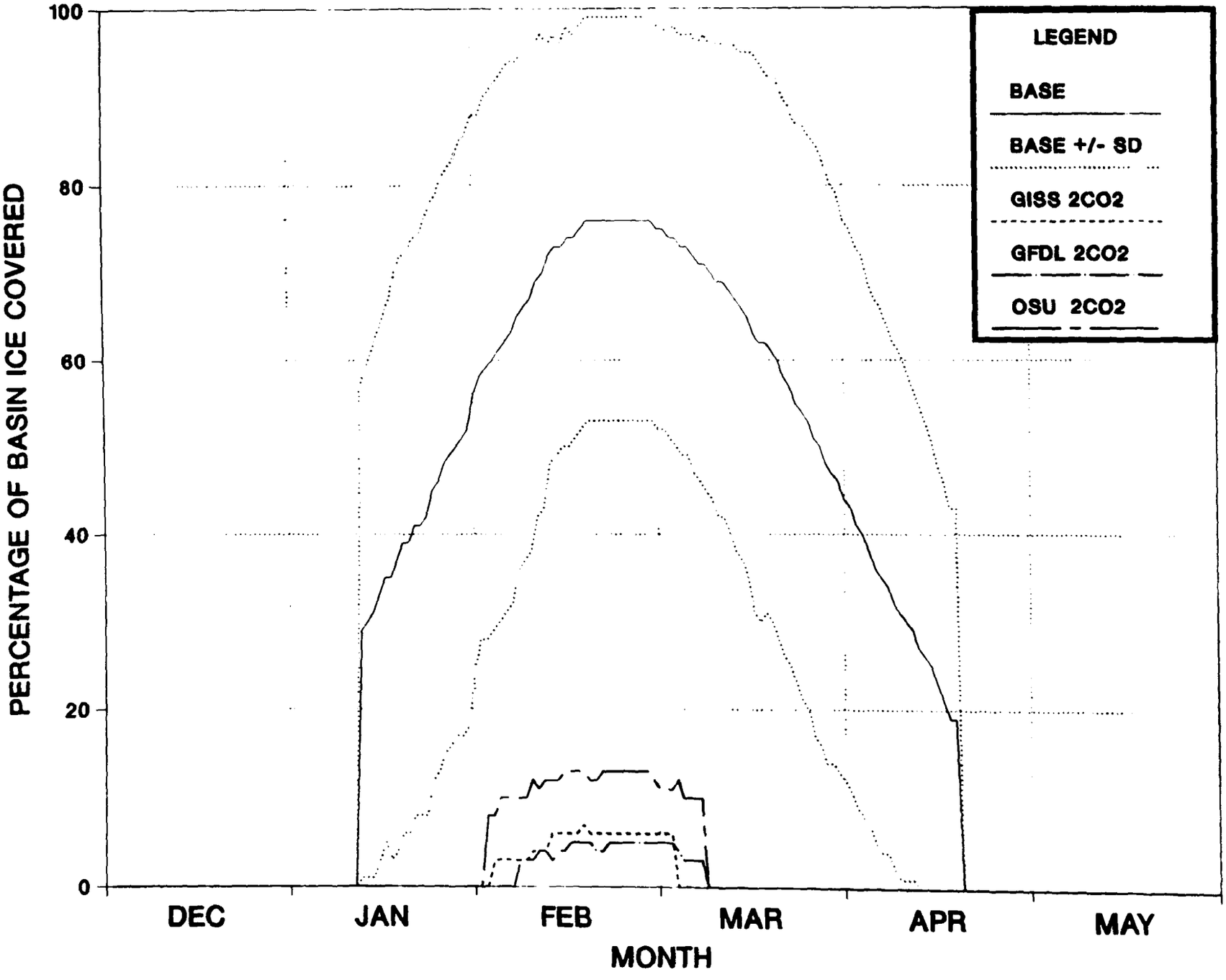

Assel

FIGURE 8

DAILY AVERAGED ICE COVER 1951-80 BASE & 2CO2 SCENARIOS LAKE SUPERIOR WEST BASIN

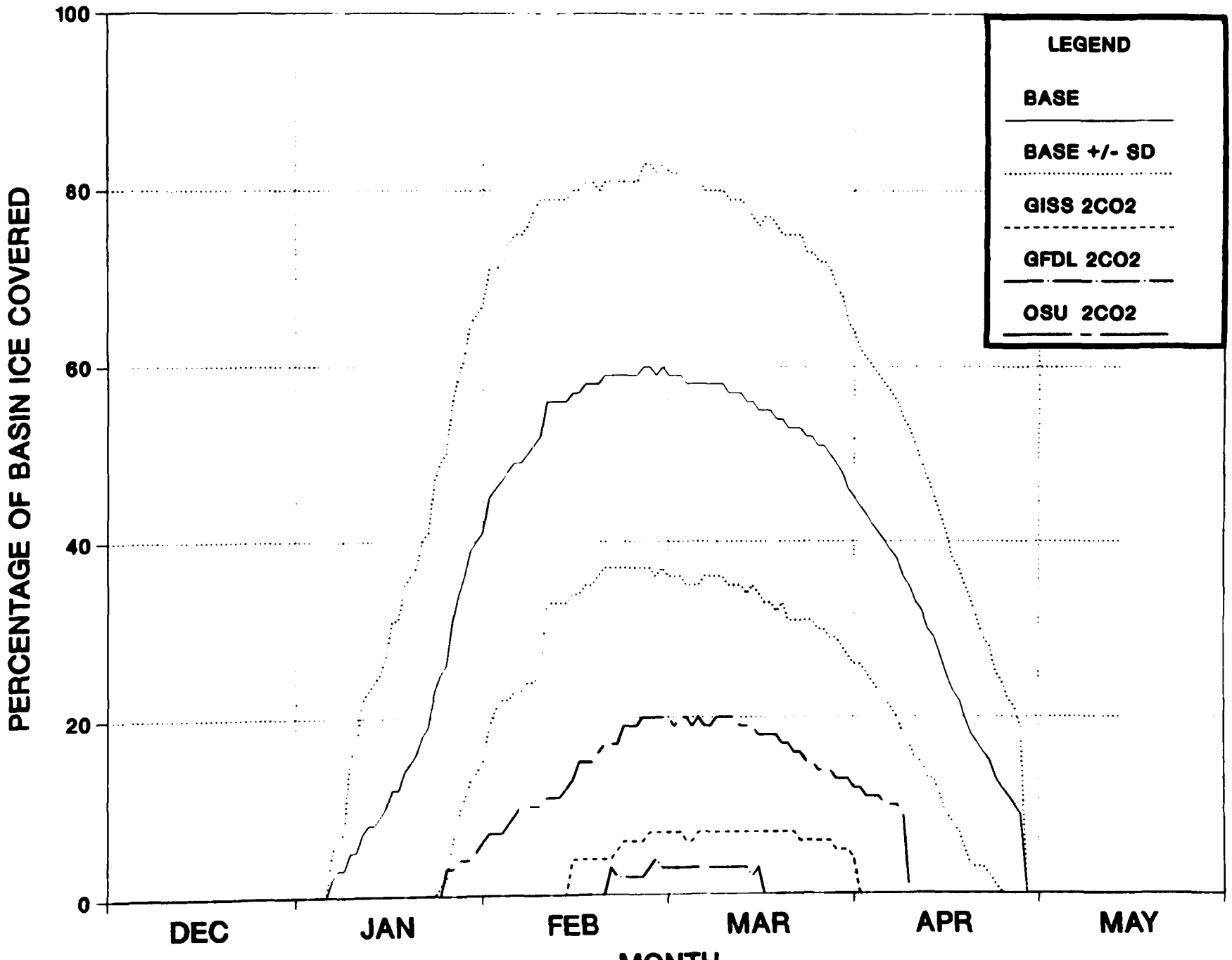

Assel

FIGURE 9

DAILY AVERAGED ICE COVER 1951-80 BASE & 2CO2 SCENARIOS LAKE SUPERIOR EAST BASIN

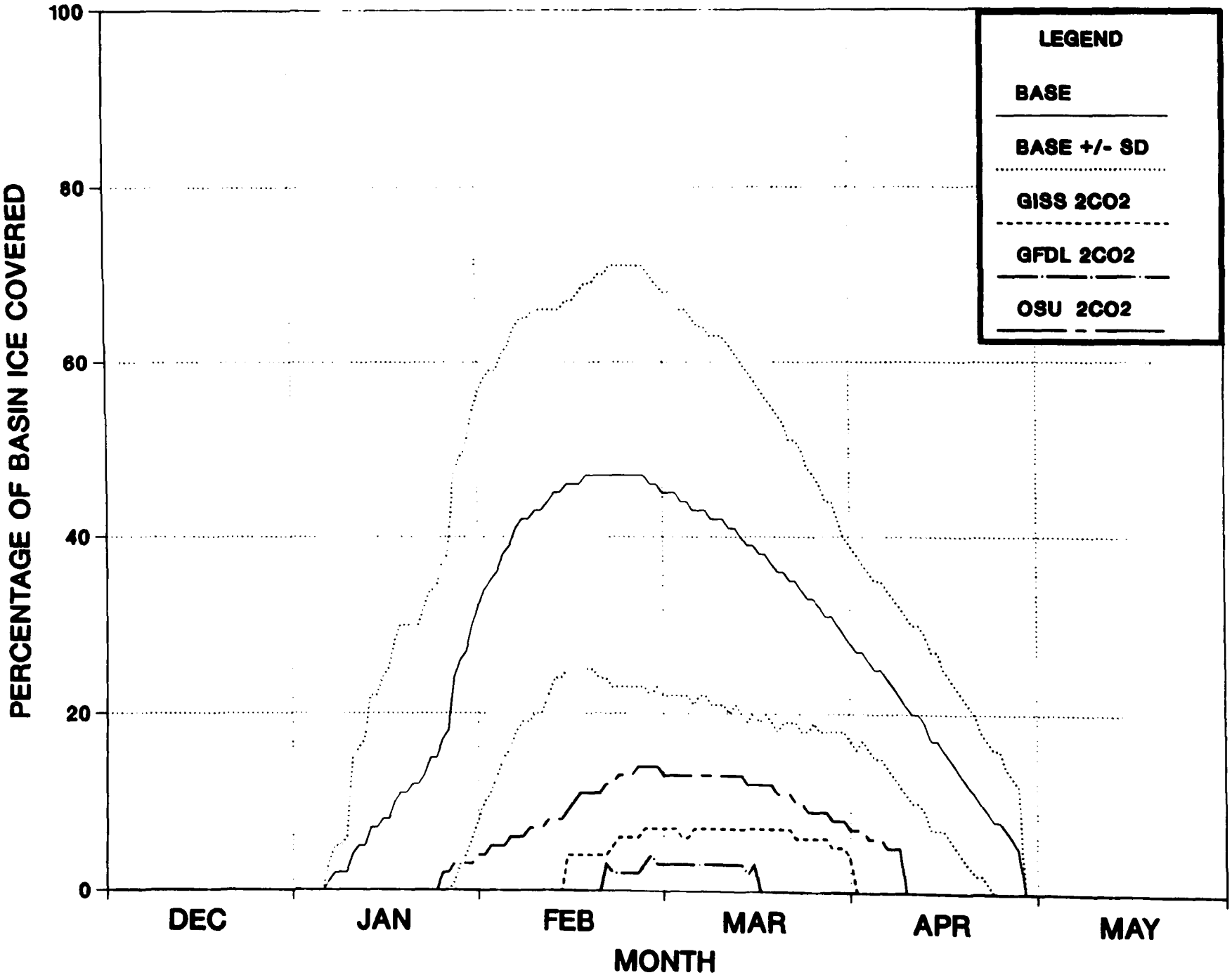

Assel

FIGURE 10

DAILY AVERAGED ICE COVER 1951-80 BASE & 2CO2 SCENARIOS LAKE SUPERIOR AT WHITEFISH BAY

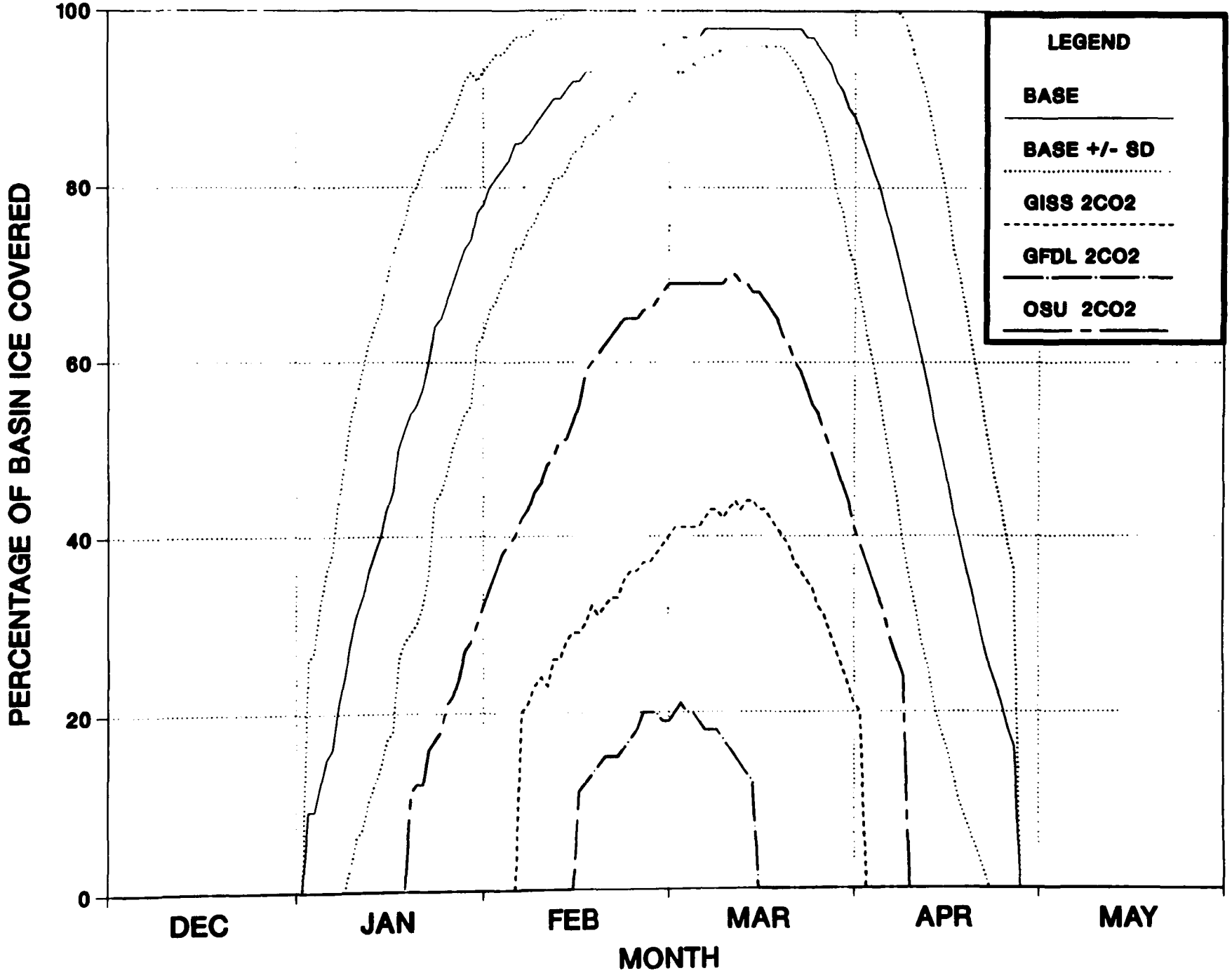

Assel

CHAPTER 4

INTERPRETATION AND LIMITATIONS OF RESULTS

INTERPRETATION

Winter duration is much shorter, ice cover less extensive, and frequency of winters without ice cover much greater under doubled CO_2 warming scenario winters relative to the 1951-80 base period. Average winter duration for the 1951-80 base period was 13 to 16 weeks; under the doubled CO_2 scenarios, the average winter duration is 5 to 13 weeks shorter. Daily average ice cover under all of the doubled CO_2 scenarios is likely to be limited to the shore area and shallows of each lake basin because these are the first areas to form ice and because maximum average daily ice concentration (30 year average) is less than 30% for all basins except Whitefish Bay. The frequency of winters without ice cover is much greater in the East and Central Basins of Lake Erie relative to the West Basin because of their greater mean depth. Ice concentration and duration trends followed the air temperature trends of the three doubled CO_2 scenarios; that is, the coldest scenario (OSU) had the greatest ice concentration with the longest ice cover duration, and the warmest scenario (GFDL) had the smallest ice concentration with the shortest ice season duration. Under the 79-year transient CO_2 scenario (1981-2059), only Lake Erie basins have winters without ice cover; during the last three decades of the transient (2030-59), 30 to 80% of the winters for Lake Erie's Center and East Basins are without ice cover. Transient scenario daily ice concentration, averaged for the years 2010-39, is significantly less than the base period for all lake basins. However, extensive ice cover will occur under many transient CO_2 winters, particularly during the first 29 years (1981-2009). Average ice cover duration is 3 to 7 weeks shorter during the next 30 years of the transient 2010-39 relative to the 1951-80 base period. During the last decade of the transient scenario (2050-59), decadal-averaged ice concentration and ice cover duration is similar to the doubled CO_2 scenarios. Ice cover simulation of an analog climate warming period (1930-39) shows that average ice cover duration was 1/2 to 1 week shorter than the 1951-80 base period for Lake Superior and about 3 to 4 weeks shorter for the Center and East Lake Erie basins. Annual maximum ice concentration was less then the base period but greater than the doubled CO_2 scenario.

LIMITATIONS

The ice cycle models do not account for the effects of wind, nor do they consider the entire annual heat budget of Lakes Superior and Erie. If the climate warming scenarios have significantly higher winds or greater frequency of severe storms, then models may over-estimate ice concentration; if wind speeds are lower, models may under-estimate ice concentration. Lake heat storage increases under global warming may result in threshold FDD developed for the 1960-79 base period no longer being representative of time of ice formation. Two points should be kept in mind regarding this limitation: (1) there were winters in the 1960-79 calibration period for the ice cycle analysis in which only shore ice formed in Lakes Erie and Superior so that the threshold FDD accumulations approximate winters in which no ice cover forms, and (2) the threshold FDD values verified well over independent data for a winter without ice cover and for a winter with only shore ice. The threshold FDD simulated a no ice cover condition for mild 1952-53 winter, no ice cover formed in the East and Central Bases of Lake Erie that winter, and the models verified well for the mild 1982-83 winter season in which ice cover formed later than normal. Another potential limitation is associated with the average daily ice melt rates developed during the regression analysis. The melt rates used to estimate ice loss may under-estimate melt rates during CO_2 warming scenarios. But the threshold FDD values and ice melt rates represent at the very least an upper limit of potential ice concentration and ice duration under global warming, and they are considered a good first approximation to ice conditions under doubled CO_2 warming scenarios.

The uncertainty in simulated ice concentration and ice duration (standard error analysis) is estimated to range from 20 to 30% for ice concentration and from 2 to 4 weeks for ice cover duration. The models are sensitive to the magnitude and number of consecutive days with air temperature below freezing. If FDD accumulations fluctuate about the value needed for initial ice formation all winter, the models show intermittent periods of ice formation and loss. In such cases, ice cover and ice duration can be either over- or under-estimated.

Information on the spatial and temporal distribution of the ice cover is limited by the calculation of basin mean ice concentration. This is a significant limitation in studies where spatial details on ice concentration are needed, as in ecological studies where the date and extent of initial ice cover and duration of shore-fast ice is important.

CHAPTER 5

IMPLICATIONS OF RESULTS

ENVIRONMENTAL IMPLICATIONS

We are just beginning to understand the importance of ice cover to lake ecology. Freeberg and Taylor (in press) observed that year-class strength of lake whitefish is related to winter severity. Under the doubled CO_2 scenarios, the Great Lakes may not have ice cover some winters. If ice cover is missing, whitefish and perhaps other cold water fish species may vanish from the Great Lakes. Bolsenga (in press) has observed that some biological activity actually increases under the protection of the ice cover in the shore zones of the Great Lakes; the loss of the ice cover therefore may result in a reduction in the annual abundance of some micro-organisms and perhaps significantly affect larger life forms that prey on them. The ice cover also protects some shore areas against the impact of high-energy waves that might otherwise cause shore erosion (Zumburge and Wilson, 1953).

SOCIO-ECONOMIC IMPLICATIONS

The ice cover impedes and eventually stops most navigation in the Great Lakes during the winter months. Aids to navigation that would be damaged by ice are removed in late fall and reinstalled the following spring. Ice booms, which help prevent ice jams, are installed at the head of the St. Marys and Niagara Rivers to aid the formation of stable ice cover lakeward of the head of these rivers (International Niagara Working Committee, 1983). The U.S. and Canadian Coast Guard and hydropower authorities are involved in this activity; the Coast Guard also assists ships beset in the ice. The results shown here indicate the navigation season could be extended to 10 months or perhaps even 12 months under a doubled CO_2 climate warming. Thus a considerable cost savings may be associated with reduced Coast Guard and hydropower authority activity and increased shipping activity in the winter months. The greatly reduced extent and duration of ice cover will likely result in higher evaporation from Lake Superior and lower lake levels during the winter months (Croley and Hartmann, in press). The higher lake evaporation during winter implies an increase in snowfall in the Snow Belt regions of the Great Lakes. There is a considerable amount of winter recreational activity on ice-covered bays and harbors of the Great Lakes -- ice boating, ice fishing, snowmobile racing. Much if not all of this activity would be reduced or discontinued completely with reduced ice cover.

CHAPTER 6

POLICY IMPLICATIONS

The management of the Great Lakes fishery should be reviewed relative to commercial and sports fishing since there may be loss or reduction of some fish species and increases or introduction of other fish species. Port and harbor facilities may need to be upgraded to support increased ocean-going and local shipping activities that would become possible with year-round navigation. New regulation plans may need to be developed for controlling flows through the St. Marys, Niagara, and St. Lawrence Rivers.

GLOSSARY

LAKE & BASIN ABBREVIATIONS

Sup = Lake Superior
Eri = Lake Erie
WB = West Basin
CB = Center Basin
EB = East Basin
WFB = Whitefish Bay

UNITS ABBREVIATIONS

C = Celsius
cm = centimeters
m = meters
km = kilometers

SCENARIO AND AGENCY ABBREVIATIONS

EPA = United States Environmental Protection Agency
2CO2 = double carbon dioxide scenario
1CO2 = single carbon dioxide scenario
GCM = Global Circulation Model
GISS = Goddard Institute of Space Science
2CO2 GCM GISS-A = Goddard institute of Space Science transient
CO2 GCM GFDL = Geophysical Fluid Dynamics Laboratory
2CO2 GCM OSU = Oregon State University 2CO2 GCM

ADDITIONAL TABLE, FIGURE, AND TEXT ABBREVIATIONS

Eq. = equation
C1,C2,C3 = coefficients of regression in Table 2
FDD = the accumulated freezing degree-days (C) on a given date
FDDCRIT = a critical FDD accumulation for a given day in the annual Great Lakes ice cycle; if FDD exceeds this value ice cover remains at 100 percent.
BFDD = a threshold value of FDD representing (1) the date of the end of fall overturn in Eq. 1 and (2) the number of FDD needed to cool the near shore water to 0 degrees C for Lake Erie basins, Eq. 2.
FZFAC = a on/off switch for ice formation in Eq. 2, ice is not permitted to form until FDD equals BFDD. Before that time FZFAC=1000, after that time FZFAC=0.
JD = a day counter, the ice cycle starts (JD=1) the first day FDD is greater than BFDD
MFDD = the annual maximum FDD accumulation
DMFDD = the date of the annual maximum FDD accumulation
MELT = the average daily ice melt rate (cm/day)

ARITHMETIC OPERATORS

* = multiplication / = division
\+ = addition - = subtraction
> = greater than < = less than
sqrt = square root
exp = exponential function (base e)

STATISTICAL ABBREVIATIONS

RMSE = Root Mean Square Error
SD = Standard Deviation

REFERENCES

Assel, R.A. "A Computerized Data Base of Ice Concentration for the Great Lakes." NOAA Data Report ERL GLERL-24, NOAA Great Lakes Environmental Research Laboratory, Ann Arbor, Michigan, 1983. 26 pp.

Assel, R.A., "Great Lakes Degree-day and Winter Severity Index Update: 1897-1983." NOAA Data Report ERL GLERL-29, NOAA Great Lakes Environmental Research Laboratory, Ann Arbor, Michigan, 1986. 54 pp.

Assel, R.A., F.H. Quinn, G.A. Leshkevich, and S.J. Bolsenga. "NOAA Great Lakes Ice Atlas." PB84160811, National Technical Information Service, Springfield, Virginia. 1983. 115 pp.

Assel, R.A., C. R. Sinder, and R. Lawrence. "Comparison of 1982-83 Winter Weather and Ice Conditions with Previous Years." Mon. Wea. Rev. 113(3):291-303, 1985.

Bilello, M.A., "Method for Predicting River and Lake Ice Formation." J. Applied Meteorology 3(1):38-44, 1964.

Bolsenga, S.J. "Nearshore Great Lakes Ice Cover." J. Cold Regions Sci. and Tech. 15:99-105, 1988.

Bolsenga, S.J. "An Under Ice Ecology Pilot Program, Operations and Preliminary Scientific Results." J. Great Lakes Res. (in press).

Brownlee, K.A. "Statistical Theory and Methodology in Science and Engineering", second edition. John Wiley & Sons, Inc. New York, New York, 1967. pp. 295-305.

Croley T.E.,II, and H.C. Hartmann. "Effects of Climatic Changes on the Laurentian Great Lakes Levels." NOAA Great Lakes Environmental Research Laboratory, Ann Arbor, Michigan (in press).

Diaz H.F., and Quayle R.G. "The Climate of the United States Since 1895: Spatial and Temporal Changes." Mon. Wea. Rev. 108(3):249-266, 1980.

Freeberg M.H., and W. Taylor. "The Impact of Egg and Larval Mortality on Year Class Strength of Lake Whitefish." Department of Fisheries and Wildlife, Michigan State University, East Lansing, Michigan (in press).

Lewis, P.J. "Severe Storms Over the Great Lakes: A Catalogue summary for the Period 1957-1985." Canadian Climate Center Report No. 87-13, Atmospheric Environment Service, Downsview, Ontario, Canada.

Howe, D.A., D.S. Marchand, and C. Alpaugh. "Socio-economic Assessment of the Implications of Climatic Change for Commercial Navigation and Hydro-electric Power Generation in the Great Lakes St. Lawrence River System." Great Lakes Institute, University of Windsor, Windsor, Ontario, Canada. 1986. 118 pp.

International Niagara Working Committee. "1982-83 Operations of the Lake Erie-Niagara River Ice Boom." U.S. Army Corps of Engineers. Buffalo District, Buffalo, New York. 1983. 7 pp.

Oak, W.W., and H.V. Myers. "Ice Reporting on The Great Lakes." Weatherwise 6(1):7-10, 1953.

Palecki M.A., and Barry, R.G. "Freeze-up and Break-up of Lakes as an Index of Temperature Changes during the Transition Seasons: A Case Study for Finland." J. Climate and Applied Meteorology 25:893-902, 1986.

Richards, T.L. "Meteorological Factors Affecting Ice Cover on the Great Lakes." In: Proceedings of the Sixth Conf. on Great Lakes Research. International Association for Great Lakes Research, Ann Arbor, Michigan, 1963. pp. 204-215.

Rogers, J.C. "Long-range Forecasting of Maximum Ice Extent of the Great Lakes." NOAA Tech. Memo. ERL GLERL-7. National Technical Information Service, Springfield, Virginia. 1976. 15 pp.

Sleator, F.E. "Ice Thickness and Stratigraphy at Nearshore Locations on the Great Lakes." NOAA Data Report ERL GLERL-1-2. NOAA Great Lakes Environmental Research Laboratory, Ann Arbor, Michigan, 1978. 434 pp.

Snider, R.C. "Great Lakes Ice Forecasting." NOAA Tech. Memo. NWS OSD 1. National Technical Information Service, Springfield, Virginia, 1971. 106 pp.

Tramoni F., R.G. Barry, and J. Key. "Lake Ice Cover As A Temperature Index for Monitoring Climate Perturbations." Zeit. Gletscherkunde 21:43-49, 1985.

Williams, G.P. "Correlating Freeze-up and Break-up with Weather Conditions." Canad. Geotech. J. 11(4):313-326, 1965.

Williams, G.P. "Predicting the Date of Lake Ice Breakup." Water Resour. Res. 7(2):323-333, 1971.

Zumburge, J.H., and J.T. Wilson. "The Effects of Ice on Shore Development." In: Proceeding of the Fourth Conf. Coastal Engineering, Chicago Ill., J. W. Johnson, ED. Council on Wave Research, The Engineering Foundation, University of California, Berkeley, California, 1953. pp. 201-205.

POTENTIAL CLIMATE CHANGES TO THE LAKE MICHIGAN THERMAL STRUCTURE

by

Michael J. McCormick
NOAA/GLERL
2205 Commonwealth Blvd.
Ann Arbor, MI 48105

Interagency Agreement No. DW13932957-01-0

CONTENTS

Page

FINDINGS 6-1

CHAPTER 1: INTRODUCTION 6-2

CHAPTER 2: METHODS 6-4
The Mixed Layer Model 6-4
Model Development 6-4
The Scenarios 6-7

CHAPTER 3: RESULTS 6-8
Base Climatology Simulation 6-8
Impacts of Climate Change 6-11

CHAPTER 4: DISCUSSION, CONCLUSIONS, AND SPECULATIONS 6-23
Interpretation of Results 6-23
Speculations 6-24

REFERENCES 6-25

FINDINGS[1]

A one-dimensional numerical model after Garwood (1977) was used to estimate the vertical climatological temperature structure in Lake Michigan. The climatology was based on the model output from simulations of the 1981-1984 offshore temperature field. Quasi-two-dimensional effects were also accounted for by the model by prescribing a weak upwelling velocity during the winter months. Once the climatology was estimated, several different global circulation model (GCM) scenarios were examined. Three different GCM scenarios of doubled CO_2 ($2xCO_2$) and one transient scenario were simulated. They were (1) Goddard Institute of Space Sciences (GISS) $2xCO_2$, (2) the Geophysical Fluid Dynamics Laboratory (GFDL) $2xCO_2$ scenario, (3) the Oregon State University (OSU) $2xCO_2$ scenario, and (4) GISS Transient scenario A corresponding to the 2010-19 decade (GISS A).

In general, the GISS, GFDL, and OSU simulations suggest the following impact on Lake Michigan. The winter heat content of the lake will be significantly higher than under current climate estimates. The summer heat content will, in general, be higher than the current climate too but not to the same extent as seen during the winter months. The higher winter heat content will cause an earlier setup for thermal stratification by as much as two months and thus a much longer stratified season will result. The earlier onset of stratification coupled with little change in the wind stress pattern will yield stronger stratification. Thus, the greatest differences between the $2xCO_2$ and the present climatology are for an earlier, longer duration, and stronger stratification.

The monthly averaged mixed layer depth (mld) may be deeper in the winter and shallower during the summer than current seasonal averages. However, for the winter months this is not true at less than monthly time scales. At higher than monthly frequencies, the present mlds may penetrate to the lake bottom any time during late fall through spring in response to storms and strong surface cooling, while the $2xCO_2$ calculated mlds do not. In general, the $2xCO_2$-derived mlds are restricted from penetrating deep waters because of the persistence of higher than present water column temperatures (>4°C), which results in less potential energy being converted into mechanical energy to aid the mixing and deepening process. Thus, the true range in mixed layer depth may well be severely decreased in the future, with only infrequent to rare episodes where the surface mixed layer encroaches on the deep lake bottom, i.e., no turnover. The shallow summer mixed layer will be warmer and more buoyant than presently observed, making it more difficult for entrainment and/or mixing to occur.

The most critical parameter controlling the thermal structure is the wind stress. Calculations of the potential climate impacts were made using uncertain future scenario winds that differ little from the present climate. Should future windspeeds be reduced from those used here, then sensitivity analyses suggest that all of the previously described impacts may underestimate the true impact on the annual thermal cycle.

Simulation results based on the GISS A scenario suggests that some of these effects may be evident 20 to 30 years from now.

---

[1]Although the information in this report has been funded wholly or in part by the U.S. Environmental Protection Agency under Interagency Agreement No. DW13932957-01-0, it does not necessarily reflect the Agency's views, and no official endorsement should be inferred from it.

CHAPTER 1

INTRODUCTION

Lake Michigan is a large lake covering over 57,000 km^2 with a maximum depth of 281 meters and a mean depth of 85 meters. Because of its large size, the dominant controlling physics of the lake environment is more similar to oceanic situations than it is to "small" lakes. Water temperature is one of the most fundamental physical properties, and accurate knowledge of its distribution is often critical to oceanographic and limnological problems. Despite the importance of temperature, little is known of its climatology in the Great Lakes and in particular that of Lake Michigan. Feit and Goldenberg (1976) determined surface water temperature climatologies for Lakes Superior, Huron, Erie, and Ontario, but the record lengths were short, ranging from only 4 to 10 years. While water intake temperature records of much longer duration exist for many locales in the Great Lakes, their nearshore proximity makes them a poor candidate for constructing meaningful climatologies. Other temperature data sets from more favorable locations exist, but their poor temporal coverage precludes their usage as well.

The most comprehensive data set to date, describing Lake Michigan temperatures in offshore waters, was obtained by the National Data Buoy Center (NDBC) in the central southern basin of the lake from 1981-1984. However, these data too do not fulfill all of the needs for generating a water temperature climatology because of gaps in their temporal coverage and limited spatial coverage as well. In particular, these data only cover the top third of the water column (i.e., 50 meters of the 150-meter mooring depth), and since the mooring is deployed only during the ice-free season, no data exist for the winter months. Consequently, the only alternative is to estimate the climatology by modeling the temperature field, and to use the NDBC data for model testing.

The Garwood (1977) model is used herein to estimate the water temperature climatology for Lake Michigan and potential changes to it that may occur should the climate change. Intermodel comparisons by McCormick and Meadows (1988) and Martin (1985) found the Garwood model to be successful for simulating the seasonal temperature cycle for inland seas and in open ocean applications, respectively. Figure 1 shows the study location and an idealized temperature profile with a shallow surface mixed layer.

The remainder of this report will describe the model development, results, conclusions, and speculations on the Lake Michigan simulations under various future climate scenarios hypothesized by several GCMs.

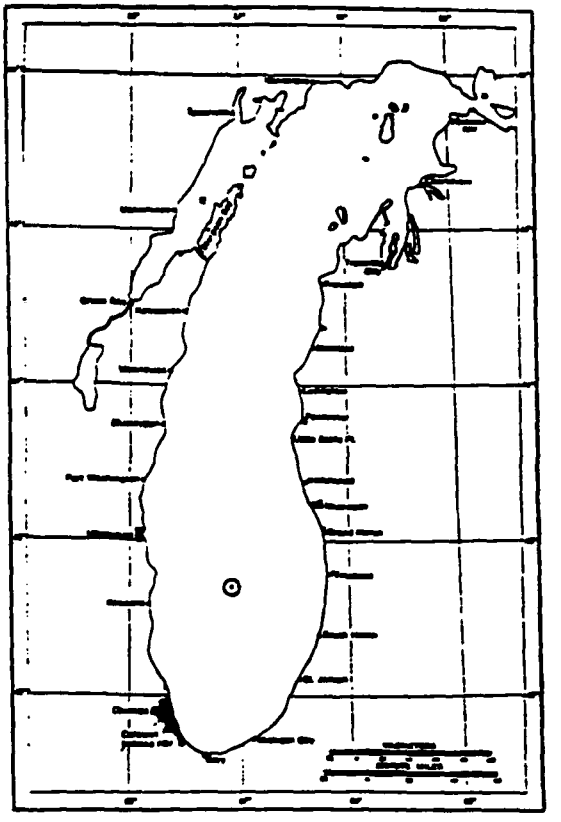

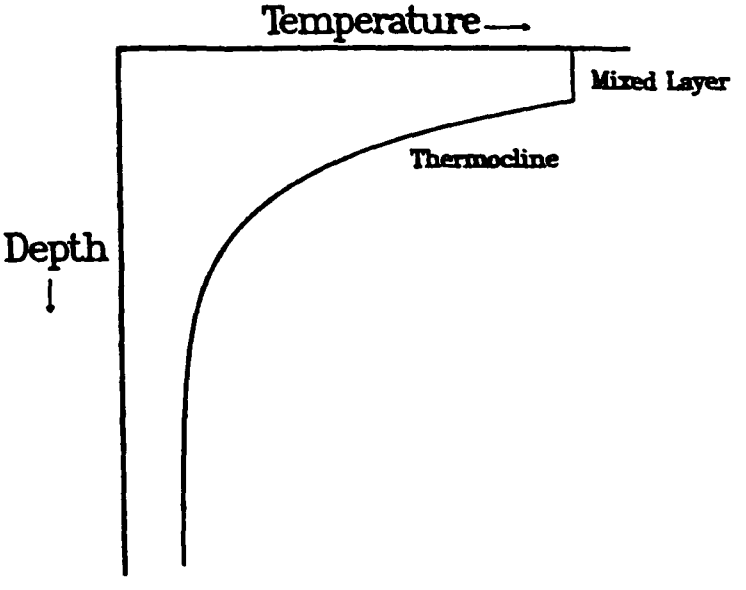

Figure 1. Lake Michigan study location (top) and an idealized temperature profile showing a shallow surface mixed layer (bottom).

CHAPTER 2

METHODS

The Mixed Layer Model

The Garwood model version used here is described in McCormick and Meadows (1988). First though, a brief description of the model is in order. The model is one-dimensional in the vertical and is based on the turbulence kinetic energy (TKE) budget. During the summer months, the thermal structure at any given time in general is dependent on the dynamic balance between the wind stress, which tends to destabilize the water column and mix it, and a positive surface heat flux, which warms the surface waters and tends to stabilize the water column and retard mixing. During the winter months when the lake is cooling and the surface heat flux is negative, the wind stress effects on mixing are aided in their efforts by convective mixing, generated from gravitational instabilities due to the surface cooling. These and other important processes are expressed in the TKE equation.

Two of the processes in the TKE budget which also affect the vertical distribution of temperature are viscous dissipation and entrainment due to shear instabilities at the mixed layer base. This version of the Garwood model allows for mixed layer deepening due to turbulent erosion and shear mechanisms. McCormick and Meadows (1988) added the shear instability source to Garwood's model and assumed the major shear source to be from wind-generated pure inertial oscillations. Observations on the frequency distribution of kinetic energy in the Great Lakes support this interpretation (e.g., Saylor et al., 1980; Boyce and Chiocchio, 1987). To estimate this contribution to the TKE budget, the shear strength was estimated from one-dimensional momentum equations after Thompson (1976).

If mixed layer deepening is to be realistically described for all possible forcing conditions, then energy dissipation must be explicitly included in the TKE budget. Garwood parameterizes dissipation on two scales. First, energy is removed in proportion to the magnitude of the total TKE, and in the second dissipation process, energy loss is proportional to both the TKE and the depth of the mixed layer. This parameterization of dissipation is advantageous to long-term simulation by avoiding the possible carry-over and buildup of potential energy over annual time scales. Thus, under well-behaved forcing conditions, cyclic solutions are possible.

Model Development

No process-oriented models have been used to do multi-year simulations of temperature in Lake Michigan. Making the transition from seasonal to annual length simulations has been problematic and shortcomings still remain. The time and place chosen for testing and enhancing the Garwood model was 1981-1984 at the site of the NDBC meteorological buoy in the center of the southern basin with a depth of 150 meters. During the ice-free months of 1981-1984, the NDBC hung a thermistor string from their buoy. Nine thermistors were positioned at approximately 5 meters spacing covering the top 50 meters of the water column. Temperatures were recorded at hourly intervals, but the data return and quality were less than ideal. At no time during the 1981-1984 period were all thermistors operational. At various times, as few as two thermistors and as many as seven were recording useful data. Furthermore, analyses of the low frequency response of the data suggests that their accuracy is no better than 0.5°C. Nonetheless, it is the best available data set for this study.

Hourly meteorological data were assembled for a period spanning 30,359 hours from 16 July 1981 through 31 December 1984. (The 16 July date was the date of the first NDBC temperature record.) No offshore water temperature records are available for the 1951-80 period. The meteorological data were obtained from the NDBC buoy and from airport meteorological stations at Milwaukee, Wisconsin, and Muskegon, Michigan. The airport data were averaged with respect to each other and were used whenever buoy meteorological data were missing. Airport meteorological data were used for December in 1981, for January through March and October through December in 1982, and for 1983 and 1984 January through March and for the month of December. Both the airport windspeeds and directions were adjusted for overwater conditions following Schwab (1983).

Hourly observations of windspeed and direction, air temperature, dew point temperature, and total cloud cover were used to force the model. Data on the shortwave global radiation (290-4000 mm) were unavailable and thus were estimated from an empirical model after Cotton (1979). The NDBC meteorological buoy had no provisions for measuring the dew point temperature, essential for estimating the latent heat flux, so all dew point data were taken from shore-based data and were corrected for over-water conditions after Philips and Irbe (1978). Once the meteorological data were assembled, the model testing and development began.

The Garwood model was forced with hourly meteorological data, and numerically integrated over one-hundred-fifty 1-meter-thick grid points at one-hour time steps. The initial conditions were estimated from the 16 July 1981 data and the solution was marched in time for 30,359 hours to the end of 1984. Simulation of the winter regime revealed the need to reevaluate the model physics.

First, the cold winter temperatures of 1982 drove the surface water temperature to freezing conditions on several days. No facilities are included in the model to properly account for ice formation, buildup, and decay. Therefore, the surface temperature was artificially constrained to always be greater than or equal to zero. The modeled surface heat flux during these episodes was set equal to the surface irradiance only and thus does not represent the true surface heat flux. Fortunately, these episodes were infrequent enough in their occurrence so as to not seriously bias the monthly averaged surface heat flux estimate. Second, Farmer and Carmack (1982) noted the importance of the nonlinear pressure temperature term on the density when temperatures are near the temperature of maximum density. The interaction between pressure and temperature has a strong influence on the mixed layer depth in deep lakes, like Lake Michigan, during the winter months. Hence, in contrast to most mixed layer modeling efforts, it was deemed necessary that pressure effects be explicitly accounted for by the equation of state. The equation of state after Pickett and Herche (1984) was used and is shown here in the following equation,

$$\rho = 999.968 - .00773T_0^2 + .526\times10^{-4}T_0^3 + .0492P - .00021PT_0 \qquad (1)$$

where, ρ = density (kg/m^3), T_0 = temperature °C (T-3.98), and P = pressure (bar).

Simulations of the 1982 Lake Michigan springtime transition to thermal stratification with mixed layer models after Denman (1973), Garwood (1977), McCormick and Scavia (1981), and Thompson (1976) suggested the need for yet additional physics. Each model was premature in its timing of the spring transition. Studies of the velocity profile at several locations in the benthic boundary layer of the southern basin by James Saylor of the Great Lakes Environmental Research Laboratory (GLERL) in Ann Arbor, Michigan, has revealed the presence of an Ekman boundary layer. Mass balance calculations suggest that significant upwelling velocities, We, (due to a convergence of the Ekman boundary layer) should persist during the winter months in the region where this study was made, and thus it may be an important source/sink of heat to surface waters which must be accounted for by the mixed layer model. The steady-state Ekman pumping velocity, W_e, is given as

$$W_e = (\rho f)^{-1}\mathrm{Curl}(\tau_b) \qquad (2)$$

where, f = Coriolis force and τ_b = bottom stress vector. The Curl of the bottom stress vector was estimated from current meter data from four moorings surrounding the central portion of the southern basin. This final model modification was implemented by prescribing W_e for January through May of each year. Constant monthly values were used with a peak velocity of 1 m/day used for March. The monthly velocities are listed in Table 1. The upwelling details will be described in a forthcoming paper.

Specifically, the heat flux due to upwelling, when it occurs, is handled at each time step by first calculating the temperature profile without any consideration of upwelling. Then the temperature change, ΔTi, at level i, is calculated by equation (3),

$$\Delta T_i = (T_{i+1} - T_i)W_e\Delta t/\Delta Z \qquad (3)$$

where, Δt is the time step and ΔZ is the grid size. Equation (3) is applied from the surface (i=1) to near bottom (i=n-1). Thus, when surface waters are colder/warmer than those at depth, the upwelling heat flux is positive/negative. Although this is a coarse approximation of the true upwelling structure, it nonetheless has

TABLE 1. Model Inputs

WIND SPEED (m/s) ($2xCO_2$ - GCM Control)

Model	Jan	Feb	Mar	Apr	May	Jun	Jul	Aug	Sep	Oct	Nov	Dec
(1)	-.4	-0.5	-1.7	-0.6	-0.8	-0.3	-0.1	0.0	0.1	1.0	1.1	-1.2
(2)	-.3	-1.0	0.3	-0.4	-1.6	-1.6	1.6	0.9	-0.7	-0.6	-0.1	-0.7
(3)	-.5	-0.3	0.3	0.4	-0.2	-0.2	-0.6	0.2	-0.3	-0.4	-0.1	-0.1
(4)	-.1	-0.2	1.0	-0.4	0.1	-0.5	0.1	1.0	0.6	0.1	-0.2	0.1

OVER-WATER AIR TEMPERATURE (°C)
(GCM - Base Climatology)

Model	Jan	Feb	Mar	Apr	May	Jun	Jul	Aug	Sep	Oct	Nov	Dec
(1)	8	8	6	5	3	3	2	3	6	4	7	8
(2)	7	7	6	5	4	8	9	5	6	6	7	8
(3)	6	4	3	3	3	3	3	3	2	3	3	3
(4)	3	3	0	3	0	0	0	0	0	0	0	3

HUMIDITY RATIOS ($2xCO_2$/GCM Control)

Model	Jan	Feb	Mar	Apr	May	Jun	Jul	Aug	Sep	Oct	Nov	Dec
(1)	1.82	1.49	1.64	1.40	1.30	1.28	1.07	1.28	1.39	1.23	1.54	1.50
(2)	1.56	1.44	1.43	1.37	1.25	1.18	0.97	1.16	1.12	1.31	1.56	1.58
(3)	1.13	1.06	1.05	1.04	1.12	1.17	1.11	1.18	1.25	1.18	1.09	1.14
(4)	1.16	1.20	1.13	1.17	1.06	1.09	1.13	1.14	1.09	1.01	1.05	1.29

SHORTWAVE SOLAR RADIATION RATIOS ($2xCO_2$/GCM Control)

Model	Jan	Feb	Mar	Apr	May	Jun	Jul	Aug	Sep	Oct	Nov	Dec
(1)	0.92	1.04	0.98	1.03	1.00	0.99	0.98	1.04	1.04	1.12	1.03	0.99
(2)	2.05	1.15	1.15	0.93	1.05	1.05	1.02	1.01	1.01	1.01	1.07	1.74
(3)	1.05	1.04	1.07	1.09	1.03	0.99	1.01	0.98	1.00	1.02	1.00	1.01
(4)	0.97	0.90	1.01	1.01	0.99	0.96	0.93	0.97	1.01	0.99	1.03	0.86

FRACTIONAL CLOUD COVER RATIOS ($2xCO_2$/GCM Control)

Model	Jan	Feb	Mar	Apr	May	Jun	Jul	Aug	Sep	Oct	Nov	Dec
(1)	1.03	0.93	.97	0.98	1.07	1.09	1.08	1.00	1.06	0.85	1.00	0.93
(2)	1.13	1.18	.92	1.09	0.90	0.83	0.95	0.82	0.90	1.00	1.09	0.92
(3)	0.76	0.83	.74	0.61	0.68	0.94	0.85	1.17	0.83	0.81	0.90	0.91
(4)	1.00	1.05	.97	1.04	0.98	1.19	1.44	1.11	0.92	1.04	1.05	1.03

UPWELLING VELOCITY (m/day) (For All Simulations)

Jan	Feb	Mar	Apr	May	June through December
0.2	.55	1.0	.45	0.3	0.

Model (1) = GISS $2xCO_2$
Model (2) = GFDL $2xCO_2$
Model (3) = OSU $2xCO_2$
Model (4) = GISS A (Transcient Scenario for 2010-19)

enabled more accurate simulation of the upper water column thermal structure when tested over short time periods. An ongoing effort to understand the offshore upwelling structure is presently being addressed at GLERL using a three-dimensional circulation model.

The remaining processes are included in the local heat budget: sensible, latent, net longwave, and shortwave global radiation. The sensible and latent heat fluxes are calculated after bulk aerodynamic formulas with atmospheric stablity-dependent exchange coefficients. The stability dependence is based on the work of Businger et al. (1971), and the program is documented in Schwab et al. (1981). The net longwave radiation is calculated after Wyrtki (1965), and the penetrating components of the solar irradiance are approximated after Ivanoff (1977). The extinction coefficients for the visible and infrared radiation bands were 0.21 m-1 and 2.85 m-1, respectively.

The Scenarios

Three different GCM results and one transient result were used and compared against the Base climatology, as estimated by the previously described simulation. The three GCM simulations, corresponding to a climate with an effective doubling of atmospheric CO_2 concentration, were made with the following models: (1) GISS, (2) GFDL, and (3) OSU. The transient run was made using a decadal average corresponding to 2010-19 with scenario A. This run is identified in the tables and figures as GISS A.

The $2xCO_2$ meteorology used to drive the Lake Michigan simulations was estimated from model output from the $1xCO_2$ and $2xCO_2$ GCM simulations. These data were formed into a ($2xCO_2/1xCO_2$) ratio and then used to adjust the Base climatology as described below. The $1xCO_2$ GCM simulations were run for a 30-year period corresponding to 1951-1980. The $2xCO_2$ general circulation model simulations were also done for a 30-year period, but with a doubling of the atmospheric concentration of CO_2 and other greenhouse gases. Monthly averages were formed for each meteorological parameter, at each grid point, for each simulation. A $2xCO_2/1xCO_2$ ratio for each parameter was formed by dividing the monthly averaged quantity from the $2xCO_2$ simulation by the $1xCO_2$ one. The transient (GISS A) simulation was handled in the same manner. The GCM model output from the grid point closest to central southern Lake Michigan was used to represent the future climate inputs for Lake Michigan. Five different parameters were used from the GCM output: (1) windspeed, (2) air temperature, (3) humidity, (4) incident solar radiation at ground level, and (5) fractional cloud cover. The hourly base meteorological data from 1981 to 1984 were adjusted by multiplication with the applicable ($2xCO_2/1xCO_2$) GCM ratios. The GCM ratios were held constant on monthly time scales.

The windspeed adjustments were made differently. The supplied GCM monthly windspeed estimates were made by vector averaging rather than by scalar averaging the GCM winds. Thus, when the $2xCO_2/1xCO_2$ GCM wind ratios were formed, the calculated ratios were often very large. If the Base climatology winds were multiplied with these ratios, then hurricane force winds would have occurred for at least 2 months out of every simulation year. Therefore, to avoid potentially disastrous results and yet still salvage some of the information in the GCM winds, the differences between the monthly averaged $2xCO_2$ and $1xCO_2$ windspeeds were used in place of their ratio. These differences were then added to the Base climatology winds. The resulting changes to the wind stress in the Base meteorology were small and more consistent with expectations from other studies (Cohen, 1986). The monthly averaged GCM inputs are shown in Table 1.

CHAPTER 3

RESULTS

Base Climatology Simulation

McCormick and Meadows (1988) simulation of Lake Erie temperatures with the Garwood model found the optimal model constants to be identical to those found by Martin (1985) in his simulation of North Pacific Ocean data. The success of this model in such diverse environments instills confidence in the model parameterizations of the governing physics. Thus, all of the model simulations for the Base and future climate scenarios were made without altering the model coefficients.

The Base climatology simulations are shown against surface water temperature data in Figures 2 and 3. The surface temperatures are illustrated for the entire time periods for which the NDBC data were available. For clarity, less than 5% of the approximately 19,000 observations are depicted in the figures.

The lack of time series data throughout the water column and winter temperature data limits the ability to fully evaluate model performance. Nonetheless, from Figures 2 and 3 some of the effects of offshore upwelling and model sensitivity to windspeed are made clear. In Figure 2, low-pass filtered surface temperatures generated by the mixed layer model with no upwelling (i.e., 0.0 meter/day) are shown against data. The effects of a 10% decrease (top of Figure 2) and 10% increase (bottom of Figure 2) in windspeed (WS) are shown as well. The rms error for the 0.0-meter/day simulation was over 4°C for surface temperatures. It is evident that much of this error is contributed by the poor simulation of the 1982 data.

Significant improvement in the surface temperature simulation was made by using a weak upwelling velocity (i.e., "Variable Upwelling" in Figure 3), which was held constant on monthly time scales and operational from January through May (Table 1 and Figure 3). The rms error was approximately 3°C overall, with the 1982 data once again being the most difficult to simulate. Additional improvement in the surface temperature simulation was made in the 0.0-meter/day case with a 10% reduction in windspeed. The overall rms error for these simulations was approximately 2°C, with the major difference between this and the other simulations occurring in 1982. The 1981, 1983, and 1984 rms errors were either similar or slightly worse than the 0.0-meter/day or variable upwelling simulations with unaltered winds. The 2°C rms error was half of the error seen in the 0.0-meter/day simulation and better than 1°C in rms error compared to the simulation with upwelling. The improved rms error occurred because of significant improvements in simulating the spring 1982 data. That year was the coldest winter in this study, and the reduced winds compensated for model shortcomings by reducing lake heat losses during the winter and thus enabled better agreement between model and data during the spring transition period.

If the objective were to solely fit surface temperature data, then the represenative choice for our Base climatology would have been obvious. However, there is no physical justification for arbitrarily reducing the windspeeds. And although the rms errors with variable upwelling were larger than the 0.0-m/day case with reduced winds, there is mounting evidence, as described earlier, to justify the use and necessity of upwelling to properly describe the offshore heat budget. Therefore, the simulation with variable upwelling was judged to be the most represenative of the region under study and consequently became the "Base" climatology referred to throughout this work.

Again it is important to note here that in terms of surface water temperature simulation of the effects of the "no upwelling" versus the "variable upwelling" cases, either one could be made to mimic the other by adding either a positive or negative 10% bias to the windspeed data. This illustrates that the windspeed is most critical for accurate determination of the Base climatology, and for estimating any possible future alterations to it as well.

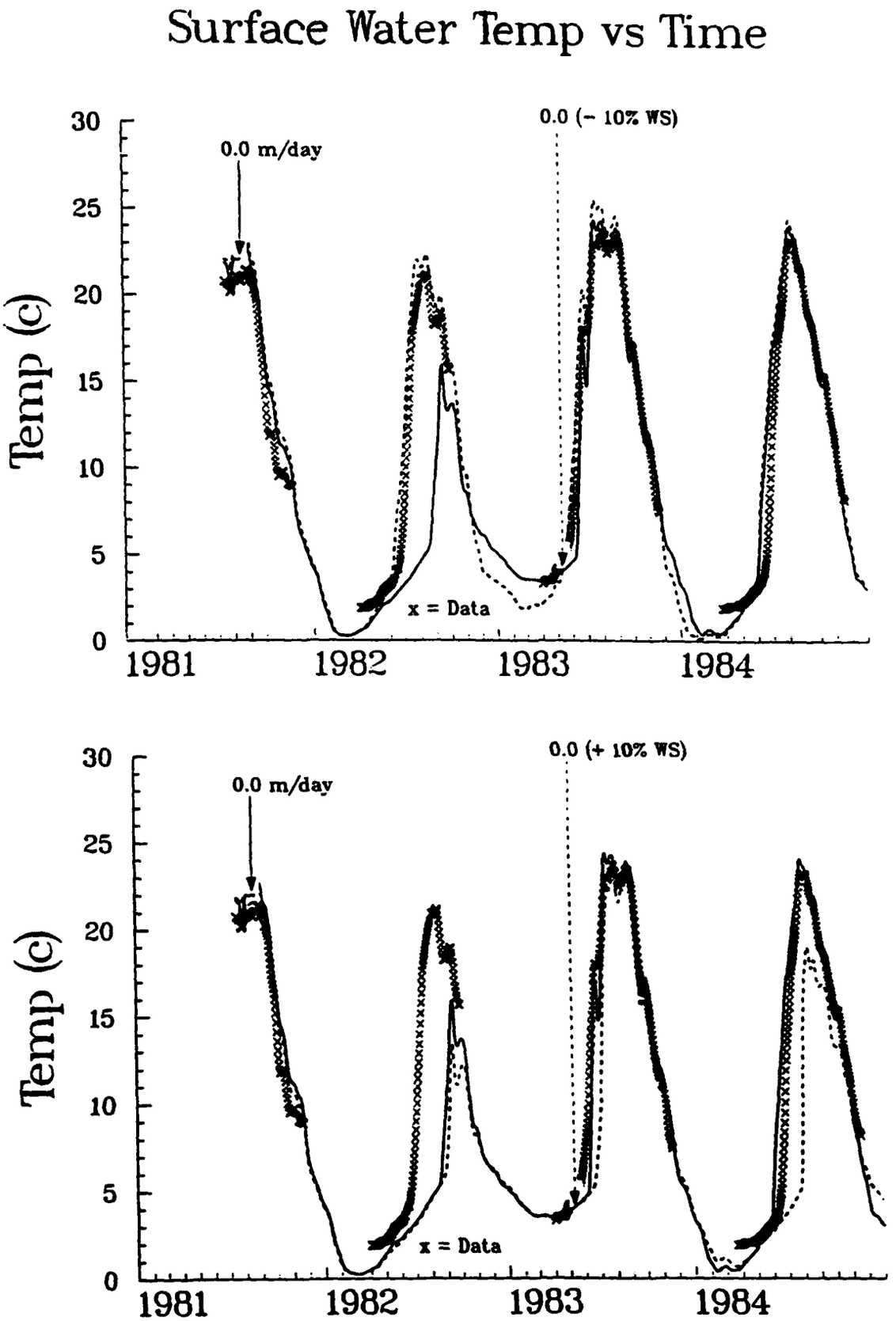

Figure 2. Low-pass filtered (336-hr cutoff) surface temperatures with no upwelling and under different wind conditions. Each curve pattern is duplicated by the line joining it to its label.

Surface Water Temp vs Time

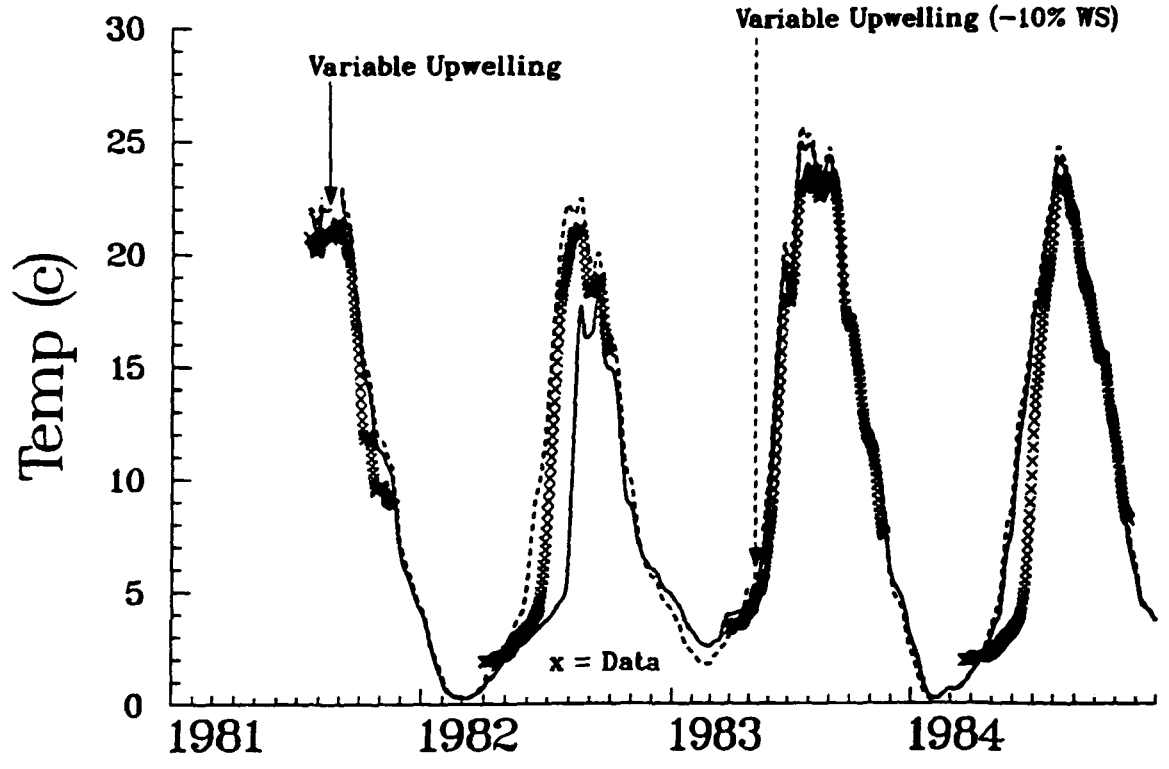

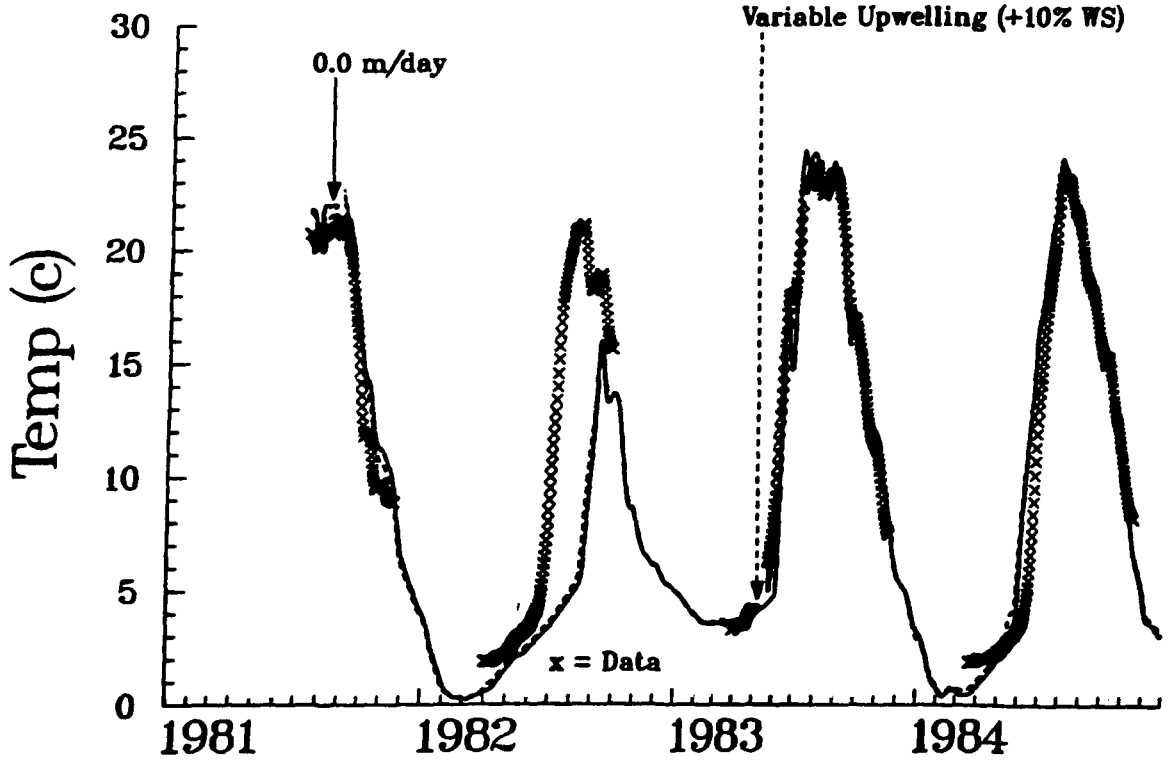

Figure 3. Low-pass filtered (336-hr cutoff) surface temperatures with variable upwelling and under different wind conditions. Each curve pattern is duplicated by the line joining it to its label.

Impacts of Climate Change

Table 2 and Figures 4-11 summarize the model results. Each figure shows the full simulation and its yearly average. Each figure has also been low-pass filtered to better identify possible trends.

Figures 4 and 5 show the net surface heat flux as calculated by the various model simulations. These plots have been low-pass filtered with a 720-hour cutoff period. When upwelling is nonexistent in the simulations (June through December), the net surface heat flux is the only source/sink of heat for the water column. An accurate accounting of the change in heat content from January to June, however, requires that the upwelling heat flux be included in the budget. Table 2 shows monthly estimates of this term, and it should be noted that the method used to estimate it, for Table 2, is subject to error since it involves multiplication of small differences between large numbers.

Two points are of interest in these figures. First, the close similarity between the surface heat fluxes throughout much of the year, particularly during late summer and early fall. And second, the very large heat losses seen in December and January of the first and third winters in the Base simulation (top of Figures 4 and 5). The monthly averaged heat flux components are listed in Table 2 and are discussed below.

Of the five heat flux components, the net longwave and shortwave global radiation terms appear to be the most consistent in their phase and magnitude from model to model (Table 2). The remaining three processes, sensible, latent, and upwelling, show less model to model agreement. The sensible heat flux loss is greatest during January for each model except OSU, where it occurs during December. The latent heat loss reaches its maximum during January for Base and GISS A, while it occurs significantly earlier in the other three models, i.e., October for GISS, September for GFDL, and November for OSU. The averaged upwelling flux shows large model to model differences. In the Base simulation, the upwelling flux, in general, represents a heat source, while in GISS, GFDL, and OSU it is a heat sink. Only in GISS A is the upwelling term positive when averaged over the 5-month period in which it is operational. However, when all the flux terms are summed the net heating rate that results suggests that the annual averaged net heat flux is within 10 W/m2 of being zero for all cases. More importantly, the maximum difference between the annual net heat flux under a GCM scenario and Base is only 8 W/m2. This emphasizes how the persistence of small changes in the net heat flux can lead to dramatic changes to the environment, and because of the uncertainties surrounding these estimates, why they often lead to controversy.

Figures 6 and 7 show the low-pass filtered surface water temperature. In Figure 6 the Base, GISS, GFDL, and OSU climatologies are shown. These GCM results suggest higher surface temperatures throughout the year. Comparison of the transient scenario for 2010-19 (Figure 7) suggests that higher surface temperatures will prevail from January through July. During the remainder of the year, there is little difference in temperature between GISS A and Base.

As we proceed down in the water column we can begin to estimate more and more of the potential climate impact on Lake Michigan. The mixed layer depth comparisons (Figures 8 and 9) together with Figures 6 and 7 suggest how the heat content of the upper water column may behave in the future. Under the GCM scenarios the mixed layer depth will in general be deeper in the early winter months and will shallow in spring much sooner than in the Base results. This suggests that thermal stratification will begin much earlier than is presently observed. If the interannual variability seen in the top of Figure 8 is truly representative of the Lake Michigan climatology, then the transition to summer stratification under the GCM scenarios may occur two or more months earlier than under the present climate.

This is well illustrated after the first cold winter (Figure 8). In that case, the GCM results (GISS, GFDL, and OSU) suggest that thermal stratification will begin in April rather than the late June date seen in Base. The GISS A results (Figure 9) shows this same tendency but not to the same degree.

TABLE 2. Monthly and annual averaged heat flux components from the Base climatology and GCM simulations

SENSIBLE HEAT FLUX (W/m2)

Model	Jan	Feb	Mar	Apr	May	Jun	Jul	Aug	Sep	Oct	Nov	Dec	Annual
(0)	-231	-80	-54	0	9	-2	-2	-2	-23	-26	-70	-169	-54
(1)	-88	-9	0	6	-10	-16	-8	-4	-1	-15	6	-43	-15
(2)	-117	-25	5	9	-8	-12	19	3	-5	-4	-22	-41	-16
(3)	-79	-42	-20	11	-5	-22	-10	-4	-25	-20	-45	-106	-30
(4)	-152	-33	-73	17	5	-9	-4	-4	-31	-30	-72	-96	-40

LATENT HEAT FLUX (W/m2)

Model	Jan	Feb	Mar	Apr	May	Jun	Jul	Aug	Sep	Oct	Nov	Dec	Annual
(0)	-141	-63	-65	-24	0	0	-32	-62	-104	-89	-107	-130	-68
(1)	-86	-56	-32	-23	-11	-16	-56	-80	-124	-136	-91	-90	-66
(2)	-125	-51	-66	-23	-17	-49	-116	-126	-145	-112	-96	-97	-85
(3)	-127	-71	-82	-36	-21	-27	-61	-84	-112	-105	-128	-124	-81
(4)	-126	-49	-69	-14	0	1	-18	-54	-108	-96	-100	-92	-60

NET LONGWAVE RADIATION (W/m2)

Model	Jan	Feb	Mar	Apr	May	Jun	Jul	Aug	Sep	Oct	Nov	Dec	Annual
(0)	-81	-62	-61	-48	-41	-53	-32	-40	-55	-60	-64	-72	-55
(1)	-57	-48	-47	-44	-58	-63	-49	-37	-30	-57	-40	-52	-48
(2)	-60	-45	-50	-39	-67	-70	-17	-31	-37	-44	-47	-52	-46
(3)	-72	-65	-66	-61	-70	-73	-57	-36	-59	-64	-64	-67	-62
(4)	-68	-49	-65	-35	-47	-59	-41	-43	-61	-60	-64	-57	-54

SHORTWAVE GLOBAL RADIATION (W/m2)

Model	Jan	Feb	Mar	Apr	May	Jun	Jul	Aug	Sep	Oct	Nov	Dec	Annual
(0)	58	86	134	185	212	254	248	218	170	112	70	50	150
(1)	52	102	138	197	205	241	235	226	170	148	72	57	153
(2)	109	91	177	165	252	297	264	247	188	114	71	101	173
(3)	84	116	193	276	292	264	275	198	194	139	82	60	181
(4)	56	75	143	183	217	223	193	200	185	108	70	42	141

UPWELLING FLUX (W/m2)

Model	Jan	Feb	Mar	Apr	May	Jun	Jul	Aug	Sep	Oct	Nov	Dec	Annual
(0)	17	100	128	27	-13	0	0	0	0	0	0	0	21
(1)	-21	-30	-75	-59	-90	0	0	0	0	0	0	0	-22
(2)	-23	-33	-66	-49	-109	0	0	0	0	0	0	0	-23
(3)	-2	9	6	-22	-91	0	0	0	0	0	0	0	-8
(4)	9	41	70	11	-24	0	0	0	0	0	0	0	8

Table 2. (continued)

	NET HEATING (W/m2) (Equals sum of all fluxes)												
Model	Jan	Feb	Mar	Apr	May	Jun	Jul	Aug	Sep	Oct	Nov	Dec	Annual
(0)	-379	-20	83	140	167	199	183	113	-12	-63	-172	-321	-7
(1)	-200	-41	-16	77	36	146	123	105	16	-60	-52	-130	0
(2)	-214	-62	0	64	52	166	151	93	1	-46	-95	-89	1
(3)	-195	-52	31	168	105	142	147	74	-2	-50	-156	-238	-2
(4)	-281	-14	5	163	151	156	130	100	-15	-78	-166	-203	-4

Model (0) = Base Climatology; Models (1)-(4) are the same as in Table 1.

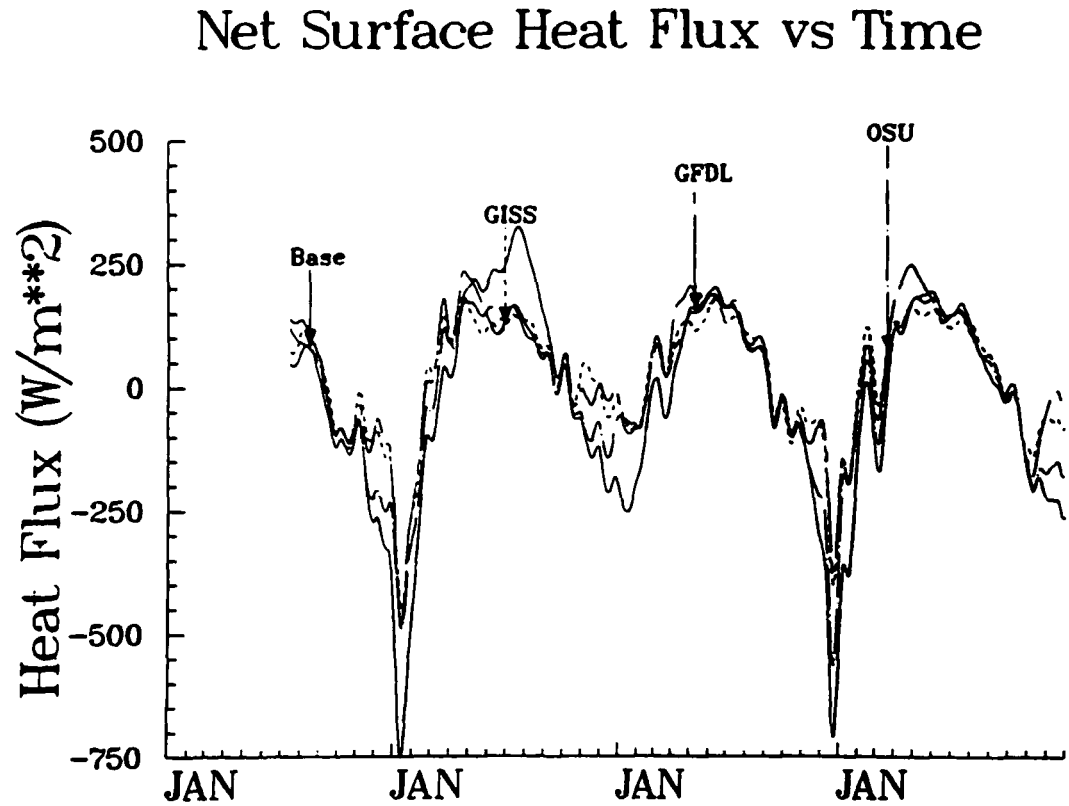

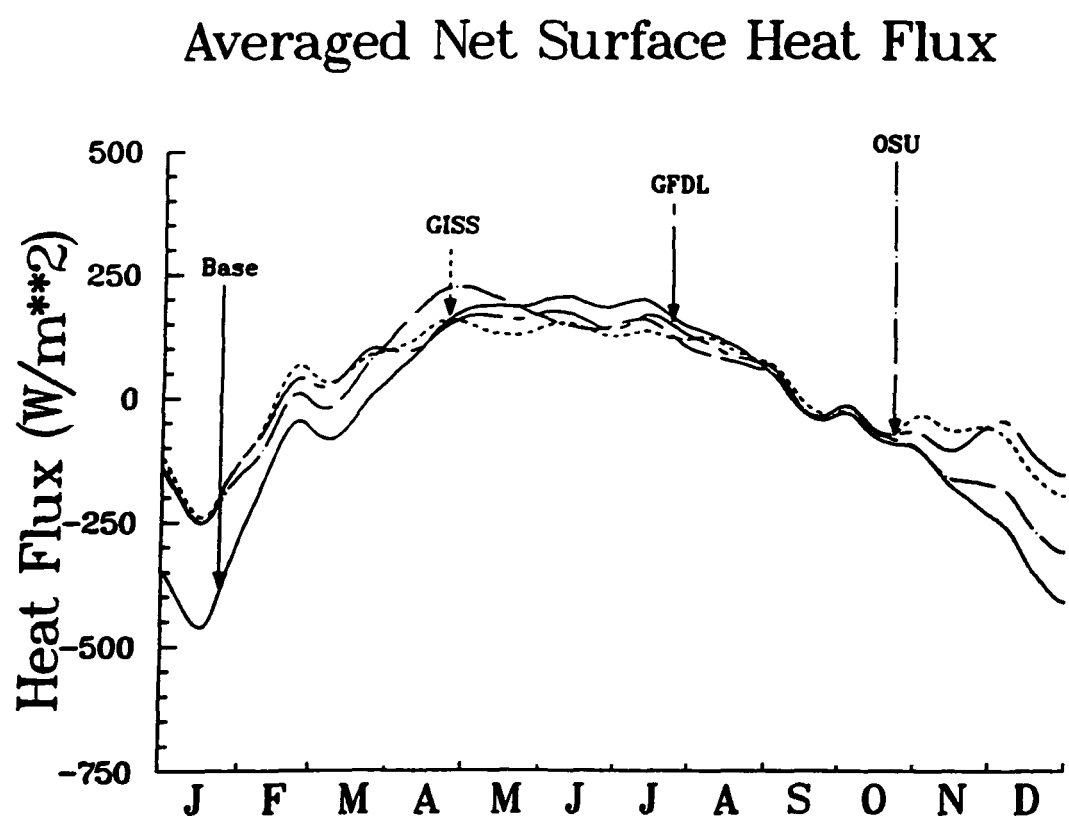

Figure 4. Low-pass filtered (720-hr cutoff) net surface heat flux.

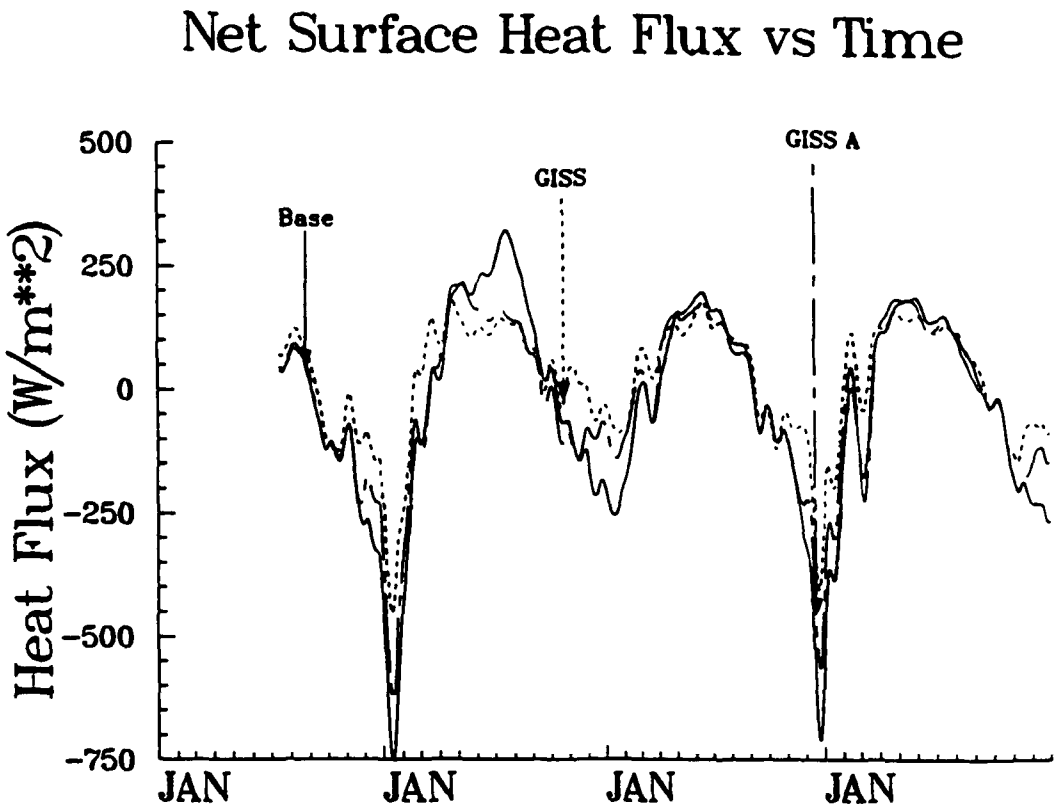

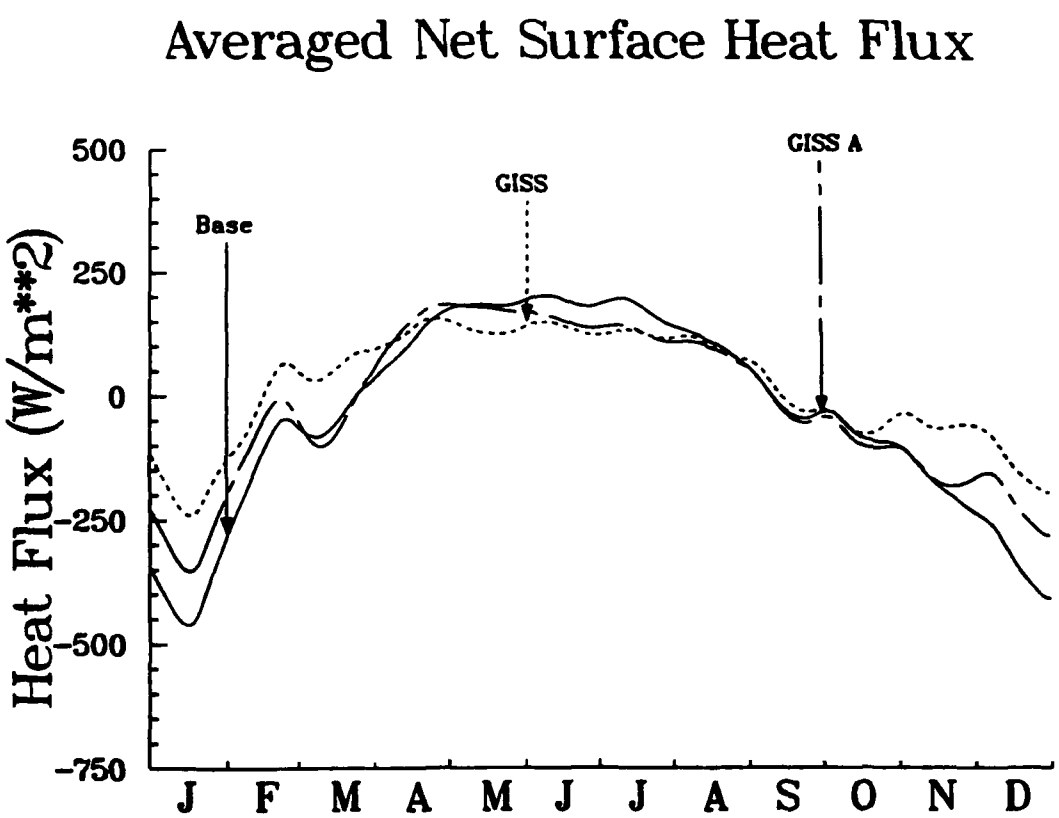

Figure 5. Low-pass filtered (720-hr cutoff) net surface heat flux.

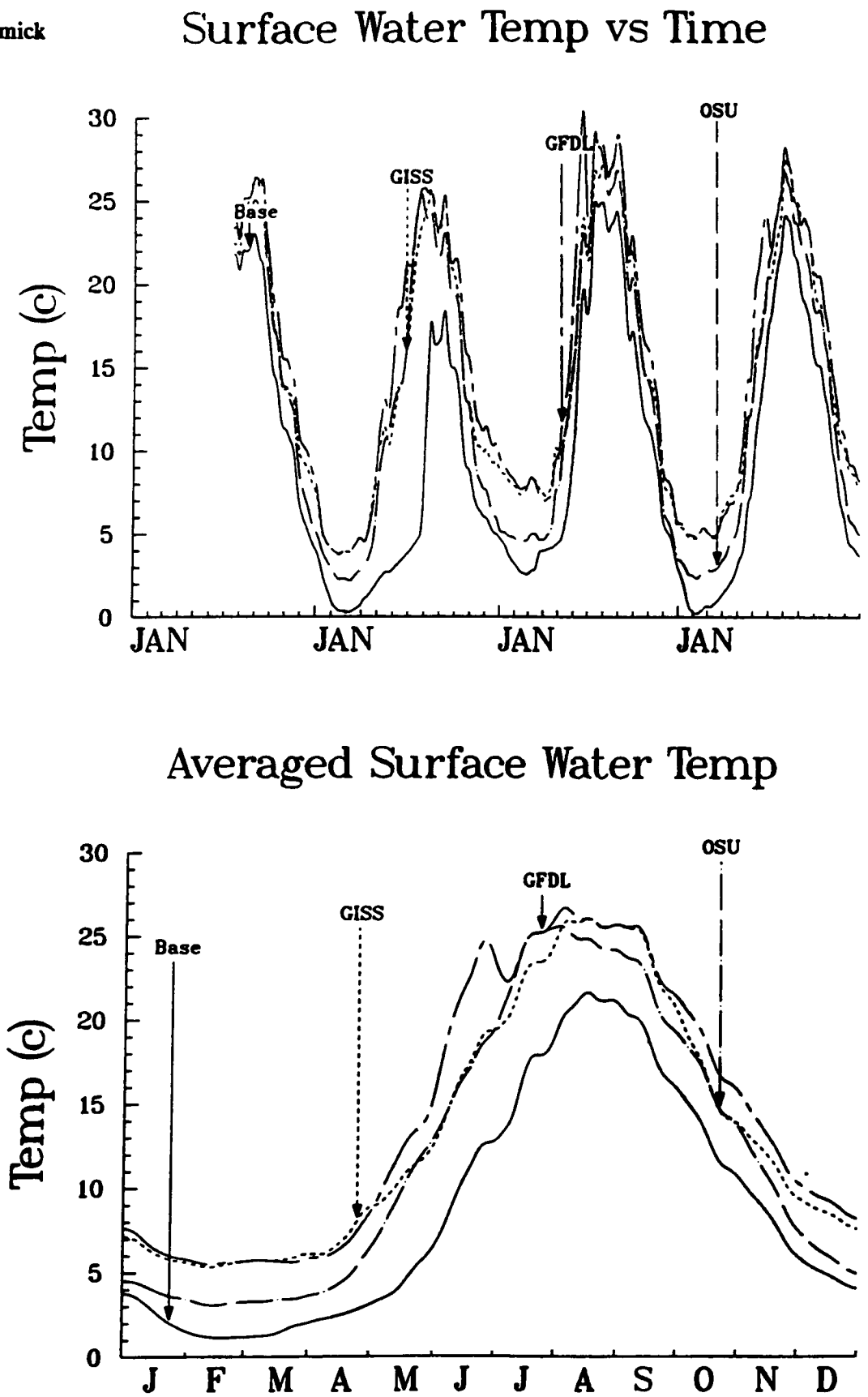

Figure 6. Low-pass filtered (336-hr cutoff) surface water temperature.

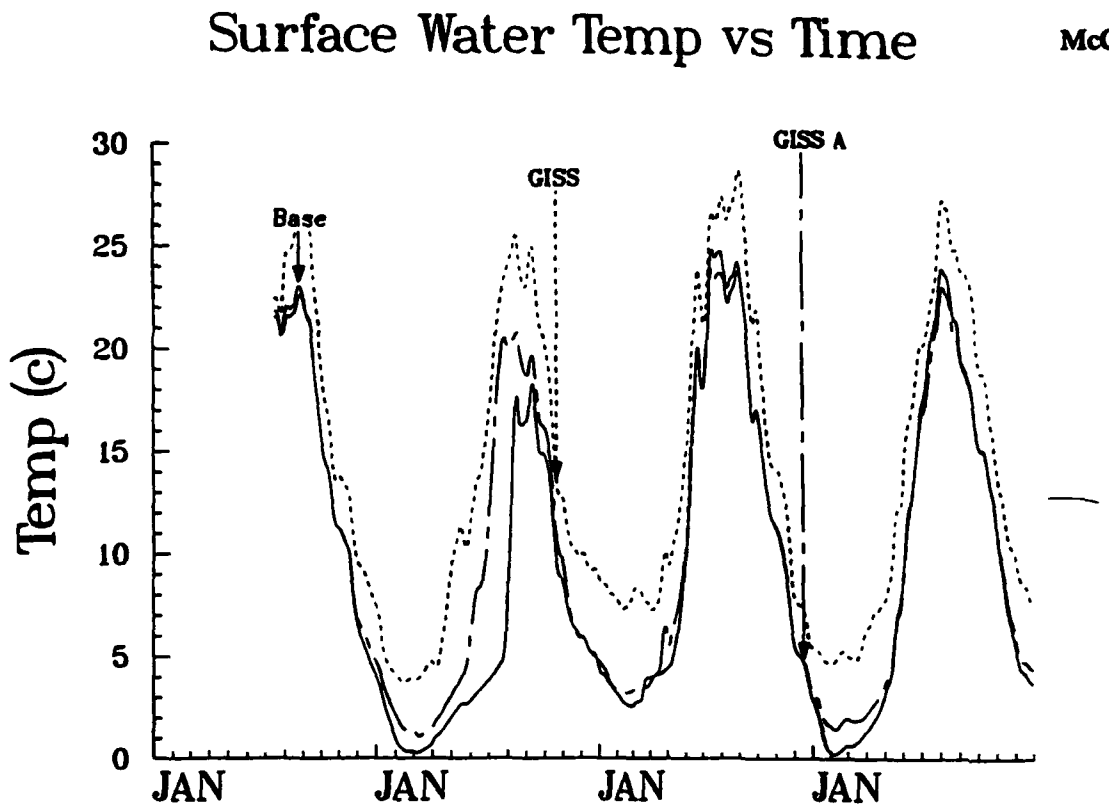

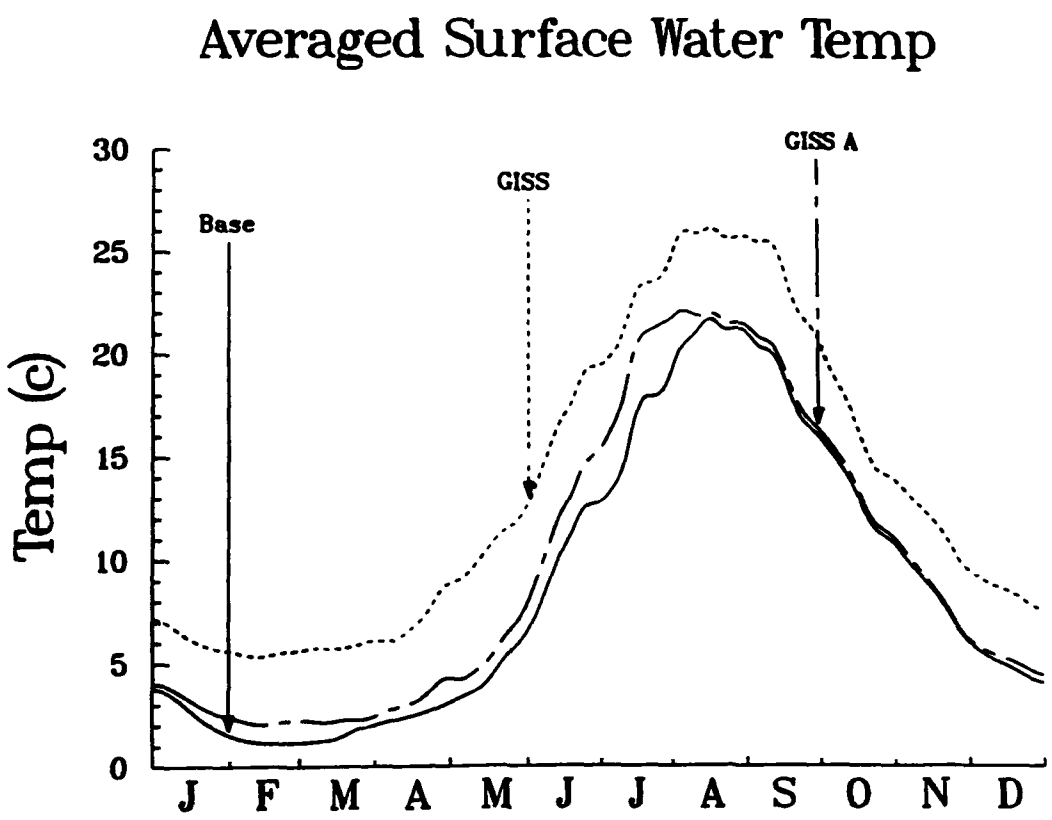

Figure 7. Low-pass filtered (336-hr cutoff) surface water temperature.

During the cooling season, the mixed layer depths deepen at approximately the same rate as seen in the current climatology. This reflects the similarity in surface heat content and that changes to the net surface heat flux are smallest during the summer months. Deepening proceeds until late fall when the GCM results suggest an overall cessation of further deepening.

Recall that the simulation is performed for a water column of 150 meter depth. The mixed layer depths in the Base climatology encroach on the bottom for significant periods. Figures 8 and 9 were low-pass filtered with a 720-hour cutoff period; thus mixed layer depth fluctuations with shorter time periods are lost. The mixed layer depths under the GCM scenarios do penetrate to the bottom, on occasion, but not anywhere nearly as often as in the Base simulation.

Figures 10 and 11 show potential climate effects on the heat content of the entire water column. This is shown in terms of the vertically averaged water temperature. The GISS and GFDL scenarios show a consistently greater heat content than Base. The biggest differences occur during the winter months when the vertically averaged temperature is significantly higher than that seen in Base. During summer and early fall, however, the heat content increase is less pronounced, with smaller relative increases over the present climatology.

The OSU and GISS A scenarios depart from GISS and GFDL. GISS A (Figure 11) while showing a general warming during the winter and spring, also shows a possible slight decrease in heat storage during the summer months. However, the decreased heat content is small enough to not merit speculation.

The OSU simulation is more similar to the GISS A results than it is to the GFDL and GISS simulations. The OSU run tends to mimic that depicted by GISS A but is displaced to slightly warmer temperatures such that the yearly averaged heat content (Figure 10) shows only zero to positive increases in heat content over Base at all times.

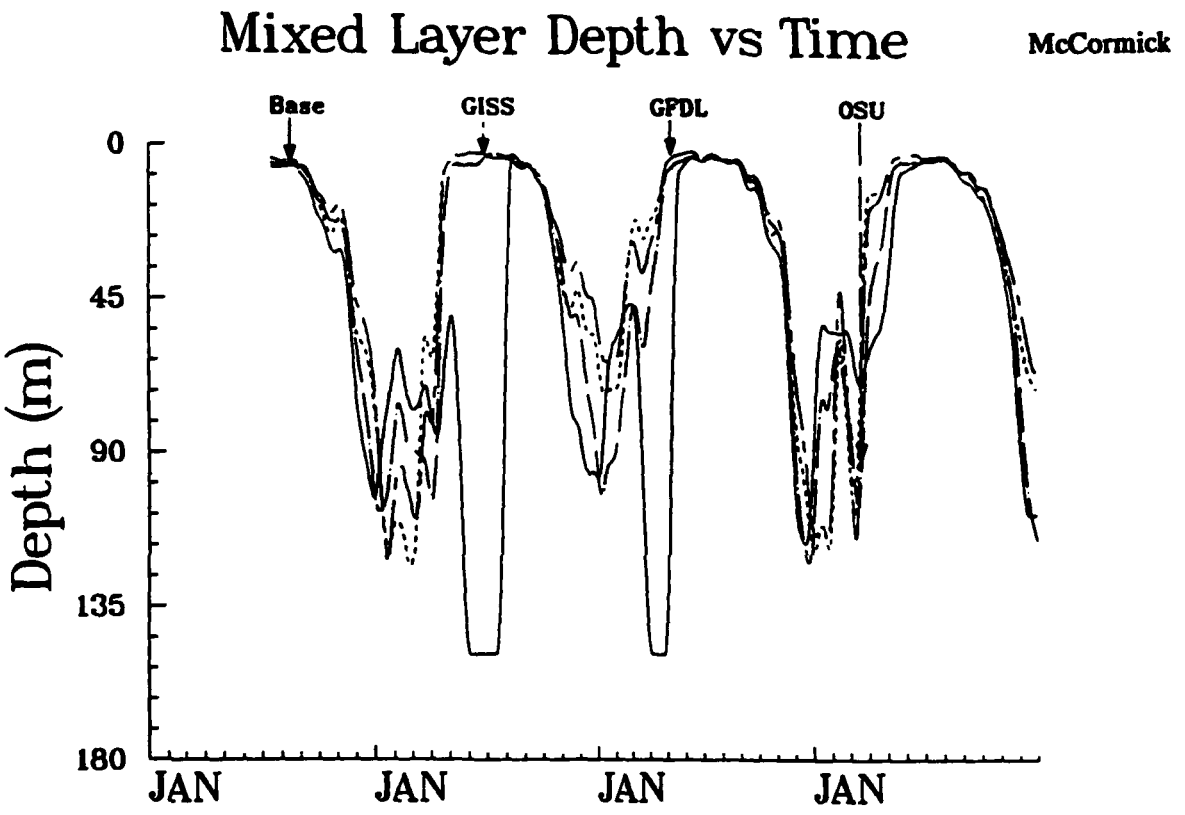

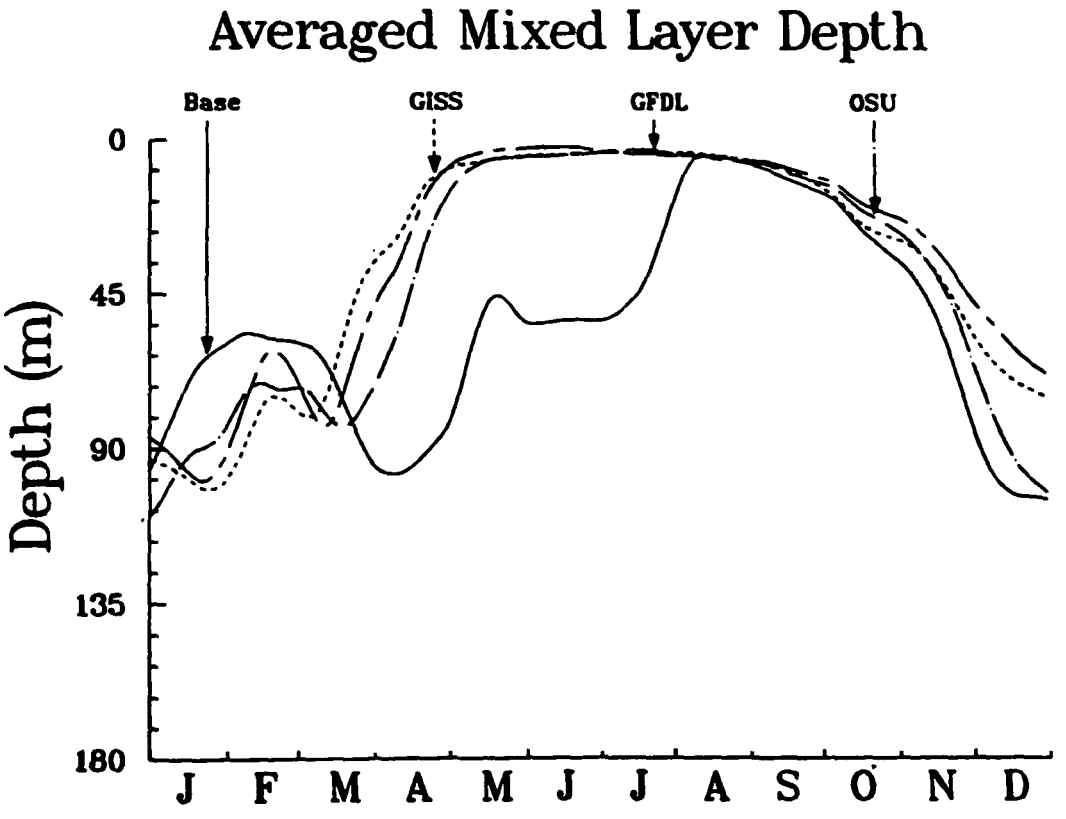

Figure 8. Low-pass filtered (720-hr cutoff) mixed layer depth.

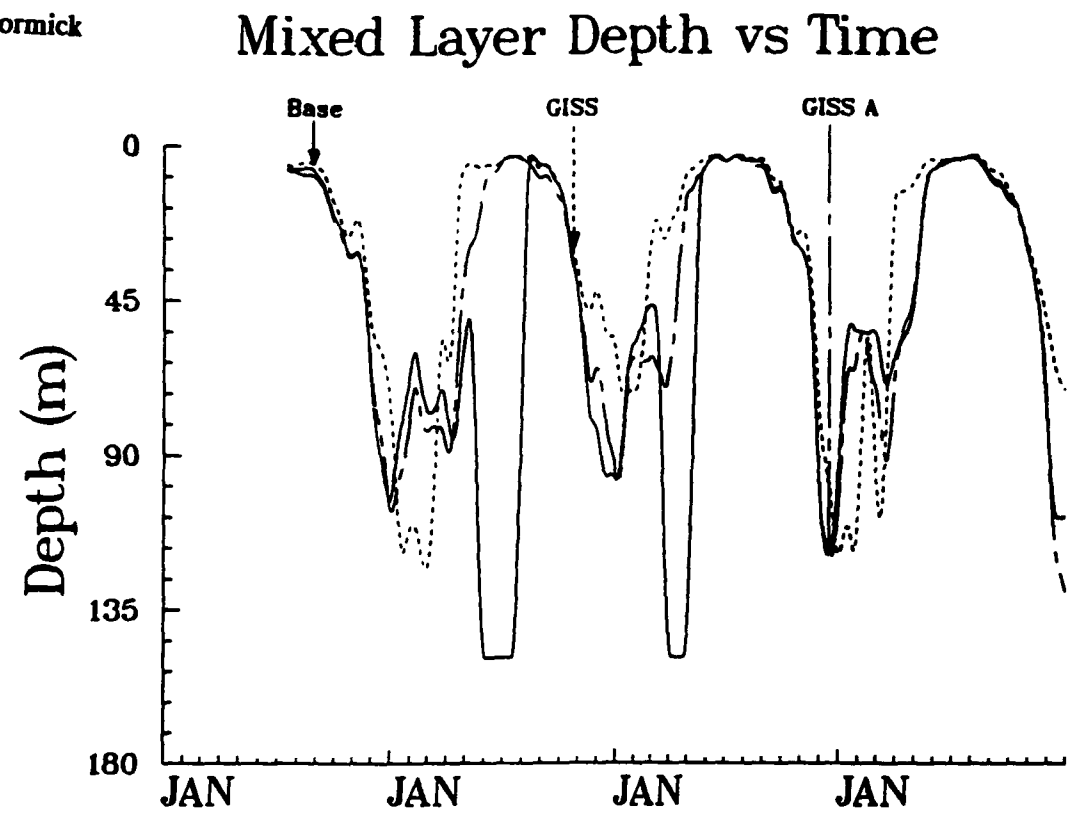

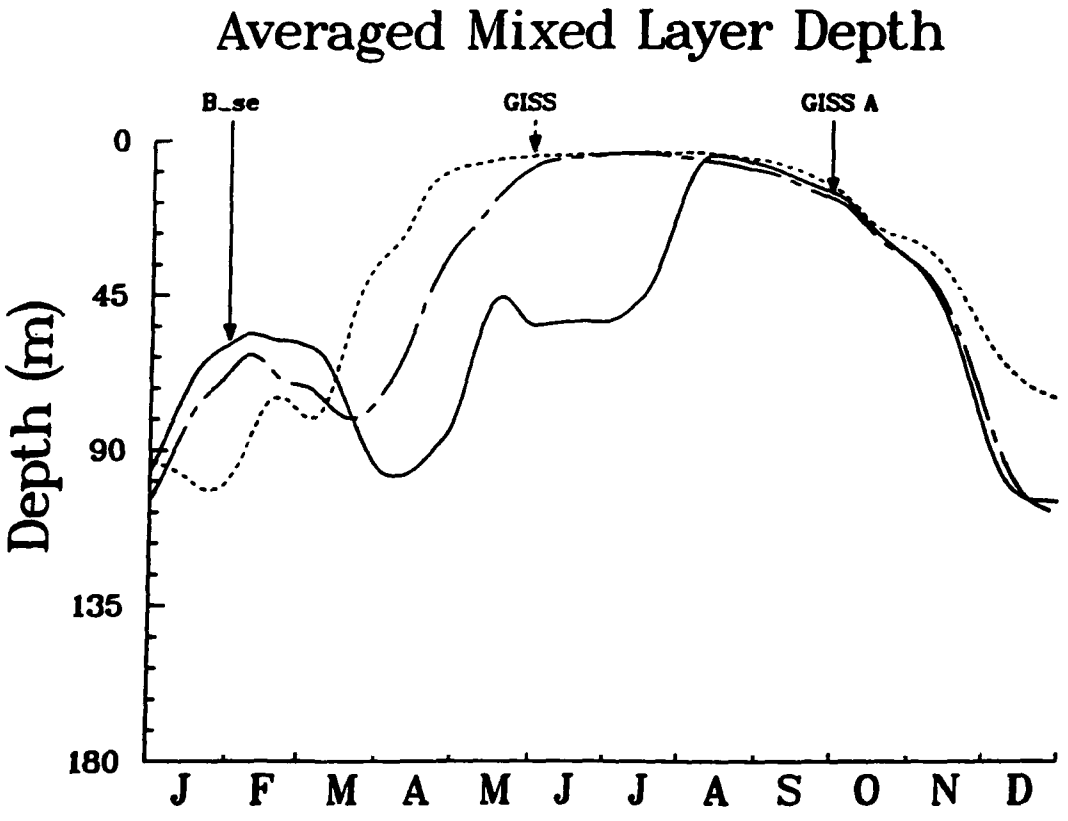

Figure 9. Low-pass filtered (720-hr cutoff) mixed layer depth.

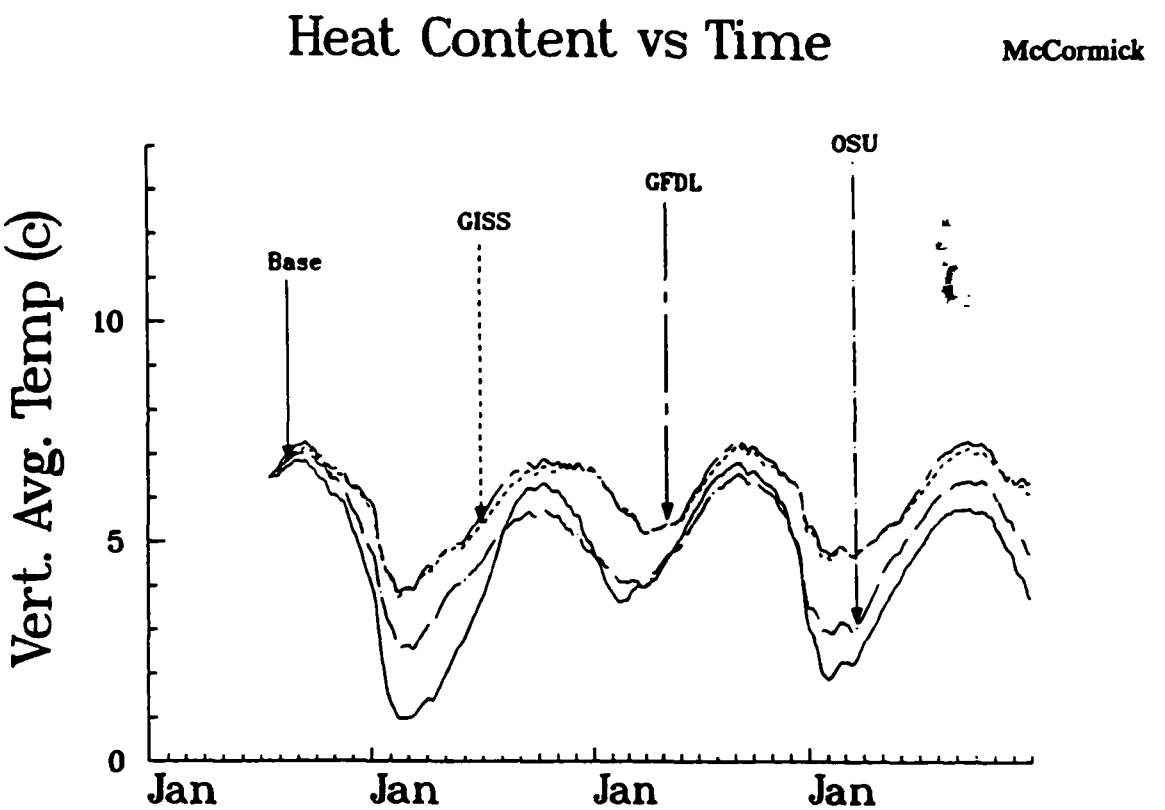

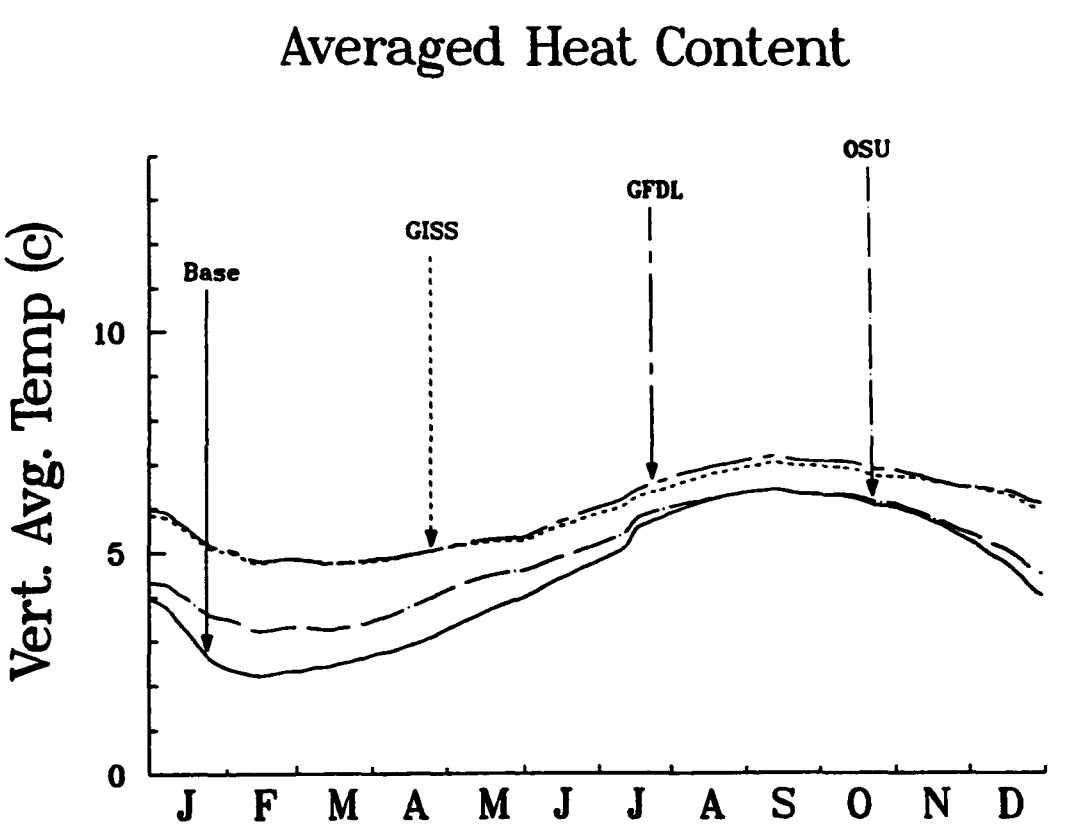

Figure 10. Low-pass filtered (168 hr cutoff) heat content.

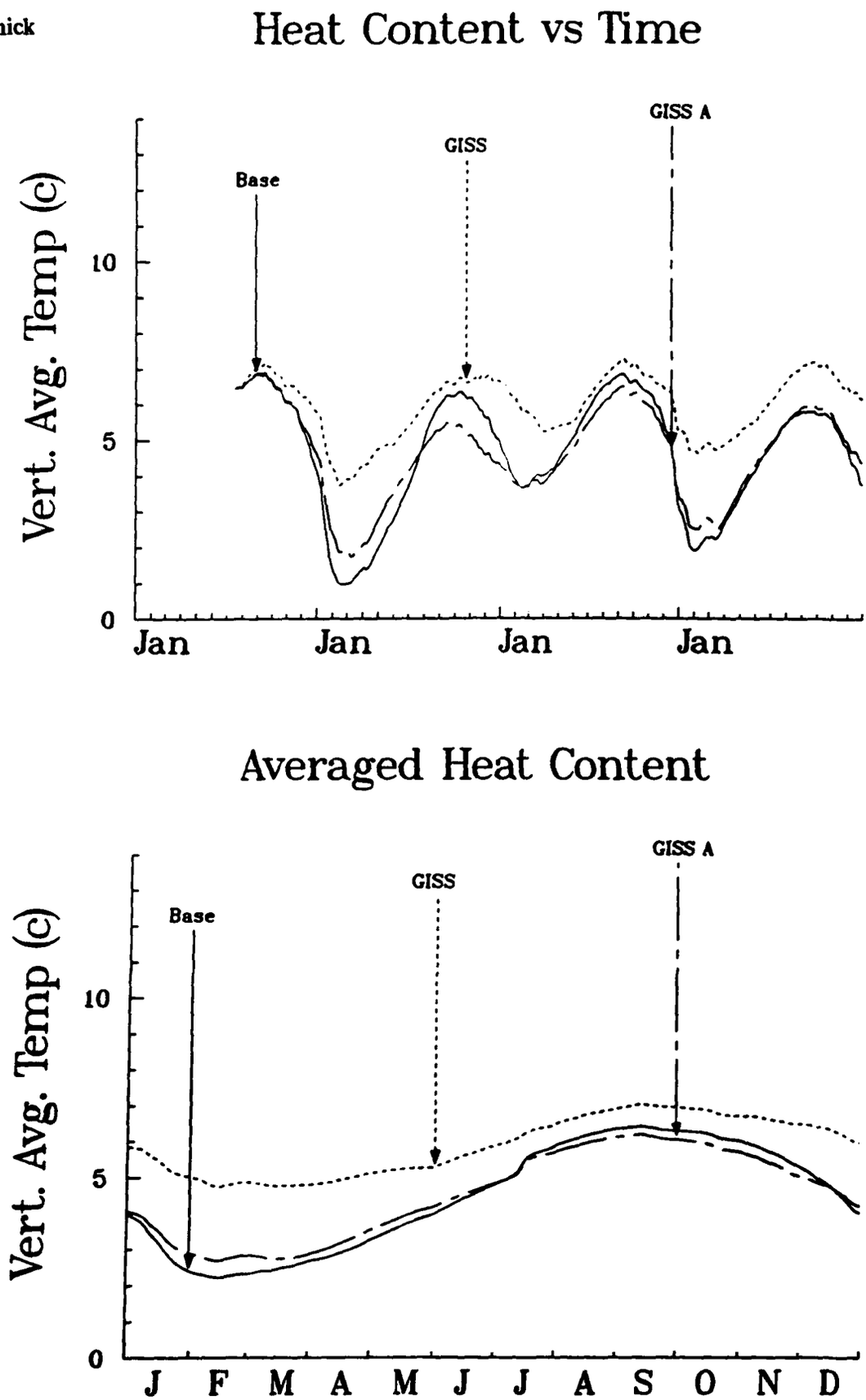

Figure 11. Low-pass filtered (168 hr cutoff) heat content.

CHAPTER 4

DISCUSSION, CONCLUSIONS, AND SPECULATIONS

Interpretation of Results

Tables 1 and 2 suggest that the primary action driving the changes in the GCM simulations is the increased air temperature. Indeed, on a yearly averaged basis the sensible heat flux showed the greatest absolute change from the Base simulation. The large monthly increases in air temperature were up to 8°C (see Table 1) and were responsible for the change in the sensible heat flux. The additional air temperature increase (relative to the GCM output) resulted from over-water modification of the land-based temperature, which was mandated in the Base climatology simulations to avoid excessively large surface heat losses. For consistency purposes, the GCM inputs were treated in an identical fashion.

In general, the GCM results suggest that the mixed layer depth will be shallower than Base. There is one exception to this. In the early winter season (see January and February in Figures 6 and 7), the GCM mixed layer depths are deeper than those in Base, yet still far above the bottom. The reason for the deeper mixed layer during this time period stems from weaker "reverse" stratification in the GCM simulations. In Base, the temperature contrast between surface and bottom waters is much greater than in the GCMs. The strong surface cooling in Base during early winter results in stronger early winter stratification and a shallower surface mixed layer. However, this scene quickly reverses as the lake gains heat. The GCM-simulated mixed layer begins to shallow while the Base generated one deepens. This interesting behavior occurs because of the relationship between the total heat content, as generated by the various simulations, and the temperature of maximum density.

Wind stress has been shown (Adamec and Elsberry, 1984) to be the most sensitive term in controlling thermal structure. For example, in Figure 2 a negative 10% bias in windspeed could cause a 50% improvement in the rms error of surface temperature. In these simulations, however, the wind plays no greater role in the GCM calculations than in the Base simulation. This was supported by comparing the GCM simulations using GCM winds, versus GCM simulations using the Base climatology winds. Differences in the model results were insignificant. However, this by no means suggests that future wind fields are unimportant with respect to present conditions. All it does say is that the monthly vector averaged windspeeds are unimportant and inappropriate for assessing GCM wind sensitivity.

An additional area of concern is the use of monthly averaged data. McCormick and Meadows (1988) have shown that over 90% of the energy associated with mixed layer deepening occurs at daily and higher frequencies. Thus if an accurate assessment of mixing impacts on water quality or other limnological problems is to be made, then the spectral distribution of the wind stress must be well represented. There are numerous examples in the literature where the distribution of physical and chemical tracers is strongly influenced by the frequency and severity of storm events. Therefore, if the physics is to be described through process-oriented models, as used in this study, then the episodic nature of mixing requires high frequency information on all the driving forces, particularly the wind. Although this information was lacking, it does not invalidate this study so much as it points out the need for further study.

Of the heat flux components, the net longwave radiation was the least sensitive to change in the GCM scenarios. This is a consequence more of the empirical formulation used to estimate it than it is a confident estimate of the true response. In fact, there is a growing body of literature suggesting that most empirical longwave radiation formulations are not accurate enough for climatological applications (Frouin et al., 1988; Fung et al., 1984).

The net longwave radiation term is not the only term subject to uncertainty. The surface heat flux can be expected to be in error by as much as 20-30 W/m2 on monthly time scales (Wyrtki and Uhrich, 1982). This

uncertainty could mask the effects of climate change. The present state of knowledge is too uncertain for quantifying climate change. Yet by using verified, process-oriented models and by referencing the GCM simulations to the Base simulation, the model and data uncertainties are minimized such that greater confidence can be placed on the relative changes. Thus the direction, and not magnitude, of change has been the focus throughout this study.

In conclusion, in each of the GCM scenarios the change is in the direction of significantly higher heat content, particularly during the winter, a deeper mixed layer depth in early winter followed by a shallower one in summer, an earlier onset to density stratification, a longer stratified season, a more buoyant surface mixed layer resulting in less energy available for mixing, and, in general, higher surface water temperatures. The transient scenario suggests that some of these effects may be evident 20-30 years from now.

Speculations

If the GISS or GFDL scenarios are realized, then surface temperatures in offshore waters may never decrease below 4°C. In other words, the lake may not fully overturn during mild winters and thus bottom waters may remain isolated from surface exposure for significant lengths of time. It is possible that the deeper regions of the Great Lakes (i.e., >100 meters deep) may experience a permanent thermocline with a shallower seasonal one occurring in surface waters, just like much of the world's oceans. In areas where the bottom depths are deep enough for this to occur, and if these regions are polluted, then the reduction in large-scale vertical mixing, as implied by the GCM simulations, may result in anoxic environments being formed where they have never before existed.

Wherever temperature effects are important, impacts will be felt. For example, the earlier warming of surface waters may result in changes to fish recruitment. Undoubtably, there too must be a reduction in the amount and duration of ice cover. Reducing the ice cover may result in less shoreline protection and increased erosion. And finally, profound changes may occur in the biota through changes in the composition of the food chain to those species which would gain a competitive advantage from changes to the seasonal thermal structure.

REFERENCES

Adamec, D. and R. L. Elsberry. 1984. Sensitivity of mixed layer predictions at ocean station PAPA to atmospheric forcing parameters. J. Phys. Oceanogr. 14:769-780.

Boyce, F. M. and F. Chiocchio. 1987. Inertial frequency oscillations in the central basin of Lake Erie. J. Great Lakes Res. 13:542-558.

Businger, J. A., Wyngaard, J. C., Izumi, Y. and E. F. Bradley. 1971. Flux-profile measurements in the atmospheric surface layer. J. Atmos. Sci. 28:181-189.

Cohen, S. J. 1986. Impacts of CO_2-induced climatic change on water resources in the Great Lakes basin. Climatic Change. 8:135-153.

Cotton, G. F. 1979. ARL models of global solar radiation. p. 165-184. National Climatic Center. In: Hourly solar radiation - surface meteorological observations. Solmet Vol. 2. - Final Report. Dept. of Energy. 184 pp.

Denman, K. L. 1973. A time-dependent model of the upper ocean. J. Phys. Oceanogr. 3:173-184.

Farmer, D. M. and E. Carmack. 1982. Wind mixing and restratification in a lake near the temperature of maximum density. J. Phys. Oceanogr. 11:1516-1533.

Feit, D. M. and D. S. Goldenberg. 1976. Climatology of surface temperatures of Lakes Superior, Huron, Erie and Ontario. U. S. Dept. of Commerce. NOAA. NWS. TDL Office Note TDL-76-16. Silver Spring, Md. 14 pp.

Frouin, R., Gautier, C. and J. Morcrette. 1988. Downward longwave irradiance at the ocean surface from satellite data: methodology and in situ validation. J. Geophys. Res. 93:597-619.
Fung, I., Harrison, D. E. and A. A. Lacis. 1984. On the variability of the net longwave radiation at the ocean surface. Rev. Geophys. 22:177-193.

Garwood, R. W., Jr. 1977. An oceanic mixed layer capable of simulating cyclic states. J. Phys. Oceanogr. 7:455-468.

Ivanoff, A. 1977. Oceanic absorption of solar energy. p. 47-72. In: Modelling and prediction of the upper layers of the ocean. E.B. Kraus, ed. New York: Pergamon Press. 325 pp.

Martin, P. J. 1985. Simulation of the mixed layer at OWS NOVEMBER and PAPA with several models. J. Geophys. Res. 90:903-916.

McCormick, M. J. and D. Scavia. 1981. Calculation of vertical profiles of lake-averaged temperature and diffusivity, in lakes Ontario and Washington. Water Resour. Res. 17:305-310.

McCormick, M. J. and G. A. Meadows. 1988. An intercomparison of four mixed layer models in a shallow inland sea. J. Geophys. Res. 93:6774-6788.

Phillips, D. W. and J. G. Irbe. 1978. Lake to land comparison of wind, temperature and humidity on Lake Ontario during the International Field Year for the Great Lakes (IFYGL). Fisheries and Environment Canada. Atmospheric Environment. CLI-2-77. 51 pp.

Pickett, R. L. and L. R. Herche. 1984. A simple density equation for Great Lakes Waters. 27th Conf. on Great Lakes Res. St. Catherines, Ontario: Brock University. May 1 - 3.

Saylor, J. H., Huang, J. C. K. and R. O. Reid. 1980. Vortex modes in southern Lake Michigan. J. Phys. Oceanogr. 10:1814-1823.

Schwab, D. J., Bennett, J. R. and A. T. Jessup. 1981. A two-dimensional lake circulation modeling system. NOAA Tech. Mem. ERL GLERL - 38. Ann Arbor, Mi. 79 pp.

Schwab, D. J. 1983. Numerical simulation of low-frequency current fluctuations in Lake Michigan. J. Phys. Oceanogr. 13:2213-2224.

Thompson, R. O. R. Y. 1976. Climatological numerical models of the surface mixed layer of the ocean. J. Phys. Oceanogr. 6(4):496-503.

Wyrtki, K. 1965. The average annual heat balance of the North Pacific Ocean and its relation to ocean circulation. J. Phys. Oceanogr. 18:4547-4559.

Wyrtki, K. and L. Uhrich. 1982. On the accuracy of heat storage computations. J. Phys. Oceanogr. 12: 1411 - 1416.

THE EFFECTS OF CLIMATE WARMING ON LAKE ERIE WATER QUALITY

by

Alan F. Blumberg
Dominic M. Di Toro
HydroQual, Inc.
1 Lethbridge Plaza
Mahwah, NJ 07430

Contract No. 68-01-7288

CONTENTS

Page

FINDINGS 7-1

INTRODUCTION 7-3

METHODOLOGY 7-4
Thermocline Model 7-4
Lake Erie Eutrophication Model 7-5
Thermocline/Eutrophication Model Interaction 7-9
Climate Scenarios 7-9

RESULTS 7-13
Verification of the Thermocline Model 7-13
Thermal Response to Scenarios 7-19
Water Quality Response to Scenarios 7-22

REFERENCES 7-27

FINDINGS[1]

Simulations of the water quality in the Central Basin of Lake Erie with a coupled hydrodynamic and water quality model have been used to quantify the response of the system to possible global climate warming trends. It appears that no matter what the detailed changes of the lake stratification dynamics may be, climate warming will lead to a degradation in water quality. Losses of 1 mg/L of dissolved oxygen in the upper layers and losses of 1 to 2 mg/L in the lower layers can be expected. There will also be a concomitant increase in the area of the lake that is anoxic. Even for the historically oxygen-rich periods which occur during windy years, the impact of climate warming will be to produce a depletion in the dissolved oxygen levels.

An area-averaged thermocline model constructed from the more general hydrodynamic equations of motion has been used to estimate the lake temperatures and thermocline variability as forced by surface heating and winds. The highly variable vertical turbulence mixing processes are parameterized by the use of a second-moment, turbulence closure submodel with no adjustments from previous applications to its requisite coefficients. Applications of the thermocline model succeed reasonably well in reproducing the physical behavior of the lake during two very different periods, 1970 and 1975. An already calibrated Lake Erie eutrophication model using the vertical mixing information emanating from the thermocline model formed the basis of the water quality analysis.

Climate scenarios from three different atmospheric general circulation models are used to drive the coupled thermocline/water quality model. The general circulation models estimate the equilibrium climate induced by a doubling of the atmospheric CO_2 concentration. All the models show global warming trends of 2.8 to 4.2°C in surface air temperature; however, considerable uncertainties exist in the other hydrometeorological parameters (Cohen, 1986). While there is a need to improve the state-of-the-art in simulating equilibrium climate change, the range of conditions used in this study encompasses a large part of the expected atmospheric response.

An analysis of the results from the coupled model forced by the climate warming scenarios and specifically designed sensitivity experiments suggest that there will be a significant decline in the lake's water quality. The decline is due to the expected warmer lake temperatures which increase the rate of bacterial activity in the hypolimnion waters and sediment enough to drive the system to lower dissolved oxygen levels independent of the depth at which the thermocline becomes established, that is, the dynamics of the lake stratification. Water quality criteria for ambient dissolved oxygen for fresh water fish (cold water criteria) specifies a one day minimum of 3.0 mg/L for adult fish life stages and 8.0 mg/L minimum for early life stages, (EPA, 1985). A 1.0 mg/L reduction in the epilimnion dissolved oxygen as projected by all of the warming scenarios would not greatly affect fish life. However, the losses of dissolved oxygen in the hypolimnion as projected by the scenarios could lead to dissolved oxygen levels of 3.0 mg/L or less, which would certainly pose a threat to adult fish life. For a comprehensive review of the impacts of this predicted loss of dissolved oxygen and more generally, the impacts of warming on water resources, the reader is referred to Cohen (1986).

The conclusions reached here must be tempered with the following caveats. First, there is the possibility that the eutrophication model has been exercised beyond the range of data (specifically water temperature) for which it was calibrated and validated. This should lead to increased uncertainty in the magnitude of the results for the various climate warming scenarios, but should not affect the direction of change. In addition, the conclusions apply to the Central Basin only. The Eastern Basin, being much deeper, and the Western Basin, being much shallower, are certain to have different responses to the climate warming. Indeed, some caution should be exercised in attempting to extend the conclusions of this study to the Great Lakes in general. Dissolved oxygen concentrations in lakes are very dependent on site-specific characteristics such as

---

[1]Although the information in this report has been funded wholly or partly by the U.S. Environmental Protection Agency under Contract No. 68-01-7288, it does not necessarily reflect the Agency's views, and no official endorsement should be inferred from it.

morphometry, prevailing wind conditions, nutrient enrichment, light extinction, and the time history of external loadings, as reflected in the composition of the sediments. While it is true in general that dissolved oxygen depletion rates would be expected to increase with increasing temperature, site-specific studies, like the one conducted here, would probably be necessary to develop actual predictions for a particular lake. Other caveats to the conclusions include the fact that while the two base years encompass a wide range of baseline anoxic conditions, they do not represent a full range of climate variability. No change is assumed in nutrient loadings from the base years, and the analysis does not incorporate the estimated drop in lake levels expected (see Cohen, 1987). Lower lake levels would reduce the volume of the lower layer in lake Erie, increasing eutrophication. The models were not run for the winter, but the sensitivity of results to higher water column temperatures in the spring was tested and it was found that no significant difference resulted.

In future efforts, it may be possible to estimate the reductions in the total phosphorus loading that would be required to return the lake to its present conditions. However, simulations with the water quality model of five years or longer need to be made so that the long-term response of the sediment can be properly incorporated. These simulations, once conducted, can be analyzed to establish target loadings for phosphorus that would eliminate the anoxia in the Central Basin.

INTRODUCTION

Atmospheric accumulations of greenhouse gases, of which carbon dioxide (CO_2) is the major constituent, has led to concern that the earth's climate may be undergoing a global warming in response to these accumulations. An assessment by Schlesinger and Mitchell (1987) suggests that if current trends in the emissions of these gases continue, the earth could experience a global mean warming of 2.8 to 4.2°C in the next century or so. It becomes important to identify and quantify the potential impacts of the possible climate change so that alternative strategies may be developed to cope with the warming. This study addresses a very specific issue within the realm of water resources. It seeks to determine how climate warming will change the present water quality in Lake Erie, a valuable natural resource. The conclusions of this study are more general and could perhaps lead to results that have Great Lakes-wide implications, especially for certain embayments and nearshore areas.

The effect of increases in nutrient inputs to all the Great Lakes, and to Lake Erie in particular, has been to increase the production of algal biomass. When the lake thermally stratifies with the formation of a thermocline, the lower part of the lake, the hypolimnion, is isolated and the dissolved oxygen (DO) concentration begins to decrease owing to the respiratory consumption of oxygen by the algae. If the algae population is excessive, there may be enough respiration to deplete the oxygen completely causing anoxic conditions that are fatal to all aerobic organisms including fish. Since the joint U.S.-Canada agreement on Great Lakes Water Quality chose the elimination of anoxia as the goal for phosphorus control for Lake Erie (International Joint Commission, 1978), this study will use changes in DO as the measure of changes in overall water quality.

The consequences of increased atmospheric temperature may be dramatic since changes in surface heating to the lake can lead to different lake stratifications. The extent of oxygen depletion is very sensitive to the depth at which the thermocline develops. If the thermocline sets up nearer the surface, the hypolimnion is deep, more oxygen is trapped and the depletion is less intense. If, however, the thermocline sets up nearer to the bottom, then the volume of the hypolimnion is reduced and depletion will occur sooner. The actual occurrence of anoxia is a balance between the rate of oxygen depletion and the destratification of the lake in the fall. Hence, if thermoclines set up nearer to the bottom for longer periods of time, anoxia becomes a more probable event. The warmer lake temperatures could also lead to anoxia or to at least lower levels of DO by increasing the rate of bacterial activity in the sediments, by increasing the biological productivity and respiration in the water column, and by decreasing dissolved oxygen saturation values. Thus, the reduction in the area of anoxia that has been achieved via the phosphorus control measures instituted at (very) large cost may be reversed by a systematic warming of the lake.

The purpose of this investigation is to examine the relationships between climate changes and the water quality of the Central Basin of Lake Erie. Data from 1970 and 1975 observations in the Central Basin form the basis for much of this investigation. These years form a unique set because, in terms of water quality, these years were quite different. There was considerable anoxia present in the deeper portions of the lake in 1970, while the DO distribution in 1975 showed no areas where the oxygen had been depleted. The principal difference between 1975 and 1970 was the shallow depth at which the thermocline developed in 1975. In addition, the use of these two particular years makes possible the direct application of a Lake Erie eutrophication model. The model, described in Section 2, has been calibrated and verified for these years. The use of different years in this analysis probably would not change the conclusions of this study because 1970 and 1975 bracket the range of possible conditions with respect to dissolved oxygen.

METHODOLOGY

Two existing, well-tested modeling frameworks will be used in the analysis. To estimate the warmer water temperatures and the thermocline variation produced by climatic changes, a thermocline model of the Central Basin of Lake Erie has been built. The relevant quantities emanating from this model are then input to an already calibrated Lake Erie eutrophication model through the use of a consistent model coupling procedure. Once the various climate change scenarios are identified, simulations and analyses can be performed.

Thermocline Model

There is little doubt that turbulent vertical mixing of heat is the primary factor in determining the vertical temperature and pollutant structure of a lake. The discussion that follows describes a thermocline model which, to good approximation, can predict the vertical distribution of mixing, currents, and temperature in a lake in response to winds and surface heating/cooling.

The most important cause of motion and mixing in a lake is the wind blowing at the surface. The water column is usually thermally stratified, and as a result, causes the vertical mixing due to winds to be limited to the surface layers in the majority of cases. In narrow lakes, the currents in the surface layers are in the same direction as the wind. Below the surface, wind-mixed layer, there is a compensating and oppositely directed current pattern established through conservation of volume. In wide lakes, the structure of the surface currents and deep compensating flows are more complex and considerably modified by depth variations. If the winds are strong and persistent enough, and/or the vertical stability of the water column is weak enough, the thickness of the wind-mixed layer will be gradually increased and the wind-induced currents spread out over a larger portion of the water column. The vertical distribution of currents and turbulent mixing, and the bottom stress, can be computed fairly well from a knowledge of the surface wind stress in conjunction with a one-dimensional (vertical direction) thermocline model.

The area-averaged, governing equations, assuming that the Rossby number is sufficiently small so that the nonlinear acceleration terms can be discarded, are:

$$(1) \qquad A \frac{\partial U}{\partial t} - fVA = \frac{\partial}{\partial z} [A (K_M + \nu) \frac{\partial U}{\partial z}] + \frac{\Delta(BP)_x}{\rho_o}$$

$$(2) \qquad A \frac{\partial V}{\partial t} + fUA = \frac{\partial}{\partial z} [A (K_M + \nu) \frac{\partial V}{\partial z}] + \frac{\Delta(BP)_y}{\rho_o}$$

and

$$(3) \qquad A \frac{\partial \theta}{\partial t} = \frac{\partial}{\partial z} [A (K_H + \nu) \frac{\partial \theta}{\partial z}]$$

where z and t are the vertical space coordinate and time, A(z) is the horizontal area U, and V are the velocities in the east-west and north-south directions, respectively, θ is the temperature, and ρ_o is the fluid density. The surface compensating return flow at depth is produced through the right-hand-most terms in Equations (1) and (2), where Δ(BP) is the difference in pressure between the east and west (north and south) ends of the basin

integrated along their respective north-south (east-west) end boundaries. These pressure terms are obtained by appealing to the steady form of the vertically integrated continuity equations, which imposes the condition that the vertical integrals of U and V vanish. The use of the steady form basically assumes that both the surface gravity and internal waves generated by the end boundaries instantaneously propagate to the center of the basin and set up the sea surface and pycnocline. Currents that occur on time scales greater than a day or so are thus properly accounted for, while higher frequency motions are probably not.

The vertical turbulent mixing coefficients for momentum and heat are K_M and K_H, and are computed from the turbulence closure submodel of Mellor and Yamada (1982). The closure submodel contains nondimensional empirical constants that are fixed by reference to a small subset of the available laboratory data and, as such, are independent of the particular thermocline model application. A background mixing, to presumably account for internal waves and other unresolved physical processes, is denoted as υ and is equal to 0.01 cm^2/s for this application. The boundary conditions at the surface are:

$$(4) \qquad \rho_o \, (K_M + \nu) \left[\frac{\partial U}{\partial z} , \frac{\partial V}{\partial z} \right] = \left[\tau_x^w , \tau_y^w \right]$$

$$(5) \qquad (K_H + \nu) \frac{\partial \theta}{\partial z} = H$$

and at the bottom:

$$(6) \qquad \rho_o \, (K_M + \nu) \left[\frac{\partial U}{\partial z} , \frac{\partial V}{\partial z} \right] = \left[\tau_x^b , \tau_y^b \right]$$

$$(7) \qquad (K_H + \nu) \frac{\partial \theta}{\partial z} = 0$$

where τ^w and τ^b denote the wind stress at the surface and the frictional stress at the bottom, H denotes the surface heat flux, and where the subscripts x and y denote components in the easterly and northerly directions, respectively.

No heat transfer to the sediments is permitted by the use of Equation (7) although it has been pointed out by Heinrich et al. (1981) that such a heat transfer can have a significant effect on near-bottom temperatures of shallow lakes. The process of heat transfer between the sediments and overlying waters is poorly understood and is therefore not considered here. The bottom stress is obtained by matching the computed near-bottom velocity to that of the logarithmic law of the wall. This approach for deducing currents, mixing and bottom stresses has been used successfully many times in the literature (see for example, Kraus, 1977; Martin, 1985). A variation of this approach, whereby the temperature structure is computed without calculating the details of the velocity field, has been successfully used in Lake Erie by Lam and Schertzer (1987). For details concerning the numerical solution technique used here, the reader is referred to Blumberg and Mellor (1983).

Lake Erie Eutrophication Model

The Lake Erie eutrophication model consists of a set of mass balance equations that quantify the mass transport and kinetic interactions of the biota (phytoplankton and zooplankton), nutrients (phosphorus, nitrogen and silica), and computes the DO consequences that result from these reactions. The model is fully documented (Di Toro and Connolly, 1980) and has been employed by others for more detailed examinations of phosphorus availability (De Pinto et al., 1986). Similar models have been developed and applied to other Great Lakes settings (Thomann et al., 1975; Bierman, 1976; Lam et al., 1983). In a recent study, Di Toro et al. (1987) have presented a retrospective analysis of the Lake Erie model performance over a 10-year period. That analysis further supported the model's predictive capability.

The model is based upon a segmentation of Lake Erie into volumes that represent the epilimnion, hypolimnion, and an active sediment layer of the three major basins (Figure 1). The active sediment layer is explicitly included to more realistically account for the oxygen demand exerted by the sediment (SOD). The kinetics employed are designed to simulate the annual cycle of phytoplankton production, its relation to the supply of light and available nutrients, and the effect on DO. The calculation is based on formulating the kinetics that govern the interactions of the biota and the available and unavailable forms of the nutrients, and applying these kinetics to the regions of Lake Erie within the context of conservation of mass equations. The 15 variables for which these calculations are performed are:

Phytoplankton

1. Diatom chlorophyll-a
2. Non-Diatom chlorophyll-a

Zooplankton

3. Herbivorous zooplankton carbon
4. Carnivorous zooplankton carbon

Nitrogen

5. Detrital and dissolved organic nitrogen
6. Ammonia nitrogen
7. Nitrate nitrogen

Phosphorus

8. Unavailable phosphorus
9. Soluble reactive phosphorus

Silica

10. Unavailable silica
11. Soluble reactive silica

Carbon, Hydrogen, Oxygen

12. Detrital organic carbon
13. Dissolved inorganic carbon
14. Alkalinity
15. Dissolved oxygen

Comparisons of the model results with extensive field data from 1970 and 1975 demonstrated that the calculation can reproduce the major features of the seasonal distribution of phytoplankton and nutrients over a range of observed concentrations. The fact that the Western, Central, and Eastern Basin distributions are all reasonably well reproduced, using the same kinetic structure and coefficients, suggests that the calculation has a certain generality and can reproduce conditions as distinct as those in the Western and Eastern Basins.

The dissolved oxygen comparisons for 1970 and 1975 in the Central Basin are shown on Figure 2. The agreement is quite good with the computation duplicating all the major features of the temporal oxygen distribution. As can be seen, the epilimnion dissolved oxygen follows the saturation oxygen concentration very closely during the entire year except for a small oxygen peak of supersaturation appearing in early July. This is due to photosynthetic production resulting from the increase in phytoplankton chlorophyll taking place at this

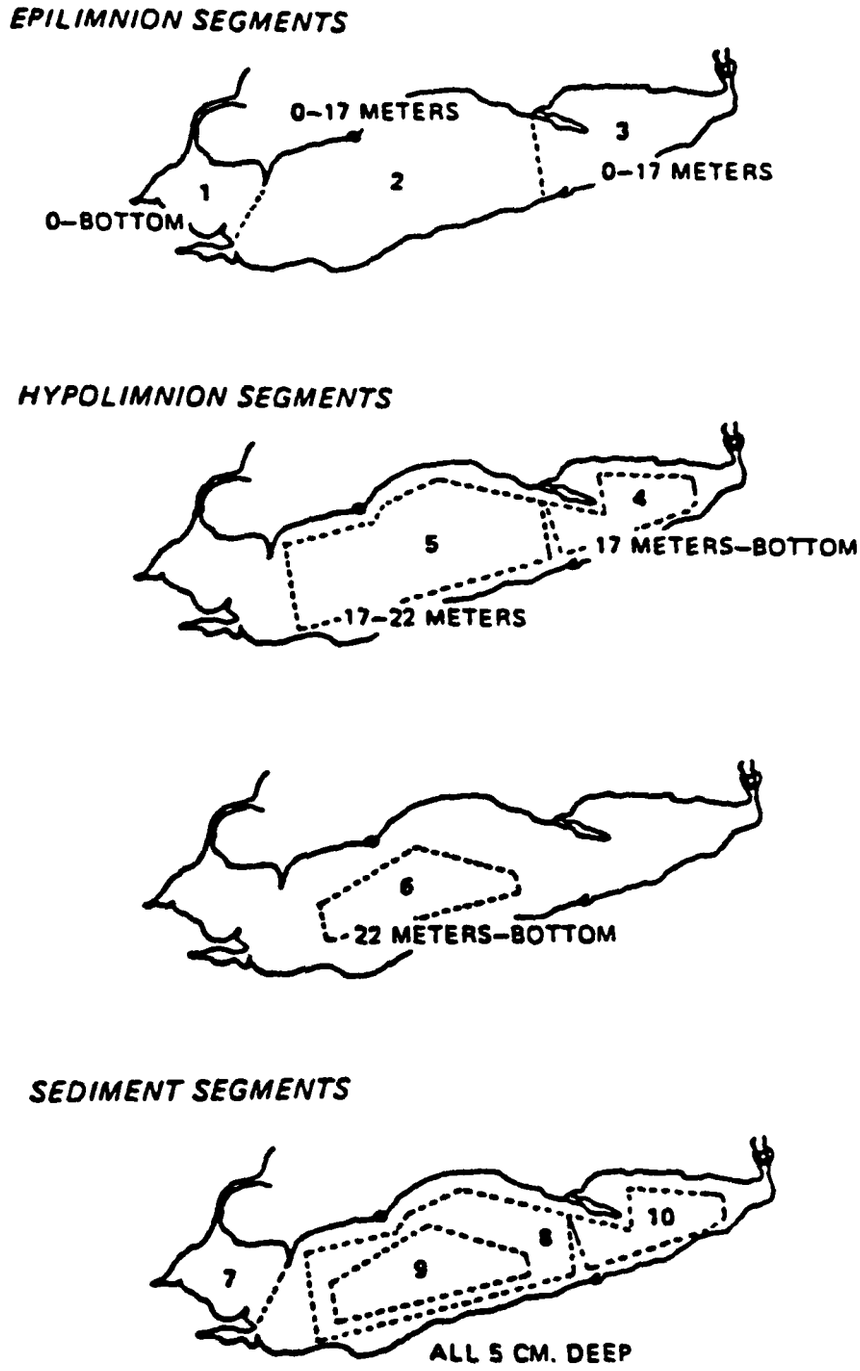

Figure 1. Lake Erie model segmentation of Western, Central, and Eastern basins: water segments 1-6, sediment segments 7-10.

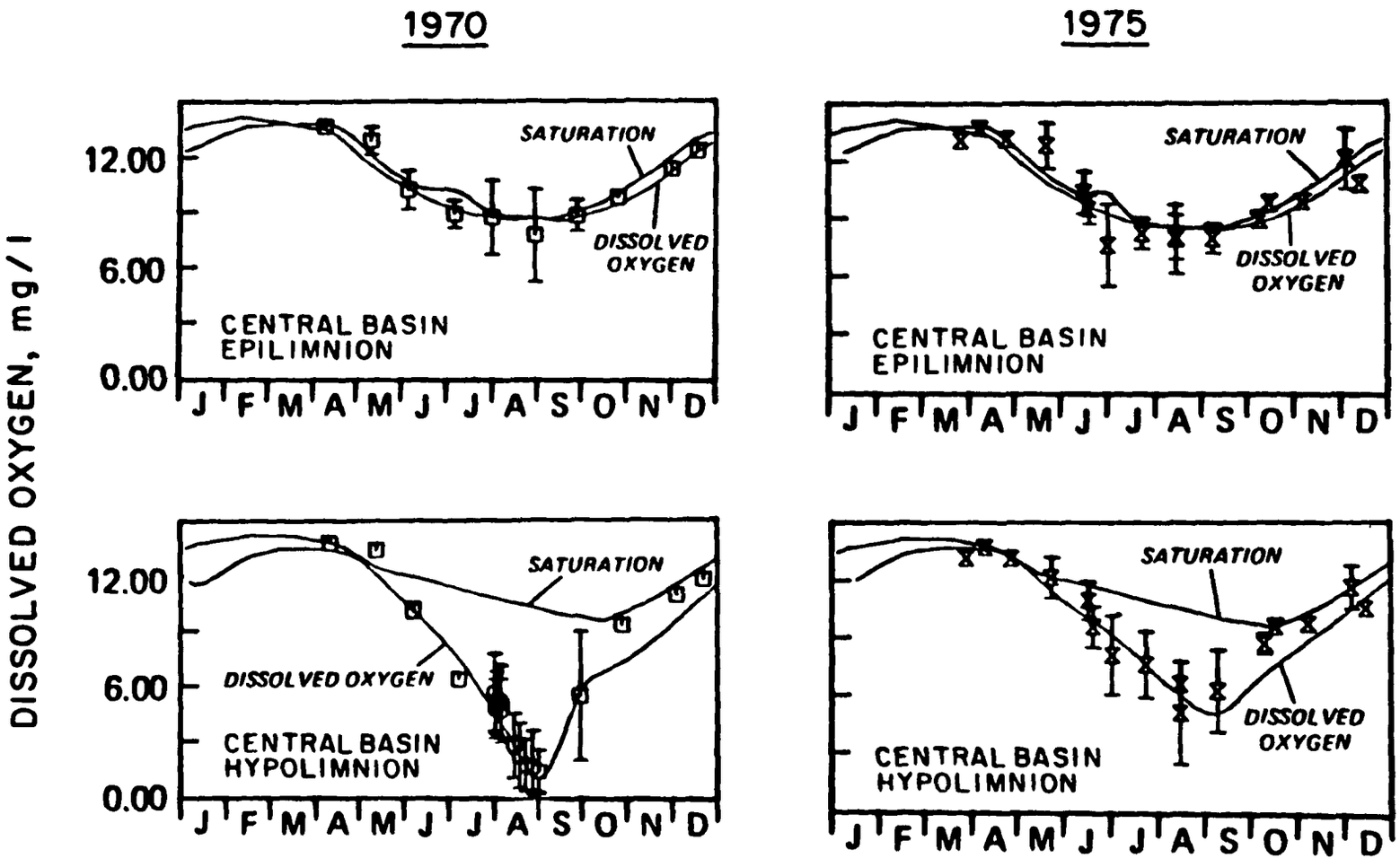

Figure 2. Comparison of predicted and observed surface and bottom layer dissolved oxygen distributions for 1970 and 1975. The data are plotted as the mean over the layer ± 1 standard deviation.

time. In the hypolimnion, the low oxygen values during the summer months of 1970 are caused by a combination of phytoplankton decay within the hypolimnion and the oxygen demand exerted by the sediment. The increasing temperature, which results in increasing reaction rates, the sinking of the phytoplankton, which have grown in the epilimnion, and stratification, which inhibits transfer of oxygen from the epilimnion to the hypolimnion, all contribute to the oxygen decline. The decline continues until overturn in early fall. At this time, there is a rapid increase in the hypolimnion dissolved oxygen, which continues to the end of the year. The higher oxygen concentrations in 1975 are basically due to the larger volume of the hypolimnion in that year. As shown by Di Toro and Connolly (1980), the sediment oxygen demand, which is a constant on an areal basis, would result in a smaller volumetric depletion rate in 1975. The maximum anoxic area of the Central Basin for 1970 is reported to be 6600 km^2, and this agrees well with the September maximum in the model of 6800 km^2.

Thermocline/Eutrophication Model Interaction

To use the eutrophication model in a predictive mode for the analysis of the various climate scenarios, three ingredients are required. The first is the expected water temperatures since they affect all the kinetic rates in the eutrophication model. The second is the depth of the thermocline and hence, the volumes of the epilimnion and hypolimnion. The third ingredient is the bulk vertical dispersive exchange between the epilimnion and the hypolimnion. The first two ingredients can be directly extracted from the thermocline model results. The dispersive exchange, on the other hand, needs to be computed using the temperature fields from the thermocline model run, averaged over the epilimnion and the hypolimnion, in conjunction with a temperature balance equation similar to Equation (3) structured for a two layer system.

The area integration of Equation (3) over the hypolimnion gives,

$$V_H \frac{\partial \theta_H}{\partial t} = A_i K_i \frac{\partial \theta_i}{\partial z} \tag{8}$$

where V_H and θ_H are the volume and volume-averaged temperature of the hypolimnion, respectively, and where i denotes the interface between the epilimnion and the hypolimnion. The interfacial dispersion coefficient, K_i, is readily computed from Equation (8) given the results from a thermocline model run.

Climate Scenarios

Three simulations of the changes in the equilibrium climate induced by a doubling of the atmospheric CO_2 ($2xCO_2$) concentration have been performed using atmospheric general circulation models (GCMs). These simulations were performed with the Goddard Institute for Space Studies (GISS) GCM by Hansen et al. (1984), the Geophysical Fluid Dynamics Laboratory (GFDL) GCM by Manabe and Wetherald (1986), and the Oregon State University (OSU) GCM by Schlesinger and Zhao (1988). Climate scenarios in the form of monthly averaged data over an annual cycle have been obtained for this study from the three GCM simulations. The relevant data are selected for the grid point closest to Lake Erie. The results of control runs using the present-day CO_2 concentration ($1xCO_2$) were also provided as a means of quantifying the predicted climate changes. A transient scenario using the GISS model was also included and involved the results of two 100-year runs in the form of decadal mean value differences (for each month) for the last 80 years of the simulations.

To use the GCM results in this study, the results were expressed as changes in surface air temperature and changes in surface windspeed. Figure 3 and Table 1 contain these values for each of the $2xCO_2$ and transient scenarios investigated. The values represent the deviation from the control, or base runs ($1xCO_2$). For the $2xCO_2$ scenarios the surface air temperature changes were calculated by subtracting the control run values from the $2xCO_2$ run values. The transient scenario decadal changes were calculated from the ratio between the temperature (in °K) of the scenario and the temperature (in °K) of the base run. The temperature differences from the GISS and GFDL $2xCO_2$ scenarios shown on Figure 3 are similar with the exception of June and July when the GFDL values are double those of GISS. Both $2xCO_2$ model runs show an increase in average monthly surface temperature of 3 to 7°C. The OSU $2xCO_2$ scenario, on the other hand, exhibits much less

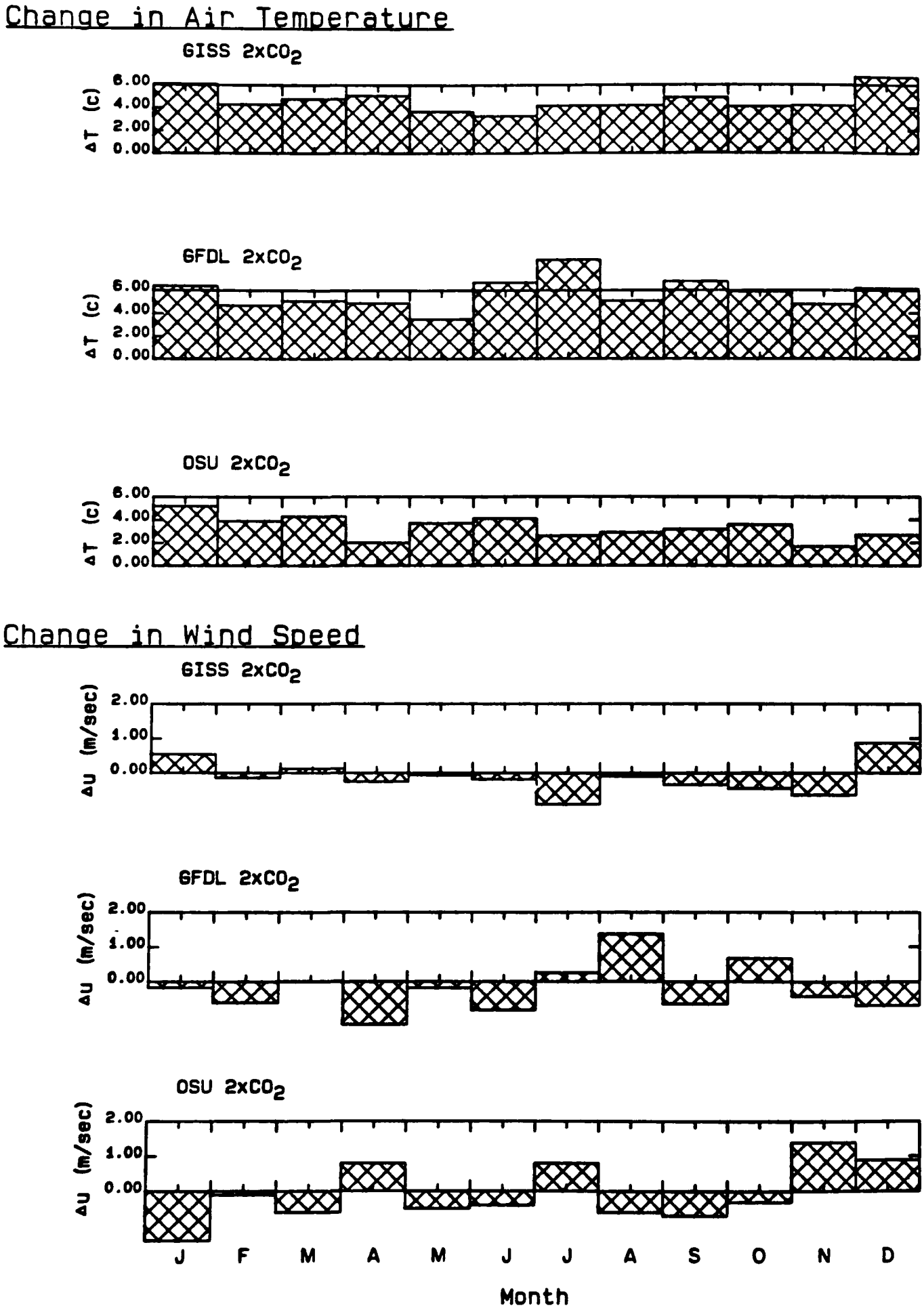

Figure 3. The monthly changes in surface air temperature and wind speed resulting from the three climate model simulations.

Table 1. Change in Air Temperature and Wind Speed for the Transient Scenario A

Change in Air Temperature (°C)

Scenario/Month	January	February	March	April	May	June	July	August	September	October	November	December	Average
Scenario A (1980-1989)	1.35	0.27	0.27	0.84	0.85	-0.29	1.17	0.29	0.00	-0.84	0.00	-0.54	0.28
Scenario A (1990-1999)	0.81	-0.27	0.00	0.00	0.65	0.87	1.46	0.29	0.00	0.56	1.37	1.35	0.61
Scenario A (2000-2009)	0.27	1.08	0.27	1.12	0.85	0.58	1.46	0.29	0.29	0.28	1.09	1.08	0.72
Scenario A (2010-2019)	1.35	2.98	1.65	1.68	1.13	0.58	1.75	0.59	0.87	0.84	2.46	3.24	1.59
Scenario A (2020-2029)	1.08	2.17	2.47	2.52	1.70	1.15	1.75	2.36	1.74	0.84	1.91	2.16	1.82
Scenario A (2030-2039)	2.96	4.07	2.47	3.37	2.55	2.31	2.92	1.47	3.19	1.40	2.46	3.24	2.70
Scenario A (2040-2049)	2.42	3.25	4.39	3.65	3.40	2.31	2.92	2.06	4.06	3.09	3.83	4.05	3.29
Scenario A (2050-2059)	5.38	5.69	4.67	3.65	4.53	3.17	4.09	5.30	4.35	4.21	5.74	5.94	4.73

Change in Wind Speed (m/s)

Scenario/Month	January	February	March	April	May	June	July	August	September	October	November	December	Average
Scenario A (1980-1989)	-0.67	-0.83	-0.60	-0.29	-0.23	0.19	-0.37	0.11	0.74	0.27	1.66	0.57	0.05
Scenario A (1990-1999)	0.14	-0.59	0.09	-0.21	-0.09	0.46	-0.34	-0.16	0.46	-0.06	0.71	0.65	0.09
Scenario A (2000-2009)	0.26	-1.02	0.64	-0.54	0.14	0.16	0.30	0.00	0.54	-0.38	0.77	0.94	0.15
Scenario A (2010-2019)	-0.46	-1.41	0.16	0.07	-0.20	0.17	-0.26	0.10	0.51	-0.40	0.34	0.09	-0.11
Scenario A (2020-2029)	0.38	-0.74	0.05	-0.45	-0.04	0.52	0.08	-0.21	0.45	0.05	0.81	0.94	0.15
Scenario A (2030-2039)	0.19	-0.11	0.35	0.29	-0.46	0.19	-0.45	-0.11	0.85	-0.05	0.83	0.84	0.20
Scenario A (2040-2049)	0.19	-0.56	-0.28	0.04	-0.46	-0.25	-0.57	0.18	0.58	-0.24	0.65	1.08	0.03
Scenario A (2050-2059)	0.20	-0.42	0.25	-0.51	0.08	0.06	-0.08	-0.06	1.16	0.11	0.83	0.46	0.17

temperature change, about half of the GISS and GFDL cases. Temperature changes of 2 to 4°C are thus predicted. The transient scenario average monthly changes in air temperature increase from the 1980-1989 decade to the 2050-2059 decade. At the end of the eighth decade (2050-2059), temperatures increased between 4 and 6°C from the control run.

The wind data available from the GCM data files are vector mean wind speeds instead of the more appropriate scalar mean wind speeds. Vector mean speeds are often significantly less than the true mean wind speed and will thus underestimate wind-induced mixing. This error is somewhat reduced here because the winds in the GCMs exhibit little directional variability within each scenario. The changes in wind speed for the $2xCO_2$ scenarios shown on Figure 3 are small and typically negative, suggesting that the winds will become weaker under the various climate scenarios. The OSU $2xCO_2$ scenario, it should be noted, has larger winds occurring in the critical spring and summer periods; increases of 1 to 1.5 m/sec are indicated. The largest increase in wind speed is about 1.7 m/sec, which occurs in November of Transient Scenario A (1980-1981) as shown in Table 1.

The heat fluxes and wind stresses required as input by the thermocline model were computed according to:

$$Q = Q_o + \frac{\partial Q}{\partial T} \Lambda T \tag{9}$$

and

$$\tau = \tau_o + \frac{\partial \tau}{\partial W} \Lambda W \tag{10}$$

where Q is the heat flux, τ is the wind stress, T is the air-lake temperature difference, and W is the wind speed. The o subscript denotes the base case, either 1970 or 1975, and Λ denotes the $2xCO_2$-$1xCO_2$ difference. The rate of change of heat flux Q from the lake with respect to the air-lake temperature difference has been computed by Gill (1982) based on the ideas of Haney (1971) for the world ocean. It appears that a value of 32 Watts m^{-2} is appropriate for the latitude of Lake Erie. The rate of change of wind stress with respect to wind speed is readily estimated to be 3×10^{-3} gm $cm^{-2}s^{-1}$.

RESULTS

Before proceeding to an assessment of the thermal and water quality response of Lake Erie to the various climate warming scenarios identified in the previous section, it becomes important to assess the skill of the thermocline model itself. The water quality model as utilized by Di Toro and Connolly (1980) used temperatures, thermocline depths, and bulk dispersion coefficients deduced from observations. Projections to future conditions are thus not possible without some predictive capability for these important inputs. In this section, the skill of the thermocline model is demonstrated, and then the model is used to estimate what the thermal response of Lake Erie would be under the various scenarios. Water quality projections follow using the computed thermal regimes for the various climate warming scenarios.

Verification of the Thermocline Model

The thermocline model presented above was applied to Lake Erie for the years 1970 and 1975. All simulations started on April 1 and terminated on December 31 to avoid considering the extensive ice cover which normally occurs during January through March. There are 40 vertical levels in the model with finer spacing near the surface than in the deeper regions. A time step of 30 minutes is used. The model is forced by hourly estimates of the surface wind stress and by monthly estimates of the surface heat flux. A continuous series of hourly wind speed and direction observations for 1970 and 1975 were obtained at the Erie, Pennsylvania, and Cleveland, Ohio, airports. These observations were corrected from overland to overwater winds (see Schwab and Morton, 1984) and turned into wind stresses using a quadratic drag law and a drag coefficient based on the work of Large and Pond (1981). The surface heat fluxes have been calculated by Di Toro and Connolly (1980) for 1970 and 1975 on a monthly basis using estimates of the heat storage. These values, illustrated on Figure 4, were linearly interpolated to form a set of daily values and are consistent with those computed by Derecki (1976) and Schertzer (1987) using hydro-meteorological data. The initial temperature profile was a vertically homogeneous 2.0°C.

A comparison of the predicted and observed surface and near-bottom temperatures for each of the two years is shown on Figure 5. The predicted and observed temperatures agree fairly well throughout the annual cycle. It appears that the model misses the onset of stratification by a month or so in 1970, while the correct onset is predicted in 1975. The peak in the hypolimnion temperatures, which occurs in September/October, well after the surface peak temperatures, is modeled quite well. The rapid fall deepening of the epilimnion due to surface cooling and convection is also captured by the model. However, the timing of this overturn event is off by two to three weeks with the model being later than the observations. The model appears to reproduce the maximum stratification in both years. In 1970, the data for August (typically the most stratified month) show bottom and surface temperatures ranging from 11 to 22°C for a temperature difference of $\Delta T = 11°C$. The 1970 model values are 12 to 24°C for a temperature difference of $\Delta T = 12°C$. In 1975, the data for the same monthly time period shows bottom and surface temperatures ranging from 13 to 22°C, for a $\Delta T = 9°C$. The 1975 model values are 13 to 20°C, for a $\Delta T = 7°C$. Thus, while the model is not perfect, it does capture most of the large observed top to bottom difference and it does so at the proper time of the year.

Another measure of model skill is to compare vertical profiles between prediction and observation. Such a comparison is made on Figure 6 where the average temperature in two meter sections of the Central Basin are shown for July cruises in 1970 and June cruises in 1975. The model reproduces the vertical structure observed in 1970 very well. However, the model has a tendency to produce slightly warmer bottom temperatures, perhaps because there is no mechanism in the model to transfer heat to the sediment. The comparison of the 1975 case is not as good. The month of June is a transitional period when the lake goes from vertically mixed to stratified. Errors in the timing of the onset of stratification can lead to the kinds of comparisons indicated for 1975. The seasonal variation of the vertical structure of the lake is shown in the upper portions of Figure 7 for 1970 and Figure 8 for 1975. The mixed layer is shallow in summer owing to intense solar heating and typically weak winds, but deepens rapidly in the fall. The isotherms deepen slowly in the spring and summer owing to downward diffusion and rise rapidly in fall owing to convection. It has been observed that 1970, with its stronger winds and larger surface heating, has a greater thermocline depth than 1975.

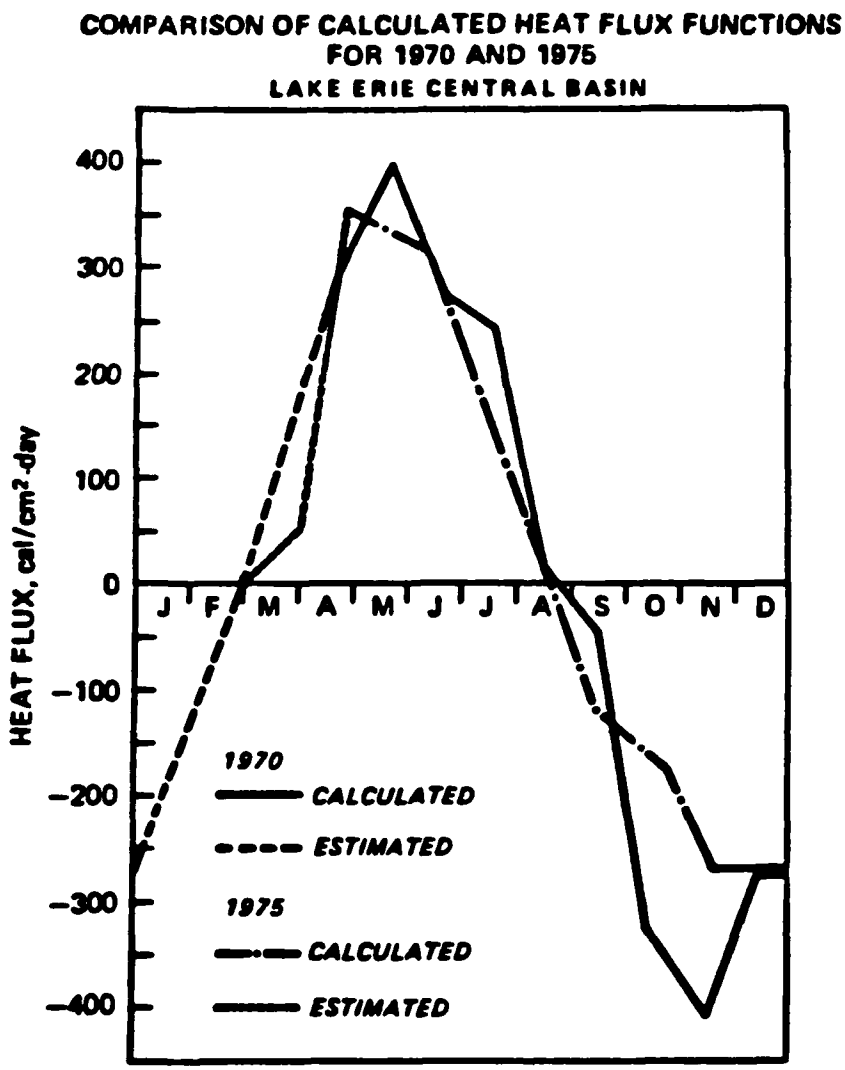

Figure 4. Calculated heat flux (cal/cm^2-day) to the central basin using observed temperatures for each cruise. During the winter period, the net heat flux shown is estimated.

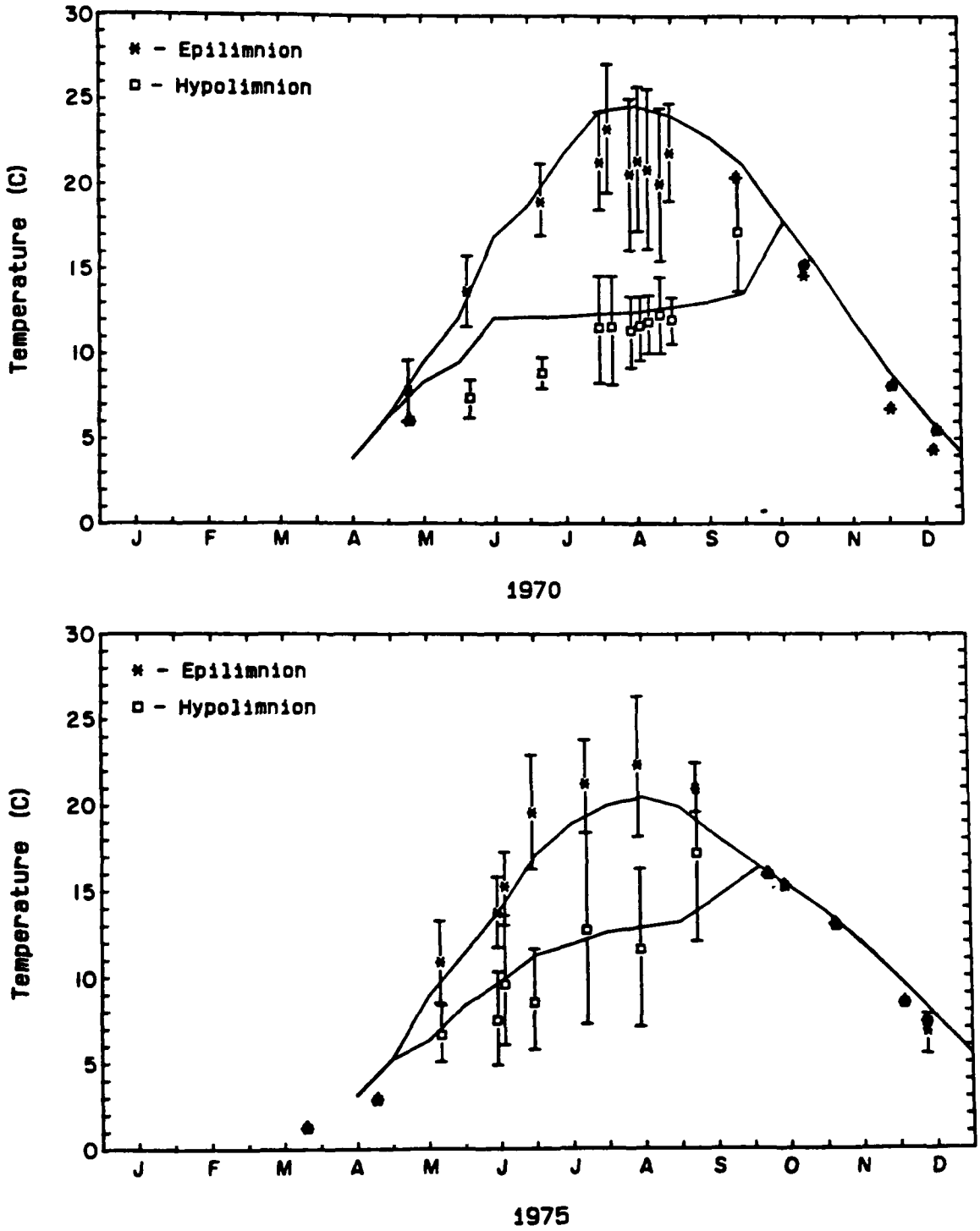

Figure 5. Comparison of predicted and observed surface and bottom temperatuers for 1970 and 1975 over the annual cycle. The data are plotted as the mean over the layer ± 1 standard deviation; lines are the computations.

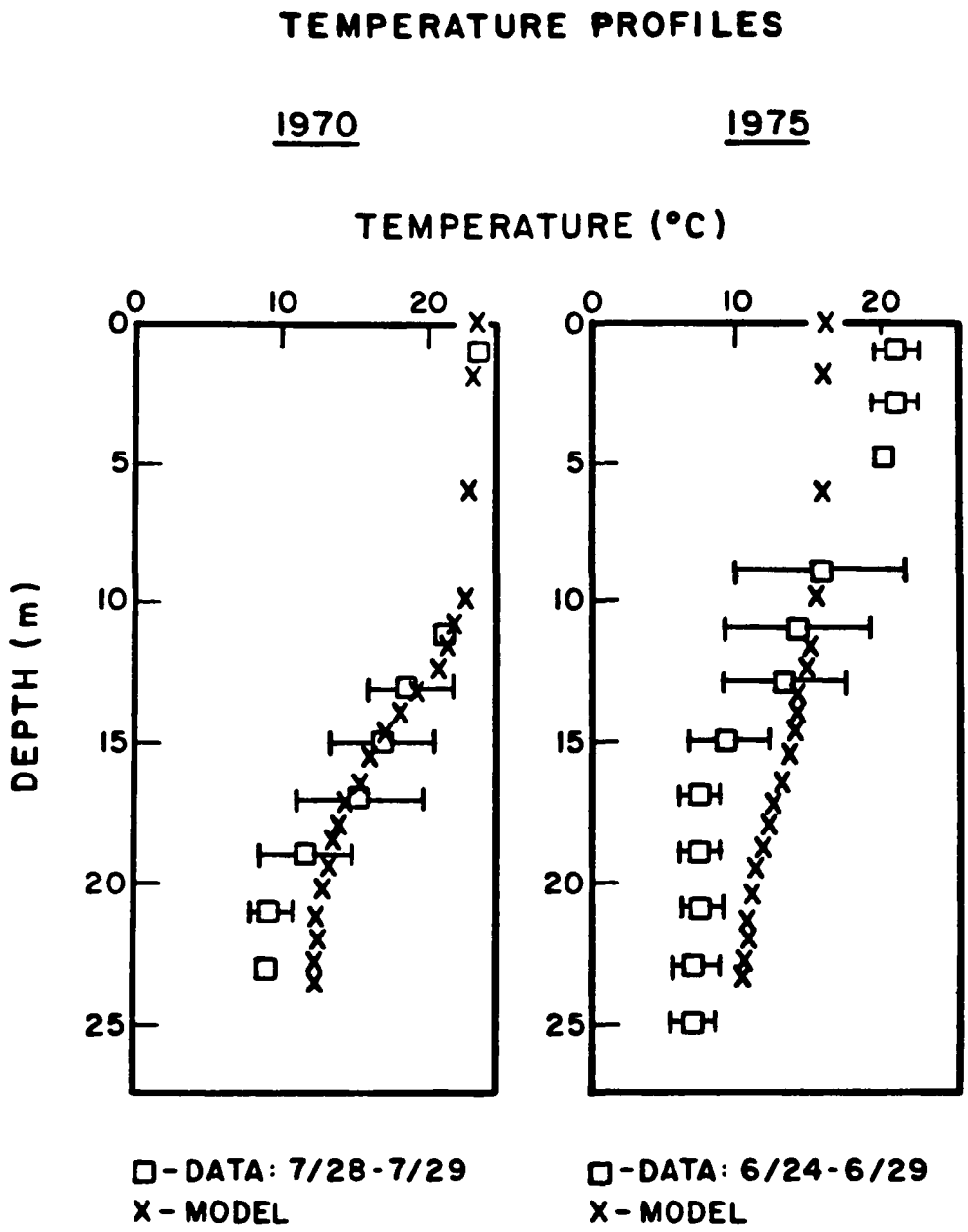

Figure 6. Comparison of the predicted and observed thermal vertical structure for July 1970 and June 1975. The data are plotted as the mean over a two-meter layer ±1 standard deviation. Much of the June 1975 error can be attributed to errors in the timing of the onset of stratification.

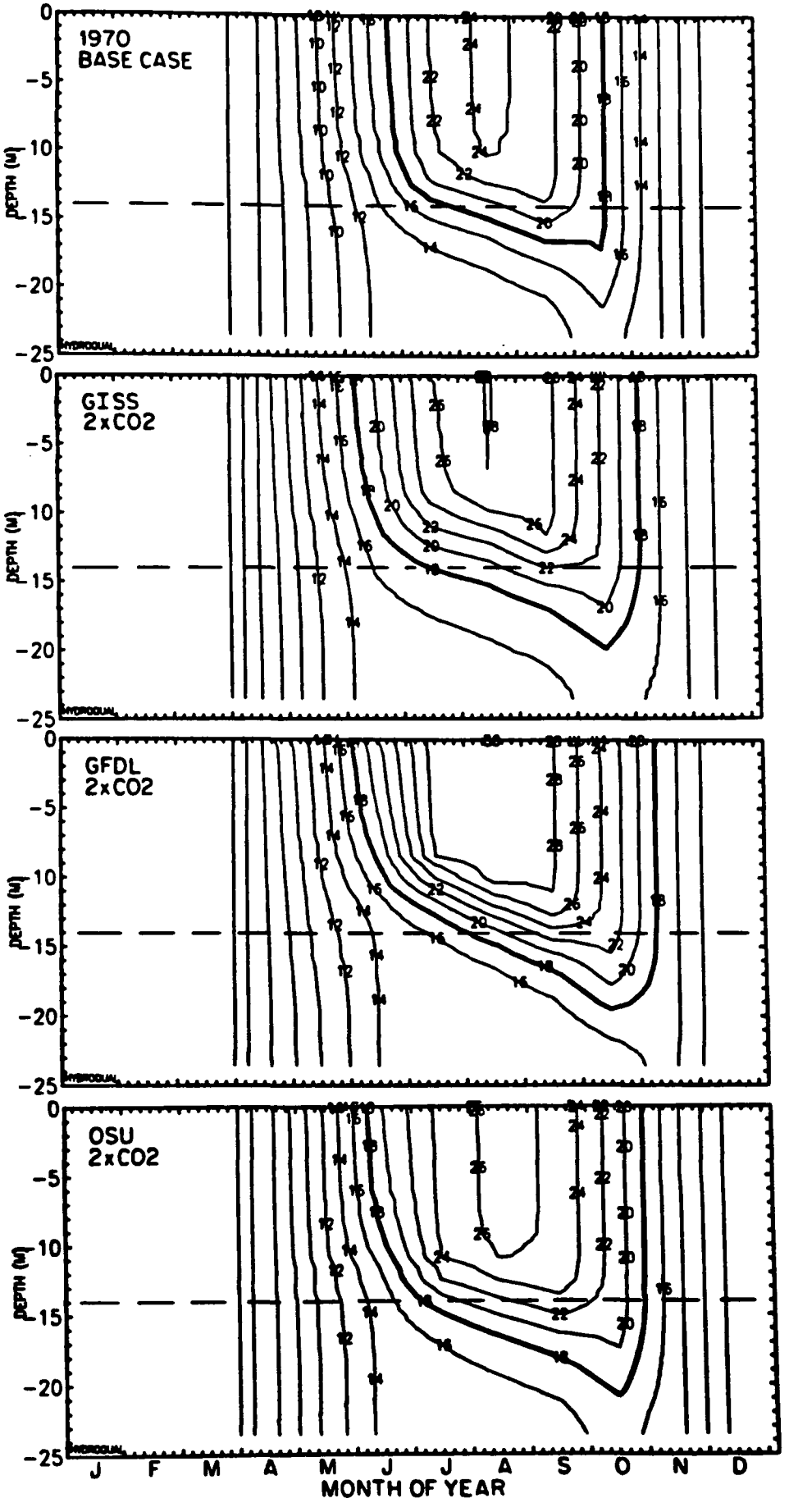

Figure 7. The seasonal variation of the thermal vertical structure for the 1970 cases. Contour in °C. Dashed line is the mixed layer depth for the base case.

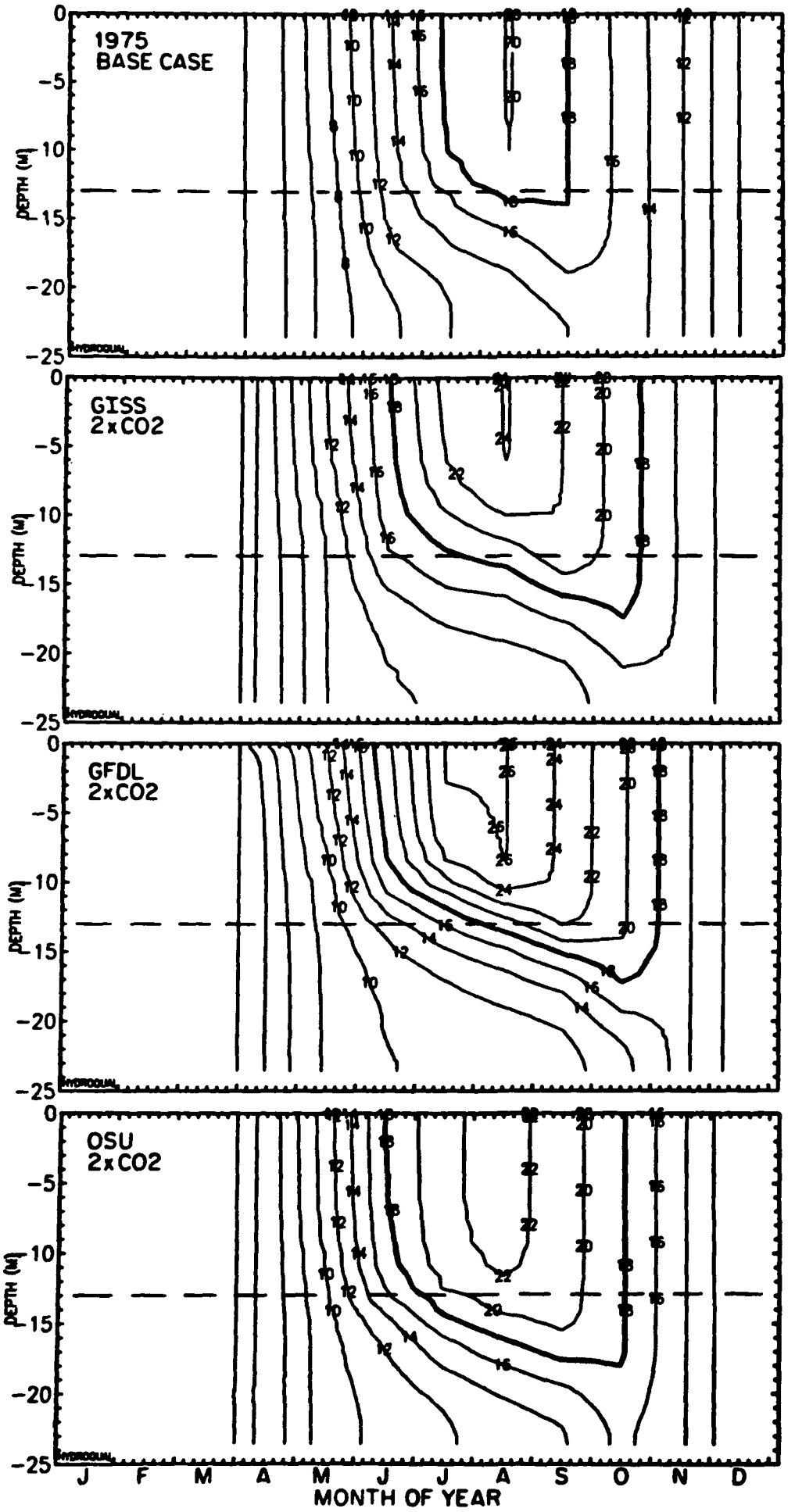

Figure 8. The seasonal variation of the thermal vertical structure for the 1975 cases. Contour in °C. Dashed line is the mixed layer depth for the base case.

To explain the difference between the observed and computed thermal structure, it is important to realize that there are no coefficients available in the thermocline model that can be adjusted in order to improve model performance for these applications. One must look toward improving model physics or assembling better model forcing data. While some improvements in the exchange processes between the water column and the sediment can be envisioned, the model physics based on areally averaged dynamics appear well established for basin-wide problems. On the other hand, the data available for model forcing, especially the wind fields, are subject to considerable uncertainty. Mid-basin wind stresses are estimated from observations of wind speed and direction at weather stations around the lake. The model error in this study is probably due to the use of only two stations. Since the timing of the formation and subsequent destruction of the thermocline are dependent on details in the wind field, the use of perhaps six stations around the lake would be necessary to incorporate the spatial variability of the wind fields into the mid-basin average.

Thermal Response to Scenarios

The calibrated and skill assessed thermocline model was run using the climate warming scenarios presented earlier. The evolution of the vertical structure over an annual cycle is illustrated on Figures 7 and 8 for the GISS, GFDL, and OSU $2xCO_2$ scenarios. It is evident from these results that the $2xCO_2$ scenarios produce a warmer, longer lasting warming regime in the lake. The heating season, as defined by the presence of surface water with temperatures greater than or equal to 18°C, lengthens about 40 days using 1970 as the base case and almost doubles to between 64 and 135 days using 1975 as the base. When comparing scenarios to their base cases, the climate scenarios using the 1975 base case begin heating some four weeks earlier and heat six weeks longer than the base, while those using the 1970 base case begin heating about two weeks earlier and heat approximately two weeks longer than the base. The maximum surface temperature increases by about 5°C in all scenarios.

The thermocline, defined as the depth of maximum vertical temperature gradient in August (the warmest month), becomes shallower by about 2 m for the GISS and GFDL $2xCO_2$ cases. The OSU $2xCO_2$ scenario results in a slightly deeper thermocline in spite of its smaller air temperature change. Apparently the increase in wind speeds can mix the extra surface heating deeper into the water column than can the lesser wind speeds and greater surface heating of the GISS and GFDL $2xCO_2$ scenarios. The change in volume of the hypolimnion for the various scenarios is tabulated in Table 2. Because of the shape of the Central Basin, a 1- to 2-meter rise in the thermocline leads to 50 to 100 percent increases in volume. The 1975 based OSU $2xCO_2$ scenario with its deeper thermocline actually has a 20 percent smaller hypolimnion volume. Table 2 provides a summary of the results from all the scenarios. The use of the transient scenarios, it will be noted, produces decadal mean values that exhibit much variability. The trend, however, is clearly toward warmer waters throughout the April to December period.

The change in epilimnion and hypolimnion temperature is shown on Figure 9. Most of the extra heat is confined to the epilimnion where changes are on the order of 4°C. The waters of the hypolimnion increase about 1 to 2°C with an even greater increase of about 3 to 4°C occurring in the later part of the year. The temperature difference across the epilimnion-hypolimnion interface, therefore, increases by 2 to 3°C, as shown in Table 2. This difference is certain to reduce the dispersive exchange between the upper and lower layers of the lake.

The results from a number of sensitivity runs have also been analyzed. These runs included running the base cases with different combinations of forcing. For example, experiments were run where the 1970 winds were used in conjunction with the 1975 heating and vice versa. As illustrated in Table 2, the runs showed that the location of the thermocline is a delicate balance between wind stirring and surface heating. Increasing the wind stirring by having stronger winds causes the thermocline to form deeper and at a later time. Conversely, weaker winds or larger surface heating will produce a shallower thermocline at an earlier time. These ideas are further substantiated by the differences between the OSU and GISS/GFDL $2xCO_2$ results. Other cases have been conducted to address the findings of Assel (1988) who showed that under the $2xCO_2$ scenarios it is likely that the central basin of Lake Erie will be void of its now characteristic winter ice cover. Results from simulations with initial temperature profiles of 4°C and 8°C indicated that the summertime conditions for these cases were identical to those of the benchmark case, which used a 2°C initial profile.

Table 2. Summary of Climate Scenario Calculations

Run	Mixed[a] Layer Depth	Length of Heating Season[b] Start Date	End Date	Duration Days	Temperature Maximum (°C)	Temperature[c] Difference (°C)	Vertical[d] Dispersion (cm^2s^{-1})	Increase in[e] Hypolimnion Volume (%)
1970 Base Case	14	6/23	10/14	113	25	9	0.02	-
1975 Base Case	13	7/10	09/12	64	20	5	0.12	-
1970 GISS ($2xCO_2$)	10	6/05	10/31	148	28	10	0.02	90
1970 GFDL ($2xCO_2$)	12	5/30	11/05	159	30	12	0.02	50
1970 OSU ($2xCO_2$)	14	6/04	10/27	145	27	9	0.02	10
1975 GISS ($2xCO_2$)	10	6/14	10/20	128	24	7	0.06	40
1975 GFDL ($2xCO_2$)	11	5/31	10/31	153	27	11	0.07	30
1975 OSU ($2xCO_2$)	14	6/15	10/14	121	23	6	0.09	-20
1970 Winds/1975 Heating	15	7/14	09/09	57	19			
1975 Winds/1970 Heating	12	6/19	10/14	117	26			
1970 Transient								
Scenario A (1980-1989)	12	6/21	10/10	111	25			
Scenario A (1990-1999)	13	6/20	10/14	116	25			
Scenario A (2000-2009)	14	6/20	10/15	117	25			
Scenario A (2010-2019)	13	6/18	10/16	120	25			
Scenario A (2020-2029)	14	6/17	10/19	124	26			
Scenario A (2030-2039)	12	6/11	10/22	133	26			
Scenario A (2040-2049)	12	6/07	10/27	142	26			
Scenario A (2050-2059)	12	6/05	11/03	151	29			

[a]Based on depth of the maximum vertical temperature gradient during August.
[b]Based on presence of water with temperatures $\geq$ 18°C at the surface.
[c]Based on averages over the epilimnion and the hypolimnion.
[d]Based on August values.
[e]Relative to base case.

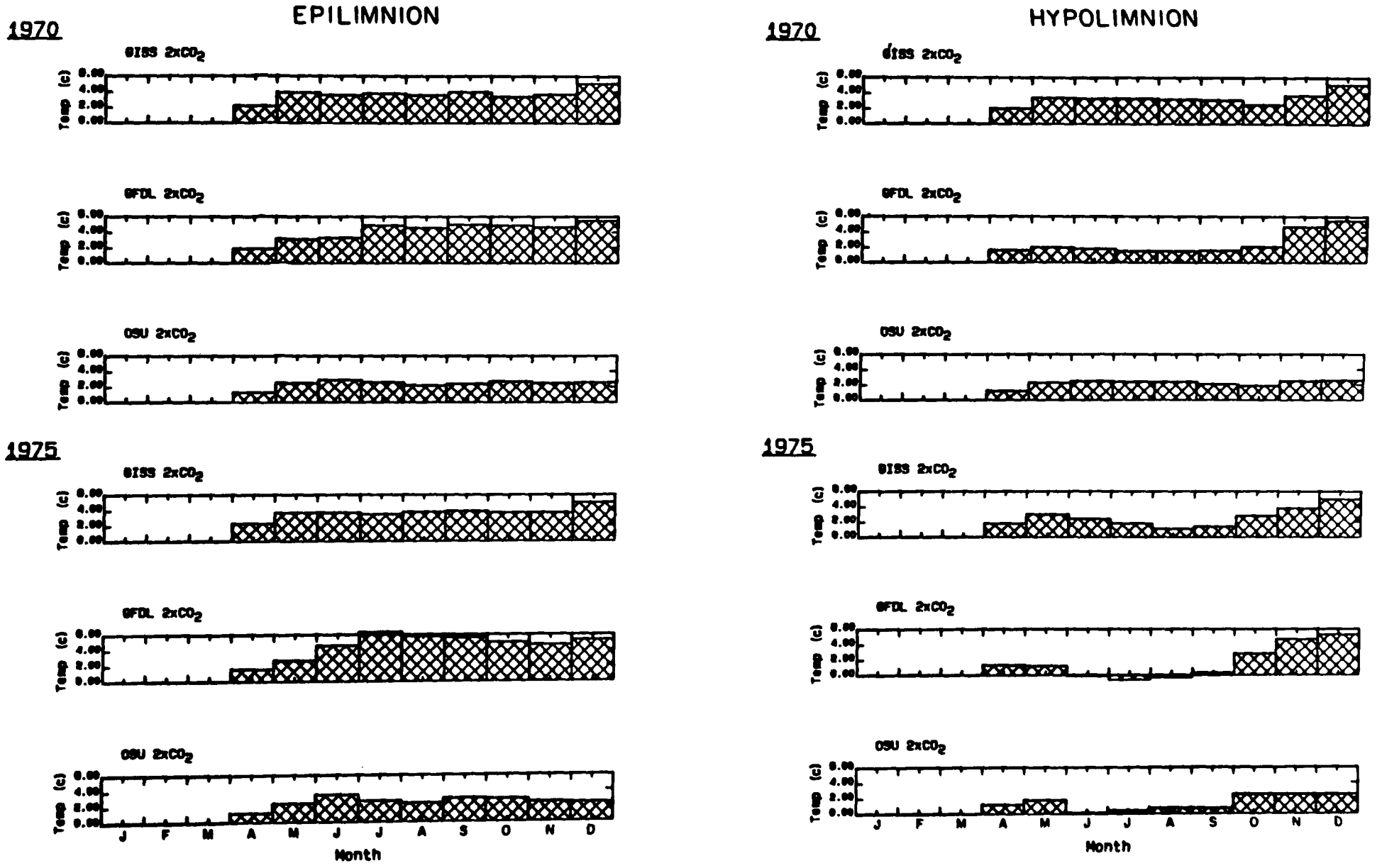

Figure 9. The monthly difference in temperature (°C) between the climate scenario and its base case for the epilimnion (left) and the hypolimnion (right).

Water Quality Response to Scenarios

Given the epilimnion and hypolimnion temperatures resulting from the climate warming scenarios, it is a straightforward task to estimate how water quality responds to the warming. The dispersion coefficients computed from Equation (8) that are consistent with the new temperatures are shown in Table 2. There is little scenario to scenario variation in the coefficients for the 1970-based cases. The temperature difference between the epilimnion and hypolimnion is great enough in every 1970-based case to prevent mixing. On the other hand, the 1975-based cases show much scenario to scenario variation. The increase in the temperature difference reduces the vertical exchange by a factor of 2 or so, from 0.09 cm^2/s to 0.06 cm^2/s, during times of maximum stratification.

The projected[2] epilimnion and hypolimnion DO for the GISS, GFDL, and OSU scenarios are shown on Figure 10 along with the observations for 1970 and 1975. The epilimnion DO worsens by about 1 mg/L in every case with respect to the observed values. This decrease is primarily due to the change in the saturation level for DO. For example, a 4°C increase in epilimnion temperature produces an approximately 0.6 mg/L decrease in the level of DO for each scenario. The hypolimnion DO, as shown on Figure 10, decreases dramatically, losses of 1 to 2 mg/L being typical under the various scenarios. The 1975-based cases, for which the observation did not reach the anoxic level, show losses of up to 5 mg/L of DO. The 1970 observations have very low levels of DO already, so a small loss leads immediately to anoxia. It is interesting to note that the GISS $2xCO_2$ scenario using 1970 as the base year leads to a three-month period of higher levels of DO.

The overall decrease in DO can be explained by noting that the sinks of oxygen in the hypolimnion, the benthic respiration rate due to the decay of organic material, and bacterial metabolism of organisms in the water column are strong functions of temperature. In fact, the increase in hypolimnion temperatures due to the climate warming increases the SOD, the largest part of the oxygen sinks, considerably overwhelming any decrease in dissolved oxygen saturation. On the other hand, the volume of the hypolimnion has increased (see Table 2), and there is now a greater volumetric reservoir of dissolved oxygen available to meet water column and benthic oxygen demand. The results of the scenario simulations indicate that the volumetric depletion rate becomes greater despite increases in the volume of the hypolimnion, which in the absence of any change in SOD, would result in a smaller volumetric depletion rate and higher levels of DO. Figure 11 illustrates the volumetric depletion rates for the model scenarios and the base cases. An experiment, whereby the thermal structure of the 1970-based GFDL $2xCO_2$ scenario was used in conjunction with the observed, and somewhat cooler, 1970 temperatures showed that high levels of DO would be present. This suggests that the major decline in the lake's water quality is due to the warmer lake temperatures, which increase the rate of bacterial activity in the sediment enough to produce apparently significant increases in the SOD. The OSU $2xCO_2$ scenario produces the worst DO distributions because the thermocline depth changed little while the SOD became much greater, again due to the elevated temperatures. It appears that no matter at what depth the thermocline forms, the increased lake temperatures will lead to degradation in the water quality.

The change in the areal extent of anoxia, defined here as 0 mg/L, in the Central Basin can be computed using the empirical method developed by Di Toro and Connolly (1980). Figure 12 shows, as monthly averages, the percentage of the Central Basin that observationally is anoxic and the percentage that is projected to become anoxic under each of the scenarios. The 1970-based scenarios produce areas of anoxia that encompass considerable portions of the lake. The areas of anoxia also occur two weeks or so sooner than those of the base case. The 1970 observations indicate only a month of severe anoxia, and only about 65 percent of the basin is affected. The OSU $2xCO_2$ scenario, with the smallest change in air temperature, produces the worst case in terms of extra anoxia for both the 1970- and 1975-based cases. It should be remembered that under the present climate conditions 1975 had ample DO, and now with the warming both the GFDL and OSU $2xCO_2$ 1975 based scenarios are showing large regions (20 to 50 percent) of anoxia for periods of a month and greater.

---

[2]The projected values are obtained by adding the difference between those values computed using the $2xCO_2$ scenarios and the $1xCO_2$ scenarios to the original observations.

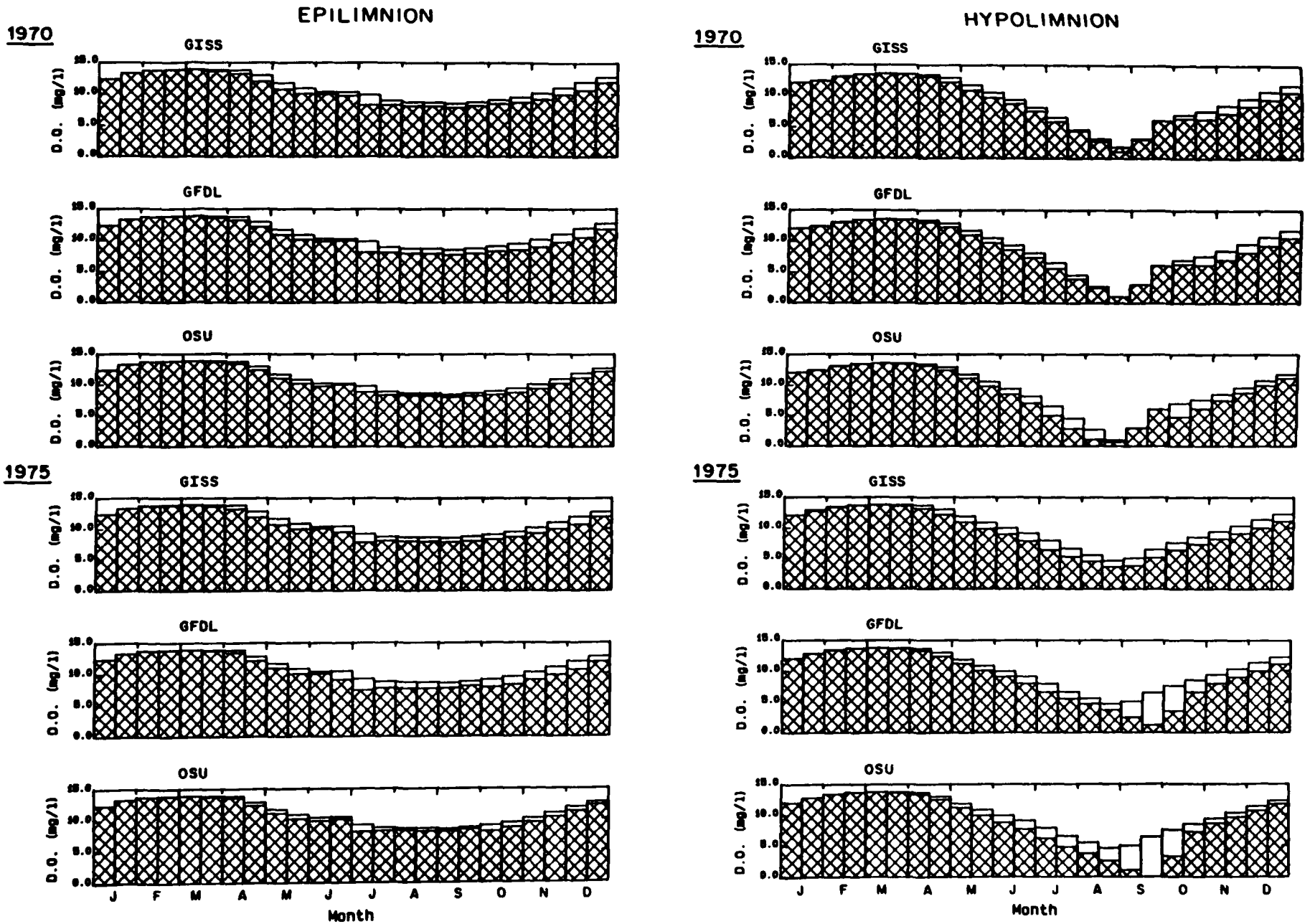

Figure 10. The monthly averaged dissolved oxygen (mg/L) or the epilimnion and hypolimnion of the Central Basin. The hatched bars denote the projections, while the clear bars are observations. The difference between these bars is the climate warming-induced change.

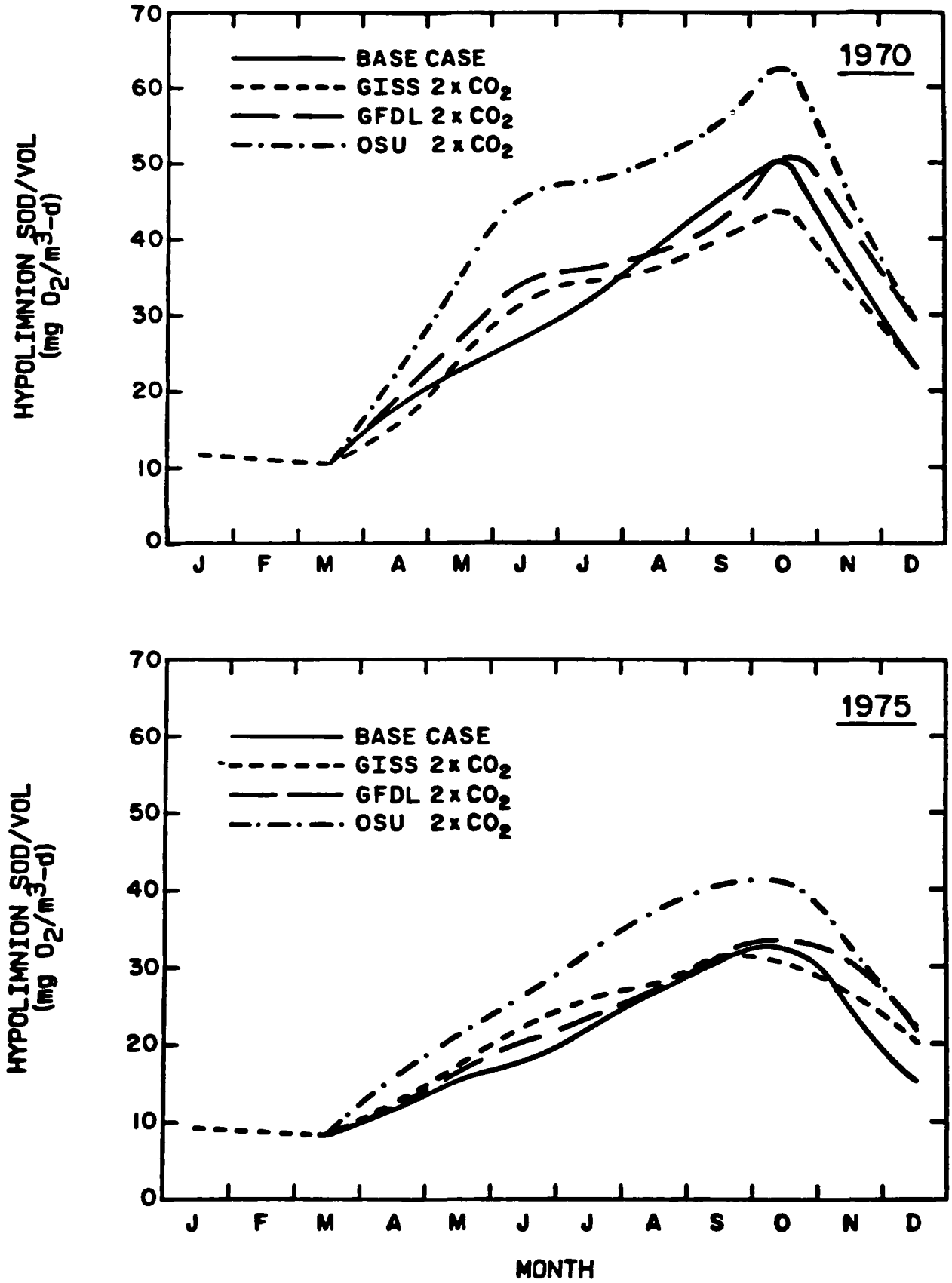

Figure 11. A comparison of the annual cycle of volumetric hypolimnion SOD between base case and the various climate warming scenarios.

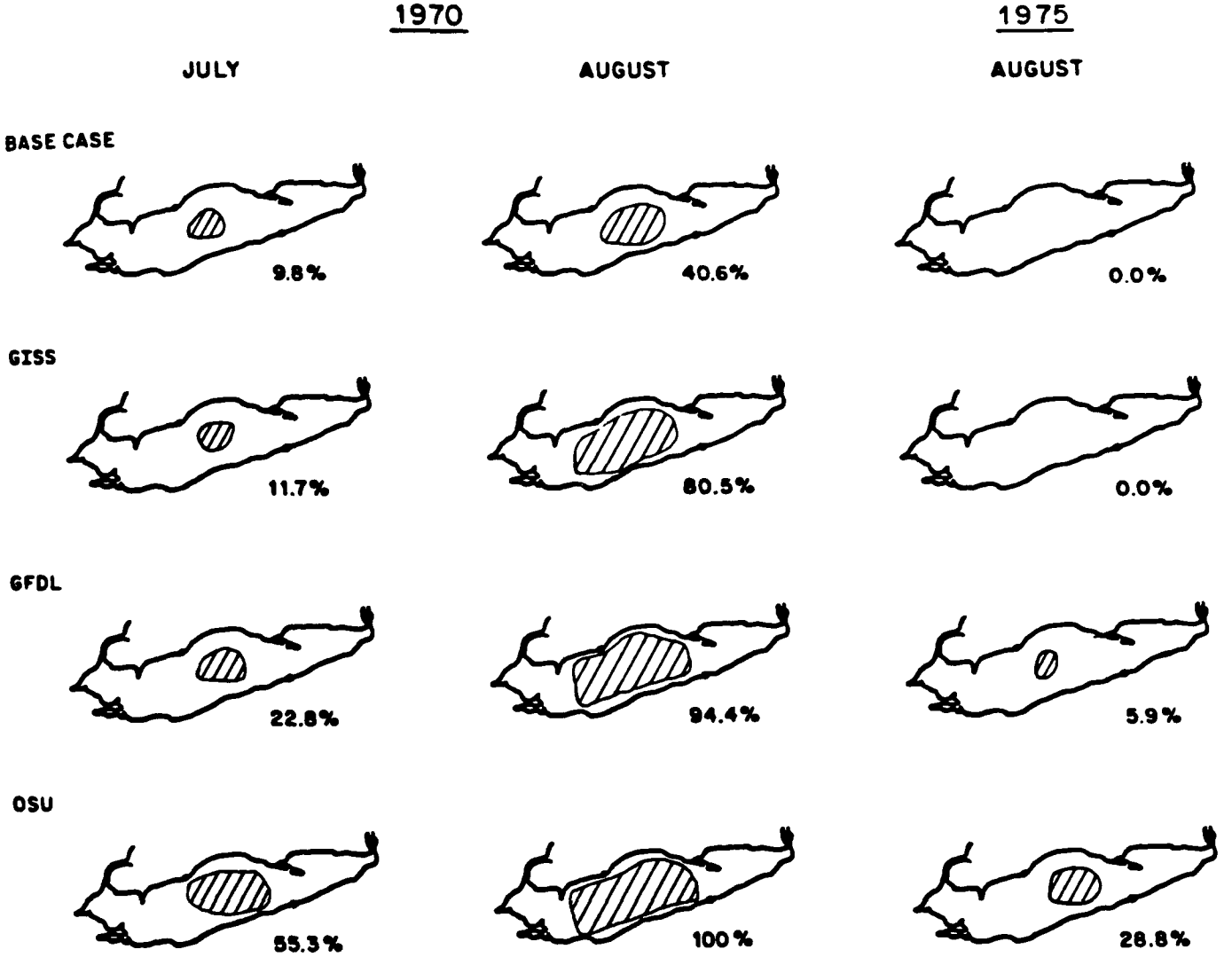

Figure 12. A comparison of the monthly average percentage of anoxia in the Central Basin between the base years and the projections from various climate warming scenarios. The hatched areas represent the regions of anoxia.

Since the lake turns over each year, there appears to be little thermal carryover from year-to-year. The transient scenarios thus become a series of steady-state ones similar to the $2xCO_2$ cases. It is possible then to make some comments about the resulting water quality for each decade in the transient series. As Table 2 illustrates, all of the transient scenarios have thermocline depths and heating season durations that are bounded by the 1970-based $2xCO_2$ cases. The resulting DO distributions and changes in areal extent of any anoxia are thus also bounded by the 1970 based cases and the conclusions reached previously apply here. The transient scenario cases were not run in the thermocline model for the 1975 base case and, as such, no additional comments can be provided.

REFERENCES

Assel, R.A., Impact of Global Warming on Great Lakes Ice Cycles. NOAA/ERL/GLERL Report, Ann Arbor, Mich., 1988.

Bierman, V.J., Mathematical model of the selective enhancement of blue green algae by nutrient enrichment. In: Modeling Biochemical Processes in Aquatic Ecosystem, Ed. R. Canale, Ann Arbor, Mich: Ann Arbor Science, 1-32, 1976.

Blumberg, A.F., and Mellor, G.L., Diagnostic and prognostic numerical circulation studies of the South Atlantic Bight. J. Geophys. Res., 88, 4579-4592, 1983.

Cohen, S.J. Impacts of CO_2-induced climatic change on water resources in the Great Lakes basin. Climatic Change, 8, 1986, 135-153.

Cohen, S.J. Influences of Past and Future Climates on the Great Lakes Region of North America. Water International, 12, 163-169, 1987.

De Pinto, J.V., Young, T.C., and Salisbury, D.K., Impact of phosphorus availability on modeling phytoplankton dynamics. Hydrobiological Bulletin, 20, 225-243, 1986.

Derecki, J.A., Heat Storage and Advection in Lake Erie. Water Resources Res., 12, 1144-1150, 1976.

Di Toro, D.M., and Connolly, J.P., Mathematical Models of Water Quality in Large Lakes. Part 2: Lake Erie. USEPA EPA-600/3-80-065, Duluth, Minnesota, 230 pp., 1980.

Di Toro, D.M., Thomas, N.A., Herdendorf, C.E., Winfield, R.P., and Connolly, J.P., A Post Audit of a Lake Erie Eutrophication Model. J. Great Lakes Res., 13, 801-825, 1987.

Gill, A.E., Atmosphere-Ocean Dynamics, Academic Press, New York, New York, 1982.

Haney, R.L., Surface Thermal Boundary Conditions for Ocean Circulation Models. J. Phys. Oceanogr., 1, 241-248, 1971.

Hansen, J., Lacis, A., Rind, D., Russell, G., Stone, P., Fund, I., Ruedy, R., and Lerner, J., Climate Sensitivity: Analysis of Feedback Mechanisms. In: Climate Processes and Climate Sensitivity, Geophys. Monogr. Ser., 29, Eds. J.E. Hansen and T. Takahashi, AGU, Washington, DC, 130-163, 1984.

Heinrich, J., Lick, W., and Paul, J., Temperatures and Currents in a Stratified Lake: A Two-Dimensional Analysis. J. Great Lakes Res., 7, 264-275, 1981.

International Joint Commission, Great Lakes Water Quality Agreement of 1978, Washington, DC and Ottawa, November 22, 1978. International Joint Commission, Windsor, Ontario, 1978.

Kraus, E.B., Modelling and Prediction of the Upper Layers of the Ocean. Pergamon Press, Ed. E.B. Kraus, p. 325, 1977.

Lam, D.C.L., and Schertzer, W.M., Lake Erie Thermocline Model Results: Comparison with 1967-1982 Data and Relation to Anoxic Occurrences. J. Great Lakes Res., 13, 757-769, 1987.

Lam, D.C.L., Schertzer, W.M., and Fraser, A.S., Simulation of Lake Erie Water Quality Responses to Loading and Weather Variations. Scientific Series No. 134, National Water Research Institute, Canada Centre for Inland Waters, Burlington, Ontario, 1983.

Large, W.G., and Pond, S., Open Ocean Momentum Flux Measurements in Moderate to Strong Winds. J. Geophys. Res., 11, 324-336, 1981.

Manabe, S., and Wetherald, R.T., Reduction in Summer Soil Wetness Induced by an Increase in Atmospheric Carbon Dioxide. Science, 232, 626-628, 1986.

Martin, P.J., Simulation of the Mixed Layer at OWS November and Papa with Several Models. J. of Geophys. Res., 90, 903-916, 1985.

Mellor, G.L., and Yamada, T., Development of a turbulence closure model for geophysical fluid problems. Rev. Geophys. and Space Phys., 20, 851-875, 1982.

Schertzer, W.M., Heat Balance and Heat Storage Estimates for Lake Erie, 1967 to 1982. J. Great Lakes Res., 13, 454-467, 1987.

Schlesinger, M.E., and Mitchell, J.F.B., Climate Model Simulations of the Equilibrium Climatic Response to Increased Carbon Dioxide. Rev. Geophys., 25, 760-798, 1987.

Schlesinger, M.E., and Zhao, Z.-C., Seasonal Climate Changes Induced by Doubled CO_2 as Simulated by the OSU Atmospheric GCM/Mixed-Layer Ocean Model. Climate Research Institute Report, Oregon State University, Corvallis, Oregon, 84 pp., 1988.

Schwab, D.J., and Morton, J.A., Estimation of Overlake Wind Speed from Overland Wind Speed: A Comparison of Three Methods. J. Great Lakes Res., 10, 68-72, 1984.

Thomann, R.V., Di Toro, D.M., Winfield, R., and O'Connor, D.J., Mathematical Modeling of Phytoplankton in Lake Ontario, 1. Model Development and Verification. Environmental Protection Agency, EPA 660/3-75-005. Corvallis, Oregon, 177 pp., 1975.

U.S. Environmental Protection Agency, Ambient water quality criterion for dissolved oxygen: freshwater aquatic life. Federal Register 50, 15634-15668, 1985.

IMPACTS OF GLOBAL WARMING ON RUNOFF IN THE UPPER CHATTAHOOCHEE RIVER BASIN

by

David K. Hains
C. F. Hains, Hydrologist, Inc.
Northport, AL 35476

Contract No. CR814637

CONTENTS

Page

FINDINGS 8-1

CHAPTER 1: INTRODUCTION 8-3
HYDROLOGY OF A SOUTHEASTERN HEADWATER BASIN 8-3
RELATED REPORTS 8-3
ORGANIZATION OF THIS REPORT 8-3

CHAPTER 2: METHODOLOGY 8-6
THE SACRAMENTO MODEL 8-6
Development of the Model 8-6
Limitations Resulting from the Model 8-8
THE SCENARIOS 8-9
Scenarios Used 8-9
Issues Resulting from the Scenarios 8-9

CHAPTER 3: RESULTS 8-10
IMPACTS OF CLIMATE CHANGE 8-10
Direction and Magnitude of Changes 8-10
Transient A Scenario 8-13

CHAPTER 4: INTERPRETATION OF RESULTS 8-22

CHAPTER 5: IMPLICATIONS OF RESULTS 8-24
ENVIRONMENTAL IMPLICATIONS 8-24

LIST OF ABBREVIATIONS 8-25

REFERENCES 8-26

APPENDIX A 8-27

FINDINGS[1]

This report presents the results of modeling studies of the hydrology and the effects of climate change on the Apalachicola-Chattahoochee-Flint (ACF) River system in the southeastern United States. Two separate studies were performed on the system. A detailed hydrologic study was performed on the upper Chattahoochee River, a small headwater portion of the system. A more general statistical study was done on the entire river system near its outlet to the Gulf of Mexico to provide flow estimates needed by other researchers.

For several years, atmospheric scientists have been studying the effects of carbon dioxide (CO_2) on climate change using general circulation models (GCMs). For this report results in the form of weather variables from three of these modeling groups have been used as inputs to a hydrologic analysis to determine the range of effects which can be predicted in the hydrology of a major southeastern river system as a result of global warming and climate change driven by increasing CO_2 concentrations. Three different GCMs were used to develop steady-state scenarios, each based on doubling of CO_2 concentrations in the atmosphere. The three models used were the Goddard Institute for Space Studies (GISS) model, developed by NASA; the Geophysical Fluid Dynamics Laboratory (GFDL) model, developed at Princeton University; and the Oregon State University (OSU) model. One transient scenario was used in the GISS model based on a gradually increasing concentration of CO_2 following the current trend.

The Sacramento Model, developed by the National Weather Service (NWS), was used to model the hydrology and the effects of climate change for the Upper Chattahoochee River Basin at Buford Dam on Lake Lanier in Georgia. Although the Sacramento Model is intended to be a continuous simulation model, its usual application is for flood forecasting by the River Forecast Centers of the National Weather Service. As a result, existing calibration data for most watersheds have been optimized to give most accurate results for flood peaks. The version of the Sacramento Model used in this study was obtained from the University of Washington where parallel studies are being conducted for catchments on the Pacific Coast. This version of the model has been set up for computer-assisted calibration to minimize the percent error in all ranges of flow. The Sacramento Model takes rainfall and pan evapotranspiration as time series inputs and applies them to the watershed being modeled using equations to describe the process yhat are partially based on the physical nature of the process and partially based on empirical data.

Although this study was originally intended to stop with the computation of inflow to Lake Sidney Lanier on the upper Chattahoochee River, other investigators participating in this report to Congress required an estimate of the effects of climate change on the freshwater flows in the Apalachicola River at Blountstown, Florida. An autoregressive, multiple correlation model was applied to the long record of historical monthly flows of the Apalachicola River at Chattahoochee, Florida, along with historical monthly rainfall and pan evaporation data. This autoregressive model was used along with climate change data to estimate the effects on the flow of the Apalachicola River at Blountstown.

The results were quite mixed. In general, we found that the various GCM outputs indicated a decrease in rainfall and an increase in temperature, and thus pan evaporation, when CO_2 is increased. For these cases, the hydrologic model showed a decrease in average annual runoff ranging from 14 to 27%. However, the GISS2X GCM output showed an increase in precipitation and resulted in a decrease in pan evaporation, with the result that the hydrologic model used on the upper Chattahoochee showed an increase in average annual runoff while the regression model used on the Apalachicola showed a small decrease under nearly identical scenarios. These differences appear to be due to differences in the hydrologic settings of the two study areas rather than differences in the behavior of the models themselves. Transient A GCM output had some unexpected fluctuations in the first decade before the CO_2 was changed very much. However, in the later

---

[1]Although the information in this report has been funded wholly or in part by the U.S. Environmental Protection Agency under contract no. CR814637, it does not necessarily reflect the Agency's views, and no official endorsement should be inferred from it.

decades of this run, the precipitation tends to decrease slightly and evaporation shows robust increases of up to 25%, and the hydrologic model shows a gradual but obvious decrease in runoff of as much as 30%.

Although any reduction in runoff seems severe during a drought of record proportions such as that experienced in the Southeast in 1988, the climate change scenarios are not particularly severe from a historical and hydrologic point of view. We have experienced dry periods as severe as any predicted by the climate change scenarios. In addition to the impacts of global climate change, changes in land use over a long period of time will also affect runoff trends -- especially on the entire ACF river system. It is only on systems whose long term effects are measured in decades -- such as forests, swamps, and fish populations, systems with very long memories -- that the dominant reductions in runoff predicted here will be felt. By that time it will be too late to reverse the damage.

CHAPTER 1

INTRODUCTION

HYDROLOGY OF A SOUTHEASTERN HEADWATER BASIN

The Chattahoochee River is part of a three-river system (Chattahoochee, Flint, and Apalachicola Rivers) that arises in Georgia and Alabama and empties into the Gulf of Mexico in the Florida Panhandle as shown in Figure 1. The detailed hydrologic study is limited to the headwaters of the Chattahoochee River down to the location of the first reservoir at Buford Dam on Lake Lanier in Georgia as shown in Figure 2 and includes about 2700 square kilometers. The study area is limited to this catchment to reduce the complications of modeling the management of multiple reservoirs and because of the particular significance of Lake Lanier as the water supply for the city of Atlanta.

The Chattahoochee River arises in the Blue Ridge physiographic province in the mountains of northeastern Georgia near the South Carolina border and flows in a southwesterly direction though the hills of the Piedmont province surrounding Atlanta. Approximately 15% of the study catchment is in mountainous terrain with the highest elevations around 1370 meters above sea level. The rest of the basin is at elevations between 300 and 450 meters above sea level. The Lake Lanier catchment normally has a humid climate throughout the year. The annual precipitation is about 1400 millimeters and snowfall is rare enough to not be included in this study. There are seasonal variations in precipitation, but periods as long as a month without precipitation are extremely rare. The area is mostly used for crop and timber production. The catchment itself has very little effect from urbanization. The Southeastern States experienced a major drought in the summer of 1986 and most of the area experienced record low flows. Northeastern Georgia and the upper Chattahoochee River were the most severely affected part of the state.

RELATED REPORTS

The Corps of Engineers has produced several reports for drought management on the Apalachicola-Chattahoochee-Flint (ACF) River system (U.S. Army Corps of Engineers, 1985 and 1986) and they have funded reports on the effects of weather extremes on the hydrologic system of the Upper Chattahoochee River (Raney et. al. 1984) and the Mississippi-Alabama Sea Grant Consortium has funded analyses of the climatology of the Apalachicola, Chattahoochee, and Flint river basins (Nichols and Raney, 1984); although, none of these has considered the effect of climate change.

ORGANIZATION OF THIS REPORT

Because the modeling for the Apalachicola River at Blountstown was not originally intended to be a part of this study and because deterministic hydrologic modeling was not used there, the methods used for that study will be documented in Appendix A.

The rest of this report will describe the hydrologic model used in the detailed hydrologic study along with the methods used to develop the precipitation traces and pan evaporation data. Caveats will be given where appropriate both concerning the use of the model and the input data transformations required for the various CO_2 scenarios. The report will present and interpret the results of the detailed hydrologic study and will address the environmental implications.

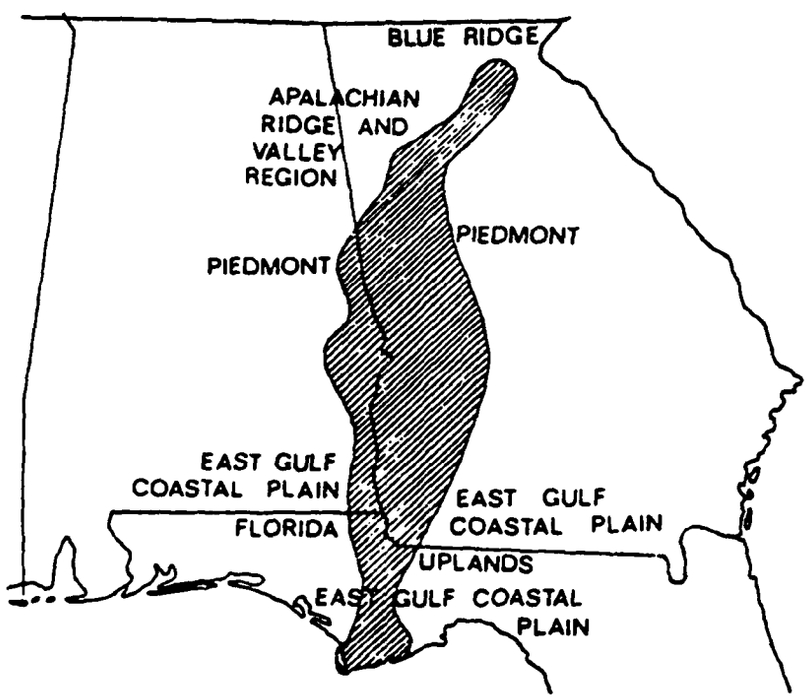

Figure 1. Location of the study area in Georgia, Alabama, and Florida.

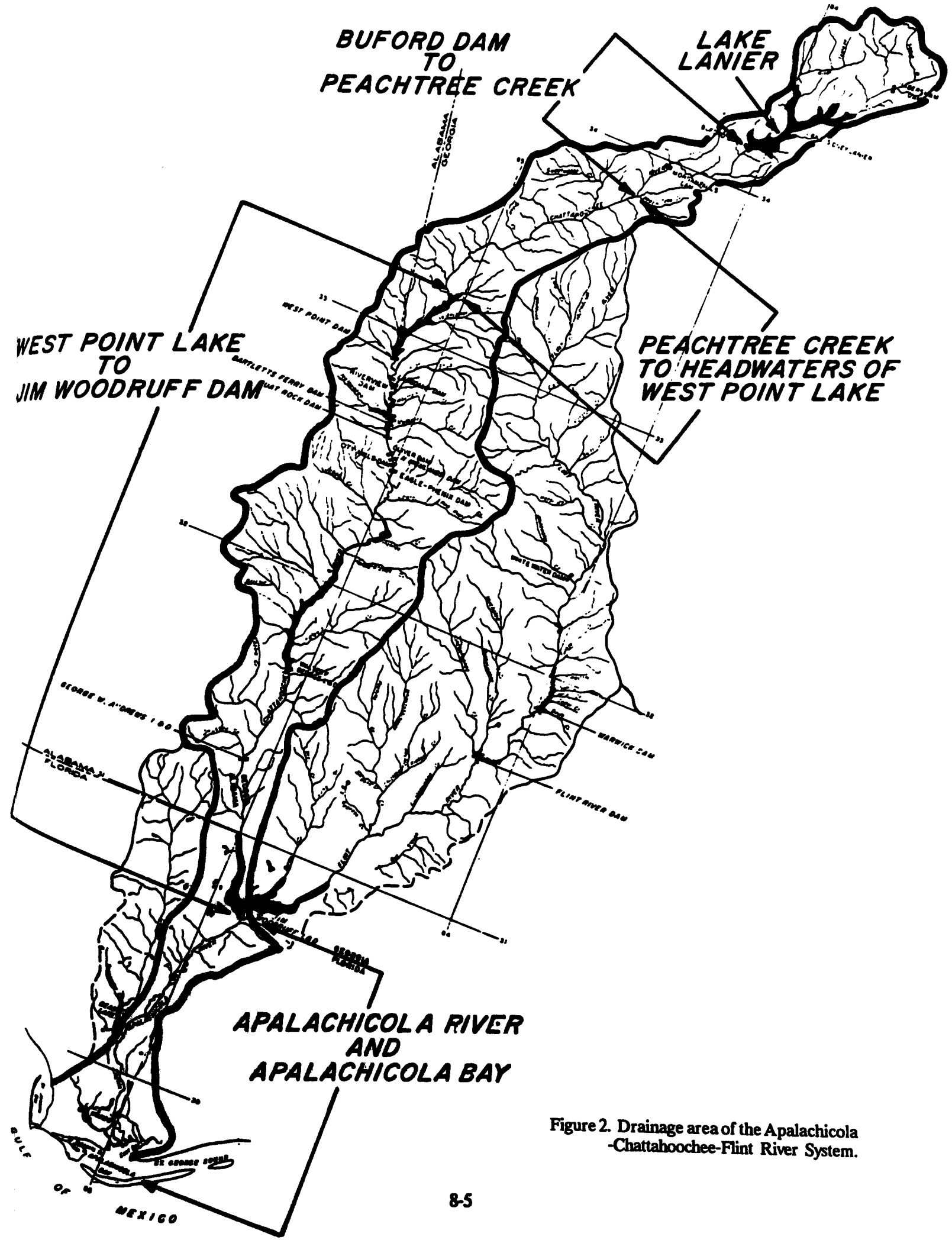

Figure 2. Drainage area of the Apalachicola -Chattahoochee-Flint River System.

CHAPTER 2

METHODOLOGY

THE SACRAMENTO MODEL

Development of the Model

The National Weather Service (NWS) has adopted the Sacramento Model (Burnash et. al., 1973) for hydrologic simulation of floods at many of the River Forecast Centers throughout the United States. This model is also used for extended streamflow prediction by NWS. Although the model is used extensively on a daily basis by NWS, there is almost no public literature related to the use and applicability of the model. Although the model is well discussed in hydrologic literature (Burnash et al., 1973; Burnash and Ferral, 1981), information on the application of the model is limited to unpublished NWS documentation and personal training by NWS at the centers where it is used.

The Sacramento Model is a deterministic hydrologic model, which attempts to parameterize soil moisture characteristics in a manner that will logically distribute applied moisture in various conditions and locations in the soil so that percolation characteristics will be reasonable when streamflow is effectively simulated.

The output of the model is streamflow runoff resulting from processing precipitation and pan evaporation through an algorithm representing the upper soil zone and the lower soils. As shown in Figure 3, the different sources of runoff are impervious runoff, surface runoff, interflow, supplementary base flow, and primary base flow. The five basic soil moisture storages in the model are upper zone and lower zone tension water storages, which are filled by infiltrated water, and the three free water storages. Upper zone free water is used for interflow and percolation to lower zones. The two lower zone free water storages receive water at the same time from percolated water but they drain independently. Potential evaporation from the basin is satisfied by the model based on availability of water on the surface and in capillary tension.

The version of the model used in this study was obtained from the University of Washington (UW) where similar studies are under way for this same report. This version is basically the same as that currently in use by NWS although it is much better suited to the research nature of this study, whereas the current NWS version is part of a very large real-time streamflow forecasting system used throughout the country. The UW version of the program includes computer-assisted parameter calibration which is specially adapted to optimize general streamflow rather than peak flow alone.

The Sacramento model was used almost as received from the University of Washington. Minor conversion was needed to install the program on a Definicon DSI020 co-processor board in an IBM AT. Two other modifications were made to the model. One was made to get it to accept pan evaporation data by months and years for the transient scenarios. As received, the model only accepted a single list of 12 monthly pan evaporation values for the complete simulation period. The other modification was to extend the model storage capacity from 20 years to 101 years. These modifications were tested to verify that they did not introduce any change in model behavior by themselves.

Precipitation data used for the calibration and the simulation were obtained from the Dawsonville, Georgia recording raingage. Other raingage locations in the catchment would have been better for this study except that they had numerous large periods of missing record. It was decided to use the more consistent record rather than the nearest record because calibration with a very intermittent record supplemented from another gage would have been like calibrating with a continually moving raingage. The Dawsonville raingage had a fairly good record although even it had a few missing periods -- some as large as three months. These deficiencies were made up without adjustment from other nearby records such as the Clermont raingage, which is in the center of the study catchment.

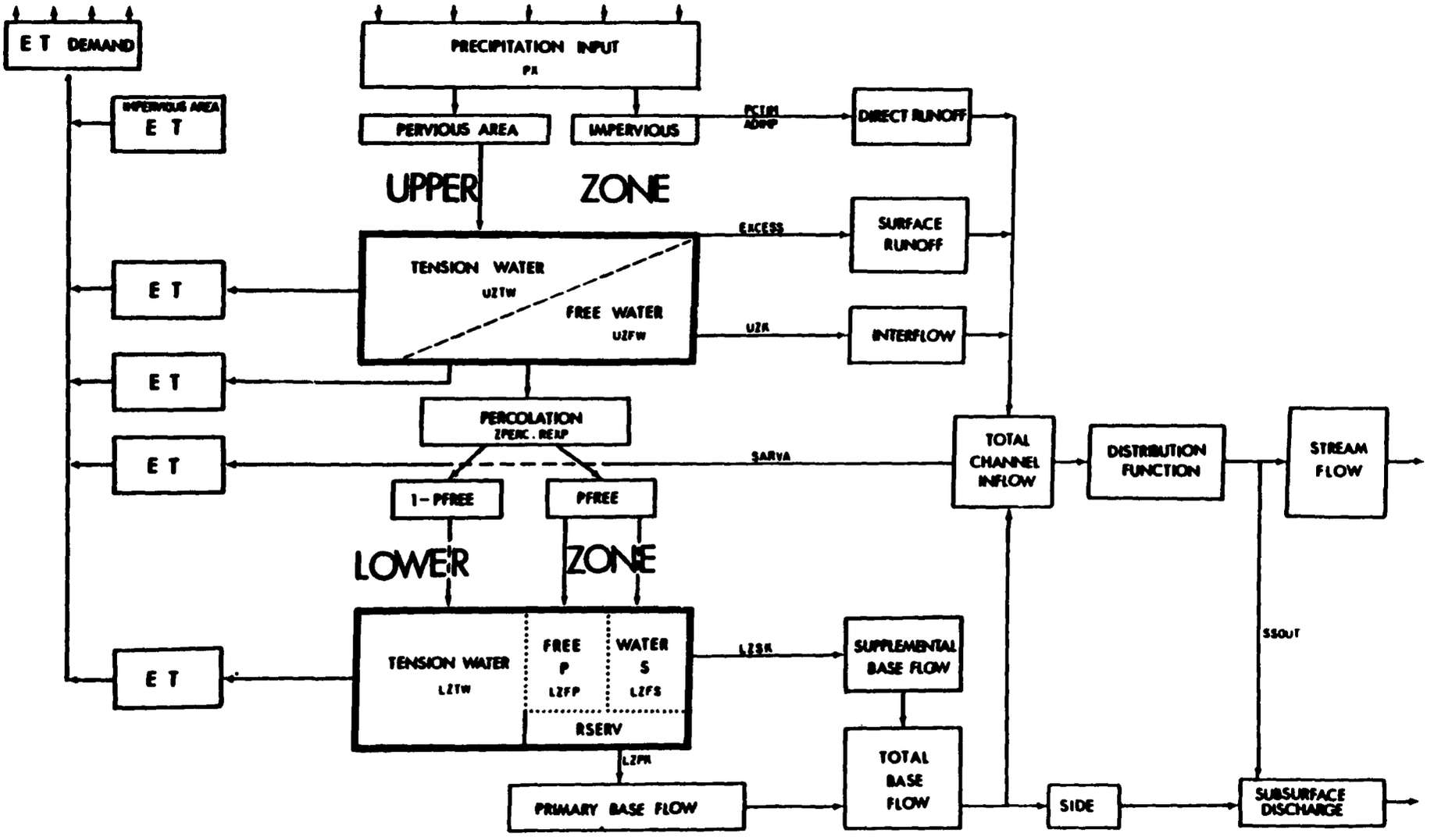

Figure 3. Flow Diagram of the Sacramento Model (Peck, 1976)

Pan evaporation data were obtained for Athens, Georgia. These data cover the period from 1947 to 1970, which is the longest period of record near the site. Long-term monthly average pan data were used in the calibration and the simulations because the data did not cover the whole period of the study.

Initial calibration parameters were obtained from the Atlanta River Forecast Center (RFC). Initial runs using the Atlanta RFC parameters showed that, while they produced good simulation of the peaks, the parameters were not optimized for low flows. Because the GCM output is presented as monthly averages to be used to modify historical meteorological data, it is not likely that the GCM effects on short-term, intense events will be preserved. The most meaningful effects from the GCM output will be on long-term events such as long-term wet or dry periods, which would have a major impact on water supply reservoirs such as Lake Lanier. As a result, the parameters received from the Atlanta RFC were optimized for general streamflow which weights low flows as well as floods. In this case, flood flows may not model quite as well but low flow events improve greatly.

The model was calibrated and verified using U.S. Geological Survey daily data for station 02334500 Chattahoochee River near Buford, Georgia for the years 1949 through 1955. These were the only years for which data were available for this location before the dam on Lake Lanier was closed. The years 1945 through 1955 were in the warmest decade of record as recorded at Atlanta, which is about 100 kilometers to the southwest of the center of the study catchment. The calibration-verification years were representative of the period of record for pan evaporation data as recorded at Athens, Georgia. Precipitation during the calibration-verification years included both the wettest year of record the two driest years prior to 1981. As a result, these years are a good sample of the hydrologic extremes experienced in this part of Georgia.

The calibration itself was performed for the years 1952-1954 using a logarithmic objective function. Average flow for these years came within one standard deviation of the long-term average flow. However, they include the third highest and the third lowest monthly flow of record up to 1984 prior to the beginning of the drought of 1988. As a result, these years represent the hydrologic extremes for this basin with the exception of prolonged drought.

Although there seems to be some difference of opinion in the hydrologic community over the amount of data required for adequate calibration, several trends seem to stand out. Donigian (1984) and Bourne (1978) suggest that 3-5 years of data should be used for calibration. Donigian (1984) says that wet years are better for calibration because they usually have more uniform rainfall over the watershed. Hassett and Lumb (1974) show on a basin near the Chattahoochee River that, as the calibration period is extended, very little improvement in calibration is achieved after 2-3 years. Johanson and Crawford (1979) explained that, although many years might be required to collect a significant number of meteorological/hydrologic events in an arid climate, 2-3 years should provide a good sampling of the hydrologic spectrum of a watershed in a subhumid climate.

Limitations Resulting from the Model

After calibration on the years 1952-1954, the period 1949-1955 was simulated and the years 1949-1951 and 1955 were used for validation. The hydrologic model did not calibrate as well as expected. Donigian (1984) gives calibration guidelines for hydrology/hydraulics modeling as: Very Good <10% difference; Good 10-15% difference; and Fair 15-25% difference between simulation and recorded values on an annual and monthly basis. In a few cases, monthly water balance errors were as high as 35% although most months were within 10 to 15% of the observed runoff. The months showing poor comparisons with observed runoff were not limited to either wet or dry months, so they probably are caused by unrepresentative rainfall. These problems with calibration would be lessened if more meteorological stations were available.

The Sacramento model does not consider CO_2 directly at all. All of the CO_2 effects are modeled only as reflected in the various GCM outputs.

Because the GCM modelers seem to place little confidence in their evaporation data, adjustments to historical pan evaporation data for the hydrologic model were made on the basis of the Penman equation (Linsley et al., 1982), which models daily pan evaporation on the basis of air temperature, wind movement, vapor pressure, and solar radiation. Monthly values for these variables were obtained from the GCM outputs, and monthly pan evaporation was computed for each scenario using the Penman equation. The same computation was done for the GCM control runs. The ratio of scenario to control Penman-computed pan evaporation data was then applied to the historical pan evaporation data on a monthly basis following the standard EPA procedure for development of the scenarios.

THE SCENARIOS

Scenarios Used

The 2X GISS, GFDL, and OSU scenarios were run as well as the GISS Transient A scenario. Time did not permit running the analogue and transient B scenarios. Precipitation ratios were used directly from the NCAR gridded data files and applied to daily historical precipitation data. Actual GCM values for wind, solar radiation, air temperature, and either specific humidity or mixing ratio were used in the Penman equation to compute pan evaporation values, which were then converted to evaporation ratios and applied to historical data monthly pan evaporation data.

The EPA standard procedure was followed for development of the scenarios. The upper Chattahoochee catchment falls within only one grid cell for each scenario. Historical daily precipitation data for Dawsonville for the years 1951 through 1980 were used along with long-term monthly averages for pan evaporation data collected during a major part of the base period. These were modified by the ratios received from NCAR for the appropriate grid cell and month for the steady-state scenarios. The 1951 data were duplicated as 1950 in the model runs to provide one year of spin up data.

Historical daily precipitation data for 1951 through 1980 were applied for the years 1981 through 2010 and repeated for 2011 to 2040 and 2041 to 2059 to develop precipitation inputs for the transient scenario. The years 1970 through 1980 historical data were applied to the years 1970 to 1980 for 11 years of spin-up time in the transient model.

Issues Resulting from the Scenarios

No particular problems arise from the use of the 1951 to 1980 historical period for the steady-state scenarios. However, several issues arise from the application of these data to the transient scenario. The use of a 30-year historical record for the 90-year period means that, except for the 30 years from 2011 to 2040, the leap years will not match. Therefore any rainfall occurring on February 29 will be ignored, and the leap year Februaries in the model runs will have one more day to runoff in base flow recession than they would have if the leap years had matched up properly. This introduces short term variations in monthly runof,f which are based on calendar irregularities rather than the climate scenarios. These will tend to reduce the long-term annual runoff very slightly, probably on the order of 1 or 2%.

The process of folding the 30-year record and reusing it introduces a 14% flow anomaly in the first month after the fold. This reduces to 1% within 4 months although because of the long persistence of base flow in this basin, it takes 3 years for this anomaly to completely disappear. This is compounded by the leap year shift problems mentioned above. The overall effect is less than 0.5% on an annual basis.

Because the GCM output is presented as monthly averages, short-term intense events are not preserved. These have been introduced into this study from the historical record. This procedure loses any variation in storm frequency, duration, or intensity resulting from climate change. If storm events were to increase in intensity, even without an increase in annual or monthly precipitation, more water would run off as surface flow instead of as base flow. This would cause increased annual runoff because less water would infiltrate and there would be less evapotranspiration.

CHAPTER 3

RESULTS

IMPACTS OF CLIMATE CHANGE

Direction and Magnitude of Changes

Any discussion of the impacts of climate change will necessarily be difficult because of the large volume of data involved in the study. In this section we will look at the effects of climate change on gross annual averages and variability, seasonal effects, and long-term annual trends.

Steady-State Scenarios

Figure 4 is a graph showing one standard deviation on either side of the average long-term annual inflow to Lake Lanier for the base period observed flows and the GCM scenario flows. The data for Figure 4 appear in Table 1.

Table 1. Annual Variability of Hydrologic Model Scenarios--Upper Chattahoochee River

	<---------- Cubic Meters per Second						---------->		
	Qbar	Std	+1 std	-1 std	Max	50%ile	Min	%ch Q	%ch Std
Base	61.84	11.95	73.79	49.89	88.26	65.19	38.82	--	--
TransA									
1980	41.99	8.52	50.52	33.47	56.10	41.03	27.78		
1990	67.00	10.62	77.62	56.38	78.92	70.03	52.13		
2000	66.20	9.26	75.46	56.95	85.77	65.13	50.66		
2010	49.33	10.62	59.95	38.71	71.27	44.49	38.74		
2020	53.01	9.80	62.81	43.21	62.35	55.73	35.88		
2030	59.89	9.88	69.77	50.01	77.28	60.26	43.78		
2040	43.38	8.98	52.36	34.40	61.14	39.36	33.33		
2050	49.95	11.19	61.14	38.77	65.95	52.90	32.28		
2X=>									
GISS	69.57	13.39	82.97	56.18	97.44	71.42	47.74	13.9%	13.2%
GFDL	45.08	10.59	55.67	34.49	68.30	43.98	28.77	-26.2%	-10.5%
OSU	49.92	10.96	60.88	38.96	74.02	54.68	27.58	-18.3%	-7.4%
TBASE	61.08	11.84	72.92	49.24	88.26	64.85	38.82		
TRANSA	54.34	12.54	66.88	41.80	85.77	55.05	32.28	-12.1%	5.0%

At first glance, it appears unusual that the GISS 2X scenario would cause a 14% increase in long-term annual flow while the GFDL and OSU 2X scenarios show decreases in long-term annual flow of 26% and 18%, respectively. However, average precipitation for the 2X GISS scenario had an increase of 12%, while the GFDL and OSU 2X scenarios had decreases of 13% and 3.6% respectively. The other input to the hydrologic model, pan evaporation, was higher in all three scenarios with the GFDL being the highest at 28% followed by the OSU at 12% and the GISS at 9%. Keep in mind that increased precipitation will cause an increase in runoff if other factors remain constant, while increased pan evaporation will normally decrease runoff.

Figure 5 presents long-term seasonal flow values for the three steady-state scenarios on the upper Chattahoochee study along with observed flow. The GISS and GFDL scenarios seem to parallel the observed flows, with the GISS intensifying both the highs and the lows and the GFDL generally decreasing the

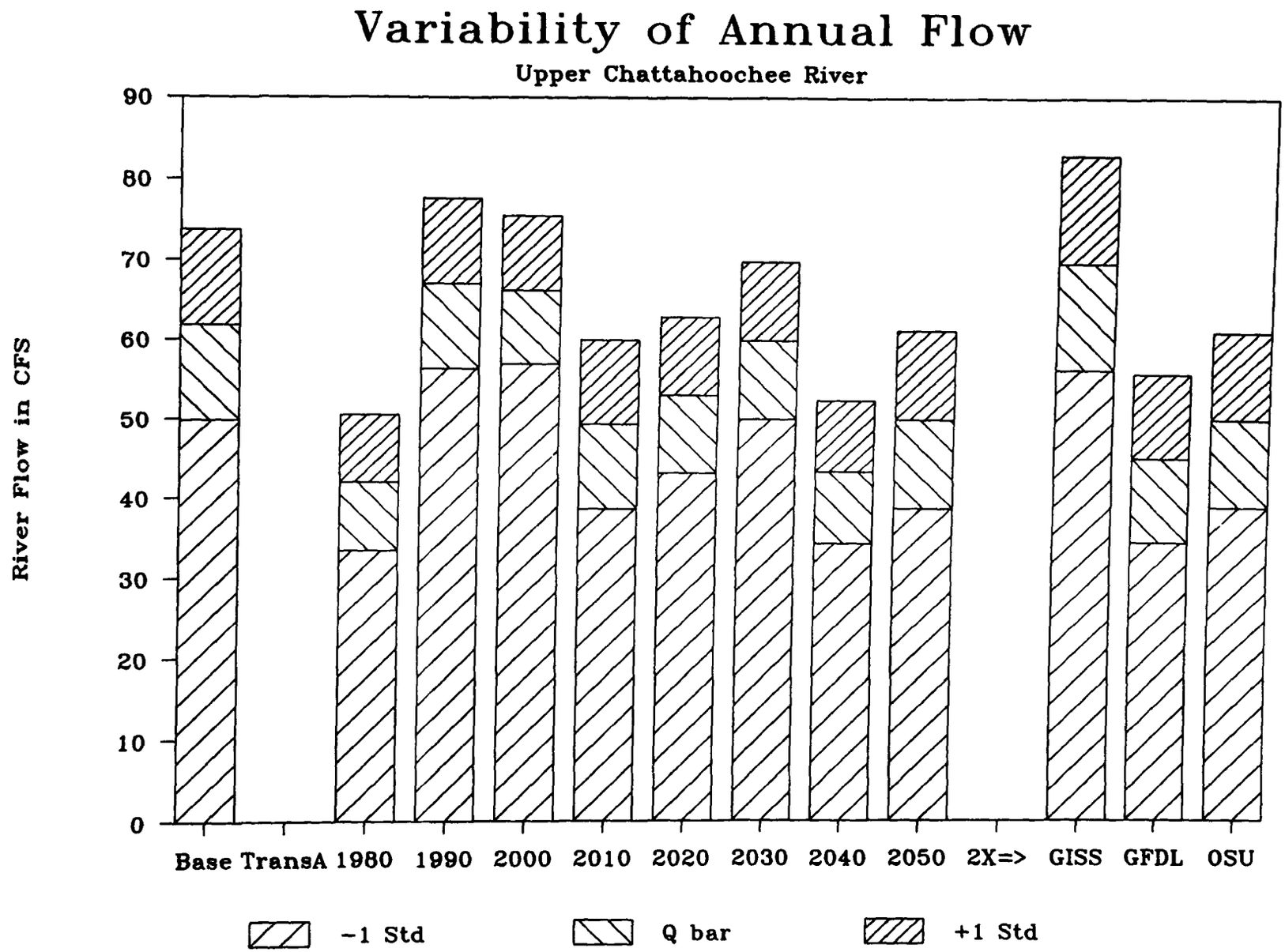
Variability of Annual Flow
Upper Chattahoochee River
River Flow in CFS
90
80
70
60
50
40
30
20
10
0
Base
TransA
1980
1990
2000
2010
2020
2030
2040
2050
2X=>
GISS
GFDL
OSU
-1 Std
Q bar
+1 Std

Figure 4

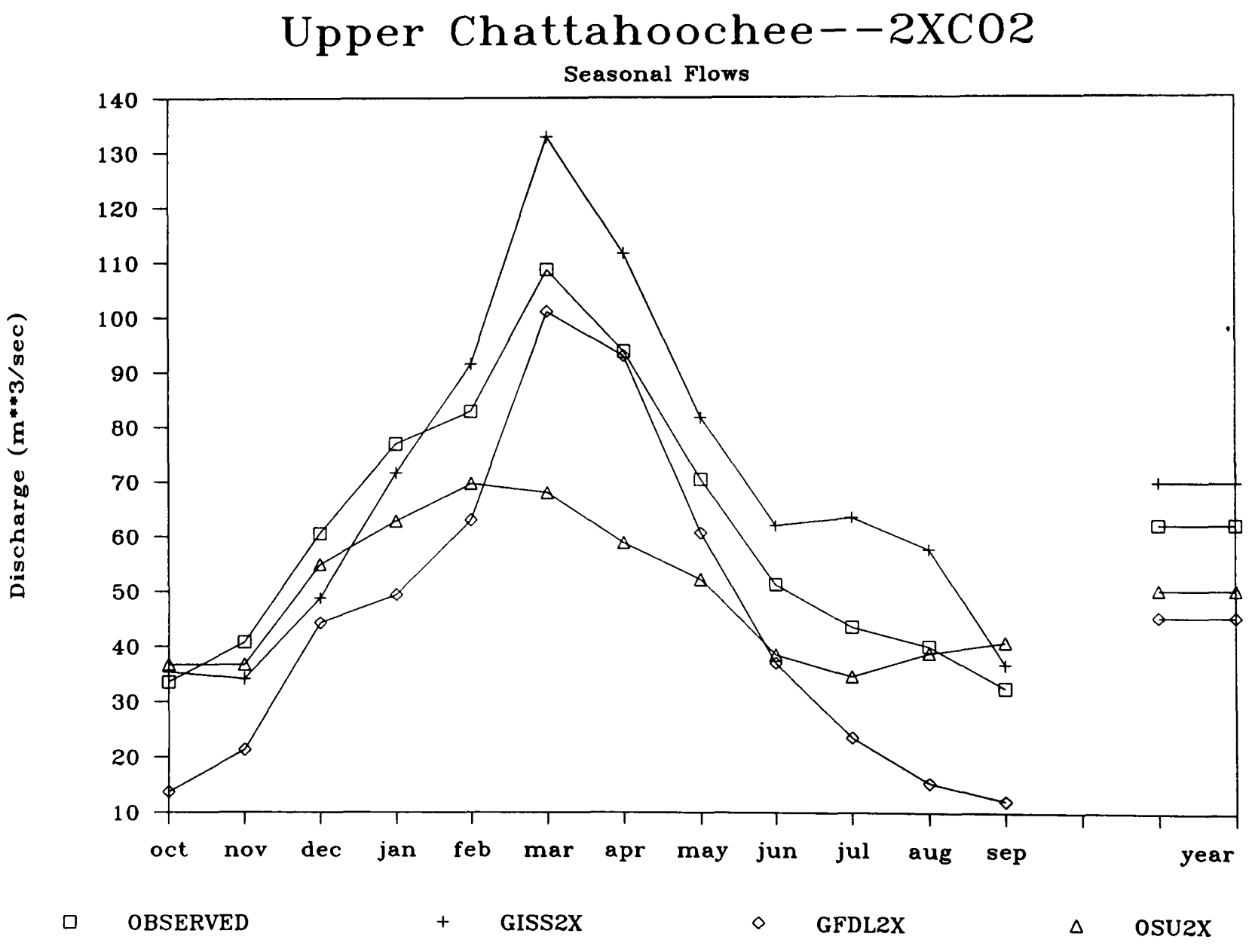
Upper Chattahoochee--2XC02
Seasonal Flows
Discharge (m**3/sec)
140
130
120
110
100
90
80
70
60
50
40
30
20
10
oct
nov
dec
jan
feb
mar
apr
may
jun
jul
aug
sep
year
OBSERVED
GISS2X
GFDL2X
OSU2X

Figure 5

high-flow months. The OSU scenario shows decreases for all monthly flows, however, the flows in the wetter spring months are decreased sufficiently more such that the wet season is shifted a month earlier. Figure 6 shows the ratio of the scenario flow/observed flow by season for the steady-state scenarios. This figure points out the strong differences between the results of the three climate models. Some have their greatest effect in the wet season, others in the dry. Some are wetter, others are drier than those observed. The largest difference between the climate models can be seen by comparing the GFDL and the OSU models, which are complete opposites.

These two effects of climate change are not the same for all months. Figures 7 through 9 present the ratio of modeled values/observed values by months averaged over the 30-year scenario period. On each graph, the climate input ratios (precipitation and pan evaporation) are shown along with the hydrologic output (flow). Figure 8 shows that even in the GISS scenario, which has an overall increase in precipitation, there are months which have reduced precipitation. In general, the months that have the greatest rainfall occur in the winter and spring months when pan evaporation is at a minimum. As a result, increases in precipitation accompanied by increases in pan evaporation will cause higher high flows and lower low flows.

The overall effect on annual runoff depends not only on the percent increase or decrease in precipitation and pan evaporation but also on the magnitude of the base precipitation and pan evaporation which is being changed. For instance, a small percentage increase in precipitation in a wet month can have more effect on annual runoff than a much larger increase in precipitation in a dry month.

The effects of the 2X scenarios are quite significant. The GISS scenario has the least effect representing an increase in annual flow of about 0.7 standard deviation. The GFDL and OSU 2X scenarios show decreases in average annual flow of about 1.4 and 1.0 standard deviation, respectively. No one climate variable seems to dominate all effects, although precipitation is assumed to have a greater effect pending further investigation.

Even though the effects are large, the period of the year in which the increases or decreases in precipitation and pan evaporation occur is significant. The hydrologic effects are extremely nonlinear, so the wetness or dryness of the catchment during an increase or decrease in precipitation or pan evaporation will alter the strength of the effect.

Changes in precipitation appear to dominate the effects of climate change on runoff. Figures 7 through 9 display the parallel between change in precipitation and change in runoff. This parallelism tends to lag about one month, so that the month with the lowest precipitation ratio is followed a month later by a month with the lowest flow ratio. This type of effect is quite consistent with the short-term memory of water storage in the system. Changes in pan evaporation have a more general effect -- bringing the annual average ratio down when the pan evaporation ratio is high. This general effect is consistent with the long-term memory of groundwater storage, which has a significant persistence in the system for several years.

Transient A Scenario

The transient scenario must be viewed from a different perspective than the steady-state scenarios. For the transient scenario, carbon dioxide in the atmosphere has been assumed to follow current trends up through 2059. As a result, the climate is changing all the time. Decadal variability of the transient A scenario is presented in Figure 4 and Table 1. Because the base period has an increasing flow trend, the results are sawtoothed at the point where the base period is repeated. As a result, it is not easy to see the GCM effects without careful consideration.

Figure 10 shows the annual ratios of transient/baseline climate inputs (precipitation and pan evaporation) and hydrologic outputs (flow) as 5-year running averages. The ratio data are easier to interpret than the flow data alone because the ratio has the particular effects of the baseline period removed. There is no clear effect of climate change on precipitation for the transient run. Precipitation ratios seem to oscillate between wet and dry trends about every 20 years, with the long-term ratio being close to one. The climate change effects for the transient run seem to be mainly associated with increases in pan evaporation which are robust and obvious.

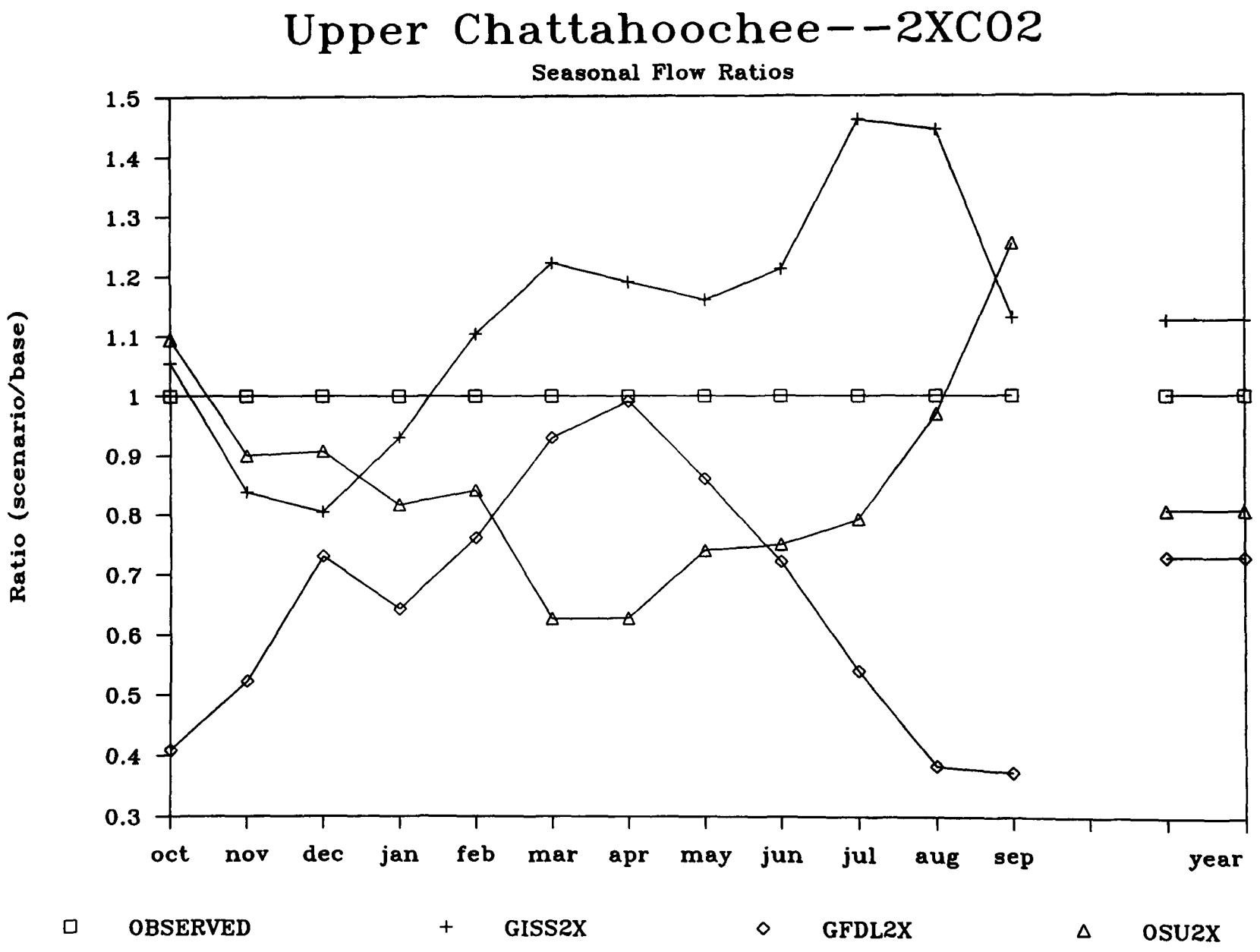
Upper Chattahoochee--2XC02
Seasonal Flow Ratios
Ratio (scenario/base)
1.5
1.4
1.3
1.2
1.1
1
0.9
0.8
0.7
0.6
0.5
0.4
0.3
oct
nov
dec
jan
feb
mar
apr
may
jun
jul
aug
sep
year
OBSERVED
GISS2X
GFDL2X
OSU2X

Figure 6

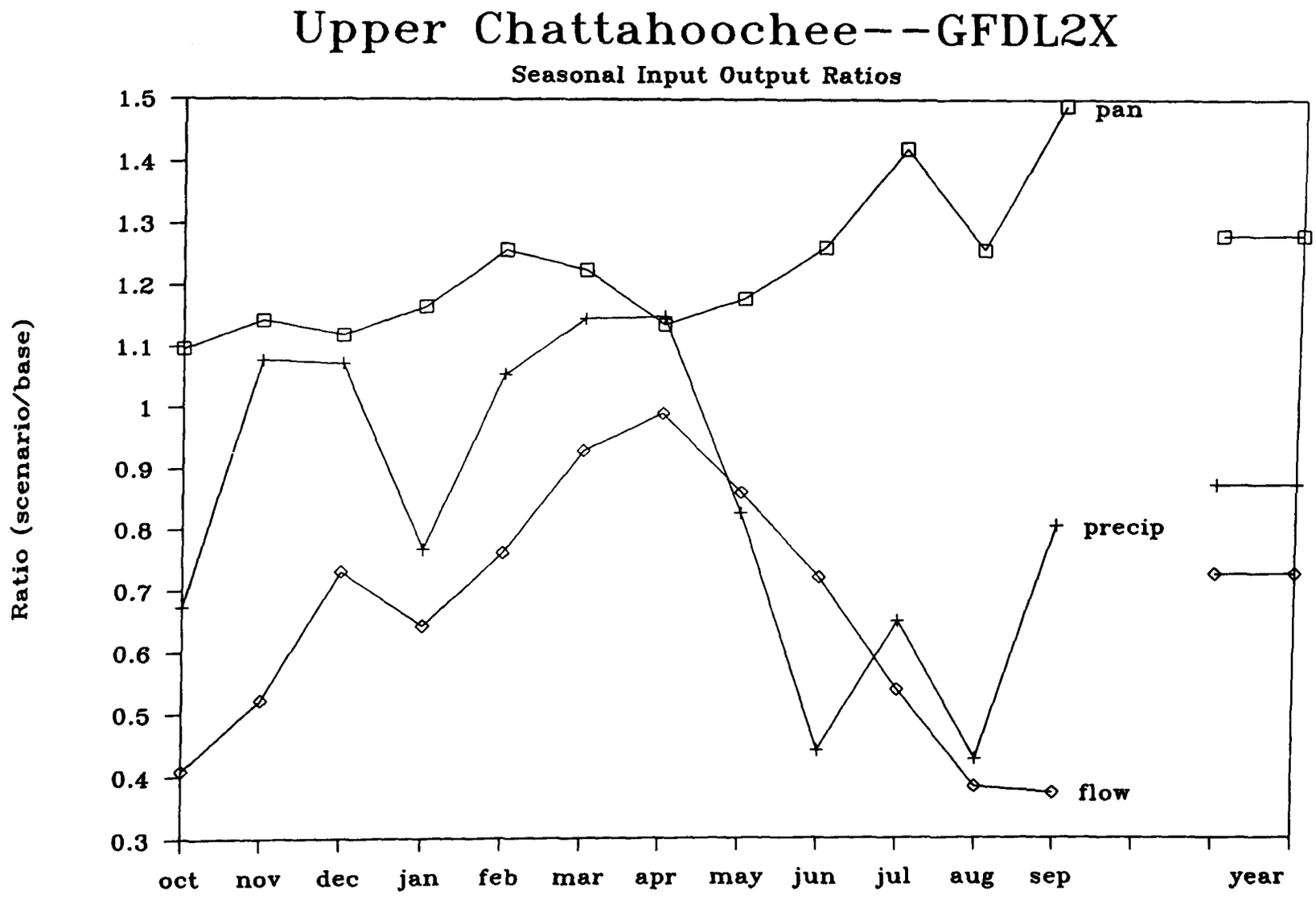
Upper Chattahoochee--GFDL2X
Seasonal Input Output Ratios
Ratio (scenario/base)
1.5
1.4
1.3
1.2
1.1
1
0.9
0.8
0.7
0.6
0.5
0.4
0.3
oct
nov
dec
jan
feb
mar
apr
may
jun
jul
aug
sep
year
pan
precip
flow

Figure 7

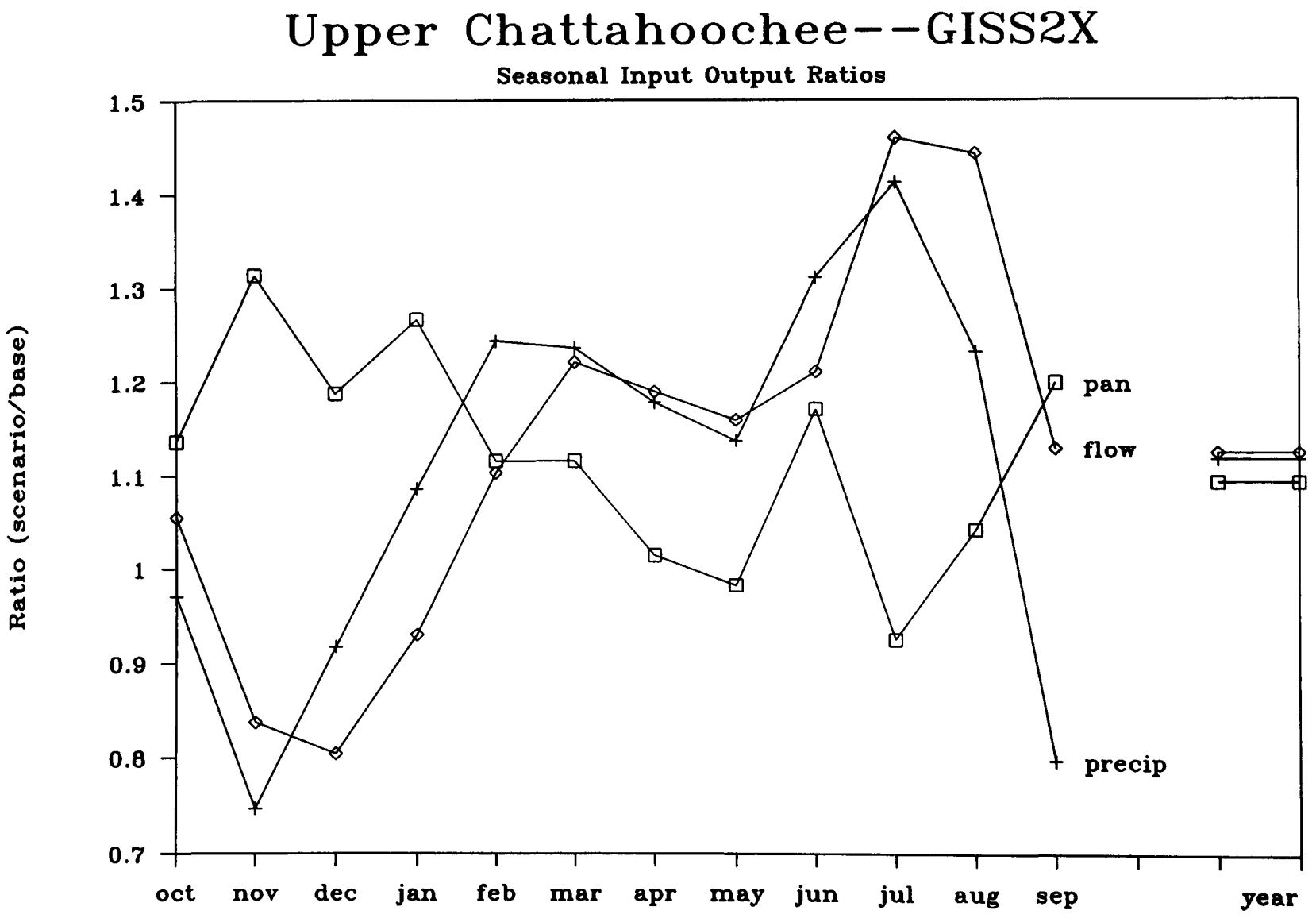
Upper Chattahoochee--GISS2X
Seasonal Input Output Ratios
Ratio (scenario/base)
1.5
1.4
1.3
1.2
1.1
1
0.9
0.8
0.7
oct
nov
dec
jan
feb
mar
apr
may
jun
jul
aug
sep
year
pan
flow
precip

Figure 8

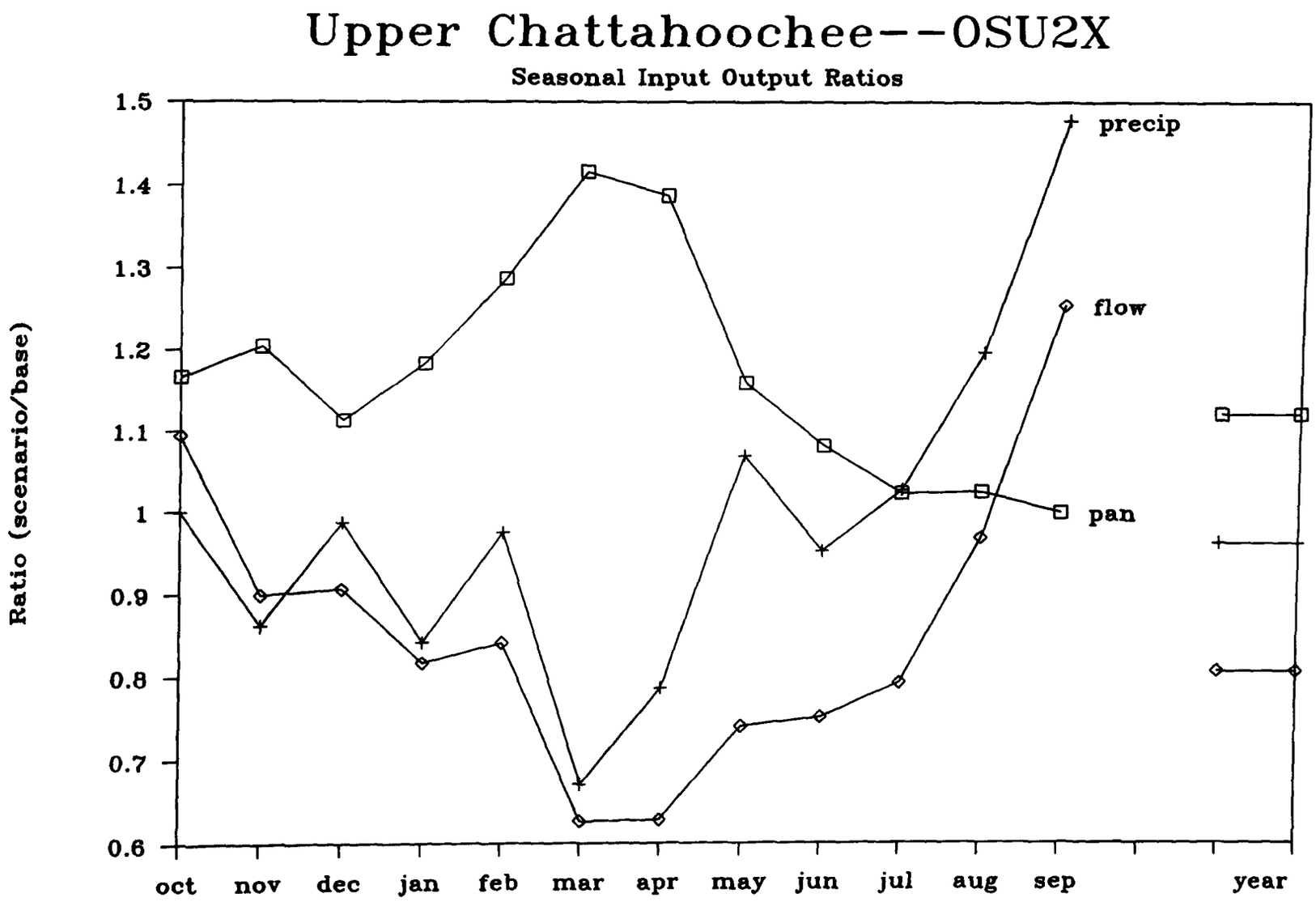
Upper Chattahoochee--OSU2X
Seasonal Input Output Ratios
Ratio (scenario/base)
1.5
1.4
1.3
1.2
1.1
1
0.9
0.8
0.7
0.6
oct
nov
dec
jan
feb
mar
apr
may
jun
jul
aug
sep
year
precip
flow
pan

Figure 9

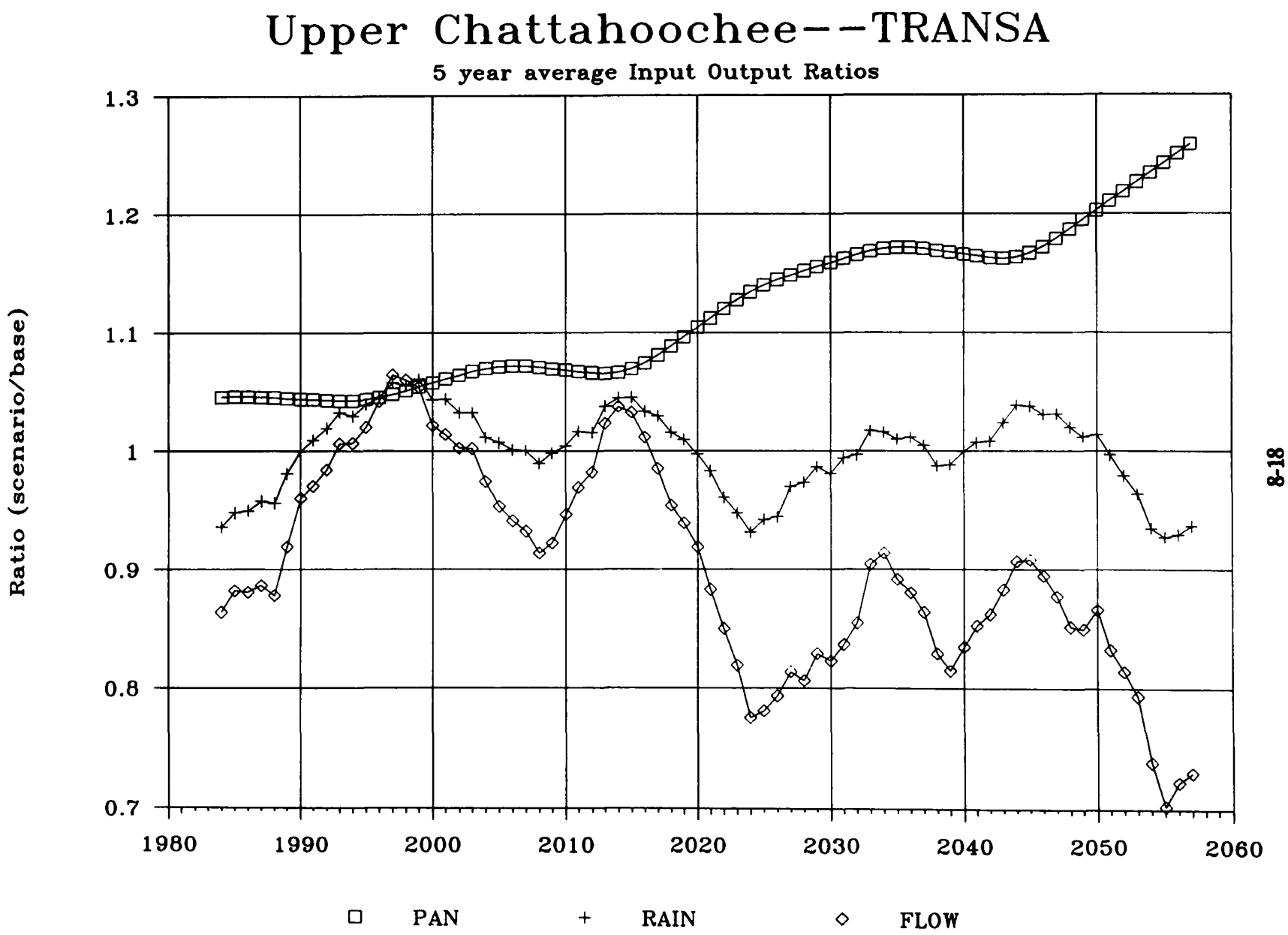
Upper Chattahoochee--TRANSA
5 year average Input Output Ratios
Ratio (scenario/base)
1.3
1.2
1.1
1
0.9
0.8
0.7
1980
1990
2000
2010
2020
2030
2040
2050
2060
PAN
RAIN
FLOW

Figure 10

During the first decade of the transient A scenario, when there was a decrease in precipitation as compared with the base period, pan evaporation was already elevated with a resulting 10% decrease in runoff. This is followed by a decade with sufficiently more precipitation than the base period so that the runoff exceeds that of the base period for several years. This seems unusual at the beginning of a transient run of the GCM when it is assumed that the CO_2 effects are minimal. The rest of the transient run follows an expected pattern of an accelerating reduction in runoff driven primarily by increases in pan evaporation. The positive excursions in rainfall appear to be less each time throughout the transient run and may possibly show a general decline in precipitation if the transient scenario is extended over a longer period.

To present the effects of the transient scenario in the clearest comparison with the identical period from the baseline data, the individual months were accumulated for both the base period and the transient scenario. These were plotted on the same graph versus time as shown in Figure 11. The effects discussed above can be seen very clearly in the departures of the transient A curve from the observed curve. The initial departure in the 1980s, the decreasing departure in 1990s and 2000s, and the robust departure beginning about 2020 are very clear.

This same behavior is displayed in Figure 12, where the two accumulated monthly curves are plotted against each other. The straight line is the slope that the curve would have if there were no effects. Where the slope is less than the straight line, the transient runoff is less than the base period runoff. Where the slope is greater than the straight line, the transient is greater than the base period runoff.

Upper Chattahoochee--TRANSA

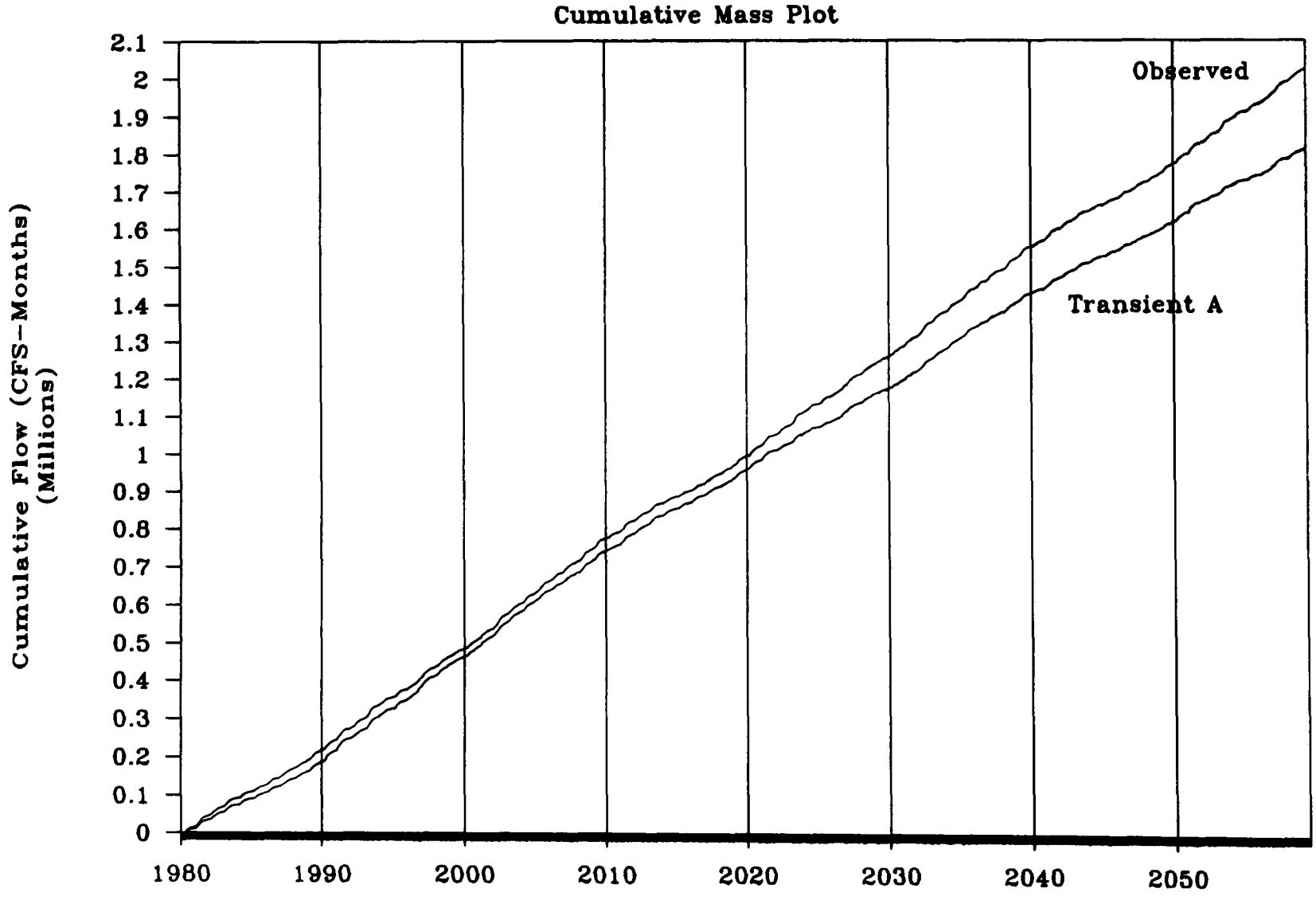

Figure 11

Upper Chattahoochee--TRANSA

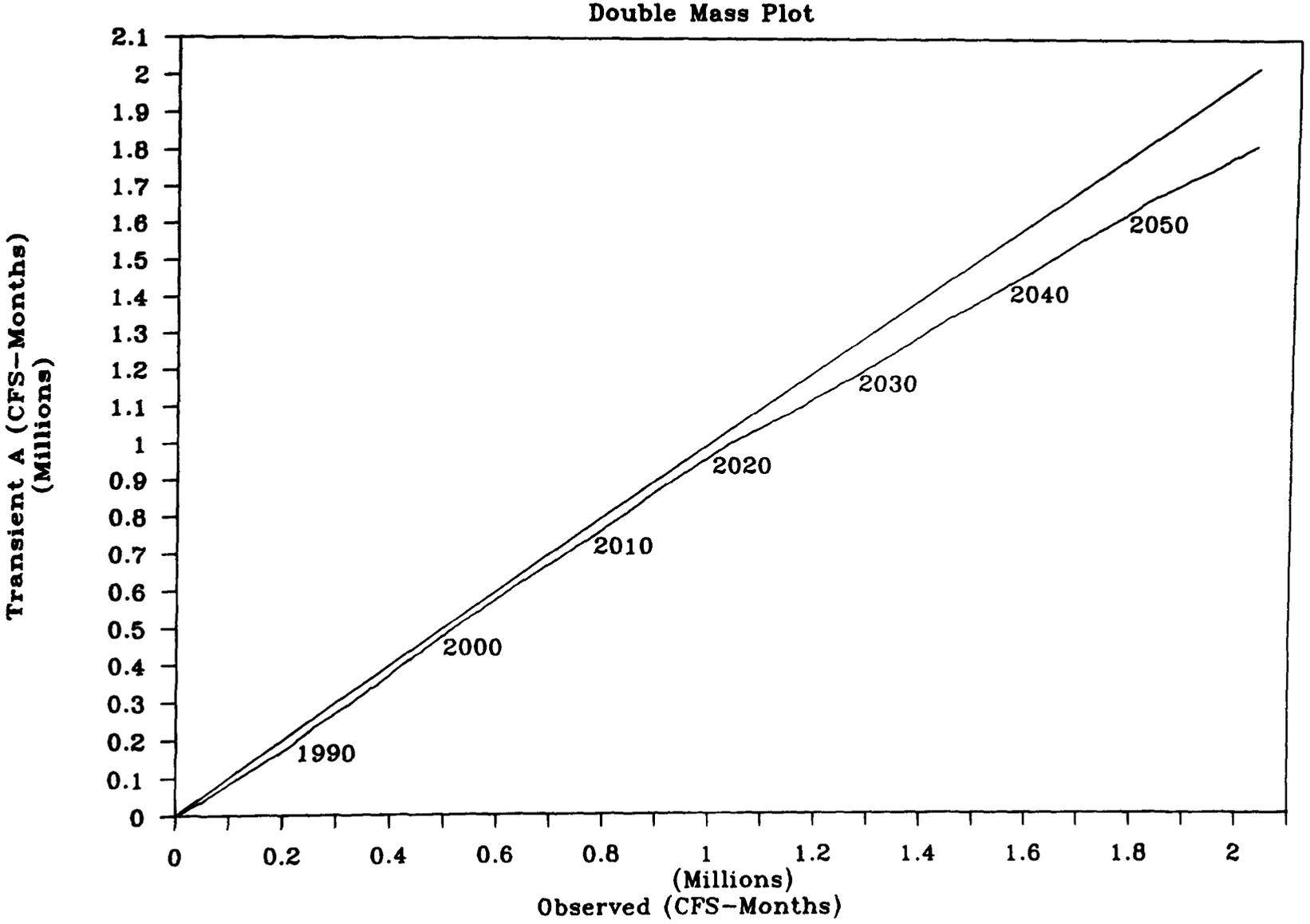

CHAPTER 4

INTERPRETATION OF RESULTS

The changes in the hydrology of the Upper Chattahoochee River for the GCM scenarios were the result of changes in precipitation and pan evaporation. The sensitivity of the hydrology to each of these variables is complex. When the system is wet, changes in precipitation and pan evaporation do not have as much effect on the streamflow as they do when the system is fairly dry. There seems to be roughly twice as much sensitivity to changes in precipitation as there is to changes in pan evaporation. The sensitivity to precipitation changes is much more immediate because the short-term moisture storages are affected. Because evaporation effects the long-term moisture storage in the system more strongly, sensitivity to this climate variable is more gradual.

Temperature, humidity, solar radiation, and wind movement have been combined using the Penman equation for pan evaporation as described above. Increases in temperature, wind movement, and solar radiation will increase evaporation, while increases in humidity will decrease evaporation. Table 2 and Figure 13 show the relative effect of each variable from the steady-state scenarios on pan evaporation. In each case, temperature has the greatest effect on evaporation. Changes in humidity have about half as much effect as changes in temperature; changes in wind movement have less than one-fifth as much effect as changes in temperature; and changes in solar radiation have less than a tenth as much effect as changes in temperature. No value is given for the effect of humidity alone on the GFDL evaporation because the GFDL2X humidity is so high that it cannot occur without the associated rise in temperature.

Table 2. Relative Effect of Each Climate Variable on Changes in Penman Evaporation

	GFDL	GISS	OSU
Partial PET change due to change in:			
Temperature	35%	19%	16%
Humidity	-15%*	-8%	-3%
Wind Movement	5%	-4%	-3%
Solar Radiation	3%	1%	1%
Total PET change	28%	9%	12%

* Estimated from combined temperature and humidity effects.

Gradual changes in CO_2 along the lines of those used in the transient A scenario might not be noticed in the hydrology of the Upper Chattahoochee River over the next 20-30 years. If the effects reported by the transient GCM run for the first 3 decades are accepted, the first effects would be a temporary decrease in precipitation with less effects on pan evaporation. This would be followed by a slight increase in precipitation followed by a long, steady increase in pan evaporation resulting in a steady decline in runoff.

Effect of Climate Variables on ET

Upper Chattahoochee

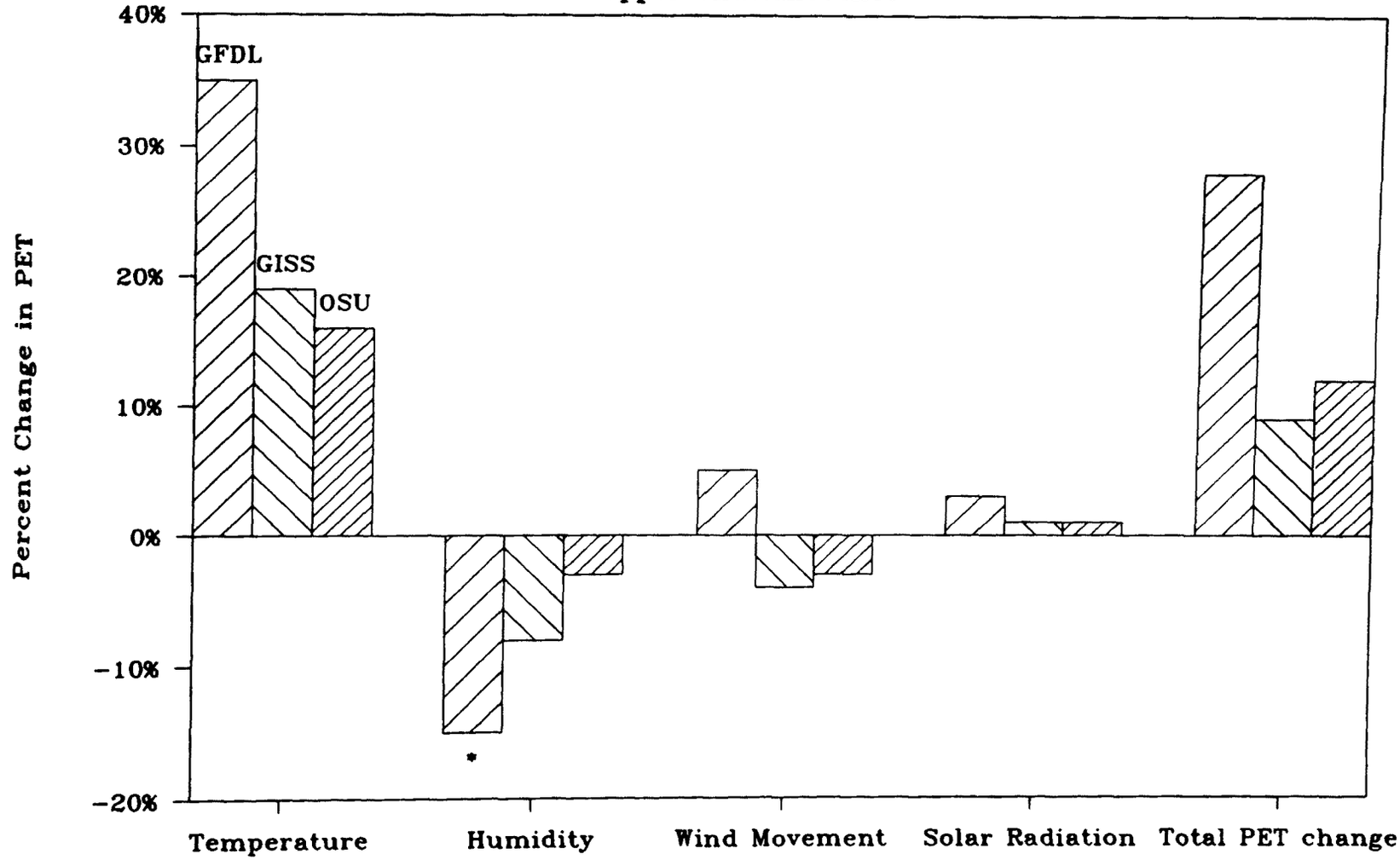

* Est. from combined Temp. and Humidity

Figure 13

CHAPTER 5

IMPLICATIONS OF RESULTS

ENVIRONMENTAL IMPLICATIONS

Because of the conflicting nature of the results of the steady-state GCM scenarios, the environmental implications of this study depend on which scenario is accepted. However, all of the scenarios show increasing pan evaporation and, with the exception of the GISS2X scenario, they show decreasing precipitation. Even the GISS model seems to suggest decreasing precipitation in the transient scenario after the first 30 years.

This suggests that there will be less water in the southeastern United States. But where does it go? The GCMs operate by balancing the energy and mass fluxes in the atmosphere for each grid cell of the model. With increased temperature, some of the moisture will simply remain in the atmosphere. The rest must show up elsewhere on the earth if the GCMs are to be given any credence at all.

It is reasonable to draw the conclusion that the current trend in CO_2 around the world will result in less runoff for the Upper Chattahoochee River Basin and for other areas nearby. This will have prominent effects on all aspects of the environment. Studies by others are in progress to assess the impact of the hydrologic effects on water supply, agriculture, forestry, biology, and other areas.

The decrease in runoff will not be clearly distinguishable from short-term trends already present in the present normal climate. The year 1988 may be the worst drought in history in the southeast United States -- drier by many times than any year in the 30-year base period used in these studies. Within a few years, we should be once again in a wet cycle. Under such conditions, who will be able to identify the current drought as the beginning of a new trend as opposed to an extreme event that is simply a statistical feature of the current normal climate? It is important to do and improve studies of the present type to assess the possibilities of global warming driven by increased carbon dioxide in the atmosphere. However, it is not likely that the effects of climate change will be first observed from its hydrologic effects. By the time hydrologic effects are clearly evident, other aspects of the environment will already have experienced irrevocable change.

LIST OF ABBREVIATIONS

ACF	--	Apalachicola-Chattahoochee-Flint River System
CO_2	--	Carbon Dioxide
GCM	--	General Circulation Model
GFDL	--	Geophysical Fluid Dynamics Laboratory
GISS	--	Goddard Institute for Space Studies
NASA	--	National Aeronautic and Space Administration
NCAR	--	National Center for Atmospheric Research
NWS	--	National Weather Service
OSU	--	Oregon State University
RFC	--	River Forecast Center

REFERENCES

Bourne, R. Gregory, Gerald N. Day, and Thomas N. Debo. " Water Quality Modeling using Hydrocomp Simulation Programming (HSP)." In: Proceedings of the 26th Annual Hydraulics Division Specialty Conference, Am. Soc. of Civil Engineers,College Park, Maryland, 1978. pp 358-362.

Burnash, Robert J. C., R. Larry Ferral, and Richard A. Mcguire. "A Generalized Streamflow Simulation System, Conceptual Modeling for Digital Computers." National Weather Service, and California Department of Water Resources, Sacramento, California, 1973. 204 pp.

Burnash, Robert J. C., R. Larry Ferral. "A Systems Approach to Real Time Runoff Analysis with a Deterministic Rainfall-Runoff Model." Proceedings of the International Symposium on Rainfall-Runoff Modeling, Mississippi State,Mississippi, 1981. pp. 107-120.

Donigian, Anthony S., John C. Imhoff, and others. "Application Guide for Hydrological Simulation Program - FORTRAN (HSPF)." EPA-600/3-84-065, U.S. Environmental Protection Agency, Athens, Georgia, 1984. 177 pp.

Hassett, Timothy, and Allen Lumb. "Use of Watershed Models to Predict Low Flows." In: Proceedings: Contribution of Irrigation and Drainage to the World Food Supply, Specialty Conference, Am. Soc. of Civil Engineers, Biloxi, Mississippi, 1974. pp. 203-217.

Johanson, Robert, Norman Crawford and others. "Hydrologic Simulation Program FORTRAN (HSPF) Workshops." Workshop sponsored by: U.S. Environmental Protection Agency and Hydrocomp, Athens, Georgia, 1979.

Linsley, Ray K., Max A. Kohler, and Joseph L. H. Paulhus. Hydrology for Engineers. Mcgraw-Hill, New York. 1982. 508 pp.

Nichols, William G., and Donald C. Raney. "1984 Water Assessment for the Apalachicola-Chattahoochee-Flint River Basin Water Management Study." U.S. Army Corps of Engineers, Mobile District, Mobile, Alabama, 1984. 114 pp.

Peck, E. L. "Catchment Modeling and Initial Parameter Estimation for the National Weather Service River Forecast System." NOAA Technical Memorandum NWS HYDRO-31, U.S. Department of Commerce, Silver Spring, Maryland, 1976.

Raney, Donald C., William G. Nichols, and Pamela S. Brandes. "An Investigation of Drought Related Factors Affecting Pool Elevation o Lake Lanier, Georgia and the Development of a Reservoir Water Availability Index." U.S. Army Corps of Engineers, Mobile District, Mobile, Alabama, 1984.

SAS Institute, Inc. "SAS/ETS User's Guide, Version 5 Edition." Cary, North Carolina, 1984. 738 pp.

U.S. Army Corps of Engineers, Mobile District. "Drought Water Management Strategy for the Apalachicola-Chattahoochee-Flint Basin." 1986.

U.S. Army Corps of Engineers, Mobile District. "Interim Drought Management Plan for the Apalachicola-Chattahoochee-Flint River Basin." 1985.

APPENDIX A

The Apalachicola River Study

The original study area for this report only included the upper Chattahoochee River down to Buford Dam on Lake Lanier. The possibility of modeling the entire Apalachicola-Chattahoochee-Flint River system (ACF) was raised prior to the beginning of these studies; however, the detailed hydrologic study was limited to the upper Chattahoochee because calibration of as many as 30 subareas and data retrieval of non digital records for 13 reservoirs would have been prohibitive in both time and expense. It is unlikely that a satisfactory model of the entire ACF system could have been produced in the 3-5 months available for the research portion of these studies.

However, other researchers involved in the current Report to Congress have important models of environmental systems that require hydrologic inputs and more specifically require assessments of the change of hydrologic inputs based on the results of the global circulation model (GCM) scenarios. The GCMs report a value for hydrologic runoff in their outputs. Unfortunately, this is one of the GCM variables for which there is no confidence within the current state of the art. The lack of confidence in the runoff outputs is best illustrated by the fact that, with the exception of the GISS model, the GCMs predict zero runoff for most months of each year for both the base case and the changed CO_2 scenarios.

In order to supply the runoff estimates required by these researchers, an autoregressive multiple correlation technique was used to develop a statistical model of the entire ACF system which would yield flow estimates as outputs from meteorological inputs and which would be responsive to the changed inputs of the GCM scenarios.

HYDROLOGY OF THE APALACHICOLA-CHATTAHOOCHEE-FLINT RIVER SYSTEM

Figure 2 in the main report shows the study area which includes the entire Apalachicola-Chattahoochee-Flint River system down to Blountstown, Florida. This system includes the headwater basin of the upper Chattahoochee River, which is the subject of the main report. The upper Chattahoochee study encompasses about 2700 square kilometers whereas this study includes about 45600 square kilometers. The ACF system includes 13 reservoirs with a combined impoundment in excess of 5 cubic kilometers. Figure 1 in the main report shows that the ACF system arises in the Blue Ridge mountains, flows through the Peidmont, across the Fall Line into the Gulf Coastal Plain. The ACF system crosses five degrees of latitude and goes over 800 kilometers from the inland mountains to the Gulf Coast. For such a large area, the climate is not uniform (Nichols and Raney, 1984). Average monthly temperatures decrease in the interior of the basin, particularly at higher altitudes, by as much as 5 degrees Celsius in the winter months and 3 degrees Celsius in the summer months. Figure A.1 shows the average annual precipitation within the ACF system which varies from about 47 inches (120 centimeters) per year to over 60 inches (150 centimeters) per year. The variation in precipitation in the basin can be attributed largely to the proximity to the mountains and the Gulf Coast and to the prevailing weather circulation patterns.

For a system the size of the ACF, even the unregulated surface water bodies will act as a filter with a long delay. With the addition of manmade impoundments and regulated flows, the memory of the system is long indeed--on the order of several months. The impacts of small storms on any part of the system will be completely lost after being stored and passed through several reservoirs.

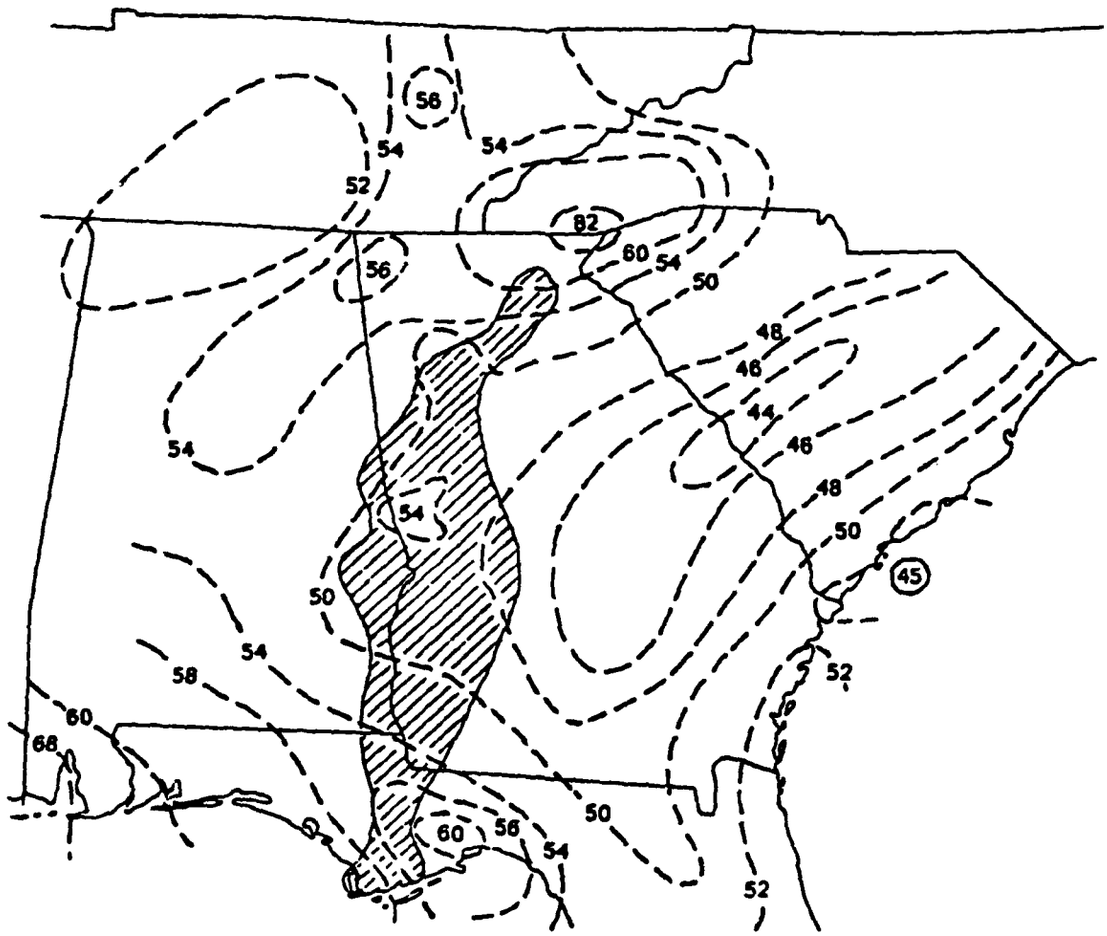

Figure A.1. Average Precipitation (inches/year) for Apalachicola, Chattahoochee and Flint River System

METHODOLOGY

Several meteorological stations in and around the ACF basin were chosen to represent the climate variation of the region in the analysis. The stations used were Tallahassee, Florida, Macon and Atlanta, Georgia, and Montgomery, Alabama, for precipitation and Tifton and Experiment, Georgia, for pan evaporation. Data from these stations were compiled into a monthly average time series for the 38 year period from 1948 to 1985.

The IDENTIFY portion of the SAS (SAS, 1984) ARIMA procedure was used initially to find the lag correlation of each of these stations with the flow on the Apalachicola River at Chattahoochee, Florida (USGS Gaging Station 02358000). This same procedure was used to find the auto correlation of the flows with themselves. The strongest correlation was the autocorrelation for the flow station itself lagged by one month. This was followed by a negative correlation with the Tifton evaporation data lagged by two months. Following these variables were the Macon and Atlanta lagged by 0 and 1 month. The Montgomery and Tallahassee rainfalls did not meet the test for significance in the regression after the other variables were entered. This is not surprising. In a system with so much delay, modeled at the gross time scale of one month, the cross-correlation of the variables will be high enough that some of them would not add any new information to the regression.

The regressions were initially performed on the untransformed monthly average data and a fairly high correlation was achieved. However, because of the logarithmic skew of hydrologic extremes, the high flow months were dominating the correlation and the low flow months were poorly modeled. To correct for the skew, the final regression was performed on the logarithms of the monthly data to give equal weight to both ends of the hydrologic extremes. The log correlation coefficient was not quite as high as the non-log correlation, although the simulation of the base period was slightly better correlated and the simulation of low flows was greatly improved. Table A.1 lists the variables included in the final multiple regression along with their regression coefficients, partial correlation and the significance of each variable in the regression. The correlation of the resulting modeled flow with observed flows is 0.83.

THE SCENARIOS

The GISS, GFDL, and OSU steady-state scenarios were run as well as the GISS Transient A scenario. The EPA standard procedure was followed for development of the scenarios. Because of its size, the ACF basin falls in more than one grid cell for each scenario. For the GISS model, both the steady-state and the transient scenario the ACF basin falls into 4 grid cells. Ratios from the GCM results were weighted on a drainage area basis for each cell to produce a composite precipitation ratio which was then applied to each historical rainfall record on a monthly basis. For potential evaporation, the Penman equation was applied here just as it was for the upper Chattahoochee study. After the evaporation ratios were determined, they were weighted on a drainage area basis for each cell to produce a composite evaporation ratio which was applied to the historical Tifton pan evaporation record on a monthly basis.

Data for the year 1950 were used to provide a year of spin up for the 1951 to 1980 steady-state scenarios. Precipitation and evaporation data for 1951 to 1980 were applied for the years 1981 to 2010 and repeated for 2011 to 2040 and 2041 to 2059 to develop inputs for the Transient A scenario. Data for the years 1970 to 1980 were applied to the year 1970 to 1980 for 11 years of spin up time in the transient scenario.

Table A.1. STEPWISE REGRESSION PROCEDURE FOR DEPENDENT VARIABLE LOGCHAT

STEP 7 VARIABLE LOGCHAT2 ENTERED R SQUARE = 0.76610469 C(P) = 8.00000000

	DF	SUM OF SQUARES	MEAN SQUARE	F	PROB>F
REGRESSION	7	21.67404930	3.09629276	206.82	0.0001
ERROR	442	6.61718772	0.01497101		
TOTAL	449	28.29123702			

	B VALUE	STD ERROR	TYPE II SS	F	PROB>F
INTERCEPT	2.47638548				
LOGATL	0.11209612	0.02355991	0.33891059	22.64	0.0001
LOGMAC	0.16853160	0.02310643	0.79643100	53.20	0.0001
LOGATL1	0.08658081	0.02411703	0.19295093	12.89	0.0004
LOGMAC1	0.10063262	0.02445807	0.25344546	16.93	0.0001
LOGTIFT2	-0.43678937	0.03542957	2.27543022	151.99	0.0001
LOGCHAT1	0.36745177	0.04683286	0.92161705	61.56	0.0001
LOGCHAT2	0.06408580	0.03769756	0.04326615	2.89	0.0898

BOUNDS ON CONDITION NUMBER: 4.180124, 105.5716

STATISTICS FOR REMOVAL: STEP 8
DF = 1,442

Table A.1 (continued)

VARIABLE	PARTIAL R**2	MODEL R**2
LOGATL	0.0120	0.7541
LOGMAC	0.0282	0.7380
LOGATL1	0.0068	0.7593
LOGMAC1	0.0090	0.7571
LOGTIFT2	0.0804	0.6857
LOGCHAT1	0.0326	0.7335
LOGCHAT2	0.0015	0.7646

SUMMARY OF STEPWISE REGRESSION PROCEDURE FOR DEPENDENT VARIABLE LOGCHAT

STEP	VARIABLE ENTERED	VARIABLE REMOVED	NUMBER IN	PARTIAL R**2	MODEL R**2	C(P)	F	PROB>F
1	LOGCHAT1		1	0.5252	0.5252	451.158	495.6473	0.0001
2	LOGTIFT2		2	0.1166	0.6419	232.767	145.5673	0.0001
3	LOGMAC		3	0.0820	0.7238	79.901	132.3429	0.0001
4	LOGMAC1		4	0.0234	0.7472	37.725	41.1504	0.0001
5	LOGATL		5	0.0114	0.7586	18.181	20.9687	0.0001
6	LOGATL1		6	0.0060	0.7646	8.890	11.2427	0.0009
7	LOGCHAT2		7	0.0015	0.7661	8.000	2.8900	0.0898

RESULTS

With the exception of the GISS scenario, the results are quite similar to those for the upper Chattahoochee study. This is encouraging because the hydrology was modeled with a much simpler method for the ACF basin than it was for the upper Chattahoochee. However, especially for the GFDL where 91% of the basin is in the same grid cell as the upper Chattahoochee river, the meteorological input ratios were very similar to those for the upper Chattahoochee, so the results should be similar if the hydrologic models are both reasonably reliable.

The results will be presented here with little discussion because most of what was said in the main report applies here as well.

Steady-State Scenarios

Figure A.2 is a graph showing one standard deviation on each side of the long-term average annual flow at Blountstown for the base period observed flows and the GCM scenario flows. The data for Figure A.2 appear in Table A.2. These results are similar to those for the upper Chattahoochee except for the GISS scenario which shows a 6% decrease in long-term average flow here as compared to a 14% increase for the upper Chattahoochee study. This difference is the result of the influence of the three additional grid cells which were used to modify the climate inputs to the model.

Figure A.3 presents long-term seasonal flow values for the 3 steady-state scenarios at Blountstown along with observed flow. Figure A.4 shows the ratio of scenario flow/observed flow by season for the steady-state scenarios. Figures A.5 through A.7 present the ratio of modeled values/observed values by months averaged over the 30 year scenario period. On each graph, the climate input ratios (precipitation and pan evaporation) are shown along with the hydrologic output (flow) ratio.

Transient A Scenario

The transient scenario must be viewed from a different perspective than the steady- state scenarios. For the transient scenario, CO_2 in the atmosphere has been assumed to follow current trends up through 2059. As a result, the climate is changing all the time. Decadal variability of the transient A scenario is presented in Figure A.2 and Table A.2. Because the base period has an increasing flow trend, the results are sawtoothed at the point where the base period is repeated. As a result, it is not easy to see the GCM effects without careful consideration.

Table A.2. Annual Variability of Hydrologic Model Scenarios--Apalachicola River

	<---------- Cubic Meters per Second ---------->								
	Qbar	Std	+1 std	-1 std	Max	50%ile	Min	%ch Q	%ch Std
Base	639.71	171.88	811.59	467.82	1003.72	642.25	326.83	--	--
TransA									
1980	482.52	133.54	616.06	348.98	671.31	513.81	290.59		
1990	647.38	185.31	832.69	462.07	959.57	608.16	444.12		
2000	728.05	108.71	836.76	619.35	921.97	710.58	623.17		
2010	530.57	124.42	655.00	406.15	690.34	580.30	328.59		
2020	595.36	174.88	770.25	420.48	901.13	552.77	395.16		
2030	629.68	93.90	723.58	535.78	803.52	603.77	530.97		
2040	462.95	109.53	572.48	353.42	61.14	39.36	289.06		
2050	536.38	156.76	693.14	379.62	65.95	505.91	803.07		
2X=>									
GISS	619.40	156.56	775.97	462.84	949.75	614.02	311.23	-6.1%	-6.0%
GFDL	512.31	132.83	645.14	379.47	800.94	513.95	247.94	-22.4%	-20.3%
OSU	567.95	142.09	710.04	425.86	856.75	565.63	282.91	-13.9%	-14.7%
TBASE	659.81	166.64	826.46	493.17	1003.72	648.17	326.83		
TRANSA	575.57	157.22	732.78	418.35	959.57	574.55	289.06	-10.0%	-8.5%

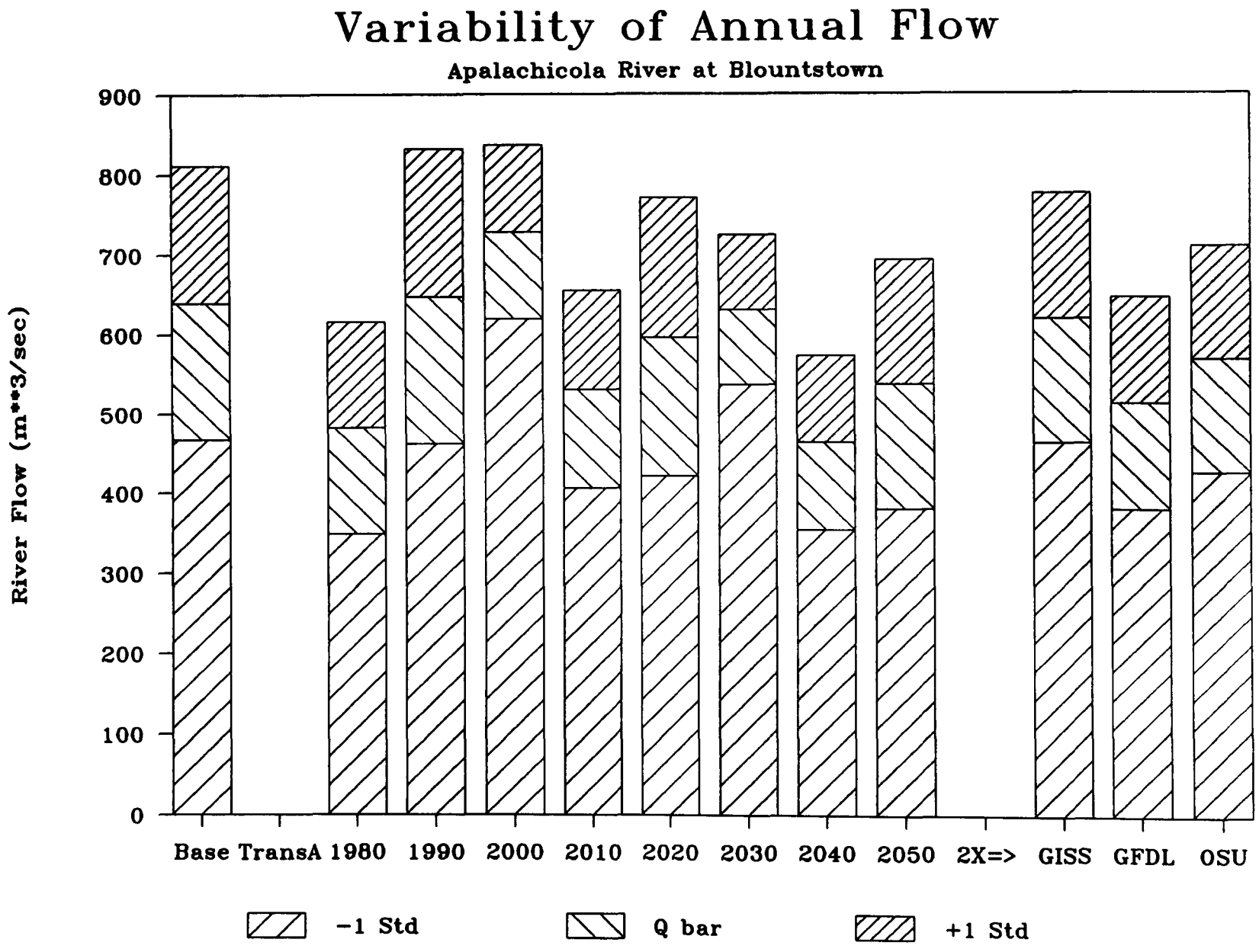
Variability of Annual Flow
Apalachicola River at Blountstown
River Flow (m**3/sec)
900
800
700
600
500
400
300
200
100
0
Base
TransA
1980
1990
2000
2010
2020
2030
2040
2050
2X=>
GISS
GFDL
OSU
-1 Std
Q bar
+1 Std

Figure A.2

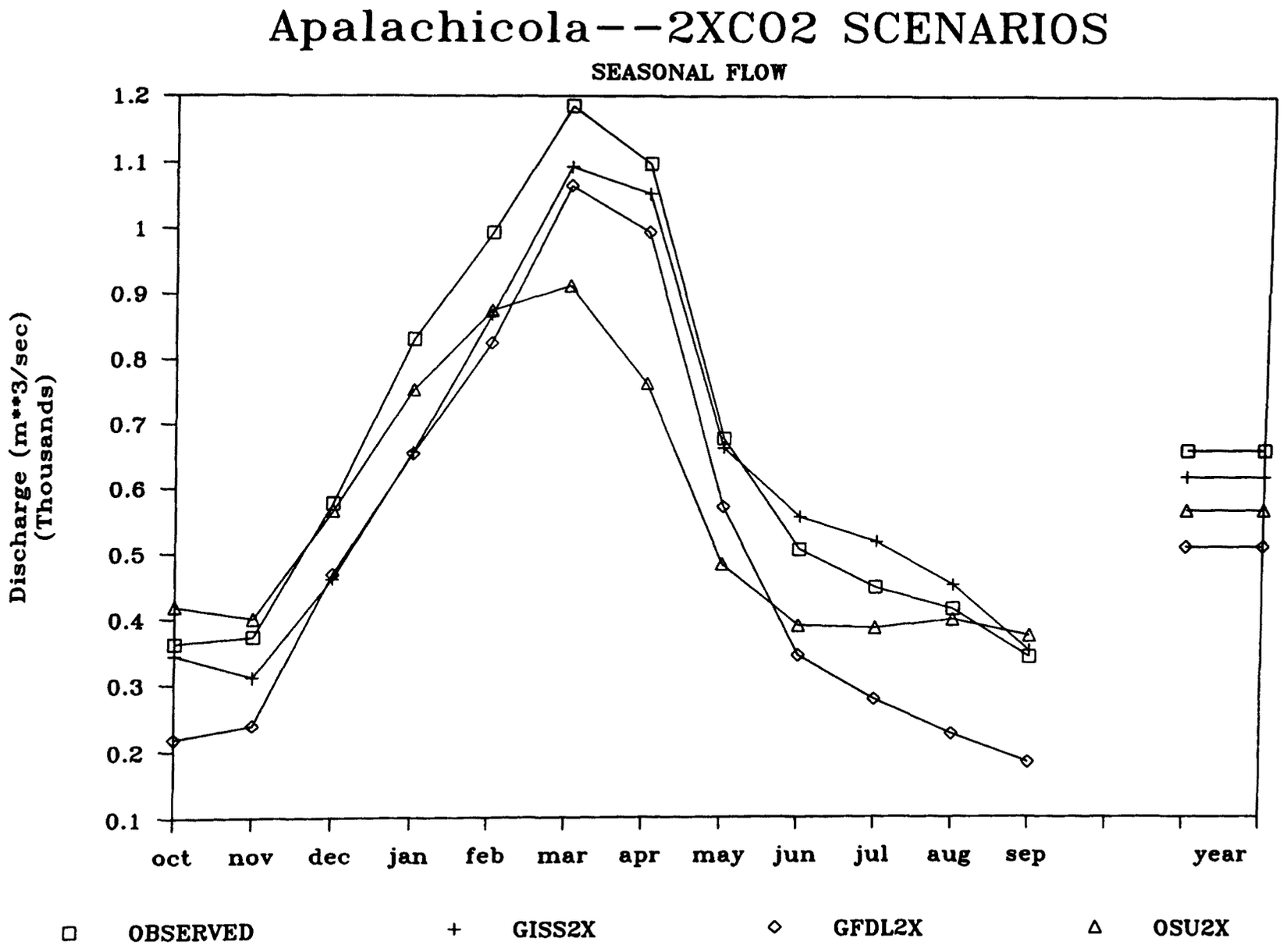
Apalachicola--2XCO2 SCENARIOS
SEASONAL FLOW
Discharge (m**3/sec)
(Thousands)
1.2
1.1
1
0.9
0.8
0.7
0.6
0.5
0.4
0.3
0.2
0.1
oct
nov
dec
jan
feb
mar
apr
may
jun
jul
aug
sep
year
OBSERVED
GISS2X
GFDL2X
OSU2X

Figure A.3

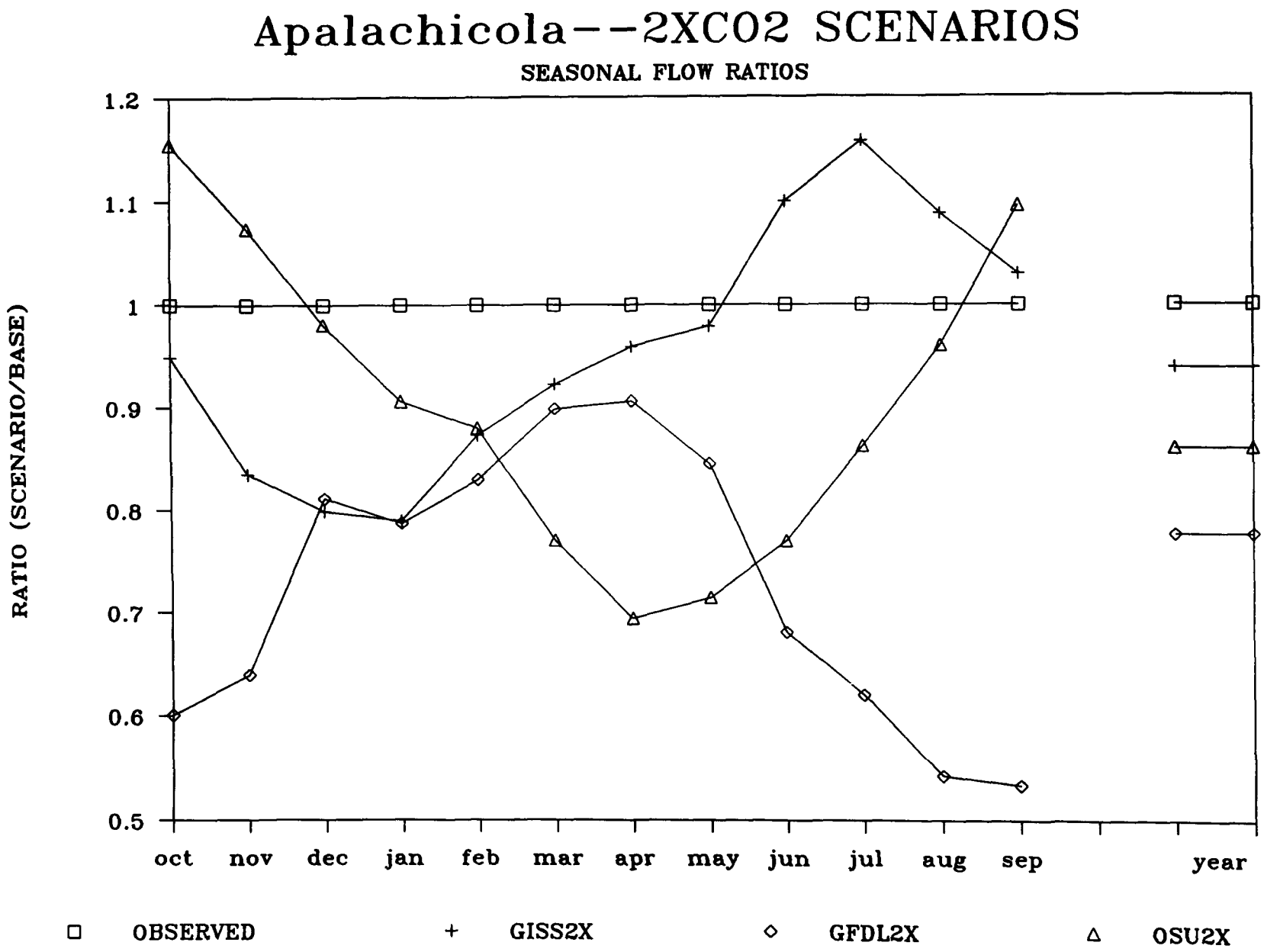
Apalachicola--2XCO2 SCENARIOS
SEASONAL FLOW RATIOS
RATIO (SCENARIO/BASE)
1.2
1.1
1
0.9
0.8
0.7
0.6
0.5
oct
nov
dec
jan
feb
mar
apr
may
jun
jul
aug
sep
year
OBSERVED
GISS2X
GFDL2X
OSU2X

Figure A.4

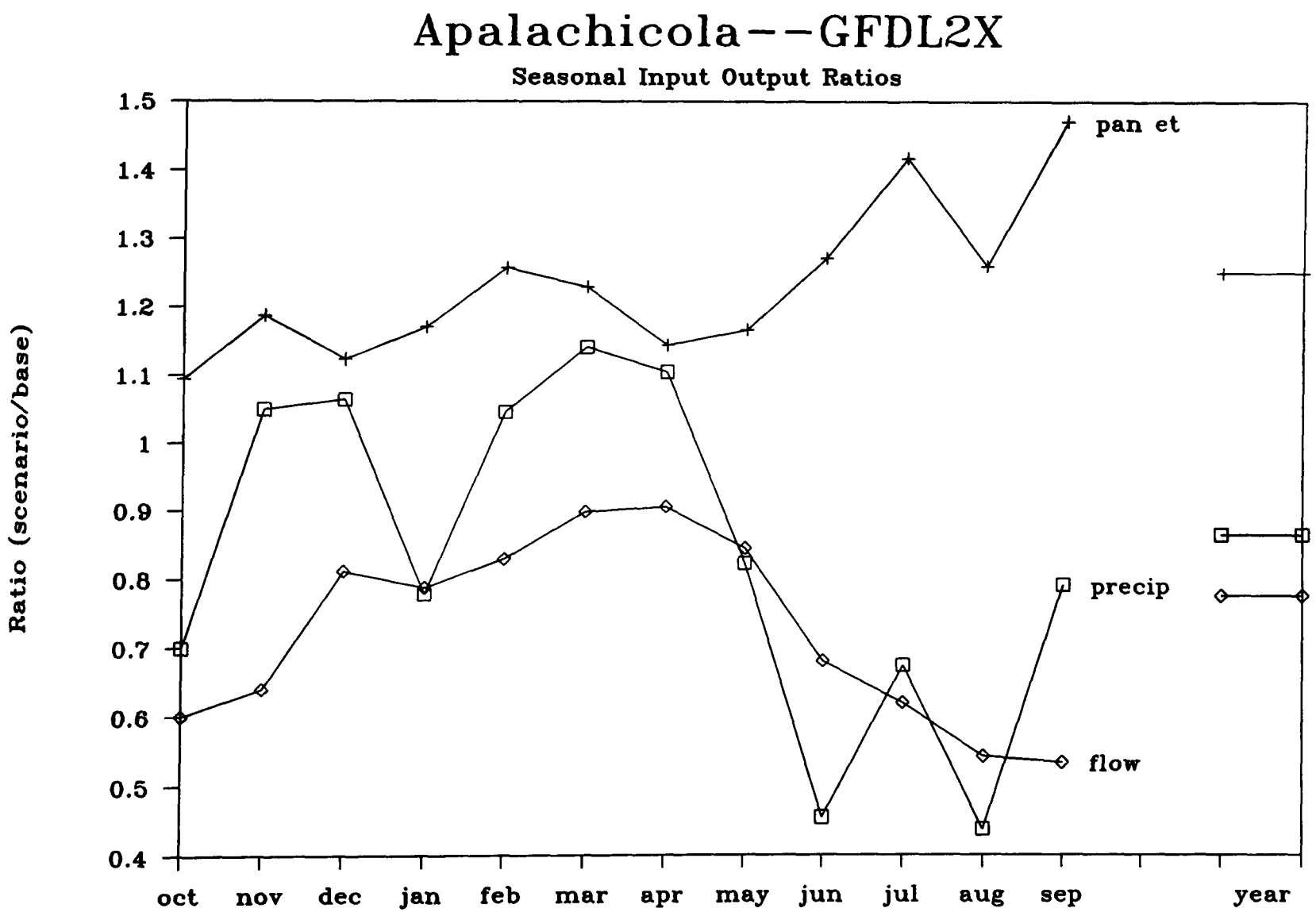
Apalachicola--GFDL2X
Seasonal Input Output Ratios
Ratio (scenario/base)
1.5
1.4
1.3
1.2
1.1
1
0.9
0.8
0.7
0.6
0.5
0.4
oct
nov
dec
jan
feb
mar
apr
may
jun
jul
aug
sep
year
pan et
precip
flow

Figure A.5

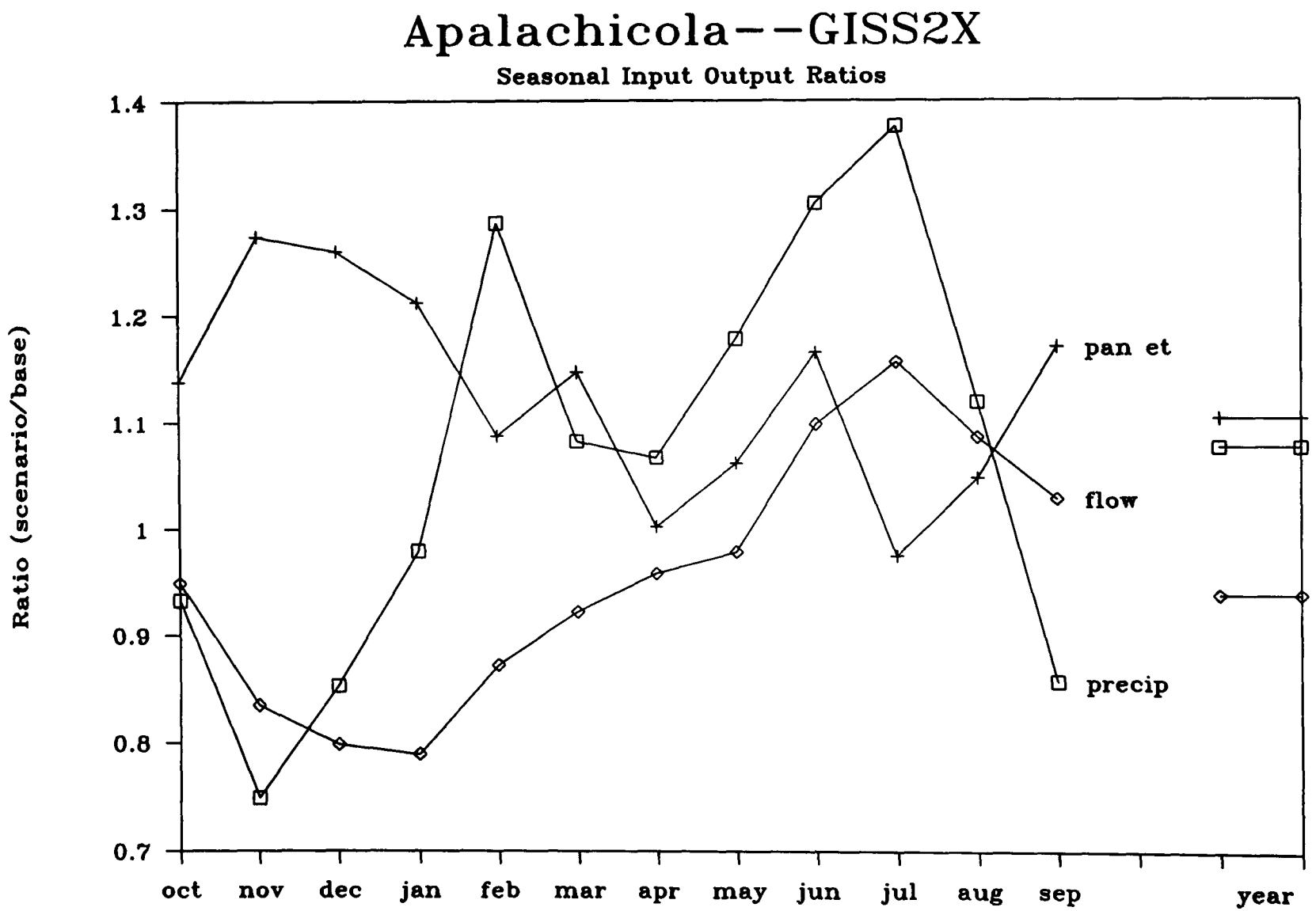
Apalachicola--GISS2X
Seasonal Input Output Ratios
Ratio (scenario/base)
1.4
1.3
1.2
1.1
1
0.9
0.8
0.7
oct
nov
dec
jan
feb
mar
apr
may
jun
jul
aug
sep
year
pan et
flow
precip

Figure A.6

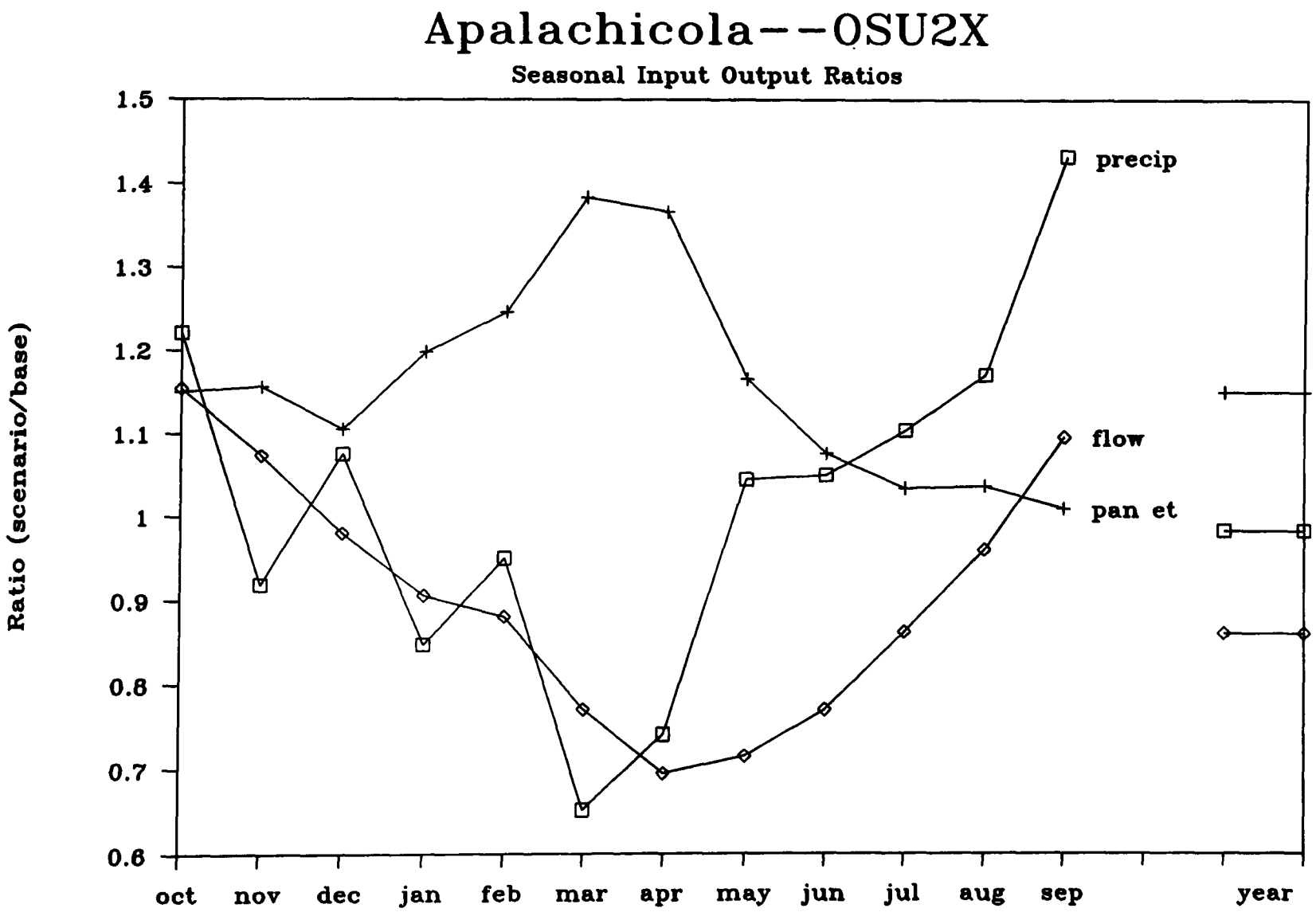
Apalachicola--OSU2X
Seasonal Input Output Ratios
Ratio (scenario/base)
1.5
1.4
1.3
1.2
1.1
1
0.9
0.8
0.7
0.6
oct
nov
dec
jan
feb
mar
apr
may
jun
jul
aug
sep
year
precip
flow
pan et

Figure A.7

Figure A.8 shows the annual ratios of transient/baseline climate inputs (precipitation and pan evaporation) and hydrologic outputs (flow) as a five year running average. The ratio data are easier to interpret than the flow data alone because the ratio has the particular effects of the baseline period removed. There is no clear effect of climate change on precipitation for the transient run. Precipitation ratios seem to fluctuate between wet and dry trends with the long-term ratio being close to one. The climate change effects for the transient run seem to be mainly associated with increases in pan evaporation which are robust and obvious.

During the first decade of the transient A scenario, when there was a decrease in precipitation as compared with the base period, pan evaporation was already elevated with a resulting 10% decrease in runoff. This is followed by a decade with enough more precipitation than the base period that the runoff almost equals that of the base period for several years. This seems unusual at the beginning of a transient run of the GCM when it is assumed that the CO_2 effects are minimal. In the fourth decade of the transient scenario the precipitation ratio reaches its highest level and then begins to decline. The rest of the transient run follows an expected pattern of an accelerating reduction in runoff driven primarily by increases in pan evaporation.

In order to present the effects of the transient scenario in the clearest comparison with the identical period from the baseline data, the individual months were accumulated for both the base period and the transient scenario. These were plotted on the same graph versus time as shown in Figure A.9. The effects discussed above can be seen very clearly in the departures of the transient A curve from the observed curve. The initial departure in the 1980's, the decreasing departure in 1990's and 2000's and the robust departure beginning about 2020 are very clear.

This same behavior is displayed in Figure A.10 where the two accumulated monthly curves are plotted against each other. The straight line is the slope the curve would have if there were no effects. Where the slope is less than the straight line, the transient runoff is less than the base period runoff. Where the slope is greater than the straight line, the transient is greater than the base period.

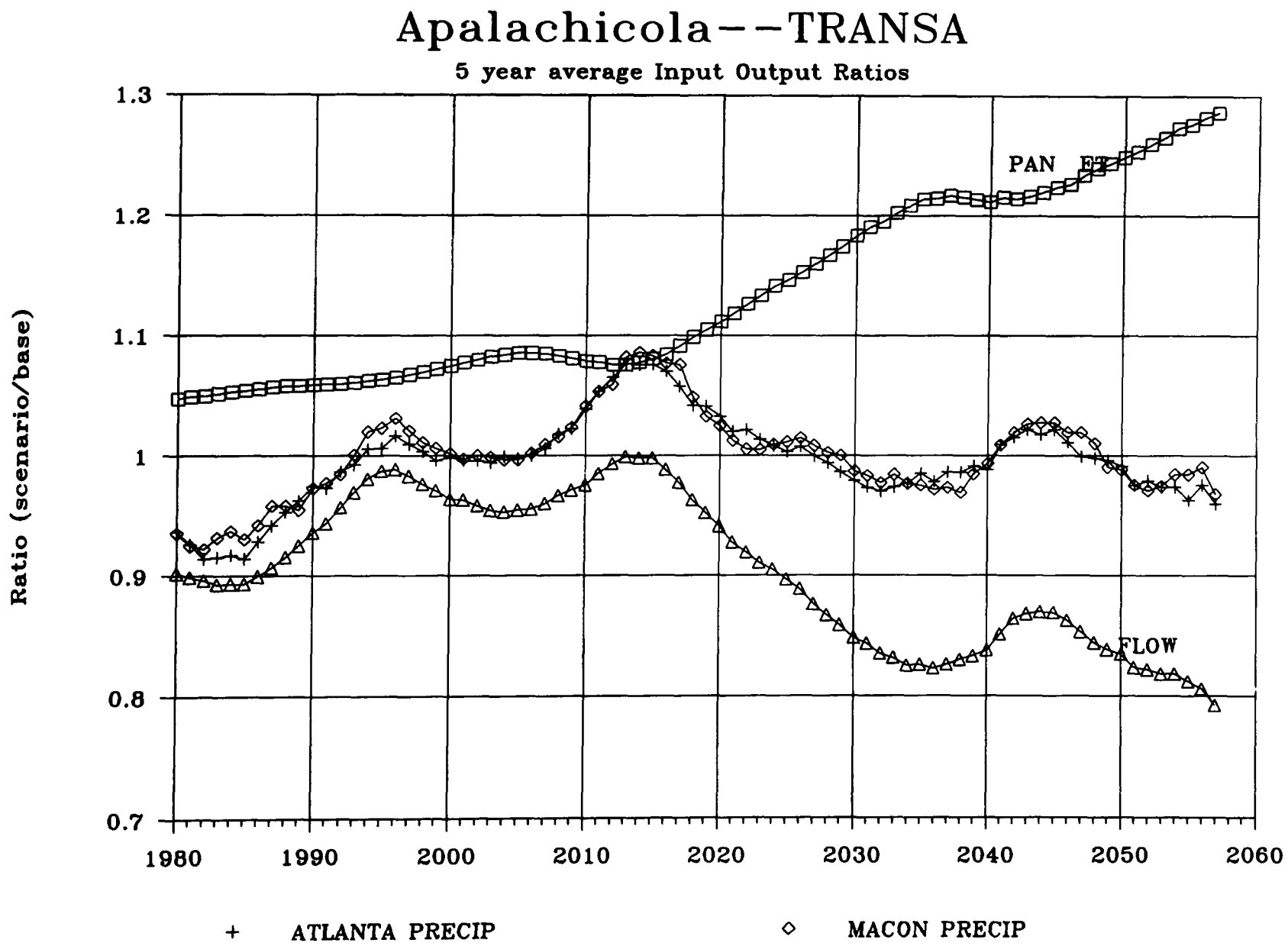
Apalachicola--TRANSA
5 year average Input Output Ratios
Ratio (scenario/base)
1.3
1.2
1.1
1
0.9
0.8
0.7
1980
1990
2000
2010
2020
2030
2040
2050
2060
PAN ET
FLOW
+ ATLANTA PRECIP
◇ MACON PRECIP

Figure A.8

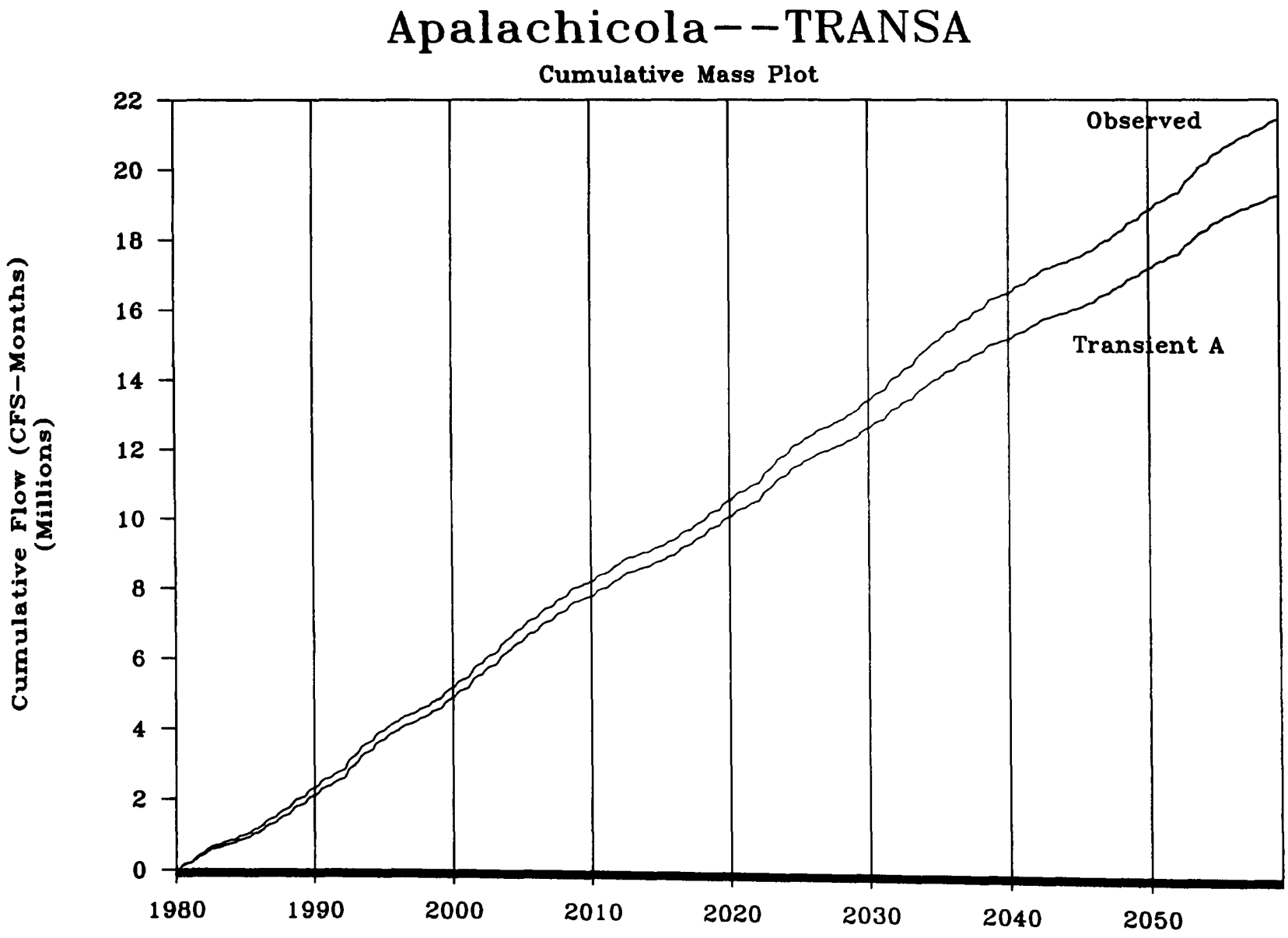
Apalachicola--TRANSA
Cumulative Mass Plot
Cumulative Flow (CFS-Months)
(Millions)
22
20
18
16
14
12
10
8
6
4
2
0
1980
1990
2000
2010
2020
2030
2040
2050
Observed
Transient A

Figure A.9

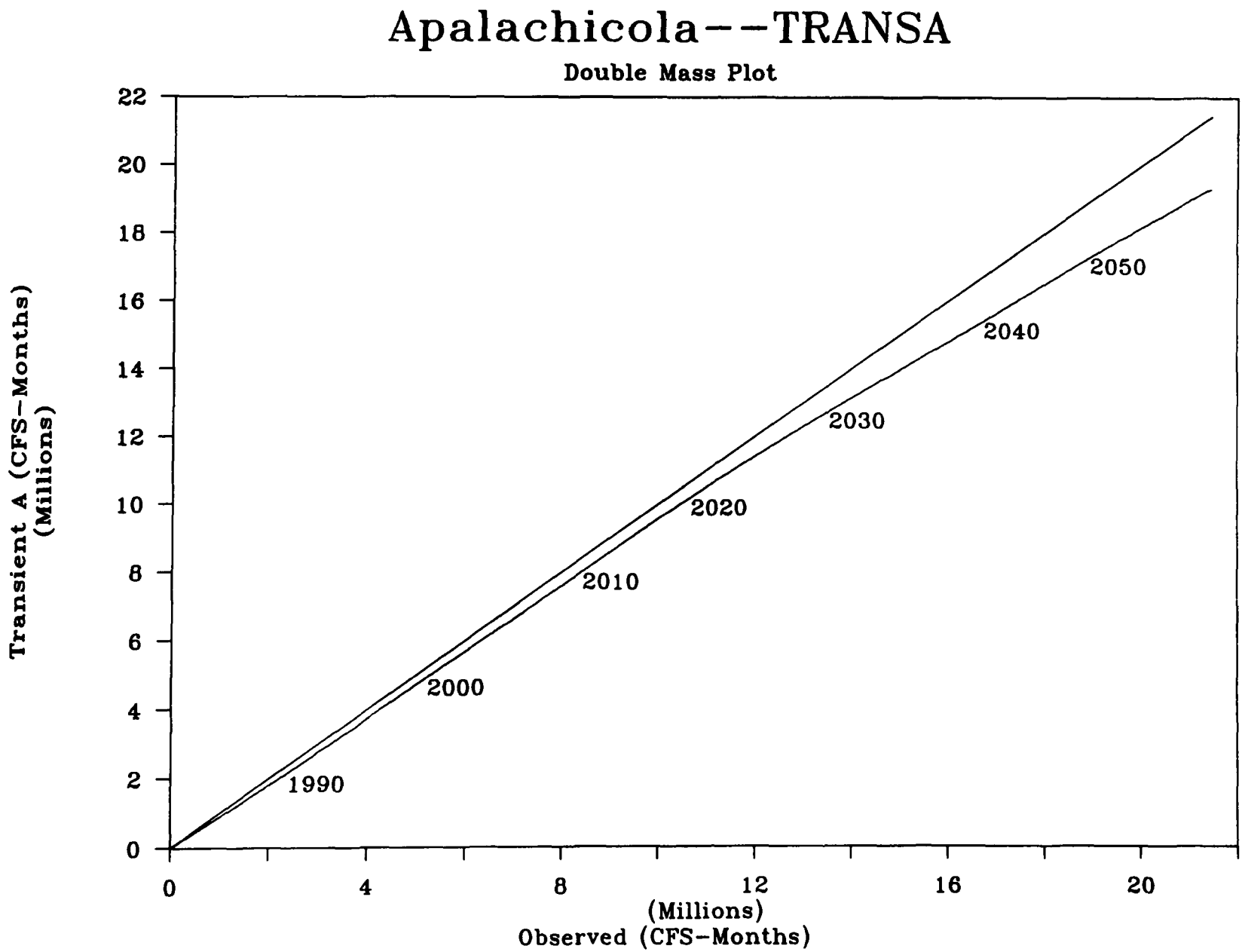
Apalachicola--TRANSA
Double Mass Plot
Transient A (CFS-Months)
(Millions)
Observed (CFS-Months)
(Millions)
0
2
4
6
8
10
12
14
16
18
20
22
0
4
8
12
16
20
1990
2000
2010
2020
2030
2040
2050

Figure A.10

POTENTIAL IMPACTS OF CLIMATE CHANGE ON THE TENNESSEE VALLEY AUTHORITY RESERVOIR SYSTEM

by

Barbara A. Miller
W. Gary Brock
Tennessee Valley Authority
Engineering Laboratory
Norris, TN 37828

Interagency Agreement #DW64932639-01-0

CONTENTS

Page

EXECUTIVE SUMMARY 9-1

CHAPTER 1: INTRODUCTION 9-3
GLOBAL CLIMATE CHANGE 9-3
PROJECT OBJECTIVES 9-3

CHAPTER 2: BACKGROUND 9-4
THE TVA SYSTEM 9-4
Elements of the Integrated Reservoir System 9-4
Managing the Reservoir System 9-9
Sensitivity of the TVA Reservoir System to Climate Change 9-9

HYDROLOGIC OVERVIEW OF THE TENNESSEE RIVER BASIN 9-11
Historical Precipitation 9-11
Historical Runoff 9-11

CHAPTER 3: METHODOLOGY 9-13
THE WEEKLY SCHEDULING MODEL 9-13
Background and Development of the Model 9-13
Application of the Model 9-14
SUPPLEMENTARY MODELS 9-14
CLIMATE CHANGE SCENARIOS 9-14
LIMITATIONS OF THE METHODOLOGY 9-19

CHAPTER 4: IMPACTS OF CLIMATE CHANGE ON THE TVA RESERVOIR SY9-22
RESULTS OF THE WEEKLY SCHEDULING MODEL 9-22
Reservoir Operations 9-22
Flooding at Chattanooga 9-24
Power Operations 9-29
IMPLICATIONS FOR TVA SYSTEM OPERATIONS 9-31
Reservoir Operations 9-31
Navigation 9-31
Flood Control 9-32
Dam Safety 9-32
Power Operations 9-33
Water Quality 9-33
Recreation 9-35
Water Supplies 9-35

CHAPTER 5: SUMMARY AND CONCLUSIONS 9-37
METHODOLOGY 9-37
IMPACTS OF CLIMATE CHANGE ON THE TVA SYSTEM 9-38
CONCLUSIONS 9-45

LIST OF ABBREVIATIONS, SYMBOLS, AND DEFINITIONS 9-46

REFERENCES 9-47

EXECUTIVE SUMMARY[1]

The objective of this project was to identify the sensitivity of the Tennessee Valley Authority (TVA) reservoir system to global climate change. The range of potential impacts on reservoir operations, navigation, flood control, hydropower production, water availability, water quality, and recreation were evaluated for the Tennessee River Basin. Implications of these changes and potential adaptive strategies were also outlined for the reservoir system and related TVA programs.

The Weekly Scheduling Model (WSM), a reservoir planning model, was used to assess climate change impacts on the TVA reservoir system. Monthly ratios for surface runoff ($2xCO_2$/CONTROL) provided by the Environmental Protection Agency (EPA) for two climate scenarios were used to adjust historical local inflows into each project for the 30-year study period (1951-1980). The weather scenarios, based on data generated by NASA's Goddard Institute for Space Studies (GISS) general circulation model (GCM), represent potential climate changes resulting from a doubling in atmospheric CO_2 concentrations (possible by the mid-21st century).

The first GISS scenario predicts a warmer and wetter climate for the Tennessee Valley region. East of Chattanooga, runoff increases 31% annually. In this eastern basin, which contains all the large tributary storage reservoirs, flows are exaggerated during the traditional flood season (75% in March) and decreased during a dry time of the year (-28% in November). West of Chattanooga, monthly ratios are more variable, but the integrated effect of changes in runoff to the Tennessee River is to increase local inflows most of the year.

The second scenario, GISS Inverse, simulates a warmer and significantly drier climate for the TVA region. In the eastern basin, runoff is substantially reduced during the traditional flood season and only modestly increased during the dry period of year. The net effect is a 31% reduction in average annual runoff and low inflow rates throughout the year. West of Chattanooga, runoff ratios are more variable, but the general trend is to reduce runoff from current levels.

The increased runoff predicted by the GISS scenario results in higher reservoir elevations throughout the year at all major projects in the TVA system. At the large storage projects in the eastern basin, normal operating levels are met or exceeded in the fall; normal maximum levels are exceeded in wet years during the traditional flood season; and summer full pools are maintained for an extended period of time. Exceedence of normal maximum reservoir levels would likely result in spillage from dams and increased flooding in the Tennessee Valley. Flood-prone urban areas in Tennessee such as Chattanooga and low-lying agricultural areas could be particularly vulnerable to flood damage. Safety issues at dams and nuclear power plants would also need to be reevaluated.

Primary benefits of the GISS scenario include a 16% average annual increase in hydropower production, valued at $54 million; enhanced recreational opportunities; and improved water availability for water supplies and minimum flow requirements. Water quality impacts would be variable and site specific, depending on the relative influence of increased flows and assimilative capacity versus increased nonpoint source pollution.

Under the GISS Inverse scenario, decreased runoff would result in an overall decline in storage and water availability at major projects in the TVA system. At the tributary storage reservoirs, lake levels are lowered throughout the year, with median levels up to 9 meters (30 feet) below the base case and minimum levels often below normal minimum pool levels during dry years. Due to constraints in the WSM, mainstem reservoirs are filled to normal operating levels and minimum downstream flow and navigation requirements are met, but at the expense of severely reducing water levels at the tributary projects.

---

[1]Although the information in this report has been funded wholly or in part by the U.S. Environmental Protection Agency under Interagency Agreement #DW64932639-01-0, it does not necessarily reflect the Agency's views, and no official endorsement should be inferred from it.

Adverse impacts of the GISS Inverse scenario include a 24% decrease in annual average hydropower generation with a replacement value of $87 million dollars; seriously impaired water quality; degraded recreational opportunities; and decreased water availability for water supplies. The ability of many TVA projects to fulfill their present multipurpose functions could be threatened. The benefits of this scenario are primarily related to reduced flood potential and the reduced probability of dam failure.

Both climate scenarios could significantly impact the operation of the TVA reservoir system. Substantial changes in the reservoir guide curves and operating philosophy, as well as potential structural changes and/or additions to the system, would be required to respond to an altered climate. Under the wetter GISS scenario, flood control and safety issues would predominate with the need to create additional flood capacity through operational changes, dam modification, and/or flood protection works. Added turbine capacity could be justified, while more pumped-storage could be needed for peaking purposes. Nonpoint source pollution control programs would need to be expanded; while enhanced recreational opportunities would encourage economic development.

Under the drier GISS Inverse scenario, drought-related issues would increase in significance. Difficulty in satisfying project purposes would necessitate a reordering of TVA priorities. Alternative sources of energy would need to replace lost hydropower potential, while fossil and nuclear plants may be unable to meet thermal and/or safety standards owing to decreased flows and elevated water temperatures. Industrial and municipal treatment facilities could be subject to more stringent waste standards. Increased power costs, decreased recreation revenues, and increased industrial restrictions could have significant adverse impacts on the Tennessee Valley economy.

The project objective was to assess the sensitivity of the TVA reservoir system to extreme climate changes and to identify the implications of these changes. The study was not intended to predict the future climate in the TVA region. Given the noted sensitivity of the TVA reservoir system to climate change, the recent extended drought in the Tennessee Valley, and the general scientific consensus that atmospheric changes are highly probable, this issue should be investigated in more detail. Climate change issues should have an increasing role in TVA long-range planning and capital expenditures.

CHAPTER 1

INTRODUCTION

GLOBAL CLIMATE CHANGE

Concern over changes in global climate caused by rising concentrations of CO_2 and other greenhouse gases has increased in recent years. A doubling in CO_2 concentrations, possible as early as 2030, could increase global air temperatures by 1.5 to 4.5°C (National Academy of Sciences, 1987). Increases in temperature are likely to be accompanied by changes in the frequency and distribution of other climate variables such as precipitation, wind, evapotranspiration, and runoff. Consequent alterations in regional hydrologic cycles would necessitate a reevaluation of the priorities and operating philosophies of water resources systems to meet the competing demands of energy production, flood control, water supply, navigation, recreation, and environmental quality.

To assess the potential range and sensitivity of regional effects of climate change, the Environmental Protection Agency (EPA) contracted with TVA to evaluate the impact of two climate scenarios on the TVA reservoir system. This project was one of approximately 50 case studies sponsored by EPA to evaluate potential climate change impacts in the United States.

PROJECT OBJECTIVES

The Tennessee Valley was selected by the EPA for a case study of potential climate change impacts because it represents a large, comprehensively managed water resources system. Based on hypothetical climate scenarios provided by EPA, the TVA Engineering Laboratory proposed to evaluate the sensitivity of the TVA reservoir system to extreme climate changes. The range of potential impacts to reservoir operations, flood control, navigation, hydropower production, water availability, water quality, and recreation are evaluated for the Tennessee River Basin. In the assessment of climate change impacts, model results are extrapolated where feasible to determine potential impacts on the need for capital expenditures and/or other system alterations.

The results of this study are not intended to predict precise changes, but to identify the elements of the TVA reservoir system and related programs most sensitive to climate change. A more detailed version of this report is provided by Miller and Brock (1988).

CHAPTER 2

BACKGROUND

THE TVA SYSTEM

The Tennessee River drainage basin encompasses a seven-state area in the southeastern United States, including parts of Tennessee, Mississippi, Alabama, Georgia, North Carolina, Virginia, and Kentucky. The 105,931 square kilometer (40,900 square mile) area includes a population of approximately 5 million people. The TVA, a multiple-purpose Federal Agency, operates a wide variety of programs within the region, including water resources and reservoir management; power production; regional agricultural and industrial development; and natural resource conservation and protection. A map of the Tennessee River Basin and the TVA power service area, which is almost twice the size of the basin, is shown in Figure 1. Summary statistics of major TVA activities are given in Table 1.

The TVA reservoir system, which is comprehensively managed as an integrated system, includes 42 major dams and reservoirs. The TVA Act of 1933 directs that TVA operate these dams and reservoirs primarily for the purposes of navigation, flood control, and hydroelectric power generation. Additional considerations include recreation, water supply, resource conservation, and environmental management. Major climate changes could have profound effects on the operation of such a multipurpose system.

Elements of the Integrated Reservoir System

Thirty-three of the major dams and reservoirs operated by TVA are shown schematically in Figure 2. Although all dams and reservoirs within the TVA system serve multiple functions, major projects can be categorized based on their primary purpose: single-purpose power projects; tributary multipurpose reservoirs; or mainstem multipurpose reservoirs.

Twelve reservoirs within the system were built or acquired strictly as hydroelectric generating facilities. These reservoirs are generally relatively small with minimal flood storage capacity.

The 21 tributary multipurpose reservoirs in the Tennessee Valley were built to ensure adequate flows for mainstem navigation, flood control, and power production. These reservoirs are deep and provide key flood storage capacity for the system. Flood control dominates the annual operating cycle, and the tributary reservoirs are operated to fit the historical annual streamflow cycle in the region. As illustrated in Figure 3, tributary reservoirs are lowered to flood control levels by January 1 to provide storage for the heavy flows of winter and early spring. Normally, spring rains are allowed to fill the reservoirs from mid-March until full-pool levels are reached by the end of May or early June. During the summer, when streamflows are typically low and power demands high, lake levels are lowered significantly. Reservoir levels continue to recede through the fall until winter flood control levels are once again reached by January 1.

The nine major reservoirs on the mainstem of the Tennessee River constitute the third category -- mainstem multipurpose reservoirs. In addition to hydroelectric facilities, each of these nine projects has navigation locks. The locks and dams create a navigation channel with a minimum depth of 3.3 meters (11 feet). This inland waterway, which extends 1,046 kilometers (650 miles) from Knoxville, Tennessee, to Paducah, Kentucky, links the Tennessee River with the Ohio and Mississippi Rivers.

Navigation constraints affect the operation of these mainstem reservoirs. Pool fluctuations are severely limited to maintain the minimum navigation channel depth. The typical mainstem drawdown range between summer "full pool" and winter flood minimum levels is only 0.6 to 2 meters (2 to 7 feet). In contrast, some of the deeper tributary reservoirs are drawn down by as much as 23 to 30 meters (75 to 100 feet) (see Figure 3).

Figure 1

Map of the Tennessee River Valley

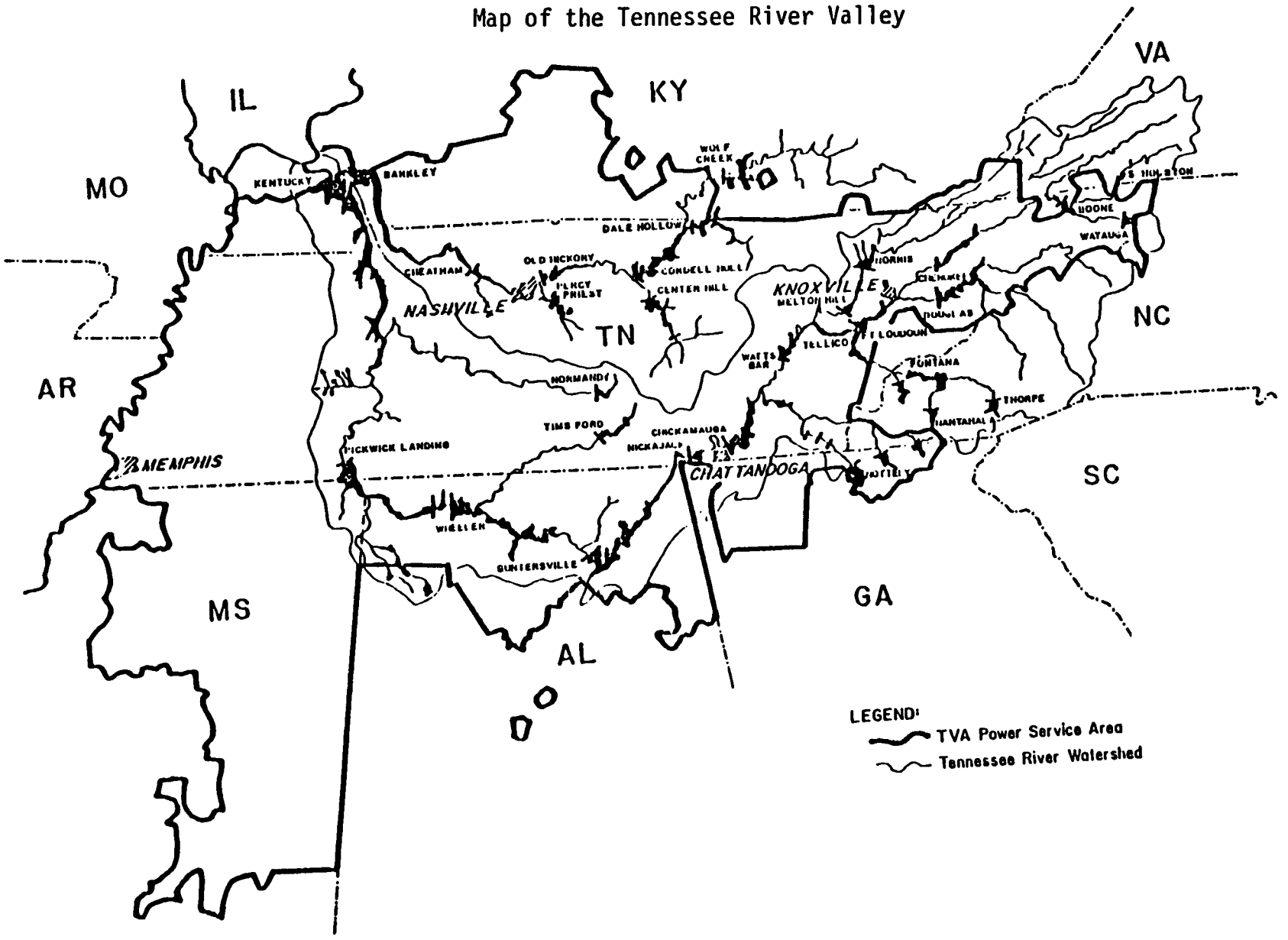

ENG LAB 1988

Table I

Summary of Major TVA Programs*

PROGRAM	GENERAL INFORMATION
1. Reservoir Operations	Major Dams and Reservoirs: 31 TVA 4 Alcoa 8 Cumberlands Water Surface: 259,590 hectares (641,455 acres) Shoreline: 18,012 km (11,195 mi)
2. Navigation	Length of Waterway: 1,050 km (676 mi) Channel Depth: 3.3 m (11 ft) Traffic (1983): 25.4 million metric tons (28 million tons) Private Investment (1933-1984): $4.8 billion
3. Flood Control	System Detention Capacity: Jan 1: 14.7 billion m^3 (11,908,860 Ac-ft) Mar 15: 12.9 billion m^3 (10,548,260 Ac-ft) Summer: 3.3 billion m^3 (2,671,300 Ac-ft)
4. Power Production	Total Generating Capacity (1986): 32,092 MW 55% Coal-Fired 18.4% Nuclear 14% Hydro 7.8% Combustion Turbine 4.8% Pumped-Storage Power Service Area: Area: 202,000 sq km (77,992 sq mi) Population: 7.1 million Tennessee River Watershed: Area: 105,960 sq km (40,910 sq mi) Population: 4.9 million
5. Recreation	Public Access and Recreational Lands: 92,130 hectares (227,643 acres) Recreation Visits (1986): 74.7 million Value of Development and Equipment (1978): $630 million
6. Fisheries (Sport)	Fishing Trips (1986): 17.1 million/year Catch: 6.8 - 9.1 million kilograms/year (15.0-20.1 million lb/year) Cost of Goods and Services: $400 million/year

*From: TVA Handbook, 1986

Figure 2
Schematic Diagram of the TVA Water Control System

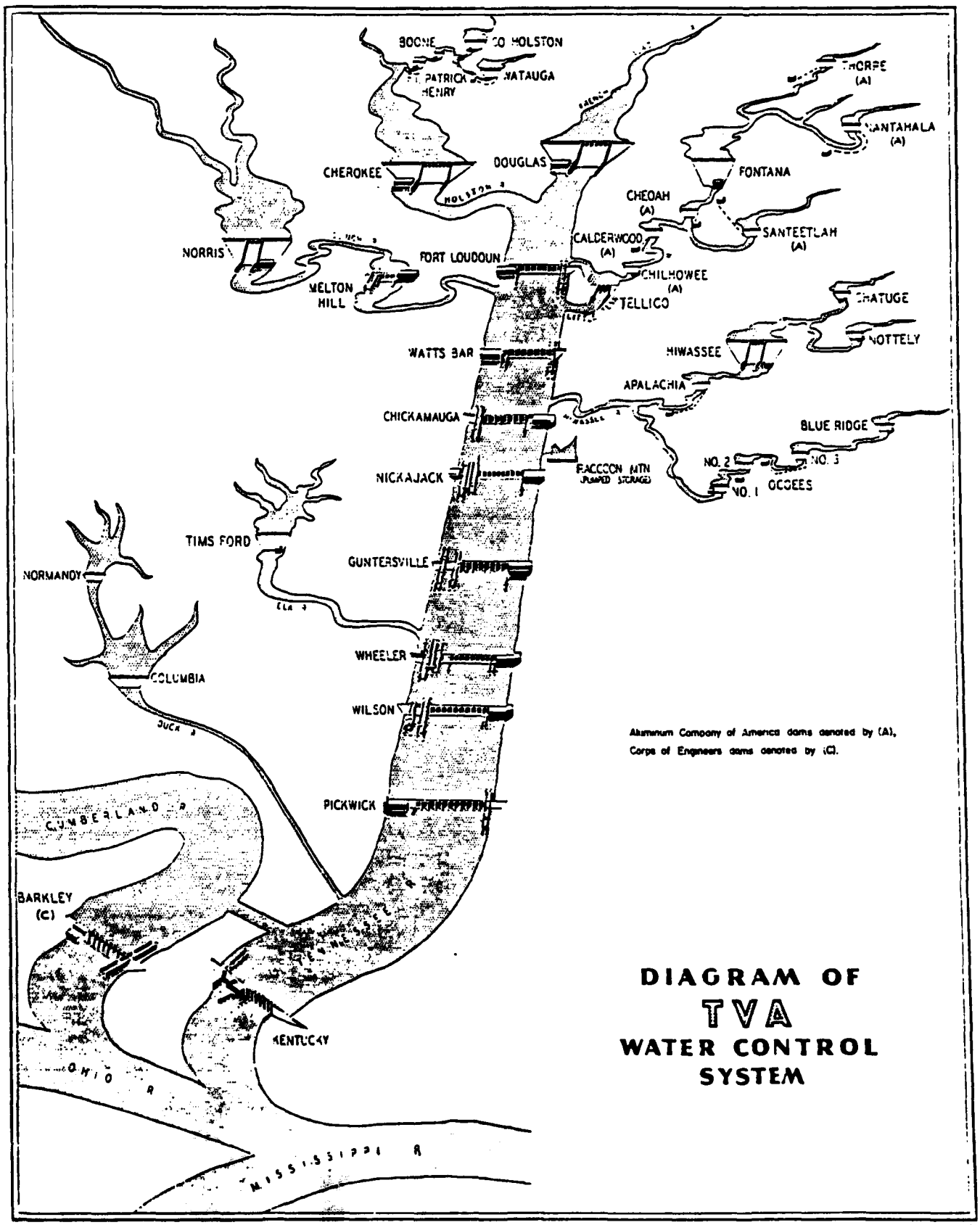

ENG LAB 1988

Figure 3
Typical Reservoir Operating Levels

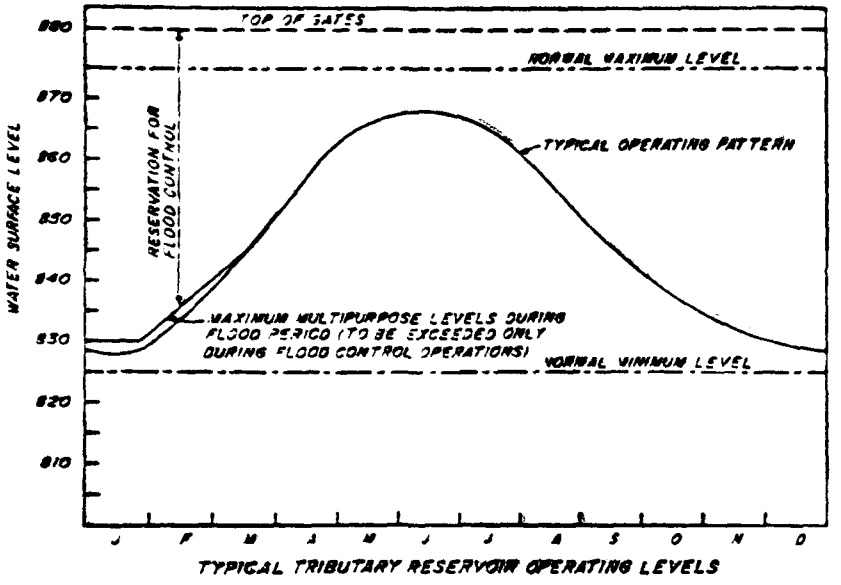

TYPICAL TRIBUTARY RESERVOIR OPERATING LEVELS

On tributary reservoirs, low lake levels provide storage capacity for the winter flood season, then normally rise to high levels by the end of spring. The stored water is gradually released to augment the smaller river flows of summer and fall for power production, water supply, and other needs.

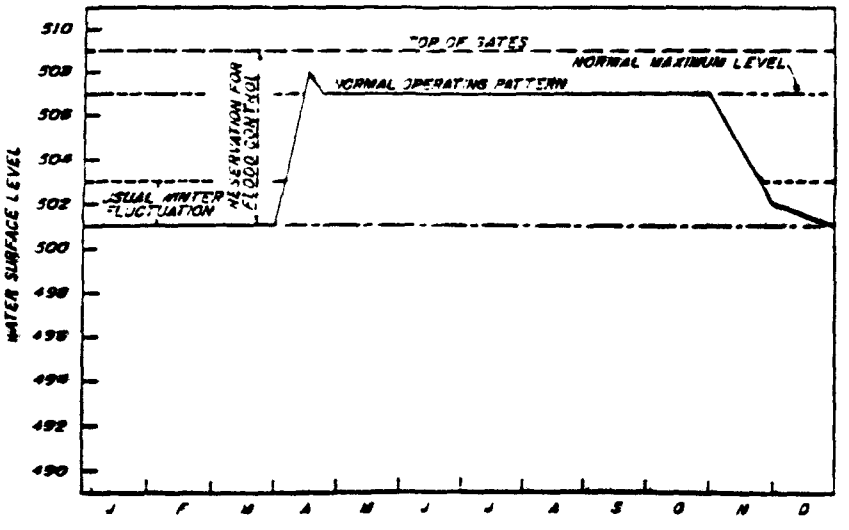

TYPICAL MAINSTREAM RESERVOIR OPERATING LEVELS

Water levels on mainstream reservoirs can fall only a few feet for winter flood control, because adequate water depths must be maintained in the navigation channel to the next dam upstream.

ENG LAB 1988

Managing the Reservoir System

Scheduling water releases from the TVA reservoirs is a complex process. Daily and seasonal operations must account for the following: the amount of water in storage; travel time through the system; unregulated local inflows; and daily weather, streamflow, and power demand variations. River control managers must determine on a daily basis the rate and quantity of water to be released from each dam to obtain maximum benefits while meeting the seasonal operating goal -- the orderly filling of reservoirs during the spring and the lowering of the reservoirs during the summer and fall. This transition from minimum winter flood levels to full pool summer levels, ideally in a manner such that minimal water is spilled and hydroelectric energy potential lost, influences operational guidelines for each reservoir in the TVA system.

Consistent with providing flood control and navigation, TVA gives emphasis to maximum production of hydroelectric power. Hydropower is a low-cost source of electricity that is unaffected by increases in fuel and construction costs. It is also the most immediately responsive source of power, which makes it ideal for peaking power, supplying additional power quickly during those times of the day when power demands are highest. Operation of the reservoir system for maximum hydroelectric production, however, involves unavoidable conflicts with other public needs and concerns such as recreation and water quality issues. TVA is presently reevaluating the operation of the reservoir system to resolve some of these conflicts in light of today's needs and changing priorities.

Sensitivity of the TVA Reservoir System To Climate Change

Major elements of the TVA reservoir system are presented schematically in Figure 4. Overland and tributary inflow rates resulting from runoff over the Tennessee River Basin directly affect reservoir pool levels and dam flow releases. Pool levels and discharge rates, in turn, directly impact the primary functions of the TVA reservoir system -- flood control, navigation, and power production -- as well as other important functions -- water supplies, recreation, the protection of wildlife and fisheries, and the enhancement of water and environmental quality.

The effects of the occurrence of extreme weather events, such as floods or droughts, under the present climate regime are illustrative of the sensitivity of the TVA reservoir system to climate shifts. Flood-producing storms force the rapid movement of huge volumes of water through the system, generally resulting in the spillage of water and the bypassing of hydroelectric generating facilities with consequent losses in power production. Under flood conditions, flood-prone areas can be inundated resulting in economic losses to urban and agricultural regions.

Conversely, droughts substantially reduce the streamflow throughout the system. Summer full pool levels become impossible to meet in some reservoirs, often resulting in the deterioration of water quality through stagnation, excess algae growth, and lowered assimilative capacity due to reduced dissolved oxygen content. During an extreme drought, water supplies could be threatened, and wildlife and fisheries adversely affected.

The current reservoir operation strategy involves the balancing of daily weather and streamflow variations against seasonal operating goals. These goals are based on 50 years of operating and flood experience determined by the historical annual streamflow cycle. Major changes in the climate regime and streamflow cycle would probably necessitate the development of alternative operational strategies to respond to new weather patterns. If altered operational strategies and policies were insufficient to meet the operating goals of the system, then alternative methodologies would need to be explored. For example, under an extremely wet climate scenario, inadequate reservoir storage could be supplemented by flood control works, such as levees, or modifications to existing dams to increase flood storage capacity. At the same time, new capacity could be added to existing hydropower facilities to take advantage of increased flows. Conversely, a significantly drier climate could mean the construction of additional storage reservoirs, more stringent environmental codes, a greater emphasis on nuclear power, and/or the reduced use of stream flow for cooling purposes at existing fossil plants. It must be emphasized, however, that the frequency and distribution of extreme events is as important as changes in long-term average conditions in determining the overall impact on the TVA system.

Figure 4
Primary Functions of the TVA Reservoir System

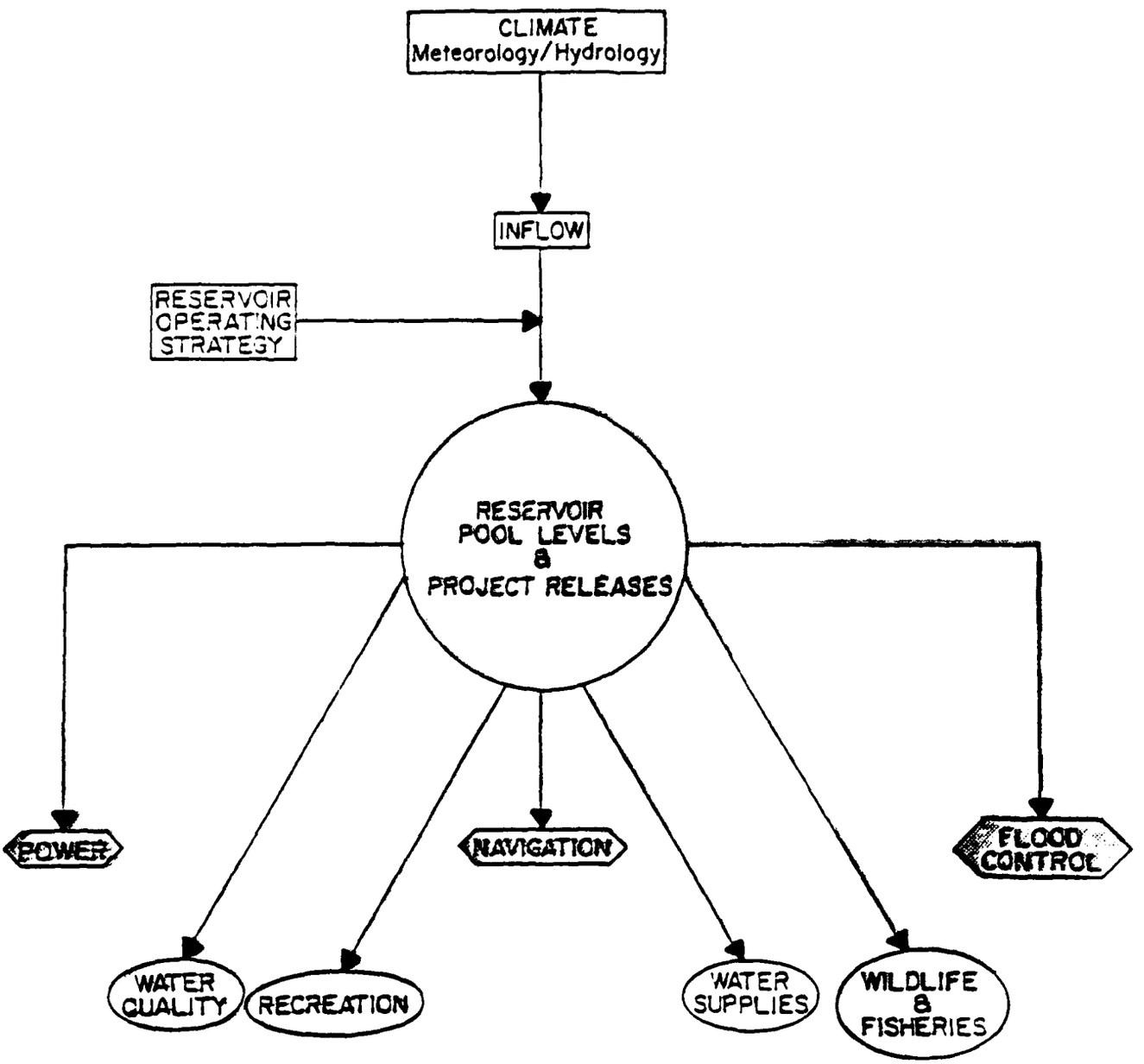

ENG LAB 1988

HYDROLOGIC OVERVIEW OF THE TENNESSEE RIVER BASIN

Historical Precipitation

The TVA region is one of the wetter regions in the United States. Long-term (1890-1986) average annual precipitation in the basin is 130 centimeters (51 inches) per year, although average annual precipitation may vary in the eastern mountainous regions from 254 centimeters (100 inches) to 102 centimeters (40 inches) in more sheltered areas. March is generally the wettest month, while September and October are likely to be the driest.

Hydrologically, the TVA basin can be divided into two distinct regions: the mountainous region to the east of, or above, Chattanooga; and the relatively flatter region to the west of, or below, Chattanooga. While the two regions presently receive approximately the same total annual precipitation, the annual distribution varies. Intense summer storms are more likely to occur in the eastern region, while the western basin generally receives higher precipitation in the winter and spring.

Historical Runoff

Long-term (1903-1986) mean annual runoff in the Tennessee River Basin is 56 centimeters (22 inches). Annual amounts, however, have varied from 28 centimeters (11 inches) in an extremely dry year to 84 centimeters (33 inches) in the wettest year. For the 1951 to 1980 study period, approximately 58 centimeters (23 inches) of mean annual runoff was observed in the Tennessee River Basin. The annual variation in runoff for the historical and study periods is shown in Figure 5. The study period typifies the long-term record; however, it does not incorporate the extremely dry periods during 1904, 1941, 1981, or the current drought beginning in 1984.

The annual distribution of runoff is influenced by rainfall, soil conditions, and evapotranspiration patterns. Runoff is heaviest in the winter and early spring (December-May) when the vegetation is dormant and the ground is saturated. As the growing season commences, infiltration and evapotranspiration increase, and runoff decreases substantially through the summer and early fall.

Figure 5
Annual Runoff in the Tennessee River Basin from 1903-1986

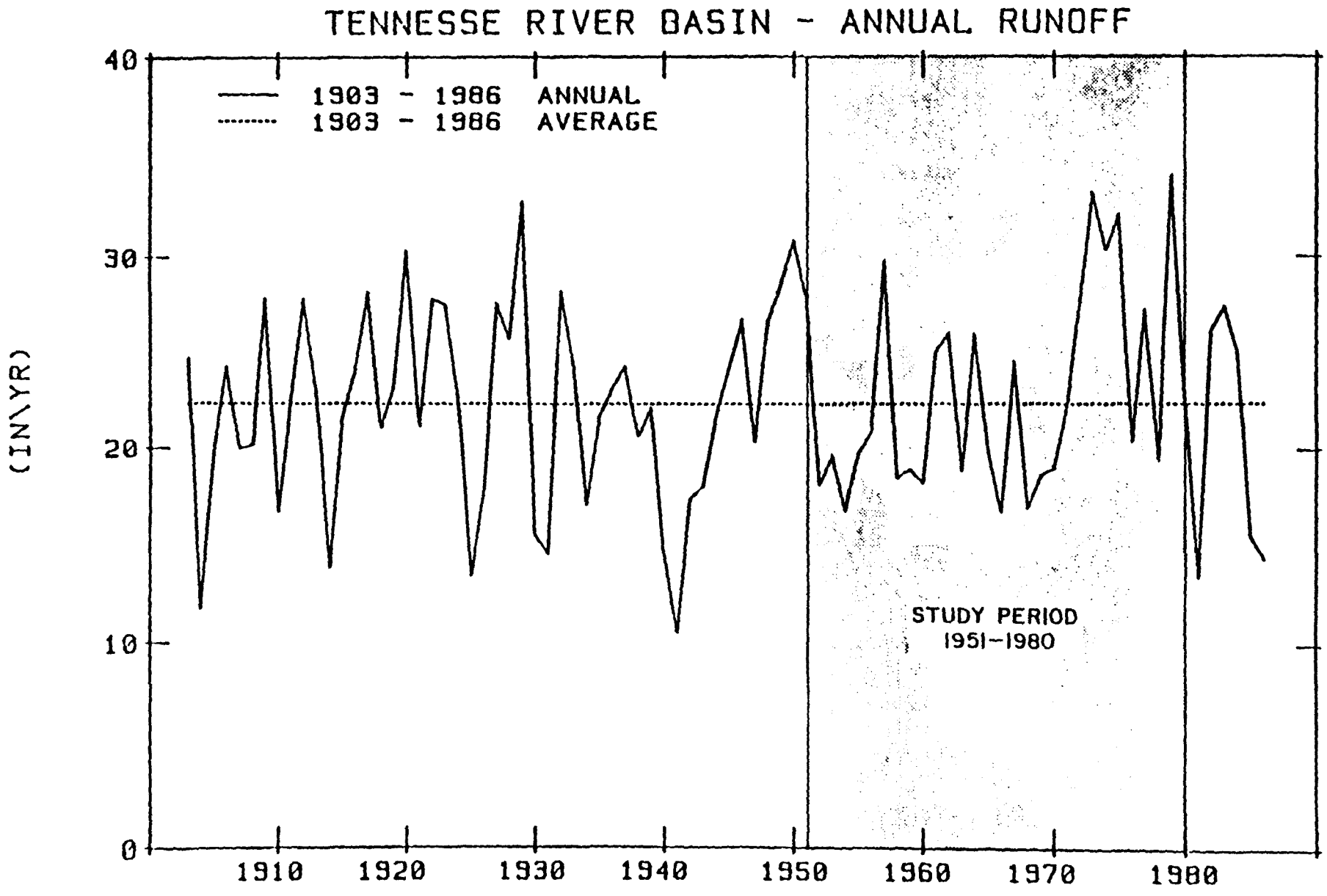

Miller

ENG LAB 1988

CHAPTER 3

METHODOLOGY

THE WEEKLY SCHEDULING MODEL

Background and Development of the Model

The Weekly Scheduling Model (WSM), an operational planning model, was the primary model used to assess climate change impacts on the TVA reservoir system. This model was developed by TVA to simulate long-term, week-to-week variations in water level, discharge, and power production for 42 reservoirs operated within the system. Typical uses of the model include power system scheduling; reservoir operations planning; and assessment of new or modified operating policy. A brief description of WSM follows; more detailed information concerning the development and application of the model has been provided by Shane and Gilbert (1981), Gilbert and Shane (1982), Shane (1984), and Waffel (1985).

The model is based upon a linear programming algorithm, which is used to schedule the reservoir system in weekly time steps. This algorithm selects a weekly reservoir schedule for each reservoir in the TVA system by sequentially satisfying a series of operating objectives in a prescribed order of priority. Each objective is satisfied to the greatest extent possible without causing a deterioration in higher level objectives. Current operating policy, as defined by the TVA Act, is simulated to minimize deviation from historically normal operating levels, subject to reservoir release and level constraints imposed to meet navigation, flood control, water supply, power generation, water quality, and recreational requirements. These operating constraints and long-range guides are summarized in the model as weekly ideal operating bounds on project release, headwater elevation, and power generation. Deviations from current policy are modeled by eliminating individual objectives, changing priorities, or adding special objectives.

For each week, local inflows for the week are specified at all reservoirs. At 23 reservoirs, storage at the end of the week is predetermined based on headwater elevation guides. These 23 prescribed reservoirs are primarily mainstem reservoirs or tributary power projects with minimal storage capacity, which have restricted operating curves. In the remaining 19 reservoirs, which are primarily larger, multipurpose tributary reservoirs, the end-of-the-week storage is simulated based on satisfying model constraints and objectives. The model selects release schedules that satisfy operating objectives to the extent possible while satisfying simple continuity expressions. The 19 storage values computed for the end of the week are used as starting water elevations for the following week and the process is repeated.

Based on the end-of-week storage, reservoir headwater elevations are computed based on mathematical formulas derived for level water surface conditions. Average weekly hydrogeneration, spill, plant capability, and power production costs can be derived from storage and release information. This output data can be interactively plotted to examine the operations at individual reservoirs or to analyze system performance data.

The WSM will model the reservoir system operation for each hydrologic year selected by the user from an unbroken hydrologic record of local inflows. In the TVA system, this record extends from 1903 to the present. Generally, the entire hydrologic record is used for model simulation to develop a range of probable operations based on the historical streamflow pattern. The resulting envelope of curves, referred to as probabilistic pool level forecasts, is used to evaluate weather and/or policy impacts on the operations of a specific reservoir. These curves are described in the List of Abbreviations, Symbols, and Definitions.

Application of the Model

A primary input into the WSM is historical local flow into each reservoir in the TVA system. Local inflows result from unregulated overland and tributary flows into each project. It was assumed that changes in runoff

are directly proportional to changes in local flows. Consequently, in the application of the WSM, monthly ratios ($2xCO_2$/CONTROL) for surface runoff provided by EPA for two climate scenarios were used directly to adjust historical local inflows into the TVA system for the 30-year study period (1951-1980). As dictated by EPA, it was also assumed that the monthly ratios applied equally to each week within a month in the WSM.

Results of the WSM are presented for a base case and the two climate scenarios. Historical inflows for the study period are used for the base case, while appropriately adjusted inflows are used for the climate scenario runs. Due to the integrated management of the TVA reservoir system, the model must be applied to the entire system.

In the application of the WSM it was also assumed that existing guide curves, or normal operations, defined the target or preferred operating conditions for each reservoir. Furthermore, the set of constraints used with the WSM were based upon current operating policy.

SUPPLEMENTARY MODELS

Supplementary models to the WSM were used to perform power cost analysis and to assess flooding potential at Chattanooga, an urban area with a high damage potential. In the power cost analysis, results of the WSM were used to determine average weekly peak and offpeak hydrogeneration cost differences for the base case and climate change scenario using projected cost data for 1988.

Estimated changes in flood stages at Chattanooga were determined using a model (FLDRT) developed to estimate weekly tributary release constraints for the WSM. The model is not an operational flood routing model used for day-to-day operations. The model uses historical daily average inflows (unregulated local inflows to Ft. Loudoun-Tellico, Watts Bar, and Chickamauga, the three main river reservoirs above Chattanooga), as well as fixed generating rule curves and balanced storage principles, to estimate how much tributary release from seven upstream tributaries could be accepted during these historical events without exceeding flood stage criteria at Chattanooga. These constraints are then used in the WSM for the long-term simulations, and the WSM observes these constraints to the extent possible without violating higher priority constraints (e.g., the WSM will not fill tributary reservoirs to the top of gates to avoid the inception of minor flood damage at Chattanooga). After the WSM simulation has been performed, the resulting tributary releases for the historical flood events can be routed back through the FLDRT model to determine what the resulting peak flood stage at Chattanooga would be.

For both the GISS and GISS Inverse scenarios, historical runoffs were multiplied by the ratios referenced earlier. Whether these "average" ratios are applicable for larger flood events is still a matter of speculation that cannot be adequately addressed within the scope of this study. For the GISS scenario, it is possible that just the increase in unregulated main river local inflows is sufficient to cause appreciable increases in flood stage at Chattanooga as compared to base case events. Since the tributaries are also receiving increased inflow, there are occasions when they cannot store all the extra runoff, so they are forced to release water to the main river reservoirs, which compounds the problem and increases flood damage even more.

CLIMATE CHANGE SCENARIOS

Data for the climate change scenarios were generated by NASA's Goddard Institute for Space Studies (GISS) general circulation model. The model simulates the physical processes of the atmosphere and oceans to estimate global climate. The GISS model has global coverage on a 10° longitude by 8° latitude grid. The GISS data provide monthly average (taken over a 10-year period) values for key climate parameters, including surface temperature, precipitation, runoff, humidity, solar radiation, cloud cover, and wind speed. For each parameter, monthly average values for a control run, a $2xCO_2$ run and the ratio ($2xCO_2$/control) were provided. The control run was based on a $1xCO_2$ level of 315 mg/L, which was valid around 1958. The $2xCO_2$ levels represent the endpoint effects of a doubling in CO_2 atmospheric concentrations (630 mg/L). The computed

ratios, which were applied to the TVA historic data for the study period 1951-1980, reflect potential climate changes on climate variables due to this doubling of CO_2 concentrations.

The TVA region extends from approximately 34°-37°N latitude and from 81°-89°W longitude. Consequently, the TVA region falls within two of the GISS grids, which are defined by 35.22°N latitude-90°W longitude and by 35.22°N latitude-80°W longitude. The grid point at 35.22°N defines an area extending from 31.30°N to 39.13°N, which encompasses the entire TVA region in the north-south direction. In the east-west direction, the 80°W grid point defines a region extending from 75° to 85°W, which essentially includes the portion of the Tennessee River Valley east of Chattanooga. The 90°W grid point, extending from 85° to 95°W, includes the portion of the Valley west of Chattanooga. This east-west division at Chattanooga closely parallels the two major hydrologic units in the Tennessee Valley.

In interpreting the GISS data it is important to note that the grid sizes are large and incorporate a wide range of topography and local climate variation. The GCM model also has a relatively smooth terrain and does not account for sharp hills and mountains like the real earth. Furthermore, while the 90°W grid has 100% land coverage, the 80°W grid extends into the Atlantic Ocean and has only 76% land coverage.

GISS Scenario. The GISS scenario, provided by EPA, simulates a warmer and wetter climate for the Tennessee Valley region. Based on the given ratios for temperature, precipitation and runoff, the effects of the GISS scenario data on TVA historical data are presented in Figures 6 and 7. In the eastern portion of the Valley (80°W), the GISS model predicts a 4.0°C (7.1°F) increase in average annual temperature. Monthly temperature increases range from 2.1°C (3.7°F) in August to 6.2°C (11.2°F) in March. Precipitation increases in the winter through summer months, with a slight decrease occurring in the fall. The greatest monthly precipitation increases occur in July (41%) and in February and March (24%), while the largest decrease (-25%) occurs in November. Average annual precipitation increases by 12% in the eastern basin.

Runoff follows a similar pattern in the eastern region, with a general increase in the winter through summer months and decrease in the fall. The largest increase in runoff occurs in March (73%), which coincides with the traditional flood season. The largest decrease in runoff occurs in November (-28%), currently one of the driest times of the year. The net effect in the eastern basin of the GISS runoff ratios is to exaggerate peak flows during the wettest period of the year and further decrease flows during the driest period. Average annual runoff increases in the eastern basin by 31%. These effects are illustrated in Figure 8, which compares median natural streamflows for current and postulated $2xCO_2$ conditions. The flows at Cherokee Dam are indicative of the effects on the Upper Holston River Basin, while Chickamauga Dam illustrates the effects on the entire eastern basin.

West of Chattanooga (90°W), the monthly ratios reveal some variability and more extreme ratios. On a seasonal basis, the general trends in the west are similar, though less pronounced, to those for the eastern valley. The GISS model predicts an average annual temperature increase of 5.3°C (9.5°F). Monthly temperature increases range from 3.5°C (6.3°F) in May to 8.5°C (15.3°F) in November. Minimal change in the average annual precipitation is predicted in the western basin. On a seasonal basis, precipitation increases through the spring and summer, and slightly decreases in the fall and winter. Average annual runoff in the western basin increases by 10%. The greatest monthly increases in runoff occur in February (126%) and July (148%), while the largest decreases occur in October (-25%) and November (-27%).

Effects of the GISS runoff ratios on median natural flows at Kentucky Dam are presented in Figure 8. As Kentucky Dam is located at the mouth of the Tennessee River, these flows reflect the integrated influence of the GISS data on the entire Tennessee River Basin. Increased peak flows in the early spring and decreased peak flows in the fall result from the influence of GISS data in the eastern basin, while the variability in the data results from the influence of the GISS data in the western basin.

GISS Inverse Scenario. The original intention of this project was to evaluate potential impacts of two different climate scenarios based on runoff data provided by the EPA. The runoff data for the second scenario, generated by the Princeton University Geophysical Fluid Dynamics Laboratory (GFDL) global circulation model, appeared

Figure 6

Effect of GISS Scenario on Average Surface Temperature and Precipitation in the Western (90°W) and Eastern (80°W) Basins

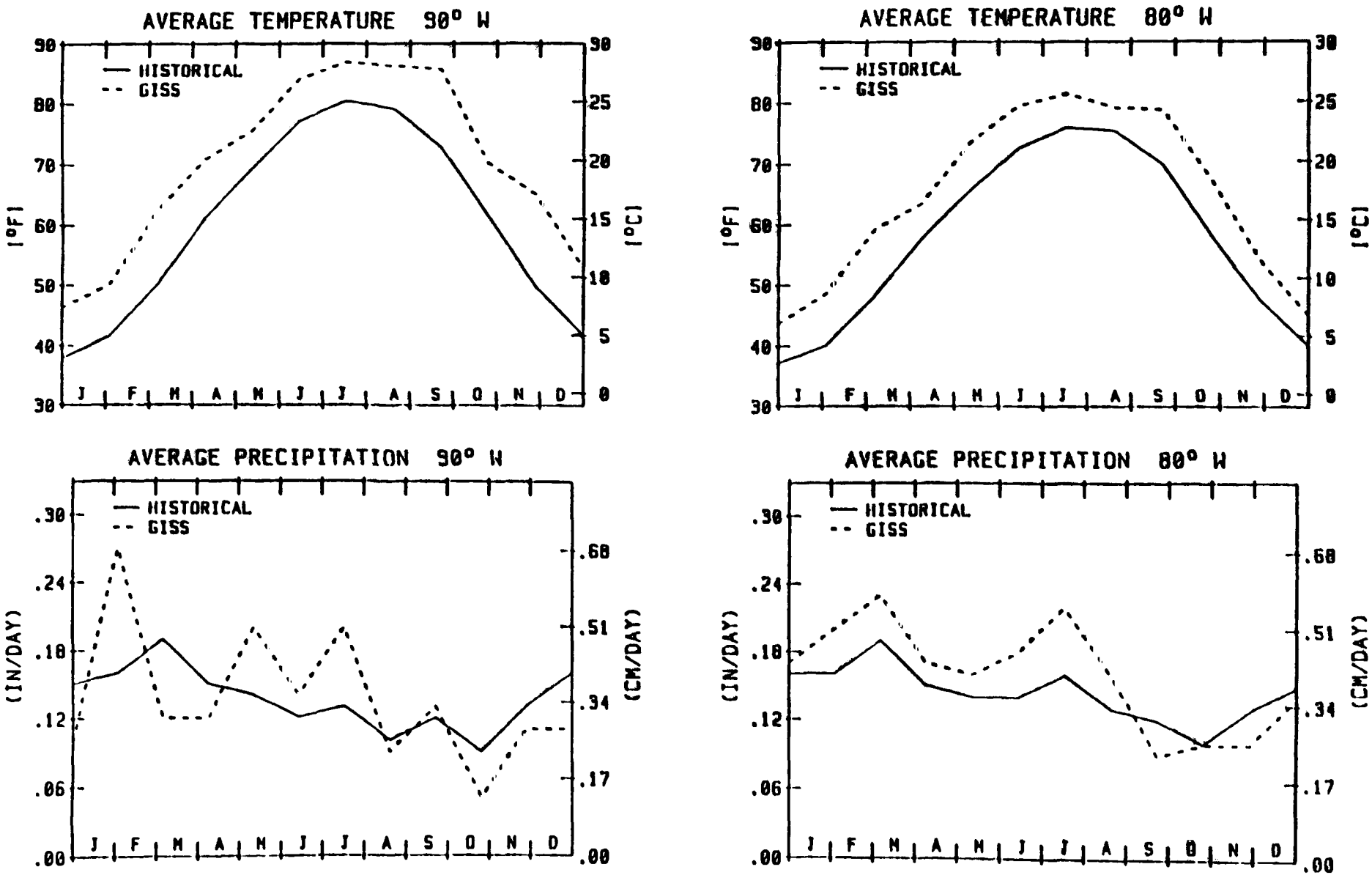

Miller

ENG LAB 1988

Figure 7
Effect of GISS Scenarios on Average Runoff in the Western (90°W) and Eastern (80°W) Basins

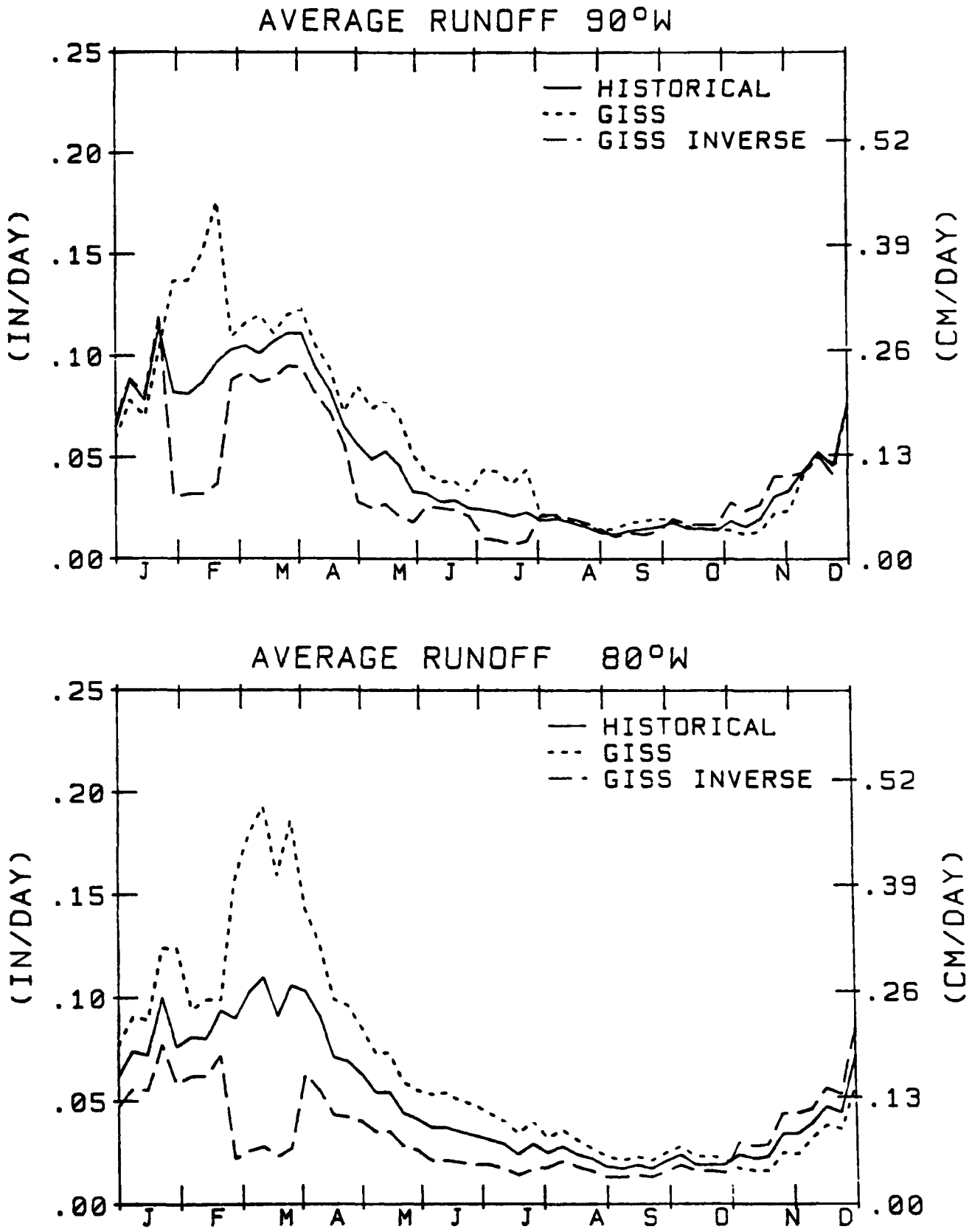

ENG LAB 1988

Figure 8
Effect of GISS Scenarios on Median Natural Streamflow
at Cherokee, Chickamauga and Kentucky Dams

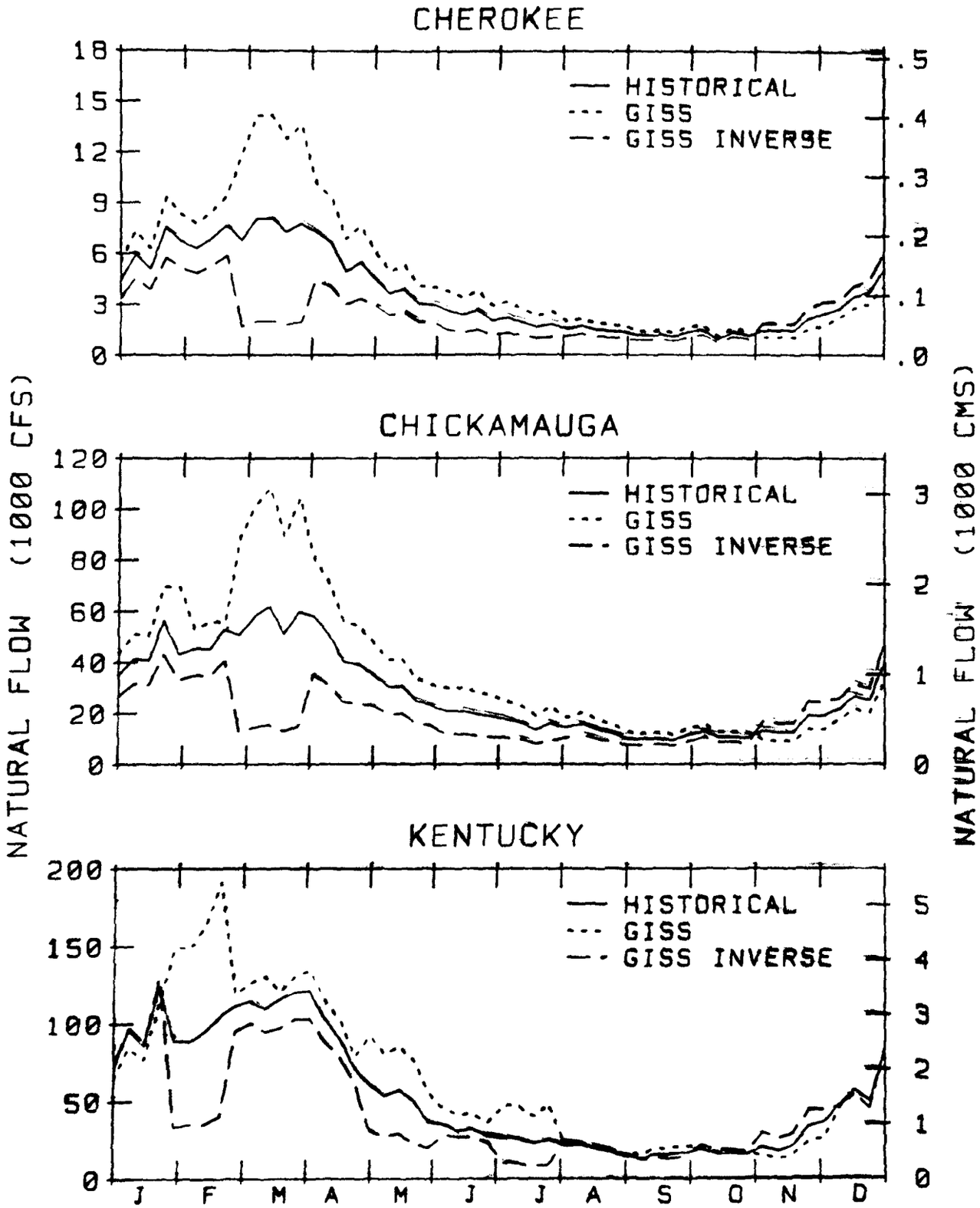

ENG LAB 1988

nreasonable for the TVA region. Although ample precipitation was apparent throughout the year, the runoff values indicated up to seven months of zero runoff in both the control and $2xCO_2$ model runs.

Experiments with the GISS $2xCO_2$ model indicate that predicted water availability in the United States is highly variable and influenced by model sensitivity, model resolution, and sea surface temperature gradient (Rind, 1988). Consequently, to meet EPA project objectives and time limitations, EPA and the model developers recommended utilizing the inverse of the GISS runoff values. For example, if GISS runoff values indicated a 24% increase in runoff in January for the eastern basin, then GISS Inverse runoff ratios would be computed on the basis of a 24% decrease in runoff. While this approach does not show impacts of a particular model run, the runoff values are within the range of the sensitivity analysis of the GISS model. Furthermore, the approach illustrates the potential effects of a warmer and significantly drier climate, which has been predicted by other GCM and hydrologic models used in the southeast (Hains, 1988). The two scenarios together, therefore, represent the full spectrum of impacts from the extremes of a wetter vs. drier climate.

The runoff ratios for the GISS Inverse scenario for the eastern and western basins are presented in Table 2. In the eastern basin, runoff decreases from January through October, with the largest decrease (-75%) occurring in March. Runoff increases by 18 and 28% during November and December, respectively. The effect of these changes in the eastern basin on median natural streamflow are illustrated in Figure 8 for Chickamauga Reservoir. Flows during March, the traditional flood season, are significantly reduced. Flows during November and the beginning of December, while somewhat increased, remain at relatively low levels. Under the GISS Inverse scenario, the peak flows are reduced over the base case and shifted from the winter through spring to the winter. The net effect of GISS Inverse in the eastern basin is to produce relatively low inflows throughout the year.

In the western basin, changes in runoff are more variable. The largest decreases in runoff (-100%) occur in February and July, resulting in no runoff during those months. The greatest increase in runoff (52%) occurs in March. The impact of these changes on median natural streamflow at Kentucky Reservoir, the last reservoir in the TVA system, is shown in Figure 8. Flows are reduced during February, May, and July; are similar to the base case from August through October; and are slightly increased in November. Peak flows, which are reduced from the base case, occur in January and from March through April. The overall effect is to reduce runoff and natural streamflow for most of the year.

LIMITATIONS OF THE METHODOLOGY

Results of the WSM provide an excellent overview of the response of the TVA reservoir system, as an integrated system, to changes in historical inflow or runoff. As noted previously, however, the application of the model was based upon use of existing guide curves and operating policies. Furthermore, analysis of the results of the WSM were based on current water use levels and seasonal patterns of power demand. In the event of major climate shifts, current operating guides would most probably be adjusted to reflect changes in weather patterns; model constraints would probably be modified to reflect changes in operating policies and priorities; and temperature changes would alter water use patterns and power demands.

In this scoping level study, which was conducted to assess sensitivity of TVA operations to climate change, GCM runoff ratios provided by EPA were used directly to adjust historical inflow data in the WSM. This methodology assumes that changes in runoff are directly proportional to changes in local inflow. This approach is reasonable to assess general trends in a large, complex system such as the TVA reservoir system. However, in a more detailed analysis of climate impacts, precipitation, temperature, and other climate variables should be used to generate more site-specific runoff data using hydrologic models. Furthermore, groundwater effects, which were not addressed in this study, should be evaluated.

In the application of the monthly runoff ratios there is also an implicit assumption that the distribution of historical runoff remains the same. It is highly probable that, in a major climate shift, the distribution and frequency of precipitation and runoff would be altered. The operation of a reservoir system such as TVA is very

Table 2

Runoff Ratios for the GISS Scenarios

WESTERN BASIN RUNOFF
90°W LONGITUDE - 35.22°N LATITUDE

	GISS		GISS INVERSE	
	RATIO	% DIFFERENCE	RATIO	% DIFFERENCE
JAN	0.600	-40.0	1.400	40.0
FEB	2.264	126.4	0.000	-100.0
MAR	0.482	-51.8	1.518	51.8
APR	0.850	-15.0	1.150	15.0
MAY	1.723	72.3	0.277	-72.3
JUN	1.060	6.0	0.940	-6.0
JUL	2.477	147.7	0.000	-100.0
AUG	0.692	-30.8	1.308	30.8
SEP	1.299	29.9	0.701	-29.9
OCT	0.748	-25.2	1.252	25.2
NOV	0.727	-27.3	1.273	27.3
DEC	1.171	17.1	0.829	-17.1

EASTERN BASIN RUNOFF
80°W LONGITUDE - 35.22°N LATITUDE

	GISS		GISS INVERSE	
	RATIO	% DIFFERENCE	RATIO	% DIFFERENCE
JAN	1.237	23.7	0.763	-23.7
FEB	1.233	23.3	0.767	-23.3
MAR	1.750	75.0	0.250	-75.0
APR	1.392	39.2	0.608	-39.2
MAY	1.353	35.3	0.647	-35.3
JUN	1.436	43.6	0.564	-43.6
JUL	1.407	40.7	0.593	-40.7
AUG	1.272	27.2	0.728	-27.2
SEP	1.228	22.8	0.772	-22.8
OCT	1.186	18.6	0.814	-18.6
NOV	0.719	-28.1	1.281	28.1
DEC	0.813	-18.7	1.187	18.7

sensitive to the spatial and temporal distribution of precipitation and runoff events, particularly under extreme drought or flood conditions. For example, in regard to flood control and dam safety issues, an evenly distributed increase in runoff for each week of the month is easier to accommodate than a significant increase concentrated in a short duration, such as the 3- or 9-day critical flood period. Similarly, it is easier to manage large storm volumes emptied over multipurpose tributary reservoirs with significant flood storage capacity than the same volume emptied over mainstem reservoirs with more limited storage capacity. These types of issues are beyond the scope of this study.

Finally, direct use of the GISS runoff ratios implies some degree of confidence in general circulation model predictions of climate variables. These models, which are based on the fundamental physical laws governing conservation of mass, momentum, and energy, incorporate a great range of time and space scales and must approximate numerous, complex physical processes on a global basis. At present, the available general circulation models provide a reasonable qualitative representation of large-scale climate features, but are less reliable in representing the detailed regional and seasonal evolution of climate variables. Temperatures can be predicted with a greater degree of confidence than more complex variables such as rainfall or runoff. The current generation of general circulation models are useful for predicting perturbations to long-term average conditions; they cannot, however, predict detailed weather 50 to 100 years in the future (MacCracken, 1986; Grotch, 1988).

Some of the problems associated with using general circulation model results on a regional basis are evident in the western basin (90°W) runoff data. The monthly ratios are highly variable and may suggest oscillations in the GISS model for that grid point. In the TVA region, all of the large multipurpose tributary reservoirs are located in the eastern basin (80°W) above Chattanooga, where the runoff ratios appear to be more reasonable. These tributary reservoirs have the greatest flexibility in operation and display the largest impacts to the climate change scenarios. The eastern basin reservoirs also have the most direct impact on flood control at Chattanooga. Consequently, in this analysis, the variability in the western basin runoff data had minimal effect on the overall results and conclusions of the project. These problems emphasize, however, that this report represents a "first cut" assessment of the sensitivity of the TVA reservoir system to climate change and does not attempt to predict the future climate for the Tennessee Valley.

CHAPTER 4

IMPACTS OF CLIMATE CHANGE ON THE TVA RESERVOIR SYSTEM

RESULTS OF THE WEEKLY SCHEDULING MODEL

The Weekly Scheduling Model (WSM) was used to evaluate TVA systemwide impacts on reservoir operations due to changes in runoff predicted by the GISS and GISS Inverse scenarios. Model application and methodology are explained in Chapter 3, while the results of the model runs are described below.

Reservoir Operations

In the WSM, operations on the mainstem reservoirs and single-purpose projects are restricted and operated according to fixed guide curves. Operations at the remaining 19 multipurpose tributary reservoirs are simulated by the WSM to account for system constraints and runoff patterns, using normal operating curves as target elevations. Operations at these 19 tributary reservoirs, however, are flexible and consequently reveal the largest impacts due to climate change.

For illustrative purposes, the results of the GISS scenarios at Norris Reservoir are presented in the probabilistic pool level forecast in Figure 9. Norris Reservoir, a large tributary storage reservoir located on the Clinch River in eastern Tennessee, is typical of the multipurpose tributary reservoirs in the Tennessee Valley.

GISS Scenario. Runoff predicted by the GISS scenario results in higher projected elevations at Norris Reservoir for all probabilistic plots for most of the year. In the eastern grid (80°W), although the GISS scenario predicts slightly decreased runoff in November and December, the increased runoff and subsequent storage earlier in the year enable Norris to meet its discharge requirements and still maintain slightly higher elevations during the late fall.

The projected median curve is higher throughout the year and at times more than 3 meters (10 feet) higher than observed in the base case. It is also significant that the projected median elevations remain at or near the normal maximum level providing full summer pool levels from the beginning of April into July. The upper envelope curve, showing maximum elevations, indicates the reservoir will often be above the normal maximum level during the traditional flood season and during very wet periods will fill to its total capacity. These higher maximum levels from February through May greatly increase the probability of spill at Norris and downstream projects, with likely flooding and possible dam safety implications.

The lower envelope curve indicates that minimum elevations at Norris generally will be higher, by up to 3 meters (10 feet), under the GISS scenario. Only during November and December, when GISS predicts decreased runoff in the eastern basin, are the minimum elevations similar for the base and climate change scenario. The significant drops in minimum elevations in April, noted in both the base and GISS scenarios, are caused by the annual spring filling of mainstem reservoirs from tributary flows.

The results at the other multipurpose tributary reservoirs, most of which lie east of Chattanooga in the 80°W grid, are similar in nature. In general, the higher runoff predicted by GISS in the winter through summer months in this area results in the following:

- Higher median projected reservoir elevations for most of the year;
- Extended operations at higher levels during the summer, with median elevations often at or near normal maximum levels;

Figure 9

Probabilistic Pool Level Forecasts for Norris Reservoir

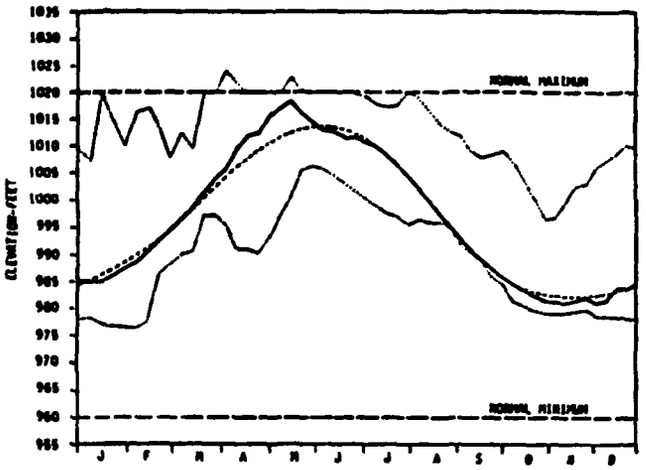

Base Case

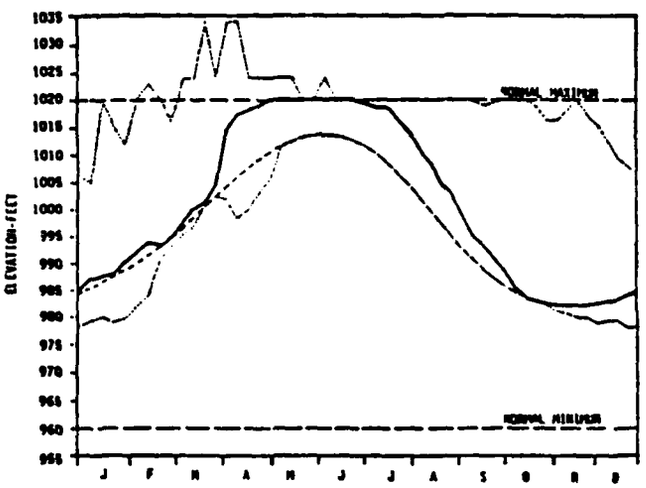

GISS Scenario

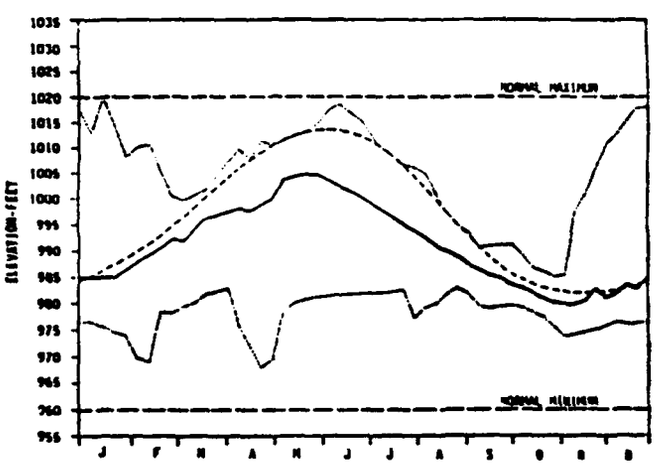

GISS Inverse Scenario

LEGEND:

—— Median Projection - - - Normal Operations ····Upper & Lower Envelope

ENG LAB 1988

Higher reservoir elevations in the fall, where the additional water can be used to satisfy downstream minimum flow requirements;

- Higher maximum elevations, particularly during the traditional flood season, resulting in increased probability of spill at tributary and mainstem projects; and

- Higher minimum reservoir elevations throughout most of the year.

As indicated by the generally higher reservoir elevations, the decreased runoff predicted in the eastern portion of the basin in the late fall is more than compensated for by the increased runoff and storage earlier in the year. The variable runoff predicted for the western basin does not appear to significantly affect the eastern tributary reservoirs.

GISS Inverse Scenario. Runoff predicted by the GISS Inverse scenario results in lower projected reservoir elevations for Norris Reservoir, as illustrated in Figure 9. The probabilistic plots indicate reservoir levels would be lower throughout the year, except during late fall and early winter when the GISS Inverse scenario predicts increased runoff.

The projected median curve is lower most of the year and at times is approximately 5 meters (15 feet) lower than observed in the base case. From November into January, the GISS Inverse median curve is projected to be approximately the same as the base case. The upper envelope indicates that Norris did not exceed its normal maximum pool level during this analysis and often approached the base case normal levels. During late fall and early winter, the maximum curve is predicted to exceed base case levels, at times up to 3 meters (9 feet). The lower envelope curve indicates that minimum elevations at Norris would be lower throughout the year, by up to 8 meters (25 feet), under the GISS Inverse scenario.

The results at the other tributary reservoirs are similar in nature. The runoff into these reservoirs is predicted to be lower from January to November and results in the following:

- Lower projected median reservoir elevations for most of the year;

- Maximum reservoir elevations never exceeding normal maximum pool levels, often approaching current normal levels; and

- Much lower minimum elevations, with most reservoirs being drawn to or below normal minimum pool levels.

In this analysis, Norris Reservoir was not drawn to minimum pool levels because of constraints in the WSM. In actual operation it could also be drawn to its normal minimum level under this scenario.

Flooding at Chattanooga

GISS Scenario. Under the GISS scenario, during exceptionally wet years, storage at the tributary reservoirs is inadequate during the flood season to provide the present level of control, and spillage from dams is likely to occur. During these flood periods, local flows into the mainstem reservoirs would also be increased, resulting in an increased probability of flooding at Chattanooga, Tennessee, a major city on the Tennessee River with the greatest urban damage potential in the Valley. Under present conditions, the protection of Chattanooga against excessive flooding is a major priority of the flood control system in the eastern basin. There is currently about a 20% annual chance of minor flood damage and a 5% chance of substantial flood damage at Chattanooga.

To assess the increased flood potential at Chattanooga, estimated daily regulated inflows from the upstream reservoirs, as well as historical daily unregulated local inflows into the mainstem reservoirs Ft. Loudoun-Tellico, Watts Bar, and Chickamauga, were routed past Chattanooga for both the base case and climate change scenarios (see Chapter 3 for more detailed methodology). The results of this analysis are summarized in Figure 10 and Table 3. These results, which are based on simplified models, show relative effects between the current base case and the climate change scenarios, and may not agree exactly with historical flood stages.*

The flow duration curve presented in Figure 10 indicates that under the GISS climate change scenario, large-magnitude flows would occur more frequently near Chattanooga on the Tennessee River at Chickamauga Dam. The figure can also be interpreted as implying that flow magnitudes increase at each duration.

The potential effects of these increased flow magnitudes on river stages at Chattanooga are summarized in Table 3 in a comparison of estimated flood peaks for five historic floods. Floods exceeding a 9.1 meters (30 feet) stage cause serious flood damage in the city of Chattanooga. At a 7.6 meters (25 feet) flood stage, barge terminals and docking facilities are flooded, resulting in some economic losses. Under the climate change scenario, flood stages are increased for four of these floods. During the estimated historic floods, river stages, though above 7.6 meters (25 feet), were still less than 9.1 meters (30 feet) and were contained within the banks of the Tennessee River. Under the GISS scenario, during two of these floods, river stages exceed 9.1 meters (30 feet) and severe flooding would occur in Chattanooga.

The most dramatic effect occurs with the 1973 March flood where estimated historic river peak stages at Chattanooga would increase from 9.0 to 17.1 meters (29.6 to 56.3 feet) and peak flows from 5,093 cms (181,900 cfs) to 14,700 cms (525,500 cfs). This represents an 8.1 meter (26.7 foot) increase in stage and 9,621 cms (343,600 cfs) increase in flow. The largest runoff ratio for the GISS model occurs in March, which in this instance coincides with a major flood event. This estimated GISS flood is greater than the largest recorded flood in Chattanooga, which occurred in 1867 with a peak flow of 12,850 cms (459,000 cfs). It should also be noted that the maximum probable flood (regulated) for Chattanooga under current climate conditions has an estimated flow of 17,000 cms (610,000 cfs), which is only 16% greater than the 14,700 cms (525,500 cfs) flow estimated with the GISS scenario. A map of Chattanooga showing the maximum probable floodplain is presented in Figure 11.

Based on a flood damage curve for Chattanooga, the following shows the range of potential damages:

Potential Flood Damage at Chattanooga

Stage (feet)	Estimated Damage (1988 dollars)
34	> 1 million
40	~100 million
56	~1 billion

Consequently, for the two largest floods shown in Table 3, damages to Chattanooga, in 1984 dollars, could range from slightly under $100 million to $1 billion.

*Actual peak flood stage for the March 1973 flood exceeded 9.1 meters (30 feet) and caused serious damage in Chattanooga.

Figure 10

Flow Duration Curves for the Tennessee River at Chickamauga Dam

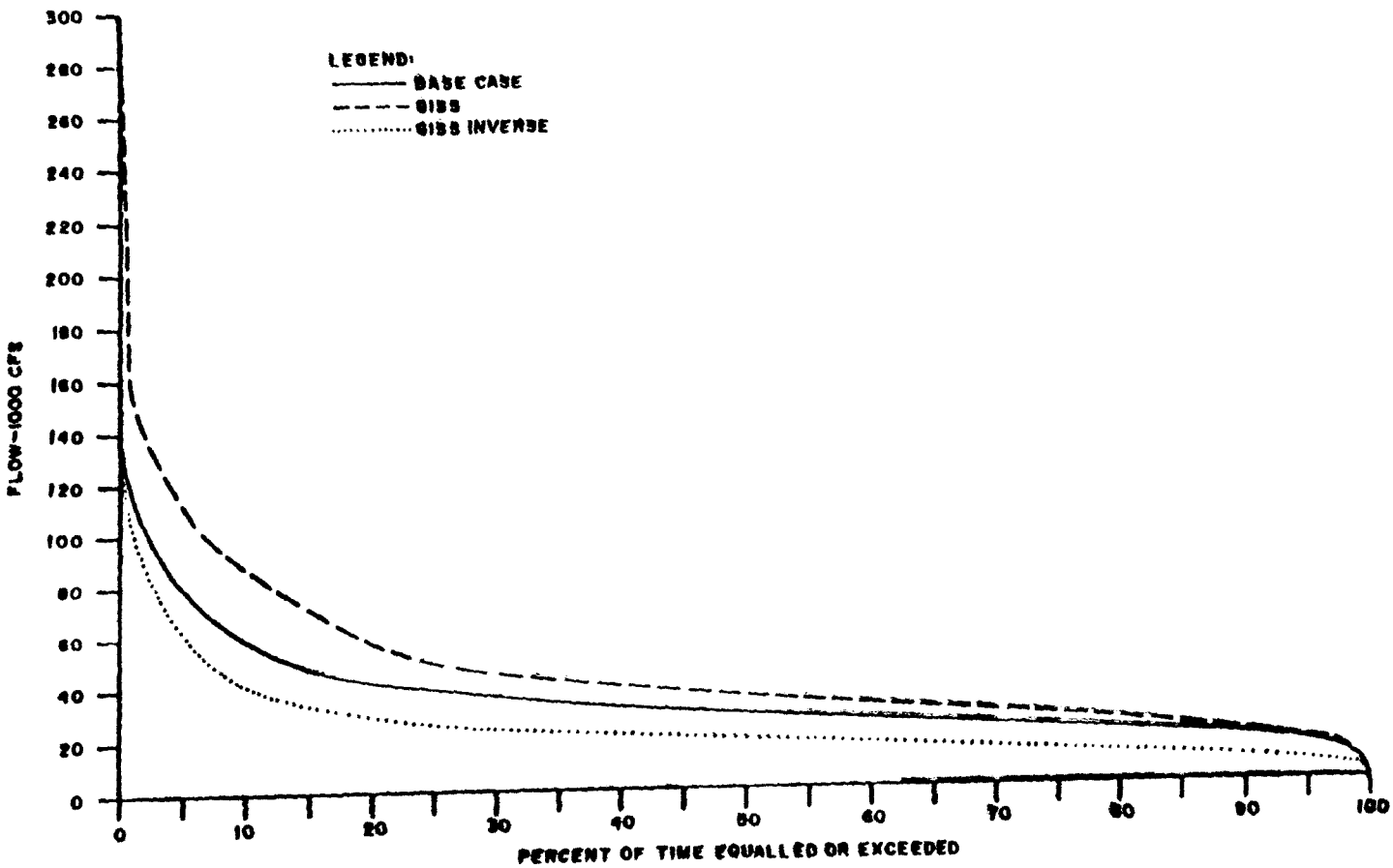

ENG LAB 1988

Table 3
Potential Effects of GISS Scenarios on Flood Stages at Chattanooga

YEAR	DATE	ESTIMATED* HISTORIC FLOOD		ESTIMATED* GISS FLOOD		ESTIMATED CHANGE DUE TO GISS CLIMATE CHANGE		ESTIMATED* GISS INVERSE FLOOD		ESTIMATED CHANGE DUE TO GISS INVERSE CLIMATE CHANGE	
		STAGE** (FT)	FLOW (1000 cfs)	STAGE** (FT)	FLOW (1000 cfs)	STAGE** (FT)	FLOW (1000 cfs)	STAGE** (FT)	FLOW (1000 cfs)	STAGE** (FT)	FLOW (1000 cfs)
1912	APR 2-APR 8	26.9	155.0	29.4	180.2	2.5	25.2	18.6	76.4	-8.3	-78.6
1936	MAR 26-APR 8	26.8	154.5	26.9	155.0	0.1	0.5	18.6	77.2	-8.2	-77.3
1957	JAN 29-FEB 11	26.9	155.0	26.9	155.0	0.0	0.0	26.9	155.0	0.0	0.0
1973	MAR 12-MAR 18	29.6	181.9	56.3	525.5	26.7	343.6	20.2	92.1	-9.4	-89.8
1975	MAR 26-APR 1	26.9	155.0	46.1	384.5	19.2	229.5	16.0	52.1	-10.9	-102.9

*Flood stage is computed by a daily model and is intended for order of magnitude comparative purposes only. The three main river pools are assumed to be at the bottom of their winter operating zones at the beginning of each event.

**Bank overflows at 30-ft stage.
Damage to docking facilities at 25-ft stage.

Figure 11

Maximum Probable and 1867 Floodplains in the Chattanooga Area

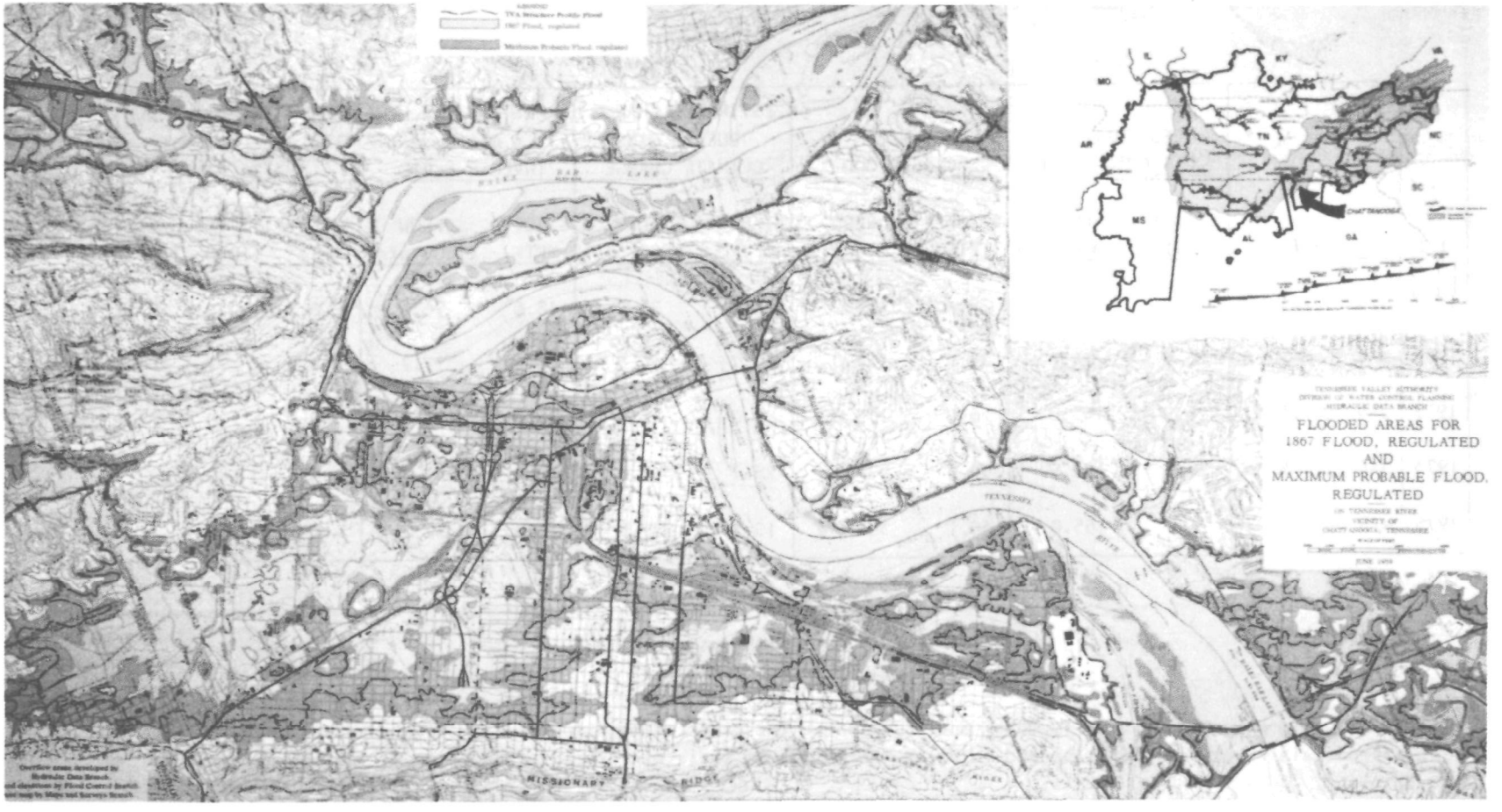

GISS Inverse Scenario. Under this climate change, even during wet periods, flood storage in the tributary reservoirs and local inflows into the main stem are reduced sufficiently to greatly decrease the probability of flooding at Chattanooga. The flow duration curve presented in Figure 10 indicates that the magnitude of flows at each duration would decrease at Chickamauga Dam near Chattanooga.

The potential effects of these decreased flows on river stages at Chattanooga are summarized in Table 3. Under this scenario, flood stages would be reduced for four of the five simulated floods, with the other flood having the same stage as the estimated historic flood. The estimated stages for all five of these simulated GISS Inverse floods are below 30 feet, the stage where serious flood damage begins.

Power Operations

GISS Scenario. For the GISS scenario, a major impact of the increased runoff predicted for most of the year is an increase in system hydropower generation. As indicated in Figure 12, the average weekly total system generation would increase substantially from January through October, and decrease slightly in November and early December. Weekly average offpeak and peak generation follow a similar pattern, except peak generation also declines slightly in February. Maximum system generation also increases substantially throughout most of the year, approaching system capability from January through June.

The results of the power cost analysis indicate that the enhancement in system generation under the GISS scenario represents an average annual energy gain of 16%, or approximately 3,100,000 MWh (3,100 gigawatt hours (GWh)). This includes an increase of 503 GWh during peak hours and 2,630 GWh during offpeak hours. This energy gain produces an average annual power benefit of about $54.7 million in 1988 dollars with $11.4 million attributable to peak hour generation increases and $43.3 million to offpeak generation increases. Each year of modeled hydrology experienced a power benefit, ranging from a low of $35.8 million for 1975 hydrology to a high of $66.1 million for 1976.

Although the GISS scenario has positive effects on system power operations, the increases in generation would have been greater if the mainstem projects were able to utilize more of the predicted flows for power generation. During the winter and spring, the GISS flows often exceed the turbine discharge capacities of the mainstem projects; therefore, the excess flows cannot be used for power production. The increased spill volume and tailwater levels also decrease the operating head and therefore the power output. Increased spill frequency also affects the operating flexibility of the mainstem projects, causing more operation at plant capacity. This decreases the usefulness of these projects to satisfy peak load demands.

GISS Inverse Scenario. The decreased runoff predicted for this scenario results in a decrease in system hydropower generation. As indicated in Figure 12, the average weekly total system generation would decrease substantially from January through November. Weekly average offpeak and peak generation follow a similar pattern. It should be noted that a substantial loss in dependable hydrosystem capacity also occurred in this scenario because of the reduced inflows and reduced operating heads. Expected seasonal capacity losses were observed for virtually all years, with summer losses about four times higher than winter losses. Summer capacity losses reached more than 1,700 MW for 1966 hydrology.

The results of the power cost analysis for this scenario indicate that the reduced system generation represents an average annual energy loss of approximately 4,697,000 MWh (4,697 GWh), or 24%. This includes a decrease of 1,980 GWh during peak hours and 2,717 GWh during offpeak hours. These decreases in energy production result in benefit losses of $87.2 million in 1988 dollars with $42.9 million attributable to peak generation losses and $44.3 million to offpeak generation losses. Each year of modeled hydrology experienced a loss of power benefit, ranging from a loss of $69.1 million for 1957 hydrology to a high of $106.8 million for 1975 hydrology.

Figure 12
Climate Change Impacts on System Generation

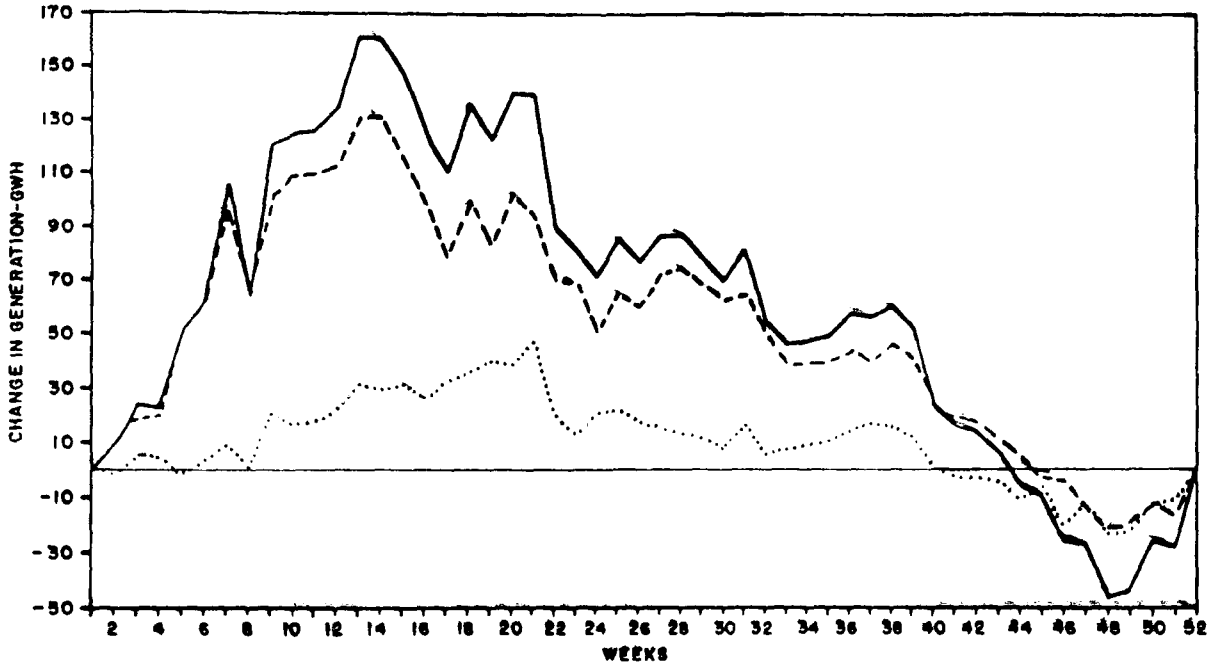

GISS

LEGEND:
PEAK — OFFPEAK — TOTAL

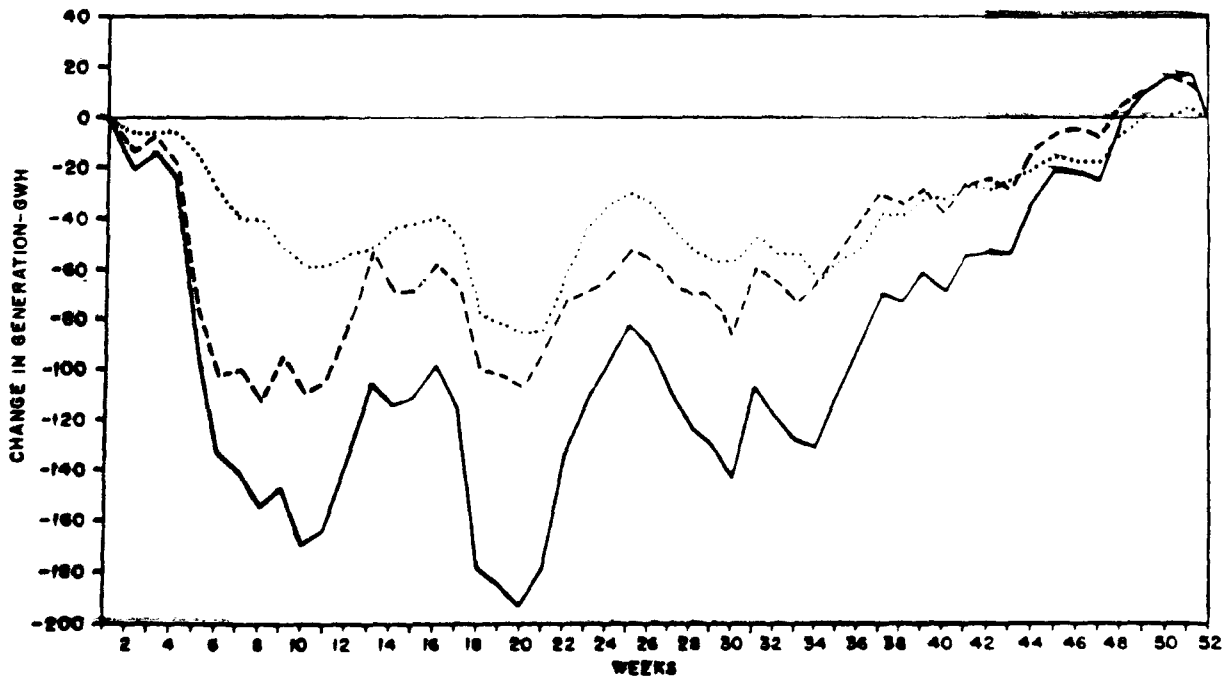

GISS INVERSE

IMPLICATIONS FOR TVA SYSTEM OPERATIONS

The results of the WSM and associated analysis reveal that the increased flows predicted by the GISS climate scenario and the decreased flows predicted by the GISS Inverse scenario could have major effects on TVA operations. The programs or areas of activity which would experience the greatest impacts, based on current operating policy, can be summarized as follows:

Reservoir Operations

The reservoir guide curves presently used to operate the reservoir system were developed based on historical weather patterns and flood experience. The curves, which allocate storage space to be held in reserve during the flood season (except when used for flood regulation), provide target reservoir elevations for different times of the year to meet navigation, flood control, and power demand constraints.

GISS Scenario. In the GISS scenario, the increased runoff predicted in the eastern region during the winter through summer months resulted in higher minimum, median, and maximum elevations throughout most of the year. The higher maximum elevations indicate a high probability of spillage at all major tributary reservoirs during exceptionally wet years. During the fall months when the GISS model predicted reduced runoff, the increased storage from earlier months generally enabled the reservoirs to maintain higher fall reservoir levels. These trends indicate that the current reservoir guide curves and operating philosophy would need to be reevaluated to provide more storage capacity during the flood season; take advantage of the opportunity for longer summer full pool levels; adjust to changes in power load demands due to seasonal changes in temperature; etc. Any reevaluation of the guide curves would also need to take into consideration the likelihood of increased variability in the occurrence of extreme events and potential changes in the Probable Maximum Precipitation.

GISS Inverse Scenario. In this climate change scenario, the decreased runoff predicted in the eastern basin generally results in lower minimum, median, and maximum elevations throughout the year. These lower elevations indicate more reservoir storage would be available for flood control operations than in the base case and should reduce the probability of downstream flooding. However, satisfying the other project purposes would be more difficult to accomplish. During very dry periods it probably would be impossible to satisfy all the competing purposes, and the very low reservoir levels would create adverse public reaction.

The current operating philosophy and guides should be reevaluated in order to determine appropriate normal minimum and normal maximum levels; determine the required flood storage for the GISS Inverse floods and reallocate flood storages if necessary; and develop operating strategies that would minimize the adverse impacts of this scenario.

A total reevaluation of the operation of a complex reservoir system that includes 42 major dams and reservoirs and serves multiple functions is a major undertaking. A comprehensive review of TVA reservoir operations and planning is currently in progress to provide policy guidelines for operation of the agency into the 21st century. The purpose of the study is to evaluate operational priorities, such as flood control, navigation, and power vs. water quality and recreational needs in order to ensure that the agency is responsive to the changing needs and values of the region. Major changes in the climate regime, and whether these changes are incorporated into the project, could have an impact on the findings and policy implications of the reservoir review study.

Navigation

GISS Scenario. Increased high-flow periods with greater flow magnitudes in the mainstem reservoirs could result in more instances of flooding of industrial and docking facilities. The higher flow velocities associated with high-flow periods could necessitate the suspension of navigation during certain times of the year. Under median-flow conditions, however, the flow needs of the mainstem reservoirs for navigation purposes would be easily met or exceeded under the climate change scenario.

GISS Inverse Scenario. This climate change scenario would have little effect on navigation. Minimum pool levels on the mainstem reservoirs, which were maintained in this scenario, provide ample depth for navigation. However, as illustrated in Table 3, the decreased runoff of the GISS Inverse scenario generally results in reduced flow magnitudes during flood events. This will reduce the frequency of flooding of docking facilities and the interruption of navigation due to very high flow velocities.

Flood Control

GISS Scenario. The results of the WSM and the analysis of major flood events at Chattanooga indicate that increased flooding could be a major impact of the GISS climate scenario. As indicated in the previous section, flood damages at Chattanooga for a major flood event could range from slightly under $100 million to $1 billion in 1984 dollars. In addition to Chattanooga, other flood-prone areas in Tennessee, such as Lenoir City, Knoxville, Kingsport, Clinton, Charleston-Calhoun, and the agricultural area surrounding Savannah, would be vulnerable to flood damages.

Increased flood control could be addressed by adjusting the reservoir guide curves or reservoir operating elevations to create more seasonal flood storage; modifying existing dams to provide flood storage above existing levels; or building additional dams to regulate flood flows. The cost of modifying existing dams, depending on the type of dam and alteration required, can range from $5 to $25 million in 1987 dollars.

Alternatively, flood control structures, such as dikes or levees, could be constructed to protect flood-prone areas such as Chattanooga. The cost of levee construction is approximately $1.5 million dollars per mile (1988 dollars) for a 7.6-meter (25-foot) levee.

A major impact of a significantly wetter climate such as the GISS scenario, would be the need to reevaluate the Probable Maximum Precipitation (PMP) and Probable Maximum Flood (PMF). All recently constructed major structures in the TVA system, including the nuclear power plants, were designed to withstand the PMF. Any significant increase in this flood would entail a reevaluation of the safety of these projects.

GISS Inverse Scenario. In general this climate change scenario has favorable impacts on flood control. The results of the WSM and the analysis of major flood events at Chattanooga indicate that the frequency and magnitude of floods would be reduced. This could result in opportunities for additional development along floodplain areas of the Tennessee River Valley. However, before such activities are undertaken new floodplain management studies should be made.

Dam Safety

GISS Scenario. The increased likelihood of the major dams operating at or above normal maximum levels for extended periods of time would necessitate a reevaluation of dam safety at these projects. Individual projects could need increased storage capacity; increased capacity of existing spillways; additional spillways; or strengthening and/or raising of the dam structures. Dam safety analysis would also need to take into account possible changes in the PMF.

A complete analysis of dam safety is presently under way at TVA, and a number of dams are being retrofitted to meet current safety standards. Safety modifications have been completed or are in the construction phase at 11 dams, with project cost ranging from $300,000 to $11 million. Over the next decade, an additional 15 dams will be upgraded. Given the higher flows predicted and increased hydropower potential predicted by the GISS scenario, the question arises whether present dam rehabilitation work and capital expenditures should be based upon historical hydrology or take into account the possibility of future climate changes.

GISS Inverse Scenario. The reduced runoff predicted in this scenario decreases the likelihood of operations at or above maximum pool levels and reduces the probability of dam failure or of incurring major damage to the

TVA dams. The current dam safety program is more than adequate to ensure continued safe operation of the dams.

Power Operations

GISS Scenario. Under the GISS scenario, the estimated 16% increase in average annual system generation (3,100 GWh), valued at $54.7 million (1988 dollars), suggests that many projects could justify added turbine capacity. Given present facilities, during much of the year under the climate change scenario many hydropower projects would need to operate at full capacity to keep the reservoir levels at or below normal maximum levels. While this would increase the use of hydropower to satisfy the base power load, it would decrease the flexibility to use hydropower for peak load demands. This could mean the need for more pumped-storage facilities to supply power quickly during periods of peak demand and/or adding additional capacity at existing hydro plants.

In the TVA region the largest seasonal power demands are for summer cooling. The GISS scenario predicts higher surface temperatures throughout the year. The largest increases in temperature occur in the fall, thereby extending the period of warm weather. These changes, coupled with changes in hydrology, could necessitate the need to reevaluate future power demands and the relative mix of hydro, fossil, and nuclear power to meet these demands.

GISS Inverse Scenario. The estimated 24% loss in average annual system hydrogeneration (4,600 GWh), valued at $87.2 million, would have to be replaced with alternative sources of generation, such as coal-fired, oil, gas, or nuclear generation. Additional capacity would not be required at present to provide this generation. However, increased power demand or retirement of power plants in the future may result in the need to build additional capacity to supply this loss in hydro production. These large losses in generation and capacity on the hydro system will make it more difficult to meet peak load demands. As in the GISS scenario, additional pumped-storage plants or special fossil plants may be required to quickly supply peak power demands.

The reduced flows of the scenario could also have negative impacts on the fossil and nuclear plants. Water quality constraints on discharge water temperatures were not considered in the WSM analysis. Even though adequate volumes of water were supplied to satisfy the water quality constraints, the water may be too warm for use as cooling water and cause suspension of operations at projects such as Bull Run, Colbert, and John Sevier Fossil Plants. Although cooling towers are available at Sequoyah and Watts Bar Nuclear Plants, elevated water temperatures could exceed safety standards for Essential Raw Cooling Water (ERCW) intake.

Water Quality

GISS Scenario. The increased runoff predicted by the GISS scenario could have both positive and negative impacts on water quality. Most projects would be able to generally exceed present downstream minimum flow requirements and, through much of the year, would have greatly increased flow releases. Increased dam releases, resulting in higher flows or tailwater levels below the dams, would increase assimilative capacity of these reaches.

Tailwater dissolved oxygen (DO) levels, a key parameter in determining the biological health of a river, are largely determined by the quality of water released from the upstream dam. Most hydropower dams release water from deep in the reservoir. Consequently, during the critical summer months when many storage reservoirs in the TVA system are stratified, the DO level of the hypolimnic layer (or cold bottom layer) of the reservoir determines the DO content of the releases.

Hypolimnic DO levels result from the complex interaction of a number of physical, biological, and chemical factors including the temperature and quantity of inflows to the reservoir; the residence time through the reservoir; and the organic loading rate from internal and external sources. Generally, increases in organic and nutrient loadings and warmer hypolimnic temperatures increase the rate and extent of hypolimnic DO depletion. Conversely, shorter residence times, or more throughflow (inflow/outflow) through the reservoir, elevate hypolimnic DO levels. The increased runoff predicted by the GISS scenario will increase inflow quantities and

most probably erosion rates, thereby raising inflow temperatures, increasing organic loading rates, and decreasing residence times through the reservoir. These effects will have contradictory impacts on hypolimnic DO levels, and the overall net impact will vary with specific reservoir geometry, time of year, and the relative balance between opposing factors.

Due to the complexity of reservoir dynamics, it is difficult to predict the impact of the GISS model on overall reservoir water quality without detailed site-specific investigations to study the dynamics of each reservoir. It is highly probable, however, that the increased runoff predicted by the GISS scenario would increase nonpoint source pollution, or the sediment, nutrient, and other chemical loads, into the reservoirs. The effect of these higher loading rates could mean lower DO levels, higher turbidity levels, and/or excessive algae growth. On the other hand, increased inflows could improve overall reservoir water quality by increasing reservoir mixing, shortening the residence time through the reservoir, and/or providing a larger volume of water for dilution of negative impacts.

GISS Inverse Scenario. The reduced runoff predicted by the GISS Inverse scenario is likely to have an adverse impact on the water quality of TVA streams and reservoirs. In a typical TVA reservoir, reduced inflow volumes, increased residence times, and low lake levels will result in a deterioration of the water quality. Owing to increased air temperatures and solar radiation predicted by GISS Inverse, the normally warm upper layer of water, the epilimnion, is likely to have increased water temperatures. As cold water in the lower level of the reservoir (hypolimnion) is withdrawn for downstream releases, the warmer epilimnion will become larger and deeper. Increased residence times allow natural processes to deplete more of the available oxygen resources, resulting in a reduction of the DO content of the hypolimnion.

The reduced runoff will likely decrease erosion, initially producing improved water clarity in the reservoirs. Ultimately, however, the increased light penetration may promote luxuriant algal growths, causing decreases in clarity and large diurnal variations in DO and pH. Increased clarity could also promote the growth of aquatic weeds at locations not previously infested.

The severity of these water quality changes may be magnified by the normal assimilation of treated municipal and industrial waste, particularly if waste and heat loads remain at current levels. The lower flows, higher temperatures, and lower DO levels will reduce the ability of the reservoirs to assimilate permitted wasteloads. The situation could be further complicated by the addition of waste pollutants such as color, dissolved solids, and toxins.

The tailwaters, or riverine reaches below dams, will also be adversely impacted by the increased temperature, reduced DO content, and decreased magnitude of the released flow. Many of the streams also provide for the assimilation of municipal and industrial wastewater after appropriate treatment. Although treatment levels are theoretically stringent enough to protect beneficial water uses under low-flow conditions, the extremely reduced runoff produced by the GISS Inverse scenario may diminish streamflow below the critical levels normally used in allocating wastes. The situation may become particularly severe at facilities that are incapable of achieving satisfactory levels of treatment under present conditions.

Several papermill plants in the TVA region depend on dilution of their highly colored wastewater to avoid aesthetically objectionable conditions downstream of their discharges. Following treatment of paper wastes, the plants coordinate waste discharges from large storage lagoons with releases from TVA dams. Under low-flow conditions, the plants must reduce the volume of discharged wastewater and subsequently increase storage in the treatment lagoons. Under the GISS Inverse scenario, during dry periods, prolonged low-flow conditions may force these plants to cut back on production, increase the storage capacity of the treatment lagoons, or be in noncompliance with color requirements for the Tennessee River.

For water quality purposes, TVA has agreed to maintain minimum daily flows of 56 cms (2,000 cfs) at Knoxville, 17 cms (600 cfs) at Charleston, 168 cms (6,000 cfs) at Chattanooga, 39 cms (1,400 cfs) below Chilhowee dam, and 10 cms (350 cfs) or 1/3 of the plant intake at John Sevier Fossil Plant (JSF) for the bypass requirement. These constraints have high priority in the WSM, and the required flows are maintained under

the GISS Inverse scenario. As discussed previously, however, during dry periods, reservoirs are drawn as necessary (sometimes below acceptable levels) to meet these requirements.

Recreation

GISS Scenario. Under present operating policy, full-pool reservoir levels are generally reached by May or early June. Through the summer months, when streamflows are typically low and power demands high, lake levels are significantly lowered. Under the GISS scenario, the results of the WSM indicate that the increased runoff in the winter through summer months would produce extended operations at higher levels during the summer. The ability to maintain summer full-pool levels for longer periods of time would greatly enhance recreation benefits, particularly on the eastern tributary reservoirs. Extended summer pool operations increase opportunities for boating, fishing, and other water-based activities, which is important in promoting tourism and economic development. The priority assigned, and who should pay, to maintaining summer full-pool levels is at present a major issue in reservoir operations. Recreation proponents are interested in maintaining summer pool levels from April through October.

Under current operating conditions, the TVA reservoir system received approximately 74.7 million recreation visits in 1986. Recreational development and equipment in the reservoir system were valued at greater than $630 million in 1978. Extended summer pool levels could increase these numbers substantially.

The increased flows predicted by the WSM would not only increase recreational uses of the reservoir, but could also enhance recreational benefits in the tailwaters below the dams. Increased flows could increase boating, fishing, canoeing, and/or rafting opportunities. At present, special weekend recreational releases are made at several dams, such as Ocoee and Chatuge Dam, to enhance downstream floating activities. Under the climate change scenario these types of releases would be more commonplace.

GISS Inverse Scenario. Assuming the reduced lake levels and streamflows produced by the GISS Inverse scenario are similar to conditions evaluated by the 1986 drought plan (Clark et al., 1986), adverse impacts on recreation in the Tennessee Valley can be expected. The reduced assimilative capacity of streams and lakes may result in higher concentrations of sewage bacteria, causing increased health hazards in high recreational use areas. Higher water temperatures will increase the survival time of sewage bacteria resulting in further potential for contamination. Increased color levels, particularly below industrial discharges, and algal growths may produce aesthetically objectionable conditions and discourage swimming and recreational boating.

As TVA reservoir levels decline, exposing mudflats and extensive shoreline, the attractiveness of the reservoirs will also decline. Recreational users of the reservoirs may also be discouraged by increased turbidity and odor levels. The incidence of navigation hazards on tributary and some mainstem reservoirs is likely to increase if reservoir levels are significantly below normal summer full-pool levels.

Fish and aquatic life will also be adversely impacted by the lower lake levels and associated negative impacts on water quality. As aquatic habitat is reduced, fish stocks are likely to become depressed, particularly in tailwaters and tributary reservoirs. Reduced fish stocks, along with loss of aesthetic appeal of the reservoirs, will probably result in large losses in recreational fishing.

Commercial recreation operators and other commercial services that depend on recreation visitors to TVA reservoirs could be severely impacted by decreased recreational opportunities. Facilities such as boat launches will be impaired by lower lake levels. The $630 million (1978 dollars) investment in recreational development and equipment in the Tennessee Valley could be threatened.

Water Supplies

GISS Scenario. In general, the higher runoff predicted by the GISS scenario would benefit water supplies by increasing reservoir levels and flow magnitudes below dams, and recharging groundwater supplies.

GISS Inverse Scenario. Based on the results of drought studies conducted in the TVA area (Clark et al., 1986), it can be extrapolated that the reduced streamflows and reservoir levels associated with the GISS Inverse scenario will have negative impacts on the quality and quantity of water supplies in the Tennessee Valley. Water supply studies in the Tennessee Valley portion of Tennessee, Alabama, and Kentucky identified 49 public and 40 self-supplied commercial and industrial water users that would be adversely effected by prolonged drought conditions. All of these systems, which would primarily experience water shortage problems, are served by groundwater sources or small tributary streams.

Water supplies located in TVA reservoirs or below TVA dams would probably have sufficient water to meet demands, but could experience operational difficulties and customer dissatisfaction due to degraded water quality conditions. Taste and odor problems and complaints about higher water temperatures are likely to increase. Increased dissolved solids and algae growths may clog treatment plant filters. Several water intakes in TVA reservoirs are located immediately above waste discharges. During extended low flow conditions there are increased opportunities for wastes to backflow upstream to water supply intakes.

CHAPTER 5

SUMMARY AND CONCLUSIONS

The objective of this project was to identify the sensitivity of the TVA reservoir system to global climate change. Potential changes in reservoir operations, navigation, flood control, hydropower production, water availability, water quality, and recreation were evaluated for the Tennessee River Basin. Implications of these changes, as well as potential adaptive strategies, were also outlined for the reservoir system and related TVA programs.

METHODOLOGY

The Weekly Scheduling Model (WSM) was used to assess climate change impacts on the TVA reservoir system. WSM is a planning model used to simulate long-term, week-to-week variations in water level, discharge, and power production for the 42 reservoirs operated within the system. Based on a linear programming algorithm, the model selects a weekly reservoir schedule for each reservoir by sequentially satisfying a series of operating objectives in a prescribed order of priority. The primary objective is to minimize deviation from historical normal operating levels, subject to reservoir release and level constraints imposed to meet navigation, flood control, water supply, power generation, water quality, and recreational requirements.

A primary input into the WSM is historical local flow into each reservoir in the TVA system. Local inflows result from unregulated overland and tributary flows into each project. It was assumed that changes in local flows were directly proportional to changes in runoff. Consequently, in the application of the WSM, monthly ratios ($2xCO_2$/CONTROL) for surface runoff provided by EPA for two climate scenarios were used directly to adjust historical local inflows to each project for the 30-year study period (1951-1980). It was also assumed that monthly runoff ratios applied equally to each week within the month; existing guide curves defined the target operating conditions for each reservoir; and current operating policy defined the set of model constraints.

The two weather scenarios provided by EPA are based on the NASA Goddard Institute for Space Studies (GISS) general circulation model. The GISS model grid divides the TVA basin into two regions that coincide with major hydrologic units: the portion of the Tennessee Valley east of Chattanooga (80°W grid); and the portion west of Chattanooga (90°W) grid. For each grid, GISS provides monthly average values for key climate variables for a control run, a $2xCO_2$ run, and the ratio ($2xCO_2$/CONTROL). The $2xCO_2$ levels, and therefore ratios, represent the endpoint effects of a doubling in CO_2 atmospheric concentrations.

The first scenario is based on GISS model data directly provided by EPA. This GISS scenario predicts a warmer and wetter climate for the Tennessee Valley. In the eastern basin average annual runoff increases 31%. On a seasonal basis, runoff increases in the winter through summer months and decreases in the late fall. The largest predicted increase occurs in March (73%) and the largest decrease in November (-28%). The net effect in the eastern basin, which contains all of the large tributary storage reservoirs, is to exaggerate peak flows during the traditional flood season and further decrease flows during a dry period of year. West of Chattanooga, runoff ratios are more variable. On a seasonal basis, runoff increases in the winter and summer and decreases slightly in the spring and fall. The integrated effect of eastern and western basin runoff on the Tennessee River is to increase local inflows throughout the year except during November and December.

Runoff data initially provided by EPA for the second weather scenario were generated by Princeton University's Geophysical Fluid Dynamics Laboratory (GFDL) general circulation model. The GFDL runoff data, however, appeared unreasonable for the Tennessee Valley. To meet EPA project objectives and time constraints, EPA and the GISS model developers recommended utilizing the inverse of the GISS runoff values. This approach, referred to as GISS Inverse, uses runoff values in the range of model sensitivity and illustrates the potential impacts of a warmer and significantly drier climate. The two scenarios together, therefore, represent

the full spectrum of impacts from the extremes of a wetter versus drier climate. Both of these extremes have been predicted for the southeast by other GCM and hydrologic models (Hains, 1988).

In the eastern basin, average annual runoff decreases 31% under the GISS Inverse scenario. On a seasonal basis, runoff decreases from January through October, with the largest decrease (75%) in March, while runoff increases during November (18%) and December (28%). As runoff is reduced substantially during the traditional flood season and only modestly increased during a dry period of the year, the net effect in the eastern basin is to create low inflows throughout the year. In the western basin, the runoff ratios are more variable, but the net effect is also to reduce runoff from current levels.

The methodology applied in this project provides an overview of the response of the TVA reservoir system, as an integrated system, to changes in historical local inflow. There are, however, several important limitations to the methodology, including the following: existing guide curves and current operating policy were used in the WSM; runoff ratios provided by the general circulation model were applied directly; current water use and power demand patterns were assumed in the analysis; the historical distribution of runoff was assumed to remain the same; and the spatial and temporal distributions of runoff and precipitation events, particularly under extreme drought or flood conditions, were not considered. In a more detailed analysis of climate impacts model constraints should be modified to reflect changes in operating policies and priorities; temperature effects on power and water use patterns should be evaluated; temperature, precipitation, humidity, and other climate variables should be used with hydrologic models to generate more site-specific runoff data; groundwater issues should be addressed; and the distribution of rainfall and runoff events should be considered.

IMPACTS OF CLIMATE CHANGE ON THE TVA SYSTEM

GISS Scenario. The impacts of the GISS scenario on the TVA system are summarized in Table 4 and Figure 13. The generally increased runoff predicted by GISS results in higher reservoir elevations throughout the year at all major projects in the Tennessee Valley. However, the impacts of this scenario are most apparent in the large storage reservoirs located in the eastern portion of the Tennessee Valley. Although runoff is slightly decreased in November and December, the additional storage earlier in the year enables the reservoirs to meet or exceed normal operating levels during the fall. During the traditional flood season (December-March), normal maximum levels are exceeded several times during wet years at the tributary projects. During the summer, full-pool levels are generally maintained for an extended period of time.

The major adverse impact of the GISS scenario is to increase spill, particularly during wet years, at tributary and mainstem projects during the traditional flood season. This would result in increased flood potential throughout the Valley. At Chattanooga, Tennessee, a major city on the Tennessee River with the greatest urban damage potential in the Valley, the river stage of four out of five major historical floods is increased. During two of these flood events, stages would exceed the Tennessee River banks and could cause damages in the range of $100 million to $1 billion (1984 dollars).

Extended operations at or above normal maximum levels would also necessitate the reevaluation of dam safety at TVA projects. Additionally, potential changes in the Probable Maximum Precipitation and Probable Maximum Flood resulting from a major climate shift could have significant safety implications at dams and nuclear power plants.

Primary benefits of the GISS scenario include increased power production; enhanced recreational opportunities; and improved water availability for water supplies and minimum flow requirements. Average annual system generation would increase by 3.1 million MWh, or 16%, at an annual value of $54.7 million (1988 dollars). The increased opportunity to maintain extended full summer pools would greatly enhance recreational opportunities, particularly on the tributary storage reservoirs. The general increase in water availability and storage would improve water supplies, the assimilative capacity of lakes and streams, and the ability to exceed minimum flow requirements for water quality. The overall effect on water quality, however, would be site-specific depending on the relative influence of increased inflows versus the potential for increased nonpoint source pollution (NPS).

Table 4. Potential Impacts of the GISS Scenario on the TVA Reservoir System

Activity	Impact	Implications	Potential Alternatives and/or Modifications	Cost Information
Reservoir Operations	- Higher levels throughout the year - Elevations above normal maximum during traditional flood season - Extended full summer pool - Higher fall reservoir levels	- Increased storage and and water availability - Increased likelihood of spill and downstream flooding - Enhanced recreational opportunities - Improved ability to meet minimum flow requirements	- Reevaluate reservoir guides and operating philosophy to better utilize available water and provide additional storage capacity during flood season	
Navigation	- Minimum navigation levels exceeded throughout the year - Increased periods of high flow	- Minimal overall effect - Increased incidences of flooding dock facilities and suspension of navigation		- $4.8 billion private investment (1933-1984)
Flood Control	- Increased spill at tributary and mainstem reservoirs during flood season - Increased flood peaks at Chattanooga (March 1973 peak flood stage increased by 26.7 ft); overflow banks during major floods	- Increased flooding potential throughout Valley - Increased flood damage at Chattanooga	- Adjust reservoir guide curves to provide more seasonal flood storage - Modify existing dams - Construct additional dams - Construct flood control structures (levees) in flood-prone areas (Chattanooga)	- $100 million - $1 billion (1984 dollars) potential damage at Chattanooga for major event - $5-27 million (1987 dollars) to modify existing dams - $1.5 million/mile (1988 dollars) to construct levees
Dam Safety	- Dams operate at or above normal maximum levels for extended periods of time	- Reevaluate dam safety - Potential impacts on Probable Maximum Precip (PMP) and Probable Maximum Flood (PMF)	- Adjust reservoir guide curves - Increase reservoir storage capacity - Increase spillway capacity - Construct additional spillways - Strengthen or raise existing dams	- $5-27 million (1987 dollars) to modify existing dams

Table 4. Potential Impacts of the GISS Scenario on the TVA Reservoir System (continued)

Activity	Impact	Implications	Potential Alternatives and/or Modifications	Cost Information
Power Operations	- 3.1 million MWh or 16% increase in average annual system generation - Full capacity operation required at many plants for extended periods - Increased spill	- Improved hydropower generation - Increase use to satisfy base load, but loss of flexibility for peaking operations - Decreased operating heads and power output during periods of spill	- Justify added capacity - Construct more pumped-storage facilities for peaking purposes - Reevaluate future power needs and relative mix of hydro, fossil and nuclear - Reevaluate maintenance schedules	- $54 million annual value of increased energy (1988 dollars)
Water Quality	- Variable impact on DO, temperature, and general water quality - Improved assimilative capacity in tailwaters - Exceed minimum flow requirements - Increased nonpoint source pollution (NPS)	- Relative influence of increased inflows vs increased NPS will determine general water quality - Site specific impacts		
Recreation	- Extended full summer pools - Increased tailwater flows	- Enhanced reservoir recreation (boating, fishing, swimming) - Enhanced tailwater recreation (canoeing, rafting, etc) - Potential for increased tourism & economic development	- Reevaluate reservoir guide curves to provide full summer pools April through September - Encourage economic development of recreation opportunities	- $630 million (1978 dollars) current value of recreational development & equipment
Water Supplies	- Increased water availability & storage	- Adequate water supplies		

Figure 13
Summary of Probabilistic Pool Level Forecasts for Norris and Watauga Reservoirs

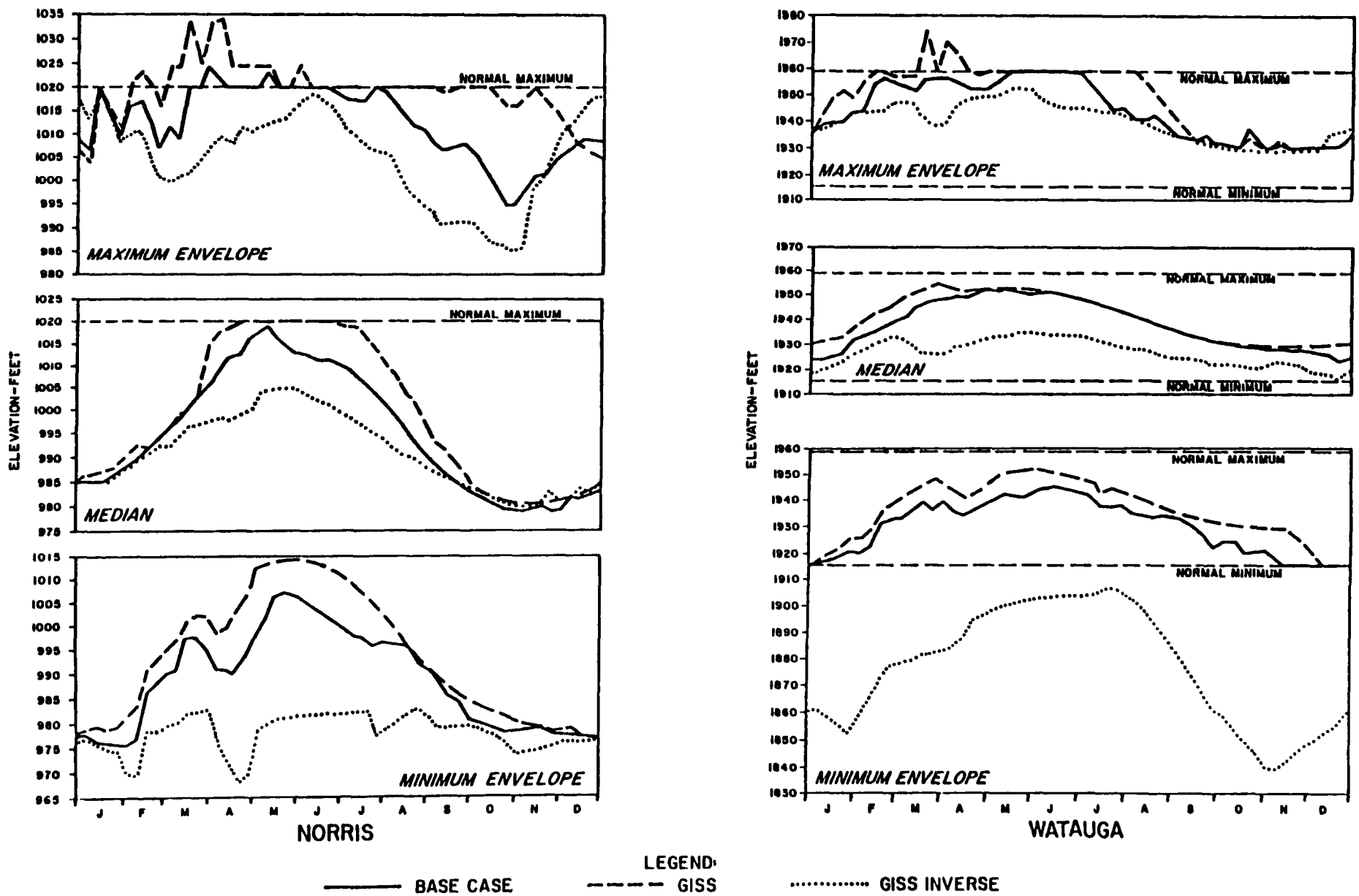

ENG LAB 1988

Miller

A climate change similar to GISS would likely result in a reevaluation of the current reservoir operating philosophy and guide curves to better utilize the increased water availability and to provide additional storage capacity during the flood season. Added turbine capacity could be justified, while more pumped-storage or special fossil plants could be needed for peaking purposes. It is likely that major dams would need to be modified to meet safety standards and/or create additional flood storage capacity. Finally, programs to control or mitigate the adverse impacts of increased nonpoint source pollution would need to be expanded.

GISS Inverse Scenario. The results of the GISS Inverse scenario are summarized in Table 5 and Figure 13. Under the GISS Inverse scenario, runoff is decreased throughout most of the year resulting in a general decrease in storage and water availability. At the tributary storage reservoirs, lake levels are lowered throughout the year. Median reservoir levels are up to 9 meters (30 feet) lower than the base case and, during dry years, minimum reservoir levels are often below normal minimum pool levels.

Based on current operating policy, the WSM is constrained to fill the mainstem reservoir to normal operating levels and to meet minimum downstream flow requirements for water quality. Consequently, these specific objectives are met under the GISS Inverse scenario; however, this is accomplished at the expense of severely reducing reservoir levels in the tributary storage reservoirs. The adverse impacts of these reduced levels include reduced power generation; impaired water quality; degraded recreational opportunities; and decreased water availability for water supplies.

Under the GISS Inverse scenario, average annual system power generation is decreased by 4.7 million MWh, or 24%. As hydropower, the least cost source of energy, must be replaced by more expensive sources of energy such as fossil or nuclear power, this loss in energy has an $87.2 million (1988 dollars) replacement value. Not only is system generation reduced, but owing to the reduced heads and flows, system hydropower capacity would also be reduced. Additionally, owing to decreased flows and elevated water temperatures, operations at several fossil and nuclear plants could be restricted because of thermal and/or safety limits.

The reduced reservoir levels and tailwater flows would likely result in significant deterioration of the water quality in TVA lakes and streams. The reduced DO levels, increased temperatures, and reduced assimilative capacity would adversely affect aquatic biota, fish, and wildlife, as well as recreational uses. The reduced water availability is likely to result in water shortages for groundwater water supply systems, while operational difficulties and customer dissatisfaction are likely to be experienced by supply systems withdrawing reservoir water.

The benefits of the GISS Inverse scenario are related to reduced flood potential and associated damages. Current normal maximum levels would rarely be exceeded and flood stages at Chattanooga would be reduced. Increased development of current floodplain areas may be possible. The probability of dam failure or major damage would be substantially reduced.

To deal with the significant reduction in water availability predicted by GISS Inverse, current operating philosophy and reservoir guides would need to be reevaluated to increase storage during the wet periods and conserve water during the extended dry periods of the year. Drought-related issues would increase in significance as compared to management of the reservoir system for flood control. It would be difficult to satisfy project purposes at many reservoirs, and a reordering of TVA priorities would probably be required. Alternative sources of energy would need to replace lost hydropower potential, while it is likely that industrial and municipal treatment plants would need to adhere to more stringent waste standards. Adverse economic impacts on the Tennessee Valley could be significant resulting from increased power costs, decreased recreational revenues, and increased industrial restrictions.

Table 5
Potential Impacts of the GISS Inverse Scenario on the TVA Reservoir System

Activity	Impact	Implications	Potential Alternatives and/or Modifications	Cost Information
Reservoir Operations	- Lower levels throughout the year - Maximum levels never exceed existing normal maximum pool levels, often resemble current normal levels - Median levels up to 30 feet lower than base case levels - Minimum levels often at or below existing normal minimum pool levels	- Decreased storage and water availability - Decreased likelihood of uncontrolled spill and downstream flooding - More difficult to satisfy project purposes - Create adverse public reaction	- Reevaluate reservoir guides, normal maximum and minimum levels, and operating philosophy to better utilize the decreased runoff	
Navigation	- Minimum pool levels maintained on mainstem reservoirs	- Minimum navigation levels maintained		- $4.8 billion private investment (1933-1984)
Flood Control	- Decreased maximum reservoir levels - Decreased flood stages at Chattanooga	- Decreased flooding throughout valley - Minimal flood damage at Chattanooga	- Reevaluate reservoir guide curves to reallocate flood storage (increase normal minimum levels) - Increased development of current floodplain areas	
Dam Safety	- Decreased likelihood of operations at or above maximum pool levels	- Reduced probability of dam failure or major damage - Potential impacts on PMP and PMF	- Evaluate current dam safety program and need to retrofit older dams	
Power Operations	- 4.7 million MWh or 24% decrease in average annual system generation - Reduced flows and increased water temperatures	- Reduced hydropower generation and capacity - Loss of hydropower for reliable peaking operations - Potential problems with meeting thermal and/or safety limits at some fossil and nuclear plants	- Increased reliance on nuclear and fossil plants - Construct alternative means to satisfy peaking demands (pumped-storage and fossil plants with peaking capability) - Increased use and/or construction of closed-cycle cooling systems	- $87 million annual loss in benefits (1988 $) - $75 million (1985 $) to retrofit John Sevier Fossil Plant with cooling towers (costs at other plants would vary)

Table 5
Potential Impacts of the GISS Inverse Scenario on the TVA Reservoir System

(continued)

Activity	Impact	Implications	Potential Alternatives and/or Modifications	Cost Information
Water Quality	- Reduced reservoir levels - Reduced tailwater flows - Reduced nonpoint source pollution	- Deteriorated reservoir water quality (reduced DO and increased temperatures) - Degraded water quality in tailwaters - Reduced assimilative capacity in lakes and streams - Adverse impacts to fish and wildlife - Increased health hazards from reduced assimilative capacity	- More stringent waste treatment standards and/or cut-backs in industrialized production - Improved situation assessment and monitoring techniques to identify critical problems	
Recreation	- Reduced reservoir levels - Reduced tailwater flows	- Degraded recreational opportunities in lakes and streams - Adverse economic effects on commercial operations and recreational developments	- Reevaluate reservoir guide curves to minimize adverse effects - Target specific reservoirs for recreational use	- $630 million (1978 $) current value of recreational development and equipment
Water Supplies	- Reduced reservoir levels	- Water shortages experienced by groundwater or small tributary stream systems - Operational difficulties and customer dissatisfaction for systems on large reservoirs - Increased waste treatment costs	- Encourage conservation through education and economic incentives - Improve water conservation/ leak detection in distribution systems - Recycle industrial process and cooling water - Total metering of public water supplies	

CONCLUSIONS

Results of this study indicate that a major shift in the global climate could have significant impacts on the TVA reservoir system. The warmer and wetter climate suggested by the GISS scenario could benefit the Tennessee Valley through increased power production, enhanced recreational opportunities, and increased water availability. However, flood control, as well as dam and nuclear plant safety, could become major issues. Conversely, the significantly reduced water availability resulting from the GISS Inverse warmer and drier climate could threaten the ability of many TVA projects to fulfill their current operating goals and purposes. Under both climate scenarios, significant changes in the reservoir guide curves, as well as potential structural changes and/or additions to the system, would be required to respond to an altered climate.

The results of this study are based on runoff data generated by a general circulation model and represent potential climate changes from a doubling of atmospheric CO_2 (possible by the year 2030). The study is intended to assess the sensitivity of the TVA reservoir system to extreme climate changes and to identify the implications of these changes. The project objective was not to predict the future climate in the TVA region. Scientists concur that significant global climate changes -- increased global mean surface temperatures and precipitation -- are highly probable (NAS, 1987). It is, however, currently impossible to accurately predict the magnitude of the change or climate impacts on a regional basis. Furthermore, given the normal cycles of wet and dry periods in the historical record, it is difficult to distinguish long-term changes from natural weather variations.

The Tennessee Valley is presently experiencing the worst drought on record. Precipitation and runoff have been significantly below average for more than four years. The question arises, "How many years of abnormal weather constitute a long-term change in climate?" Given the noted sensitivity of the TVA reservoir system to climate change, the recent weather patterns in the Tennessee Valley, and the general scientific consensus that atmospheric changes are highly probable, this issue should be investigated in more detail.

Future climate change studies should include an in-depth hydrologic study of the TVA region based on temperature, precipitation, and other climate variables generated by general circulation models. Based on potential changes in hydrology and temperature, detailed assessments should be conducted to address TVA reservoir and power system impacts; Tennessee Valley social and economic development; and institutional and legal ramifications. Finally, potential adaptation strategies need to be identified and methodologies need to be developed for incorporating climate change issues and uncertainties into TVA's long-range planning and decision-making process.

LIST OF ABBREVIATIONS, SYMBOLS, AND DEFINITIONS

ABBREVIATIONS

ALCOA	--	Aluminum Company of America
cfs	--	cubic feet per second
cms	--	cubic meters per second
DO	--	dissolved oxygen
EPA	--	Environmental Protection Agency
ft	--	feet
GFDL	--	Geophysical Fluid Dynamics Laboratory
GISS	--	Goddard Institute of Space Studies
GWh	--	gigawatt hours
m	--	meters
MWh	--	megawatt hours
NPDES	--	National Pollutant Discharge Elimination System
PMF	--	Probable Maximum Flood
PMP	--	Probable Maximum Precipitation
TVA	--	Tennessee Valley Authority
WSM	--	Weekly Scheduling Model

SYMBOLS

CO_2	--	carbon dioxide
N_xO_y	--	nitrogen oxide
CFC	--	chlorofluorocarbons

DEFINITIONS*

lower envelope--minimum weekly reservoir elevations for given period of record

median projection--median of WSM projected operations based on given period of record

normal operations--normal reservoir operations based on 15 years of operation experience (1972-86); target elevation for each year of simulation

normal maximum level--elevation above which a reservoir would not be operated except during periods of high flow; extended operations above normal maximum levels often result in spillage

normal minimum level--elevation below which a reservoir would not be operated except under extreme drought conditions

upper envelope--maximum weekly reservoir elevations for given period of record

---

* Definition of curves used in Probabilistic Pool Level Forecasts

REFERENCES

Clark, L. R. et al., "TVA's Response to Drought Related Water Quality Impacts in the Tennessee River System," Water Quality Drought Task Force, TVA, Knoxville, Tennessee, 1986.

Gilbert, K.C., and R.M. Shane, "TVA Hydro Scheduling Model: Theoretical Aspects," ASCE Journal of the Water Resources Planning and Management Division, Vol. 108, No. WR1, pp 21-36, March 1982.

Grotch, S.L., "Regional Intercomparisons of General Circulation Model Predictions and Historical Climate Data," Department of Energy Report No. NBB-0084, Dist. Category UC-11, Washington, D.C., 1988.

Hains, D.K., "Impacts of Runoff in the Upper Chattahoochee River," (EPA National Assessment of Climate Change Effects), C.F. Hains, Hydrologist, Inc., 1988.

MacCracken, M.C., "The Reality of the Greenhouse Effect," Lawrence Livermore National Laboratory, Livermore, California, Preprint UCRL-95580, 1986.

Miller, B.A., and W.G. Brock, "Sensitivity of the Tennessee River Valley to Global Climate Change," Report No. WR28-1-680-101, Engineering Laboratory, Norris, Tennessee, 1988.

National Academy of Sciences, "Current Issues in Atmospheric Change: Summary and Conclusions of a Workshop, October 30-31, 1986," National Academy Press, 1987.

Rind, D., "The Doubled CO_2 Climate and the Sensitivity of the Modeled Hydrologic Cycle," Journal of Geophysical Research (in print), 1988.

Shane, R.M., "Weekly Scheduling Model for the TVA Reservoir System," Report No. WR28-1-500-126, TVA Engineering Laboratory, Norris, Tennessee, 1984.

Shane, R.M., and K.C. Gilbert, "A Weekly Time Step Scheduling Model for the TVA Operated Reservoir System," Water Resources Publication, Littleton, Colorado, 1981.

Waffel, Heinz-Dieter, "Operation Objectives in TVA's Weekly Scheduling Model," Report No. WR28-2-590-119, TVA Engineering Laboratory, Norris, Tennessee, 1985.